RESEARCH ACTIVITIES I
Department of Theoretical Studies

I-A Development of New Theoretical and Numerical Techniques in the Study of Molecular Structures

Theories of the electronic structure of molecules have been extensively developed for last four decades. The theories are in some senses at a matured stage. However, there are plenty of challenging and practically important problems to be solved.

I-A-1 Generalization of the Coupled-Cluster Response Theory to Multireference Expansion Spaces; an Application of the Coupled-Cluster Singles and Doubles Effective Hamiltonian

Seiichiro TEN-NO, Suehiro IWATA, Sourav PAL *(Nat. Chem. Lab. India and IMS)* **and Debashis MUKHERJEE** *(Indian. Assoc. Cult. Sci.)*

[*Theor. Chem. Acc.* (Prof. Fukui's memorial issue), in press]

Employing separate cluster ansatz in time-independent and dependent wave-operators, the coupled-cluster (CC) response theory is generalized to the multireferecne expansion spaces. For state energies, this corresponds to the multireference secular problem with an arbitrary similarity transformed effective Hamiltonian, $\tilde{H} = \Omega^{-1}H\Omega$. The effective Hamiltonian can be generated via the size-extensive CC methods. And thus the states in the multireference linear response theory (MRLRT) maintain the core-extensive properties as in the usual CC ones. We have used the Gelfand unitary group basis of the spin-adapted configurations to construct the matrix of $\tilde{H}$ in the MR excitation space.

As a preliminary application, the CC singles and doubles effective Hamiltonian is applied to excitation and photo-ionization energies of the CH^+ and N_2 molecules, compared with experimental results and those from other numerical procedures including conventional CC linear response theory (CC-LRT), multireference and full configuration interaction (MRCI and FCI) methods. The numerical results indicate that the MRLRT reproduces valence- and external-excited states quantitatively, combining best features of the CC-LRT and MRCI.

I-A-2 Modified McMurchie-Davidson Method for the Calculation of the Two-Electron Integral and its Derivatives

Feiwu CHEN and Suehiro IWATA

In the McMurchie-Davidson(MD) method, the product of two Gaussian functions are expanded as a linear combination of Hermit Gaussians. In the original procedure, the expansion coefficients are calculated recursively starting from the zero-th order function. We have shown that these coefficients are expressed explicitly without invoking any recursive procedure. Thus, the evaluation of two-electron integrals for higher angular momentum functions becomes more efficient than the original MD method. The derivatives of the two-electron integral respected to the nuclear coordinates are also expressed explicitly. The present extension of the MD method is expected to be very useful both for direct methods and for parallel computations in the Master-Slave mode.

I-A-3 A New Perturbation Expansion for Solution of Higher Roots in Quasi-Degenerate Problems

Feiwu CHEN and Suehiro IWATA

Quasi-degenerate perturbation theory (QDPT) using effective Hamiltonian theory is one of the most important approaches in modern quantum chemistry and dates back to the early partitioning technique by Löwdin. Based on the partitioning technique, we have derived an energy expression for the higher roots, which has a similar form with the conventional non-degenerate perturbation expansion. With perturbation parameter λ, Hamiltonian matrix can be partitioned as follows

$$\begin{pmatrix} H^0_{PP} + V_{PP} & \lambda V_{PQ} \\ \lambda V_{PQ} & H^0_{QQ} + \lambda V_{QQ} \end{pmatrix}, H_{PP} = H^0_{PP} + V_{PP}, H_{PQ} = V_{PQ}, H_{QQ} = H^0_{QQ} + V_{QQ}$$

The size of H_{PP} is n, and the eigenvalues of H_{PP} are $\varepsilon^{(0)}_p$, $p = 1,2,\cdots,n$. After some manipulation, the perturbation expansion for the p-th eigenvalue $E(\lambda,p)$ is expressed as

$$E(\lambda,p) = \varepsilon^{(0)}_p + \frac{1}{\sum_{j=1}^{n} A_{jj}(\varepsilon^{(0)}_p)} \left\{ \sum_{i=1}^{n} \sum_{a}^{Q-space} \frac{A^a_i(\varepsilon^{(0)}_p) V_{ai}}{\varepsilon^{(0)}_p - \varepsilon^{(0)}_a} \lambda^2 + \sum_{i=1}^{n} \sum_{a,b}^{Q-space} \frac{A^a_i(\varepsilon^{(0)}_p) V_{ab} V_{bi}}{(\varepsilon^{(0)}_p - \varepsilon^{(0)}_a)(\varepsilon^{(0)}_p - \varepsilon^{(0)}_b)} \lambda^3 + \cdots \right\}$$

where $A_{jj}(\varepsilon^{(0)}_p)$is the cofactor of determinant $|H^0_{PP} + V_{PP} - \varepsilon^{(0)}_p \mathrm{I}|$, and $A^a_i(\varepsilon^{(0)}_p)$ is a variant of the same determinant with the i-th column replaced by the first n elements of the a-th column of matrix V_{PQ}. A uniqueness of this expansion is that it converges to any of p-th eigenvalue ($p \le n$), and that the re-diagonalization within the model space P is not required.

I-A-4 Photodetachment Cross Section of Anions

Feiwu CHEN, Takeshi TSURUSAWA and Suehiro IWATA

A method to evaluate the photodetachment cross

section using L^2 basis set and conventional ab initio MO CI wave functions is developed. To augment the Gaussian type functions, we introduce a set of eigenfunctions of a particle-in-box potential (PIBF) to describe the excess electron as well as the ejected electron. We code a new integral calculation package, in which the molecular integrals for the mixed basis set of the Gaussian and PIBF are evaluated. To reduce the number of integrals to be evaluated, only the coulomb (gg'|kk') and exchange (gk|g'k') types of two-electron integrals are calculated, where g and g' stand for the Gaussian functions, and k and k' for PIBF. Under this limitation of the integrals, we introduce a series of the approximations for many-electron wave functions of the initial and final states. Since the role of the electron correlation in the wave functions of the anion (initial state) and of the neutral (final state after an electron ejection) is different, special cares should be taken in developing the approximations. Because we use the discrete k values for PIBF, the hybrid basis set is still a L^2 basis set. To evaluate the photodetachment cross section, we use the Stieltjes Imaging (Lanczos Recursive) method.

I-A-5 Iterative Method for Spectral Decomposition

Tsutomu IKEGAMI and Suehiro IWATA

A method for the spectral decomposition of a ket state $|\boldsymbol{v}\rangle$ with respect to a set of eigen states of Hamiltonian H (or any hermitian operators) is developed. First, a Chebyshev series $T_n(H)|\boldsymbol{v}\rangle$ is generated through a sequential operation of H on $|\boldsymbol{v}\rangle$. From the Chebyshev series, $\exp(iHt)|\boldsymbol{v}\rangle$ is evaluated approximately for several value of t. By taking an inner-product of $\exp(iHt)|\boldsymbol{v}\rangle$ with the original $|\boldsymbol{v}\rangle$, we obtain an auto correlation function for $|\boldsymbol{v}\rangle$, whose Fourier transformation gives the spectral density. If $\exp(iHt)|\boldsymbol{v}\rangle$ itself is Fourier-transformed, the eigen states are obtained as a function of energy (or the others depending on the hermitian operator). The method is applied for the vibrational state of the Morse potential, and both the discrete and the continuum states are well described. The method works also well for one-dimentional multi-state problems.

I-B Water Clusters and Their Complexes with Atomic Ions

I-B-1 Dipole-Bound and Interior Electrons in Water Dimer and Trimer Anions: Ab Initio MO Studies

Takeshi TSURUSAWA and Suehiro IWATA

[*Chem. Phys. Letters* **287**, 95-110 (1998)]

Two types of structures of water dimer and trimer anion are found in the ab initio molecular orbital study with an extensively diffuse basis set. The first type is the dipole-bound anion, and the excess electron is distributed exteriorly, or on the surface of water clusters. In the second type of dimer and trimer anions, the excess electron is internally trapped between two waters. The electron correlation contributes to stabilizing the latter anions. The calculated vertical detachment energies for both types of trimers are positive.

I-B-2 A New Form of Stable Excess Electron: {e}·(HO) bonds

Takeshi TSURUSAWA and Suehiro IWATA

It has been known that two types of molecular anions are stable; one is dipole-bound anion and the other is valence anion. A typical example of the dipole bound anions is water dimer anion. The excess electron is trapped under the electrostatic field made by a dipole. The distribution of the excess electron is very diffuse and the detachment energy is very small. The other characteristics of the anion are that the geometric structure of the anion is nearly identical with that of the neutral. An example of the valence anions is C_2^- and $(CO_2)_2^-$. The excess electron occupies a bonding or non-bonding orbital. Contrary to the dipole-bound anion, the structure of the anion changes from that of the neutral species. While studying small water cluster anions, we have found a new form of excess electron. The electron is confined within a space surrounded by HO bonds of water molecules. Examples are interior type isomers of water dimer anion $(OH_2)\{e\}(H_2O)$ and trimer anions $\{e\}(H_2O)_3$; all water molecules being equivalent. A peculiarity of this form of anions is no direct hydrogen bonds between the water molecules surrounding the excess electron {e}. Therefore, after the photo-detachment the clusters of this form might be broken. One of the stable isomers of water tetramer anion has a form of $(OH_2)_2\{e\}(H_2O)_2$. In fact, the OH·{e}·HO structure is ubiquitous. In $(H_2O)_6^-$ and $(H_2O)_{12}^-$ studied by Kim's group, some of the isomers have the similar structure. Most importantly this form of anion is found in the ion pair state in metal-water clusters. The electron correlation contributes to stabilizing this form of anions. The calculated vertical detachment energies for this form is always positive.

I-B-3 Electronic Structure of $Li(H_2O)_n$ and $Na(H_2O)_n$ for n=3, 4 and 5

Takeshi TSURUSAWA and Suehiro IWATA

We have investigated the structures and the energies of $Li(H_2O)_n$ and $Na(H_2O)n$ for n = 3, 4 and 5 using *ab initio* MO method. The structures are optimized with the MP2/6-311++G(d,p) level of approximation. It turns out that both $Li(H_2O)_n$ and $Na(H_2O)_n$ can form similar structures and that the vertical ionization energies of the corresponding structures are almost independent of the metal atom included in the clusters. The main differences between the structures of $Li(H_2O)_n$ and $Na(H_2O)_n$ are the bond distance between the metal atom and oxygen atoms. R(Li-O) is about 1.9 Å and R(Na-O)

is about 2.3Å. Although this difference is not small, its influence on the electronic and geometric structures are small. The structures of the isomers are classified to three types by the shape of the SOMO and its surrounding water molecules; '*internal*', '*semi-internal*' and '*surface*' types. This classification also corresponds to the classification by the vertical ionization energies (VIE); VIE of the *surface* is less than 3.4eV, VIE of *semi-internal* about 3.5eV and VIE of *internal* about 3.9eV. The *surface* (A), *semi-internal* (B) and *internal* (C) isomers of $Na(H_2O)_4$ are shown in Figure 1. In the figure 50% of the electron density in the singly occupied orbital (SOMO) is contained within a shaded bowl. The figures clearly indicate that the metal is fully ionized. The difference in the isomers is the electronic structure of the ejected electron {e} in SOMO. In *semi-internal* and *internal* types, the SOMO electron is surrounded by two water molecules as (HOH){e}-(HOH). The internal type becomes possible for $n \geq 4$. Indeed, Hashimoto et.al. showed in their paper that one of the isomers of $Li(H_2O)_n$ n = 6 and 8 have this structures.[1)] We conclude that the VIE of $M(H_2O)_n$ is determined mainly by the shape of the SOMO and its surrounding water molecules and not affected by the metal atom. The role of the alkali metal atom is only to make the base structure of larger cluster. Our theoretical finding may explain a mystery of the observed constant ionization threshold energy for all of $M(H_2O)_n$ (M=Li, K and Cs) of $n \geq 4$.

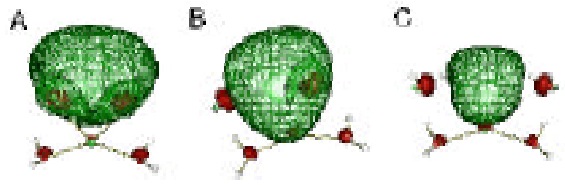

Reference:

1)K. Hashimoto and T. Kamimoto, *J. Am. Chem. Soc.* **120**, 3560 (1998).

I-B-4 Ab-Initio Monte Carlo Simulation Using Multicanonical Algorithm: Temperature Dependence of the Average Structure of Water Dimer

Pradipta BANDYOPADHYAY *(Grad. Univ. for Advanced Studies and IMS)***, Seiichiro TEN-NO and Suehiro IWATA**

[*Molecular Physics* in press (1998)]

Theoretical studies of finite temperature effects on molecular spectra and properties are rare but extremely important. Ab-initio simulation techniques, though promising, suffer from the enormous computational cost to study the finite temperature effects. Multicanonical algorithm/reweighting technique is an efficient tool to study finite temperature effects. In this algorithm the system can explore any part of the potential energy surface with equal ease and get the reweighted canonical distribution for any temperature from only a single run making finite temperature studies computationally tractable. In this series of works the algorithm are combined with the ab initio MO calculations.

As a test example it was first applied to water dimer. The potential energies have been calculated at the RHF/6-31G* level of theory. Analysis of the radial and angular distribution functions show how with the increase of temperature thermally accessible states contribute to the average structure. With the increase of temperature structures, similar to the C_i transition state contributes considerably to the average structure.

I-B-5 Theoretical Assignments of the Photo-Dissociation Excitation Spectra of Mg^+ Ion Complexes with Water Clusters: Multi-Reference CI Studies

Hidekazu WATANABE *(Grad. Univ. for Advanced Studies, IMS and RIKEN)* **and Suehiro IWATA**

[*J. Chem. Phys.* **108**, 10078 (1998)]

With the ab initio multi-reference CI method, electronic excitation energies of $Mg^+(H_2O)_n$ clusters have been calculated in order to analyze the photo-dissociation excitation spectra reported by Fuke and his co-workers. Observed bands for $n \geq 2$ are assigned to the $s \rightarrow p$ transitions of the most stable isomer of $Mg^+(H_2O)_n$, with all waters directly bonded to the metal ion. For n = 3, 4 and 5, the dominant bands are also those of the most stable isomer, $[Mg^+(H_2O)_3](H_2O)_{n-3}$, which have three water molecules in the first hydration shell. There are, however, shoulders and weak peaks in the experimental spectra, and the calculations prove that these are due to the $s \rightarrow p$ transitions of less stable isomers. The calculated spectra clearly indicate the coexistence of a few isomers for $n \geq 3$ in molecular beam experiments.

I-B-6 Ab Initio MO Monte Carlo Simulation of $[X(H_2O)]^-$ (X = F, Cl , Br, I)

Katsuhiko SATOH and Suehiro IWATA

Theoretical study of hydrated anion clusters $[X(H_2O)_n]^-$ (X = F, Cl, Br, I, n = 1) has been performed using ab initio MO Monte Carlo simulation. The molecular dynamic simulation for these systems is sensitive to the quality of the potential energy. Experimentally the clusters have a thermal energy even under molecular beam conditions. It is thus necessary to examine the thermal effect based on the accurate potential energy. The MO calculation at each MC step is at the second-order Moller-Plesset (MP2) level with the 6-31+G** basis set. The statistical averages on structural properties are evaluated at the several temperatures to examine the dependence of temperature and of halides (F, Cl, Br and I). Ab initio vibrational frequencies and intensities are calculated for canonical ensembles. The spectra are compared with the recent experimental spectra.

I-C Structures and Vibrational Frequencies of Infinite Polymer Chains

I-C-1 Analytical Second Derivatives in Ab Initio Hartree-Fock Crystal Orbital Theory of Polymers

So HIRATA *(Grad. Univ. Adv. Stud. and IMS)* **and Suehiro IWATA**

[*J. Mol. Struct. (THEOCHEM)* **451**, 121 (1998)]

In the framework of ab initio Hartree-Fock crystal orbital theory of polymers, the formulas for the analytical second derivatives of energy with respect to in-phase (k = 0) nuclear coordinates are derived. The coupled perturbed Hartree-Fock (CPHF) equation is iteratively solved by using the direct (recomputation of two-electron integrals) atomic-orbital-based algorithm. Frequencies of the Brillouin zone center (k = 0) vibrations of all-*trans* polyethylene are calculated by using the STO-3G, 3-21G, and 6-31G* basis sets. The dependence of the frequencies on the number of neighbors included in the lattice summations, on the number of momentum sampling points in the first Brillouin zone, and on the convergence criterion for the CPHF solutions is examined. In our implementation, the use of analytical second derivatives is more efficient than the use of the finite differences of analytical first derivatives.

I-C-2 Analytical Energy Gradients in Second-Order Møller-Plesset Perturbation Theory for Extended Systems

So HIRATA *(Grad. Univ. for Advanced Studies and IMS)* **and Suehiro IWATA**

[*J. Chem. Phys.* in press (1998)]

The spin-restricted formulas for the analytical gradients of the second-order Møller-Plesset (MP2) perturbation energy are presented within the framework of ab initio crystal orbital theory of infinite one-dimensional lattices (polymers). The coupled perturbed Hartree-Fock equation for polymers is solved iteratively using the atomic-orbital-based algorithms. The MP2 energy and its gradient contributions are evaluated by the disk-based algorithms with the aid of the two-particle density matrix. The analytical-gradient method at the MP2 level as well as the analytical first- and second-derivative methods at the Hartree-Fock level is applied to calculate the equilibrium structures and harmonic vibrational frequencies of all-trans polyacetylene. The deviations of the calculated frequencies from the observed ones for the in-phase C=C stretching modes are reduced by about 70 % on going from HF/6-31G to MP2/6-31G theory.

I-C-3 Ab Initio Hartree-Fock and Density Functional Studies on the Structures and Vibrations of an Infinite Hydrogen Fluoride Polymer

So HIRATA *(Grad. Univ. Adv. Stud. and IMS)* **and Suehiro IWATA**

[*J. Phys. Chem. A* in press]

Structural parameters, binding energies, and frequencies of the infrared- and Raman-active vibrations are calculated for an infinite zigzag chain of hydrogen fluoride molecules by ab initio crystal orbital theory with the analytical energy gradient scheme. The Becke-Lee-Yang-Parr (BLYP), Becke3-Lee-Yang-Parr (B3LYP), and Hartree-Fock (RHF) levels are used in conjunction with the 6-311++G(d,p) basis set. Molecular orbital calculations at the BLYP, B3LYP, RHF, and the second-order Møller-Plesset perturbation (MP2) levels with the same basis set are carried out on linear HF oligomers containing up to six molecules, in order to examine the chain-length dependence of the energetic and structural properties. The predicted chain-length dependence is found significantly smaller in the RHF results than in the BLYP and B3LYP results. The RHF level substantially underestimates the downward frequency shifts in the intramolecular H-F stretching modes on going from the monomer to the polymer, while the shifts calculated at the BLYP and B3LYP levels are much closer to the experimental findings, although they are slightly overestimated. The RHF level strongly underestimates the intramolecular H-F bond length and overestimates the intermolecular F···H and F···F distances of the HF polymer, while the structural parameters predicted at the BLYP and B3LYP levels are in good agreement with the experimental results. It is concluded that the RHF level seriously underestimates the cooperative binding effects of consecutive hydrogen bonds, whereas the BLYP and B3LYP levels slightly overestimate this behavior; but these latter levels provide much better description than the former. Vibrational assignment of librational modes of HF crystals is reexamined on the basis of the calculated frequencies. The observed frequencies of the librational and pseudo-translational modes fall between the corresponding frequencies calculated at the RHF and density functional levels.

I-D Structures and Reations of Atomic and Molecular Clusters

I-D-1 Photodissociation Dynamics of Argon Cluster Ions

Tsutomu IKEGAMI and Suehiro IWATA

The photodissociation process of argon cluster ions is studied by using Tully's MDQT (molecular dynamics with quantum transition) method. It is demonstrated that the non-adiabatic transitions play an important role in the process. The lifetime of the initial photo-excited state and the recovery time to the electronic ground state are obtained for several cluster sizes and excitation energies. The decay curve of the photo-excited state is composed from the gaussian-like decay followed by an exponential decay. The initial gaussian-like delay of the decay may be attributed to the acceleration time of the nuclei. The number of the non-adiabatic transitions required for the recovery to the ground state increases with the excitation energy, while the rate of each transition decreases. As a result, the recovery to the ground state becomes faster for the lower excitation energy. The low rate at the higher excitation energy may be explained from the low density of states in the energy range.

I-D-2 Theoretical Investigation of the Structure and Spectroscopy of Silicon-Carbon Mixed Clusters

Pradipta BANDYOPADHYAY *(Grad. Univ. for Advanced Studies and IMS)***, Seiichiro TEN-NO and Suehiro IWATA**

Pure Silicon and Carbon clusters have been studied extensively over the years both theoretically and experimentally. However, the same is not true for mixed Silicon-Carbon clusters. The mixed clusters demand interest not only because of its importance in material science but also because of the inherent complexity associated with its structures and spectra. It has been suggested that the complex photoelectron spectra of Silicon-Carbon anion clusters are due to the presence of several isomers at the experimental condition.[1] In the present work mixed Silicon-Carbon clusters $Si_mC_n^-$ where $m + n = 4$ have been studied theoretically. Ab initio molecular orbital calculations at the CASSCF and MRCI level have been performed to determine the vertical detachment energies (VDE). It has been found that the VDEs are very much sensitive to the levels of electronic structure calculation. For $Si_2C_2^-$, the highly complex photoelectron spectra is presumably from the contribution of linear and ring structures. As enormous computational cost prohibits ab initio simulation with reliable electronic structure calculation for this system, the relative contributions of two structures have been evaluated by the quantum cluster equilibrium model.[2]

References

1)A. Nakajima et. al., *J. Chem. Phys.* **103**, 2050 (1995).

2)F. Weinhold, *J. Chem. Phys.* **109**, 367 (1998).

I-D-3 Model Study of H-Bonded ROH $(NH_3)_5$ Clusters: A Search for Possible Ground-State Proton Transfer Species

Michail V. VENER *(Karpov Institute of Physical Chemistry, Russia and IMS)* **and Suehiro IWATA**

[*Chem. Phys. Letters* **292**, 87 (1998)]

Model studies have been made of the non-transferred (reactant) and proton-transferred (product) species of the ground-state hydrogen-bonded clusters $ROH(NH_3)_5$, where ROH is an aromatic alcohol. The structure, relative energies and vibrational frequencies of this species were obtained at the HF/6-31G* level of theory. It was found that proton transfer can proceed in the case of phenols with the electron-withdrawing substituents. A low-frequency vibration, which corresponds to the synchronous motion of the solvation shell, does exist in these clusters. The energy of the lowest π-π^* transition is calculated for aromatic alcohols and their anions at the CASPT2 level with a VDZ basis set.

I-D-4 Ab Initio MO Studies of van der Waals Molecule $(N_2)_2$: Potential Energy Surface and Internal Motion

Akira WADA *(Tokyo Inst. Tech)***, Hideto KANAMORI** *(Tokyo Inst. Tech and IMS)* **and Suehiro IWATA**

[*J. Chem. Phys.* in press (1998)]

The equilibrium structure, potential energy and van der Waals (vdW) mode vibration of dimer of nitrogen molecule $(N_2)_2$ have been studied with high levels of ab initio calculations. The most stable structure is found to be a 45 degree canted parallel structure of C_{2h}. On the other hand, neither T-shape of C_{2v} nor cross shape of D_{2d} is a stable structure, but they are transition state structure, contrary to the previous calculations. The out-of-plane motion changing from the 45 canted parallel structure of C_{2v} to the cross shape of D_{2d} has a higher barrier than the in-plane motion. The binding energy of two N_2 molecules is about 80 cm^{-1} and the fundamental frequency of vdW stretching mode is estimated to be 22 cm^{-1}. A very small energy difference by 5 cm^{-1} between the C_{2h} and C_{2v} structures implies that two molecules move coherently like a gear rotation in the plane. This internal freedom of motion should make the rotational energy states extremely modulated, and therefore, a very complex spectral patter could be expected.

I-D-5 Theoretical Studies of Clusters of H_2 Molecules at High Pressure

Debasis MUKHOPADHYAY *(R. K. Mission Vidyamandira,*

India) **and Pradipta BANDYOPADHYAY** *(Grad. Univ. Adv. Stud. and IMS)*

Assemble of hydrogrn molecules at high pressure was predicted to form an atomic and presumably a metallic solid and this prediction has motivated experimental and theoretical studies over the years. We focused our attention on the observation of a dramatic (> 1000 fold) enhancement of the infrared (IR) intensity at the high pressure phase above 150 Gpa, characterized by a discontinuity of the vibrational frequency. It is noteworthy that Raman intensity shows only monotonic increase in this region. Such intense IR has been attempted to be explained by electron-vibration coupling to postulated charge-transfer (CT) states. In a recent study by Soos and Mukhopadhyay direct evaluation of the dipole derivative for overlapping H_2 dimer, with intermolecular distance corresponding to the pressure of 150 Gpa, has been seen to be consistent with the experimental IR oscillator strength, with hexagonal-close-packed lattice structure of molecular solid hydrogen. It was found that for a H_2 molecule with all its nearest neighbors, only one pair has important contribution. We take this dimer as 'good' dimer. In order to test the extensibility of the understanding within the dimer picture to the actual case of molecular solid, we have studied some fabricated structures obeying the geometry of the hcp lattice with ab initio MO methods. The MCSCF and closed shell HF wavefunctions are used. The models we have studied (I) *n* 'good' dimers oriented along z-axis for *n* = 2, 3, 4, (ii) a 'good' dimers with complete nearest neighbour environment, and (iii) two hexagonal planes of 7 pairs H_2 molecules, each dimer having orientation of the 'good' dimer. For case (i) we have dipole derivative consistently as *n* times that of the single 'good' dimer. Notably, extra interactions arising from the assembles are found to be not important. For case (ii) we have the dipole derivative of the order of magnitude of the 'good' dimer stripped of the neighbors. This is interesting, in particular, as here effective contribution from the interaction of the nearest neighbor molecules has seen to be negligibly small and practically null.

I-E Accurate Studies of Excited States of Small Molecules

I-E-1 A Theoretical Study of the Electronic Structure and Spectroscopic Properties of the Low-Lying Electronic States of the Molecule AlSi

Fernando R. ORNELLAS *(Departmento de Oulmica Fundamental. Insliluto de Qulmica, Universidade de Sa-a Paulo, Brazil)* **and Suehiro IWATA**

[*Chem. Phys.* **232**, 95 (1998)]

Twenty-one lowest-lying electronic states of the species AlSi are described theoretically using the internally contracted multi-reference configuration interaction approach and natural orbitals generated from a state-averaged density matrix. Correlated consistent valence quadruple-zeta (cc-pVQZ) atomic functions are used in the expansion of the one-electron basis. Potential energy curves are presented for all the states as well as a description of the electronic structure characterizing the most relevant ones. Dissociation and excitation energies, and dipole moment functions complete the electronic structure description. Solution of the radial nuclear equation allowed the determination of vibrational energies, and vibrational and rotational constants. For the ground state ($X^4\sum^-$), R_e = 2.424 Å and D_e = 2.53 eV. The first excited quartet is a $A^4\Delta$ located 2.29 eV (T_e) higher in energy, with a longer equilibrium distance (2.887 Å), and smaller, D_e, 0.24 eV. The first quartet directly accessible by a one-photon transition is the $B^4\prod$ (T_e = 2.3l eV, R_e = 2.520 Å, D_e = 0.22 eV); the transitions $X^4\sum^- - B^4\prod$ are expected to fall in the green region of the visible spectrum. Higher-lying $^4\prod$ states show very noticeable changes in the potential function due to avoided crossings. Within ~ 1.2 eV from the ground state there are located five doublet states; the lowest one a $^2\sum^-$. with T_e = 0.72 eV, R_e =2.415 Å, and D_e = 1.81 eV. For selected states, transition dipole moments, transition probabilities and radiative lifetimes are also presented. Crossings of various states and the energetic closeness of others are expected to play non-negligible perturbative effects in the spectra. The global picture of the electronic states presented will certainly be an important aid to experimentalists in the spectroscopic investigation of this species.

I-E-2 The Variety of [Fe,N,O] Isomers. A Theoretical Study

Andreas FIEDLER and Suehiro IWATA

[*J. Phys. Chem.* **102**, 3618 (1998)]

The stationary points on the potential energy hyper surfaces of triatomic [Fe,N,O] have been systematically studied using an economic combination of a density functional/Hartree Fock hybrid method, i.e. the B3LYP functional, and the multi-reference averaged quadratic coupled cluster approach. The global minimum is linear FeNO ($^2\Delta$) which is not adiabatically connected to the neutral ground state fragments Fe and NO. Side-on and oxygen bound isomers have low barriers for rearrangement, however, might be stabilized due to ligand effects. Inserted OFeN (^{4}A") is kinetically stable although it lies considerably higher in energy than the other isomers. The calculations indicate near-degenerate ground states for all isomers. We discuss the implications for the reported experimental observations. Furthermore, the findings are rationalized using valence-bond and molecular-orbital theories.

I-E-3 Theoretical Studies of Highly-Excited Valence States of N_2^+ Molecule Ion

Kazutoshi OKADA *(Grad. Univ. for Advanced Studies)*, **G. K. JARVIS** *(Iowa State Univ., U.S.A.)*, **Cheuk Y. NG** *(Iowa State Univ., U.S.A.)* **and Suehiro IWATA**

Recently highly-excited valence states of nitrogen cation have been studied with synchrotron radiation source. In particular, the $C^2\sum_u^+$ state of N_2^+ has been examined with various types of photoelectron spectra. In the present studies, we have calculated the accurate potential energy curves of the doublet and quartet states lying 90,000 cm^{-1} above the zero vibrational level of the ground state $X^2\sum_g^+$. The basis set used in the multi-reference configuration interaction (MRCI) calculations is [5111/211/21/2]. The calculated dissociation energy D_0 of the neutral molecule is > 9.5eV, and is very close to the experimental energy (9.754 eV). The error in the excitation and ionization energies at the dissociation limit is also within 200 cm^{-1}. The accurate description near the dissociation limit for the $B^2\sum_u^+$ state is required in the present purpose, because its highly-lying vibronic levels is expected to interact with the vibronic levels of the $C^2\sum_u^+$ state. Vibrational and rotational levels for each electronic state are calculated with our FEM1D program. In our calculation the vibrational level v = 32 of the *B* state lies just above v = 0 of the *C* state. The highest vibrational level of the *B* state is 46, and it lies above v = 2 of the *C* state. Experimentally the rotational constant B_v for each vibrational level of the *C* state is determined, and an abnormal v dependency is found for $v \leq 2$. This is consistent with our calculated inter-relation of vibrational levels of two $^2\sum_u^+$ states; the radial coupling of vibronic levels causes the change of the rotational constants.

I-E-4 Theoretical Study on Spectroscopic Properties of Positive, Neutral, and Negative Species of BCl_2 and $AlCl_2$

Kyoung K. BAECK *(Kang-Nung Univ. and IMS)* **and Suehiro IWATA**

Accurate and predictive values of the bond lengths, bond angles, dipole moments, vibration frequencies, and IR intensities of positive(X $^1\sum_g^+$), neutral(X $^2A_1$), and negative(X $^1A_1$, a $^3B_1$) species of BCl_2 and $AlCl_2$, are calculated by Becke's three parameter density-functional-theory method, B3LYP-DFT, with the augmented correlation consistent triple- and quadruple-zeta (aug-cc-pvtz and aug-cc-pvqz, respectively) basis sets. The coupled-cluster singles, doubles, and noniterative triples method, CCSD(T), with aug-cc-pvtz is also used to augment the B3LYP-DFT results. The ionization energies and electron affinities are also evaluated by the B3LYP-DFT/aug-cc-pv5z method at the B3LYP-DFT/aug-cc-pvqz geometry and the CCSD(T)/aug-cc-PVQZ method at the CCSD(T)/aug-cc-pvtz geometry, as well as by the G1, G2, CBS-4, and CBS-Q methods. It is shown that the negatively charged species, which have never been studied experimentally, are stable both in singlet and triplet spin states. The Franck-Condon factors within the harmonic approximations are calculated for the electron detachment processes of anions, and the simulated photoelectron spectra for singlet and triplet states of BCl_2^- and $AlCl_2^-$ are given.

I-E-5 The Electronic Structures of HCCS and NCS

Yumin LI and Suehiro IWATA

The number of valence electrons of HCCS and NCS are fifteen, and therefore, the similarity of the electronic structures is expected, though the number of atoms is different. The ground and first excited states of both molecules are $^2\prod$ and the next state is $^2\sum^+$. Three of states of NCS are linear, and Renner-Teller splittings of two $^2\prod$ states are very small. The UHF wavefunction has a large spin contamination, and the multi-reference description is required. The calculated bond lengths with MRCI calculations are 1.166 for NC and 1.634 for CS in the ground state $^2\prod$, and 1.232 for NC and 1.650 for CS in the first excited state $^2\prod$. The wavefuctions indicate that the ground state and the first excited state are π radical, and mixture of $(2\pi)^4(3\pi)^3$ and $(2\pi)^3(3\pi)^4$. In terms of valence bond structures they are N≡C−Ṡ and Ṅ=C=S̈. The second excited state $^2\sum^+$ is the σ radical, $(9\sigma)^1(2\pi)^4(3\pi)^4$, and N≡C−S̈·. These are also true for three states of HCCS. Because HCCS is tetra-atomic molecules and two bending angles, Renner-Teller effects become complex. The potential energy surfaces for two bending angles are created, and the coupling of two bending angles with the dihedral angle is also examined.

I-E-6 The Electronic Structures of HCCN and HCCP

Yumin LI and Suehiro IWATA

HCCN and HCCP are isovalent molecules, and both are of astronomical interest. The geometric and electronic structures of the ground and low-lying excited states are studied with high levels of ab initio MO methods. The differences and similarities of two molecules are discussed. The ground state of both molecules is the triplet state. The HCC angle of the triplet ground state $^3A''$ of HCCN is about 140 degree, and on the other hand, the CCN angle is almost linear, 175 degree in our best estimate. The optimized bond lengths for CC (1.316 Å) and CN (1.223 Å) suggest the allenic backbone, which is contrary to some of the recent theoretical publication, but agrees with the recent experimental work in Saito's laboratory, IMS. The energy difference between the linear and bent configuration is 1.10 eV. At the linear configuration, the lowest singlet state $^1\Delta$ lies above 8900 cm^{-1}, and the state ordering among the triplet states is $A^3\Delta$, $B^3\sum^-$, $C^3\sum^+$ and $D^3\prod$; they are accessible from the ground state by near-UV excitations. The character of the ground triplet state $X^3\sum^-$ of HCCP is different from that of HCCN. The molecule is linear, and the calculated harmonic frequencies of two bending modes are 296 and 586 with CCSD(T)/cc-pvtz level of approximation.

The calculated bond lengths of CC (1.231 Å) and CP (1.716 Å) and the electronic wavefunction suggest that the C-C bond is close to a triple bond and the molecule has phosphonic structure H–C≡C–P. The lowest singlet state $^1\Delta$ lies above 8460 cm^{-1} from the bottom of the ground state. The state ordering among the low-lying triplet states is $A^3\Sigma^-$, $B^3\Delta$, $C^3\Sigma^+$ and $D^3\Pi$

I-F Application of Ab Initio Molecular Orbital Methods to Experimentally Relevant Systems

I-F-1 Theoretical Studies of Geometric and Electronic Structures of Novel Molecular Anion $CH_3CO_2I^-$

Morihisa SAEKI *(Univ. Tokyo)*, **Lei ZHU, Tatsuya TSUKUDA** *(Univ. Tokyo)*, **Suehiro IWATA and Takashi NAGATA** *(Univ. Tokyo)*

[*Chem. Phys. Lett.* **280**, 348 (1997)]

Geometric and electronic structure of acetyloxy iodide anion $CH_3CO_2I^-$, which is produced in the reactions of $(CO_2)_N^-$ with CH_3I, are investigated by ab initio MO calculation. It was found that $CH_3CO_2I^-$ is composed as a molecular anion, where acetyloxyl framework binds the I atom through an O-I bond to share the excess electron. The excess electron in the ground state ($1^2A'$) is accommodated into an anti-bonding orbital formed between the $CH_3CO_2^-$ and I. The electron configuration of $CH_3CO_2I^-$ is $\cdots(13a')^2$-$(14a')^2(3a'')^2(15a')^2(4a'')^2(16a')^1$. Based on a simple MO correlation diagram, these orbitals are classified. Interaction of MOs between $CH_3CO_2^-$ and I leads to formation of bonding and antibonding orbitals, which correspond to the 13a' and 16a'. The electronic distribution of 14a' and 3a'' orbitals is localized on $CH_3CO_2^-$, while that of 15a' and 4a'' is localized on I. On the basis of vertical detachment energies (VDEs) evaluated, two peaks in photoelectron spectrum are attributed to electron detachment from the 16a' and 4a'' orbitals. On the other hand, based on the excitation energy and transition dipole moments calculated by MR-CI method, two absorption bands of $CH_3CO_2I^-$ are assigned to electronic transitions of $3^2A' \leftarrow 1^2A'$ and $4^2A' \leftarrow 1^2A'$. These correspond to electronic excitation of 14a' → 16a' and 13a' → 16a'. Photodissociation of $CH_3CO_2I^-$ showed production of $CH_3CO_2^-$ and I, whose branching fraction depends on excitation energy. State correlation diagram of $CH_3CO_2I^-$ indicates crossing of two potential curves, which leads to avoided crossing. The avoided crossing of potential curves results in the energy dependence of branching ratio.

I-F-2 Theoretical Studies of Internal Methyl Rotations in *m*-Xylene: Comparison of Franck-Condon Factors with the Experimental Spectra

Tadayoshi SUZUKI *(Grad. Univ. for Advanced Studies and IMS)*, **Tsutomu IKEGAMI, Masaaki FUJII and Suehiro IWATA**

[*J. Molec. Struct. (THEOCHEM)* in press (1999)]

The potential energy surfaces of internal rotations of two methyl groups were calculated with *ab initio* MO method for the *m*-xylene (1,3-dimethylbenzene) in the ground (S_0), first excited (S_1), and cation ground (D_0) states. The internal rotation levels and their wave-functions on the theoretically calculated potential energy surfaces were obtained by solving Schrödinger equation for double methyl rotors. The Franck-Condon factors for $D_0 \leftarrow S_1$, and $S_1 \leftarrow S_0$ transitions were calculated and compared with the experimental spectra. A good agreement was obtained not only in level spacings but also in relative intensities in the spectra. The interaction between two methyl rotors was also found to be small, and the rotational levels can be labeled by the irreducible representation of the direct product $G_6 \times G_6$ group.

I-F-3 Theoretical Studies of Internal Methyl Rotations in *o*-Xylene: Coupled Internal Rotation

Tadayoshi SUZUKI *(Grad. Univ. for Advanced Studies and IMS)*, **Tsutomu IKEGAMI, and Suehiro IWATA**

The potential energy surfaces of internal rotations of two methyl groups in *o*-xylene (1,2-dimethylbenzene) are calculated with ab initio MO method for the ground (S_0), first excited (S_1), and cation ground (D_0) states. The internal rotation levels and their wavefunctions on the potential energy surfaces are obtained by solving Schrodinger equation for double methyl rotors. As is expected, the interaction between two methyl rotors is very strong in all states, and the internal rotation levels have to be labeled by the irreducible representation of G_{36} group. A single transition with no change of quantum numbers of the internal rotation dominates the calculated Franck-Condon factors for $D_0 \leftarrow S_1$, and $S_1 \leftarrow S_0$ transitions. Nevertheless, theoretical calculations suggest that weak side bands could reveal the correlated motion of two methyl groups, if they would be ever observed.

I-F-4 Reaction of $OCrO^+$ with a H_2 Molecule

Andreas FIEDLER, Detlef SCHRöDER *(Tech. Univ. Berlin)* **and Suehiro IWATA**

In a tight collaboration with the mass spectrometry group in Berlin the mechanism of the reaction of the chromium dioxide cation with a molecular hydrogen was theoretically examined. We used the B3LYP method to locate possible intermediates and the

corresponding transition structures. The resulting qualitative picture for the characteristic critical points on the PESs shall than be verified by further experiments. In the gas phase under thermal conditions $OCrO^+$ slowly activates H_2 (and hydrocarbons) to produce CrO^+ and H_2O. The chromium dioxide cation has already been calculated to have a low-spin doublet ground state and a rather high-lying excited quartet state. The B3LYP approach reproduces these high level calculations in good agreement. An encounter complex with H_2 is a doublet ground state. From a chemical point of view, there are four possible routes for the following σ-bond activation. (1) Oxidative insertion of the metal center into the H-H bond to form a high-valent dihydro-dioxo-chrome compound, (2) A [2+2] pathway, i.e. H-H σ-bond methateses along one Cr-O unit, to generate a oxo-hydro-hydroxo-chrome species, (3) A [3+2] path via a five memberd ring where both oxygen centers simultaneously abstract a hydrogen atom resulting the dihydroxy-chrome cation, (4) A reductive elimination of Cr to form a complex of molecular oxygen, molecular hydrogen, and the chrome cation, followed by H_2 activation. The last two mechanisms are energetically excluded. Products from [2+2] and [2+3] activation paths are much more stable. Both cationic oxo-hydro-hydroxo-chrome and dihydroxy-chrome are low-lying minima on the doublet PES. In addition, the quartet ground state of dihydroxy-chrome is the global minimum. We did not find a stable quartet oxo-hydro-hydroxo-chrome isomer. However, regarding the bottlenecks for these reactions only the [2+2] transition structure (doublet) is located below the entrance channel whereas the [2+3] TS is not accessible at thermal energies. The quartet states are computed to be much higher in energy. Thus, the only viable reaction is the [2+2] activation path on the doublet PES. This is implicitly leading to the doublet oxo-hydro-hydroxo-chrome cation. However, since the dihydroxy isomer is more stable and has a quartet ground state, rearrangement and/or curve crossing to the quartet surface take place after the initial H-H bond breaking. Furthermore, the final reaction product CrO^+ and H_2O implies a further intermediate, i.e., complex of water and chromium oxide cation. The later isomer also has a low-lying quartet ground state. On the doublet PES both TSs for hydrogen shifts in oxo-hydro-hydroxo-chrome cation are calculated to be at the same energy level. The barrier for rearrangement between both products is lower in energy. All located TSs for the hydrogen shifts on quartet and doublet PESs are lower than the lowest TS for the H_2 activation. Thus, after the initial [2+2] activation of H_2 fast rearrangements can take place, probably accompanied by curve crossing to the high-spin PES.

I-G Prediction of Protein Tertiary Structures from the First Principles

Prediction of the three-dimensional structures of protein molecules by computer simulations is a very challenging problem in theoretical molecular science. The difficulty of the problem lies in two facts: (1)the inclusion of accurate solvent effects is non-trivial and time-consuming (2) there exist huge number of local minima in the energy function, forcing conventional simulations to get trapped in states of energy local minima. We have been exploring the strategies that allow us to overcome these difficulties.

I-G-1 Effects of Side-Chain Charges on α-Helix Stability in C-Peptide of Ribonuclease A Studied by Multicanonical Algorithm

Ulrich H. E. HANSMANN and Yuko OKAMOTO

[submitted for publication]

We have performed multicanonical Monte Carlo simulations of C-peptide of ribonuclease A. Three analogues of the peptide with charged and neutral side chains were used to study the role of side-chain charges in the stability of the observed α-helix. Two dielectric functions, distance-dependent and constant, are considered to study the effects of solvent contributions. The results are found to be in accord with the implications of CD and NMR experiments of C-peptide where it was found that this peptide has high α-helix content in aqueous solution and that the removal of the side-chain charge of Glu-9^- enhances helix formation. The lowest-energy conformation obtained by our simulations has an α-helix from Ala-4 to Gln-11 in complete agreement with the corresponding structure deduced from an X-ray crystallography experiment of ribonuclease A. The salt bridge between the side chains of Glu-2^- and Arg-10^+, which is known to exist from both NMR and X-ray experiments, is formed only when the side chains are properly charged. Its formation is greatly enhanced when the solvation effects are taken into account.

I-G-2 Stochastic Dynamics Simulations in a New Generalized Ensemble

Ulrich H. E. HANSMANN and Yuko OKAMOTO

[*Chem. Phys. Lett.* in press]

We develop a formulation for molecular dynamics, Langevin, and hybrid Monte Carlo algorithms in the recently proposed generalized ensemble that is based on a physically motivated realisation of Tsallis weights.

The effectiveness of the methods are tested with an energy function for a protein system. Simulations in this generalized ensemble by the three methods are performed for a penta peptide, Met-enkephalin. For each algorithm, it is shown that from only one simulation run one can not only find the global-minimum-energy conformation but also obtain probability distributions in canonical ensemble at any

temperature, which allows the calculation of any thermodynamic quantity as a function of temperature.

I-G-3 The Folding Funnel Landscape for the Peptide Met-Enkephalin

Ulrich H. E. HANSMANN, Yuko OKAMOTO and José N. ONUCHIC *(Univ. Calif. San Diego, U.S.A.)*

[*Proteins* in press]

We study the free energy landscape of the small peptide Met-enkephalin.

Our data were obtained from a *generalized-ensemble* Monte Carlo simulation taking the interactions among all atoms into account.

We show that the free energy landscape resembles that of a funnel, indicating that this peptide is a good folder. Our work demonstrates that the energy landscape picture and folding concept, developed in the context of simplified protein models, can also be used to describe the folding in more realistic models.

I-G-4 Finite-Size Scaling of Helix-Coil Transitions in Poly-Alanine Studied by Multicanonical Simulations

Ulrich H. E. HANSMANN and Yuko OKAMOTO

[*J. Chem. Phys.* in press]

We report results from multicanonical simulations of poly-alanine.

Homopolymers of up to 30 amino acids were considered and various thermodynamic quantities as a function of temperature calculated. We study the nature of the observed helix-coil transition and present estimates for critical exponents.

I-G-5 Singular Behavior of the RISM Theory Observed for Peptide in Salt Solution

Masahiro KINOSHITA *(Kyoto Univ.)***, Yuko OKAMOTO and Fumio HIRATA**

[*Chem. Phys. Lett.* in press]

We examine the reference interaction site model theory applied to a peptide-salt solution system, with the assumption that a zwitterionic dipeptide (Ala-Ala) is present in NaCl solution at the infinite-dilution limit. For some sets of the parameters in the peptide-cation and peptide-anion potentials, the theory exhibits singular behavior: as the salt concentration decreases, the ionic concentration around the peptide increases and the theory eventually loses its solution. The singularity is interpreted as a signal of the ion condensation. A trend of aggregation of peptide molecules is also found.

For other sets of the potential parameters, however, no such singularity occurs. As far as the salt effects are concerned, the qualitative aspects of the conclusions are somewhat sensitive to the potential parameters employed.

I-G-6 Analysis on Conformational Stability of C-Peptide of Ribonuclease A in Water Using the Reference Interaction Site Model Theory and Monte Carlo Simulated Annealing

Masahiro KINOSHITA *(Kyoto Univ.)***, Yuko OKAMOTO and Fumio HIRATA**

[submitted for publication]

Solvation structure and conformational stability of the C-peptide fragment of ribonuclease A in pure water have been analyzed using the full reference interaction site model (RISM) theory. The charged groups in the side chains of Lys-1^+, Glu-2^-, Lys-7^+, Arg-10^+, and His-12^+ (in particular, the four like-charged groups) play substantial roles in stabilizing the conformations. The solvation free energy and the conformational energy are governed by the contribution from the electrostatic interaction with water and the intramolecular Coulombic energy, respectively, and the conformational stability is determined by competition of these two factors.

The contribution from the hydrophobic hydration and the van der Waals and torsion terms in the conformational energy are less important, which is in contrast with the result for Met-enkephalin. The Monte Carlo simulated annealing combined with the RISM theory has been applied to the C-peptide using an almost fully extended conformation as the initial one. The conformation first changes in the direction that the charged groups in the side chains are more exposed to water, and in particular, the positively charged groups are closer together. Thus, the solvation free energy decreases greatly in the initial stage. Although this leads to significant increase in the intramolecular Coulombic repulsion energy, the decrease in the solvation free energy dominates. In the later stage, however, further decrease in the solvation free energy gives rise to even larger increase in the intramolecular Coulombic repulsion energy, and the conformational change is greatly decelerated. The conformations thus stabilized in four different runs of the combined program are quite similar. The peptide conformation in water is stabilized far more rapidly than in gas phase.

I-G-7 β-Sheet Formation in BPTI(16-36) by Monte Carlo Simulated Annealing

Yuko OKAMOTO, Masato MASUYA, Miho NABESHIMA *(Nara Women's Univ.)* **and Takashi NAKAZAWA** *(Nara Women's Univ.)*

[submitted for publication]

Performing Monte Carlo simulated annealing simulations from randomly chosen intial conformations, we have obtained a β-sheet structure as the lowest-energy conformation. The solvent effects were included by the term that is proportional to the solvent-accessible surface area. This lowest-energy structure has a type II' β-turn and three characteristic intrachain hydrogen bonds that connect the two β-strands. It turns out that the positions of these β-turn and hydrogen bonds are in

remarkable agreement with the implications of an NMR experiment of the same fragment.

I-H Theoretical Studies of Chemical Reaction Dynamics

I-H-1 Cumulative Reaction Probability without Absorbing Potentials

Oleg I. TOLSTIKHIN *(Lebedev Physical Inst. and IMS)*, **Valentin N. OSTROVSKY** *(Univ. St. Petersburg and IMS)* **and Hiroki NAKAMURA**

[*Phys. Rev. Lett.* **80**, 41 (1998)]

Cumulative reaction probability, introduced in the collision theory by W. H. Miller [*J. Chem. Phys.* **62**, 1899 (1975)], characterizes a net efficiency of a rearrangement process as a function of the total energy of the collision system. We derive a formula that expresses this quantity in terms of the outgoing wave Green function. Our formula is free from the ambiguities of previous formulations; in particular, no absorbing potentials are required for its implementation. The formula has a potentially wide range of applications in atomic and molecular collision physics. As an illustration, we consider the rearrangement processes in the $dt\mu$ system for the energies up to the $n = 6$ threshold.

I-H-2 Hyperspherical Elliptic Coordinates for the Theory of Light Atom Transfer Reactions in Atom-Diatom Collisions

Oleg I. TOLSTIKHIN *(Lebedev Physical Inst. and IMS)* **and Hiroki NAKAMURA**

[*J. Chem. Phys.* **108**, 8892 (1998)]

We formulate and demonstrate a new method for quantum 3D calculations of light atom transfer reactions in atom-diatom collisions. The method follows a general scheme of the hyperspherical method, in common with other hyperspherical formulations in the field. The main novelty consists in the hyperspherical elliptic coordinates (ξ,η) used to parametrize the hypersphere. These coordinates have been introduced recently for studying three-body Coulomb systems, and here we apply them to study a system of three atoms. The coordinates are defined and their relation with the Smith-Whitten and Delves coordinates is explored. On account of a big difference between vibrational and rotational excitation energies in molecules, the hyperspherical adiabatic Hamiltonian allows adiabatic separation between ξ and η. This not only greatly facilitates solution of the hyperspherical adiabatic eigenvalue problem, but also provides an approximate classification of the states by a pair of indices (n_ξ, n_η) representing vibrational and rotational quantum numbers simultaneously for a reagent and product. Another novel technology exploited here is the Slow/Smooth Variable Discretization (SVD) method. The SVD is used for treating nonadiabatic couplings between the ξ and η motions, as well as between the motions with respect to the hyperradius and the hyperangular variables. The whole scheme is illustrated by calculations for the reaction $O(^3P)+HCl \rightarrow OH + Cl$ for zero total angular momentum. It is shown to be very efficient, accurate, and providing a framework of choice for elucidating light atom transfer reaction mechanisms.

I-H-3 Quantum Mechanical Elucidation of Reaction Mechanisms of Heavy-Light-Heavy Systems: Role of Potential Ridge

Katsuyuki NOBUSADA, Oleg I. TOLSTIKHIN *(Lebedev Physical Inst. and IMS)* **and Hiroki NAKAMURA**

[*J. Chem. Phys.* **108**, 8992 (1998)]

A new idea to elucidate quantum reaction dynamics of heavy-light-heavy (HLH) systems is proposed on the basis of the hyperspherical elliptic coordinate approach. This coordinate system has a big advantage of nicely expressing good vibrational adiabaticity in the HLH systems. Taking this advantage, the concept of potential ridge is introduced, for the first time, in three-dimensional reactions. The potential ridge is proved to be very useful to extract some important avoided crossings which dominate the reaction dynamics. In fact, qualitative features of the reaction dynamics can be interpreted in terms of non-adiabatic transitions at those important avoided crossings near the potential ridge. Examples are: (i) onset of reaction for specified initial rotational states, and (ii) major reactive transition for a specified initial rotational state. Avoided crossings to the left of the potential ridge are also useful to interpret certain aspects of reactions accompanying vibrational transitions. The new idea mentioned above is applied to a typical HLH reaction $O(^3P)+HCl \rightarrow OH + Cl$ with the use of two types of potential energy surfaces.

I-H-4 Quantum Reaction Dynamics of Cl + HCl → HCl + Cl: Vibrationally Nonadiabatic Reactions

Katsuyuki NOBUSADA, Oleg I. TOLSTIKHIN *(Lebedev Physical Inst. and IMS)* **and Hiroki NAKAMURA**

[*J. Mol. Str. (THEOCHEM)* in press]

Quantum reaction dynamics of Cl + HCl → HCl + Cl for J (total angular momentum) = 0 is studied with use of the hyperspherical *elliptic* coordinate approach recently proposed by the authors. Thanks to the numerical efficiency of this approach, the reactions involving vibrational quantum jumps up to three are calculated accurately. Actually, all transitions among the states up to $v = 3$ and $j = 15$, in other words up to the total energy $E = 1.3$ eV, are covered, where v and j

represent vibrational and rotational quantum numbers, respectively. Because of the symmetry of the system, the vibrationally adiabatic reactions are generally more probable than the nonadiabatic ones. However, some specific vibrationally nonadiabatic reactions even with two or three vibrational quantum jumps are found to occur efficiently. The concepts of potential ridge and nonadiabatic transitions at avoided crossings near the ridge lines enable us to comprehend the reaction mechanisms nicely.

I-H-5 Semiclassical Treatment of Resonances in the Collinear O + HO Exchange Reaction

Gennady V. MIL'NIKOV *(Inst. Structual Macro - kinetics, Russia and IMS)*, **Chaoyuan ZHU, Hiroki NAKAMURA and Vladimir I. OSHEROV** *(Inst. Chem. Phys., Russia and IMS)*

[*Chem. Phys. Lett.* **293**, 448 (1998)]

Feshbach type sharp resonances appearing in the O + HO collinear reaction are analyzed by the newly completed semiclassical theory for the Landau-Zener-Stueckelberg type curve crossings. Not only the resonance positions, but also the widths are nicely reproduced in comparison with the exact numerical calculations, even when the widths are as small as $10^{-8} \sim 10^{-11}$ *a.u.* The semiclassical theory is extended so as to be applicable to the case that the bottom of upper adiabatic potential is higher than the crossing point.

I-H-6 Four Mathematical Dimensional Quantum Mechanical Studies of Tetra-Atom Systems: State-to-State $J = 0$ Probabilities for the $H_2 + OH \rightarrow H_2O + H$ Reaction

Henrik SZICHMAN *(Soreq NRC, Israel and IMS)*, **Michael BAER** *(Soreq NRC, Israel)* **and Hiroki NAKAMURA**

[*J. Chem. Phys.* **107**, 3521 (1997)]

This paper presents reactive state-to-state $J = 0$ probabilities for the title system as obtained in a four-mathematical-dimensional quantum mechanical treatment. The present treatment differs from our previous one by the fact that in addition to the three Jacobi radial coordinates also the angular coordinate related to the H_2 axis is treated as coordinates. As a result only the Jacobi angle related to the OH axis is treated as a parameter and the final probabilities follow from an integration over this angle (the out-of-plane angle, β, is eliminated by using a β-averaged potential). The calculations yielded final rotational and vibrational distributions that were analyzed and discussed with respect to more accurate (i.e., five- and six-mathematical-dimensional) results.

I-I Theory of Nonadiabatic Transitions

I-I-1 Semiclassical Theory of Multi-Channel Curve Crossing Problems: Nonadiabatic Tunneling Case

Chaoyuan ZHU and Hiroki NAKAMURA

[*J. Chem. Phys.* **107**, 7839 (1997)]

Based on the new two-state theory of curve crossing recently completed by the authors, a compact and powerful theory is formulated for a general resonant multi-channel scattering with nonadiabatic tunneling (NT) type curve crossings. This theory is demonstrated to work remarkably well by comparing with the numerical solutions of close-coupling equations. Even detailed structures of overlapping resonances are nicely reproduced by the theory. Furthermore, this theory is very simple, not requiring any non-unique diabatization procedure, any complex calculus and any information on the couplings, neither diabatic nor nonadiabatic. The theory is based only on the adiabatic potentials on the real axis. Together with the previously proposed theory for the Landau-Zener (LZ) type curve crossings, the present semiclassical theory provides a complete picture of and a very powerful tool for multi-channel curve crossing problems.

I-I-2 Semiclassical Theory of Nonadiabatic Transition in a Two-State Exponential Model

Vladimir I. OSHEROV *(Inst. Chem. Phys., Russia and IMS)*, **Vladimir G. USHAKOV** *(Inst. Chem. Phys., Russia)* **and Hiroki NAKAMURA**

[*Phys. Rev. A* **57**, 2672 (1998)]

A general two-state exponential potential model is solved with use of the Bessel transformation and the WKB (Wentzel-Kramers-Brillouin) type semiclassical approximation. Accurate expressions are obtained for the nonadiabatic transition probability for one passage of the transition point and for the two dynamical phases.

Functionalities of these quantities in terms of two basic parameters are the same as those obtained before by Nikitin. The two basic parameters are, however, expressed in more general and accurate forms. Accuracies of these expressions are numerically confirmed.

The three quantities, the nonadiabatic transition probability and the two dynamical phases, constitute the nonadiabatic transition matrix and can be used to describe various (spectroscopic as well as scattering) processes not only for a two-state but also for a multichannel system. A possible generalization of the present theory is also briefly discussed to formulate a unified theory which can cover both Landau-Zener-Stueckelberg and Rosen-Zener-Demkov cases within the adiabatic state representation.

I-I-3 Improvement of the Adiabatic Phase

Integral for the Landau-Zener-Type Curve Crossing

Chaoyuan ZHU and Hiroki NAKAMURA

[*J. Chem. Phys.* **109**, 4689 (1998)]

We have established the new semiclassical theory for the two-state Landau-Zener-Stueckelberg-type curve crossing problems and have demonstrated their usefulness for various multichannel curve crossing problems in both time-independent and time-dependent cases. For both Landau-Zener (LZ) and nonadiabatic-tunneling (NT)-type transitions, our new theory can be solely based on the adiabatic potentials on the real axis and is free from searching complex crossing points and evaluating complex phase integrals. As a result, the theory can handle multichannel problems basically without any restriction to the number of crossings and channels involved. We have realized, however, that the theory in NT-type works much better than that for the LZ-type, and found that this is due to the adiabatic phase in the very strong diabatic coupling regime. In this note we report its improvement. This is quite important, because it is practically almost impossible to find complex crossing points among multichannel adiabatic potentials.

I-I-4 Patterns of Time-Propagation on the Grid of Potential Curves

Valentin N. OSTROVSKY *(Univ. St. Petersburg, Russia and IMS)* **and Hiroki NAKAMURA**

[*Phys. Rev. A* in press]

Time-propagation patterns are studied for a network formed by two bands of equidistant rectilinear parallel diabatic potential curves which cross each other. In the case of weak coupling between the bands the propagation proceeds mostly via diabatic path. In the case of strong coupling a new regime of antidiabatic propagation is revealed. For the intermediate case of coupling strength the propagation is basically described by an overlay of diabatic and antidiabatic patterns; interestingly, the adiabatic propagation is never operative. The present dynamic quantum model is compared with those models that assume reduction of the problem to a succession of pairwise transitions between the states.

I-J New Way of Controlling Molecular Nonadiabatic Processes

I-J-1 Control of Time-Dependent Nonadiabatic Processes by an External Field

Yoshiaki TERANISHI *(Grad. Univ. Adv. Stud.)* **and Hiroki NAKAMURA**

[*Phys. Rev. Lett.* **81**, 2032 (1998)]

A new idea of controlling nonadiabatic transitions by an external field is proposed. The basic principle is to periodically sweep an external field at each level crossing to make the overall transition probability from an initial state to any desirable final state equal to unity. The recently completed semiclassical theory of nonadiabatic transition enables us to analytically deal with this problem. The present idea may be applicable to various physical and chemical problems, whenever level crossings are created by an extern field.

I-J-2 New Way of Controlling Molecular Processes by a Time-Dependent External Field

Yoshiaki TERANISHI *(Grad. Univ. Adv. Stud.)* **and Hiroki NAKAMURA**

A new way of controlling molecular processes by using a time-dependent external field is proposed. As was discussed in the previous paper, the basic idea is to completely control nonadiabatic transitions at avoided crossings of potential curves by periodically sweeping the external field. The control conditions can be formulated analytically. The external field can be anything like magnetic, electric, or laser field. In the case of laser field, one can use both frequency and intensity as control parameters. Various semiclassical theories of nonadiabatic transitions can be nicely utilized to formulate the problem. As an example, a one-dimensional model of ring puckering isomerization of trimethyleneamine is discussed.

I-K Theoretical Studies of Characteristics and Dynamics of Superexcited States of Molecules

I-K-1 Characteristics and Dynamics of Superexcited States of Diatomic Molecules: General Theoretical Procedure

Miyabi HIYAMA *(Grad. Univ. Adv. Stud.)***, Nobuhiro KOSUGI and Hiroki NAKAMURA**

[*J. Chem. Phys.* **107**, 9370 (1997)]

A general theoretical procedure to analyze the characteristics and dynamics of superexcited states of diatomic molecules is developed. It utilizes the following three methods effectively: (1) quantum chemical methods to evaluate basic parameters of the

superexcited states, (2) spectroscopic experiments to improve the basic information obtained theoretically, and (3) multi-channel quantum defect theory (MQDT) to analyze couplings among various kinds of states and to clarify the dynamics. This procedure is composed of seven steps, including a method to evaluate the electronic coupling of the first king of superexcited state to ionization continuum which is newly proposed here. The two-center Coulomb function in the field of the corresponding diatomic molecular ion is used to evaluate this coupling. This can be done by incorporating the Coulomb functions into an ab initio quantum chemical code. The whole procedure is illustrated for the CO molecule.

I-K-2 Analytical Treatment of Singular Equations in Dissociative Recombination

Lukas PICHL *(Grad. Univ. Adv. Stud.)***, Hiroki NAKAMURA and Jiri HORACEK** *(Charles Univ., Czech Rep. and IMS)*

The Lippmann-Schwinger type singular integral equation, which arises in the multichannel quantum defect theory (MQDT) approach to the dissociative recombination process, is investigated. The singularity is treated analytically by introducing an energy dependent quadrature. In many cases of physical interest the energy kernel of the equation is well approximated to be separable and an analytical solution becomes possible. The solution is illustrated by taking the case of H_2^+ as an example, and is shown to be better than the other available methods such as the perturbation and the grid methods.

I-K-3 Electron Attachment and Vibrational Excitation in Hydrogen Iodide: Calculations Based on the Nonlocal Resonance Model

Jiri HORACEK *(Charles Univ., Czech Rep. and IMS)***, Wolfgang DOMCKE** *(Heinrich-Heine-Univ., Germany)* **and Hiroki NAKAMURA**

[*Z. Phys. D* **42**, 181 (1997)]

The nonlocal resonance model developed earlier for the description of the collision of low-energy electrons with HCl and HBr has been adapted to the electron-HI collision system. The parameters of the model have been determined by fitting experimental high-resolution data for the attachment cross section in HI in the energy range 0-170 meV. Moreover, ab initio electronic-structure data for the electronic ground-state potential-energy function of HI^- have been taken into account. Within the resulting model, cross sections for vibrational excitation and dissociative attachment processes in HI and DI have been calculated over a reasonably wide energy range. No high-resolution experimental data are available for comparison.

I-L Siegert Pseude-State Formulation of Scattering Theory

I-L-1 Siegert Pseude-State Formulation of Scattering Theory: One-Channel Case

Oleg I. TOLSTIKHIN *(Lebedev Physical Inst., Russia and IMS)***, Valentin N. OSTROVSKY** *(Univ. St. Petersburg, Russia and IMS)* **and Hiroki NAKAMURA**

[*Phys. Rev. A* **58**, 2077 (1998)]

Siegert pseude-states (SPS) are defined as a finite basis representation of the outgoing wave solutions to radial Schroedinger equation for cutoff potential, and the problem of their calculation is reduced to standard linear algebra easily implementable on computers. For a sufficiently large basis and the cutoff radius, the set of SPS includes bound, weakly antibound, and narrow complex-energy resonance states of the system, i.e. all the physically meaningful states observable individually. Moreover, the set is shown to posess certain orthogonality and completeness properties which qualify it as a discrete basis suitable for expanding the continuum. We rederive many results of the theory of Siegert states in terms of SPS and obtain some new relations not known previously. This not only makes the results for the first time practically applicable, but also sheds a new light on their mathematical nature. In particular, we show how the Mittag-Leffler expansion for the outgoing wave Green function and the scattering matrix can be obtained on the basis of very simple algebraic relations, without assuming them to be meromorphic functions. Explicit construction of these two fundamental objects completes the SPS formulation of scattering theory for one-channel case. The computational efficiency of this approach is illustrated by a number of numerical examples.

I-M Theoretical Studies of Ultrafast Nonlinear Optical Spectroscopy of Molecules in Condensed Phases

I-M-1 Fifth-Order Two-Dimensional Vibrational Spectroscopy of a Morse Potential System in Condensed Phases

Yoshitaka TANIMURA

[*Chem. Phys.* **233**, 217 (1998)]

The nonlinear optical response of a molecular system in the condensed phase subjected to a series of five off-resonant femtosecond laser pulses has been studied using a quantum Fokker-Planck equation. The third- and fifth-order response functions, which are equivalent to the second- and third-order correlation functions of the molecular coordinate were obtained form the equation of motion. Assuming the potential surface of a Cesium dimer [Cs_2], which is modeled by a Morse potential, and considering both the linear and nonlinear coordinate dependence of the polarizability, we calculated the third- and fifth-order response functions for various temperatures and heat-bath couplings. The temporally two-dimensional (2D) profiles of the fifth-order signal effects both the shape of potential and the coordinate dependence of the polarizability, even at strong damping. The nonlinearities caused by the anharmonic potential and by the nonlinear polarizability have different temperature dependence. This indicates that fifth-order two-dimensional spectroscopy carried out for a different temperature allows us to access information of the potential and the polarizability.

I-M-2 Pump-Probe Spectra and Nuclear Dynamics for a Dissipative Molecular System in a Strong Laser Field: Predissociation Dynamics

Yutaka MARUYAMA *(Grad. Univ. Adv. Stud.)* **and Yoshitaka TANIMURA**

[*Chem. Phys. Lett.* **292**, 28 (1998)]

The predissociation dynamics of a molecular system under a strong laser field in the condensed phase is investigated by direct numerical integration of the multi-state quantum Fokker-Planck equation. Numerical calculations of probe absorption spectra driven by a strong pump pulse are presented, and discussed. The results show dynamical Stark splitting, but, in contrast to the Bloch equations which contain an infinite-temperature dephasing, we find that at finite temperatures their peaks have different heights even when the pump pulse is on resonance. Furthermore we observe the effect of the diabatic coupling between excited and dissociative states as the peaks on the spectra.

I-M-3 Coherent Two-Dimensional Raman Scattering: Frequency-Domain Measurement of the Intra- and Intermolecular Vibrational Interactions

Minhaeng CHO *(IMS and Korea Univ.)* **Ko OKUMURA and Yoshitaka TANIMURA**

[*J. Chem. Phys.* **108**, 1326 (1998)]

A new experiment of frequency-domain coherent two-dimensional Raman scattering is theoretically proposed. By using three fields whose wave vectors and frequencies are independently controlled, one can measure the nonlinear Raman responses in either gas or condensed phases. The connection to the time-domain femtosecond two-dimensional Raman spectroscopy is completely established. By considering several limiting cases in detail, it is found that from the coherent 2D Raman scattering spectrum one can obtain quantitative information on the anharmonicity, anharmonic mode coupling, and polarizability coupling.

I-M-4 Sensitivity of Two-Dimensional Fifth-Order Raman Response to the Mechanism of Vibrational Mode-Mode Coupling in Liquid Molecules

Ko OKUMURA and Yoshitaka TANIMURA

[*Chem. Phys. Lett.* **278**, 175 (1997)]

We study coupling mechanism of inter- and intramolecular modes of liquids by using a multi-mode Brownian oscillators model. The coupling between modes comes into play through polarizability and/or potential expanded with respect to vibrational coordinates. We take into account these two causes of coupling and present analytical expressions for the Fourier transform of the time-domain fifth-order Raman signal. We demonstrate a notable sensitivity of the Fourier-transformed quantity to the coupling mechanism through numerical calculations for chloroform.

I-M-5 Two-Dimensional THz Spectroscopy of Liquids: Nonlinear Vibrational Response to a Series of THz Laser Pulses

Ko OKUMURA and Yoshitaka TANIMURA

[*Chem. Phys. Lett.* **295**, 298 (1998)]

We propose a nonlinear experiment utilizing the nonlinear interaction with THz pulses, whose generation has recently become well established. In the lowest nonlinear process, we have two controllable delay times. This is another optical analogue of the two-dimensional (2D) NMR as the recently developed 2D Raman spectroscopy. Our model calculation for liquid water demonstrates the striking capability of the proposed technique, clearly distinguishing two types of anharmonicity in the low-frequency modes.

I-M-6 Optimized Perturbation Approach to a Dissipative System: Correlation Functions of Anharmonic Oscillators

Yoko SUZUKI and Yoshitaka TANIMURA

[*Phys. Rev. E* in press]

We apply the optimized perturbation theory (OPT) to study the dynamics of a anharmonic potential system in coupled to a heat bath. The OPT combines the techniques based on the variational principle and the perturbative expansion. The first order approximation of the OPT agrees with the Feynman's variational theory developed for the polaron problem. The OPT makes it

possible to deal with anharmonic potential system in non-perturbative way. Combined with inversion method which is the technique to carry out the Legendre transformation, we take effectively into account of the information lacked in the OPT alone, for example the ansymmetry of potential. We then develop a formalism to calculate partition functions and two-time correlation functions of a coordinate which relate to the linear absorption spectrum in laser experiments. We use this procedure so as to study the dynamics of a Morse potential system and a double well potential system coupled to a heat-bath, respectively.

I-N Theoretical Studies of Molecular System Coupled to a Glass Environment

I-N-1 Spectral Random Walks and Line Broadening of Impurity Molecules in an Ising Spin Glass Environment

Yoshitaka TANIMURA, Hiroshi TAKANO *(Keio Univ.)* **and Joseph KLAFTER** *(Tel-Aviv Univ.)*

[*J. Chem. Phys.* **108**, 1851 (1998)]

Transition energy fluctuations in impurity molecules, embedded in an inhomogeneous environment, are investigated within an Ising spin model of the environment. The spatially distributed impurity molecules are assumed to interact with the Ising spin glass through dipole-dipole type of interaction. We calculate the fluctuations in the transition energies of impurity molecules, for different temperatures and various Ising parameters, and find that the spectral distribution of the fluctuations follows approximately a 1/f power law. The fluorescence spectra of the impurity molecules yield microscopic information about domain structures in the Ising environment. In the case of large disorder, the distribution of transition energies shows profiles similar to those observed in single molecule spectroscopy.

I-N-2 Absorption Line Shape of Impurity Molecule Driven by a Fractal Noise

Gautam GANGOPADHYAY and Yoshitaka TANIMURA

[*Chem. Phys. Lett.* **289**, 97 (1998)]

We have applied the quantum master equation to simulate a two-level system driven by a fractal noise in a dissipative environment. The fractal noise is assumed to be a two-state process with $\pm\Delta$ and characterized by its correlation function $1/\tau^{\beta}$ where $0 < \beta < 1$. Steady state absorption spectrum for the system is obtained analytically for a monochromatic laser excitation. A dramatic blue shift as well as a broadening of the absorption peak, due to the interference between the fractal noise and the natural damping, is observed.

I-O Ab Initio Molecular Orbital studies of Organic Conductors

I-O-1 Ab Initio MO Studies on Electronic States of DCNQI Molecules

Yutaka IMAMURA *(Grad. Univ. Adv. Stud.)*, **Seiichiro TEN-NO and Yoshitaka TANIMURA**

Electronic and geometrical structures of DR-DCNQI molecules (R = H, Cl, Br, I, Me and OMe) were studied by performing ab initio MO calculations at the HF/DZP level. We carried out DCNQI monomer calculations and found that the optimized structures are close to experimental ones within errors of 0.04 Å in a six-membered ring. We then discussed the basis set dependence of geometrical parameters and concluded that the polarization functions improve the description for double and triple bond states. Ab initio parameters such as transfer integrals were calculated for DCNQI dimers and trimers and compared with formerly calculated parameters. We found that the transfer integrals correlate well with lattice parameters of the c axis.

I-O-2 Theoretical Study on Electron Correlation of 1-D (DCNQI)2M (M = Li, Ag) Salts

Yutaka IMAMURA *(Grad. Univ. Adv. Stud.)*, **Seiichiro TEN-NO, Kenji YONEMITSU and Yoshitaka TANIMURA**

[*Chem. Phys. Lett.* in press]

We study electronic states of the (DCNQI)2M (M = Li and Ag) salts based on the ful configuration interaction (FCI) method using effective Hamiltonians derived from the ab initio molecular orbital theory. FCI results of the DCNQI tetramer and octamer models indicate that the ground state has the antiferromagnetic and charge ordering correlations. It corresponds to the 2 kF spin density wave and 4 kF charge density wave states (SDW and CDW). In the octamer model, it is also found that some low-lying excited states have similar spin-flipped CDW correlations and the antiferro-magnetic correlation is weakened.

I-P Electron and Positron Scattering from Polyatomic Molecules

The interaction potential between the positron or electron and a molecule consists of three components: electrostatic, exchange and polarization. The static potential arises from the interaction between the projectile and the electrostatic field of the molecule. Thus the static potential for the positron collision is the same as that for the electron collision except for its sign. There is no exchange interaction in the case of positron-molecule collision. In the asymptotic (long-range) region, the polarization interaction for the positron-molecule collision is exactly the same as that for the electron-molecule collision. As the projectile comes closer to the molecule, the distortion of the molecular charge cloud becomes different for different projectiles. The polarization potential at short to intermediate range, particularly its anisotropic part, should be different for the two projectiles. The polarization interaction is another example of long-range interaction, but the cumulative effects of the two types of interactions are totally different for the two projectiles (additive for one and canceling for another).

Due to the complexity of the potential, an electron is known to be temporarily captured by a molecule. This gives rise to a so called "shape resonance" in the electron scattering from a molecule. It is of much interest to see if a similar resonance can occur in the positron scattering from a molecule. The shape resonance affects also the rotational and vibrational excitation processes. Even if no shape resonance occurs, the dependence on the projectile (i.e., positron vs. electron) can appear differently in the processes of rotational and vibrational excitations. A comparative study of the positron- and electron-molecule collisions, particularly that of the rotational and vibrational excitation (and dissociation), would be fruitful in understanding the dynamics of the interaction of both the positron and electron with molecules. In this respect, collisions involving polyatomic molecules are of much interest.

I-P-1 A Comparative Study of Electron- and Positron-Polyatomic Molecule Scattering

Mineo KIMURA *(Yamaguchi Univ. and IMS)*, **Osamu SUEOKA and Akira HAMADA** *(Yamaguchi Univ.)* **and Yukikazu ITIKAWA** *(ISAS)*

The present article is concerned with polyatomic molecules than with diatomic and triatomic ones, which were mainly treated in the earlier review article by Kauppila and Stein.[1] We discuss a few new and intriguing features observed for the first time recently for positron scattering from large polyatomic molecules, and provide with an analysis from combined theoretical and experimental points of view.

All possible processes by electron and positron impacts are listed in Table 1. For electron impact, a few data are available for total, elastic, momentum transfer, rovibrational excitation, and some electronic excitation and ionization processes, while for positron impact, very limited information for total cross section for limited species of atoms and molecules and virtually no data exists for inelastic processes. From a comparative study between electron and positron impact, we can shed a light on basic schemes of interaction and scattering dynamics, and hence provide the understanding of basic physics at much deeper level.

Reference

1)W. E. Kauppila and T. E. Stein, *Adv. At. Mol. Opt. Phys.* **26**, 1 (1989).

Table 1. Processes possible for electron and positron scattering.

$e_p + AB(v,J)$	→	$e_p + AB$	elastic
	→	$e_p + e^- + AB^+$	ionization
	→	$e_p + AB^*$	electronic excitation
	→	$e_p + AB(v', J')$	rovibrational excitation
	→	AB^-	electron attachment
	→	AB^+	positron attachment (not observed yet)
	→	$(e^+e^-) + AB^+$	positronium formation (Positron only)
	→	$h\nu + AB^+$	direct annihiration (Positron only)

I-P-2 Mode-Dependence in Vibrational Excitation of CO_2 Molecule by Electron and Positron Impacts

Mineo KIMURA *(Yamaguchi Univ. and IMS)*, **Michiya TAKEKAWA** *(ISAS)*, **Yukikazu ITIKAWA** *(ISAS)*, **Hideki TAKAKI and Osamu SUEOKA** *(Yamaguchi Univ.)*

We have found theoretically, for the first time, that vibrational excitations of CO_2 molecule by electron (e^-) and positron (e^+) impacts are strongly dependent on the charge of the projectile at impact energy below 6 eV. For the symmetric-stretching mode, the excitation cross section of e^- impact is larger by two-to-three orders of magnitude than that of e^+ impact, while for bending and asymmetric-stretching modes, the magnitude of both cross sections for e^- and e^+ impacts are nearly comparable. These results are qualitatively confirmed experimentally, and are interpreted as the difference of interactions and incident-e^- or -e^+ wavefunctions.

I-P-3 Total Cross Sections of Electron and Positron Collisions with C_3F_8 and C_3H_8 Molecules, and Differential Elastic and Vibrational Excitation Cross Sections by Electron Impact on These Molecules

Hiroshi TANAKA, Yoshio TACHIBANA, Masashi KITAJIMA *(Sophia Univ.)*, **Osamu SUEOKA, Hideki TAKAKI, Akira HAMADA** *(Yamaguchi Univ.)* **and Mineo KIMURA** *(Yamaguchi Univ. and IMS)*

Total cross section for electron (e^-) and positron (e^+) scattering from C_3H_8 and C_3F_8 have been measured from 0.8 to 600 eV and 0.7 to 600 eV, respectively. We have also investigated differential elastic cross sections DCS's by electron impact from 2.0 eV to 200 eV, which are compared with the present theoretical result. For e^- scattering from C_3H_8, the cross sections are found to be larger by a factor of two than these of e^+ scattering below 20-30 eV measured and they show a large peak at 8 eV due to a shape resonance, in addition to a shoulder-like structure in the region of 20 - 40 eV. For e^- scattering from C_3F_8, the cross sections are again larger by at least a factor of two than those of e^+ scattering below 50 eV, and have two peaks at 4 and 8 eV, followed by a broad peak in the region of 20 - 40 eV. Some small structures overlies on the broad hump. Both cross sections of e^- and e^+ impacts for C_3H_8 and C_3F_8 quickly approach to each other beyond 200 eV. From DCS's study, we have been able to provide with more detailed information of shape resonances, and also have carried out some analysis of resonances in vibrational excitation results. In general, the total and integrated elastic cross sections are in good qualitative and quantitative agreement.

I-Q Electronic Structure of a Molecule in Solution

Chemical reaction is undoubtedly the most important issue in the theoretical chemistry, and the electronic structure is a key to solve the problem. As long as molecules in the gas phase are concerned, the theory for the electronic structure has been enjoying its great success. However, when it comes to molecules in solution, the stage of theory is still an infant. We have recently proposed a new method refereed to as RISM-SCF based on the integral equation theory of molecular liquids (RISM) and the ab initio electronic structure theory (SCF).[1] The integral equation approach replaces the reaction field in the continuum models by a microscopic expression in terms of the site-site radial distribution functions between solute and solvent.

$$V_\lambda = \sum_j \int \frac{q_j}{r} g_{j\lambda}(r) 4\pi r^2 dr$$

where j and λ specify solvent and solute sites, respectively, and r denotes the solvent density. The site-site radial distribution functions $g_{\lambda j}(r)$ can be calculated from the extended RISM equation. Using V_λ the solvated Fock operator is defined as,

$$F^s = F^g - \sum_\lambda V_\lambda b_\lambda$$

where b_λ is a population operator of solute atoms. The statistical solvent distribution around solute is determined by the electronic structure or the partial charges of solute, while the electronic structure of solute is influenced by the solvent distribution. Therefore, the Hartree-Fock equation and the RISM equation should be solved in a self-consistent manner. It is this self-consistent determination of the solute electronic structure and the solvent distribution around the solute that features the RISM-SCF procedure.

$$A = E_{\text{solute}} + \Delta\mu$$

The same Fock operator can be derived from a variational principle.[2] Defining the Helmholtz free energy A as follows, where E_{solute} is the energy of solute under solvent influence, and $\Delta\mu$ is the solvation free energy represented in terms of the Singer-Chandler formula. The Fock operator for a solute molecule in solvent as well as the RISM-HNC equations can be obtained as the first order variations with respect to the wave functions and the pair correlation functions under the constraint of the orthonormality to the molecular orbitals. The latest development along this line are reported below.

References

1)S. Ten-no, F. Hirata and S. Kato, *Chem. Phys. Lett.* **214**, 391 (1993); *J. Chem. Phys.* **100**, 7443 (1994).
2)H. Sato, F. Hirata and S. Kato, *J. Chem. Phys.* **105**, 1546 (1996).

I-Q-1 Molecular Theory of Solvent Effect on keto-enol Tautomers of Formamide in Aprotic Solvents: RISM-SCF Approach

Tateki ISHIDA *(Kyoto Univ.)*, **Fumio HIRATA, Hirofumi SATO and Shigeki KATO** *(Kyoto Univ.)*

[*J. Phys. Chem. B* **102**, 2045 (1998)]

By using RISM-SCF method, the optimized geometries and solvation free energies of the keto and enol tautomers of formamide were calculated in six organic aprotic solvents (CS_2, CCl_4, DME, THF, acetonitrile, and DMSO). From the analysis of the

solvation free energies, it was shown that the solute-solvent hydrogen bonding largely contributed to them and that the ability of the solvent to form hydrogen bondings is very important. It was also shown that Taft's b parameters are well-correlated to the calculated well-depth of hydrogen bonding. The results that the solvation free energies for both the tautomers showed the irregularity in acetonitrile solution are in qualitative accord with the empirically determined solvent parameters. The empirical measure of solvent ability to form hydrogen-bonding with solute is explained at a molecular level.

The solvent effects on the energy difference between the keto-enol tautomers were examined. It was found that the keto tautomer was stabilized largely compared to enol form. These tendencies are consistent with the experimental and previous theoretical results. In both tautomers, the dipole moments of solutes were enhanced in polar solvents and the geometric structures were changed, so as to increase the solute dipole moment. It was found that the tendency of solute dipole moments was correlated to Taft's parameters with respect to solvent polarity.

I-Q-2 Theoretical Study of the Solvent Effect on Triiodie Ion in Solutions

Hirofumi SATO, Fumio HIRATA and Anne B. MYERS *(Univ. Rochester)*

[*J. Phys. Chem. A* **102**, 2065 (1998)]

The free energy surfaces of I_3^- in aqueous, methanol and acetonitrile solutions as well as in the gas phase are examined in both ground and excited states by means of the *ab initio* RISM-MCSCF (reference interaction site model — multiconfigurational self consistent field) method. The $X^1\sum_g^+$ state in the gas phase has a highly symmetrical $D_{\infty h}$ geometry as its stable structure. In solution phases, the electronic structure of I_3^- is strongly affected by the surrounding solvent molecules and the energy profiles are drastically changed. Especially in aqueous solution, the ground-state free-energy surface around the gas phase equilibrium geometry becomes virtually flat, indicating an increased population of asymmetrical structure due to the solvent effect. It is suggested that this broken symmetry can explain the appearance of transitions in the IR and Raman spectra which are symmetry forbidden in the gas phase.

I-Q-3 Theoretical Study for Autoionization of Liquid Water: Temperature Dependence of the Ionic Product (pK_w)

Hirofumi SATO and Fumio HIRATA

[*J. Phys. Chem. A* **102**, 2603 (1998)]

The temperature dependence of the ionic product of water (pK_w) is investigated theoretically by means of ab initio electronic structure theory combined with the extended reference interaction site method in statistical mechanics of molecular liquids (RISM-SCF/MCSCF method). The chemical equilibrium $H_2O + H_2O = H_3O^+ + OH^-$ is studied, in which water molecules, hydronium ions, and hydroxide ions are regarded as "solute" molecules in aqueous solution. Molecular geometries, electronic structures, pair correlation functions, and free energy components of those species as well as their temperature dependence are calculated. It is shown that the hydroxide anion is polarized more easily by surrounding solvent compared to the other species. The solvent-induced electronic structure relaxes toward that in the gas phase as temperature increases. The hydroxide anion exhibits the largest temperature dependence in the electronic structure as well as in solvation structure. It is found that changes in the solvation free energies drive the chemical equilibrium toward the left-hand side (association) as temperature increases, while energies associated with solvent-induced reorganization of electronic structure make the opposite contribution. The temperature dependence of pK_w is dominated by the latter contribution, which gives rise to good agreement with the experimental results. It is suggested that the observed temperature dependence of pK_w is related to the great sensitivity of the electronic structure of OH^- on the solvent effect.

I-Q-4 The Syn-/Anti- Conformational Equilibrium of Acetic Acid in Water Studied by the RISM - SCF/ MCSCF Method

Hirofumi SATO and Fumio HIRATA

[*J. Mol. Struct.(theochem)* in press]

The syn-/anti- conformational equilibrium of acetic acid in water is studied by the RISM-SCF/MCSCF method, a hybridized method of the *ab initio* quantum chemistry and the statistical mechanics of molecular liquids. The solvent effect on the two conformers are examined in terms of the solvation free energy. Significant stabilization due to solvation was observed on the anti-conformer, while only slight decrease in the free energy is resulted in the syn-conformer. Due to the greater stabilization in the anti-conformer, the energy gap between the two conformers is dramatically reduced in solution; 1.7 kcal/mol in solution compared with 6.9 kcal/mol in gas phase. The change in the electron density of acetic acid upon transferring the solute from gas phase into aqueous solution is visualized to understand the polarization effects due to solvent.

I-Q-5 RISM-SCF Study for the Free Energy Profile of Menshutkin Type Reaction $NH_3 + CH_3Cl \rightarrow NH_3^+CH_3 + Cl^-$ in Aqueous Solution

Kazunari NAKA *(Kyoto Univ.)*, **Hirofumi SATO, Akihiro MORITA** *(Kyoto Univ.)*, **Fumio HIRATA and Shigeki KATO** *(Kyoto Univ.)*

[submitted]

The free energy profile for the Menshutkin type reaction $NH_3 + CH_3Cl \rightarrow NH_3^+CH_3 + Cl^-$ in aqueous solution is studied using the RISM-SCF method. The effect of electron correlation on the free energy profile

is estimated by the RISM-MP2 method at the HF optimized geometries along the reaction coordinate. The vibrational frequencies at the reactant, transition state and product are found to undergo a large influence by the solvation and these are utilized to calculate the zero-point energy correction of the free energy profile. The computed barrier height and reaction exothermicity are in reasonably agreement with those of the experiment and the previous calculations. The change of solvation structure along the reaction path are represented by the radial distribution functions between the solute-solvent atomic sites. The mechanisms of the reaction are discussed from the view points of solute electronic and solvation structures.

I-R Solvation Thermodynamics of Protein and Related Molecules

Concerning biomolecules such as protein, it is a final goal for the biochemistry and biophysics to explore the relation between conformations and biological functions. The first important step toward the goal would be to explain the confomational stability of biomolecules in terms of the microscopic structure of the molecules in solvent. It is an extremely difficult probelm by any means due to the overwhelmingly large degrees of freedom to be handled, including protein and solvent. As long as the small and/or short-time fluctuations of protein around the native structure is concerned, a variety of molecular simumaltion techniques is a quite powerful tool to explore the microscopic structure of protein and solvent. However, the techniques are not so effective to characterize stability of the macromolecules, to which the thermodynamic limit is concerned. The semi-microscopic approach based on the Poisson-Boltzmann equation and the scaled particle theory deserves to draw attention from such a view point.[1)] Inspite of the oversimplification employed for the model of solvent, the method could have succeeded to reproduce fundamental characteristics of the solvation thermodynamics of a protein, including the cold denaturation. An well-addressed weakness of the treatment is the less sophisticated representation of the microscopic structure of solvent water. The extended RISM theory has potential capability of overcoming the problem at least in the level of microscopic description based on the pair correlation functions. Ovbious technical difficulties which one may face in applying the theory to such a large system are not only the computation time but also the stability of the numerical solution.[2)]

Here, we present our recent effort to tackle the problem based on the two theoretical tools: extended RISM and the scaled particle theory (SPT). The studies for the solvation thermodynamics of small molecules such as ions are also included because it is regarded as elementary processes for the solvation of biomolecules, and because it is prerequisite for studying the more complicated molecules.

References

1) M. Irisa, K. Nagayama and F. Hirata, *Chem. Phys. Lett.* **207**, 430 (1993); M. Irisa, T. Takahashi, K. Nagayama and F. Hirata, *Mol. Phys.* **85**, 1227 (1995).

2) A. Kitao, F. Hirata and N. Go, *J. Phys. Chem.* **97**, 10231 (1993).

I-R-1 Calculation of Hydration Free Energy for a Solute with Many Atomic Sites Using the RISM Theory: Robust and Efficient Algorithm

Masahiro KINOSHITA *(Kyoto Univ.)*, **Yuko OKAMOTO and Fumio HIRATA**

[*J. Comput. Chem.* **18**, 1320 (1997)]

We have developed an algorithm for solving the reference interaction site model (RISM) equations for water near a solute molecule with many atomic sites (interaction sites). It is a hybrid of the Newton-Raphson and Picard methods which is judiciously constructed. Various considerations are given so that the computer time can be saved as greatly as possible. The robustness and high efficiency of the algoritm has been demonstrated for calculating hydration free energies of Met-enkephalin (a peptide with 75 sites) with different conformations. The Jacobian matrix is treated as part of the input data, and it has been found that the same matrix can be used for a considerably large set of different conformations of the solute molecule.

I-R-2 Solvation Structure and Stability of Peptides in Aqueous Solutions Analyzed by the Reference Interaction Site Model Theory

Masahiro KINOSHITA *(Kyoto Univ.)*, **Yuko OKAMOTO and Fumio HIRATA**

[*J. Chem. Phys.* **107**, 1586 (1997)]

We report results of numerical analyses on solvation structure and conformational stability of a dipeptide and Met-enkephalin in the extended simple point charge (SPC/E) model water. The reference interaction site model (RISM) theory is fully solved using our robust, highly efficient algorithm. It is shown that water structure near the peptides and the hydration free energy are greatly dependent on the peptide conformations. Stability of Met-enkephalin is examined in terms of the total energy defined as the sum of the conformational energy and the hydration free energy of the peptide. We test several different conformations including that with the minimum energy in gas phase, which takes rather compact form due to an intramolecular hydrogen bond. It is shown that a fully extended conformation has the highest stability in water. Our results are in qualitative accord with the recent nuclear magnetic resonance

(NMR) experiments which suggest fully extended conformations with large fluctuations for the solution structure of the peptide. A conformation which is similar to that obtained from the NMR experiments in miceller solutions, is much less stable when it is put in water. Thus, the peptide conformations are greatly sensitive to microscopic solvent environment, and any native treatment of the solvent such as the continuum model will end in failure.

I-R-3 First-Principle Determination of Peptide Conformations in Solvents: Combination of Monte Carlo Simulated Annealing and RISM Theory

Masahiro KINOSHITA *(Kyoto Univ.)*, **Yuko OKAMOTO and Fumio HIRATA**

[*J. Am. Chem. Soc.* **120**, 1855 (1998)]

This paper contributes to development of a microscopic approach to predicting stable conformations of proteins in solvent. We report results of the first attempt to combine Monte Carlo simulated annealing, a powerful conformational sampling technique, and the reference interaction site model (RISM) theory, a statistical-mechanical treatment for molecular fluids. In solvent the key function is the total energy defined as the sum of the conformational energy and the solvation free energy, and the RISM theory is employed to calculate the latter. Starting from an initial conformation given, our computer program samples many conformations, and then finds the conformation with the minimum total energy. Met-enkephalin in the two different solvents, a model water and a simple, repulsive-potential system, are considered. In water the solvation free energy varies greatly from conformation to conformation, while in the simple solvent it remains almost unchanged against conformational changes. In water most of the conformations with larger solvation free energies are strongly rejected and the number of probable conformations is drastically reduced, which is suggestive that Met-enkephalin is forced to take conformations favored by water far more rapidly than in gas phase and in the simple solvent. The set of stable conformations obtained in water are quite different from those in gas phase and the simple solvent: they are characterized by almost fully extended backbone structure with large fluctuations in side-chain structure, which are in qualitatively good agreement with those determined by the recent nuclear magnetic resonance (NMR) experiments.

I-R-4 Calculation of Solvation Free Energy Using RISM Theory for Peptide in Salt Solution

Masahiro KINOSHITA *(Kyoto Univ.)*, **Yuko OKAMOTO and Fumio HIRATA**

[*J. Comput. Chem.* in press]

We have developed a robust, highly efficient algorithm for solving the full reference interaction site model (RISM) equations for salt solutions near a solute molecule with many atomic sites. It is obtained as an extension of our previously reported algorithm for pure water near the solute molecule. The algorithm is a judicious hybrid of the Newton-Raphson and Picard methods. The most striking advantage is that the Jacobian matrix is just part of the input data and need not be recalculated at all. To illustrate the algorithm, we have solved the full RISM equations for a dipeptide (NH_2-$CHCH_3$-CONH-$CHCH_3$-COOH) in a 1M-NaCl solution. The extended simple point charge (SPC/E) model is employed for water molecules. Two different conformations of the dipeptide are considered. It is assumed for each conformation that the dipeptide is present either as an unionized form or as a zwitterion. The structure of the salt solution near the dipeptide and salt effects on the solvation free energy have also been discussed.

I-R-5 Singular Behavior of the RISM Theory Observed for Peptide in Salt Solution

Masahiro KINOSHITA *(Kyoto Univ.)*, **Yuko OKAMOTO and Fumio HIRATA**

[*Chem. Phys. Lett.* submitted]

We examine the reference interaction site model theory applied to a peptide-salt solution system, with the assumption that a zwitterionic dipeptide (Ala-Ala) is present in NaCl solution at the infinite-dilution limit. For some sets of the parameters in the peptide-cation and peptide-anion potentials, the theory exhibits singular behavior: as the salt concentration decreases, the ionic concentration around the peptide increases and the theory eventually loses its solution. The singularity is interpreted as a signal of the ion condensation. A trend of aggregation of peptide molecules is also found. For other sets of the potential parameters, however, no such singularity occurs. As far as the salt effects are concerned, the qualitative aspects of the conclusionsare somewhat sensitive to the potential parameters employed.

I-R-6 Analysis on Conformational Stability of C-Peptide of Ribonuclease A in Water Using the Reference Interaction Site Model Theory and Monte Carlo Simulated Annealing

Masahiro KINOSHITA *(Kyoto Univ.)*, **Yuko OKAMOTO and Fumio HIRATA**

[*J. Chem. Phys.* submitted]

Solvation structure and conformational stability of the C-peptide fragment of ribonuclease A in pure water, have been analyzed using the full reference interaction site model (RISM) theory. The charged groups in the side chains of Lys-1+, Glu-2-, Lys-7+, Arg-10+, and His-12+ (in particular, the four like-charged groups) play substantial roles in stabilizing the conformations. The solvation free energy and the conformational energy are governed by the contribution from the electrostatic interaction with water and the intra-molecular Coulombic energy, respectively, and the

conformational stability is determined by competition of these two factors. The contribution from the hydrophobic hydration and the van der Waals and torsion terms in the conformational energy are less important, which is in contrast with the result for Met-enkephalin. The Monte Carlo simulated annealing combined with the RISM theory has been applied to the C-peptide using an almost fully extended conformation as the initial one. The conformation first changes in the direction that the charged groups in the side chains are more exposed to water, and in particular, the positively charged groups are closer together. Thus, the solvation free energy decreases greatly in the initial stage. Although this leads to significant increase in the intramolecular Coulombic repulsion energy, the decrease in the solvation free energy dominates. In the later stage, however, further decrease in the solvation free energy gives rise to even larger increase in the intramolecular Coulombic repulsion energy, and the conformational change is greatly decelerated. The conformations thus stabilized in four different runs of the combined program are quite similar. The peptide conformation in water is stabilized far more rapidly than in gas phase.

I-R-7 Molecular Theories of Partial Molar Volume

Fumio HIRATA, Takashi IMAI and Masayuki IRISA *(Kyushu Inst. Tech.)*

[*Rev. High Press. Sci. & Tech.* **8**, 96 (1998)]

The theoretical study for response of chemical processes to pressure change requires analyses of the partial molar volume of the chemical species in solution, since the pressure dependence of equilibrium constants is closely related to the difference in the partial molar volumes between reactants and products. The pressure denaturation of protein is one of outstanding properties, which refutes any naive argument concerning 'volume.' According to the most naive argument based on the excluded volume, applying pressure should stabilize its native conformation, because native conformations usually have most compact structure, thereby, the least excluded volume. However, general observations tell us that protein often denatures by applying pressure. How can the paradox be reconciled? The answer to the question may be given by looking at the partial molar volumes, not the 'excluded volume,' before and after the conformational change. The partial molar volume is a thermodynamic response of the chemical potential to pressure change, to which many chemical processes contribute. For instance, some residues in protein may dissociate upon denaturing to release ions, which in turn make partial molar volume less due to so called 'electrostriction' of solvent. If that is the case, protein will unfold by applying pressure. Polar residues will contribute to pressure denaturation in the same direction, if the residues are exposed to solvent upon unfolding. Hydrophobic residues may gives rise to the same effect. It is safe to say that what leads to pressure denaturation of protein are changes in the partial molar volume due to structural change in protein as well as in water. A large volume of experimental works have been devoted to the partial molar volume, but relatively few thoretical studies have been reported. In this report, we have developped two thories for the partial molar volume of protein in water, one based on the extended scaled particle theory and the other based on the Kirkwood-Buff solution theory coupled with RISM equation. Effect of conformational change of a peptide to the partial molar volume is examined by the method.

I-S Spatial and Temporal Density Fluctuation in Molecular Liquids

The latest development in the experimental techniques including the high resolution NMR and a variety of techniques in the time-resolved laser-spectroscopies have revealed the molecular nature of the solvent dynamics around solute or the solvation dynamics, which refuse any naive interpretation based on the continuum models. A microscopic or statistical-mechanical description for the solvation dynamics requires the formulation of the temporal as well as spatial fluctuations of solvent density around solute. A general recipe to such a problem is to use the generalized Langenvin equation (GLE). The GLE in principle gives the dynamics of a system in any resolution in space and time depending on the level of projection. However, its actual usefulness for a problem is largely determined by a choice of dynamic variables onto which other degrees of freedom are projected. It is the pair correlation functions which researves the microscopic nature of the system and yet tractable within the current development in the statistical-mechanical theory of liquids. A natural choices of the dynamic variables which lead to the density-density pair correlation function as an important ingredient in the dynamical equations is a set of the collective density field and its conjugate momentum density field. Such a choice leads to a Smoluchowsky-Vlasov type diffusion equation in the overdamped limit. As to the model for molecular diffusion in polar liquids, there are two quite different point of view. One is the traditinal rot-translational model[1)] and the other the interaction-site description which sees the diffusion of a molecule as a correlated motion of each atoms (sites).[2,3)] The interaction-site description employes the site-site Ornstein-Zernike (SSOZ) equation (or RISM equation) in order to represent the site-site direct correlation functions, which proves to be successful in a variety of application to molecualr liquid including water.[3)]

In what follows, the latest progress which we have made in the theory of the structure and dynamics of molecular liquids is reviewed. We also report our effort to formulate the non-equlibrium free energy profile along a solvent coordinate based on the extended RISM theory, which has played an essential role in the Marcus theory of

the electron transfer reaction.

References
1)D. F. Calef and P. G. Wolynes, *J. Chem. Phys.* **78**, 4145 (1983).
2)F. O. Raineri, Y. Zhou, H. L. Friedman and G. Stell, *Chem. Phys.* **152**, 202 (1991).
3)F. Hirata, *J. Chem. Phys.* **96**, 4619 (1992).

I-S-1 Interaction-Site-Model Description of Collective Excitations in Classical Molecular Fluids

Song-Ho CHONG *(Kyoto Univ.)* **and Fumio HIRATA**

[*Phys. Rev. E* **57**, 1691 (1998)]

We describe a molecular theory for liquid dynamics which provides a method for calculating dynamical correlation functions of classical molecular fluids. The theory is based on the generalized Langevin equation and on the interaction-site model for molecular liquids. A simple model for memory functions is developed by generalizing the conventional one which has been successfully applied to monatomic systems. The theory is applied to the calculation of longitudinal current spectra of a model diatomic liquid, and collective excitations in this solvent are investigated. We also clarify how these excitations originate from the translational and rotational motions of molecules.

I-S-2 Dynamics of Solvated Ion in Polar Liquids: An Interaction-Site-Model Description

Song-Ho CHONG *(Kyoto Univ.)* **and Fumio HIRATA**

[*J. Chem. Phys.* **108**, 7339 (1998)]

We present a molecular theory for friction coefficient of an ion based on the interaction-site model for molecular liquids and on the mode-coupling theory. The ionic friction is described in terms of response of collective excitations in solvent to a solute displacement, and the resultant formula expresses the friction as an amount of the energy dissipated during the relaxational processes after the solute perturbation. Utilizing this view point, the ionic friction is shown to be naturally decomposed into hydrodynamic, dielectric and their coupling contributions. It is demonstrated from theoretical calculations of the ionic frictions that both of classical pictures, the solventberg and dielectric friction pictures, are responsible for large frictions of small ions and that the coupling term, which has been disregarded in theoretical considerations so far, should also be properly taken into account in dealing with small ions.

I-S-3 Interaction-Site Representation for Collective Excitations in Diatomic Dipolar Liquid

Song-Ho CHONG *(Kyoto Univ.)* **and Fumio HIRATA**

[*J. Mol. Liq.* **77**, 105 (1998)]

We describe a molecular theory for solvent dynamics which provides a method for calculating the dynamic structure factors of molecular fluids. The theory is based on the generalized Langevin equation and on the interaction-site model for molecular liquids. A simple approximation scheme for the memory function is developed by generalizing the conventional one which has been successfully applied to monatomic liquids. The theory is applied to the calculation of longitudinal current spectra of a diatomic dipolar liquid, and collective excitations in this solvent are studied. The paper clarifies how these excitations originate from the translational and rotational motions of molecules.

I-S-4 Effect of Molecular Symmetry on Electrical Potential Fluctuations of Solvent Around Solute in Polar Liquid

Song-Ho CHONG *(Kyoto Univ.)* **and Fumio HIRATA**

[*Chem. Phys. Lett.* **293**, 119 (1998)]

We discuss how the asymmetry structure in solvent and solute affects the free energy profile governing electrical potential fluctuations of solvent around solute and characteristic parameters relevant to electron transfer reactions in solutions using the recently developed method based on the integral equation theory called ex-RISM (the extended reference interaction-site method). Since ex-RISM is inherently a nonlinear theory, we can shed some light on the possible nonlinear effects in electrical potential fluctuations.

I-S-5 Mode-Coupling Theory for Molecular Liquids Based on the Interaction-Site Model

Song-Ho CHONG *(Kyoto Univ.)* **and Fumio HIRATA**

We develop a microscopic theory for dynamics of molecular liquids which is based on the interaction-site model for polyatomic fluids, the projection-operator formalism of Zwanzig and Mori, and the mode-coupling theory. Closed nonlinear equations are derived for a self-consistent treatment of density propagation in a classical polyatomic liquid, which enable one to calculate dynamic structure factors provided the equilibrium structure functions of liquids are known.

I-S-6 Time-Correlation Functions in Molecular Liquids Studied by the Mode-Coupling Theory Based on the Interaction-Site Model

Song-Ho CHONG *(Kyoto Univ.)* **and Fumio**

HIRATA

Numerical results for longitudinal current spectra, velocity autocorrelation functions and diffusion coefficients of a model diatomic liquid are presented using the recently developed theory for dynamics of classical polyatomic fluids. The theory is based on the interaction-site model for molecular liquids, the projection-operator formalism of Zwanzig and Mori, and the mode-coupling theory. The effect of the inclusion of the slow contribution in memory kernels, represented by the mode-coupling expression, on the aforementioned dynamical quantities is discussed. The molecular dynamics simulation of the same system is also performed to test the accuracy of our theory, and the theoretical results are found to be in fair agreement with those obtained from the simulation.

I-T Liquid-Solid Interface

Due to recent progress in experimental techniques in the in situ measurements, the electro-chemistry seems making a new epoch in understanding the chemical processes at electorode-solution interfaces. For examples, the scanning tunneling microscope (STM) applied to the interface has been revealing detailed atomic structure of the interface.[1)] The surface enhanced infrared absorption spectroscopy has provided detailed picture regarding the orientation of water molecules at the surface.[2)] The information in atomic level have been combined with the traditional techniques in the electrochemistry such as the cyclic voltammogram to provide more complete picture of electrode-solution interfaces. Obviously, the traditional descriptions using electric double layer models, which are based on the continuum models of solvent, mismatch the level of detailness attained by the recent experimental techniques.

Theoretical understanding of the interface has also made great progress in the last two decades, especially, in terms of solvent configuration near electrode surfaces.[3)] The progress has been mainly driven by two theoretical methods in the statistical mechanics of liquids: the molecular simulation and the integral equation methods. The two methods have reached consistent molecular pictures regarding reorganization of the water structure in the vicinity of the flat electrode surface. Latest topics in those approaches concern the electronic structure of electrode. The methods features a self-consistent treatment of the liquid state and the electronic structure of the metal surface. Significance of such treatments will become more and more clear as the methods are extended to chemical reactions at the interface, which are primary motivation for the electrochemistry.

Although the integral equation methods have great advantage in the overall description of the electrode-solution interface both at phenomenological and molecular levels, the models which have been employed for the metal surface seems oversimplified considering the resolution attained by latest development in the experimental techniques stated above. Here, we propose a new approach for the electrode-solution interface based on the reference interaction site method (RISM) of liquids, which can handle both the structured metal surface and water in atomic level.

References

1)K. Itaya and E. Tomita, *J. Surf. Sci.* **201**, L507 (1988).
2)K. Ataka, T. Yotsuyanagi and M. Osawa, *J. Phys. Chem.* **100**, 10664 (1996).
3)L. Blum, *Adv. Chem. Phys.* **78**, 171 (1990).

I-T-1 Theoretical Study for Water Structure at Highly Ordered Surface: Effect of Surface Structure

Ryo AKIYAMA and Fumio HIRATA

[*J. Chem. Phys.* **108**, 4904 (1998)]

Liquid structures of water at electrode-solution interface were investigated by RISM integral equation, putting special stress on the effect of surface structure. Two types of surface geometry were examined: Au(111)-like geometries which is characterized by the threefold hollow sites in which a water molecule can fit, and flat-like surface geometry. The orientation of water molecules in the vicinity of surface depends strongly on the surface structure. Especially, the difference is significant in the case of negatively charged surface. At Au (111)-like surface with negative charges, angles between the surface normal and both of the two O-H vectors are around 108 degree. The result agrees with that proposed experimentally by surface enhanced infrared absorption spectroscopy (SEIRAS) applied to Au(111) surface in aqueous solution of perchloric acid. On the other hand, in the case of flat-like surface the angle between the surface normal and one of the O-H vector is 180 degree, H-atom is available for hydrogen-bonding with bulk water. In the present study, the hydrogen end of water becomes more oriented toward the solution phase above the potential of zero charge (pzc). Those features qualita- tively agree with results proposed by the SEIRAS experiment. However, the orientation of water molecules undergoes significant changes due to the coadsorption of perchlorate ion at a surface with very positive potential.

I-T-2 Solution of the Three-Dimensional RISM/HNC Equations for SPC Water by the Modified Method of Direct Inversion in the Iterative Subspace

Andriy F. KOVALENKO, Seiichiro TEN-NO and

Fumio HIRATA

[*J. Comput. Chem.* submitted (1998)]

We proposed a modified procedure of the direct inversion in the iterative subspace (DIIS) method to accelerate convergence in the integral equation theory of liquids. We update the DIIS basis vectors at each iterative step by using the approximate residual obtained in the DIIS extrapolation. The procedure is tested by solving the three-dimensional (3D) generalization of the reference interaction site model (RISM) equation together with the hypernetted chain (HNC) closure as well as their one-dimensional version. We calculated the 3D site distribution of water, represented by the simple point charge (SPC) model, around one water molecule considered as a central particle.

I-T-3 Three-Dimensional Density Profiles of Water in Contact with a Solute of Arbitrary Shape: A RISM Approach

Andriy F. KOVALENKO and Fumio HIRATA

[*Chem. Phys. Lett.* **290**, 237 (1998)]

We obtain three-dimensional density profiles of interaction sites of a molecular liquid in an external field by generalizing the solute-solvent equation of the Reference Interaction Site Model (RISM) at infinite dilution. The equation complemented with the analogue of the hypernetted chain (HNC) closure is solved on a three-dimensional grid by employing the dynamic relaxation technique. The distribution of water, represented by the Simple Point Charge (SPC) model, around the central water molecule is obtained and discussed. The water density profiles near a (111) FCC crystalline surface are studied. The preferential location and orientation of adsorbed water molecules are discussed.

I-T-4 Extended States of a Shallow Donor Located near a Semiconductor-Insulator Interface

Andriy F. KOVALENKO

[*Intern. J. Quant. Chem.* in press (1998)]

Scattering of a conduction electron by a charged shallow donor located near a semiconductor-insulator interface in the semiconductor or by a charged center embedded in the insulator is considered within the model of a hydrogen-like atom in a semi-infinite space. The interface influence is allowed for by spatial confinement of the electron envelope wavefunction. The impurity electrostatic image at the interface is taken into account. The problem is separable in prolate spheroidal coordinates and thus is solvable exactly. A rapidly convergent expansion is proposed for the angular eigenfunctions. The radial eigenfunctions are calculated directly by numerical integration of the radial boundary value problem. Expansions of the scattering wavefunction and the scattering amplitude in terms of the eigenfunctions of the problem are obtained. Using the extended and localized state wavefunctions, the photoionization cross-section of a shallow donor near a semiconductor-insulator interface is calculated. It is presented as a superposition of the oscillator strengths of transitions to the partial extended eigenstates that constitute the scattering wavefunction. Near the interface, the cross-section is enhanced significantly and redistributed over the direction of photoionized electron escape. The photoionization threshold follows the localized state energy varying with the donor — interface distance.

I-T-5 The Structure and Adsorption of the Four Bonding Sites Model for Associating Fluids in Disordered Porous Media from Replica Ornstein-Zernike Integral Equation Theory

Andriy F. KOVALENKO and Orest PIZIO
(National Autonomous Univ. of Mexico)

[*J. Chem. Phys.* **108**, 8651 (1998)]

We have studied a model for an associating fluid in which each of the particles have four sites available for bonding, thus a network of bonds can be formed. This fluid intrinsically possesses liquid-gas transition in the absence of any long-range nonassociative interactions. The model is considered in a disordered porous media that corresponds to an equilibrium configuration of hard spheres. The model is investigated by means of the associative extension of Replica Ornstein-Zernike (ROZ) equations, with the Percus-Yevick (PY) and hypernetted chain (HNC) approximations. Those are supplemented by the ideal network approximation. We have obtained the pair distribution functions and the structure factors of the model. We have obtained the adsorption isotherms using a system of hard spheres adsorbed in a hard sphere matrix as a reference. The associative contribution is obtained similarly to Wertheim's thermodynamic perturbation theory, however, with monomer fraction that follows from the ROZ equations. The liquid-vapor coexistence curve has been obtained complementing the adsorption isotherms by Maxwell construction. We have obtained that with increasing matrix density the critical temperature, if scaled w.r.t.the bulk value, decreases for few percent. The critical density is more sensitive to the density of adsorbent, it substantially decreases with increasing matrix density. We discuss the prepeak on the structure factor at small wave vectors in the adsorbed network-forming fluid at fixed chemical potential dependent on matrix density.

I-U Dimensional Crossovers in Doped Ladder Systems, Organic Conductors and Cuprate Superconductors

Electronic states in pure one dimension and those in two or three dimensions are very different from each other. In many organic conductors and copper oxides, dimensionality is controlled by applying external or chemical pressure. The induced dimensional crossovers are classified by what kind of transverse coherence is restored by increasing dimensionality, i.e., one-particle coherence or two-particle coherence. Which coherence is restored depends on the asymptotic property of the corresponding one-dimensional system. For example, the Tomonaga-Luttinger liquid is known to be unstable against interchain hopping since the transverse one-particle coherence is easily restored. However, in some other one-dimensional phases, the transverse one-particle process is strongly suppressed by electron correlation, and then the transverse two-particle coherence is relatively easily restored. One example is the doped ladder system, $Sr_{14-x}Ca_xCu_{24}O_{41}$, where the spin gap suppresses the transverse one-particle coherence and the two-particle crossover is then accompanied by the superconducting transition. Another example is the quasi-one-dimensional organic conductor, $(TMTTF)_2X$, where the charge gap suppresses the transverse one-particle coherence and the two-particle crossover is then accompanied by the antiferromagnetic transition. More interestingly, the high-T_c copper oxide, $Bi_2Sr_2CaCu_2O_8$, has a partially flat Fermi surface (thus dimensionality depends on the momentum), which anisotropically suppresses one-particle coherence and induces a pseudogap.

I-U-1 Spin Gap and Superconductivity in Weakly Coupled Ladders: Interladder One-Particle vs. Two-Particle Crossover

Jun-ichiro KISHINE and Kenji YONEMITSU

[*J. Phys. Soc. Jpn.* **66**, 3725 (1997)]

Effects of the interladder one-particle hopping, $t_\perp$, on the low-energy asymptotics of a weakly coupled Hubbard ladder system have been studied, based on the perturbative renormalization-group approach. We found that for finite intraladder Hubbard repulsion, U, there exists a crossover value of the interladder one-particle hopping, $t_{\perp c}$. For $0 < t_\perp < t_{\perp c}$, the spin gap metal (SGM) phase of the isolated ladder transits at a finite transition temperature, T_c, to the d-wave superconductor (SCd) phase via a two-particle crossover. In the temperature region, $T < T_c$, interladder *coherent Josephson tunneling* of the Cooper pairs occurs, while the interladder coherent one-particle process is strongly suppressed. For $t_{\perp c} < t_\perp$, around a crossover temperature, T_{cross}, the system crosses over to the two-dimensional (2D) phase via a one-particle crossover. In the temperature region, $T < T_{cross}$, the interladder coherent band motion occurs.

I-U-2 One-Particle vs. Two-Particle Crossover in Weakly Coupled Hubbard Chains and Ladders: Perturbative Renormalization Group Approach

Jun-ichiro KISHINE and Kenji YONEMITSU

[*Int. J. Mod. Phys. B* in press]

Physical nature of dimensional crossovers in weakly coupled Hubbard chains and ladders has been discussed within the framework of the perturbative renormalization-group approach. The difference between these two cases originates from different universality classes which the corresponding isolated systems belong to.

I-U-3 Dimensional Crossovers in the Doped Ladder System: Spin Gap, Superconductivity and Interladder Coherent Band Motion

Jun-ichiro KISHINE and Kenji YONEMITSU

[*J. Phys. Soc. Jpn.* **67**, 1714 (1998)]

Based on the perturbative renormalization group (PRG) approach, we have studied dimensional crossovers in Hubbard ladders coupled via weak interladder one-particle hopping, $t_\perp$. We found that the one-particle crossover is strongly suppressed through growth of the intraladder scattering processes which lead the isolated Hubbard ladder system toward the spin gap metal (SGM) phase. Consequently when $t_\perp$ sets in, there exists, for any finite intraladder Hubbard repulsion, $U > 0$, the region where the two-particle crossover dominates the one-particle crossover and consequently the d-wave superconducting transition, which is regarded as a bipolaron condensation, occurs. By solving the scaling equations for the interladder one-particle and two-particle hopping amplitudes, we give phase diagrams of the system with respect to U, $t_{\perp 0}$ (initial value of $t_\perp$) and the temperature, T. We compared the above dimensional crossovers with those in a weakly coupled chain system, clarifying the difference between them.

I-U-4 Antiferromagnetic Phase Transition and Crossover to Fermi Liquid Phase in a Weakly Coupled Half-Filled Chain System

Jun-ichiro KISHINE and Kenji YONEMITSU

[*J. Phys. Soc. Jpn.* **67**, 2590 (1998)]

Effects of the intrachain electron-electron umklapp process and the interchain one-particle hopping, $t_\perp$, in a weakly coupled half-filled chain system have been studied, based on the perturbative renormalization-group approach. By solving the scaling equations, we found that the intrachain umklapp process strongly suppresses an interchain one-particle process and causes a finite critical value for $t_\perp$, $t_{\perp c}$. For $t_\perp < t_{\perp c}$, as the temperature decreases, the system undergoes a phase

transition into an antiferromagnetic long-range-ordered phase at a transition temperature T_N which increases with the increasing $t_\perp$. On the other hand, for $t_\perp > t_{\perp c}$, the system undergoes a crossover to the Fermi liquid phase where the interchain coherent propagation of quasi-particles occurs.

I-U-5 Effects of Dimerization and Interchain One-Particle Hopping in a Weakly Coupled Dimerized Chain System at Quarter Filling

Jun-ichiro KISHINE and Kenji YONEMITSU

[*Synth. Met.* submitted]

Effects of the intrachain dimerization and the interchain one-particle hopping, t_b, in a quasi-one-dimensional dimerized chain system at quarter filling have been studied, based on the perturbative renormalization group (PRG) approach. Based on the results, we discuss difference in the low-energy properties between TMTTF and TMTSF compounds.

I-U-6 Geometry, Universality and Dimensional Crossovers in Weakly Coupled One-Dimensional Conductors

Jun-ichiro KISHINE and Kenji YONEMITSU

[*Synth. Met.* submitted]

We discuss dimensional crossover phenomena in weakly coupled one-dimensional conductors, in terms of the universality classes of the corresponding isolated one-dimensional systems.

I-U-7 Renormalization-Group Study of Competition between Density Waves and Pairing in Quasi-One-Dimensional Electron Systems

Kenji YONEMITSU

[*Synth. Met.* submitted]

We study crossover from the doped two-leg ladder system to a quasi-one-dimensional system by an inter-ladder one-particle process and stability of the superconductor phase, using a renormalization-group method and differentiating the contributions from the particle-particle channel and those from the particle-hole channel. Effects of electron-$2k_F$ phonon and electron-$4k_F$ phonon couplings are also investigated.

I-U-8 Anisotropic Suppression of Quasiparticle Weight in Two-Dimensional Electron System with Partially Flat Fermi Surface: Two-Loop Renormalization-Group Analysis

Jun-ichiro KISHINE and Kenji YONEMITSU

[*Phys. Rev. B* submitted]

Two-loop renormalization-group analysis for a two-dimensional electron system with a partially flat Fermi surface has been carried out. We found that, irrespective of pairing mechanism, the quasiparticle weight is anisotropically suppressed due to logarithmically singular processes in the flat regions of the Fermi surface. When the energy scale decreases, the quasiparticle weight is the most strongly suppressed around the center of the flat region, which qualitatively agrees with the anisotropic pseudogap behavior suggested through the angle-resolved photoemission spectroscopy experiments for underdoped $Bi_2Sr_2CaCu_2O_8$.

I-V Magnetic Properties of Metal-Assembled Complexes with Two Different-Dimensional Bands

Antiferromagnetism and superconductivity are realized in strongly correlated, organic materials. In κ-(BEDT-TTF)$_2X$, the two-dimensional quarter-filled HOMO band is effectively regarded as a half-filled band due to strong dimerization. Strong dimerization is realized in the metal-assembled complex, $Me_4Z[Pd(dmit)_2]_2$, also. In the latter, however, there are a rather one-dimensional LUMO band and a two-dimensional HOMO band, both of which are largely split due to the dimerization. So far, we do not know which band is responsible to the pressure-induced metal and superconductor phases. Meanwhile, the phase diagram is richer than that of κ-(BEDT-TTF)$_2X$ in that applied pressure induces a metal or superconductor phase and then an insulator phase again. Whether the origins of the two insulator phases are the same or not is currently of particular interest. We study this problem using a mean-field theory and a strong-coupling expansion as a first step, showing the two phases may correspond to two possible magnetic phases. We have found the exchange interactions are not simple as one usually expects. For example, some exchange interaction is ferromagnetic due to the mechanism which causes flat-band ferromagnetism. Whether the exchange interaction is ferromagnetic or antiferromagnetic depends on the symmetry of the molecular orbitals.

I-V-1 On the Effects of On-Site Coulomb Interaction in Strongly Dimerized Two Band Systems

Hiori KINO *(JRCAT-ATP)*, **Tsuyoshi MIYAZAKI** *(NRIM)*, **Michiyasu MORI and Kenji YONEMITSU**

[*Proceedings of the JRCAT Conference*]

We consider the strongly dimerized two-band organic solids, $Me_4Z[M(dmit)_2]_2$ (dmit=2-thioxo-1,3-dithiole-4,5-dithiolate), where Z = N, P, As, Sb and M = Ni, Pd (β polytype in the $Pd(dmit)_2$ salts). A phase diagram is shown in the plane of the on-site Coulomb

interaction and the level splitting between the HOMO and the LUMO of the $M(dmit)_2$ molecule, based on the results of the Hartree-Fock (HF) approximation. The nature of the phase transition is discussed. The results of the exact diagonalization for small clusters is also presented to check the validity of the HF approximation.

I-V-2 Possible Magnetic Phases in Two-Band Systems with Different Dimensionality

Michiyasu MORI, Kenji YONEMITSU and Hiori KINO *(JRCAT-ATP)*

[*Synth. Met.* submitted]

The ground states of the molecular conductors $Me_4Z[M(dmit)_2]_2$, which have strong dimerization and two bands with different dimensionality, have been studied based on the Hartree-Fock approximation. The results indicate that two different magnetic orders appear depending on both the energy difference between the two bands and the strength of the Coulomb interaction. To clarify the origin of the magnetic orders, exchange interactions between dimers have been calculated within the second-order perturbation theory with respect to the inter-dimer transfer integrals. We have found that the different magnetic orders are due to the different symmetry of the molecular orbitals.

I-V-3 Effective Exchange Interactions in Dimerized Systems

Michiyasu MORI and Kenji YONEMITSU

In our previous work, it has been clarified that the ground states of $Pd(dmit)_2$ salts have two different antiferromagnetic (AF) orders depending on both the energy difference between molecular orbitals and the strength of the Coulomb interaction. These orders have uniform charge density, i.e., 0.5 electron per site, and it can be considered as AF orders between dimers. Thus, we have calculated the exchange interactions between dimers within the second-order perturbation theory with respect to the inter-dimer transfer integrals. The results indicate that one magnetic order is dominated by HOMO (highest occupied molecular orbital) and the other originates from LUMO (lowest unoccupied molecular orbital). The molecular orbitals HOMO and LUMO have different symmetry and result in the different magnetic orders. In the case of LUMO, interestingly, the ferromagnetic coupling is also possible in a particular direction. The origin of such ferromagnetic exchange interaction is equivalent to the mechanism of flat-band ferromagnetism. Our calculation is also applicable to BEDT-TTF salts and other dimerized systems.

I-V-4 From Possible Magnetic Orders to Quantum Disorder

Michiyasu MORI and Kenji YONEMITSU

The anion radical salt $(Et_xMe_{4-x}Z)[Pd(dmit)_2]_2$ exhibits a metal (superconductor)-insulator transition at low temperature and under pressure. For such phase transitions, cation effects play significant roles. The system with cation Me_4P is always an insulator even under pressure, while the system with cation Et_2Me_2P becomes a superconductor under pressure, for example. At ambient pressure, however, the system with any cation behaves as an insulator. Thus, in this present paper, the cation effects in the insulator phases have been investigated. The magnetic properties of $Pd(dmit)_2$ salts can be described by a dimer spin model, in which the dimer is a site for the localized spins. The exchange interactions between dimers are calculated in our previous papers. We have found that the cation effect is considered as the frustration for the spin system on the triangular lattice. Then, we have calculated the stability of antiferromagnetic (AF) orders based on the spin wave approximation for the frustrated spin systems. The results indicate that in the case of Me_4P the AF order is stable, while in the case of Et_2Me_2P the AF order is unstable and goes into a quantum disordered phase because of the frustration. These results are consistent with the experiment of the magnetic susceptibility at ambient pressure.

I-W Metal-Insulator and Superconducting Transitions in Strongly Correlated Electron Systems Coupled with Localized Spins or Phonons

Electronic states are influenced by the presence of local degrees of freedom such as localized spins or phonons. Especially, when the conduction electrons are confined in low dimensions and strongly correlated, the problems are highly nontrivial. Here, we study the effect of exchange coupling with localized spins in a one-dimensional quarter-filled system (Heisenberg-Kondo lattice) and the effect of electron-phonon coupling in a two-dimensional doped antiferromagnet (Holstein-Hubbard polaron system). The former system corresponds to the one-dimensional π-d electron system, $CoPc(AsF_6)_{0.5}$, while the latter system is compared with the high-T_c copper oxides. In the former system, the exchange coupling alone does not produce an insulator phase, but long-range repulsion can induce an insulator phase with the help of the exchange coupling at least when the localized spins are antiferromagnetically ordered. In the latter system, the electron-phonon coupling produces self-trapped polarons which attract each other and form d-wave pairs. Berry phases are convenient tools to explain the symmetry, quantum numbers and statistics of polarons and polaron pairs. The properties of these polarons are very different from those of ordinary polarons and may explain the strange isotope effect observed in the high-T_c copper oxides.

I-W-1 Conductivity and Magnetic Properties of One-Dimensional Heisenberg-Kondo Lattice

Takuhiro OGAWA and Kenji YONEMITSU

[*Synth. Met.* submitted]

Using the one-dimensional quarter-filled Heisenberg-Kondo lattice model for a π-*d* electron system, $CoPc(AsF_6)_{0.5}$, we study the effects of long-range Coulomb interaction among π electrons on the conductivity. The density-matrix renormalization-group method is employed. As a first step, we regard the localized spins of *d* electrons as classical ones, and then, as quantum $S = 1/2$ spins, which are coupled antiferromagnetically with each other. In the former case, *d* electrons produce a static staggered magnetic field for π electrons. It is pointed out that the next-nearest-neighbor repulsion among π electrons and the magnetic coupling between π and *d* electrons are essential to open a charge gap.

I-W-2 Superconductivity and Magnetism in Quasi-One-Dimensional Two-Band Systems

Kenji YONEMITSU, Jun-ichiro KISHINE and Takuhiro OGAWA

[*Rev. High Pressure Sci. Technol.* **7**, 490 (1998)]

We study crossovers from one to quasi-one dimensions in doped two-leg ladder systems, using a renormalization group method. When quasi-one dimensionality is regarded as controlled by incomplete interference between the Cooper and Peierls channels, we obtain spin-density wave, *d*-wave superconductor, and metal phases with decreasing dominance of the Peierls channel. When transverse single-particle hopping is treated perturbationally, we obtain a one-particle crossover from incoherent to coherent transverse motion for weak interaction and a two-particle crossover from short- to long-range ordering of a *d*-wave superconductor for strong interaction. We also study a magnetic property in a doped Heisenberg-Kondo chain, using the exact diagonalization method. A fully saturated ferromagnetism in the ferromagnetic Kondo chain is destroyed by rather weak antiferromagnetic Heisenberg coupling between localized $S = 1/2$ spins.

I-W-3 Berry Phases and Pairing Symmetry in Holstein-Hubbard Polaron Systems

Kenji YONEMITSU, Jian ZHONG *(Univ. Georgia)* **and Heinz-Bernd SCHÜTTLER** *(Univ. Georgia)*

[*Phys. Rev. B* in press]

We study the tunneling dynamics of dopant-induced hole polarons which are self-localized by electron-phonon coupling in a two-dimensional antiferromagnet. Our treatment is based on a path integral formulation of the adiabatic (Born-Oppenheimer) approximation, combined with many-body tight-binding, instanton, constrained lattice dynamics, and many-body exact diagonalization techniques. The applicability and limitations of the adiabatic approximation in polaron tunneling problems are discussed in detail and adiabatic results are compared to exact numerical results for a two-site polaron problem. Our results are mainly based on the Holstein-*tJ* and, for comparison, on the Holstein-Hubbard model. We also study the effects of 2nd neighbor hopping and long-range electron-electron Coulomb repulsion. The polaron tunneling dynamics is mapped onto an effective low-energy Hamiltonian which takes the form of a fermion tight-binding model with occupancy dependent, predominantly 2nd and 3rd neighbor tunneling matrix elements, excluded double occupancy, and an effective intersite charge interactions. Antiferromagnetic spin correlations in the original many-electron Hamiltonian are reflected by an attractive contribution to the 1st neighbor charge interaction and by Berry phase factors which determine the signs of effective polaron tunneling matrix elements. In the two-polaron case, these phase factors lead to polaron pair wave functions of either d_{x2-y2}-wave symmetry or *p*-wave symmetry with zero and nonzero total pair momentum, respectively. Implications for the doping dependent isotope effect, pseudo-gap and T_c of a superconducting polaron pair condensate are discussed and compared to observed properties of the cuprate high-T_c materials.

I-X Coexistence of or Competition between Different Density Waves in One-Dimensional Quarter-Filled Organic Conductors

Quasi-one-dimensional organic conductors show a variety of phases due to the instability of a metallic state described by the Fermi liquid theory. Many phases are understood within mean-field theories for tight-binding models with short-range repulsion. When coexistence of purely electronic spin-density and charge-density waves was suggested in $(TMTSF)_2PF_6$ by X-ray experiments two years ago for the first time, many scientists regarded this phenomenon as mysterious since one usually expects only one type of long-range order except $4k_F$ charge ordering. We show that this is due to a cooperative effect of long-range repulsion (especially, next-nearest-neighbor repulsion) which are usually neglected and dimerization which lowers the symmetry of electronic states. Such importance of long-range repulsion has been pointed out for the charge ordering in a quarter-filled π-electron system, $(DI\text{-}DCNQI)_2M$ (M = Li, Ag), and for the insulator phase in a quarter-filled π-*d* electron system, $CoPc(AsF_6)_{0.5}$. For $(DCNQI)_2M$ (M = Li, Ag), we apply the full configuration interaction method to an effective

Hamiltonian whose parameters are derived from the ab initio molecular orbital theory. Antiferromagnetic correlation and $4k_F$ charge ordering in these systems are reproduced.

I-X-1 Coexistence of SDW and Purely-Electronic CDW in Quarter-Filled Organic Conductors

Nobuko KOBAYASHI *(Univ. Tokyo)*, **Masao OGATA** *(Univ. Tokyo and IMS)* **and Kenji YONEMITSU**

[*J. Phys. Soc. Jpn.* **67**, 1098 (1998)]

We have performed a mean field calculation in order to determine the ground state of a modified Hubbard model of a quarter-filled one-dimensional chain. It is found that the coexistence of $2k_F$ spin density wave (SDW) and purely-electronic $2k_F$ charge density wave (CDW) is realized due to the effect of next-nearest-neighbor Coulomb repulsion. Phase diagrams are obtained as the values of nearest- and next-nearest-neighbor Coulomb interaction energies are varied. Competition between the two coexistent states with $2k_F$ CDW and with $4k_F$ CDW is revealed, which gives a first order transition. Our result supports the X-ray result confirming the presence of a coexisting phase of purely-electronic $2k_F$ CDW and $2k_F$ SDW in $(TMTSF)_2PF_6$, a quarter-filled one-dimensional chain in terms of holes.

I-X-2 Coexistence of SDW and Purely-Electronic CDW in Quarter-Filled Organic Conductors at Finite Temperatures

Masao OGATA *(Univ. Tokyo and IMS)*, **Nobuko KOBAYASHI** *(Univ. Tokyo)* **and Kenji YONEMITSU**

[*Synth. Met.* submitted]

Recently an X-ray experiment reported a coexisting phase of purely-electronic $2k_F$ charge density wave (CDW) and the conventional $2k_F$ spin density wave (SDW) in $(TMTSF)_2PF_6$. In order to understand such coexistence, we have performed a mean-field calculation for a Hubbard-type model of a quarter-filled one-dimensional chain. It is found that the coexistence of $2k_F$ SDW and *purely-electronic* $2k_F$ CDW is realized due to the effect of next-nearest-neighbor Coulomb repulsion. Phase diagrams are obtained as a function of nearest- and next-nearest-neighbor Coulomb interaction energies. Competition between the two coexistent states with $2k_F$ CDW and with $4k_F$ CDW is revealed, which gives a first order transition. It turns out that the internal degrees of freedom inside a dimer (consisting of two TMTSF molecules) play an important role. Our result supports the X-ray result of a coexisting phase in $(TMTSF)_2PF_6$. When the coexistent state with $2k_F$ CDW is realized, the critical temperature for $2k_F$ SDW is slightly higher than that for $2k_F$ CDW. These two transition temperatures are close enough to explain the experimental result.

I-X-3 Exact Diagonalization Study of $(DCNQI)_2M$ (M = Li, Ag) Clusters Based on Ab Initio Molecular Orbital Parameters

Yutaka IMAMURA *(Grad. Univ. Adv. Stud.)*, **Seiichiro TEN-NO, Kenji YONEMITSU and Yoshitaka TANIMURA**

[*Chem. Phys. Lett.* submitted]

We study electronic states of the $(DCNQI)_2M$ (M = Li and Ag) salts based on the full configuration interaction (FCI) method using effective Hamiltonians derived from the ab initio molecular orbital theory. FCI results of the DCNQI tetramer and octamer models indicate that the ground state has the antiferromagnetic and charge ordering correlations. It corresponds to the $2k_F$ spin density wave and $4k_F$ charge density wave states (SDW and CDW). In the octamer model, it is also found that some low-lying excited states have similar spin-flipped CDW correlations and the antiferromagnetic correlation is weakened.

I-Y Electron Correlation and New Photoinduced Phenomenon in Polymers

Electron correlation is important in conducting polymers also, in order to understand the relation between electron correlation and the strength of dimerization, and to understand the symmetry of the lowest excited state. The latter is crucial to luminescence and its applications to electronic devices. First, we study the effect of the off-diagonal part of the electron-electron interaction on the ground state and on the coherence length, going beyond a mean-field theory. Next, we point out a possibility of negative polarizability in photoexcited polymers of nondegenerate ground states which have biexcitons. Here, the proximity of the mid-gap states is crucial. Note that negative polarizability is impossible in a gas or condensed matter in an equilibrium state, but it is not prohibited in principle in a molecule in an excited state.

I-Y-1 Effect of Electron Correlation on Competition between BOW and SDW in Polymer

Xin SUN *(Fudan Univ. and IMS)*, **Xiaohua XU** *(Fudan Univ.)*, **Kun HU** *(Fudan Univ.)* **and Kenji YONEMITSU**

[*Phys. Lett. A* **239**, 191 (1998)]

Because π electrons in polymers possess a broad band, the off-diagonal part of the electron interaction, which is omitted in the extended Hubbard model, plays an essential role in the competition between bond-order waves (BOWs) and spin-density waves (SDWs). Our study, which goes beyond the extended Hubbard model and the Hartree-Fock approximation, shows that this competition depends on the range of the electron interaction; a short interaction range, where the off-diagonal part is more effective, is in favor of SDW. It is also shown that the correlation effect works against the exchange effect in building up the SDW.

I-Y-2 Off-Diagonal Interactions and Spin-Density Waves in Polymers

Xiaohua XU *(Fudan Univ.)***, Rongtang FU** *(Fudan Univ.)***, Kun HU** *(Fudan Univ.)* **Xin SUN** *(Fudan Univ. and IMS)* **and Kenji YONEMITSU**

[*Phys. Rev. B* in press]

In order to clarify the effects of electron interaction on the competition between SDW (spin-density wave) and BOW (bond-order wave), the existing theories are improved in two aspects: (1) The electron interaction in polymers, which possess a broad band, is described by screened Coulomb potential rather than the extended Hubbard model, which is a good approximation only for narrow-band systems. (2) A spin-dependent CBF (correlated-basis-function) method is developed to calculate the correlation effect, which goes beyond the HF (Hartree-Fock) approximation. Our study shows that the off-diagonal interaction substantially influences the competition so that shortening of the interaction range greatly enhances the SDW; meanwhile the correlation effect promotes the BOW against the SDW.

I-Y-3 A Correlated-Basis-Function Study of SDW in Polymers

Xiaohua XU *(Fudan Univ.)***, Rongtang FU** *(Fudan Univ.)***, Xin SUN** *(Fudan Univ. and IMS)* **and Kenji YONEMITSU**

[*Synth. Met.* submitted]

We study SDW in polymers, using screened Coulomb potential to describe full electron interaction in the broad-band systems and developing a spin-dependent correlated-basis-function method to handle the correlation effect. The SDW is shown to be sensitively enhanced with shortening interaction range and suppressed by the correlation effect.

I-Y-4 Making a Molecule with Negative Polarizability

Xin SUN *(Fudan Univ. and IMS)***, Rouli FU** *(Nat'l Lab. of Infrared Phys.)***, Kenji YONEMITSU and Keiichiro NASU** *(IMSS)*

Many novel phenomena have been found in excited states by ultrafast technology. One more is proposed here. The molecular magnetic susceptibility can be positive or negative. But, so far, the electrical susceptibility α of all observed molecules is always positive. Can a molecule with negative α exist? Our study shows it can be realized by photoexcitation, one candidate is the polymer with a bipolaron. It is a new photoinduced phenomenon — photoinduced polarization inversion, an ultrafast process with relaxation time of 2×10^{-13} second. The molecule with negative α possesses anomalous charge transfer, whose direction is opposite to that expected by the Coulomb's Law.

I-Y-5 Polarization and Dissociation of Exciton in Luminescent Polymers

Xin SUN *(Fudan Univ. and IMS)***, Rouli FU** *(Nat'l Lab. of Infrared Phys.)***, Lei LI** *(Fudan Univ.)* **and Kenji YONEMITSU**

[*Synth. Met.* submitted]

It is shown in this paper that the exciton in polymers possesses very large polarizability, and when the electric field is strong enough, the exciton in luminescent polymers is dissociated into a pair of charged polarons. This dissociation can quantitatively interpret the experiment that the luminescence of polymer is heavily quenched by strong electric field.

RESEARCH ACTIVITIES II
Department of Molecular Structure

II-A Laboratory and Astronomical Spectroscopy of Transient Molecules

Vast, cold, and low-density space environment is a unique laboratory, whose physical and chemical conditions are rarely attained in the laboratory on Earth. The unique space laboratory is favorable to the existence of transient molecules such as molecular ions, free radicals, and unstable molecules, most of which are very exotic and nonterrestrial. These exotic transient molecules are generally difficult and challenging problems for laboratory spectroscopy. Laboratory spectroscopy may be enriched by astronomical studies on non-terrestrial transient species which represent new developments in high-resolution molecular spectroscopy. On the other hand, detailed knowledge about new transient molecules obtained by laboratory spectroscopy is essential to a deeper understanding of physical and chemical processes in space. We developed a high-sensitivity submillimeter-wave and far-infrared spectrometers suitable for high-resolution spectroscopy of transient molecules of astronomical interest. We expect that our laboratory spectroscopy may accelerate the mutually beneficial aspect between laboratory spectroscopy, and astrochemistry and astrophysics.

II-A-1 Experimental Determination of the Ground-State Inversion Splitting in D_3O^+ by Microwave Spectroscopy

Mitsunori ARAKI *(Grad. Univ. Adv. Stud.)*, **Hiroyuki OZEKI and Shuji SAITO**

[*J. Chem. Phys.* **109**, 5707 (1998)]

The hydronium ion, H_3O^+, is one of the most fundamental species in aqueous acid-base chemistry and also in gas-phase interstellar chemistry. The ion is isoelectronic to ammonia showing an "umbrella inversion motion" and has been extensively studied spectroscopically. Liu and Oka[1] measured the crucial inversion separation in the $v_2 = 1$ state, $1^- \text{-} 1^+$, and derived the ground state splitting.

In the present study, inversion-rotation transitions of the fully deuterated hydronium ion, D_3O^+, were observed for the first time by microwave spectroscopy (see Figure 1). The ion was generated in a hollow cathode cell by dc-glow discharge of a mixture of D_2O and D_2. Twenty six P- and Q-branch transitions were measured precisely for the lowest pair levels of inversion motion in the frequency region of 220-565 GHz. The ground-state inversion splitting and effective molecular constants for the upper and lower levels were determined by a least-squares fit of the measured line frequencies. The inversion splitting was determined to be 15.3555044(45) cm^{-1}, where the number in parentheses denotes three standarad deviations of the fit. Furthermore, the inversion splitting in the $v_2 = 1$ state was calculated to be 191.3887(30) cm^{-1} from the present value, combined with IR band data by Petek et al.[2] The ground-state and $v_2 = 1$ state inversion splittings of D_3O^+ obtained in the present study are essential to a deep understanding of the inversion potential of H_3O^+.

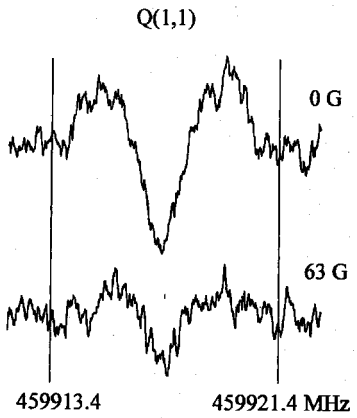

Figure 1. The Q(1,1) transition of D_3O^+. The integration time was 290 s (1600 scans). The upper trace was recoreded with no magnetic field, whereas the lower trace with a field of 63 G.

II-A-2 Microwave Spectroscopic Detection of a New Transient Phosphorus-Bearing Molecule, H_3PO

Imtiaz K. AHMAD, Hiroyuki OZEKI and Shuji SAITO

[*J. Chem. Phys.* **110** (1999) in press]

Experimental studies of simple intermediates in the oxidation of phosphorus are few in number. PH, PH_2, PO, PO_2, HPO, and H_2PO[1] have been studied and characterized mainly using microwave spectroscopy. There still remain several key and interesting transient molecules en route to the final product, H_3PO_4. The transient molecule H_3PO is such an example and has to date eluded gas-phase spectroscopic detection. Many sophisticated quantum chemical calculations so far carried out have concluded that its geometrical isomer H_2POH is more stable than H_3PO with an energy

References

1) D.-J. Liu and T. Oka, *Phys. Rev. Lett.* **54**, 1787 (1985).
2) H. Petek, D. J. Nesbitt, J. C. Owrutsky, C. S. Gudeman, X. Yang, D. O. Harris, C. B. Moore and R. J. Saykally, *J. Chem. Phys.* **92**, 3257 (1990).

difference of 6.5 kcal/mol,[2] though the trifluoride and trichloride of H_3PO are known to be symmetric-top molecules from their spectroscopic studies, and trialkylphosphines are easily changed into the corresponding phoshine oxides by autoxidation.

In the present study H_3PO was detected in the gas phase for the first time by using microwave spectroscopy. The spectral lines of H_3PO, which was generated by dc-glow discharge in a mixture of PH_3, CO_2 and H_2, showed a pattern clearly indicative of a symmetric top molecule. The observed rotational constants (see Table 1) of three isotopic species, H_3PO, D_3PO, and $H_3P^{18}O$, were used to determine the r_0 structure: $r_0(PO)$ = 1.4763 Å, $r_0(PH)$ = 1.4406 Å and HPO = 114.26˚. These strucural parameters deviate significantly from the most recent result predicted by ab initio calculations, and are compared and discussed with those of related molecules.

References

1) T. Hirao. S. Saito, and H. Ozeki, *J. Chem. Phys.* **105**, 3450 (1996).
2) J. A. Boatz, M. W. Schmidt and M. S. Gordon, *J. Phys. Chem.* **91**, 1743 (1987)

Table 1. Molecular Constants of H_3PO, D_3PO, and $H_3P^{18}O$ (MHz)[a,b]

Constant	H_3PO	D_3PO	$H_3P_{18}O$
B_0	17426.6217(20)	14599.8519(21)	16268.6646(22)
D_J	0.015205(13)	0.0104509(95)	0.013332(12)
D_{JK}	0.248390(87)	0.138966(56)	0.218681(75)
H_{JK}	0.0000054(13)	0.00000180(54)	0.00000490(87)

[a] MHz(3σ)
[b] The latest ab initio prediction, J. S. Kwiatkowski and J. Leszczynski, *J. Phys. Chem.* **96**, 6636 (1992): B = 17168.8860 MHz for H_3PO.

II-A-3 Microwave Spectrum of Silicon Trifluoride, SiF_3

Mitsutoshi TANIMOTO *(Shizuoka Univ. and IMS)* **and Shuji SAITO**

Silicon trifluoride SiF_3 is isovalent to CF_3 and one of rarely known symmeytric-top free radicals showing very complex fine and hyperfine structures in their rotational spectrum.[1] Transient SiF_3 and other members of SiF_n have been supposed to be important intermediate species in the silicon etching process. Stable SiF_4 and transient SiF and SiF_2 molecules have extensively been studied with various spectroscopic techniques. On the other hand, silicon trifluoride SiF_3 was investigated with matrix isolation IR spectroscopy as well as matrix and single crystal ESR spectroscopy. Gas phase spectrum was observed only in low resolution with UV-visible emission spectroscopy.

Previously we observed the microwave spectra of silicon trifluoride in the submillimeter region (300 GHz region) with a source modulation spectrometer by glow-discharging in 200 mTorr of Si_2F_6. The SiF_3 species yielded many spectral lines due to the spin-rotation and dipolar hyperfine interactions. In high frequency transitions many overlapping lines hindered the unambiguous K assignment. Subsequent observation of the rotational spectra down to the 105 GHz frequencies still did not allow the definite assignment of the hyperfine structures.

Recently we succeeded in observing the microwave spectrum in the 90 (N = 6-5) and 75 (N = 5-4) GHz regions with a spectrometer of improved sensitivity. In these transitions the K = 1 hyperfine components were found to show distinct splitting and thus the assignment of the K quantum number was made. It is found that the sign of the spin-rotation interaction constant is different from that of the iso(valence)electronic carbon trifluoride radical, CF_3 (Table 1).

Reference

1) Y. Endo, C. Yamada, S. Saito and E. Hirota, *J. Chem. Phys.* **77**, 3376 (1982).

Table 1. Molecular Constants of SiF_3 and CF_3[a]

Constant	SiF_3[b]	CF_3[c]
B_0	7509.0867(28)	10900.9118(52)
D_N	0.010014(28)	0.013882(87)
D_{NK}	-0.017118(30)	-0.02343(17)
D_K	0.0055(fixed)	
H_N (10^6)	0.329(93)	
H_{NK} (10^6)	-0.164(45)	
H_{KN} (10^6)	0.181(85)	
F_N (10^9)	-0.291(88)	
ε_{bb}	36.015(33)	-36.500(42)
ε_{cc}	4.766(108)	3.35(15)
a_F	386.57(118)	408.5(16)
T_{cc}	115.38(22)	320.01(20)
$T_{aa} - T_{bb}$	122.1(95)	40.1(49)

a MHz(2.5σ)
b Present study
c Reference 1.

II-A-4 The Pure Rotational Spectra of TiO($X^3\Delta$) and TiN($X^2\sum^+$)

Kei-ichi NAMIKI *(Grad. Univ. Adv. Stud. and Arizona State Univ.)***, Shuji SAITO, J. Scott ROBINSON** *(Arizona State Univ.)* **and Timothy C. STEIMLE** *(Arizona State Univ. and IMS)*

[*J. Mol. Spectrosc.* **191**, 176 (1998)]

The pure rotational transitions of TiO ($^3\Delta_r$) and TiN ($^2\Sigma^+$) have been observed in the 220-460 GHz spectral range with the submillimeter-wave spectrometer at IMS, as briefly reported in the former Annual Review.[1)] In addition, the two lowest rotational transitions of TiO at 63 and 94 GHz have been observed using molecular beam pump/probe microwave optical double resonance (PPMODR) technique. An improved set of spectroscopic parameters for TiO ($X^3\Delta_r$) was generated by combining the new PPMODR and submillimeter-wave absorption measurements. Similarly, an improved set of spectroscopic parameters for TiN ($X^2\Sigma^+$) was generated by combining the new submillimeter-wave absorption measurements with the previously recorded PPMODR measurements.[2)] The determined Δ-type doubling parameter for TiO ($X^3\Delta_1$) is effectively modeled using the fourth-order perturbation expression given by Brown et al.[3)]

References

1) K. Namiki, T. C. Steimle and S. Saito, *Ann. Rev.* II-A-6 (1996).
2) D. A. Fletcher, C. T. Scurlock, K. Y. Jung and T. C. Steimle, *J. Chem. Phys.* **99**, 4288 (1993).
3) J. M. Brown, A. S. -C. Cheung and A. J. Merer, *J. Mol. Spectrosc.* **124**, 464 (1987).

II-A-5 Microwave Spectrum of the PD_2 Radical in the $^2B_1$ Ground Electronic State

Tsuyoshi HIRAO *(Grad. Univ. Adv. Stud. and IMS)*, **Shin-ichi HAYAKASHI** *(Nagoya Univ.)*, **Satoshi YAMAMOTO** *(Univ. Tokyo)* **and Shuji SAITO**

[J. Mol. Spectrosc. **187**, 153 (1998)]

The PH_2 radical is isovalent to NH_2 and one of the fundamental bent triatomic free radicals in molecular spectroscopy. The PH_2 and NH_2 radicals are two examples showing the Renner-Teller effect in the nonlinear triatomic molecules. The NH_2 radical has been extensively studied by various high-resolution spectroscopic methods[1)] in the regions from optical to microwave, whereas spectroscopic studies on PH_2 have been relatively limited.

In the present study, the rotational spectrum spectrum of the PD_2 radical in the $^2B_1$ ground electronic state was measured to determine its force field and then the accurate r_z molecular structure PH_2 and PD_2. One hundred thirty fine and hyperfine components of 20 b-type rotational transitions were measured and analyzed by least-squares methods. The detailed molecular constants including the rotational constants, centrifugal distortion constants, the spin-rotation coupling constants, and the hyperfine coupling constants of both the phosphorus and the deuterium nuclei were precisely determined. The harmonic force field of PH_2 was derived from centrifugal distortion constants, inertial defects, and the reported vibrational frequencies for PH_2 and PD_2. The determined force field was used to make harmonic corrections to the observed moments of inertia, and the r_z structures for both species were derived:for PH_2, r_z(PH) = 1.43365(23) Å, and θ_z(HPH) = 91.622(32)˚, and for PD_2, r_z(PD) = 1.42852(17) Å, and θ_z(DPD) = 91.646(23)˚, where errors are due to residual inertial defects of the corrected moments of inertia.

References

1) M. Tonooka, S. Yamamoto, K. Kobayashi and S. Saito, *J. Chem. Phys.* **106**, 2563 (1997).

II-B Development of a Mt. Fuji Submillimeter-Wave Telescope

Shuji SAITO, Hiroyuki OZEKI, Hideo FUJIWARA, Satoshi YAMAMOTO *(Univ. Tokyo)*, **Yutaro SEKIMOTO** *(Univ. Tokyo)*, **Junji INATANI** *(National Space Developing Agency)*, **Masatoshi OHISHI** *(National Astronomical Observatory)* **and Norio KAIFU** *(National Astronomical Observatory)*

In recent years the submillimeter-wave to far infrared region has attracted much attention in the field of astronomy because the initial stage of star forming activity or in other words, the final stage of molecular cloud contraction shows various physical and chemical phenomena in the energy region of this wavelength. Several submillimeter-wave telescopes have now been developed to study astrophysics and astrochemistry of the star-forming regions through atomic and molecular spectral lines. Since atmospheric attenuation, mainly due to water vapor, becomes high in the submillimeter-wave to far infrared region, astronomical observations should be made at a high-altitude site with a cold environment.

We are building a submillimeter-wave telescope at the summit of Mt. Fuji. The main scientific purpose of our project is (1) a survey of the neutral carbon line at 492 GHz, and (2) a search for new simple and fundamental molecules, especially related to interstellar dust chemistry, which will help us to understand evolutionary physical and chemical processes of molecular clouds as a whole.

II-B-1 Development of a Backend System for Mt. Fuji Submillimeter Wave Telescope: An IF Band Synthesis Unit and a New Data Accumulator

Hiroyuki OZEKI, Hideo FUJIWARA and Shuji SAITO

The backend system of Mt. Fuji Submillimeter-wave telescope consists of a wideband acousto-optical spectrometer (AOS) and a data accumulator. Although this basic system has been developed and used since

October '97, it can be applied only to normal 'Position Switching' observation. To meet demands for various kind of observation, we are constructing two additional units for the backend system; one is an IF synthesis unit and the other is new data accumulator for OTF (on the fly) mapping.

The IF synthesis unit is an apparatus which enables one spectrometer to observe spectral lines of multiple frequency bands. In the present system, two IF signals coming from 345 GHz and 492 GHz SIS mixers are shaped with high-order band pass filters and are mixed to synthesize new IF signal by a diplexer. We will be able to observe both CO (J = 3-2, 345.796 GHz) and CI ($^3P_1$ - $^3P_0$, 492.161 GHz) emission lines simultaneously with the IF synthesis unit. This will contribute to investigate the physical evolution of molecular clouds to stars through an elucidation of the chemical evolution of carbon.

OTF (on the fly) mapping is an efficient method in survey observation, which is different from a conventional 'position switching' method. In OTF observation, the spectral data was acquired continuously with an antenna being swept the object to be observed in a constant velocity. Various overheads can be avoided in the observation process such as antenna positioning, observation efficiency is expected to be greatly improved. A new type of data accumulator must be necessary which can process a huge amount of spectral data ejected continuously from the AOS. The new data accumulator is equipped with analog-to-digital converters and ultra-fast interface units to take raw data. The processed spectral data will be shared with a host computer by NFS in which the client and the host are directly connected with 100Mbps network. The data acquisition program of the data accumulator is accessible through the network, and can be further developed after the installation of the system to the telescope site. This is fairly convenient for such a telescope that the site is difficult of access in the winter season.

II-C Laser Cooling and Trapping of Neutral Atoms

When an atom absorbs or emits a photon, the atom is accelerated or decelerated because a photon has momentum. On the other hand, a strong radiation field modifies the internal energy of an atom, so that an atom in an inhomogeneous radiation field receives a force from the field. The former mechanism allows us to decrease the translational temperature of neutral atoms down to an extremely low temperature by laser radiation, and the latter enables the spatial control of neutral atoms with lasers. As the translational temperature goes down to the nano kelvin region, the atomic de Broglie wavelength becomes a macroscopic size, and macroscopic quantum-mechanical collective motion of atoms can then be expected to occur. The long de Broglie wavelength also enables us to realize an atomic interferometry. On the other hand, easy control of atomic spatial position and velocity with lasers is expected to open the possibility of various applications. For these reasons, we have been studying the laser cooling and trapping of neutral atoms.

II-C-1 Isotopic Differences in Rate Coefficients of Cold Penning Collisions between Optically Trapped Metastable He Atoms

Mitsutaka KUMAKURA and Norio MORITA

We have confined about 10^5 triplet metastable ^{4}He and ^{3}He atoms separately in magneto-optical traps at a temperature of 0.5 mK and number density of 10^9 cm^{-1}, and have measured rate coefficients of cold Penning collisions between the trapped atoms ($He^* + He^* \rightarrow He^+ + He + e^-$) by counting ions produced in the traps. In cold collisions, collisional processes can considerably be modified by near-resonant laser light. To obtain both modified and unmodified rate coefficients, ions produced in the presence and absence of trapping laser light have been counted by turning the trap laser on and off repeatedly. By fitting a phenomenological rate equation for ionization to the atomic density dependence of ion count rates, the unmodified rate coefficient has been determined to be $(3.8 \pm 1.1) \times 10^{-10}$ cm^3/s for ^{4}He and $(1.1 \pm 0.4) \times 10^{-9}$ cm^3/s for ^{3}He (denoted by k_4 and k_3, respectively), and the modified ones are $(2.1 \pm 0.6) \times 10^{-8}$ cm^3/s for ^{4}He and $(3.5 \pm 1.3) \times 10^{-8}$ cm^3/s for ^{3}He (denoted by k_4^M and k_3^M, respectively). The ratios k_3/k_4 and k_3^M/k_4^M are about 2.9 and 1.7, respectively, and the former ratio is much larger than the latter, which is almost equal to the one expected for the normal temperature collision. Moreover, the ratios k_3^M/k_3 and k_4^M/k_4 are about 32 and 55, respectively, and the latter ratio is much larger than the former. To understand these remarkable isotopic differences, we have theoretically calculated the rate coefficients, examining the number of potentials for colliding helium atoms. The calculated rate coefficients k_3, k_4, k_3^M, and k_4^M are 1.0×10^{-9} cm^3/s, 2.0×10^{-10} cm^3/s, 1.3×10^{-8} cm^3/s, and 1.1×10^{-8} cm^3/s, respectively, and these are all in good agreement with the experimental values. Through this calculation, it has been found that only s-waves can contribute to the unmodified Penning collision at this cold temperature owing to the presence of high centrifugal barriers for higher partial waves, and a large isotopic difference in the number of the s-waves that can contribute to the ionization results in the remarkable difference between k_3 and k_4, which is unclear because of averaging over many partial waves at a normal temperature or in the presence of the laser-modification.

II-D Spectroscopy of Ions and Atoms in Liquid Helium

Ions and atoms in liquid helium are known to reside in bubble-like cavities due to the Pauli repulsive force between electrons. Physical properties in these exotic surroundings are determined by the potential energy of impurity-He_n system, the surface tension energy of the liquid helium, and the pressure-volume energy. Spectroscopic study of ions in liquid helium is expected not only to give information on the structure and dynamics of the bubbles, but also to contribute to the study on the property of superfluid liquid helium. Moreover, if ions are trapped in liquid helium by a radio-frequency trap or just below the liquid helium surface by a static electronic field, this kind of study is expected to break a new way in the experimental physics of low temperature and low dimensional plasma.

II-D-1 Laser Spectroscopy of Yb^+ Ions in Liquid Helium

Yoshiki MORIWAKI and Norio MORITA

Although spectroscopic observations of many neutral atoms in liquid helium have so far been demonstrated, there have been no such observations on ions other than Ba^+. This may be because of difficulties in optical detection of ions in liquid helium: for example, low density of foreign ions due to the Coulomb repulsion between the ions and also due to recombination with electrons, and low detection efficiency due to extraordinarily broadened spectra. However, the first difficulty can be overcome by implanting ions in liquid helium with laser sputtering of a metal tip in a strong electric field, which is applied to prevent ions from recombination with electrons. With this method, we have successfully observed emission and absorption spectra of the $4f^{14}6s^2S_{1/2}$ - $6p^2P_{1/2}$ (D1) and $4f^{14}6s^2S_{1/2}$ - $6p^2P_{3/2}$ (D2) transitions of Yb^+. Properties of the observed spectra are as follows: (1) The excitation spectrum of the D1 transition shows some broadening and blue shift in comparison with those of free ions. The shift and width of the emission spectrum are smaller than those of the excitation spectrum. (2) The excitation spectrum of the D2 transition is doubly peaked. In addition, the emission from the $4f^{14}6p^2P_{1/2}$ state is clearly observed after the excitation to the $4f^{14}6p^2P_{3/2}$ state. The fine structure splitting in the $4f^{14}6p^2P_j$ state of Yb^+ (3330 cm^{-1}) is expected to be much larger than the interaction potential between the Yb^+ ion in the $4f^{14}6p^2P_j$ state and the He atom, and this means that an ion bubble in the $4f^{14}6p^2P_{1/2}$ state is spherical. An ion bubble in the $4f^{14}6s^2S_{1/2}$ state is, of course, also spherical, so that a simple model for transitions between spherical bubbles can explain property (1). On the other hand, a vibration of the ion bubble in a deformed mode leads to energy level splitting in the $4f^{14}6p^2P_{3/2}$ state (dynamic Jahn-Teller effect). The splitting of the excitation spectrum of the D2 transition (property (2)) can be explained by this picture. However, transitions between the $4f^{14}6p^2P_j$ states have not been clearly understood yet. The ^2P state of Yb^+-He is expected to have a potential minimum, as is the case in the pair state of alkali-He. After the excitation to the $4f^{14}6p^2P_{3/2}$ state, the He atom approaches the potential minimum point. If some relaxation occurs at the potential minimum, the D1 emission spectrum should be more broadened and its center wavelength should be more red shifted than the observed ones. This is because the interaction between Yb^+-He is so large at the minimum point that, instead of spherical bubble formation, an exciplex is expected to be formed. Therefore transitions between the $4f^{14}6p^2P_j$ states are expected to occur in a very early stage after the ^2P state is created, and this means that the transition rate between the $4f^{14}6p^2P_j$ states is considerably large. For further analysis, detailed theoretical calculations on the Yb^+-He potential are necessary.

II-D-2 Laser Spectroscopy of Yb atoms in Liquid Helium

Yoshiki MORIWAKI and Norio MORITA

Spectra of the Yb atom in liquid helium have been observed. It has been found that excitation spectra of the $4f^{14}6s^2\ ^1S_0$ - $4f^{14}6s6p\ ^1P_1$ and $4f^{14}6s^2\ ^1S_0$ - $4f^{13}(^2F_{7/2})5d_{5/2}6s^2(7/2,5/2)_1$ transitions show extremely small spectral width (~ 0.1nm), while in other atoms in liquid helium spectral widths are usually very large. For the latter transition, this property can be explained by the fact that electrons in inner shells are shielded by outer electrons with respect to the perturbation caused by surrounding helium atoms. On the other hand, it needs further analyses to explain the spectrum of the former transition, in which a valence electron is excited.

II-D-3 Theoretical Analyses of the Spectrum of Mg Atoms in Liquid Helium

Yoshiki MORIWAKI and Norio MORITA

In our previous experiment, it was found that the emission spectrum of the $3s3p\ ^1P_1 \rightarrow 3s^2\ ^1S_0$ transition of Mg atoms in liquid helium shows an extraordinary broadening and a large red-shift in comparison with atomic bubble transitions so far observed. This cannot be explained by the usual bubble model in which a continuous bubble interface is assumed. We have instead proposed an exciplex formation model, in which we assume that He atoms localize near the Mg atom in the nodal plain of the $3p$ electron and form a ring structure. Minimization of the total energy has shown that the most probable form of the exciplex is Mg-He_{10}. By using the spectral method, we have calculated an emission spectrum of the transition from this exciplex to the bound free ground state. As a result, it has been found that the shift is well explained, and that this model provides much improvement in the spectral broadening in comparison with the bubble model. This means that the exciplex model is more suitable for understanding the dynamics in the $3s3p\ ^1P_1 \rightarrow 3s^2\ ^1S_0$

transition than the bubble model does. This is the first evidence for the formation of exciplexes in a ring-like structure. We have also calculated emission spectra of the same type exciplexes of Na, Mg^+, and Ca^+ in the np^2P_j state. This will be helpful in the experimental search for spectra of these atoms and ions in liquid helium, which have not been observed yet.

II-E Structure and Function of Respiratory Terminal Oxidases

In the aerobic respiratory chain of *Escherichia coli*, there are structurally unrelated two terminal oxidases. A heme-copper oxidase, cytochrome *bo* is predominantly expressed under highly aerated growth conditions while an alternative oxidase, a putative heme-heme oxidase, cytochrome *bd*, is predominant under microaerobic conditions. Both oxidases catalyze the two-electron reduction of ubiquinol-8 and the four-electron reduction of dioxygen, whereas only cytochrome *bo* exhibits vectorial proton transport. However, only a little structural information has been given for these ubiquinol oxidases. To clarify the molecular mechanism of electron transfer, chemical reaction of dioxygen, and proton pumping in the two respiratory terminal oxidases, we utilize various molecular spectroscopic techniques (*e.g.*, resonance Raman, EPR, FTIR) in conjuction with methods of molecular biology and biochemistry.

II-E-1 Fluoride-Binding to the Oxidized *Escherichia coli bd*-Type Ubiquinol Oxidase Studied by Visible Absorption and EPR Spectroscopies

Motonari TSUBAKI *(Himeji Inst. Tech. and IMS)*, **Tatsushi MOGI** *(Univ. Tokyo)* **and Hiroshi HORI** *(Osaka Univ.)*

Escherichia coli produces cytochrome *bo*- and *bd*-type ubiquinol oxidases, both of which reduce molecular oxygen to water, whereas only *bo*-type oxidase exhibits vectorial proton transport. It is believed that the *bd* type oxidase contains two heme *b* centers (heme b_{558} and heme b_{595}) and one heme *d* center. To clarify the structure of the reaction center, we analyzed the purified *bd*-type oxidase in oxidized state with visible absorption and EPR spectroscopies using fluoride ion as a monitoring probe. The observed visible spectral changes upon fluoride-binding (blue shifts of high-spin charge-transfer bands from 743 and 595 nm to 708 and 575 nm, respectively) were typical of those observed for other ferric iron-chlorin species, indicating that fluoride ion binds at the ferric heme *d* center. In EPR spectra, fluoride-binding to the oxidized enzyme caused a complete disappearance of low-spin signals and a formation of a rhombic high-spin signal at g = 6.3, 5.5, and 2.00. Each component of the high-spin signal showed a doublet (with splitting of 3.5, 2.9, and 10.8 mT, respectively) which arises from interaction of the unpaired spin of iron with the nuclear magnetic moment of ^{19}F, which has a spin of one-half.[1),2)] This unexpected result establishes that the rhombic high-spin signal previously assigned to ferric heme b_{595} is actually derived from the ferric heme *d* center.

References

1) H. Morimoto and M. Kotani, *Biochim. Biophys. Acta* **126**, 176 (1966).
2) J. Peisach, W. E. Blumberg, S. Ogawa, E. A. Rachmilewitz and R. Oltzik, *J. Biol. Chem.* **246**, 3342 (1971).

II-E-2 Azide- and Cyanide-Bindings to the *Escherichia coli bd*-Type Ubiquinol Oxidase Studied by Visible Absorption, EPR and FTIR Spectroscopies

Motonari TSUBAKI *(Himeji Inst. Tech. and IMS)*, **Tatsushi MOGI** *(Univ. Tokyo)* **and Hiroshi HORI** *(Osaka Univ.)*

To clarify the structure of the reaction center of *bd*-type ubiquinol oxidase, we analyzed the oxidized enzyme with visible absorption, EPR and FTIR spectroscopies using azide and cyanide ions as monitoring probes. Azide-binding to the oxidized enzyme caused a formation of a new EPR low-spin signal characteristic to low-spin ferric iron-chlorin-azide species. In the g6 region, there was no appreciable change. In visible absorption spectra, a disappearance of high-spin charge-transfer bands (595 and 643 nm) and an appearance of a new band at 650 nm were observed. These results suggest that the primary binding site of azide is the heme *d* center. FTIR spectra gave a new bound azide antisymmetric stretching band at 2010.5 cm^{-1}, presumably derived from a low-spin species. This azide band showed anomalies upon azide [^{15}N]-isotopic substitution, suggesting some effects from surrounding protein residues or from heme b_{595} in close proximity. The bound azide infrared band disappeared completely upon addition of cyanide. The visible spectral change upon cyanide-binding was typical of those observed for ferric iron-chlorin species with diol substituents in macrocycles. However, we could not observe any corresponding low-spin EPR signal. Instead, a derivative-shaped signal at g = 3.19 was observed. This unusual signal could be arising from the heme $d(Fe^{3+})$-CN-heme $b_{595}(Fe^{3+})$ moiety. Thus, the present study confirmed our previous proposal[1)] that heme *d* and heme b_{595} forms a binuclear metal center.

Reference

1) M. Tsubaki, H. Hori, Mogi, T. Mogi and Y. Anraku, *J. Biol. Chem.* **270**, 28565 (1995).

II-F Biomolecular Science

Elucidation of a structure-function relationship of metalloproteins is a current subject of this group. The primary technique used for this project is the stationary and time-resolved resonance Raman spectroscopy monitored by near IR to UV lasers. The main themes that we want to explore are (1) mechanism of oxygen activation by enzymes, (2) mechanism of active proton translocation and its coupling with electron transfer, (3) coupling mechanism of proton- and electron transfers by quinones in photosynthetic reaction center, (4) higher order protein structures and their dynamics, and (5) reactions of biological NO. In category (1), we have examined a variety of terminal oxidases, cytochrome P450s, and peroxidases, and also treated their enzymatic reaction intermediates by using the mixed flow transient Raman apparatus and the Raman/absorption simultaneous measurement device. For (2) the third generation UV resonance Raman (UVRR) spectrometer has been constructed and we are going to use it to the peroxy and ferryl intermediates of cytochrome c oxidase. In (3) we succeeded in observing RR spectra of quinones A and B in bacterial photosynthetic reaction centers for the first time and in assigning them with Raman spectra of electronically reduced isotope-labeled quinones. For (4) we developed a novel technique for UV resonance Raman measuremnts based on the combination of the first/second order dispersions of gratings and applied it successfully to 235-nm excited RR spectra of several proteins including mutant hemoglobins and myoglobins. Nowadays we can carry out time-resolved UVRR experiments with nanosecond resolution to discuss protein dynamics. We have succeeded in isolating the spectrum of β37-Trp and α42-Tyr of Hb A separately and their changes upon quaternary structure transition. For (5) we purified soluble guanylate cyclase from bovine lung, characterized it and observed its RR spectra.

II-F-1 Resonance Raman Characterization of Nitrosylheme in Myoglobin and Its Mutants

Takeshi TOMITA *(Grad. Univ. Adv. Stud.)*, **Shun HIROTA** *(Nagoya Univ.)*, **Takashi OGURA, John S. OLSON** *(Rice Univ.)* **and Teizo KITAGAWA**

Resonance Raman spectra have been observed for wild-type nitrosylmyoglobin (MbNO) and H64G, H64L, L29W, V68W, and V68T mutants at neutral and acidic pH. Raman excitation in resonance with the Soret band enabled us to detect the Fe-NO (ν_{Fe-NO}) and N-O stretching (ν_{NO}) and Fe-N-O bending (δ_{FeNO}) bands of nitrosylmyoglobins. The ν_{Fe-NO}, δ_{FeNO}, and ν_{NO} bands of wild type sperm whale MbNO at neutral pH were observed at 560, 452, and 1613 cm^{-1}, respectively, and substitution of the distal His64 to Gly or Leu caused an upshift of ν_{NO} to 1633 ~ 1636 cm^{-1} but no change in ν_{Fe-NO}. This change in ν_{NO} for the substitution is due to removal of hydrogen bonding between His64 and bound NO. Substitution of Leu29 with tryptophan altered ν_{Fe-NO} but caused no change in ν_{NO} at neutral pH. These properties are somewhat similar to those in MbO_2 but contrast with those of MbCO, for which the Fe-CO and C-O stretching frequencies have an inverse linear correlation. In the case of L29W-MbNO, the change in ν_{Fe-NO} is probably caused by tilting of the Fe-N bond from the heme normal due to steric hindrance with the large indole ring but not by changes in the Fe-N-O bond angle. When pH is lowered below 4, Mb(II)NO adopts the five-coordinate structure due to cleavage of the Fe-His bond. Accordingly, the Raman maker bands, ν_3 and ν_{10}, shift from 1500 and 1636 cm^{-1} at pH 7.4 to 1509 and 1646 cm^{-1} at pH 4 which are in agreement with those of a five-coordinate Fe-proto-porphyrin-NO complex in detergent micelles at neutral pH. The ν_{Fe-NO} and ν_{NO} bands of acidic MbNO are observed at 520 and 1668 cm^{-1} and exhibit no shift when the distal His is replaced by Gly or Leu. The latter observation supports previous X-ray crystallographic, infrared, and resonance Raman spectroscopic measurements which show that the distal histidine becomes protonated at pH 4 and swings out into the solvent away from the bound ligand.

II-F-2 Infrared Evidence for Cu_B Ligation of Photodissociated CO of Cytochrome *c* Oxidase at Ambient Temperatures and Accompanied Deprotonation of a Carboxyl Side Chain of Protein

Tadashi IWASE *(Grad. Univ. Adv. Stud.)*, **Constantinos VAROTSIS** *(Crete Univ. and IMS.)*, **Kyoko SHINZAWA-ITOH** *(Himeji Inst. Tech.)*, **Shinya YOSHIKAWA** *(Himeji Inst. Tech.)* **and Teizo KITAGAWA**

FTIR "light" minus "dark" difference spectra were measured for the CO complex of bovine fully reduced cytochrome *c* oxidase in H_2O and D_2O. Unexpectedly, the CuB-bound CO was identified at ambient temperatures in the photo-steadystate only for the D_2O solution, and simultaneously a difference peak was observed at 1737 cm^{-1}, indicating that the lifetime of the Cu_BCO is much longer in D_2O than in H_2O and that deprotonation of a carboxylic side chain occurs upon photodissociation of CO from heme a_3. However, the frequency and intensity of the CO stretching band remained unchanged in H_2O and D_2O between pH 6.8 and 9.2. Time-resolved IR diode laser spectrophotometry demonstrated that the protein structural changes have finished within the response time of the instrument (3 ms).

II-F-3 Interaction of Phosphatidylinositol 3-Kinase SH3 Domain with Its Ligand Peptide Studied by Absorption, UV Resonance Raman and Circular Dichroism

Nobuyuki OKISHIO *(Kanazawa Univ.)*, **Ryuji FUKUDA** *(Kanazawa Univ.)*, **Masako NAGAI** *(Kanazawa Univ.)*, **Shigenori NAGATOMO and Teizo KITAGAWA**

Absorption, UV resonance Raman and circular dichroism (CD) spectroscopies were applied to examine selectively the environmental and structural changes of Trp and Tyr residues in the binding cleft of phosphatidylinositol 3-kinase (PI3K) SH3 domain induced by ligand association. Comparison of the spectra of PI3K SH3 in the presence or absence of its ligand peptide RLP1 (RKLPPRPSK) indicated that RLP1 binding placed Trp55 of the SH3 in a polar environment and disrupted its H-bonding, and made Tyr residues to form a new H-bond in a hydrophobic environment. The D21N mutant (Asp21 changed to Asn) of the SH3 yielded the near-UV CD distinct from that of the wild-type, and its spectral changes induced by RLP1 were smaller and different compared with those of the wild-type, suggesting that the mutation of conserved Asp21 affected the conformation of the ligand affinity. These data provide a direct evidence for the occurrence of some environmental and structural alterations in the binding cleft of PI3K SH3 by the ligand association and the D21N mutation.

II-F-4 Quaternary Structure Sensitive Tyrosine Residues in Human Hemoglobin: UV Resonance Raman Studies of Mutants at α140, β35 and β145 Tyrosine

Masako NAGAI *(Kanazawa Univ.)*, **Henri WAJCMAN** *(Hopital Hneri Mondor)*, **Anges LAHARY** *(CHRU of Rousen)*, **Takashi NAKATSUKASA** *(Osaka Univ.)*, **Shigenori NAGATOMO and Teizo KITAGAWA**

Recent studies noted the contribution of α42 Tyr to the T-R dependent UV resonance Raman (UVRR) spectral changes of HbA [M. Nagai et al.; *J. Mol. Struct.* **379**, 65-75 (1996); Huang, et al. *Biochemistry* **36**, 6197-6206 (1997)], but the observed UVRR changes of Tyr residue can not be fully interpreted by α42 Tyr alone. To identify the remaining contributions the 235-nm excited UVRR spectra of mutant Hbs at α140, β35, and β145 were investigated here. The Fe-His stretching mode demonstrated that all these mutant Hbs take the T structure in the deoxy form under the present experimental conditions. UVRR change of Trp residue of these mutants upon the T-R transition was the same as that in HbA, indicating that the T-R dependent UVRR change of β37 Trp is not due to stacking with Tyr residues but is owing to changes in the surrounding hydrophobicity. Recombinant Hb (β35Tyr → Phe) gave an identical UVRR spectrum with that of Hb A, indicating that β35Tyr is not responsible. In the spectra of des(β146His, β145Tyr)Hb with IHP, the frequenccy shift of Tyr RR bands was the same as that in HbA but the intensity enhancement in the CO-form was small, suggesting that β145Tyr contributes partly to the intensity change, but scarcely relates to the frequency shift. In the spectra of Hb Rouen (α140Tyr → His), the frequency shifts of bands at 1617 (Y8a) and 1177 (Y9a) cm^{-1} following ligation were half of those in HbA, while the intensity enhancement was not detected. This results indicates that α140Tyr is resposible for both the frequency shift and the intensity changes. It is sugggested that the frequency shift of Tyr RR bands on the T → R transition is due to the changes of hydrogen bonding state of α42 and α140 Tyr, the intensity enhancement is due to the environmental chage of the penultimate Tyr in both α and β subunits (α140 and β145).

II-F-5 A Superoxodicopper(II) Complex Oxidatively Generated by a Reaction of Di-μ-Hydroxodicopper(II) Complex with Hydrogen Peroxide

Masahito KODERA *(Doshisha Univ.)*, **Yoshimitsu TACHI** *(Nagoya Univ.)*, **Shun HIROTA** *(Nagoya Univ.)*, **Kou KATAYAMA** *(Tokyo Inst. Tech.)*, **Hisashi SHIMAKOSHI** *(Tokyo Inst. Tech.)*, **Koji KANO** *(Tokyo Inst. Tech.)*, **Kiyoshi FUJISAWA** *(Tokyo Inst. Tech.)*, **Yoshihiko MORO-OKA** *(Tokyo Inst. Tech.)*, **Yoshinori NARUTA** *(Kyushu Univ.)* **and Teizo KITAGAWA**

[Chem. Lett. 798 (1998)]

Di-μ-hydroxodicopper(II) complex with a hexapyridine dinucleating ligand, $[Cu_2(OH)_2(hexpy)](CF_3SO_3)_2$ (hexpy = 1,2-bis[2-bis(2-pyridyl)methyl)-6-pyridyl]ethane), reacts with H_2O_2 in $MeCN/CH_2CL_2$ to give a superoxodicopper(II) complex. Its visible absorption (Figure 1) and resonanace Raman spectra (Figure 2) were observed.

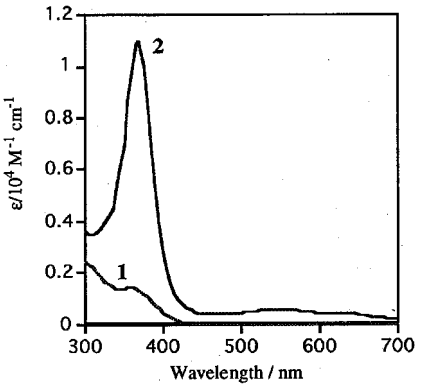

Figure 1. UV-vis spectra of **1** and **2** in $MeCN/CH_2CL_2$ (1:9, v/v) at-40˚C.

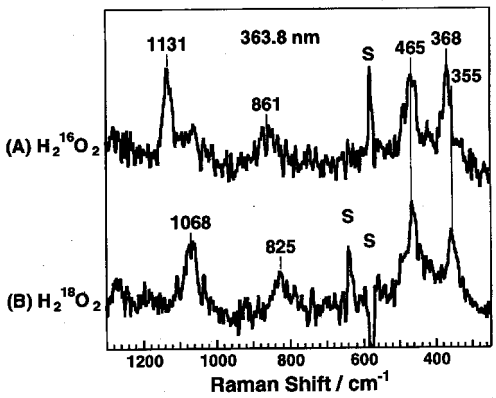

Figure 2. Resonance Raman spectra of **2** generated by the reaction of **1** with (A) $H_2{}^{16}O_2$ and (B) $H_2{}^{18}O_2$ in MeCN /CH_2Br_2 (1:9, v/v) at -30˚C. **S** denotes solvent (CH_2Br_2) bands.

II-F-6 Structural and Spectroscopic Characterization of a Mononuclear Hydroperoxo-Copper(II) Complex with Tripodal Pyridylamine Ligands

Akira WADA *(Nagoya Inst. Tech.)*, **Manabu HARATA** *(Nagoya Inst. Tech.)*, **Koji HASEGAWA** *(Nagoya Inst. Tech.)*, **Koichiro JITSUKAWA** *(Nagoya Inst. Tech.)*, **Hideki MASUDA** *(Nagoya Inst. Tech.)*, **Masahiro MUKAI, Teizo KITAGAWA and Hisahiko EINAGA** *(Nagoya Inst. Tech.)*

[*Angew. Chem. Int. Ed.* **37**, 798 (1998)]

Hydroperoxo-copper species are key intermediates in biological oxidations catalyzed by copper enzymes such as dopamine β-hydroxylase, glactose oxidase and superoxide dismutase. To confirm the structural characterization of the Cu(II)-OOH^- species, we prepared a mononuclear copper complex with a new designed tripodal pyridylamine ligand, bis(6-pivalamide-2-pyridylmethyl)-(2-pyridylmethyl)amine (bppa) and subjected it to reaction with hydrogen peroxide. Here we present the first example of an isolated copper-hydroperoxo species, $[Cu(II)(bppa)-(OOH^-)]^+$. The resonance Raman spectra of the reaction product of $Cu(bppa^-)]ClO_4$ with excess H_2O_2 in MeCN excited at 441.6 nm gave a strong Raman band at 856 cm^{-1}, which shifted to 810 cm^{-1} when ^{18}O-labeled H_2O_2 was used. Accordingly, the oxygen-isotope sensitive band is assigned to an O-O stretch of a hydroperoxo species. The crystal structure of this compound was also analyzed.

II-G Fast Dynamics of Photoproducts in Solution Phases

Picosecond time-resolved resonance Raman (ps-TR^3) spectroscopy is a promising technique to investigate ultrafast structural changes of molecules. However, this technique has not been used as widely as nanosecond TR^3 spectroscopy, mainly due to the lack of light source which has suitable repetition rates of pulses and wavelength tunability. In order to obtain qualified TR^3 spectra, first we need two independently tunable light sources for pump and probe pulses. Second, the repetition rate should be higher than kilohertz to keep a moderate average laser power without allowing the photon density of probe pulse too high. We succeeded in developing light sources for ps-TR^3 spectroscopy having wide tunability and kHz repetition, and applied them to study fast dynamics of photo-excited molecules. For carbonmonoxy myoglobin (MbCO), vibrational relaxation with the time costant of 1.9 ps was observed for CO-photodissociated heme. For Ni-octaethylporphyrin in benzene, different population rises in vibrationally excited levels were observed in the anti-Stokes spectra for different vibrational modes. For the same molecule in piperidine, coordination of two solvent molecules was observed in the transient (d,d) excited state. Nanosecond time-resolved Raman spectra were investigated for photodissociation of various mutant myoglobins. The UV ns-TR^3 experiments on MbCO demonstrated the presence of a transient open form of the ligand pathway.

II-G-1 Photo-Induced Solvent Ligation to Nickel(II)-Octaethylporphyrin Probed by Picosecond Time-Resolved Resonance Raman Spectroscopy

Yuki UESUGI *(Grad. Univ. Adv. Stud.)*, **Yasuhisa MIZUTANI and Teizo KITAGAWA**

[*J. Phys. Chem. A* **102**, 5809 (1998)]

Pump/probe picosecond time-resolved resonance Raman spectra of nickel(II)-octaethylporphyrin (NiOEP) in pyridine were observed in the time range -5 to 1000 ps. The spectra demonstrate generation of the vibrationally and electronically excited (d,d) state (B_{1g}) immediately after the excitation to the $\pi\pi^*$ state of the macrocycle, subsequent vibrational relaxation, and the formation of six-coordinate exciplex, $B_{1g}(L)_2$ (L: pyridine). Singular value decomposition analysis was applied to a series of picosecond time-resolved Raman spectra to investigate whether a five-coordinate complex was generated prior to the formation of the six-coordinate species. The results indicate insignificant population of the five-coordinate species preceeding the formation of $B_{1g}(L)_2$ and suggest concerted coordination of two solvent molecules to axial positions of the (d,d) excited NiOEP. The formation process of the $B_{1g}(L)_2$ species is discussed.

II-G-2 Time Resolved Resonance Raman Evidence for the Exciplex Formation of Free-Base Porphyrin with an Electron Acceptor

Anandi L. VERMA *(North-Eastern Hill Univ.)*, **Shin-ichiro SATO** *(JAIST)* **and Teizo KITAGAWA**

[*Chem. Phys. Lett.* **267**, 507 (1997)]

Pump/probe time-resolved resonance Raman experiments (TR^3) on free-base tetraphenylporphyrin (H_2TPP) in benzene and benzene plus CCl_4 mixed solvents were carried out to probe the mechanistic details and transient species involved in the photo-oxidation of H_2TPP. We have detected spectral features due to the π-radical cation, and exciplex tansient species in the singlet and triplet excited states at different time-scales in the presence of CCl_4 under laser irradiation. A mechanism for the photooxidation of porphyrins is discussed.

II-G-3 Comment on: Polarization Effects in Time Resolved Incoherent Anti-Stokes Raman Spectroscopy

Yasuhisa MIZUTANI

[*J. Chem. Phys.* in press (1998)]

The theoretical inspection on anti-Stokes Raman measurements following strong vibrational excitation by Hofmann et al. [M. Hofmann, R. Zürl and H. Graener, *J. Chem. Phys.* **105**, 6141 (1996)] was reexamined. It is found that the depolarized intensity is dependent on the incident angle of the pump pulse in the case of perpendicularly polarized pumping. Therefore one can observe "rotation-free" depolarized scattering only with some particular incident angle, which was not described in their paper. In addition to that, it is suggested to use the definition of depolarization ratio for polarized probe light instead of that for unpolarized light, since currently laser is a light source for this kind of experiments.

II-G-4 Saturation Raman Spectrosocpy as a Tool for Studying the Excited States of Complex Organic Molecules: Application to Nickel Octaethylporphyrin

Sergei G. KRUGLIK *(B. I. Stepanov Inst. and IMS)***, Alexander G. SHVEDKO** *(B. I. Stepanov Inst.)* **and Teizo KITAGAWA**

[*Asian J. Phys.* in press]

The nanosecond saturation resonance Raman (RR) technique has been reviewed and its peculiarities have been examined on the basis of a well-known molecular system, nickel octaethylporphyrin [Ni(OEP)] in solution. The results of mathematical treatment of saturation RR spectra of Ni(OEP) in weakly coordinating pyridine solvent suggest that the quantum yield of photogeneration of the six-coordinate Ni(OEP)(pyridine)$_2$ species is low, with the rate of complexation process being about one tenth of the rate of excitation deactivation within the manifold of four-coordinate species.

II-H Molecular and Electronic Structures of Metallofullerenes and the Fullerene Radical Anions

The continued interest in radical ions of fullerenes and metallofullerenes has resulted from the discovery of superconductivity in the CT complexes of alkali metals with fullerenes. Spectroscopic information concerning the molecular structure of the metallofullerene of La@C_{82} has been obtained by EPR and ENDOR measurements. From the comparison between the two results some dynamics of La metal ion within the carbon cage were also deduced.

II-H-1 ENDOR Measurements of La@C_{82}

Tatsuhisa KATO, Kazunobu SATO *(Osaka City Univ.)***, Takeji TAKUI** *(Osaka City Univ.)***, Deanna HURUM** *(Univ. Rochester)***, Robert W. KREILICK** *(Univ. Rochester)***, Shingo OKUBO** *(Niigata Univ.)* **and Takeshi AKASAKA** *(Niigata Univ.)*

^{13}C enriched La@C_{82} (^{13}C-La@C_{82}) sample was produced by the conventional arc-discharge procedure with electrodes of ^{13}C enriched LaC composite rods. The most abundant isomer of La@C_{82} was purified by a two stage HPLC purification procedure with Buckyprep and PBB columns. The ENDOR spectrum of toluene solution of La@C_{82} observed at 200 K is shown in the figure, and the most intense peak at 3.7 MHz was assigned to the ENDOR signal of ^{139}La nucleus, and several peaks between 3.75 MHz and 6.25 MHz to ^{13}C nuclei at the different site of the C_{82} cage. The ENDOR spectrum due to ^{13}C nuclei was well reproduced by the simulation with the ^{13}C hfc constants, as shown by a stick diagram and by a dotted line in the figure. The simulation is consistent with that for the ^{13}C satellite of the ESR spectrum for natural La@C_{82}. The ENDOR measurements could also indicate the dynamics of La metal ion inside the carbon cage. The ENDOR spectrum observed at the lower magnetic field exhibit relatively smaller ^{139}La peak than that at higher field. The fact reflects on the different relaxation rate for ^{139}La and ^{13}C.

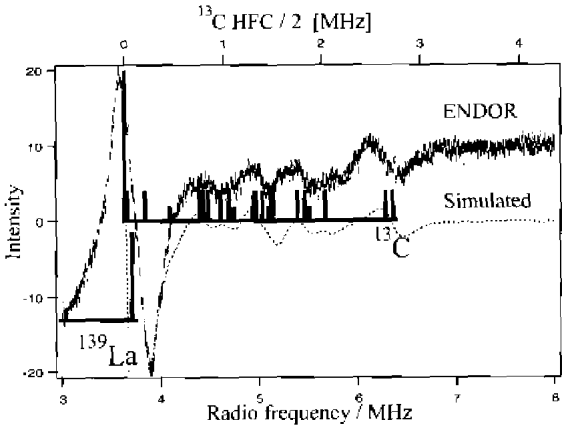

Figure 1. The ENDOR spectrum of toluene solution of purified ^{13}C enriched La@C_{82} (^{13}C-La@C_{82}) sample observed at 200 K. A stick diagram and a dotted line are the simulation with the ^{13}C hfc constants.

II-I Site Selective Spectroscopy in Solid Crystals

The line broadening due to the variation of the environment over the some sites in the crystal structure prevents from determining small energy splitting between pair of closely spaced levels with high accuracy. However the

broadening effects give a nice prove to investigate the intermolecular interaction in the crystal structure. On the other hand some techniques of the site selective spectroscopy to eliminate the disturbance were proposed. We are applying the technique of the heterodyne detection of optical magnetic double-resonance to some systems of crystal.

II-I-1 Coherent Raman Spectroscopy of Nuclear Quadrupole Resonance of La around Pr^{3+} in LaF_3

Michio MATSUSHITA, Akiko MUTOH *(Kitasato Univ.)* **and Tatsuhisa KATO**

[*Phys. Rev. B* **58** in press (1998)]

Coherent Raman spectroscopy was applied for an optical-rf double resonance study of LaF_3 crystal doped with Pr^{3+}. The coherent nuclear spin Raman scattering was detected as a function of the applied rf frequency. Exciting the resonance condition of the $^3H_4 \rightarrow {}^3P_0$ transition of Pr^{3+} (20925 cm^{-1}), only the La nuclei surrounding the Pr^{3+} ion were observed through their nuclear quadrupole resonance (NQR). The double resonance between the optical transition of the ion and the NQR transition of its neighboring nucleus is theoretically described by analyzing the magnetic dipolar interaction that is affected by the optical excitation. Under a certain restriction, which the present system fulfills, the intensity of the Raman heterodyne signal can be described by an analytical function of the internuclear vector and the orientation of the electric field gradient (EFG) at the Pr and La nuclei. Five different neighboring La nuclei were observed. They are different from the bulk La in both magnitude and orientation of the EFG. In addition, it was found that the laser frequency jitter affects the relative signal intensity of the different La NQR transitions through the optical pumping of the La spin levels.

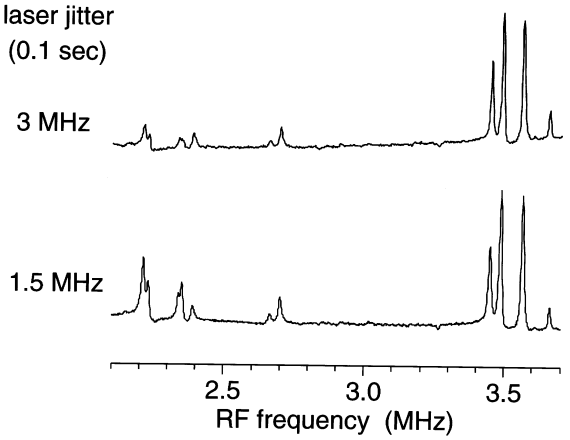

Figure 1. Influence of the laser frequency jitter on the Raman heterodyne signals. Comparison of the spectra between jitter of 3 MHz and 1.5 MHz. The NQR transitions whose frequencies are below the laser jitter are suppressed due to the optical pumping effect on the La spins.

II-I-2 Coherent Raman Scattering from a Delocalized Excitation in Molecular Crystal of 1,4-Dibromonaphthalene

Michio MATSUSHITA and Tatsuhisa KATO

Since its first application to NMR study of Pr^{3+} in LaF_3 in 1983, coherent Raman spectroscopy has been almost exclusively applied to rare earth impurity ions in inorganic crystals. The technique was for the first time shown to be applicable to magnetic resonance study of delocalized excitation in a molecular crystal. Optical-RF double resonance of the triplet exciton in 1,4-dibromonaphthalene (20192 cm^{-1}) was detected as coherent Raman scattering. One of the ESR transitions of the triplet exciton and the NQR transitions of ^{79}Br and ^{81}Br in the excited state were observed. The structure of the ESR transition and the intensity of the NQR transitions reflect the nature of the exciton through the hyperfine interaction between the delocalized electron spin and the Br nuclear spins.

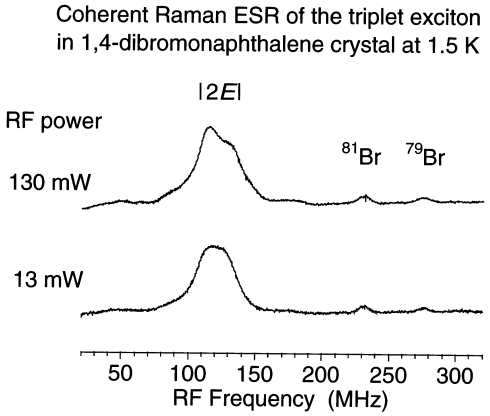

Figure 1. Raman heterodyne detected zero-field magnetic resonance of the triplet exciton in 1,4-dibromonaphthalene at 1.5 K. A cw laser was tuned to excite the triplet exciton at 20192 cm^{-1} (495.2 nm) and coherent Raman scattering was measured as a function of the frequency of the applied RF. Transition around 120 MHz is the $|2E|$ ESR transition of the triplet exciton. The transitions at 232 and 276 MHz are the NQR transitions of ^{81}Br (I = 3/2) and ^{79}Br (I = 3/2) in the exciton state, respectively.

II-J State Correlated Raman Spectroscopy

The vibrational Raman polarizability tensor responds to molecular reorientational relaxation process, and the structural environment in condensed media. The measurement of Raman scattering is a powerful technique for the study of molecular motion and of the mechanism of phase transition. We've built up the system of multichannel type detection of Raman scattering combined with the temperature controlled cell.

II-J-1 Polarized Raman Scattering Measurements of MHPOBC

Naoki HAYASHI and Tatsuhisa KATO

Polarized Raman scattering was measured on the successive smectic phase, SmA, SmC_α*, SmC*, SmC_γ* and SmC_A* of MHPOBC. 2nd and 4th order parameters of the Raman tensor, $<P_2>$ and $<P_4>$, were evaluated. The C=C stretching mode of phenyl rings and C=O stretching modes of carbonyl groups in core and chiral parts of each smectic phase were investigated. The tilt angle for spiral axis was taken into consideration for the analysis of the order parameters. $<P_2>$ and $<P_4>$ obtained were plotted with respect to the temperature. It was noticed that the values of the order parameters, especially of $<P_4>$, exhibited considerable dip at the temperature range of the SmC* phase. It is supposed that the molecular ordering was influenced by the ferroelectric molecular interaction. Moreover $<P_4>$ obtained for the C=O stretching mode of chiral CO group showed a prominent decrease comparing with the others, while $<P_2>$ showed a similar change. This fact suggests the specific dynamics for the chiral CO group in the process of the transition around SmC* phase.

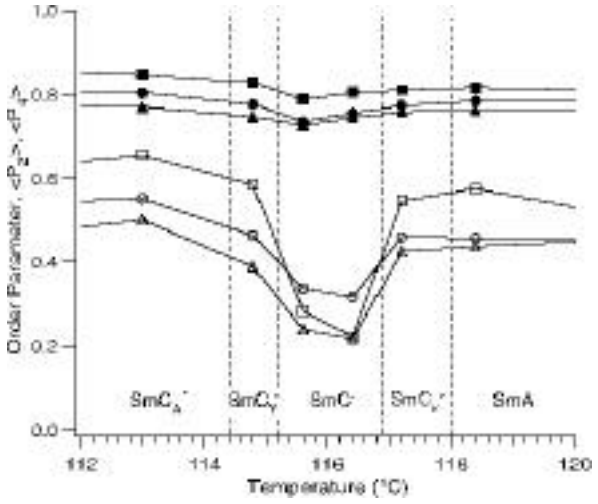

Figure 1. The order parameters of $<P_2>$ and $<P_4>$. ■: $<P_2>$ for the chiral C=O, □: $<P_4>$ for the chiral C=O, ●: $<P_2>$ for the phenyl C=C, ○: $<P_4>$ for the phenyl C=C, ▲: <P2> for the core C=O, △: $<P_4>$ for the core C=O.

II-K Double Resonance Spectroscopy Using Two Phase-Locked Lasers

Optical-Optical double resonance (OODR) is one of the most sophisticated techniques in high resolution spectroscopy. It is as precise as microwave spectroscopy and provides detailed information which is often complementary to other spectroscopic information. Most of OODR experiments observe change of the population induced by irradiation of two laser fields resonant with two transitions of a three level system. However, if we could control the phase relation between the two laser fields and could detect phase dependent signals, it would give direct information on the phase in the quantum state excited by two phase-controlled coherent radiations. In order to perform this coherent OODR experiment, we are developing a light source system where the difference frequency between two lasers is kept phase-1ocked to a microwave frequency standard.

II-K-1 Direct Observation of the Quantum Phase Induced by Third-order Nonlinear Susceptibility Using Phase-Locked OODR Spectroscopy

Motohiro KUMAGAI *(Tokyo Inst. Tech.)***, Hideto KANAMORI** *(Tokyo Inst. Tech. and IMS)***, Michio MATSUSHITA and Tatsuhisa KATO**

Optical-optical double resonance (OODR) is one of most sophisticated techniques in high-resolution spectroscopy. Two laser radiation makes a coherent quantum state in materials. However, most of OODR experiments have observed only the change in the population among the three levels interacting with the two lasers. If we utilize coherency of the quantum system, we can get direct information on the phase of the quantum state.

We have been developing a phase-locked OODR spectrometer using two CW single mode lasers. All the components of experimental system are schematically shown in Figure 1. The difference frequency of two Titanium-sapphire ring lasers was phase-locked to a tunable MW frequency standard. A hyper-fine structure in the D_2 line of Rubidium atom in a Zeeman cell was coherently excited by these master and slave radiation. The optical beat signal after the interaction with the atoms was detected by a high speed photodiode, and the phase shift from the original optical beat was picked up by a double balanced mixer. Figure 2. shows cosine and sine components of the optical beat signal obtained by the phase sensitive detection. The narrower structures with sub-Doppler width appeared in the upper and lower traces correspond to the imaginary and the real part of the third order nonlinear susceptibility, respectively.

This quantum phase monitoring technique in the frequency domain will be developed further for studies of dephasing process in an excited molecule and phase controlled reaction dynamics.

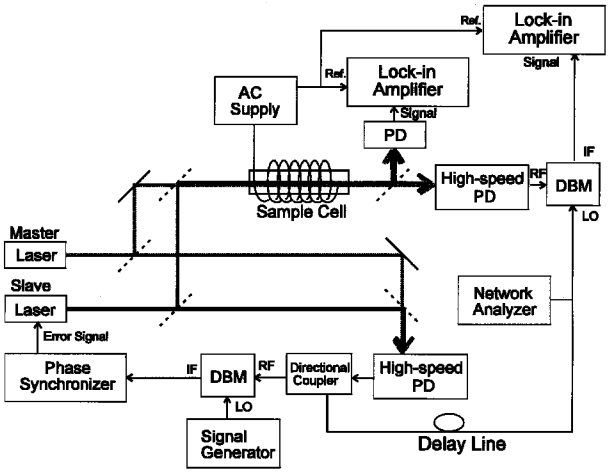

Figure 1. Block diagram of phase-locked OODR spectroscopy system. Zeeman modulation method was used to improve the sensitivity.

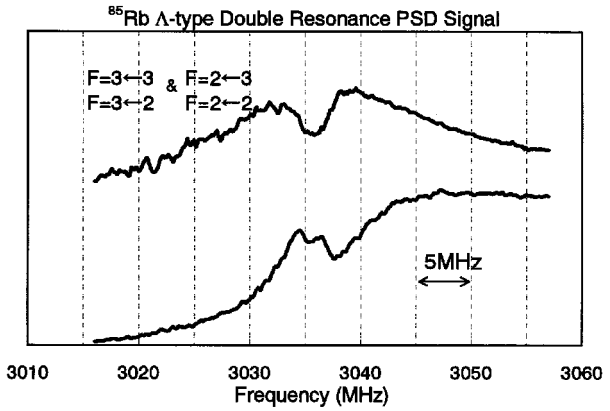

Figure 2. Cosine and sine components of the optical beat obtained by phase sensitive detection of the double resonance spectrum of ^{85}Rb around 3.035 GHz. The upper and lower signals correspond to the imaginary and real parts of the third-order susceptibility, respectively.

RESEARCH ACTIVITIES III
Department of Electronic Structure

III-A States of Molecular Associates in Aqueous Environment

Because of its large dipole moment, smallness of the molecule, and structure making and network formation abilities, water can dissolve various molecules in the liquid state. Although we know phase separation of hydrophobic liquids from aqueous solutions at critical concentrations, it is not so well understood how solute molecules are dissolved in water, particularly at a solute molar fraction in the region of 10^{-2}-10^{-3}. Despite of extreme importance of the study on the intermolecular interaction in the solution, spectroscopic approach for capturing evident structural information has been limited to provide indirect information on the states of molecular associates. In particular, the observation of intermolecular vibrations in solution systems is highly important, although the depolarized Rayleigh wing spectra are normally just broad and give almost structureless feature. The development of theoretical approach and the use of $R(\bar{\nu})$ representation for the Raman spectra has changed this situation drastically. For the development of a new type of spectroscopy by means of synchronized femto (low resolution) and pico(high resolution) multi-beam laser system, our study is now concentrated to finding good molecular systems with interesting and functional molecular association in the aqueous environment.

III-A-1 Low Frequency Raman Spectra of Crystalline and Liquid Acetic Acid and its Mixtures with Water: Is the Liquid Dominated by Hydrogen-Bonded Cyclic Dimers?

Kentaroh KOSUGI *(Grad. Univ. Adv. Stud.)*, **Takakazu NAKABAYASHI and Nobuyuki NISHI**

[*Chem. Phys. Lett.* **291**, 253 (1998)]

Crystalline acetic acid has a melting point at 16.6 ˚C (= 289.8 K). The crystalline structure has a chain form with the C=O oxygen atom doubly coordinated with an O-H hydrogen atom of a neighboring acetic acid and a methyl hydrogen of another molecule. Low frequency Raman spectra of crystalline and liquid acetic acid are presented in the form of the relative scattering activities, $R(\bar{\nu})$ spectra in Figure 1. The crystalline spectrum at 286 K shows five distinctive bands at 48, 78, 91, 122, and 180 cm^{-1}, and at least two weak bands at 30, and 40 cm^{-1}. The 78 and 91 cm^{-1} bands show difference in the polarization. At a specific crystal angle these bands become as strong as other three bands. Upon the melting of the crystal, however, the liquid exhibits conspicuous difference in its appearance. The intensity at lower frequencies increases drastically and a new but weak component appeared at 170 cm^{-1}. However, the main spectral feature is unchanged on the melting: the $R(\bar{\nu})$ spectrum of the liquid shows two strong peaks and a shoulder at wavelengths similar to those of the crystalline bands. The spectral change does not directly support the dominance of the cyclic dimers in the liquid. We attribute the observed and analyzed components to the fragment clusters with structures similar to the parts of the crystalline networks.

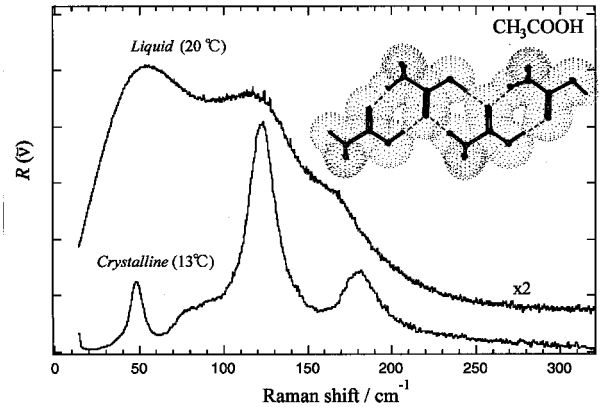

Figure 1. $R(\bar{\nu})$ spectra of crystalline acetic acid at 13 ˚C (bottom) and liquid acetic acid at 20 ˚C (top).

III-A-2 Effects of Intermolecular Hydrogen-Bonding Interactions on Raman Spectra of Crystalline and Liquid Acetic Acid: Ab Initio Molecular Orbital Study

Takakazu NAKABAYASHI, Kentaroh KOSUGI *(Grad. Univ. Adv. Stud.)* **and Nobuyuki NISHI**

Hydrogen bonding molecular crystals usually melt with a heat of fusion fairly smaller than the energy of hydrogen bonding. An ice melts with 25% of a single hydrogen bond energy, while acetic acid melts with 20% of the dimerization energy. This indicates that the liquid maintains large parts of the network structure as clusters, fragments of the chains. We observed the change of the low-wavenumber Raman spectrum of acetic acid on melting and came to assign the peaks to the clusters with structures similar to that of the crystal. In order to confirm this assignment we performed ab initio molecular orbital calculations of intermolecular vibrational wavenumbers and their Raman intensities of various clusters of acetic acid. The calculated low-wavenumber Raman spectra ($R(\bar{\nu})$ representation) for the cluster species at the HF/6-31G(d,p) level are shown

in Figure 1. The observed $R(\bar{\nu})$ spectrum of solid acetic acid is also shown in this figure. Crystalline acetic acid has been shown to have infinite chains, which involve C-H···O as well as O-H···O hydrogen bonds. The intensity pattern in the $R(\bar{\nu})$ spectrum of solid acetic acid is well reproduced by the $R(\bar{\nu})$ spectra calculated for the chain clusters which contain C-H···O and O-H···O hydrogen bonds. The features of the $R(\bar{\nu})$ spectra calculated for the chain clusters are independent of the aggregate size, but are different from the spectrum of the cyclic dimer which contains two O-H···O hydrogen bonds. The melting of the solid leads to a broadening of the $R(\bar{\nu})$ spectrum and an increase in the intensity in the low-wavenumber region (≈ 50 cm^{-1}), however, it does not affect the main peak positions of the $R(\bar{\nu})$ spectrum. These spectral changes are reproduced by the $R(\bar{\nu})$ spectra calculated on the assumption that a variety of chain sizes are produced on the melting of the solid. From the results described above, we conclude that the liquid acetic acid is mainly composed of the chain clusters, not the cyclic dimer, near the temperature of the melting point and at room temperature. On going from the solid to the liquid state, the C=O stretching band (≈ 1670 cm^{-1}) becomes broadened toward the higher-wavenumber side and exhibits an obviously asymmetric shape. This result is attributable to the increase in the number of C=O bonds which are shortened due to weakened hydrogen bonding interactions with the breaking of the chain on the melting. Calculated frequencies of the C=O stretches for the clusters support the above conclusion.

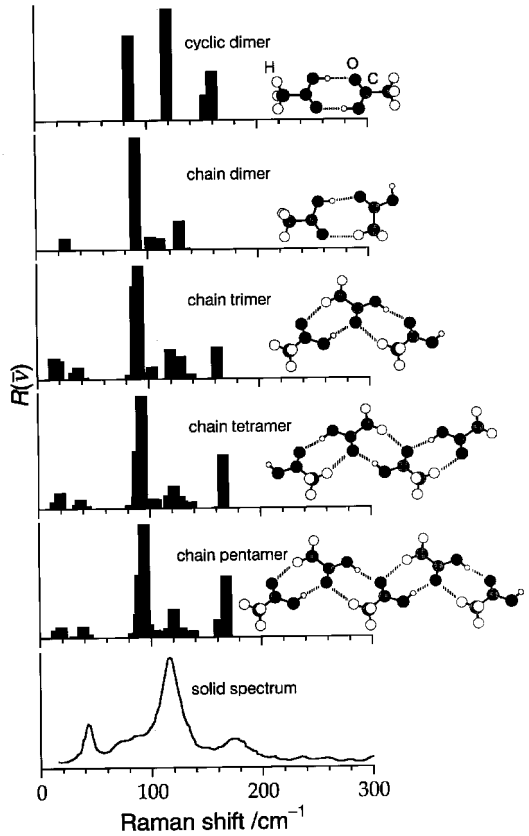

Figure 1. Optimized geometries and $R(\bar{\nu})$ spectra of the cluster species of acetic acid. Observed $R(\bar{\nu})$spectrum of solid acetic acid is shown in the bottom.

III-A-3 States of Acetic Acid and Water Molecules in Aqueous Mixture Studied by Low Frequency Raman Spectroscopy

Kentaroh KOSUGI *(Grad. Univ. Adv. Stud.)*, **Takakazu NAKABAYASHI and Nobuyuki NISHI**

Acetic acid has been believed to form a cyclic dimer with the methyl groups at the both ends even in aqueous solution. From the theoretical point of view, such a cyclic dimer with a negligible dipole moment is hardly stabilized in polar environment. Figure 1 shows the spectral change in $R(\bar{\nu})$ representation of acetic acid-water binary mixtures with varying molar fraction of acetic acid (χ_A). The $R(\bar{\nu})$ spectra at $0 < \chi_A < 0.5$ are found to be reproduced by linear combinations of the spectra at $\chi_A = 0$ and 0.5, indicating that the intermolecular compounds responsible for the Raman signals contain the same structure (or intermolecular bindings) in this concentration range. Interestingly, the $R(\bar{\nu})$ spectrum of acetic acid-methanol mixture with $\chi_A = 0.5$ shows nearly the same spectral shape except for the some intensity extension on the lower energy side and methanol signals around 250 cm^{-1}. This spectral similarity in the two systems strongly suggests that an acetic acid dimer pair or a dimer structure is responsible for the spectra. Intermolecular vibrational frequencies and Raman intensities are calculated by Gaussian 94 at the HF/6-31G(d,p) level. The structure that reproduces the observed Raman spectrum is inserted in Figure 1. The two acetic acids are not equivalent to each other. One C=O is hydrogen-bonded, while the other C=O is free producing a large dipole moment as a dimer. This result is in accord with the spectral change of the intramolecular C=O stretching band on varying the acid concentration. The asymmetric band around 1700 cm^{-1} observed for the mixture with $\chi_A = 0.3$ is decomposed into two components: a narrow band at 1715 cm^{-1} and a broad band with a peak at 1685 cm^{-1} and an extended wing to the lower frequencies. The former component is attributed to non-bonded C=O and the latter to the hydrogen-bonded C=O. Most interestingly, the O-H stretching bands of water exhibit that hydrogen bonds of waters are dissociated with increasing the acid.

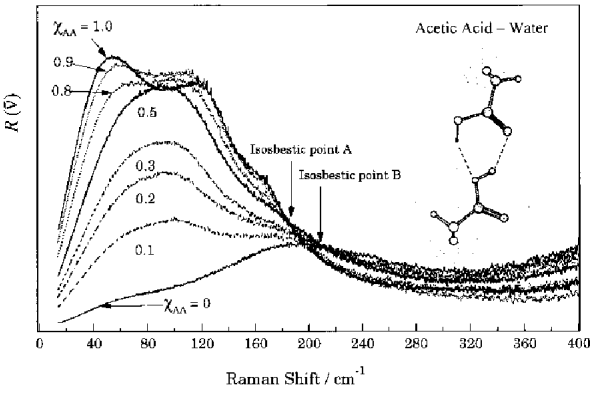

Figure 1. Mixing ratio dependence of the $R(\bar{\nu})$ spectra in acetic acid -water binary system.

III-B Spectroscopic and Dynamical Studies on Charge Delocalization and Charge Transfer in Aromatic Molecular Clusters

Charge transfer processes resulting in dynamical charge delocalization such as consecutive proton or electron hopping in molecular clusters and even in pure liquids are highly interesting in relation to the charge transportation in insulating materials. Not only in aromatic molecular liquids but also in pure water itself electric conductivity is very low when they do not contain impurities of ionic atoms or molecules. We demonstrated that a positive charge in a pure benzene cluster is localized in a dimer unit where the charge resonance (CR) interaction makes the two molecules share an electron forming an intermolecular bond. One of the hot topics in this project is the finding of the charge hopping in vibrationally excited benzene trimer cations. This means the dimer cation core in the trimer is switching, probably periodically concerted with an asymmetric stretching motion of the three benzene molecules.

III-B-1 Vibrational Predissociation Spectroscopy of Phenol-Benzene Dimer Cation

Yoshiya INOKUCHI, Nobuyuki NISHI and James M. LISY *(Univ. Illinois and IMS)*

Vibrational predissociation spectroscopy is one of the most powerful methods to investigate geometric structures of cluster ions. In a hetero-dimer cation of (phenol-benzene)$^+$, the charge is expected to be localized on the phenol site. Then, the hydrogen atom of the hydroxyl group is thought to be coordinated with the π-electron cloud of the neutral benzene. In order to examine this situation, we have measured a vibrational predissociation spectrum of (phenol-benzene)$^+$ in the region of 2900-3500 cm^{-1}. The experiment is done by using a tandem mass spectrometer, which consists of two quadrupole mass analyzers. Mass-selected ions of (phenol-benzene)$^+$ are irradiated with an IR output of a commercial OPO laser. The photoexcited dimer cation immediately dissociates into a cation and a neutral. Resultant fragment phenol ions are mass-analyzed and detected by an MSP. Thus, the vibrational predissociation spectrum of the dimer cation is obtained from the yields of the fragment ions with varying the excitation laser wavenumber.

A photodissociation study of (phenol-benzene)$^+$ in the 750-1250 nm region already showed that the positive charge is localized on the phenol site. Such an electronic spectrum, however, cannot provide detailed information on the structure of cluster ions. Figure 1 shows a vibrational predissociation spectrum of (phenol-benzene)$^+$. The spectrum shows a single peak at 3239 cm^{-1} and the apparent width of 67 cm^{-1} (FWHM). The peak can be attributed to the OH stretching vibration of (phenol-benzene)$^+$. The reported OH stretching frequency of a bare phenol ion is 3534 cm^{-1}. The observed OH stretching frequency of the dimer cation shows a 295-cm^{-1} red-shift from that of the bare phenol ion. The red shift indicates that the hydrogen atom of the hydroxyl group is coordinated with the π-electrons of the benzene. Such a π-hydrogen bonding is known in benzene-water or benzene - methanol neutral clusters. The present result disagrees with the spectrum reported by Mikami and co-workers. In their spectrum, a peak emerges at 3060 cm^{-1} with a width of approximately 120 cm^{-1} (FWHM), almost twice as large as the present observation. The difference in the spectra is thought to be originated from the difference of the temperature of the cluster ions. Now we are investigating such a large temperature effect on the structure of the cations.

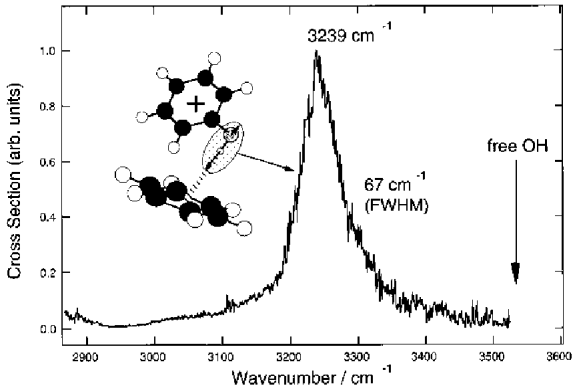

Figure 1. Vibrational predissociation spectrum of (benzene-phenol)$^+$.

III-B-2 Electronic Structure of Solvent Benzene in (Phenol-Benzene)$^+$

Yoshiya INOKUCHI, Nobuyuki NISHI and James M. LISY *(Univ. Illinois and IMS)*

Presence of a π-hydrogen bond in (phenol-benzene)$^+$ is expected to perturb the electronic structure of benzene chromophore. The electronic structure of solvent benzene in (phenol-benzene)$^+$ has been investigated by photodissociation spectroscopy in the region of 23500-40650 cm^{-1} where the electronic transitions of neutral benzene and cationic phenol are expected to appear.

First in order to find the absorption bands of phenol ion chromophore, the electronic spectrum of (phenol-water)$^+$ was observed by the photodissociation method. In this cluster, the charge is localized on phenol. Thus, we assumed that the observed electronic spectrum is characteristic of the phenol cation. The phenol cation spectrum is subtracted from the photodissociation spectrum of (phenol-benzene)$^+$. Figure 1 shows the subtracted spectrum, which is regarded as an electronic spectrum of benzene site in (phenol-benzene)$^+$. This absorption band is ascribed to the $\pi^* \leftarrow \pi$ transition of the benzene site. The $\pi^* \leftarrow \pi$ transition of the benzene site in (phenol-benzene)$^+$ is approximately 1600-cm^{-1} red-shifted from that of the neutral benzene. Such a

large red-shift of the $\pi^* \leftarrow \pi$ transition could be an evidence that the π-orbitals of the benzene are perturbed so much because of the π-hydrogen bonding. In Figure 1, an absorption spectrum of benzene vapor is also shown for comparison with the positional shift by 1600 cm^{-1} to the red from the original position. From the comparison of these spectra, one can find that the vibrational sequence in the cluster spectrum is almost the same as that of benzene vapor spectrum, except for the band at 36470 cm^{-1}. On the basis of the spacing corresponding to the ν_6 and ν_1 vibrations, this band is attributed to the 0-0 band of the $\pi^* \leftarrow \pi$ transition. In a benzene-water neutral dimer with a π-hydrogen bond, the 0-0 band is not observed because the sixfold symmetry of benzene is kept due to the free rotation of the water molecule along the sixfold axis. In (phenol-benzene)$^+$, therefore, the interaction between the positive charge on the aromatic ring of phenol ion and the π-electrons of neutral benzene may fix the intermolecular configuration, strongly breaking the sixfold symmetry.

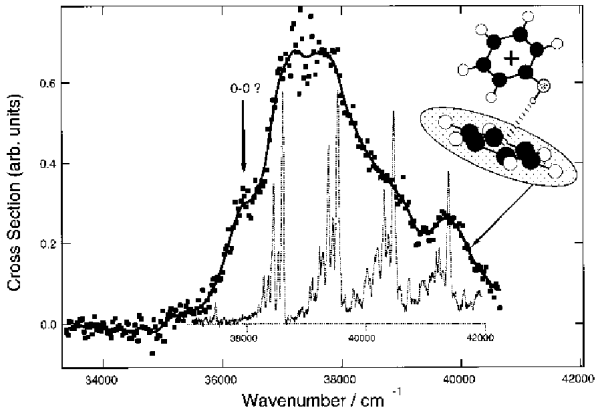

Figure 1. Electronic spectrum of the benzene chromophore in (phenol-benzene)$^+$ and absorption spectrum of benzene vapor (dotted curve).

III-B-3 Photodissociation Dynamics of $(C_6H_6)_3^+$: Role of the Extra Benzene Molecule Weakly Bound to the Dimer Core

Kazuhiko OHASHI *(Kyushu Univ. and IMS)* **and Nobuyuki NISHI**

[*J. Chem. Phys.* in press]

Benzene trimer ion has a charge-localized structure, $(C_6H_6)_2^+\cdots C_6H_6$, where $(C_6H_6)_2^+$ is the dimer core. The trimer ion is photodissociated by excitation of the charge resonance transition of the dimer core. Branching ratios and translational energies of the product ions, $(C_6H_6)_2^+$ and $C_6H_6^+$, are measured as functions of photon energies ($h\nu$ = 0.99-1.80 eV). At the lowest photon energy studied, the dominant dissociation channel is the formation of $(C_6H_6)_2^+$ and C_6H_6. In this process, only a small fraction (7-8 %) of the available energy is partitioned into the translational energy of the products. The branching ratio of the $(C_6H_6)_2^+$ product decreases smoothly with increasing photon energy from 0.90 at $h\nu$ = 0.99 eV to 0.04 at 1.80 eV. The behavior is consistent with the following two-step model for the formation of $C_6H_6^+$. The photo-excited $(C_6H_6)_3^+$ ion first ejects one C_6H_6 molecule, yielding the transient dimer ion. If the dimer ion has sufficient internal energy, it further dissociates into $C_6H_6^+$ and C_6H_6. Statistical theories for unimolecular reactions are applied to predict the translational energies and the branching ratios. A comparison of the theoretical branching ratios with the experimental data suggests that a part (30-35%) of the product internal energy is distributed to the intramolecular vibrations of the extra C_6H_6 molecule. As far as the energy partitioning is concerned, the extra C_6H_6 molecule is no longer a spectator.

III-B-4 Photodissociation Spectroscopy of $(Benzene\text{-}Toluene)^+$. Charge Delocalization in the Hetero-Dimer Ion

Kazuhiko OHASHI *(Kyushu Univ. and IMS)*, **Youko NAKANE** *(Kyushu Univ.)*, **Yoshiya INOKUCHI, Yasuhiro NAKAI** *(Kyushu Univ.)* **and Nobuyuki NISHI**

[*Chem. Phys.* in press]

The electronic spectrum of the benzene-toluene hetero-dimer ion is measured in the 380-1400 nm region. The spectrum shows intense bands around 1175 and 670 nm and a weaker band around 920 nm, which correspond to charge resonance (CR) bands of homo-dimer ions. The observation indicates that the positive charge stays on the benzene part in some probability, although the ionization potential of benzene is 0.4162 eV higher than that of toluene. A local excitation (LE) band is observed around 420 nm, where a $\pi \leftarrow \pi$ transition is locally excited in the charged benzene or toluene molecule. On the basis of the positions of the CR-like bands as well as the intensity of the LE band relative to that of homo-dimer ions, the probability of finding the charge on the benzene molecule is analyzed to be approximately 36 %.

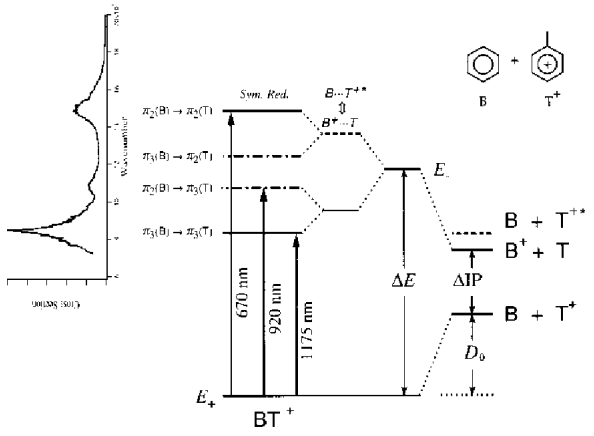

Figure 1. Energy level diagram for analyzing near-resonance interactions in BT^+. The $B^+ + T$ dissociation limit is located above the $B + T^+$ limit by ΔIP (0.4162 eV). The dissociation energy of BT^+ into $B + T^+$ is determined to be D_0 = 0.53 eV. Near-resonance interaction between $B\cdots T^*$ and $B^*\cdots T$ locates the hypothetical excited state 0.53 eV (= D_0) above the $B^+ + T$ limit. Near-resonance interaction between $B^+\cdots T$ and

$B\cdots T^{+}$*(a LE state correlating to the $B + T^{+}$* limit) makes the energy gap of the two excited states much wider. Each of the two states further splits into two levels due to the lift of the degeneracy (symmetry reduction) of $\pi_2(B)$ and $\pi_3(B)$. Although the energy difference (0.11 eV) between $B^+ + T$ and $B + T^{+}$* is neglected, the transition energy from the ground state to the hypothetical excited state ($\Delta E = 2D_0 + \Delta IP = 1.48$ eV) is in good agreement with the average (1.45 eV) of the transition energies observed for the 1175 and 670 nm bands. Main configurational changes of the SOMO electron upon the four types of excitations are also shown on the left side with the observed spectrum.

III-B-5 Photodissociation Spectrum of Cyanobenzene Dimer Cation. Absence of Intermolecular Resonance Interaction

Kazuhiko OHASHI *(Kyushu Univ. and IMS)*, **Masaharu NISHIGUCHI** *(Kyushu Univ. and IMS)*, **Yoshiya INOKUCHI, Hiroshi SEKIYA** *(Kyushu Univ.)* **and Nobuyuki NISHI**

[*Res. Chem. Intermed.* **24**, 755(1998)]

Electronic spectra of a homo-molecular dimer cation, $(C_6H_5CN)_2^+$, are measured by photodissociation spectroscopy in the gas phase. Broad feature appeared in the 450-650 nm region are characteristic of $\pi_3 \rightarrow \pi_{CN}$ transition of the $C_6H_5CN^+$ chromophore. No intense band is observed in the 650-1300 nm region, where other aromatic dimer cations show charge resonance bands. Two component molecules of $(C_6H_5CN)_2^+$ cannot take a parallel sandwich configuration suitable for the resonance interaction, because of geometrical constraints due to other stronger interactions.

III-C Ultrafast Dynamics of Photoexcited Molecules by Transient Absorption Spectroscopy

Ultrafast transient absorption spectroscopy is now an universal and popular method for the study of reaction pathways induced by electronic excitation of organic or metal complex molecules. Although we are going to introduce a new femto-pico synchronized multi-laser beam system in the coming spring, we have improved the specification of the old style dye amplifier system that will take a role of a complementary equipment particularly for the use of strong subpicosecond light source around 300 nm. This system is used for collaborative studies with organic chemists.

III-C-1 Construction of a Subpicosecond Time-Resolved Absorption Spectrometer Using a Dye Amplifier

Takakazu NAKABAYASHI and Nobuyuki NISHI

Although Ti:sapphire laser systems are widely used as ultrafast light sources, dye laser systems remain attractive sources because a tunable visible light with a high pulse energy cannot be easily obtained by using Ti:sapphire lasers at the present stage of development. We have thus constructed a subpicosecond time-resolved absorption system using an amplified dye laser, to the experiments for which visible light pulses are needed. A beam from a frequency-doubled cw mode-locked Nd:YAG laser is used to excite a synchronously pumped, hybridly mode-locked dye laser. Light pulses with 800 fs duration and 1 nJ pulse energies are obtained at a repetition rate of 76 MHz. The laser wavelength is tunable between 560 and 670 nm. Pulses from the dye laser pass through a dye amplifier, and amplified pulses with pulse energies of 1 mJ are obtained at a repetition rate of 10 Hz. The dye amplifier is excited by the second harmonic output from a pulsed Nd:YAG regenerative amplifier. The second-harmonic output of the dye amplifier is used as a pump beam, and the visible radiation that remained unconverted is focused into a cell containing water to generate a white light continuum. The generated continuum is split into two parts, one for a probe beam and the other for a reference. After passing through fixed (for the pump beam) and variable (for the probe beam) optical delay lines, the pump and probe beams are focused onto the sample cell. The continuum light intensities are detected by multichannel photodiodes and collected at a 10 Hz repetition rate synchronized with the light source. Time-resolved absorption spectra of some polyatomic molecules have been observed by using this spectrometer.

III-C-2 Time-Resolved Absorption Studies on Photochromism of 2H-Chromene Derivatives

Yoichi KODAMA *(Univ. Tsukuba and IMS)*, **Takakazu NAKABAYASHI, Nobuyuki NISHI and Hirochika SAKURAGI** *(Univ. Tsukuba)*

Spiropyrans being one of the most typical photochromic compounds have been extensively studied because they have potentially important applications as optoelectronic devices. Since these structures are too large to be analyzed quantitatively, little is known about reaction pathways in the photochromism of spiropyrans. We have therefore studied photoexcitation dynamics of 2H-chromenes (benzopyrans), which are simplified models of spiropyrans, by femto to microsecond time-resolved absorption spectroscopy. Figure 1 shows transient absorption changes of 2,4-diphenylchromene in various time regions. The transient absorption spectrum of 2,4-diphenylchromene (closed form) exhibit peaks at 390, 410, and 470 nm, all of which are attributed to the open form. The open form is shown to form within 2 ps and return to the closed form on the microsecond timescale. Four relaxation processes are observed with a time constant of 20 ps, 200 ps, 700 ns, and 50 μs, respectively. They are attributed to

vibrational relaxation (20 ps) and the lifetimes of three dynamically distinct open isomers (200 ps, 700 ns, 50 μs). The reaction mechanism describing the photochromism of 2H-chromenes is discussed on the basis of the observed results.

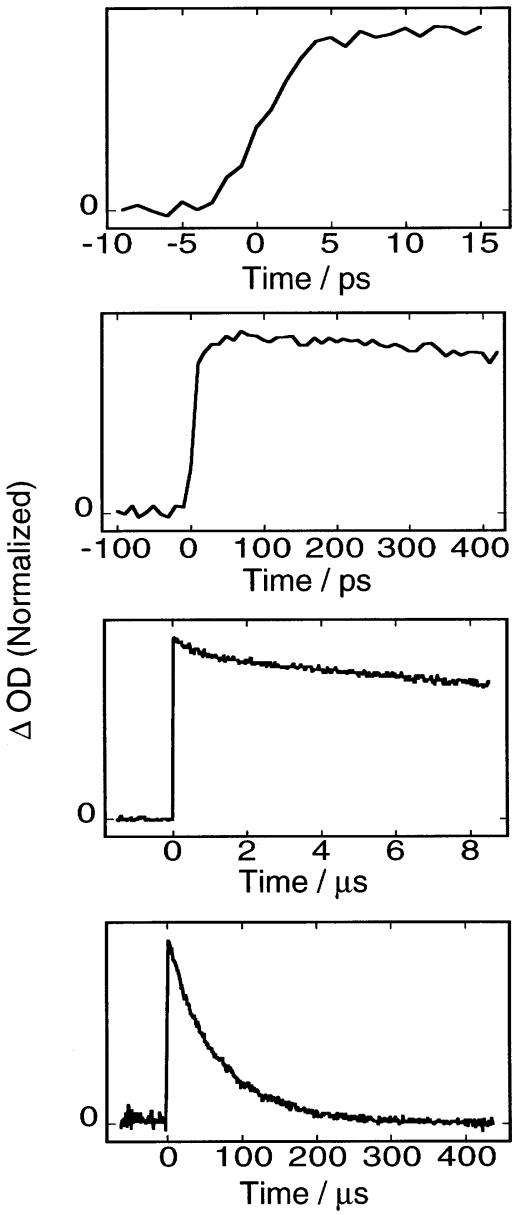

Figure 1. Transient absorption signals obtained from 2,4-diphenylchromene in cyclohexane in various time regions (probe, 400 nm).

III-D Photochemistry on Well-Defined Surfaces

Upon the irradiation of light in the wavelength range from visible to ultraviolet, a number of adsorbed molecules on metal surfaces reveal variety of photochemical processes, including photo-stimulated desorption, rearrangement of adsorbed states, photodissociation, and photo-initiated reactions with coadsorbates. A central and fundamental question in the surface photochemistry is to clarify how adsorbate-substrate systems are excited by photon irradiation. In addition, since photo-initiated reactions can be induced without any thermal activation of reactants, they may provide good opportunities for studying a new class of surface reactions which may not be induced thermally. We have studied photochemistry of various adsorption systems on well-defined metal and semiconductor surfaces mainly by temperature-programmed desorption (TPD), x-ray photoelectron spectroscopy (XPS), work function measurements, near edge x-ray absorption fine structure (NEXAFS) and angular-resolved time-of-flight (TOF) spectroscopy of photodesorbed species associated with pulsed laser irradiation. We have shown that methane weakly adsorbed on Pt(111) and Pd(111) is dissociated or desorbed by irradiation of 6.4-eV photons, which is far below the excitation energy for the first optically allowed transition of methane in the gas phase. In this year, we have started extensive investigations of photodesorption of rare gas atoms from semiconductor surfaces. This

physisorption system is very similar to methane on the transition metal surfaces in a sense that the photo-induced processes take place at the wavelengths where there is no absorption band in the gas phase.

III-D-1 Photodesorption of Xe Adsorbed on Clean and Oxidized Si(100) Surfaces

Kazuya WATANABE and Yoshiyasu MATSUMOTO

Rare gas weakly adsorbs on solid surfaces. The ionization potential is larger than typical polyatomic molecules and the first electronic excited state is also located at higher energy. Its electron affinity is negative. Thus, no photo-induced processes are expected under the irradiation of photon whose energy less than 6 eV. However, we have observed for the first time that Xe weakly adsorbed on clean and oxidized Si(100) surfaces is desorbed by the irradiation of photon with the energy ranging from 1.2 to 6.4 eV. Xe is adsorbed on the surfaces at 50 K. UV and visible photons are irradiated onto the surfaces. Post-irradiation TPD is observed as a function of irradiated photon numbers. The area of TPD peaks decreases with increase of the number of photons, indicating the coverage of Xe is reduced by the photon irradiation. Figure 1 shows that the TOF distributions of Xe photodesorbed by 6.4-eV photons. Thus, it is clear that Xe is desorbed by the photon irradiation. The TOF distribution of Xe from the clean Si(100) surface is well represented by Maxwell-Boltzmann distribution with a mean kinetic energy of 0.06 eV. On the other hand, the TOF distribution from the oxidized Si(100) surface shows multiple velocity components with mean kinetic energies of 0.8 eV and 0.3 eV. Those TOF distributions do not show any significant dependence on laser wavelength and fluence. Since Xe is weakly adsorbed on the surfaces, thermal heating by substrate photon absorption may induce desorption. However, the observed mean kinetic energies are all higher than the temperature attainable by the photon irradiation. Furthermore, if the thermal heating is a true origin of the desorption, the TOF distribution should depend on the laser fluence. However, the observed results are not consistent with these expectations. Thus, the Xe desorption from these surfaces are not simply induced by thermal heating by photon irradiation. In order to clarify the excitation mechanism, we will measure more carefully the wavelength dependence of effective cross sections and TOF distributions.

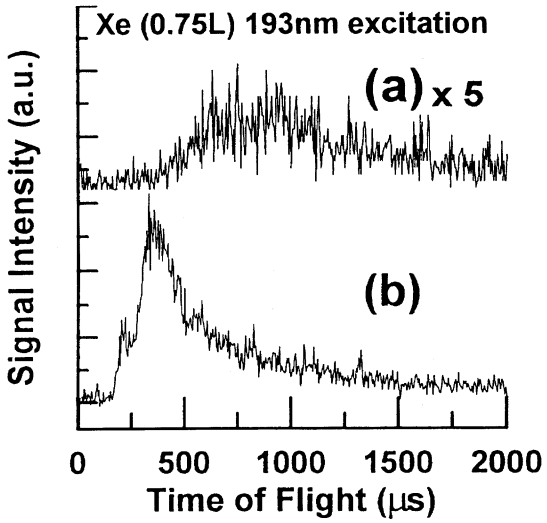

Figure 1. Time-of-flight distributions of Xe desorbed from (a) a clean Si(100) and (b) an oxidized Si(100). The surfaces are irradiated by 6.4 eV (193 nm) excimer laser pulses.

III-E Photochemistry of Adsorbates on Thin Films and Clusters of Metals

An isolated atom has a set of discrete energy levels. On the other hand, as a result of mutual interactions of atoms, the electronic structure of a bulk solid is composed of a set of energy bands. Ultra-thin films and microclusters provide a unique opportunity for studying how the electronic structure changes from one to the other. In such nano-structured materials electronic levels are still discrete and photo-induced energetic electrons likely show ballistic motions rather than stochastic ones. Thus, they may show unique electronic properties and chemical reactivities. We have concentrated on how molecules interact with bulk metal surfaces and how they are excited by photons as described in the previous section. From this year we have started a project to study how the electronic properties and reactivities depend on the size and thickness of the spatially confined systems; these are more relevant to real world chemistry, i.e. catalysis.

III-E-1 Photochemistry of Methane adsorbed on Pd/Al_2O_3 Model Catalysts

Kazuo WATANABE, Margarethe KAMPLING *(Fritz-Haber-Institut der Max-Planck-Gesellschaft)***, Katharina AL-SHAMERY** *(Fritz-Haber-Institut der Max-Planck-Gesellschaft)***, Hans-Jochaim FREUND** *(Fritz-Haber-Institut der Max-Planck-Gesellschaft)* **and Yoshiyasu MATSUMOTO**

Conversion of methane into useful chemical reagents has been extensively studied for several decades owing to the increasing industrial and environmental importance. However, methane is the most stable hydrocarbon and the previous efforts to break the methane C-H bond thermally have not necessary been successful regarding the efficiency and costs even with sophisticated catalysts. Recently, we have discovered that methane physisorbed on Pt(111) and Pd(111) surfaces is photodissociated into methyl

and hydrogen by 193-nm (6.4 eV) ArF excimer laser irradiation despite gaseous methane is transparent at this wavelength.[1)] The electronic interaction between methane and metal surfaces in the unoccupied states plays an important role in this photoexcitation. To further investigate the mechanism of this new photochemistry, we study adsorption states and photoreactions of methane adsorbed on Pd clusters deposited on thin Al_2O_3 films on a NiAl(110) substrate. Depending on the size and the structure of Pd-clusters, the strength of interaction between methane and Pd-clusters changes significantly, and consequently the photoreaction cross section and the branching ratios of reaction (photodissociation/photodesorption) change dramatically.

Reference

1) Y.Matsumoto, Y.A.Gruzdkov, K.Watanabe and K.Sawabe, *J. Chem. Phys.* **105**, 4775 (1996).

III-F Reaction Dynamics on Well-Defined Surfaces

Vast majority of surface reactions studied so far has been interpreted in terms of a Langmuir-Hinshelwood mechanism; reactants are first adsorbed on a surface and a reaction takes place between two chemisorbed species. Although reactants are in equilibrium with surface atoms, the energetics of desorbed products are determined by potential energy surfaces along reaction coordinates. In particular, associative desorption, which is often a reversed process of activated dissociative chemisorption, shows interesting features manifested by a potential barrier near the exit channel. In this year, we have made an extensive study of CO_2 conversion to carbonate on Si(100) coadsorbed with N_2O and O_2.

III-F-1 Effective Conversion of CO_2 to Carbonate in Surface Oxidation Processes at Si(100)

Kazuya WATANABE, Hiroyuki KATO *(Grad.Univ. Adv. Stud.)* **and Yoshiyasu MATSUMOTO**

[*J. Phys. Chem.* in press]

It is found that effective carbonate formation occurs at a clean Si(100) surface between CO_2 and surface oxidants: N_2O and O_2. The reactions of CO_2 with N_2O or O_2 are studied by temperature-programmed desorption and X-ray photoelectron spectroscopy. CO_2 physisorbed on Si(100) desorbs exclusively at (75 K. However, when CO_2 is coadsorbed with N_2O or O_2, CO_2 is converted very effectively into surface carbonate species below 140 K. The carbonate species are dissociated to produce desorbed species of CO or CO_2 in the temperature range of 200-600 K. By using $C^{18}O_2$, it is confirmed that the carbonate is composed of the adsorbate CO_2 and one oxygen atom from the surface oxidant. In the case of N_2O/CO_2 coadsorption, the carbonate formation is mainly induced by thermal dissociation of N_2O adsorbates. In the case of O_2/CO_2 coadsorption, the carbonate formation is not only induced by dissociative chemisorption of O_2, but also proceeded with chemisorbed dioxygen that likely adsorbs in a peroxy bridging configuration.

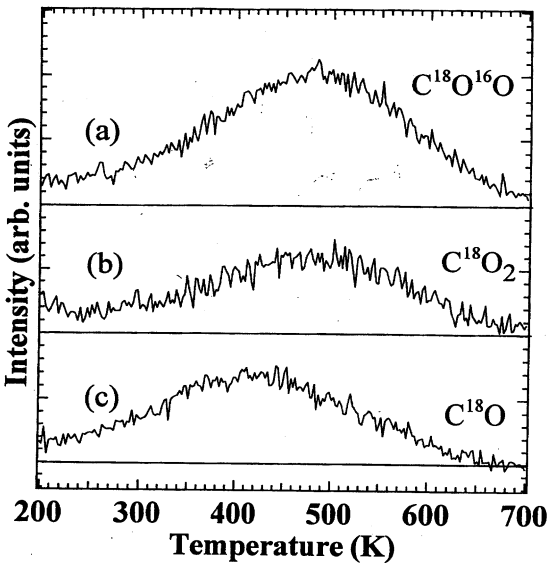

Figure 1. TPD results measured at (a) m/e=46 ($C^{18}O^{16}O$), (b) m/e=48 ($C^{18}O_2$), and (c) m/e=30 ($C^{18}O$) taken from Si(100) exposed to CO_2 (0.4 L) and O_2 (1.0 L). The surface was first exposed to CO_2 and then to O_2. The heating rate was 4.0 K/s.

III-G Dynamical Behavior of Electronically Excited States

Understanding the dynamics of photoexcited dye molecules in solution, such as the intra- and intermolecular vibrational energy relaxation, solvation dynamics and electron transfer reaction, has been an area of intense research in recent years. If the excited molecules have an excess vibrational energy, vibrational relaxation should affect the spectral evolution of the solvation dynamics within a few picosecond time scale. We investigated the internal conversion (IC) and intramolecular vibrational energy redistribution process (IVR) of coumarin 481 (C481) in solutions with a large excess energy in order to reveal how the vibrational relaxation is coupled to the solvation process.

III-G-1 Ultrafast Relaxation Processes from a Higher Electronically Excited State of a Dye Molecule in Solution: A Femtosecond Time-Resolved Fluorescence Study

Kaoru OHTA *(Kyoto Univ. and IMS)*, **Tai Jong KANG** *(Taegu Univ. and IMS)*, **Keisuke TOMINAGA and Keitaro YOSHIHARA** *(JAIST)*

[*Chem. Phys.* submitted]

We have investigated the internal conversion, intramolecular energy redistribution, and vibrational cooling of coumarin 481 in cyclohexane after the photoexcitation by a third harmonic of the Ti:Sapphire laser (267 nm). Following the photoexcitation to a higher electronic state, we observe the fluorescence up-conversion signals at several wavelengths. The experimental results show that the fluorescence signals rise with time constants of 220-280 fs at all the wavelengths, and these is no drastic change of the spectral shape within a few picoseconds. These suggest that the observed dynamics are mainly due to the internal conversion from the S_n to S_1 state and the intramolecular energy redistribution takes place much faster than the former process. We also perform the model calculation of the fluorescence spectrum by assuming three Franck-Condon active modes to obtain information on the relaxation process. A spectral change due to vibrational cooling is observed in a time scale of 10 ps, which is simulated quite well in terms of the thermal diffusion equation.

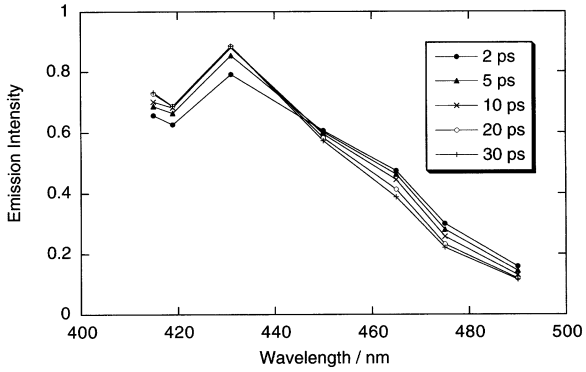

Figure 1. Time-resolved fluorescence spectrum of coumarin 481 excited at 267 nm in cyclohexane.

III-H Spectroscopy and Dynamics of Vibrationally Excited Molecules and Clusters

This research group, which started in April 1997, is planning to study spectroscopy and dynamics of molecules and clusters in higher vibrational state by two-color double resonance spectroscopy. New spectroscopic methods will also be developed to observe the higher vibrational state under collision-free condition.

III-H-1 Nonresonant Ionization Detected IR Spectrum of Jet-Cooled Phenol — Ionization Mechanism and Its Application to Overtone Spectroscopy

Shun-ichi ISHIUCHI *(Grad. School. Waseda Univ.)*, **Hiroshi SHITOMI** *(Grad. School Waseda Univ.)*, **Ken TAKAZAWA** *(National Research Institute for Metals)* **and Masaaki FUJII**

[*Chem. Phys. Lett.* **283**, 243 (1998)]

Vibrational transitions of jet-cooled phenol have been detected by nonresonant two-photon ionization due to UV laser from 3400 cm^{-1} to 14000 cm^{-1}. The UV frequency dependence of IR-UV double resonance signals is used for discussion on the mechanism of ionization. The spectrum shows a well-resolved structure due to the first to the fourth quantum of OH stretching vibrations, CH overtones and various combination vibrations. The vibrational frequency, anharmonisity and the dissociation energy of the OH stretching mode has been measured. The bandwidth of the OH overtone is found to decrease with increase in the vibrational quantum number.

III-H-2 Structure of 1-Naphthol-Water Clusters Studied by IR Dip Spectroscopy and Ab Initio Molecular Orbital Calculation

Ruriko YOSHINO *(Grad. School. Waseda Univ.)*, **Kenro HASHIMOTO** *(Tokyo Metropolitan Univ.)*, **Takuichiro OMI** *(Grad. School. Waseda Univ.)*, **Shun-ichi ISHIUCHI** *(Grad. Univ. Adv. Stud.)* **and Masaaki FUJII**

[*J. Phys. Chem. A* **102**, 6227-6233 (1998)]

IR spectrum of cis-1-naphthol, trans-1-naphthol, and 1-naphthol·$(H_2O)_n$ (n = 1-3) clusters has been measured by the IR dip spectroscopy in a supersonic jet. The spectra show clear vibrational structures of the monomers and the clusters in the energy region from 3000 cm^{-1} to 3800 cm^{-1}. Observed vibrational transitions are assigned to the OH stretching vibrations of 1-naphthol and waters in the clusters. The size dependence of the IR bands and the cluster geometries are analyzed by using the ab initio MO method at MP2/6-31G level. From the comparison between the observed and calculated IR spectra, we have concluded that the 1-naphthol acts as the proton donor and a cyclic hydrogen-bond network is formed in the n = 2 and 3 clusters.

III-I Large Amplitude Motion in Molecular Cation Studied by Pulsed Field Ionization - Zero Kinetic Energy Photoelectron Spectroscopy

Large amplitude motion is important subject in spectroscopy, and is a fundamental model to understand nonrigid motion in biological systems and that in chemical reaction. In this project, large amplitude motion, such as internal rotation, intermolecular vibration in cation radicals will be observed by using PFI-ZEKE photoelectron spectroscopy, and its change by ionization will be discussed.

III-I-1 Internal Rotation of Methyl Group in Tolunitrile Cations Studied by Pulsed Field Ionization - Zero Kinetic Energy Spectroscopy

Kazunari SUZUKI *(Grad. School Waseda Univ.)*, **Keigo YOSHIDA** *(Grad. School Waseda Univ.)*, **Yuji EMURA** *(Grad. School Waseda Univ.)*, **Hideyuki IKOMA** *(Grad. School Waseda Univ.)* **and Masaaki FUJII**

Pulsed Field Ionization-Zero Kinetic Energy (PFI-ZEKE) photoelectron spectroscopy has been applied to *o*-, *m*- and *p*- tolunitrile in a supersonic jet. The PFI-ZEKE spectra of *m*- and *p*-tolunitrile show well-resolved structure due to internal rotation of the methyl group in the corresponding cations. Level energies and transition intensities were reproduced by a one-dimensional rotor model with a free-rotor basis set, and the potential curves of the internal rotation in the cations have been determined. Analysis for *m*- and *p*-tolunitrile shows a slight increase of the barrier height for internal rotational motion from the neutral to the corresponding cation. On the other hand, no internal rotational bands was found in the PFI-ZEKE spectrum of *o*-tolunitrile. It suggests that ionization does not cause the significant change of the barrier height for the internal rotation in *o*-tolunitrile. This tendency is largely different from other toluene derivatives, such as toluidine,[1)] which shows the drastic increase of the internal rotational barrier after ionization. The substituent effect on the internal rotational motion has been discussed.

Reference

1) H. IKOMA, K. TAKAZAWA, Y. EMURA, S. IKEDA, H. ABE, H. HAYASHI and M. FUJII, *J. Chem. Phys.* **105**, 10201 (1996).

III-J Laser Investigation of Molecular Photodissociation Dynamics

Detailed studies on photodissociation dynamics provides the basis for understanding molecular photochemistry and bimolecular reactions (full collisions). This project aims at, (1) the development of new experimental techniques to obtain complete information on quantum state distributions of reaction products, and (2) the elucidation of complex dissociation dynamics of polyatomic molecules. Lasers with high intensity, good monochromaticity, and well-defined polarization provide extremely sensitive detection methods of reaction products with the capability of examining their scalar (e.g. energy) and vector (e.g. linear and angular momenta) quantities. The extensive use of laser-based techniques is the key for the elucidation of complicated dynamics. Our major effort have been directed to the development of two and three dimensional imaging techniques to visualize the scattering of atoms and molecules and also the development of theoretical treatment of vector correlation observed in imaging. By coupling the laser and imaging techniques, differential cross section can be measured with complete internal state selection.

III-J-1 Quantal and Semiclassical Analysis of Vector Correlation in Molecular Photodissociation

Yuxiang MO and Toshinori SUZUKI

[*J. Chem. Phys.* **108**, 6780 (1998)]

General semiclassical expressions for state multipoles and multipole moments have been obtained by the correspondence principle. The expression derived for low-rank multipole moments is identical with that obtained by comparing quantal and classical formulae for one- and two-photon absorption intensity of diatomic molecules. [D. A. Case, G. M. McClelland and D. R. Herschbach, *Mol. Phys.* **35**, 541 (1978)]. For molecular photodissociation, *quantal* expressions for multipole moments have been obtained by formal expansion of the density matrix by the state multipoles of fragment angular momentum both in the *velocity-fixed* (*VF*) and the *transition dipole moment fixed* (μF) frames. The formulae derived in the two frames were proved to be equivalent. Semiclassical formulae have been also obtained in *VF* and μF frames by approximating the quantal multipole moments with the *semiclassical expressions*. The expression thus obtained in the μF frame is in agreement with that reported by Dixon [*J. Chem. Phys.* **85**, 1866 (1986)].

III-J-2 Geometrical Factors of Two-Photon Absorption for the Determination of Alignment and Orientation

Yuxiang MO and Toshinori SUZUKI

[*J. Chem. Phys.* **109**, 4691 (1998)]

It is shown that the relative ratios of geometrical factors in two-photon transition are invariant to the character of the virtual states and are expressed by a simple formula for both linearly and circularly polarized light. The recognition of this simple relation would much simplify the analysis of polarization dependence of signal intensity observed.

III-J-3 Probing alignment of NO($X^2\Pi$) by [2+1] REMPI via C $^2\Pi$ state: A Test of Semiclassical Theory in 355 nm Photodissociation of NO_2

Yuxiang MO, Hideki KATAYANAGI and Toshinori SUZUKI

[*J. Chem. Phys.* in press]

A theoretical method is presented to analyze 2D and 3D imaging data of photofragments with polarized angular momentum. The theory is critically tested by comparison with the experimental data on NO from 355 nm photodissociation of NO_2. The alignment of NO($X^2\Pi$) is detected by [2+1] resonance-enhanced multiphoton ionization (REMPI) via the C $^2\Pi$ state. The angular momentum polarization of NO is described by semiclassical multipole moments expressed by vector correlation in the *velocity-fixed* frame. The geometrical factors for two-photon absorption, P_k, are derived rigorously for the intermediate coupling between Hund's cases (a) and (b), however, it is also shown that the factors for large angular momenta are independent of the coupling case and approximated by simple formulae. Excellent agreement of simulation with the experimental data proves the validity of the theory.

III-J-4 Non-Adiabatic Bending Dissociation in 16 Valence Electron System OCS

Toshinori SUZUKI, Hideki KATAYANAGI, Shinkoh NANBU and Mutsumi AOYAGI

[*J. Chem. Phys.* **109**, 5778 (1998)]

The speed, angular and alignment distributions of S($^1D_2$) atoms from the ultraviolet photodissociation of OCS has been measured by a photofragment imaging technique. From the excitation wavelength dependence of the scattering distribution of S($^1D_2$), the excited states accessed by photoabsorption were assigned to the A' Renner-Teller component of the $^1\Delta$ and the A"($^1\Sigma^-$) states. It was found that the dissociation from the A' state gives rise to high and low-speed fragments, while the A" state only provides the high-speed fragment. In order to elucidate the dissociation dynamics, in particular the bimodal speed distribution of S atoms, two-dimensional potential energy surfaces of OCS were calculated for the C-S stretch and bending coordinates by ab initio method (MCSCF/SDCI/DZP). Conical intersections of $^1\Delta$ and $^1\Sigma^-$ with $^1\Pi$ were found as adiabatic dissociation pathways. Wave packet calculations on these adiabatic surfaces, however, did not reproduce the low-speed component of S($^1D_2$) fragments. The discrepancy regarding the slow S atoms was attributed to the dissociation induced by non-adiabatic transition from A'($^1\Delta$) to A'($^1\Sigma^+$) in the bending coordinate. This hypothesis was confirmed by wave packet calculations including non-adiabatic transitions. The slow recoil speed of S atoms in the non-adiabatic dissociation channel is due to more efficient conversion of bending energy into CO rotation than the adiabatic dissociation on the upper state surface. By analyzing the experimental data, taking into account the alignment of S($^1D_2$) atoms, we determined the yield of the non-adiabatic transition from the A'($^1\Delta$) to the ground states to be 0.31 in the dissociation at 223 nm. Our theoretical model has predicted a prominent structure in the absorption spectrum due to a Feshbach resonance in dissociation, while an action spectrum of jet-cooled OCS measured by monitoring S($^1D_2$) exhibited only broad structure, indicating the limitation of our model calculations.

III-J-5 C-Br Bond Rupture in 193 nm Photodissociation of Vinyl Bromide

Hideki KATAYANAGI, Nobuaki YONEKURA and Toshinori SUZUKI

[*Chem. Phys.* **231**, 345 (1998)]

Photofragment ion imaging has been applied to 193 nm photodissociation of vinyl bromide to measure the speed and angular distributions of Br atoms. Br atoms were observed in both spin-orbit states (^2P_J; J= 1/2 or 3/2) with the branching ratio, [Br*]/[Br], of 0.06 ± 0.03. Both Br(^2P_J) distributions were dominated by anisotropic high translational energy components, which are ascribed to C-Br bond rupture via surface crossing between the optically-excited $^1(\pi,\pi^*)$ state and ^{1}(n(Br) or π(Br), σ^*(C-Br)) repulsive state(s). The anisotropy parameters of the high translational energy components, 1.3 (Br) and 1.2 (Br*), provide the direction of the transition dipole moment for the $\pi^* \leftarrow \pi$ transition to be 26 ± 3° from the C=C bond axis, in good agreement with ab initio calculations by Yamashita. Despite that the available energy is 10.5 kcal/mol smaller in the Br* channel, the peak energies of P(E_T) in the Br* and Br channels were quite similar, indicating that the fine structure branching occurs in the molecular region. Low translational energy components of Br and Br* observed are ascribed to the dissociation of VBr from the ground state, although contribution from the secondary dissociation of C_2H_2Br radical is also suggested for the Br channel. The anisotropy of low energy component implies that the lifetime of the ground state VBr is only a fraction of its rotational period.

III-J-6 Energy Barrier for the C-C Bond Rupture in Acetyl Radical Studied by Nanosecond Photofragment Imaging

Hideki KATAYANAGI and Toshinori SUZUKI

[*J. Chem. Phys.* in press (1998)]

Nanosecond photofragment imaging has been applied to UV photodissociation of acetyl chloride. From the scattering distributions of acetyl radical, the energy barrier for the C-C bond rupture in acetyl radical was estimated to be 14.5 ± 1 kcal/mol.

III-J-7 Dissociation of Metastable CH_3CO Radical Observed by Subpicosecond Time-Clocked Imaging

Takeshi SHIBATA *(Grad. Univ. Adv. Stud.)*, **Haiyang LI, Hideki KATAYANAGI and Toshinori SUZUKI**

[*J. Phys. Chem. A* **102**, 3643 (1998)]

A novel experimental technique to measure the energy-dependent unimolecular dissociation rate k(E) of radical species is presented. Internally-excited CH_3CO radicals were formed by ultraviolet photodissociation of CH_3COCl, and the subsequent decay of these radicals were detected by subpicosecond time-clocked photofragment imaging. The CH_3CO radicals with different internal energies were dispersed in space by their recoil velocities, and their decay rates were measured for each internal energy. The dissociation rates of CH_3CO radicals determined were an order of magnitude smaller than those calculated by Rice-Ramsperger-Kassel-Marcus theory.

III-J-8 Sensitized Phosphorescence Detection of Metastable Triplet Acetylene Produced by Intersystem Crossing

Yang SHI and Toshinori SUZUKI

[*J. Phys. Chem. A* **102**, 7414 (1998)]

The triplet metastable states of acetylene produced by intersystem crossing from the $\tilde{A}(^1A_u)$ state have been detected by sensitized phosphorescence (SP) method. The phosphorescence was observed in the energy region up to V^4K^2 level that is below the barrier to dissociation in the $\tilde{a}$ state suggested previously. The lifetimes of the triplet states coupled with the V^3K^1 and V^4K^1 levels in the were estimated to be 80 and 100 μs. The rotational structures of SP and LIF spectra were similar, except that weak absorption lines appear more strongly in SP spectrum, thus making SP spectrum more congested. This exemplifies complicated singlet-triplet mixing at the V^3K^1 level suggested previously. The SP signal was observed with different phosphors, where benzil provided the most intense SP signal. Using benzil, the SP spectrum was also be measured for C_2D_2. The prompt emission from Acetylene in collision with the surface was observed for all the phosphors, which is most likely to be due to intersystem crossing from the triplet to the $\tilde{A}(^1A_u)$ state. The lifetime of triplet states and the threshold energy for dissociation for C_2H_2 and C_2D_2 suggest that there is a tunneling effect in dissociation in the triplet manifold.

III-J-9 Predissociation of Acetylene from the $\tilde{A}(^1A_u)$ State Studied by Absorption, LIF and H-Atom Action Spectroscopies

Nobuhisa HASHIMOTO and Toshinori SUZUKI

[*J. Chem. Phys.* in press]

The state dependence of the fluorescence quantum yield and predissociation yield of acetylene in the $\tilde{A}$ state have been investigated. The fluorescence quantum yield decreased with the total angular momentum J at the V^3K^1 and V^4K^1 levels, while not at V^2K^1. Dissociation yield from the V^4K^1, V^5K^1, and V^6K^1 did not depend upon J. The absolute fluorescence quantum yield was found to be only 0.02 at the V^4K^1 J' = 2 level, and more surprisingly 0.13 even at the V^2K^1 J' = 2 level located 1778 cm^{-1} below the dissociation threshold to C_2H ($\tilde{X}\ ^2\Sigma^+$) + H(^{2}S). The translational energy release determined from the Doppler line shape of H atoms suggests that dissociation mainly occurs in the $\tilde{a}$ state over the barrier. Although the singlet-triplet coupling has been believed to be mediated by the $\tilde{c}$ state, the absolute fluorescence quantum yield indicates that electronic relaxation is not specific for the levels lying close to the surface crossing point between the $\tilde{A}$ and $\tilde{c}$ states. It is suggested that internal conversion also plays a role in relaxation from the $\tilde{A}$ state and the ratio of internal conversion and intersystem crossing varies as a function of energy.

III-K Laser Investigation of Bimolecular Reaction Dynamics

In order to understand chemical reactions, detailed knowledge of the dynamics of atomic and molecular collisions is needed. Crossed molecular beams provide a powerful and versatile approach for the study of reactive and inelastic encounters. However, with the conventional detection technique using electron impact ionization, differential cross sections were hardly measured with rotational resolution. This project aims at the measurement of fully state-resolved differential cross sections for reactive scattering processes via two-dimensional ion imaging. The reaction of O($^1D_2$) atoms will be investigated because of their importance in atmospheric chemistry.

III-K-1 High-Resolution Measurements of State-Resolved Differential Cross Sections in NO + Ar Inelastic Scattering at E_{coll} = 65 meV

Hiroshi KOHGUCHI, Christian GEBAUER and Toshinori SUZUKI

We have constructed a crossed molecular beam machine with a 2D ion imaging detector. Each of the two beam sources are pumped by two diffusion pumps

(2 × 2000 l/s) backed by roots blowers (250 and 500 m^3/h), while the main chamber is pumped by tandem turbo molecular pumps (1500 l/s and 500 l/s). Two pulsed supersonic beams generated by piezoelectric valves are crossed at the right angle 50 mm downstream from the nozzles, and the scattered products are interrogated by a probe laser by resonance-enhanced multiphoton ionization. The subsequent ions are accelerated by an electric field in the direction perpendicular to the relative velocity vector and projected onto a gated two-dimensional position sensitive ion detector. The angular and speed distributions of the state-selected products are observed. An acceleration field has 2-D space focusing effect, and a hexapole deflector located in the drift region compensate the center-of-mass velocity of the particles to direct them to the center of the detector. The image observed by a video-rate CCD camera is processed in real time to calculate the center of the light spot on the screen for resolution enhancement. In order to evaluate the performance of the apparatus, inelastic scattering of NO (J" = 1/2, Ω" = 1/2) + Ar → NO (J', Ω' = 1/2, 3/2) was measured at the collision energy of 65 meV. Rotationally and spin-orbit excited NO were detected by $A^2\sum$-$X^2\prod$ [1+1] REMPI. Scattering images showed the state-dependent rotational rainbow peaks.

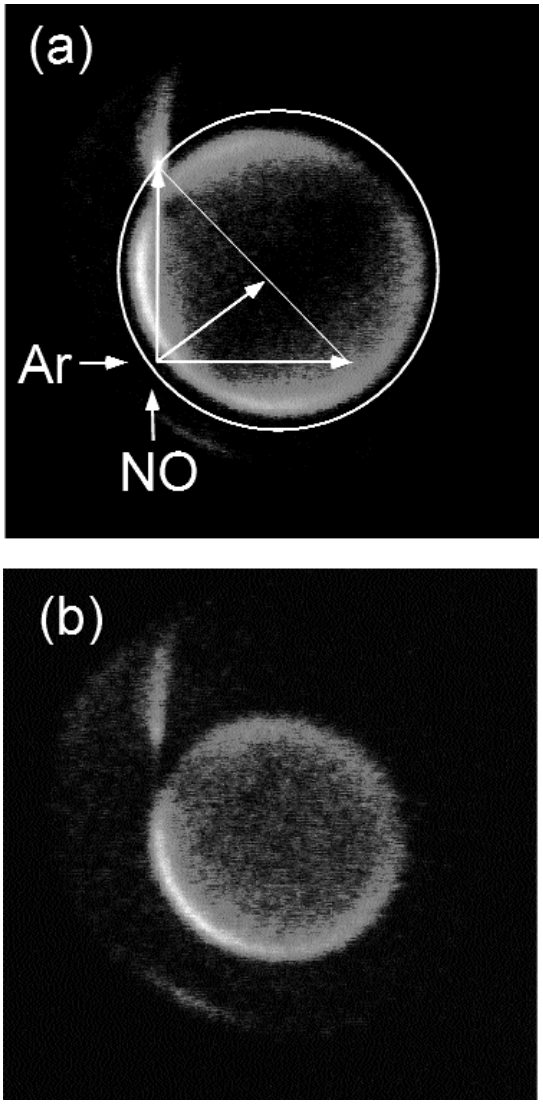

Figure 1. Two-dimensional images of NO scattered by Ar, a) Ω' = 1/2, v' = 0, J' = 8.5, and b) Ω' = 3/2, v' = 0, J' = 8.5. A Newton circle for elastic scattering limit is imposed. The images were integrated for 90 000 laser shots (60 minutes) each.

III-K-2 Development of an Intense Atomic Beam Source of O(^{1}D)

Hiroshi KOHGUCHI, Christian GEBAUER and Toshinori SUZUKI

The reactions of O(^{1}D) have large cross sections and play important roles in combustion or atmospheric chemistry. In order to study the O(^{1}D) reactions at the state-resolved differential cross section level, an intense atomic beam source of O(^{1}D) was developed. O(^{1}D) was produced by laser photolysis of O_2 molecule via Schumann-Runge band at 157nm (F_2 excimer laser, 50mJ/pulse). The intensity of the O(^{1}D) beam at the interaction region was monitored by VUV-LIF using the transition (2p O(^{1}D) → 3s O(^{1}D)) at 115.2 nm. The VUV light was generated by tripling the second harmonic of the output of a YAG-pumped dye laser. A high stagnation pressure up to 9 atm was used to confine the photolytically-generated O(^{1}D) atoms with fast recoil velocity (2200 m/s) in the molecular beam. Hellium was used as a career gas for its small quenching rate of O(^{1}D)+He → O(^{3}P)+He. Although the absolute concentration of O(^{1}D) was not deduced, the comparison with the B-X band (105.1nm) of CO indicated that the number density of O(^{1}D) is 5% of that of CO beam (5% CO/He) at the collision region.

III-L Spectroscopy and Excited State Dynamics in van der Waals Complexes

Spectroscopy and excited state dynamics in van der Waals complexes give much helpful information on the atom-molecule collision processes. We have studied two systems; 1) rare gas-NO system , which concerns with the collisional relaxation of excited NO molecule with rare gas and 2) N_2O-saturated hydrocarbon system (RH), in which $O(^1D)$ is produced in the photolysis of N_2O and the half-reactions of $O(^1D)$- RH are studied.

III-L-1 Electronic Spectroscopy and Predissociation Mechanism of Ar-NO in the 3p Rydberg States

Kazuhide TSUJI, Kosuke AIUCHI, Kazuhiko SHIBUYA *(Tokyo Inst. Tech.)* **and Kinichi OBI** *(Tokyo Inst. Tech. and IMS)*

[*Chem. Phys.* **231**, 279 (1998)]

The $\tilde{D}$ state was found to have surprisingly large D_0 values of l044 cm^{-1} for $v'_{NO} = 0$ and l004 cm^{-1} for $v'_{NO} = 1$, which are larger than 940 cm^{-1} of Ar-NO^+. From the analysis of these spectra, it was found Ar-NO in the 3p Rydberg states predissociates into NO and Ar at different rates strongly depending on the Rydberg orbital character, the vibrational quantum number (v'_{NO}) of NO moiety, and the intermolecular stretching quantum number (v'_{str}) of Ar-NO. Especially, the interaction of the 3p Rydberg states with the nearest-neighboring $\tilde{B}$ state plays an important role in these v'_{NO}- and v'_{str}- dependent predissociation of Ar-NO $\tilde{C}$ ($v'_{NO} = 0, 1, 2$) and ($v'_{NO} = 0, 1$).

III-L-2 Photochemical Reaction Dynamics of $O(^1D)$ with Saturated Hydrocarbons, CH_4, C_2H_6, and C_3H_8, under Bulk Conditions and in van der Waals Complexes

Shin-ichi WADA *(Tokyo Inst. Tech.)* **and Kinichi OBI** *(Tokyo Inst. Tech. and IMS)*

[*J. Phys. Chem. A* **102**, 3481, (1998)]

The reactions of $O(^1D)$ atom with saturated hydrocarbons (RH), CH_4, C_2H_6, and C_3H_8, were studied by monitoring the laser induced fluorescence of products OH in the $v'' = 0$ and 1 levels under bulk conditions and in van der Waals complexes, N_2O-RH. $O(^1D)$ was produced by the ArF excimer laser photolysis of N_2O. Nascent rotational distributions are bimodal in all cases; the low- and high-N components. The former is formed from a long-lived collision complex generated by the insertion process. The collision complex has enough lifetime to randomize excess energy before decomposition. The high-N component is produced in the short-lived insertion process, in which the collision energy of $O(^1D)$ atoms is reflected in the rotational energy. The spin-orbit state in the only half-reactions producing the $v'' = 0$ level shows large population in the low-lying $^2\prod_{3/2}$ state in low-N components, though spin-orbit populations are statistical in other reaction systems studied. The reaction proceeds via a transfer from a singlet reaction surface to a triplet surface keeping the conservation of the electronic angular momentum.

III-M Photochemical Processes Studied by Time-Resolved ESR

Photochemical processes generate abnormal electron spin polarization on excited molecules and free radicals, which is called as chemically induced dynamic electron spin polarization (CIDEP). We have studied photochemical reactions by probing CIDEP. We investigated the interaction in radical and triplet pairs and confirmed evidences for CIDEP generations by level crossing in triplet doublet interactions. Secondly, we succeeded in detection of singlet oxygen molecules by monitoring spin polarization generated on free radicals in the singlet oxygen-free radical systems.

III-M-1 Exchange Interaction in Radical-Triplet Pair: Evidence for CIDEP Generation by Level Crossings in Triplet-Doublet Interactions

Yasuhiro KOBORI *(Tohoku Univ.)***, Keizo TAKEDA** *(IBM)***, Kazuhide TSUJI, Akio KAWAI** *(Tokyo Inst. Tech.)* **and Kinichi OBI** *(Tokyo Inst. Tech. and IMS)*

Chemically induced dynamic electron polarization (CIDEP) generated through interaction of the excited triplet state of 1-chloronaphthalene, benzophenone, benzil, and Buckminsterfullerene (C_{60}) with 2,2,6,6 -tetramethyl-1-piperidinyloxyl (TEMPO) radical was investigated by using time-resolved ESR spectroscopy. We carefully examined what factors affect the CIDEP intensities. By comparing CIDEP intensities of TEMPO in the 1-chloronaphthalene, benzophenone, and benzil systems with that obtained in the C_{60}-TEMPO system, the absolute magnitude of net emissive polarization was determined to be -2.2, -6.9, and -8.0, respectively, in the units of Boltzmann polarization. In the 1-chloronaphthalene-TEMPO system, the viscosity effect on the magnitude of net polarization was studied by changing the temperature (226-275 K) in 2-propanol. The emissive polarization was concluded to result from the state mixing between quartet and doublet manifolds in a radical-triplet pair induced by the zero-field splitting interaction of the counter triplet molecule. The

magnitude of net polarization is much larger than the polarization calculated with the reported theory that CIDEP is predominantly generated in the region where the exchange interaction is smaller than the Zeeman energy. Our experimental results are quantitatively explained by the theory that CIDEP is generated predominantly in the regions where the quartet and doublet levels cross. We propose a theoretical treatment to calculate the magnitude of net polarization generated by the level crossings in the radical-triplet pair mechanism under highly viscous conditions and perform a numerical analysis of the net RTPM polarization with the stochastic-Liouville equation. The viscosity dependence of the net polarization indicates that the back transition from the doublet to quartet states sufficiently occurs in the level-crossing region under highly viscous conditions. The estimated large exchange interaction suggests that the quenching of the excited triplet molecules by TEMPO proceeds via the electron exchange interaction.

III-M-2 CIDEP in Radical-Singlet Molecular Oxygen System

Akio KAWAI *(Tokyo Inst. Tech.)*, **Masaaki MITSUI** *(Kyoto Univ.)*, **Yasuhiro KOBORI** *(Tohoku Univ.)* **and Kinichi OBI** *(Tokyo Inst. Tech. and IMS)*

[*Appl. Magn. Reson.* **12**, 405, (1997)]

Net absorptive CIDEP generation has been demonstrated on singlet molecular oxygen and 4-oxo-2,2,6,6-tetramethyl-1-piperidinyloxyl (OTEMPO) radical system in benzene. CIDEP generation was reasonably explained in terms of the radical-triplet pair mechanism of singlet molecular oxygen-OTEMPO pair with doublet precursor. Several excited molecule-OTEMPO systems have been investigated if this CIDEP generation contributes to their CIDEP spectra. Surprisingly strong CIDEP was produced even in the presence of trace amount of dissolved oxygen, which suggests the importance of complete degassing for CIDEP studies in general systems.

III-N Dynamics of Excited Electronic States of 4-Dimethylaminopyridine and Its Derivatives

It is well known that some aromatic molecules with electronic donor and acceptor substituent groups such as 4-(dimethylamino)benzonitrile (DMABN) show peculiar dual fluorescence. The TICT (twisted intramolecular charge transfer) model is now widely accepted as the most plausible mechanism for the appearance of dual fluorescence. Besides the TICT model, however, various mechanisms have been proposed. For example, charge transfer from solute to solvent or change in the hybridization of orbitals of amino-nitrogen atom is discussed. Dynamics of the appearance of dual fluorescence, therefore, has not been clearly elucidated. DMABN and its derivatives have been only the systems so far whose dynamics of electronically excited states have been investigated in detail in relation to the TICT state formation. In this project, dynamics of 4-dimethylaminopyridine and its derivatives is investigated in detail in order to get more information on the appearance of dual fluorescence.

III-N-1 Dual Fluorescence of 4-Dimethylamino-pyridine and Its Derivatives in Solutions

Suguru MISHINA *(Tokyo Univ. Agric. Tech.)*, **Satoshi KUDOH** *(Tokyo Univ. Agric. Tech.)*, **Masao TAKAYANAGI** *(Tokyo Univ. Agric. Tech. and IMS)*, **Munetaka NAKATA** *(Tokyo Univ. Agric. Tech.)*, **Joe OTSUKI** *(Univ. Tokyo)* **and Koji ARAKI** *(Univ. Tokyo)*

Electronic absorption and emission spectra of 4-dimethylaminopyridine (DMAP), 3-methyl-4-dimethyl-aminopyridine (MDMAP), and 3,5-dimethyl-4-dimethylaminopyridine (DMDMAP) were measured in cyclohexane (non-polar), chloroform (medium polar), and acetnitrile (highly polar) solutions. These molecules are expected to show dual fluorescence. In MDMAP and DMDMAP, dimethylamino group and pyridine ring are expected to stay in a twisted position each other even in the ground electronic state because of the steric hindrance between the dimethylamino group and the methyl groups at 3 and 5 positions. Therefore, relation between dual fluorescence and twisting motion of the dimethylamino group can be investigated by comparing the spectroscopic behaviors of these three compounds. DMAP was of commercial origin, while MDMAP and DMDMAP were synthesized, respectively, from 4-nitro-3-picoline 1-oxide and 3,5-lutidine. Charge transfer (CT) emission at longer wavelength was observed for DMAP only in acetnitrile, while those for MDMAP and DMDMAP were observed in all the three solvents as shown in Figure 1. This result suggests that the TICT mechanism is valid; i.e. twisting motion of dimethylamino group plays the important role on the CT emission. Relative energies of LE (local excited) and CT states, which are considered to depend on the twisting angle between dimethylamino group and pyridine ring and on the solvent polarity, are discussed in detail.

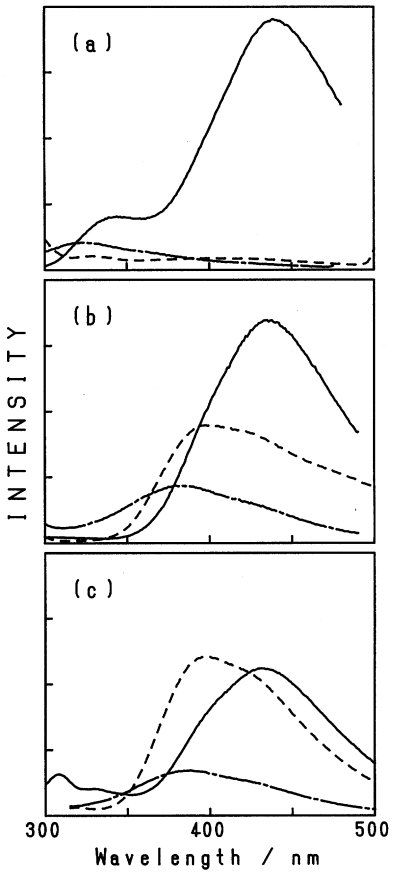

Figure 1. Emission spectra of (a) DMAP, (b) MDMAP, and (c) DMDMAP in acetnitrile (——), chloroform (– – –) and cyclohexane (–·–·–) solutions. Excitation wavelength was set at the absorption maximum around 280 nm for each solution.

III-O Conformation, Photoisomerization and Solvent Effect of Merocyanine Dyes

There has been increasing interest in the use of merocyanine dyes for photoelectric and photochemical devices. Although there have been a great deal of reports on the application of merocyanine dyes for devices, many questions still remain unanswered. For example, little has been known about the rotational isomerism of possible conformers in relation to the conjugated system. Although some merocyanine dyes show large solvent effect in their electronic absorption spectra, the effect has not been clearly interpreted in terms of intermolecular interaction and the structural change of dye molecules induced by solvents. In this project, resonance Raman, infrared absorption, electronic absorption, and fluorescence spectra of merocyanine dyes are measured in various solvents and in low-temperature Ar matrices to clarify their conformation and the mechanism of photoisomerization and solvent effect.

III-O-1 Dispersed Fluorescence and Fluorescence Excitation Spectra of Merocyanine Dyes in Low-Temperature Argon Matrices

Sumi KAWABATA *(Tokyo Univ. Agric. Tech.)*, **Masao TAKAYANAGI** *(Tokyo Univ. Agric. Tech. and IMS)*, **Munetaka NAKATA** *(Tokyo Univ. Agric. Tech.)*, **Yukihiro OZAKI** *(Kwansei-Gakuin Univ.)* **and Keiji IRIYAMA** *(The Jikei Univ. School of Medicine)*

Dispersed Fluorescence and fluorescence excitation spectra of the merocyanine dyes, 5-[2-(3-ethyl-2-benzothiazolylidene)-1-methyl-ethylidene]-3-ethyl-2-thioxo-4-thiazolidinone [Et(Me)MD] and 5-[2-(3-ethyl-2-benzothiazolylidene)ethylidene]-3-ethyl-2-thioxo-4-thiazolidinone [EtMD], in low-temperature argon matrices were measured. Four isomers in relation to the conjugated system are possible for each dye. They coexist in a solution where one isomer can be easily photoisomerized to another.[1)] It is difficult, therefore, to measure electronic absorption or fluorescence spectra of a single isomer of the dye molecules in solutions. Complexity due to the coexistence of isomers and photoisomerization can be avoided by applying the low-temperature matrix isolation technique because the photoisomerization is restricted in the matrices where a dye molecule is surrounded by inert solid rare gas. Fluorescence spectrum of a single isomer can be measured by choosing excitation wavelength, while electronic absorption spectrum of a single isomer can be measured as a fluorescence excitation spectrum by choosing the wavelength of observation.

Dye was vaporized by heating up to 120°C, mixed with argon, and deposited onto a CsI plate cooled at 15 K by a closed cycle helium refrigerator. Spectra of the

matrix sample were measured by a commercial fluorescence spectrophotometer (Shimadzu, RF-5300PC). Figure 1 shows the results for EtMD. These spectra are expected to give valuable information on the electronic structure and photoisomerization mechanism of the dyes.

Reference

1)M. Takayanagi, M. Nakata, Y. Ozaki, K. Iriyama and M. Tasumi, *J. Mol. Struct.* **405**, 239 (1997).

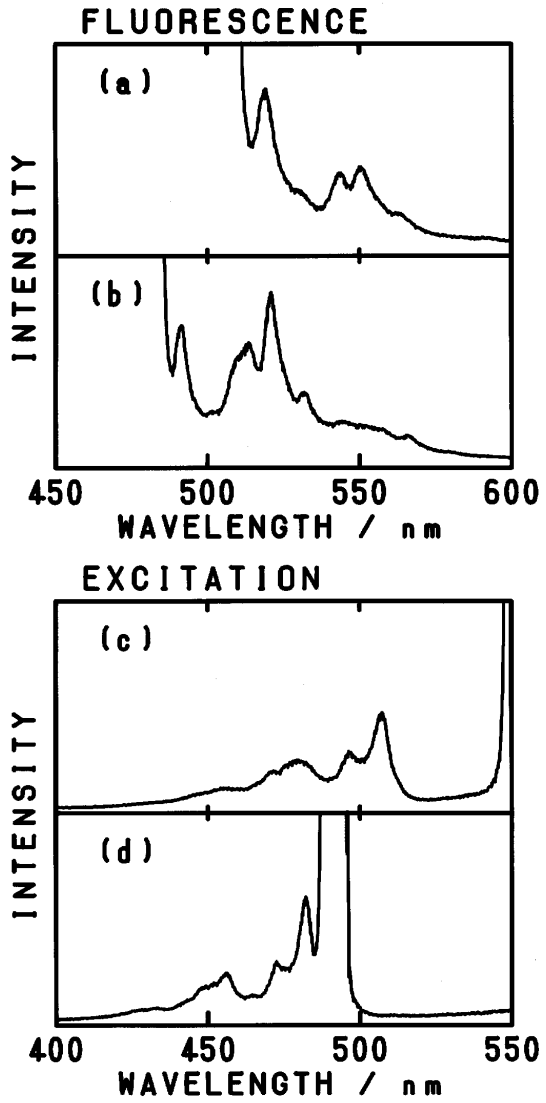

Figure 1. Spectra of EtMD in an Ar matrix. (a) and (b); dispersed fluorescence spectra measured by the excitation wavelengths of 507 and 482 nm, respectively. (c) and (d); fluorescence excitation spectra measured by probing 550 and 490 nm, respectively. Asterisks in (c) and (d) show the bands due to scattered light. Bands due to two isomers are overlapping in each spectrum.

RESEARCH ACTIVITIES IV
Department of Molecular Assemblies

IV-A Solid State Properties of Phthalocyanine Salts and Related Compounds

Some phthalocyanine molecules contain unpaired d-electrons in the conjugated π-electron system. Due to this special nature, the itinerant π-electrons and localized unpaired d-electrons coexist in solid phthalocyanine salts, in which a one-dimensional double-chain system (metal and ligand chain) is formed. Furthermore these chains make up wide (π-band) and narrow (d-band) one-dimensional bands, the energy of the narrow band being close to the Fermi energy of the wide band. The phthalocyanine conductor is thus a two-chain and two-band system. These band structure and exchange interaction of itinerant π-electrons with localized magnetic moments are new aspects in the field of organic metals. For the sake of basic understanding of these materials, where a magnetic interaction takes an important role, we prepare and characterize the solid phthalocyanine salts and related compounds.

IV-A-1 Optical Spectra of the Single Crystals of Phthalocyanine Charge-Transfer Salts $Co_xNi_{1-x}Pc(AsF_6)_{0.5}$

Yukako YONEHARA *(Grad. Univ. Adv. Stud.)* **and Kyuya YAKUSHI**

[*Synthetic Metals* in press]

$NiPc(AsF_6)_{0.5}$ is a two-band system, in which a narrow 3-d band is located just below the Fermi level of the wide π-band. This metallic compound undergoes a metal-insulator transition at *ca*. 50 K. On the other hand, the nearly isostructural $CoPc(AsF_6)_{0.5}$ is a non-metal already at room temperature. The different point between two compounds is the following: 3d-orbital of the central metal is singly occupied in $CoPc(AsF_6)_{0.5}$ whereas fully occupied in $NiPc(AsF_6)_{0.5}$. The polarized reflection spectra of the single crystals of $Co_xNi_{1-x}Pc(AsF_6)_{0.5}$ (x = 0, 0.33, 0.5, 1) are measured in the spectral region of 600-30000 cm^{-1}. In spite of the same band filling and isomorphous crystal structure, the reflection spectra of $CoPc(AsF_6)_{0.5}$ is quite different from all other compound as shown in Figure 1. The plasma edge at high wavenumber region and the reflectivity line shape suggests the formation of the one-dimensional band of $3d_{z^2}$-orbital of Co. This finding is important to understand the origin of the non-metallic nature of $CoPc(AsF_6)_{0.5}$.

At the metal-insulator transition, anomaly was found in heat capacity of $NiPc(AsF_6)_{0.5}$, which suggests the structural phase transition. Figure 2 shows that this phase transition does not accompany the usual Peierls-type lattice deformation, since the vibronic modes are not observed except the very small ones marked by arrows. The low-temperature structure analysis is necessary to understand this metal-insulator phase transition.

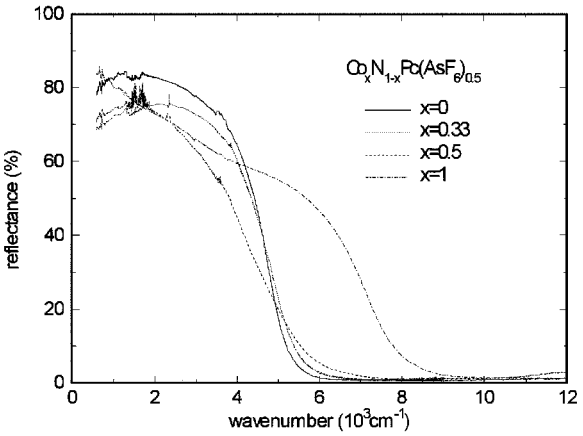

Figure 1. Reflection spectra (//*c*) of $NiPc(AsF_6)_{0.5}$, $CoPc(AsF_6)_{0.5}$, and $Co_xNi_{1-x}Pc(AsF_6)_{0.5}$ (x = 0.33, 0.5). Note that $CoPc(AsF_6)_{0.5}$ demonstrates that the plasma edge is much higher than all other compounds.

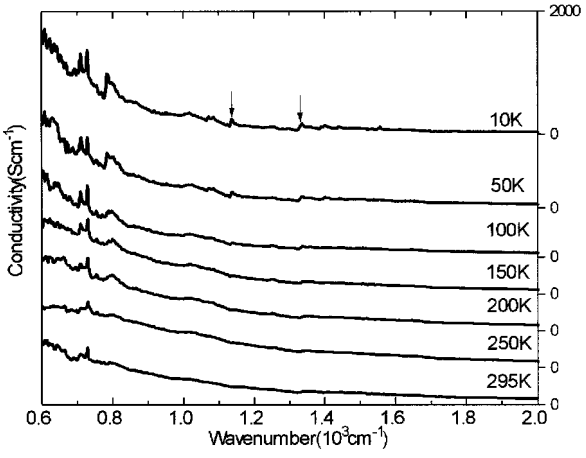

Figure 2. Temperature dependence of the //*c* optical conductivity spectrum of $NiPc(AsF_6)_{0.5}$.

IV-A-2 Optical, EPR, and Structural Properties of Solid Platinum Phthalocyanine in the Different Oxidation States of Electrochemical Process

Yukako YONEHARA *(Grad. Univ. Adv. Stud.)*, **Iakov**

L. KOGAN and Kyuya YAKUSHI

[*J. Electrochem. Soc.* submitted]

The electrochemical oxidation of solid platinum phthalocyanine (PtPc) was examined by cyclic voltammetry, X-ray diffraction, optical absorption, and EPR using two different samples of PtPc incorporated into transparent poly-bisphenol-A-carbonate (PBC) matrix. Two different films were used to evaluate the effect of particle size on the electrochemical and spectroelectrochemical phenomena: The film A consisted of PtPc electrochemically dispersed to nearly molecular level while the film B was formed from finely ground crystals. In the film A, the PtPc molecules were separated out from the crystal surface and distributed in the polymer matrix as a result of relatively fast scans of potentials during electrochemical pretreatment. These molecules were completely oxidized up to the dication state whereas the crystals of film B were only partially oxidized at the same anodic potential 0.8 V, limited by solvent decomposition. Initial PtPc composite film showed a one-step oxidation in the first cycle, whereas two-step oxidation in the second and successive ones, providing the identical product at the highest oxidation state. A large constant potential difference was observed between relevant anodic and cathodic peaks with peak potentials independent of scan rate even at a very low scan rate 0.05 mVs^{-1}. The product formed after the second oxidation step was unstable in the air and transformed into the intermediate state after 24 h of exposition. EPR signal was significantly increased by changing the potential from 0.8 to -0.12 V and reduced again at ϕ = -0.8 V.

Through this experiment we developed a electrochemical doping technique in solid state and identified the solid compound at each oxidation stage by X-ray diffraction. Although the band-filling control was attempted using this technique, the oxidized solid at intermediate electrochemical potential provided the superposition of the X-ray patterns of undoped and doped compounds. This means that the band-filling control by solid electrochemical method is difficult in $PtPc(PF_6)_x$.

IV-B Structure and Properties of Organic Conductors

The study of organic metals rapidly developed when the dimensionality of an intermolecular charge-transfer interaction is expanded. This expansion of dimensionality has been brought about by the discovery of new molecules such as BEDT-TTF or C_{60}. The most basic physical parameters are the transfer integrals which represent the dimensionality and itinerancy of the electron, and the on-site Coulomb energy and coupling constants with molecular vibration which represent the localized character of the electron. We systematically determine these parameters by polarized reflection spectroscopy assembling a microscope, multi-channel detection system, FT-IR, and liquid helium cryostat.

Another ongoing program is to look for negative-*U* organic charge-transfer compounds, the strategy of which is described in the special research project of this issue. In this research program, the most important parameter is the charge or valence of the molecule in a mixed valent state. The examination of the electronic and vibrational spectra at low temperature or high pressure is most efficient to characterize the valence. Molecular metals consisting of large or long molecules are examined by reflection and Raman spectroscopy at low temperature.

IV-B-1 Nature of the Phase Transition of Metallic DMTSA-BF_4

Jianyong OUYANG *(Grad. Univ. Adv. Stud.)***, Kyuya YAKUSHI, Kazuo TAKIMIYA** *(Hiroshima Univ.)* **and Tetsuo OTSUBO** *(Hiroshima Univ.)*

[*Synthetic Metals* in press]

A quasi-one-dimensional charge-transfer salt with a half-filled band usually becomes a Mott insulator. Because of the 1:1 chemical ratio, DMTSA-BF_4 is a half-filled band system. In contrast to this general property, DMTSA-BF_4 shows a metallic conductivity down to *ca*. 180 K and undergoes metal-insulator transition. We showed in *Annual Review 1997* that this metal-insulator transition was regarded as the Peierls transition. The temperature dependence of the //*b* (stacking axis) spectrum was re-measured and analyzed again by plotting $Re[1/\sigma(\omega)]$. Figure 1 shows the evolution of the vibronic modes. In this figure the vibronic band appearing as a dip in $\sigma(\omega)$ is transformed into a peak. It should be noted that the vibronic modes appear already at room temperature. This means that the breaking of the glide-plane symmetry occurs already above the metal-insulator transition temperature. This large fluctuation of the lattice distortion may be related to the one-dimensional Fermi surface of this compound. The low-temperature X-ray diffraction study is now going on. To determine the Peierls gap, the $\sigma(\omega)$ spectrum at 10 K was fitted by the one-dimensional phason model. The Peierls gap was estimated to be 140 meV which is much larger than twice the activation energies obtained by the resistivity (70 meV) and thermopower (80 meV) below 150 K.

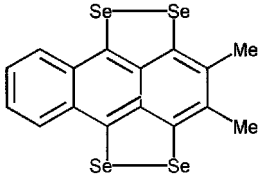

DMTSA

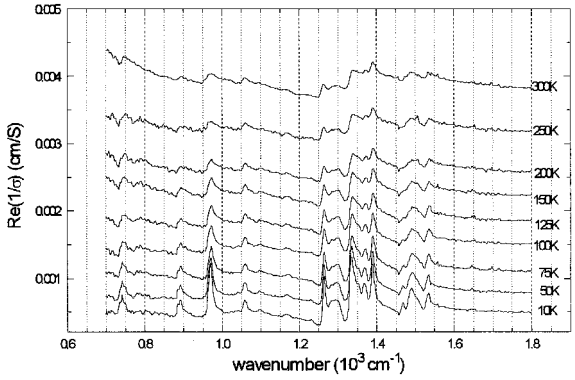

Figure 1. The evolution of the vibronic modes is shown in the plot of the real part of the inverse optical conductivity (*Re*[σ(ω)]).

IV-B-2 Charge-Transfer Transition Polarized Perpendicular to the Molecular Stack in 1:1 Metallic DMTSA-BF_4

Jianyong OUYANG *(Grad. Univ. Adv. Stud.)*, **Kyuya YAKUSHI, Kazuo TAKIMIYA** *(Hiroshima Univ.)*, **Tetsuo OTSUBO** *(Hiroshima Univ.)* **and Hiroyuki TAJIMA** *(ISSP Univ. Tokyo)*

[*Solid State Commun.* submitted]

DMTSA is stacked along the *b*-axis making a zigzag chain. The neighboring molecules are overlapped in a face-to-face fashion and slided along the long molecular axis (//*b*). From this molecular arrangement, the inter-molecular charge-transfer transition can occur in two polarizations: the directions of the stacking axis (//*c*) and long molecular axis (//*b*). Due to this molecular arrangement, the energy band is folded at the zone boundary making two branches. This band is filled up to this folded point. In this band model, the //*c* optical transition is interpreted as the intra-band transition by conduction electron and the //*b* transition as the inter-branch transition. To confirm this interpretation the inter-branch transitions are theoretically calculated based on the one-dimensional tight-binding model, and compared with the experimental observation. The optical transition from the lower filled branch to the upper branch is calculated as,

$$\sigma_{yy}(\omega) = \frac{2i}{V\hbar^3}\sum_{i,f}\frac{\langle i|[H,P_y]|f\rangle\langle f|[H,P_y]|i\rangle}{\omega_{fi}(\omega^2-\omega_{fi}^2=i\gamma\omega)}\omega$$

$$= \frac{e^2}{\nu}\frac{\sqrt{2}(\Delta b)^2 td}{\hbar^2\pi}\int_{-\pi}^{\pi}\frac{\sqrt{1+\cos(2kd)}\,\omega^2\gamma}{\left\{\omega^2-8t^2(1+\cos(kd))/\hbar^2\right\}^2+\omega^2\gamma^2}dk$$

where V is the sample volume, H the tight-binding Hamiltonian i and f lower and upper half band, ω_{fi} = $(E_f(k) - E_i(k))/$, $v$the volume of DMTSA-BF_4, Δb shift along the *b*-axis, t transfer integral, $d = c/2$. The maximum position of $\sigma_{yy}(\omega)$ gives the bandwidth, which agrees very well with the value (0.8 eV) estimated by the analysis of $\sigma_{yy}(\omega)$. We find a simple relation in the plasma frequencies or oscillator strengths of the optical transitions between the intra-band and inter-branch transitions.

$$\omega_p^2(//c)/\omega_p^2(//b)=d^2/(\Delta b)^2$$

This intensity ratio 0.19 agrees well with the geometrical relation between neighboring DMTSA molecules. In this way the calculated conductivity spectrum well reproduces the observed spectrum perpendicular to the stacking axis.

IV-B-3 Two-Dimensional Band Structure of Organic Metals (BDT-TTP)$_2$X (X = SbF_6, AsF_6) Studied by Polarized Reflection Spectroscopy

Jianyong OUYANG, Kyuya YAKUSHI, Yohji MISAKI *(Kyoto Univ.)* **and Kazuyoshi TANAKA** *(Kyoto Univ.)*

[*J. Phys. Soc. Jpn.* in press]

Polarized reflection spectra were measured on the conductive (010) plane of metallic (BDT-TTP)$_2$X (X = SbF_6, AsF_6) single crystals at room and low temperatures. Well-defined plasma edges appeared in both directions parallel (//*a*) and perpendicular (*a*) to the molecular stack, indicating two-dimensional band structures with a significant anisotropy. The intra- and inter-stack transfer integrals were estimated from the plasma frequencies in the framework of tight-binding model. The intra-stack transfer integral agrees very well with the value calculated by the extended Hückel approximation, whereas the inter-stack transfer integral is about half the calculated value. Based on these transfer integrals, the energy dispersion, density of state, and Fermi surface were calculated. The Fermi surfaces of both compounds were open in the k_c direction, which is different from the closed Fermi surface predicted by the extended Hückel calculation. This difference comes from the overestimation of the inter-stack transfer integrals in extended Hückel calculation. The temperature dependence of the transfer integrals was determined by analyzing the low-temperature spectra. The intra-stack transfer integral increased by about 30% whereas the enhancement of inter-stack transfer integral was very weak. So the system became more anisotropic at low temperatures. The strongly appeared CH stretching mode in the *a* spectra suggested that the conjugated π-electrons were extended over the hydrogen atoms of BDT-TTP molecule.

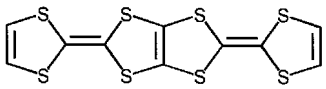

BDT-TTP

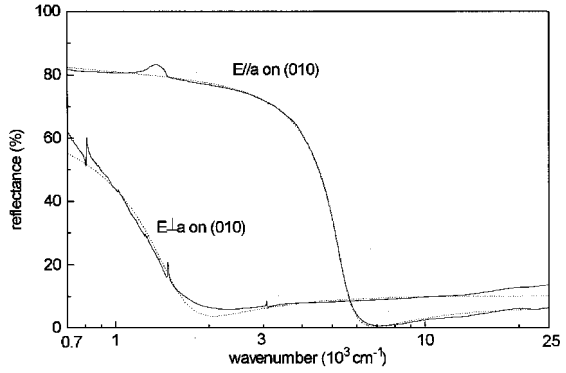

Figure 1. Polarized reflection spectrum of $(BDT\text{-}TTP)_2SbF_6$. The dotted lines are the best-fit curve by Drude model.

IV-B-4 Band Structure of Organic Metal $(BDT\text{-}TTP)_2ClO_4$ Studied by Polarized Reflection Spectroscopy

Jianyong OUYANG, Kyuya YAKUSHI, Yohji MISAKI *(Kyoto Univ.)* **and Kazuyoshi TANAKA** *(Kyoto Univ.)*

[*Synthetic Metals* in press]

Polarized reflection spectrum was measured on the conductive (100) plane of metallic $(BDT\text{-}TTF)_2ClO_4$ single crystals at room and low temperatures. Well-defined plasma edges appeared in both directions parallel (//*b*) and perpendicular (//*c*) to the molecular stack, which is very similar to $(BDT\text{-}TTP)_2SbF_6$. The similar spectrum comes from the similar β-type molecular arrangement although the space group is different. From the plasma frequencies, the intra- and inter-stack transfer integrals were estimated as 0.26 eV and -0.048 eV, which are almost the same as 0.26 eV and 0.048 eV for $(BDT\text{-}TTP)_2SbF_6$. and 0.26 eV and 0.041 eV for $(BDT\text{-}TTP)_2AsF_6$. The Fermi surfaces calculated using these transfer integrals was widely open in the k_c direction, showing the quasi-one-dimensional nature of the Fermi surface. At low temperature ω_p (//*b*: intra-stack) increases, whereas ω_p (//*c*: inter-stack) decreases in the same way as $(BDT\text{-}TTP)_2SbF_6$ and $(BDT\text{-}TTP)_2AsF_6$. This means that the system became more anisotropic at low temperatures. The strong CH stretching mode in the //*c* spectrum is split at low temperature.

IV-B-5 Spectroscopic Study of Narrow-Band Organic Metal $(BEDT\text{-}ATD)_2PF_6(THF)$

Mikio URUICHI, Kyuya YAKUSHI and Yoshiro YAMASHITA

[*J. Mater. Chem.* submitted]

The polarized reflection spectrum indicates the quasi-one-dimensional band structure of $(BEDT\text{-}ATD)_2PF_6(THF)$, which has a narrow bandwidth of *ca.* 0.2 eV. It is surprising that such a quasi-one-dimensional narrow-band system becomes metallic. The conduction-electron absorption band of $(BEDT\text{-}ATD)_2PF_6(THF)$ shows two broad peaks at *ca.* 1000 cm^{-1} and 1700 cm^{-1} which feature is quite different from the Drude model. It is concluded from the crystal symmetry that a strong correlation plays an important role for this unusual absorption band profile. In the //*b* (stacking direction) spectrum, the vibronic bands begin to grow at 100 K, which means that the screw-axis symmetry is broken below 100 K. This broken symmetry is supported by the splitting of the Raman band of a charge-sensitive vibrational mode. Unusually this structural change is not directly correlated with the thermopower and spin susceptibility which show no anomaly down to 50 K and 3 K, respectively. The intensity of some vibrational bands in the //*c* spectrum is enhanced through the coupling with the intra-molecular electronic transition at 4600 cm^{-1}. This interpretation is supported by the molecular orbital calculation of BEDT-ATD^0.

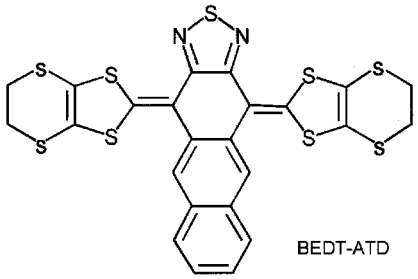

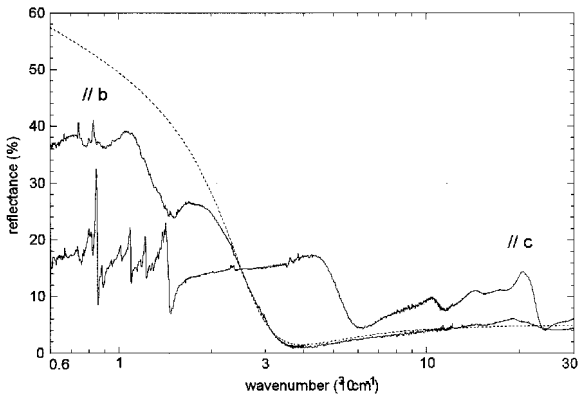

Figure 1. Polarized reflection spectrum of $(BEDT\text{-}ATD)_2PF_6(THF)$ measured on the (100) crystal face. The curve drawn by broken line is the Drude model fitted to the //*b* spectrum in the region of 2500-30000 cm^{-1}.

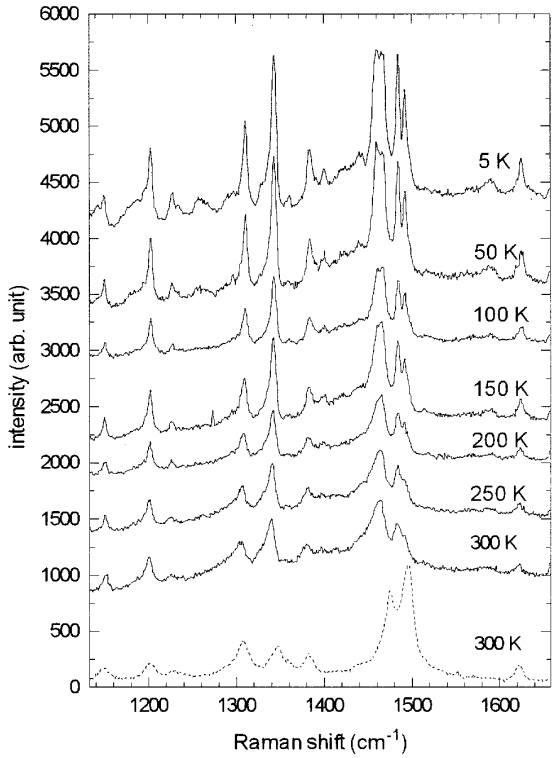

Figure 2. Temperature dependence of the Raman spectrum of $(BEDT\text{-}ATD)_2PF_6(THF)$ (solid lines) and $BEDT\text{-}ATD^0$ (broken line). One can see the softening of the C=C stretching mode by oxidation.

IV-B-6 Charge Distribution in $(Et_4N)(DMe\text{-}TCNQ)_2$ Crystal Studied by Raman and Reflection Spectroscopy

Chikako NAKANO, Kyuya YAKUSHI, Masayoshi KOHAMA *(Osaka Prefecture Univ.)*, **Kazumasa UEDA** *(Osaka Prefecture Univ.)* **and Toyonari SUGIMOTO** *(Osaka Prefecture Univ.)*

DMe-TCNQ forms a dimerized stack in (Et_4N)-$(DMe\text{-}TCNQ)_2$ with two crystallographically independent sites. Although the average charge of DMe-TCNQ is -0.5, the charge in different site has a different value such as -0.5+δ and -0.5-δ. This kind of charge separation (or ordering) is sometimes accompanied by the phase transition in organic metal such as $(DI\text{-}DCNQI)_2Ag$ and $\alpha\text{-}(BEDT\text{-}TTF)_2I_3$ and is attracting an attention as a new ground state. DMe-TCNQ is one of the compounds which have a typical charge-sensitive vibrational mode. We first examined the C=C stretching mode of DMe-TCNQ whose average charge is 0, -0.5, -0.67, and -1 and found a systematic shift. Assuming the linear relation between the shift and charge, δ was determined as 0.1. Comparison with the charge-transfer band analyzed by the polarized reflection spectrum shows that the dimer model is not sufficient to reproduce the charge separation δ = 0.1. The inter-dimer charge transfer and/or relaxation by polarization effect of the CT state should be taken into account.

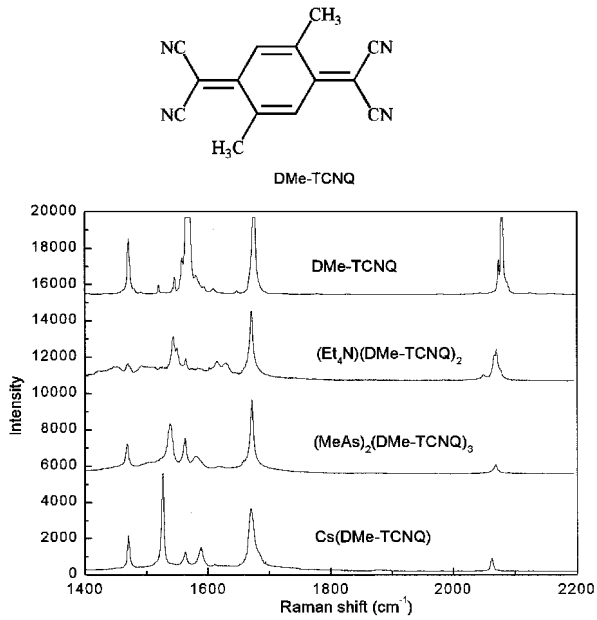

Figure 1. Raman spectra of DMe-TCNQ and its charge transfer salts with various chemical ratio.

IV-B-7 Phase Transition of $\alpha'\text{-}(BEDT\text{-}TTF)_2IBr_2$ Studied by Polarized Reflection and Raman Spectroscopy

Makoto INOKUCHI *(Yamaguchi Science Univ. Tokyo)*, **Kyuya YAKUSHI, Minoru KINOSHITA** *(Yamaguchi Science Univ. Tokyo)* **and Gunzi SAITO** *(Kyoto Univ.)*

[*Synthetic Metals* in press]

The molecular semiconductor $\alpha'\text{-}(BEDT\text{-}TTF)_2IBr_2$ is known to undergo structural phase transition at 200 K and magnetic phase transition at 60 K. In the σ(ω) spectrum, the broad band around 1200 cm^{-1} of the electronic origin abruptly decreased below 200 K, and at the same time the interference pattern is observed. The appearance of the interference pattern means that the spectral region below 1500 cm^{-1} becomes transparent, which suggests the increase of the charge gap. No change is observed at 60 K. It is well known that ν_3 (a_g) mode of BEDT-TTF is sensitive to the charge or valence and a sharp Raman band is observed at 1460-1470 cm^{-1} in $BEDT\text{-}TTF^{0.5+}$. A broad Raman band is observed at room temperature around 1470-1480 cm^{-1} in the corresponding spectral region. This band begins to split at 210 K, each component is well separated (1454 cm^{-1} and 1490 cm^{-1}) at 180 K, and high-wavenumber component shows a shoulder (1484 cm-1) at 5.4 K. This spectral feature indicates that the charge on the four BEDT-TTF molecules in the unit cell has some distribution around +0.5 at room temperature and this charge separation (disproportionation) is fixed below the structural phase transition at 200 K.

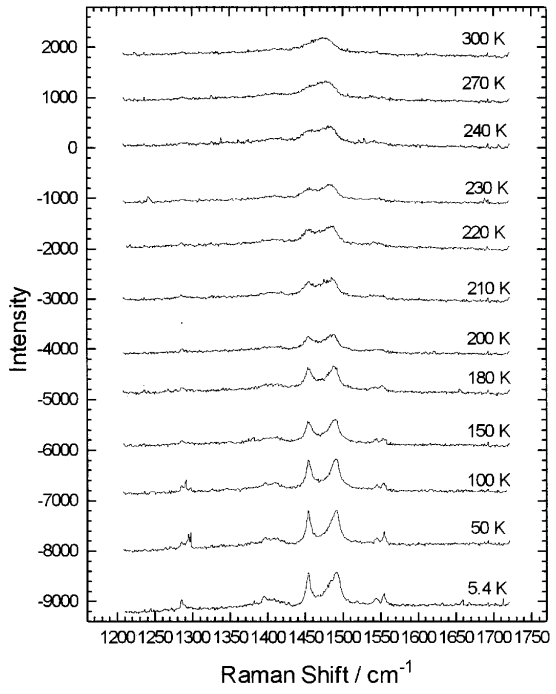

Figure 1. ν_3 mode in Raman spectrum of α'-(BEDT-TTF)$_2$IBr$_2$

IV-B-8 BEDT-TTF Being Inserted into a Layered $MnPS_3$

Chuluo YANG *(Wuhan Univ.)*, **Jingui QIN** *(Wuhan Univ.)*, **Kyuya YAKUSHI, Yasuhiro NAKAZAWA and Kenji ICHIMURA** *(Kumamoto Univ.)*

[*Synthetic Metals* in press]

BEDT-TTF was inserted into the layered $MnPS_3$ by ion exchange reaction of a new pre-intercalate $Mn_{0.86}PS_3(bipy)_{0.56}$ with (BEDT-TTF)$_2I_x$, affording a novel inorganic-organic nano-composite material, the intercalate $Mn_{0.86}PS_3(ET)_{0.46}$. The expansion of the lattice spacing is the largest in the intercalates based on MPS_3 so far. It shows a conductivity (on compressed pellet) 10^5 times higher than that of the pristine $MnPS_3$. Contrary to the ferromagnetic phase transition in $Mn_{0.86}PS_3(bipy)_{0.56}$, which was synthesized by us before, this new intercalate did not show any magnetic transition.

IV-C Thermodynamic Study of Organic Conductors

In order to get reliable information on the electron density of states and on the entropy distribution around the phase transition, specific heat studies are inevitable. In this project, we aim at constructing several types of calorimeters available at low-temperature region and also in magnetic fields and performing systematic investigation on organic materials from a thermodynamic viewpoint.

IV-C-1 Thermodynamics of BEDT-TTF Based Dimeric Salts

Yasuhiro NAKAZAWA and Kazushi KANODA *(Univ. Tokyo)*

[*Synth. Metals* Submitted]

The low-temperature electronic properties of 2:1 salts of BEDT-TTF molecules are studied by specific heat measurements, especially focusing on the dimeric systems. It is recently pointed out that when the intradimer coupling becomes larger than other overlap integrals in the BEDT-TTF layers as is typically the case of κ-, and β-type salts, a dimerization gap appears in the center of HOMO band and consequently it splits into upper-HOMO and lower-HOMO bands. The quarter-filled state of holes provided by the monovalence of anions is therefore considered as an effectively half-filled state of the upper-HOMO band. The degree of dimerization is, therefore, considered as an important parameter to control the electron correlation in this type of compounds. The C_p/T vs T^2 curves of β'-(BEDT-TTF)$_2$ICl$_2$ and the insulating salts of κ-type structure are shown in Figure 1. The absence of T-linear temperature dependence at low-temperature region demonstrates that the Mott insulating behavior is manifested itself in their electronic ground states of this material, which is consistently understood with the above picture.

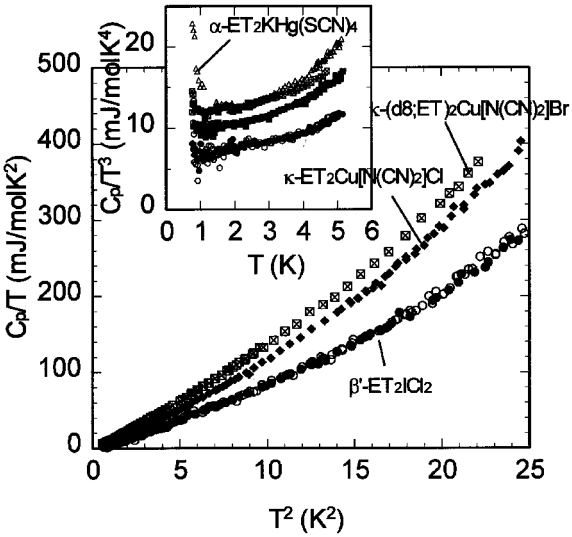

Figure 1. C_p/T vs T^2 plot of insualting salts of (BEDT-TTF)$_2$X. The inset shows C_p/T^3 vs T plots.

IV-C-2 Cooling Rate Dependence of Low-Temperature Specific Heat of Deuterated κ-(BEDT-TTF)$_2$Cu[N(CN)$_2$]Br

Yasuhiro NAKAZAWA and Kazushi KANODA *(Univ. Tokyo)*

We report the result of low-temperature specific

heat measurements of deuterated κ-(BEDT-TTF)$_2$Cu-[N(CN)$_2$]Br, which is situated at the critical region of the Mott transition between superconductive phase and insulating phase of κ-(BEDT-TTF)$_2$X system by changing cooling rate to control the volume fraction of superconductive and insulating phases. The electronic specific heat contribution do not show distinct variation by changing cooling rate from 0.07 K/min to 50 K/min. The magnetic fields dependence of the electronic specific heat is also studied up to 6T as is shown in Figure 1. Here, we do not observe drastic increase of γ term in the present accuracy of the measurement. This fact demonstrates that the density of superconducting electrons in this material, even if they exist, is smaller than those of superconducting material of hydrogenated X = Cu[N(CN)$_2$]Br and Cu(NCS)$_2$ salt.

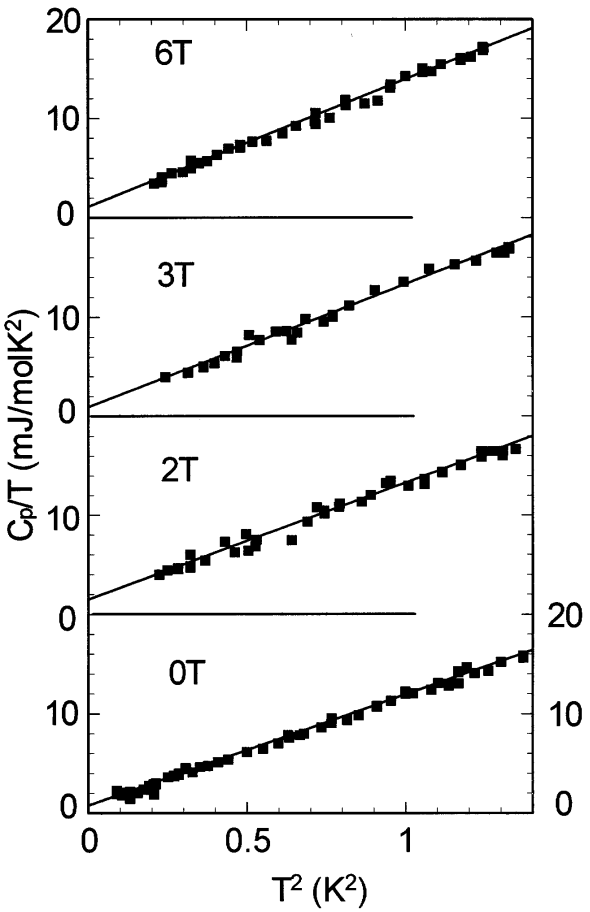

Figure 1. Magnetic field dependence of low-temperature specific heat of κ-(d$_8$;BEDT-TTF)$_2$Cu[N(CN)$_2$]Br cooled down with the rate of 0.8 K/min.

IV-D Photoelectron Spectroscopy of Organic Solids in Vacuum Ultraviolet Region

The works of ultraviolet photoelectron spectroscopy (UPS) and also of UPS with synchrotron radiation lightsource (UVSOR-UPS) of organic materials have been proceeded to find their quantitative electronic structures.

IV-D-1 Origin of the Photoemission Intensity Oscillation of C_{60}

Shinji HASEGAWA, Takayuki MIYAMAE, Kyuya YAKUSHI, Hiroo INOKUCHI, Kazuhiko SEKI *(Nagoya Univ.)* **and Nobuo UENO** *(Chiba Univ.)*

[*Phys. Rev. B* **58**, 4927 (1998)]

The photon energy dependences of photoemission intensities of C_{60} were quantitatively calculated by the single-scattering approximation for the final state and the *ab-initio* molecular orbital calculation for the initial state. The calculated results agreed well with the measured intensity oscillation in the photon energy range of hν = 18-110 eV. The calculation by the plane-wave approximation for the final state also gave the similar oscillations, which suggests that the oscillations are independent of the accuracy of the final state. These results indicated that the oscillations originate from the interference of photoelectron waves emanating from the 60 carbon atoms, *i.e.*, the multi-centered photoemission with the phase difference of each wave. Further, the analytical calculation with a simplified spherical-shell like initial state revealed that the spherical structure of C_{60} molecule and its large radius dominate the oscillations.

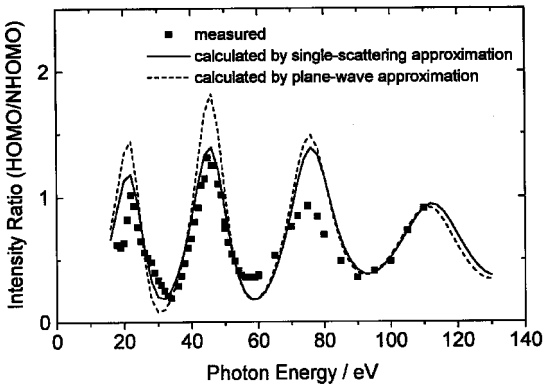

Figure 1. Photon energy hν dependences of photoemission intensity ratio of HOMO/NHOMO. The intensity oscillation of the measured results (solid squares) is in good agreement with the calculated curves. The solid line was calculated by the single-scattering approximation for the final state. The broken line was calculated by the plane-wave approximation for the final state. The initial state calculated by STO-5G MO method was used for both calculations.

IV-E Electrical Conduction and its Related Properties of Organic Solids

Two major categories of organic solids are known to offer the prospect of good electrical conduction. The first group comprises single-component materials; typical examples are polycyclic aromatic compounds and also phthalocyanines. The second group consists of charge-transfer complexes such as the perylene-bromine complexes (donor-acceptor complexes). After the accumulation of large number of works on those charge-transfer complexes, their conductivity ranges from semiconductivity to superconductivity.

To expand the research field of molecular conductors, we always consider to introduce a new category. Recently, with the introduction of gaseous elements such as hydrogen and nitrogen to the charge-transfer complexes, we are finding the third category to produce a new type of molecular conductors: Three components organic semiconductors.

In this section, therefore, we present the works on the electronic properties of single component organic semiconductors, charge-transfer complexes and also three components organic superconductor based on C_{60}. We summarize the work of molecular fastener as review article.

IV-E-1 Molecular Fastener

Hiroo INOKUCHI

A series of tetrakis (alkylthio)-tetrathiafulvalenes (TTC_n-TTF) has been prepared. These compounds constitute novel type of single component organic semiconductors. The electrical resistivities of those single crystals have been measured in a vacuum of 10^{-6} Torr; the room temperature dark resistivity reaches 10^5 Ωcm, a value that is extraordinarily low compared with those of ordinary organic semiconductors constructed with a single component. The cause of this low resistivity is close packing of molecules in crystal. From the crystal structural analysis, the shortest distance between sulfur atoms of central tetrathiotetrathiafulvalene skeleton in two adjacent molecules has been found to be 3.57 Å for TTC_9-TTF and TTC_{10}-TTF, which is considerable shorter than the sum of the van der Waals radius (3.70 Å). The central skeleton has been "fastened" strongly with the substituted four long alkyl chains. We call this type of organic semiconductors by the name of "Molecular Fastener".

IV-E-2 Na-X-C_{60} (X = N, H) Superconductors

Kenichi IMAEDA and Hiroo INOKUCHI

[*Trends in Chem. Phys.* **5**, 239 (1997)]

We found superconductivity in the sodium-X-C_{60} (X = nitrogen and hydrogen) ternary compounds. The onset T_c is observed at 13 K for $Na_xN_yC_{60}$ and 15 K for $Na_xH_yC_{60}$. In contrast to $Na_xN_yC_{60}$ composed of two face-centered-cubic (fcc) phases, $Na_xH_yC_{60}$ crystallizes in a single fcc phase. The Rietveld analysis for the powder X-ray diffraction pattern of $Na_xH_yC_{60}$ demonstrates that Na^+ ions in both the tetrahedral and octahedral sites are off-centered. Hydrogen in Na_xH_y-C_{60} is detected by solid state ^1H NMR and thermal desorption spectroscopy. $Na_xN_yC_{60}$ and $Na_xH_yC_{60}$ superconductors containing off-centered alkali-metal ions belong to the different family from the on-centered M_3C_{60} and Na_2MC_{60}.

IV-F Superconductivity and Antiferromagnetism of λ-Type BETS Conductors

Since the discovery of the semiconducting properties of molecular solids such as phtalocyanine and aromatic hydrocarbons around 1950, conducting properties of a vast of organic conductors have been studied and a great progress has been achieved in the field of organic conducting systems. The widely accepted clear evidences

showing the existence of the metal electrons in molecular crystals was obtained in the early 1970's and the first organic superconductor was reported in 1980. In addition, the first molecular superconductor based on transition metal complex molecules was discovered in 1986 and the first paramagnetic organic superconductor was reported in 1995. On the other hand, despite of the increasing number of the organic superconductors, the speed of the essential progress in the development of organic superconductors seems to be slowing down recently. For example, the highest T_c record of organic superconductors has been stopped almost 10 years since the discovery of κ-BEDT-$TTF_2Cu[N(CN)_2]Cl$ in 1990. We have examined a series of BETS (= bis(ethylenedithio)tetraselenafulvalene) conductors with tetrahalide anions, λ-$BETS_2Fe_xGa_{1-x}Br_yCl_{4-y}$. Our main interest is in the development of new conducting systems by incorporating Fe^{3+} magnetic anions. Of course the above-mentioned first paramagnetic superconductors is an excellent example of the magnetic organic conductors but the magnetic ions in this system was revealed to be almost independent of the π conduction electrons. We have recently discovered an unprecedented superconductor-to-insulator transition in λ-type BETS conductors. To our knowledge, such a transition has not been observed in the inorganic superconductors. In addition, we have found the superconductor-to-metal transition. The Fe^{3+} ions play an essential role in breaking superconductivity. It may be said that a new class of organic superconductors with non-superconducting ground states has been discovered after two decades of the first report of the organic superconductor. Furthermore, we have discovered the evidence for the first antiferromagnetic organic metal phase in λ-$BETS_2FeCl_4$.

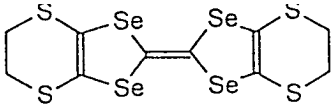

BETS (= bis(ethylenedithio)tetraselenafulvalene)

IV-F-1 Evidence of the Bulk Superconductor-to-Insulator Transition in λ-$BETS_2Fe_xGa_{1-x}Cl_4$ (x ≈ 0.45)

Hayao KOBAYASHI, Akane SATO, Emiko ARAI, Yasuhiro NAKAZAWA, Akiko KOBAYASHI *(Univ. Tokyo)* **and Patrick CASSOUX** *(CNRS)*

We have recently discovered a novel superconductor-to-insulator transition in λ-$BETS_2Fe_x$-$Ga_{1-x}Cl_4$ (x ≈ 0.45). The resistivity measurements on the system with x = 0.43 showed a superconducting transition around 4.2 K and a subsequent superconductor-to-insulator (SC-I) transition around 3 K. Since such drastic conducting phenomena have never been observed even in the inorganic systems, the microscopic mechanism of the transition will be of great interest. We have already reported the anomalous susceptibility behavior around T_{SC-I}. However we found recently the reported susceptibility was not correct for the weak field perpendicular to the needle axis of the crystal (//c) because of the "effective pressure" produced by the freezing of the grease used to keep the crystals in the glass capillary. Therefore we reexamined the susceptibility of two samples of oriented thin needle crystals very carefully. A sharp drop of the susceptibility and its recovery at lower temperature clearly showed that the crystal once transforms into superconducting state and returns to the non-superconducting state. In order to estimate the superconducting volume fraction, we measured the *ac* susceptibility and found the Meissner volume fraction to be about 75% at 4 K, which showed conclusively the bulk nature of the SC-I transition (Figure 1).

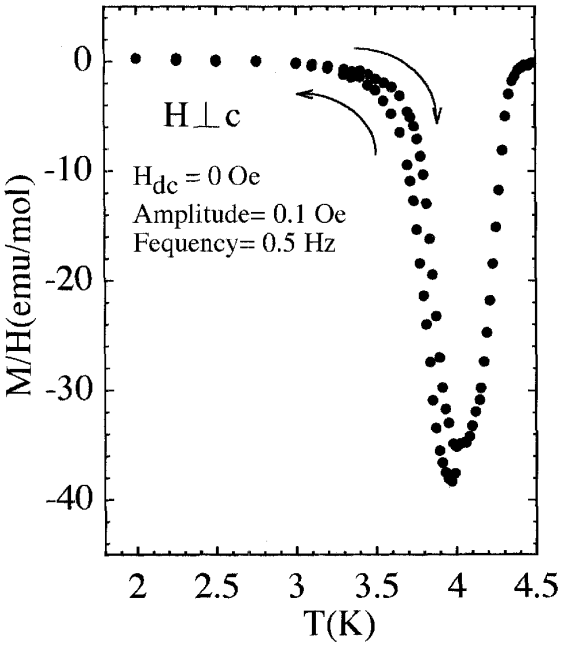

Figure 1. The ac susceptibility of λ-$BETS_2Fe_xGa_{1-x}Cl_4$ (x ≈ 0.45)

IV-F-2 Superconductor-to-Metal Transition in λ-$BETS_2Fe_xGa_{1-x}BrCl_3$ (x ≈ 0.1-0.2)

Hayao KOBAYASHI, Hisashi TANAKA *(Univ. Tokyo)***, Akiko KOBAYASHI** *(Univ. Tokyo)* **and Patrick CASSOUX** *(CNRS)*

As reported before, we have found the superconductor-to-insulator (SC-I) transition in λ-$BETS_2Fe_x$-$Ga_{1-x}Cl_4$ (x ≈ 0.45). We have also examined the resistivity of Br-containing systems λ-$BETS_2Fe_xGa_{1-x}$-$BrCl_3$. It has been reported that the exchange of Cl atoms to Br atoms produces the effectively "negative pressure" in the crystal. At ambient pressure, the crystal

showed the semiconducting behavior down to low temperature. But at high pressure, it exhibited the SC-I transition ($x \approx 0.5$ around 2 kbar) or the SC-M transition ($x \approx 0.1$-0.2 around 1.5 kbar): $T_c \approx 7$ K, T_{SC-I} or $T_{SC-M} \approx 3.5$-4 K (Figure 1). It may be said that the breaking of superconductivity occurs irrelevantly the nature of the ground state (metallic state or insulating state). Since the superconducting states of all the λ-$BETS_2GaBr_xCl_{4-x}$ systems without Fe^{3+} ions are stable down to low temperature, it is clear that Fe^{3+} ions play crucial role in breaking the superconductivity. At higher pressure, the system showed a simple superconducting behavior and then became a stable metal down to low temperature.

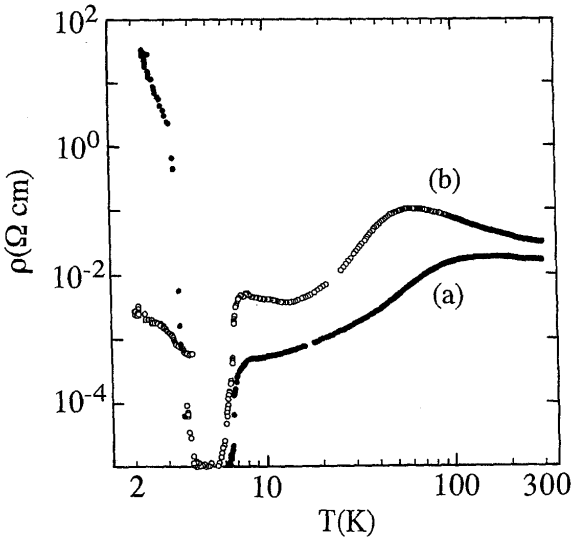

Figure 1. SC-M and SC-I transitions of λ-$BETS_2Fe_xGa_{1-x}BrCl_3$. (a) $x \approx 0.2$ (b) $x \approx 0.5$

IV-F-3 Temperature-Composition Phase Diagram of λ-$BETS_2Fe_xGa_{1-x}Cl_4$

Akane SATO, Emiko OJIMA, Hiroki AKUTSU, Hayao KOBAYASHI, Akiko KOBAYASHI *(Univ. Tokyo)* **and Patrick CASSOUX** *(CNRS)*

[*Chem. Lett.* 673 (1998)]

In order to determine the phase diagram of λ-$BETS_2Fe_xGa_{1-x}Cl_4$, the preparation, EPMA (electron probe microanalysis), resistivity measurements of λ-$BETS_2Fe_xGa_{1-x}Cl_4$ were made systematically. The crystals were grown electrochemically from the 10% ethanol-containing chlorobenzene solutions of BETS, $[(C_2H_5)_4N]FeCl_4$ and $[(C_2H_5)_4N]GaCl_4$. The Fe-rich system showed a sharp metal-insulator transition and the transition temperature (T_{MI}) decreased with decreasing Fe-content (x). In the Ga-rich system, the superconducting transition was observed. The T_c decreased with increasing x. The SC-I transition was observed at $x = 0.35$-0.5 (Figure 1). From the spin flop behavior and the anisotropy of the susceptibilities of the system exhibiting a M-I transition ($x = 1.0$, 0.7, 0.55) or a SC-I transition ($x = 0.45$), it was concluded that the system takes a characteristic π-d coupled antiferromagnetic insulating ground state at $x > 0.35$.

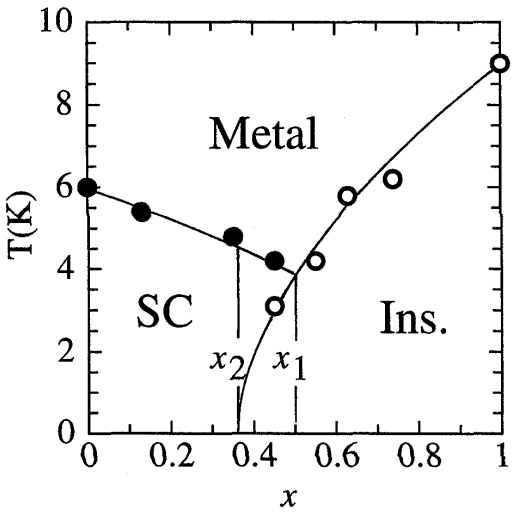

Figure 1. Temperature-composition phase diagram of λ-$BETS_2Fe_xGa_{1-x}Cl_4$

IV-F-4 Antiferromagnetic Ordering of Diluted Fe^{3+} Spins in λ-$BETS_2Fe_xGa_{1-x}BrCl_3$ ($x \approx 0.1$)

Hisashi TANAKA *(Univ. Tokyo)*, **Akiko KOBAYASHI** *(Univ. Tokyo)*, **Hayao KOBAYASHI, Akane SATO and Patrick CASSOUX** *(CNRS)*

The physical properties of λ-type BETS conductors can be controlled continuously by exchanging the metal atoms (Fe, Ga) and/or halogen atoms (Br, Cl). We have recently examined the susceptibility of λ-$BETS_2Fe_xGa_{1-x}BrCl_3$ ($x \approx 0.1$-0.2), which exhibits a semiconducting property at ambient pressure and superconducting-to-metal (SC-M) transition around 1.5 kbar. Quite unexpectedly, only 10% Fe^{3+} spins showed antiferromagnetic ordering below ca. 4 K. The spin-flop behavior was observed around 1.5 T for the field perpendicular to c (Figure 1). In the successive SC and SC-M transitions around 1.5 kbar, Fe^{3+} ion will play an important role. Since the free energy of superconducting state becomes lower than that of the metallic state at T_c (= 7 K), the low-temperature metallic state below T_{SC-I} (= 3.5 K) is considered to be more stable than the high-temperature metallic state above T_c. One possible mechanism of the stabilization of the low-temperature metallic state will be related to the antiferromagnetic ordering of Fe spins, which seems to coexist with metallic state but not with superconducting state.

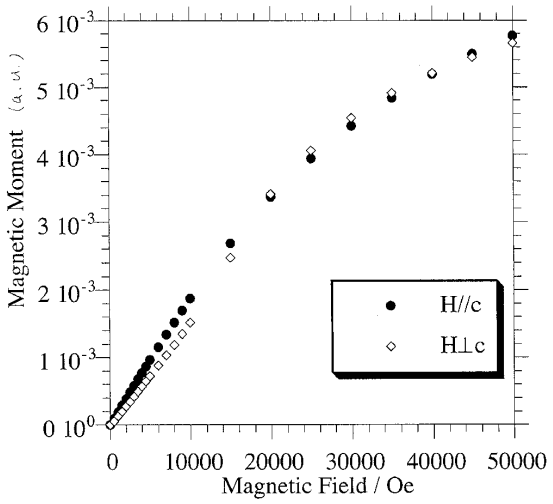

Figure 1. Magnetization of λ-$BETS_2Fe_xGa_{1-x}BrCl_3$ ($x \approx 0.1$) at 3 K

IV-F-5 The x-Dependence of Antiferromagnetic Interaction between Fe^{3+} Ions in λ-$BETS_2Fe_x$-$Ga_{1-x}Cl_4$

Akane SATO, Emiko OJIMA, Hayao KOBAYASHI, Akiko KOBAYASHI *(Univ. Tokyo)* **and Patrick CASSOUX** *(CNRS)*

The role of Fe^{3+} spins is a key factor to understand the anomalous conducting properties of λ-$BETS_2Fe_x$-$Ga_{1-x}Cl_4$. ESR and SQUID measurements showed the antiferromagnetic interaction between localized Fe spins. Since the shortest Fe···Fe distance is longer than 6 Å, the dipole-dipole interaction between Fe^{3+} spins is very small and therefore Fe-Fe interaction must be mediated by π electrons of BETS molecules. Since the Fe and Ga atoms seem to be almost ideally mixed in the crystals, the detailed studies on the magnetic interaction between diluted Fe spins in two-dimensional π conducting system will be possible in λ-$BETS_2Fe_x$-$Ga_{1-x}Cl_4$, which is very difficult in the usual organic conducting systems. Weiss temperature of λ-$BETS_2Fe_x$-$Ga_{1-x}Cl_4$ decreases with decreasing x (θ = -8K at x = 1.0) at $x > 0.35$, where the system takes insulating ground state and tends to be constant (θ = -1.8K) below 0.35, where a simple superconducting transition is observed.

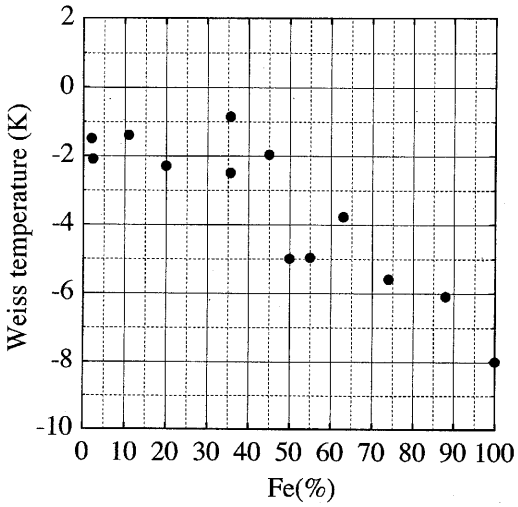

Figure 1. The x-dependence of Weiss temperature of λ-$BETS_2Fe_xGa_{1-x}Cl_4$.

IV-F-6 Easy Axis Rotation of Antiferromagnetic Structure and Phase Diagram of λ-$BETS_2FeBr_x$-Cl_{4-x}

Hiroki AKUTSU, Kiyonori KATO, Emiko OJIMA, Hayao KOBAYASHI, Hisashi TANAKA *(Univ. Tokyo)***, Akiko KOBAYASHI** *(Univ. Tokyo)* **and Patrick CASSOUX** *(CNRS)*

[*Phys. Rev. B* in press]

The electric and magnetic properties of a series of highly correlated two-dimensional organic πconductors incorporating magnetic ions (Fe^{3+} with S=5/2), λ-$BETS_2FeBr_xCl_{4-x}$ (x = 0-0.8) were examined by controlling the Br content (x). A broad resistivity maximum at 100K ($x \approx 0$) - 50K ($x \approx 0.7$) indicating the strong correlation of π-conduction electrons becomes prominent with increasing x. At the same time the metal-insulator (MI) transition temperature (T_{MI}) was enhanced from 8.5K (x = 0) to 18K (x = 0.7). At $0 < x < 0.2$, the MI transition and the antiferromagnetic (AF) transitions took place cooperatively around 8.5 K ($T_N \approx T_{MI}$). A large magnetization drop was observed at T_{MI} for the magnetic field parallel to c axis ($H//c$), which indicates the appearance of localized πspins (S=1/2) and the strong AF coupling of πand d spin systems. At $0.3 < x < 0.5$, two anomalies were observed in the magnetization-temperature (M-T) curve. The high-temperature anomaly corresponds to MI transition (T_{MI}) and the low-temperature one corresponds to AF ordering of the Fe^{3+} spins (T_N). For $x > 0.6$, the magnetization drop at T_{MI} disappeared, which shows that the πelectron system undergoes MI transition independently of the d spin systems. The disappearance of the susceptibility anomaly at T_{MI} indicates that the π electron system transforms to non-magnetic insulating state below T_{MI}. On the other hand, the anisotropy of M showing the development of AF spin structure of Fe spins was observed independently of x ($0 < x < 0.8$). Around x = 0.3-0.5, the direction of easy axis of the AF spin structure changes from parallel to c ($x < 0.2$) to perpendicular to it ($x > 0.6$). In other words, the

direction of easy axis is varied according to the magnitude of π-d coupling. The Weiss temperature (θ) determined from the *M-T* curve at $T_{MI} < T < 30$K decreased with increasing *x*.

IV-F-7 Systematic x-Dependence of the Crystal Structure and Magnetic and Electric Properties of λ-$BETS_2GaBr_xCl_{4-x}$

Hisashi TANAKA *(Univ. Tokyo)*, **Akiko KOBAYASHI** *(Univ. Tokyo)*, **Akane SATO, Hiroki AKUTSU and Hayao KOBAYASHI**

The electrical transport properties of λ-$BETS_2GaBr_xCl_{4-x}$ ($0 < x < 2$) are drastically changed by varying bromine content x and/or applying pressure. At ambient pressure, the superconducting transition could be observed at $x < 0.75$. The pressure and x dependencies of T_c were examined. The M-H curve of λ-$BETS_2GaCl_4$ at 2K indicated the almost perfect Meissner state of superconducting phase (M = magnetization; H = magnetic field). The H_{c1} is about 8 Oe for H c and 12 Oe for H//c. The magnetic susceptibility of λ-$BETS_2GaBr_xCl_{4-x}$ increases with decreasing temperature down to about 60K, below which the susceptibility becomes x-dependent and tends to be suppressed with increasing x. The isotropic decrease of the susceptibility at lower temperature observed in the insulating system with $x > 1.1$ indicates the insulating ground state to be not antiferromagnetic but probably non-magnetic. The crystal structure determinations of a series of λ-$BETS_2GaBr_xCl_{4-x}$ and the calculations of the intermolecular overlap integrals of the highest occupied molecular orbital of BETS were made to elucidate a key factor of the superconducting transition mechanism. The x dependence of intermolecular overlap integrals suggests that the magnitude of "spin gap" of non-magnetic insulating state tends to be diminished with decreasing x. There exists one intermolecular overlap integral exhibiting large temperature and x dependencies, which seems to play a crucial role in determining the nature of the ground state.

IV-G Structural Studies at Low Temperature and High Pressure

Since the molecular crystal is very soft and rich in the structural freedom, various structural phase transitions will be expected at high pressure and/or low temperature. Moreover, the electronic properties of molecular crystal are very sensitive to the structure change. Therefore the precise three-dimensional X-ray structure analyses at high pressure and/or low temperature are important in the studies on solid state properties of molecular crystals. More than several years ago we have developed X-ray imaging plate system equipped with liquid He refrigerator. Although some improvements are needed in the old type system, similar low-temperature X-ray systems become to be used in some laboratories in Japan.

As for the high pressure studies, we have made preliminary high-pressure diffraction experiments on two molecular conductors with triclinic unit cells by using beryllium cell and X-ray imaging plate system. The pressure dependence of the lattice constants and the crystal structures were determined. Although the quality of the collected X-ray reflection data were fairly good, the further improvement was needed to reduce the back ground reflections. Furthermore, the maximum pressure of the beryllium cell was too low (< 7 kbar). We are now examining a specially designed X-ray diamond anvil. A spectrometer was set up to determine the pressure by the shift of ruby fluorescence spectrum.

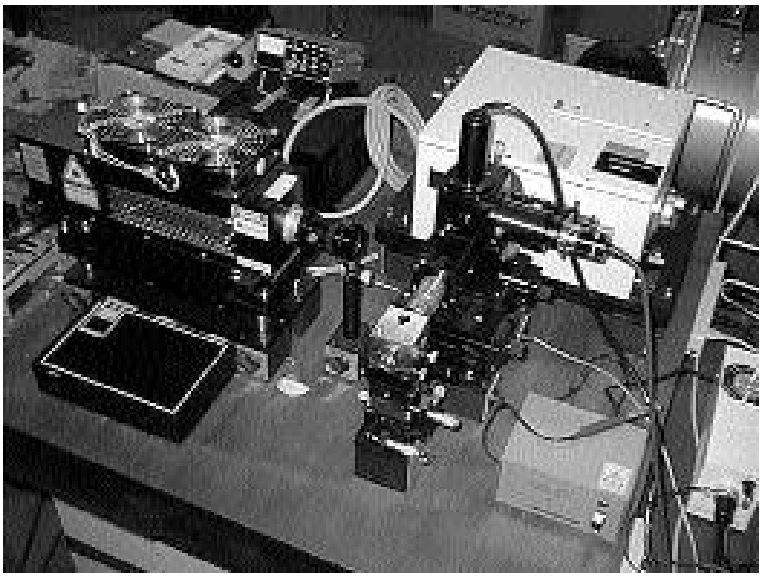

Spectrometer for monitoring the pressure of the diamond anvil cell

IV-G-1 High Pressure Structure of $[(C_2H_5)_2(CH_3)_2N][Pd(dmit)_2]_2$

Takafumi ADACHI, Bakhyt NARYMBETOV, Hayao KOBAYASHI and Akiko KOBAYASHI *(Univ. Tokyo)*

As the first step of the crystal structure studies on molecular crystals at high pressure, we tried to analyze the crystal structure of high-pressure superconductor, $[(CH_3)_2(C_2H_5)_2N][Pd(dmit)_2]_2$, which has an unusual phase diagram. Almost the same phase diagram was recently found in the similar $Pd(dmit)_2$ superconductor by Kato et al. We have proposed a HOMO-LUMO inversion mechanism to explain the reason why the insulating phase appears when the superconducting phase is suppressed by pressure. Although the three-dimensional crystal structure analysis was successfully made around 5 kbar, the maximum pressure of our Be-cylinder type cell was insufficient to examine the HOMO-LUMO inversion mechanism because the pressure-induced insulating phase appears around 9 kbar. Recently we examined the diffraction pattern of $[(CH_3)_2(C_2H_5)_2N][Pd(dmit)_2]_2$ by using specially designed diamond anvil cell and X-ray imaging plate system, which will enable us to make structure studies at higher pressure region. Unlike usual X-ray diamond anvil cell, the Be disk is not used to reduce the back ground diffraction. In the preliminary experiments, a small crystal ($0.3 \times 0.2 \times 0.04$ mm^3) was used but we could obtain sufficiently fine diffraction patterns (Figure 1).

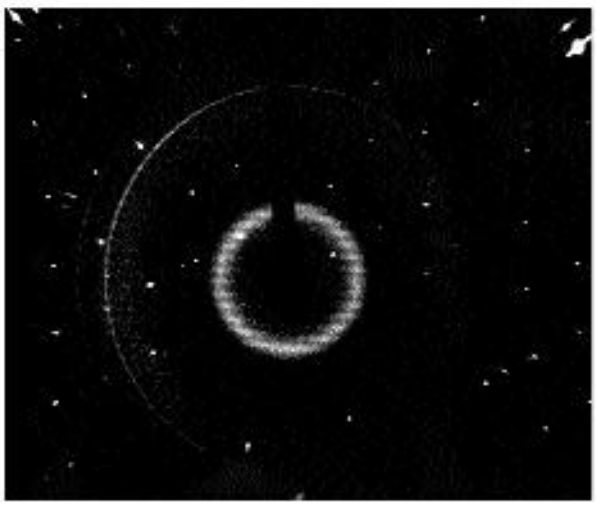

Figure 1. Diffraction pattern from the crystal of $[(CH_3)_2(C_2H_5)_2N][Pd(dmit)_2]_2$

IV-G-2 Low-Temperature Structural Analysis of α-$(BETS)_2Cu_{5-x}I_6$

Bakhyt NARYMBETOV, Hayao KOBAYASHI, Akiko KOBAYASHI *(Univ. Tokyo)***, Nataliya KUSHCH** *(Institute of Chemical Physics in Chernogolovka, Russia)* **and Eduard YAGUBSKII** *(Institute of Chemical Physics in Chernogolovka, Russia)*

α-$(BETS)_2Cu_{5-x}I_6$ is a novel organic metal compound with two-dimensional polymeric anion network. The electrical conductivity of this salt at ambient pressure has metallic behavior down to 25-30K and then undergoes M-I transition which is completely suppressed by applying a pressure about 10 kbar. After release of pressure the salt reveals the metallic properties down to 1.3K. In order to examine an existence of structural changes at low temperature we have carried out X-ray diffraction analysis of the structure at temperature below MI transition region (Figure 1). Low-temperature diffraction patterns were detected by Weissenberg type X-Ray imaging plate at 15K. There is some statistic disorder of Cu atoms in anion network and at low-temperature a little redistribution of populations of Cu atom positions are observed. Detail analysis of the structure show that there is turning of the planes forming by I and Cu atoms relatively to the planes of BETS molecule for about 1.5°.

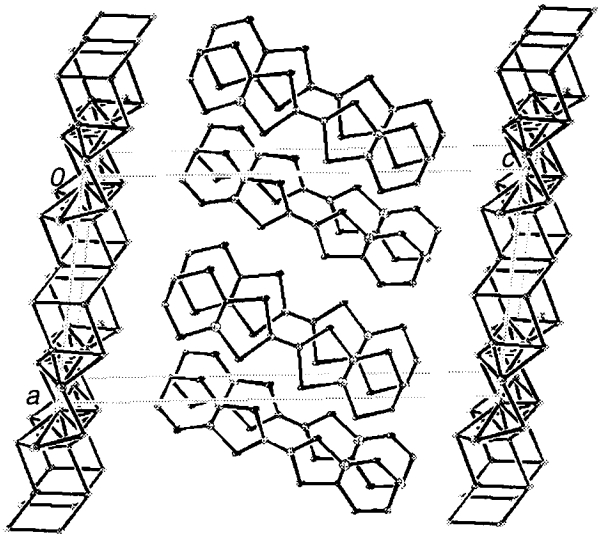

Figure 1. The crystal structure of α-$(BETS)_2Cu_{5-x}I_6$ at 15K.

IV-H Electrical Properties of Molecular Crystals at High Pressure

Pressure is one of the most important parameters in the studies of the physical properties of solids. Usually, the high-pressure resistivity measurements of molecular conductors have been made by using clamp type pressure cell up to about 20 kbar. The most convenient high-pressure apparatus at higher pressure region will be diamond anvil cell. However, despite of the pioneer work by Matsuzaki, the resistivity measurements by diamond anvil cell seems to have unsurmounted difficulties and there seems to be no report on the metallic systems. In the four-probe measurement, four leads bonded to the small fragile molecular crystal (< 0.3 mm) must be took out through metal

gasket with keeping insulation. Although the technical difficulties seem to be very large, we have recently embarked on the high pressure resistivity experiments by using a conventional diamond anvil cell. The pressure was determined by the shift of fluorescence spectra of ruby crystals put in the gasket.

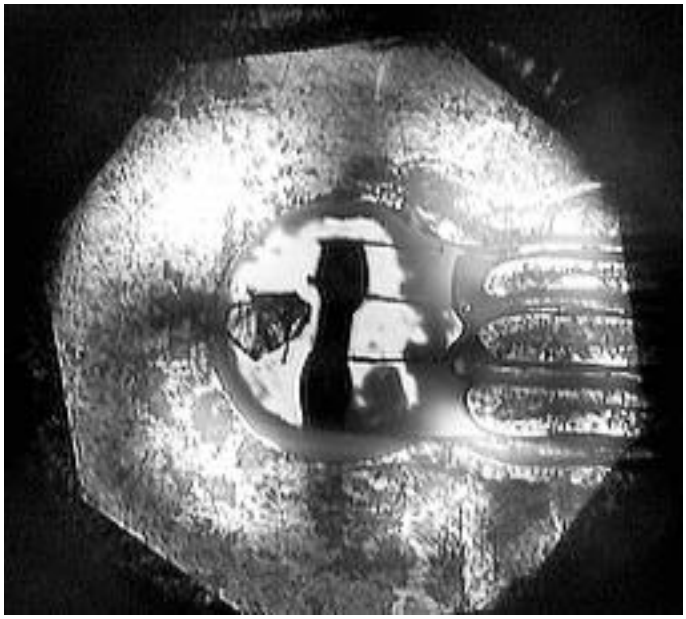

Crystal put in the gasket of the diamond anvil resistivity cell

IV-H-1 Pressure-Temperature Phase Diagram of $(TMTTF)_2PF_6$

Takafumi ADACHI, Emiko OJIMA, Hayao KOBAYASHI and Takafumi MIYAZAKI *(Toyama Univ.)*

We have recently started to try the four-probe resistivity measurements on molecular conductors by using a conventional diamond anvil cell. Our present aim is to establish the technique for four-prove resistivity measurement up to about 50 kbar. As the first sample, we have selected $TMTTF_2PF_6$ system in view of the importance of the generalized phase diagram of Bechgaard salts proposed by Jerome et al. It has been believed that in TMTTF system with spin-Peierls (SP) ground state at ambient pressure, the ground state is changed as, SP → SDW (spin density wave) → SC (superconductor) with increasing pressure. $TMTTF_2PF_6$ is a good system to confirm these successive phase transitions. In order to examine the possibility of superconducting transition of this system, the resistivity measurements up to 40 kbar down to 0.5K will be required. Recently we have succeeded to measure the resistivity up to 45 kbar down to 2K and confirmed the suppression of the insulating phase. However much effort must be paid to overcome many difficulties in the experimental procedure.

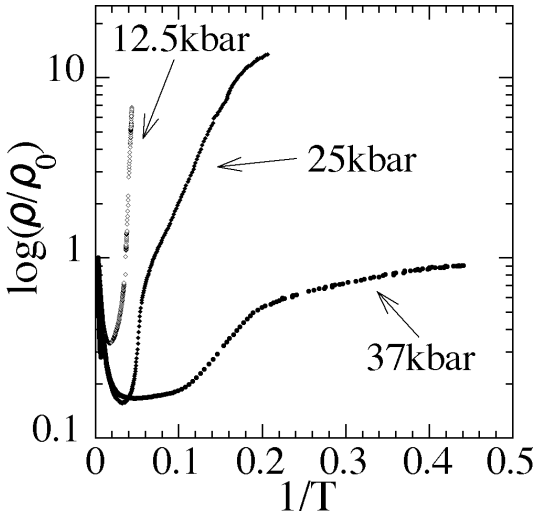

Figure 1. Pressure dependence of the resistivity behavior of $TMTTF_2PF_6$.

IV-I Development of New Molecular Conductors

The development of new materials is the most important driving force for the field of solid state chemistry. The recent progress of concept of the molecular design enriched greatly the physics and chemistry of crystalline molecular solids. The appearance of various types of molecular metals, superconductors and molecular

ferromagnets have attracted an increasing interest of chemists and physicists. We must grow out of the conventional design of molecular conductors for the future development. In these point of view we have performed the development of several types of new molecular components for organic molecular conductors. In the study of polythio-substituted TTF systems and ditellurium bridged polyacene donors we have determined the whole of the crystal structures and physical properties. We are now examining new guiding principles for designing the organic conductors. Furthermore we have developed the novel organic donor containing a stable organic radical part to investigate the interaction between itinerant electrons of the charge-transfer complexes and localized spins of the organic stable radical parts for the development of novel organic conducting-magnetic hybrid materials.

IV-I-1 Novel Stable Metallic Salts Based on a Donor Molecule Containing *Peri*-Ditellurium Bridges, TMTTeN

Emiko ARAI, Hideki FUJIWARA, Hayao KOBAYASHI, Akiko KOBAYASHI *(Univ. Tokyo)*, **Kazuo TAKIMIYA** *(Hiroshima Univ.)*, **Tetsuo OTSUBO** *(Hiroshima Univ.)* **and Fumio OGURA** *(Kinki Univ.)*

[*Inorg. Chem.* **37**, 2850 (1998)]

The first stable organic metals of the *peri*-ditellurium-bridged polyacene donor 2,3,6,7-tetramethylnaphtho[1,8-*cd*:4,5-*c'd'*]bis[1,2]ditellurole (TMTTeN) were obtained. In the crystal of $TMTTeN_2$-$M(CN)_2$ (M = Ag, Au), the donor molecules are stacked to form columns along *c*-axis of the tetragonal unit cell. They also develop three-dimensional network through the intermolecular Te···Te contacts. The salts are highly conductive (500-1000 S cm^{-1}) and keep the metallic states down to low temperature. Furthermore $Ag(CN)_2$ salt exhibited constant Pauli paramagnetic behavior down to 2K (χ(para) ≈ 2.0-2.5 × 10^{-4} emu/mol). The extended Hückel tight-binding band calculation gave the quasi-three dimensional Fermi surfaces owing to the three-dimensional Te···Te network and the tetragonal lattice symmetry. Crystal data for $(TMTTeN)(CS_2)$: $C_{15}H_{12}Te_4S_2$, triclinic, *P*-1, *a* = 10.812(5), *b* = 14.588(6), *c* = 6.295(3) Å, α = 100.49(4), β = 106.75(4), γ = 89.90(4)°, *V* = 933.5(7) $Å^3$, *Z* = 2. Crystal data for the $Ag(CN)_2^-$ salt: $TeAg_{0.12}C_{3.75}N_{0.25}H_3$, tetragonal, $P4_2/ncm$, *a* = 18.2911(9), *c* = 5.352(1) Å, *V* = 1790.5(4) $Å^3$, *Z* = 16. Crystal data for the $Au(CN)_2^-$ salt: $TeAu_{0.12}C_{3.75}N_{0.25}H_3$, tetragonal, $P4_2/ncm$, *a* = 18.322(1), *c* = 5.350(3) Å, *V* = 1795.9(9) $Å^3$, *Z* = 16.

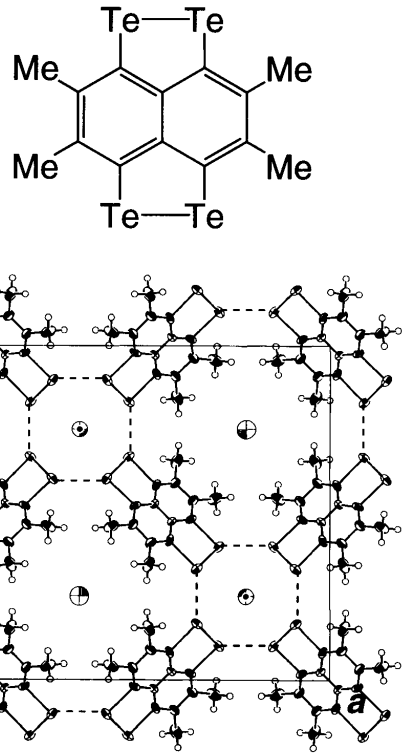

Figure 1. TMTTeN structure and crystal structure of its $Au(CN)_2^-$ salt.

IV-I-2 Synthesis and Properties of a New Organic Donor Containing an Organic Radical Part: TEMPOET

Hideki FUJIWARA and Hayao KOBAYASHI

[*Synth. Met.* in press]

Recently the interplay between the conductivity and magnetism has been focused in the research of new organic conductors. Among them, several donors containing a stable organic radical part have been prepared to investigate the interaction between itinerant electrons of the charge-transfer complexes and localized spins of the organic stable radical parts for the development of novel organic conducting-magnetic hybrid materials. We report herein the synthesis and properties of a novel organic donor TEMPOET **1**. A novel electron donor TEMPOET was synthesized from the ketone derivative as air-stable orange microcrystals in 42% yield. The ESR spectrum of benzene solutions of TEMPOET and the ketone showed three absorption lines (g =2.0061, a_N = 15.1 G) characteristic of the TEMPO radical and almost quantitative spin concentration. The static magnetic susceptibilities of the

ketone **3** and TEMPOET revealed that TEMPOET shows paramagnetic susceptibility corresponding to one spin per molecule and slightly antiferromagnetic interaction at low temperature region (θ = -1.00K). On the other hand the ketone 3 indicated very weak ferromagnetic short-range interaction (θ = +0.55K). TEMPOET shows one pair of reversible redox waves (0.88 V vs. Ag/AgCl) and three pairs of irreversible ones (+0.56, +1.17, +1.77V). The first oxidation potential, +0.56V, is almost the same as that of BEDT-TTF (+0.53 V), indicating its appropriate donating ability. Comparing its oxidation potentials to those of the corresponding tetramethylpiperidine analog (+0.55, +0.87 and +1.74 V), the oxidation of the TEMPO radical part seems to occur at the third oxidation process (+1.17 V), suggesting the possibility of the formation of its cation-radical salts with TEMPO radical part.

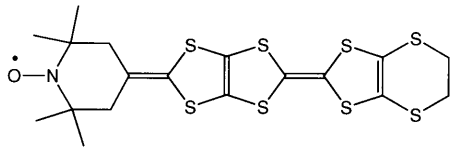

Figure 1. Structure of **1**.

IV-I-3 Synthesis, Structure and Physical Properties of Tetraalkylammonium Bis(5,6-dihydro-1,4-dithiin-2,3-diselenolato)-nickelate, (R_4N)[Ni(ddds)$_2$] (R = Me, Et and *n*-Bu) and Neutral Complex [Ni(ddds)$_2$]$_2$

Hideki FUJIWARA, Emiko OJIMA, Hayao KOBAYASHI, Thierry COURCET *(LCC-CNRS)*, **Isabelle MALFANT** *(LCC-CNRS)* **and Patrick CASSOUX** *(LCC-CNRS)*

[*Eur. J. Inorg. Chem.* in press]

Novel metal complexes (R_4N)[Ni(ddds)$_2$] (R = Me, Et and *n*-Bu, ddds = 5,6-dihydro-1,4-dithiin-2,3-diselenolate) have been prepared and their crystal structures determined. The neutral Ni(ddds)$_2$ species was obtained by electrochemical oxidation from the monoanionic (*n*-Bu_4N)[Ni(ddds)$_2$] complex. X-Ray crystal structure analyses of this neutral species show that two Ni(ddds)$_2$ are connected by the two Ni-Se bonds. Thus, the Ni(ddds)$_2$ entities form [Ni(ddds)$_2$]$_2$ dimers which are arranged face-to-face and rotated by about 90° with respect to each other (Figure 1). The electrochemical behavior of (*n*-Bu_4N)[Ni(ddds)$_2$] indicates the possible formation of cation-radical species. The room temperature magnetic susceptibility measurements showed that the (R_4N)[Ni(ddds)$_2$] complexes are paramagnetic with μ_{eff} = 1.77-1.83 μ_B, corresponding to one unpaired electron per molecular formula The temperature dependence of the magnetic susceptibility of (Et_4N)[Ni(ddds)$_2$] is indicative of weak long-range antiferromagnetic ordering below 9K. The dimerization in [Ni(ddds)$_2$]$_2$ results in a strong antiferromagnetic spin coupling within the dimer, and explain the non magnetic state observed for this compound.

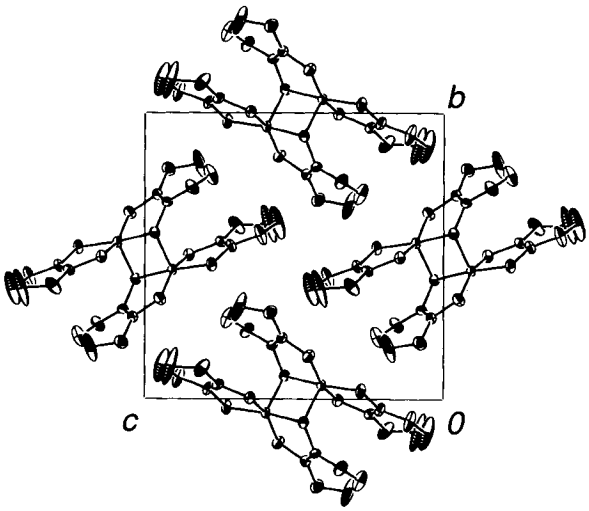

Figure 1. Crystal structure of neutral [Ni(ddds)$_2$]$_2$.

IV-I-4 Synthesis, Structure and Properties of a New Derivative of Sulfur-Bridged TTF Dimer

Hideki FUJIWARA, Emiko ARAI and Hayao KOBAYASHI

[*Synth. Met.* in press]

Synthesis of tetrathiafulvalenophane has been first reported in 1980 and extensively developed in 1990's because of its unusual molecular structure and interesting intramolecular interaction. We focused on a polysulfide chain as a bridging chain because it has more rigid framework than that of polymethylene chain and large interplanar interaction between two TTF moieties may be realized in a dimer. We report here the synthesis and structure of cyclopenteno-fused derivative of a novel cyclophane-like trisulfide-bridged TTF dimer **1** in which two TTF moieties are connected to each other by two trisulfide chains. New derivative **1** was synthesized by the same procedures of the tetrakis-(methylthio) derivative. Preparation of cation radical salts was performed by electrochemical oxidation in chlorobenzene. The composition of the PF_6^- salt of **1** is 1:1 (Donor:Anion) and donors are in the monocationic state, in other words, each TTF moieties are in the semication state. The TTF moieties have planar structure and eclipse almost perfectly to each other with comparatively short interplanar distance of 3.65 Å. Each dimers are stacked each other and formed one-dimensional columnar donor arrays of the dimer molecules along *a*-axis. This salt shows semiconducting behavior with comparatively high conductivity of σ_{rt} = 10^{-1} Scm^{-1}.

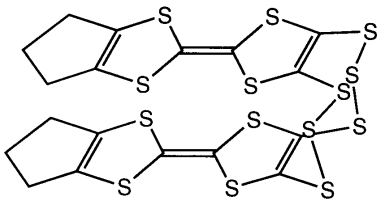

Figure 1. Structure of **1**.

IV-I-5 Synthesis, Structures and Properties of an Unsymmetrical Donor Containing Pyradino-Ring (PEDTTSeF) and Its Cation Radical Salts

Emiko OJIMA, Hideki FUJIWARA and Hayao KOBAYASHI

In the design of new molecular conducting systems, it is expected to enhance the intermolecular interaction by the condensation of hetero ring and/or the substitution of chalcogen atoms. In recent years the diazino-, pyrizino-, pyrazino- and dimethylpyrazino-condensed teterathiafulvalenes have received attention as the materials for realization of two- or three-dimensional conducting property through the S-S or S-N intermolecular contacts. From this viewpoint, we have synthesized a novel unsymmetrical donor containing pyradino-ring: PEDTTSeF. The crystal structure and electrochemical property of the neutral molecule have been investigated. The CV result indicates that the donor molecule shows two pairs of reversible redox waves (+0.85 and 1.18 V vs. Ag/AgCl in PhCN) and its electron-donating ability is lower than that of BETS by the condensation of pyradino-ring. Furthermore we prepared several cation radical salts of this new π-donor by electrochemical oxidation. The temperature dependence of the electrical resistivities of the BF_4^-, ClO_4^-, $GaCl_4^-$, PF_6^- and AsF_6^- salts are metallic down to low temperature and several of which show metal-insulator transition. The crystal structure analyses of the BF_4^- and ClO_4^- salts reveal that these salts have 2:1 composition of D:A and are isomorphous to each other. There are many short intermolecular contacts and two-dimensional networks through the hetero atoms (Figure 1). The magnetic susceptibility of the BF_4^- salt was measured by SQUID magnetometer down to 2K. The paramagnetic susceptibility is almost constant throughout the temperature range, indicating the Pauli paramagnetism of the metal electrons (*ca*. 5.0 × 10^{-4} emu/mol).

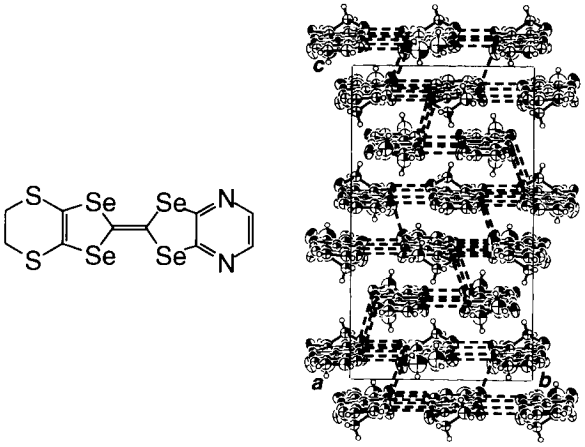

Figure 1. PEDTTSeF structure and donor arrangement of its BF_4^- salt.

IV-I-6 Development of Novel Organic Conductors Based on Tellurium Containing Donor Molecules

Emiko OJIMA, Hideki FUJIWARA, Bakhyt NARYMBETOV, Hayao KOBAYASHI and Akiko KOBAYASHI *(Univ. Tokyo)*

In the search for superior electron donors for organic conductor, the tellurium- containing TTF derivatives have drawn much attention, because the introduced tellurium atoms are expected to produce a novel metallic system in which wide bandwidth and high dimensionality may be realized due to the large van der Waals radii and electron density of tellurium atoms. Furthermore conducting salts based on tellurium-containing donor molecules are interesting because the tellurium network in the crystal is dominant for the construction of whole the crystal structure. Because of their low solubility to organic solvents and difficulty of synthesis, however, the systems based on tellurium-containing donor molecules have not recieved much attention compared to the systems based on sulfur- or selenium-containing donors as yet. Therefore we focused on the development of new tellurium-containing donors and prepared new trimethylene-ditelluro- and trimethyleneoxaditelluro-substituted dimethyl-TTF derivatives. The electrochemical properties of the neutral molecules have been investigated. The CV result indicates that trimethylene-ditelluro-substituted dimethyl-TTF derivative shows peculiar multi-redox behavior, though trimethylene-oxaditelluro-substituted dimethyl TTF derivative shows conventional two pairs of reversible redox waves. Preparation of the conducting salts and their physical property measurements are now in progress.

IV-J Development of Pulsed Field Gradient NMR Spectroscopy

Pulsed field gradient spin echo (PGSE) nuclear magnetic resonance (NMR) is a powerful method for the study of dynamics in condensed matter since it probes translational motion of molecules selectively, without being affected by vibrational or rotational motions. Due to this advantage it has been widely applied to the dynamics of molecules in liquids. However, applications of this technique to strongly dipole-coupled spin systems with short T2 or to the study of slow and anisotropic self-diffusion are still challenging works because combined techniques of line-narrowing, pulsing of sharp and intense field gradients, and two-dimensional field-gradient generation are necessary.

In the present study we applied the technique to the study of anisotropic self-diffusion in liquid crystals and also to the diffusion of lithium ions in sulfide glasses, with the use of the laboratory-made spectrometer equipped with a rotatable quadrupole gradient coil.

IV-J-1 Inversion of Self-Diffusion Anisotropy within a Smectic A Phase of Liquid Crystal

Osamu OISHI and Seiichi MIYAJIMA

A technique of PGSE-NMR coupled with a quadrupole coil rotation[1] was applied to the study of self-diffusion anisotropy in a liquid crystalline material OBBF, 4-(4-octyloxybenzoyloxy)benzylidene(4-fluoro)aniline. It was found, as shown in Figure 1, that the self-diffusion anisotropy was inverted within a smectic A (S_A) phase: The diffusion coefficient component perpendicular to the director, $D_\perp$, is larger than the component parallel to the director, $D_\parallel$ (which means the diffusion within the layer is faster than that across the layer) in the low temperature region of the S_A phase, but the anosotropy was inverted in the high temperature region. The two activation energies were significantly different, namely, 31 kJ mol^{-1} for $D_\perp$, and 55 kJ mol^{-1} for $D_\parallel$.

Reference

1) O. Oishi and S. Miyajima, J. Magn. Reson. Ser. A, 123, 64 (1996).

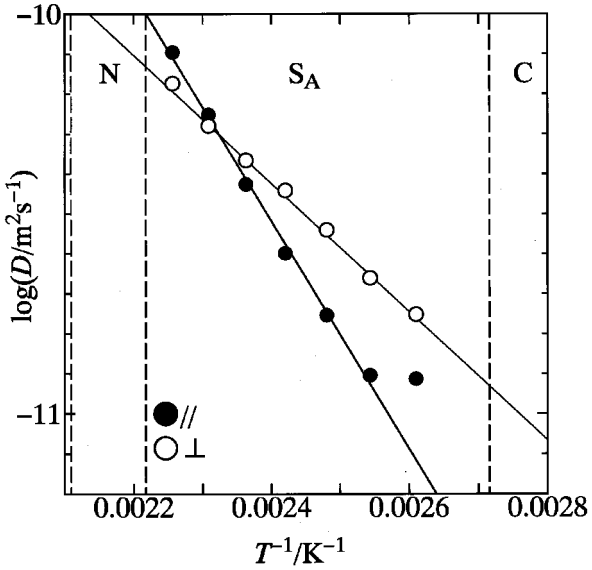

Figure 1. Components of the self-diffusion coefficient tensors, $D_\parallel$ (parallel to the director) and $D_\perp$ (perpendicular to the director), in S_A phase of OBBF.

IV-J-2 Ion Dynamics in Superionic Glasses by ^{7}Li NMR

Tomoko AKAI *(Osaka Natl. Res. Inst.)*, **Osamu OISHI and Seiichi MIYAJIMA**

[*Solid State Commun.* submitted]

Dynamics of lithium ions in superionic glasses have been investigated by ^{7}Li NMR. In the study of ionic transport mechanism, it is important to evaluate the rate of ionic hopping in the short-range and long-range transport independently because the ionic conduction is a result of correlated microscopic motions of individual ions. For this purpose, we measured spin relaxation rate and diffusion coefficient. Hopping rate of the ions was determined from the temperature dependence of spin relaxation rate. The diffusion coefficient was measured in a compound $0.7Li_2S$-$0.3B_2S_3$ by a pulsed field gradient spin echo (PGSE) method. From these data, it was suggested that considerable portion of ions move backward after the initial hoppings.

IV-K Phase Transitions and Dynamical Ordering in Liquid Crystals

Extensive high resolution NMR studies were conducted to reveal the microscopic origins of antiferroelectricity and reentrant phase transitions in liquid crystals. ^{13}C and ^{2}H NMR revealed interesting features of the antiferroelectric liquid crystalline material, especially on aspects of freezing of conformational motion and asymmetric hindrance of the chiral chain motion. Neutron diffraction study was also started for reentrant liquid crystals.

IV-K-1 Complete Assignment of ^{13}C NMR Spectra and Determination of Orientational Order Parameter for Antiferroelectric Liquid Crystal MHPOBC

Toshihito NAKAI *(Univ. Tsukuba and IMS)*, **Hiroki FUJIMORI** *(Nihon Univ. and IMS)*, **Daisuke KUWAHARA and Seiichi MIYAJIMA**

[*J. Phys. Chem. B* submitted]

Complete assignment of the ^{13}C NMR lines was accomplished for both isotropic and oriented samples of antiferroelectric liquid crystal MHPOBC (Figure 1). Two-dimensional double-quantum coherence spectroscopy (2-D INADEQUATE) in the isotropic phase, and field alignment-induced shifts (AIS) were studied. ^{19}F-^{13}C dipolar quartets were measured for TFMHPOBC, where a methyl group attached to the chiral center of MHPOBC is replaced by a trifluoromethyl group, to assist the assignment. Shielding tensor principal elements were determined for each carbon by site-separated spinning sideband spectroscopy (2-D TOSS-deTOSS). The orientational order parameter has been evaluated to be 0.73 at 403 K in S_A phase, by using the experimentally determined AIS and the tensor elements and by assuming an intramolecular free rotation model.

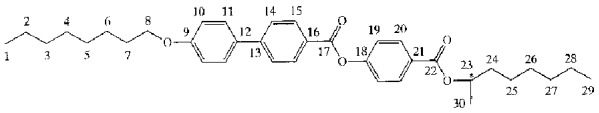

Figure 1. MHPOBC with the numbering scheme for the carbon atoms.

IV-K-2 Freezing of Intramolecular Motion around the Chiral Center of Antiferroelectric Liquid Crystal as Evidenced by Transient Oscillation in ^{13}C-^{1}H Cross Polarization Dynamics

Hiroki FUJIMORI *(Nihon Univ. and IMS)*, **Jean-Pierre BAYLE** *(Univ. Paris XI and IMS)* **and Seiichi MIYAJIMA**

[*Chem. Phys. Lett.* submitted]

Transient coherent effect is observed in the process of ^{13}C-^{1}H cross polarization when individual ^{13}C spins are dipole-coupled to a small number of protons and the spin-diffusion rate of ^{1}H is low enough. In this study we opened a new application of this transient effect to the analysis of intramolecular motion in liquid crystal. Decay time of oscillation, which is determined by ^{1}H spin-diffusion, probes how the intramolecular ^{13}C-^{1}H dipole interactions are averaged out, and hence detects the change of intramolecular motion. Figure 1 shows the oscillations observed for the aromatic protonated carbons of MHPOBC in the paraelectric smectic A (S_A) phase ((a) and (b)) and in the antiferroelectric smectic CA* (S_{CA}*) phase ((c) and (d)). It was shown that chain conformational motions around the chiral center are different in the two phases: A large amplitude motion in SA is frozen to a significant extent in S_{CA}*, and hence enables a large transverse dipole moment of a molecule to come out.

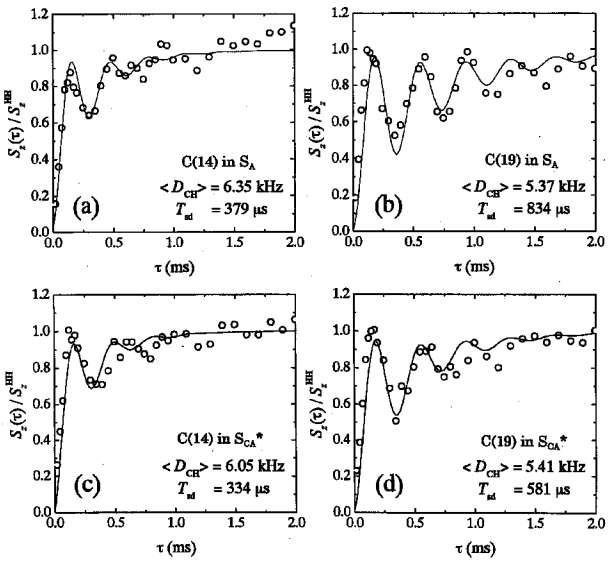

Figure 1. Time evolution of ^{13}C magnetizations of C(14) and C(19) during the ^{13}C-^{1}H double resonance in the rotating reference frame for MHPOBC. See Figure 1 of IV-b-1 for the carbon site numbers.

IV-K-3 Transient ^{13}C-^{1}H Nuclear Overhauser Effect in Liquid Crystal

Hiroki FUJIMORI *(Nihon Univ. and IMS)*, **Daisuke KUWAHARA, Toshihito NAKAI** *(Univ. Tsukuba and IMS)* **and Seiichi MIYAJIMA**

[*J. Magn. Reson.* submitted]

Significant transient ^{13}C-^{1}H nuclear Overhauser effect (NOE) was observed in liquid crystal, and was explained quantitatively by a local ^{13}C-^{1}H dipole interaction. Figure 1 shows three different pulse sequences used for the present experiment and the observed ^{13}C magnetization recoveries. The recovery

after the Hartman-Hahn signal enhancement (B) deviated significantly from the exponential behavior. Remarkably large maximum amounting to 2.5 times the equilibrium magnetization appeared in the Solomon's two-pulse sequence (C), and provided an interesting way of estimating the transition probabilities between the coupled spin states. Experimental data are obtained for an antiferroelectric chiral smectic liquid crystal MHPOBC.

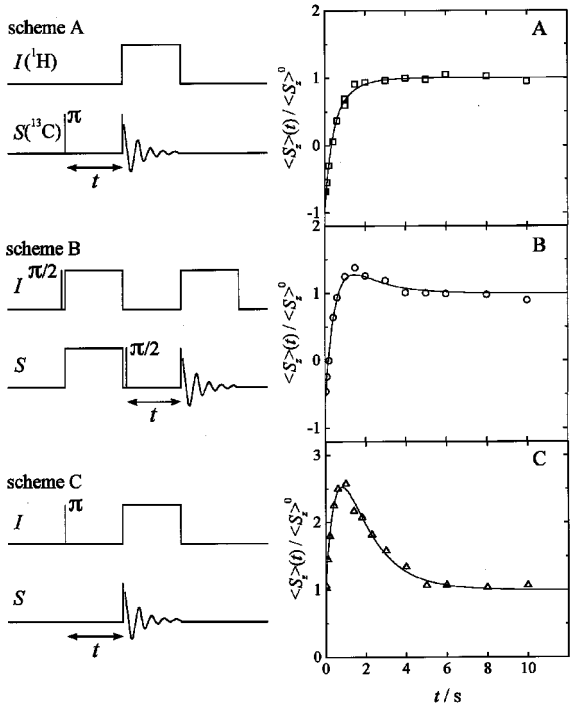

Figure 1. Three pulse sequences and the respective time-evolutions of ^{13}C magnetizations measured at C(19) for MHPOBC in S_A phase. The solid curves are drawn on the basis of coupled master equations for a dipole -coupled ^{13}C-^{1}H spin pair.

IV-K-4 Asymmetrical Hindrance of Methylene Group Rotations about the Chiral Alkyl Chain Axis in the Smectic A Phase of an Antiferroelectric Liquid Crystal as Observed by ^{2}H-NMR

Shohei YOSHIDA *(Tokyo Inst. Tech.)*, **Bo JIN** *(Tokyo Inst. Tech.)*, **Koh TOKUMARU** *(Tokyo Inst. Tech.)*, **Yoichi TAKANISHI** *(Tokyo Inst. Tech.)*, **Ken ISHIKAWA** *(Tokyo Inst. Tech.)*, **Hideo TAKEZOE** *(Tokyo Inst. Tech.)*, **Atsuo FUKUDA** *(Shinshu Univ.)*, **Tetsuo KUSUMOTO** *(Sagami Cent. Res. Center)*, **Toshihito NAKAI** *(Univ. Tsukuba)* **and Seiichi MIYAJIMA**

[*Phys. Rev. E* submitted]

A number of homologues of MHPOBC with selectively deuterated methylenes were synthesized, and the ^{2}H-NMR spectra were detected. The quadrupolar splitting widthes of methylenes in the chiral chain are about one-third of those in the achiral chain, and this result gives a clear evidence of the bent chiral chain. A most striking fact is that the chiral chain methylenes exhibited anomalously large double splittings, indicating that the two deuterons belonging to one methylene unit are not equivalent. This gives an evidence of extremely asymmetric rotational potentials of the methylenes near the chiral center.

IV-K-5 Molecular Rotation in Antiferroelectric Liquid Crystal Studied by ^{13}C-NMR Spin-Lattice Relaxation Time Measurement

Koh TOKUMARU *(Tokyo Inst. Tech.)*, **Bo JIN** *(Tokyo Inst. Tech.)*, **Shohei YOSHIDA** *(Tokyo Inst. Tech.)*, **Yoichi TAKANISHI** *(Tokyo Inst. Tech.)*, **Ken ISHIKAWA** *(Tokyo Inst. Tech.)*, **Hideo TAKEZOE** *(Tokyo Inst. Tech.)*, **Atsuo FUKUDA** *(Shinshu Univ.)*, **Toshihito NAKAI** *(Univ. Tsukuba)* **and Seiichi MIYAJIMA**

[*Jpn. J. Appl. Phys.* submitted]

Temperature dependence of the spin-lattice relaxation time T_1 was measured in an antiferroelectric liquid crystal MHPOBC by means of ^{13}C NMR. The activation energies determined by the temperature dependences of T_1 are the same for most of the carbon nuclei in the S_A and S_{CA}* phases, whereas they are different for carbon nuclei at the chiral center and at the carbonyl carbons. The overall molecular rotation about its long axis does not change through the phase change from S_A to S_{CA}*. Critical slowing down of this rotational motion was not observed.

IV-K-6 Neutron Diffraction Study of a Reentrant Liquid Crystal

Osamu OISHI, Seiichi MIYAJIMA, Michihiko NAGAO *(Univ. Tokyo)* **and Masayuki IMAI** *(Univ. Tokyo)*

When conventional liquid loses its isotropic (I) symmetry and assumes uniaxial orientational order, the nematic (N) liquid crystalline state is formed. The smectic A (S_A) state is characterized by its one-dimensional translational order in addition to the nematic order. It is therefore natural that the phase transition sequence be I-N-SA on lowering the temperature. However, the present compound, CBOBP (4-cyanobenzoyl-oxy-[4-octyl-benzoyloxy]-*p*-phenylene), exhibits a transition sequence, I-N-S_{Ad}-N-S_{A1} (doubly reentrant sequence) on lowering the temperature. The second N phase is called reentrant nematic (RN), and the S_{Ad} to RN transition means that 1-D translational lattice *melts* on lowering the temperature. Due to this peculiarity, the nature of this transition sequence has been one of the interesting topics in recent liquid crystal research.[1)]

We made neutron diffraction study to clarify the structure of the liquid crystalline phases and hence to clarify the microscopic mechanism of this phenomenon. For this purpose a compound with perdeuterated chain, CBOBP-d17 was prepared. Small angle neutron diffraction instrument (SANS-U) of JAERI at Tokai was used at an wavelength of 7.0 Å with a velocity selector.

Figures 1 shows the intensity of the smectic primary

peak. What is striking is that the peak intensity was very small in S_{Ad} phase; smaller than those in N or RN phases, and therefore the reentrant *melting* seems to accompany *increase* in peak intensity. This revealed highly disordered chain structure in the S_{Ad} mesophase, in accordance with the deuterium NMR study.[1)]

Reference

1)S. Miyajima and T. Hosokawa, *Phys. Rev. B* **52**, 4060 (1995).

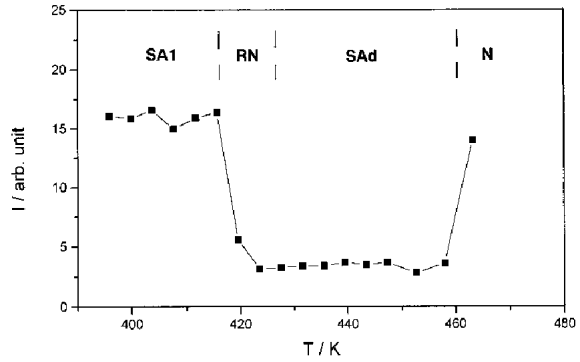

Figure 1. Temperature dependence of the diffraction intensity of the smectic primary peak for CBOBP-*d*17.

IV-K-7 ^{13}C NMR Study of a Reentrant Liquid Crystal

Hiroki FUJIMORI *(Nihon Univ. and IMS)*, **Daisuke KUWAHARA and Seiichi MIYAJIMA**

^{13}C NMR experiments were carried out for a reentrant liquid crystal CBOBP, 4-cyanobenzoyloxy-[4-octylbenzoyloxy]-*p*-phenylene, and its chain-deuterated analogue, CBOBP-*d*17. Temperature dependences of the alignment-induced shift and the transient behavior in ^{13}C-^{1}H cross-polarization dynamics were analyzed for oriented samples. It was shown, as in Figure 1, that chemical shifts for aromatic protonated carbons exhibited anomalous increase in S_{A1} phase. Transient oscillation frequency, $\langle D_{CH} \rangle$, exhibited similar behavior showing that $\langle D_{CH} \rangle$ is determined predominantly by the orientational order parameter, but the increase in S_{A1} phase is less clear.

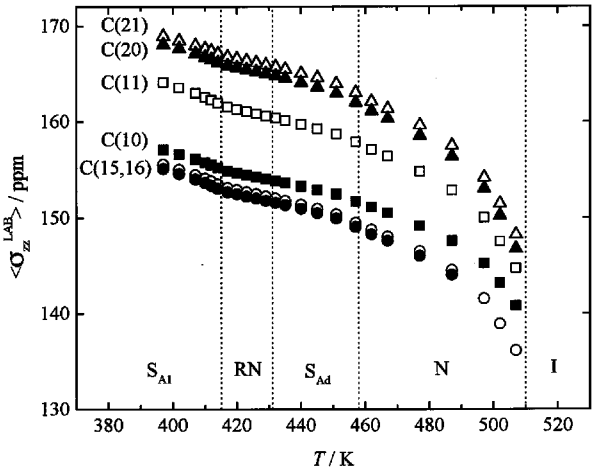

Figure 1. Temperature dependence of the ^{13}C NMR absorption position (measured from tetramethylsilane) for the aromatic protonated carbons of CBOBP.

IV-L Electronic Properties of Alkali-Hydrogen-Carbon Systems

In alkali-hydrogen-carbon ternary systems, hydrogen or alkali metal elements exhibit a variety of electronic states when doped or intercalated in the host crystal lattice. An interesting feature is how the hydrogen 1*s* state contribute to the bulk electronic properties. Structural and electronic properties were studied for sodium-hydrogen-graphite ternary compound by means of the first principle local density functional calculation of the electronic state and the electric field gradient at sodium site. Local electronic state at hydrogen atom was investigated in sodium-hydrogen-C_{60} ternary superconductor by ^{1}H NMR spin lattice relaxation time measurement. The effect of hydrogen absorption on the structural and electronic properties in K_3C_{60} superconductor was investigated by means of powder X-ray diffraction, magnetic susceptibility measurement, and solid state NMR spectroscopy. An attempt at detecting and controlling the reaction of potassium hydride with C_{60} crystal was conducted with *in-situ* ^{1}H NMR measurements. New alkali-hydrogen-C_{60} compounds were synthesized and characterized by powder X-ray diffraction and solid state NMR measurements.

IV-L-1 First-Principles Study on Structure and Electronic State of NaH-Graphite Ternary Intercalation Compound

Shin'ichi HIGAI *(Univ. Tsukuba)*, **Toyoki FUJIWARA** *(Univ. Tsukuba)*, **Shugo SUZUKI** *(Univ. Tsukuba)*, **Kenji NAKAO** *(Univ. Tsukuba)*, **Seiji MIZUNO** *(Hokkaido Univ.)*, **Hironori OGATA and Seiichi MIYAJIMA**

The structure and electronic state of NaH-graphite ternary intercalation compound have been theoretically studied based on the first-principles calculation. In order to make clear the structure of intercalated Na and H, we constructed a number of simple structural models, and calculated the total energy and the nuclear quadrupole coupling constant and asymmetry parameter of ^{23}Na. The structural model in which H exists as the H_2 molecule was found most stable, and could explain the result of ^{23}Na NMR spectroscopy. In the electronic band structure for this model, two kinds of bands form the metallic conduction states. One is the antibonding π-band of graphite, and another is the band which is composed of the antibonding 1*s* orbital of H_2 and the 3*s* orbital of Na. A part of the present calculation was performed with the IMS super computer system.

IV-L-2 ^{1}H NMR Study in Na_4HC_{60} Superconductor

Hironori OGATA, Seiichi MIYAJIMA, Kenichi IMAEDA and Hiroo INOKUCHI

The local electronic state at hydrogen atom for the Na_4HC_{60} superconductor has been investigated by spin-lattice relaxation time measurement of ^{1}H NMR. Figure 1 shows the temperature dependence of spin-lattice relaxation time (T_1) measured by the saturation recovery method at 60 MHz. No frequency dependence was observed for the value of T_1 among 60, 300 and 400 MHz in the temperature region between 120K and 340K. Below about 150K, the T_1 shows Korringa-like temperature dependence ($T_1 \times T$ = 740 s K) within experimental accuracy. This suggests that H 1*s* orbital contribute to the electronic state on the Fermi level. At about 260 K, a jump of T_1 is observed, which is caused by the increase of the density of states at Fermi level, $N(E_F)_{H_{atom}}$, above this temperature by the first order phase transition.

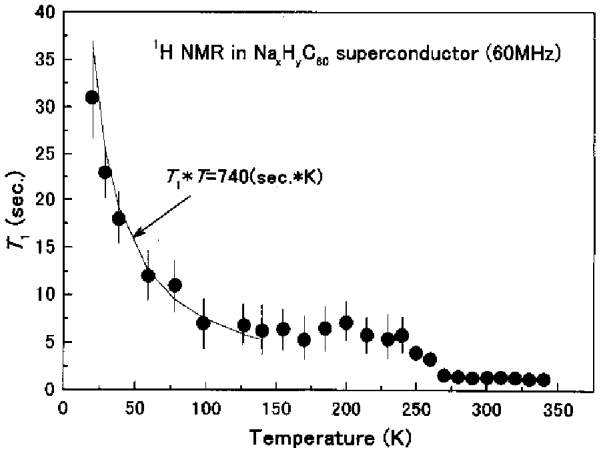

Figure 1. Temperature dependence of ^{1}H T_1 in Na_4HC_{60} superconductor.

IV-L-3 Structural and Electronic Properties of Hydrogen-Absorbed Alkali-C_{60} Compounds

Hironori OGATA and Seiichi MIYAJIMA

[*Synthetic Metals* in press]

The effect of hydrogen absorption on the structural and electronic properties of single phase K_3C_{60} superconductor was investigated by means of powder X-ray diffraction, magnetic susceptibility measurement, and solid state NMR spectroscopy. No lattice expansion as well as no structural change were observed in powder X-ray diffraction by hydrogen absorption. Superconductivity was preserved, and the superconducting transition temperature did not change by hydrogen absorption. No distinct relationship is observed between the shielding fraction and the amount of absorbed hydrogen. Peak position and line shape of ^{13}C NMR spectrum did not change by hydrogen absorption. Peak position of ^{1}H NMR spectrum suggests that hydrogen is neutral in the crystal. No significant difference was observed between K_3C_{60} and hydrogen-absorbed sample in ^{23}Na NMR spectra down to 200 K. This fact suggest that absorbed hydrogen does not occupy octahedral- or tetrahedral-site in the f.c.c. lattice. Curie-like behavior was observed in the temperature dependence of the intensity of ^{1}H NMR spectra. A possible explanation for the above experimental results would be that hydrogen reacts with C_{60} molecule on the surface of crystal grain, while the bulk samples of K_3C_{60} are free from hydrogenation for the hydrogen contents of ≤ 0.56.

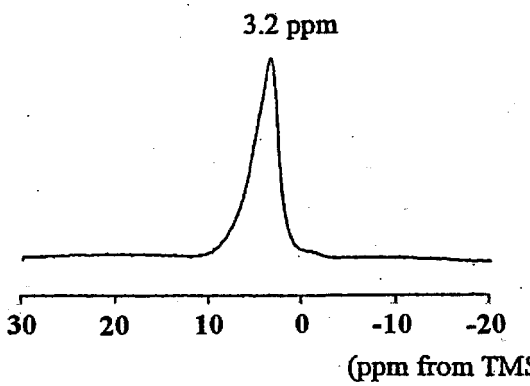

Figure 1. ^{1}H NMR spectrrum of $K_3C_{60}H_{0.56}$ at room temperature.

IV-L-4 *In-Situ* NMR Study of the Reaction Process in Alkali-Hydrogen-C_{60} Compounds

Hironori OGATA and Seiichi MIYAJIMA

An attempt at detecting and controlling the reaction process of potassium hydride with C_{60} is reported. A mixture of stoichiometric amounts of potassium hydride and C_{60} powder was evacuated and sealed in a Pyrex tube, and heated in the NMR probe in several conditions. These reaction processes were monitored by *in-situ* ^{1}H NMR measurements. Figure 1 shows the time dependence of ^{1}H NMR spectra for the sample reacted at 457 K. After eight hours' reaction, a signal at about -6 ppm appeared, which may be ascribable to decomposed hydride ions. Just after the intensity of this peak became maximum, the sample was cooled rapidly to room temperature to stop the reaction. After cooling, the hydrogen peak exhibited down-field shift, showing the change of the hydrogen states from anionic toward neutral side. Powder X-ray diffraction profile of the final product showed that crystal structure of this sample was K_3C_{60}. Furthermore, the superconducting transition temperature was 19.4 K, same as that of K_3C_{60}.

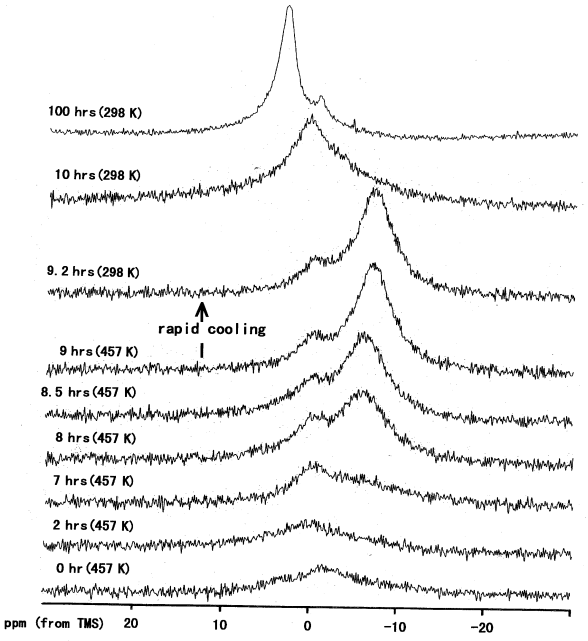

Figure 1. Time dependence of *in-situ* ^{1}H NMR apectra in the mixture of potassium hydride and C_{60} powder.

IV-L-5 Synthesis and Structural Study of New Alkali-Hydrogen-C_{60} Compounds

Hironori OGATA and Seiichi MIYAJIMA

$Li_xH_yC_{60}$, $Na_xLi_yH_zC_{60}$ and $K_xLi_yH_zC_{60}$ compounds were synthsized by the reaction of alkali metals, alkali hydrides and C_{60} solid, and characterized by powder X-ray diffraction and ^{1}H NMR. Powder X-ray diffraction profiles of these compounds showed that these crystals form single phase f.c.c. lattice. ^{1}H NMR spectra of these compounds suggest that hydrogen is in an anionic state in the crystal lattice.

IV-M Magnetic Local Structure and Magnetic Interactions in Molecule Based and Organic-Inorganic Hybrid Magnets

Organic ferromagnet is one of the realizations of great possibilities of organic molecules which can be designed to exhibit a variety of functions by chemical modifications and attracts interest of chemists in broad areas such as organic, physical, and theoretical chemistry, *etc*. Ferromagnetism of organic materials is of current interest. It is desired to clarify the mechanism of intermolecular magnetic interaction in a microscopic viewpoint to establish a leading principle to produce the ferromagnetic ordering in the crystalline phase of molecule based materials and to understanding the characters and the functions of open-cell molecules. Solid state high resolution NMR techniques provide an unique information of the magnetic local structure and the magnetic interactions in a microscopic view point. We have investigated the magnetic local structure and magnetic interaction for a variety of magnetic materials.

IV-M-1 Solid State ^{1}H-MAS-NMR and Spin Densities on Protons of the Organic Ferromagnetic Tempo Derivatives

Goro MARUTA *(Osaka Univ.)*, **Sadamu TAKEDA** *(Gunma Univ. and IMS)*, **Takashi KAWAKAMI** *(Osaka Univ.)*, **Wasuke MORI** *(Kanagawa Univ.)*, **Ron IMACHI** *(Univ. Electro-Commun.)*, **Takayuki ISHIDA** *(Univ. Electro-Commun.)*, **Takashi NOGAMI** *(Univ. Electro-Commun.)* **and Kizashi YAMAGUCHI** *(Osaka Univ.)*

[*Mol. Cryst. Liq. Cryst.* **306**, 307 (1997)]

Ferromagnetism in purely organic materials attracts a grate interest, since Kinoshita et al. reported a molecular ferromagnet at low temperature. Most examples of organic ferromagnetic crystals are based on nitroxide (N-O) radicals. Main interest of this field is to control the intermolecular magnetic interaction between N-O radical groups in the crystalline state to produce the ferromagnetic ordering. As a possible intermolecular ferromagnetic interaction path, a close contact of methyl and/or methylene protons to N-O radical group of adjacent molecules in crystal has been proposed from X-ray diffraction experiment. The methyl and methylene protons are expected to be intermolecular ferromagnetic exchange coupler via spin polarization mechanism (NO(↑)-C(↓)-C(↑)-H(↓)⋯NO(↑)). The electron spin polarized on the proton is a key point. Electron spin densities on hydrogen atoms of 4-(arylmethyleneamino)-2,2,6,6-tetramethylpiperidin-1-oxyls (abbreviated as Ar-CH=N-TEMPO), which show ferromagnetic behavior at low temperatures, were determined in their crystalline phases from the temperature dependence of the Fermi contact shift measured by high speed magic angle spinning proton nuclear magnetic resonance. This method revealed a large negative hyperfine coupling constant for the methyl and methylene protons, A = -1.0 MHz for Ar = *p*-Cl-ph and A = -1.3 MHz for Ar = ph, and very small one for the aryl group protons, $|A| < 0.01$ MHz for *p*-Cl-ph and A = +0.1 MHz for ph. The observed negative hyperfine coupling constant (negative spin density) of methyl and methylene protons matches with spin alternation for the intermolecular spin polarization mechanism through the contact of methyl and/or methylene protons to adjacent N-O radical group. This contact potentially contributes to the intermolecular ferromagnetic interaction.

IV-M-2 Solid State High Resolution NMR

Studies of Electron Spin Densities in Charge-Transfer Complex-Based Organic Ferromagnets

Goro MARUTA *(Osaka Univ.)*, **Sadamu TAKEDA** *(Gunma Univ. and IMS)*, **Kizashi YAMAGUCHI** *(Osaka Univ.)*, **Kazumasa UEDA** *(Osaka Pref. Univ.)* **and Toyonari SUGIMOTO** *(Osaka Pref. Univ.)*

[*Synth. Metals* submitted]

A variety of purely organic ferromagnets which consist of stable neutral radical species have been developed. Charge-transfer complex-based organic ferromagnets are particularly of current interest because of their potential to exhibit ferromagnetism at high temperatures. In these compounds, donor ($D^{+\bullet}$) and acceptor ($A^{-\bullet}$) can be designed to bear electron spins and electronic conduction can be also expected, so that the magnetic interaction in these salts may be different from those in neutral radical-based magnetic crystals and a novel magnetism is expected. A series of 4,4,5,5-tetramethylimidazolin-1-oxyls with 4-(*N*-R-pyridinium) groups at the 2-position (**1**$^{+\bullet}$: R = methyl, **2**$^{+\bullet}$: R = ethyl, **3**$^{+\bullet}$: R = *n*-propyl) form stable charge transfer complexes with the radical anion of $TCNQF_4$. It has been revealed by the magnetic susceptibility measurements that **1**$^{+\bullet}\cdot TCNQF_4^{-\bullet}$ and **3**$^{+\bullet}\cdot TCNQF_4^{-\bullet}$ are ferromagnets at low temperature ($T_c \sim 0.5$K), whereas **2**$^{+\bullet}\cdot TCNQF_4^{-\bullet}$ exhibits antiferromagnetic behavior. It is interesting to study the mechanism of magnetic interaction of these CT complexes. The mechanism can be elucidated from the electron spin density distribution in the magnetic crystals. In this work, we have determined the electron spin density distribution and the magnetic local structure in the salts of **1**$^{+\bullet}\cdot TCNQF_4^{-\bullet}$, **2**$^{+\bullet}\cdot TCNQF_4^{-\bullet}$ and **3**$^{+\bullet}\cdot TCNQF_4^{-\bullet}$ by solid state high resolution ^{1}H, ^{13}C and ^{19}F-NMR.

IV-M-3 Magic Angle Spinning ^{1}H-NMR Study of the Spin Density Distribution of Pyridyl Nitronyl Nitroxides in the Crystalline Phase

Goro MARUTA *(Osaka Univ.)*, **Sadamu TAKEDA** *(Gunma Univ. and IMS)*, **Akira YAMAGUCHI** *(Univ. Tokyo)*, **Tsunehisa OKUNO** *(Univ.Tokyo)*, **Kunio AWAGA** *(Univ. Tokyo)* **and Kizashi YAMAGUCHI** *(Osaka Univ.)*

[*Mol. Cryst. Liq. Cryst.* in press]

Electron spin density distribution was investigated for *p*- and *m*-pyridyl nitronyl nitroxides (*p*-PYNN and *m*-PYNN) in the crystalline phase by the temperature dependence of the solid state high resolution ^{1}H-MAS NMR spectrum. The results were compared with that of phenyl nitronyl nitroxide (PNN) for elucidating the effect of incorporation of a nitrogen atom into the aromatic group. For *p*-PYNN, the magnitude of the negative spin density at 3 and 5 positions of the pyridyl group was suppressed by 30% in comparison with that of PNN and the positive spin density at 2 and 6 positions was slightly enhanced by 10%. On the other hand, the positive spin density at 2, 4 and 6 positions of pyridyl group of *m*-PYNN was suppressed by 30% in average and the negative one at 5 was also suppressed by 20%. The DFT calculation at UBLYP/6-31G(d,p) level suggested that the molecular geometry largely contributed to the change of the spin density in addition to the effect of incorporation of the nitrogen atom. In fact, the spin density distribution of the aromatic ring of *p*-PYNN was remarkably reduced in solution compared with that in the crystalline phase.

IV-M-4 Solid State High Resolution Deuterium NMR Study of Electron Spin Density Distribution of Hydrogen-bonded Organic Ferromagnetic Compound 4-Hydroxyimino-TEMPO

Goro MARUTA *(Osaka Univ.)*, **Sadamu TAKEDA** *(Gunma Univ. and IMS)*, **Ron IMACHI** *(Univ. Electro-Commun.)*, **Takayuki ISHIDA** *(Univ. Electro-Commun.)*, **Takashi NOGAMI** *(Univ. Electro-Commun.)* **and Kizashi YAMAGUCHI** *(Osaka Univ.)*

Electron spin density distribution at hydrogen atoms of 4-hydroxyimino-2,2,6,6-tetramethylpiperidin-1-yloxyl (4-hydroxyimino-TEMPO), which has been recently found to be a molecular ferromagnet at low temperature, was determined in the crystalline phase from the temperature dependence of the Fermi contact shifts of magic angle spinning deuterium NMR spectrum to elucidate the mechanism of intermolecular magnetic interaction. The plus and minus signs of observed hyperfine coupling constants A_D of methyl hydrogens revealed two different mechanisms of electron spin distribution. Equatorial CD_3 groups show negative coupling constants (A_D = -0.24 MHz) induced by the spin polarization mechanism, whereas positive hyperfine coupling constants (A_D = +0.12 MHz) of axial CD_3 groups indicate that single occupied MO spreads out partly toward the axial CD_3 groups by the mechanism of hyperconjugation. Large negative hyperfine coupling constant (A_D= -0.45 MHz) observed for NOD group implies that the spin polarization mechanism works via intermolecular hydrogen bond in the crystalline state. These experimental results and molecular orbital calculations indicate that there exists ferromagnetic interaction in the hydrogen bonded chains and these chains are coupled through the axial methyl groups.

IV-M-5 Local Magnetic Structure of Layered Compounds $Cu_2(OD)_3X$ with Exchangeable Acid Anion X Studied by Solid State High Resolution Deuterium NMR

Sadamu TAKEDA *(Gunma Univ. and IMS)*, **Goro MARUTA** *(Osaka Univ.)*, **Katsumasa TERASAWA** *(Gunma Univ.)*, **Nobuya FUKUDA** *(Gunma Univ.)* **and Kizashi YAMAGUCHI** *(Osaka Univ.)*

[*Mol. Cryst. Liq. Cryst.* in press]

The microscopic magnetic local structure of Botallackite-type layer structured compounds $Cu_2(OD)_3X$ (X = $NO_3^-$and $HCOO^-$) exhibiting non-

equilateral planar triangular magnetic lattice was determined by the solid-state high resolution deuterium NMR of deuterated hydroxy groups in the high temperature region above 190K. The magnetic interactions in a copper ion layer were probed by the paramagnetic NMR shifts of the two chemically distinct hydroxy groups. Isotripic NMR shift of each hydroxy group showed different temperature depndence, suggesting non-uniform magnetic inetraction. It appered that the magnetic interaction in the copper layer could be decomposed to a sum of 1D-Heisenberg ferro- and antiferromagnetic chains in the high temperature region. Two distinct copper chains with ferro- and antiferromagnetic exchange interactions $J = +19 \pm 11$ and -21 ± 3K were found for X = NO_3^- from the temperature dependence of the two distinct NMR signals, while $J = +13 \pm 7$ and -13 ± 5K for X = $HCOO^-$. The derived values of J almost reproduced the temperature behavior of the magnetic susceptibility $\chi_A T$ vs. *T*.

IV-N Proton Transfer Tunneling in Interacting Hydrogen Bonds in the Solid State

Control of functional interactions, such as electronic and dynamic one, is a key to produce new functional materials. It is important to study the possibility of the functional interactions in the solid state. The nuclear magnetic resonance provides microscopic aspects of the functional interactions in the solid state. Hydrogen bond has a great capability for mediating a variety of interactions. We have investigated proton transfer dynamics in the interacting hydrogen bonds in organic quasi-conjugated π-system. Interaction between the hydrogen bonds is a key point for propagating an information of one hydrogen bond to the other hydrogen bond through molecular frame.

IV-N-1 Observation of Thermal Tautomerism of Thermochromic Salicylidene-Aniline Derivatives in the Solid State by ^{15}N CPMAS NMR down to Cryogenic Temperatures

Claudia BENEDICT *(Freie Univ. Berlin)*, **Uwe LANGER** *(Freie Univ. Berlin)*, **Hans-Heinrich LIMBACH** *(Freie Univ. Berlin)*, **Hironori OGATA, and Sadamu TAKEDA** *(Gunma Univ. and IMS)*

[*Ber. Bunsenges. Phys. Chem.* **102**, 335 (1998)]

Temperature dependence of solid state ^{15}N-CP/MAS NMR spectra of ^{15}N enriched salicylideneaniline derivatives, *N*-salicylideneaniline (SA), N,N'-bissalicylidene-p-phenylenediamine (BSP) and N,N'-di(2-hydroxy-1-naphthylidene)-p-phenylenediamine (DNP) were measured in ordrt to study possible proton transfer process in the NHO hydrogen bonds. For DNP a remarkable change of the ^{15}N chemical shift of more than 50 ppm was observed between 26 and 388 K by using the CP/MAS NMR technique down to cryogenic temperatures. The result clearly indicates very small enthalpy differences among the four tautomers associated with the combination of two possible forms, OH and NH forms, of the two NHO hydrogen bonds in a DNP molecule.

Combination of comprehensive investigations of the spin-lattice relaxation rate of proton and low temperature ^{15}N-CP/MAS NMR spectrum provides unique information of proton dynamics in two interacting NHO hydrogen bonds of solid N,N'-di(2-hydroxy-1- naphthylmethylene)-p-phenylenediamine (DNP). It was evidenced from the ^{1}H-NMR relaxation measurement that tunneling mechanism operates for the proton transfer in the hydrogen bonds. The tunneling phenomenon is closely related to the very small energy differences among the four tautomeric states accompanied with the proton transfer in the two NHO hydrogen bonds. The very small values of the energy difference, in spite of the chemically asymmetric NHO hydrogen bond, were revealed by the ^{15}N-CP/MAS NMR spectrum. This is a unique character of solid DNP. It was also suggested from the derived energy scheme of the four tautomers and activation energies of the proton transfer that an interaction exists between the two NHO hydrogen bonds linked by π-electronic molecular frame. This means that the information of one NHO hydrogen bond, *e.g*. OH-form or NH-form, propagates to the other hydrogen bond and the proton transfer in one hydrogen bond induces the change of the potential function for the proton transfer in the other hydrogen bond.

IV-N-2 Proton Dynamics in Interacting Hydrogen Bonds in the Solid State: Proton Tunneling in the NHO Hydrogen Bonds of N,N'-Di(2-hydroxy-1-naphthylmethylene)-p-phenylenediamine

Sadamu TAKEDA *(Gunma Univ. and IMS)*, **Tamotsu INABE** *(Hokkaido Univ.)*, **Claudia BENEDICT** *(Freie Univ. Berlin)*, **Uwe LANGER** *(Freie Univ. Berlin)* **and Hans-Heinrich LIMBACH** *(Freie Univ. Berlin)*

[*Ber. Bunsenges. Phys. Chem.* in press]

RESEARCH ACTIVITIES V
Department of Applied Molecular Science

V-A Molecular Mechanisms of Oxygen Activation by Heme Enzymes

By sharing a common prosthetic group, the heme enzymes such as cytochrome P450s, peroxidases, and catalases catalyze their own unique biological functions; monooxygenation, hydrogen peroxide dependent oxidation, and dismutation of hydrogen peroxide, respectively. Our efforts have been focused on the elucidation of the structure-biological function relationship of those heme enzymes by employing both enzymic systems including mutants and their model systems.

V-A-1 On the Formation and Reactivity of Compound I of the His64 Myoglobin Mutants

Toshitaka MATSUI, Shin-ichi OZAKI and Yoshihito WATANABE

[*J. Biol. Chem.* **272**, 32735 (1997)]

Myoglobin (Mb) catalyzes various two-electron oxidations; however, ferryl porphyrin cation radical equivalent to peroxidase compound I has not been identified yet. Distal histidine mutants of sperm whale Mb (His-64 → Ala, Ser and Leu) afford an apparent intermediate followed by the formation of a ferryl heme (Mb-II) in the reaction with *m*-chloroperbenzoic acid (*m*CPBA) (Figure 1). Since the intermediate exhibits characteristic absorption spectrum of compound I and bears two electron oxidizing equivalents above the ferric state, we have assigned the species as compound I of myoglobin (Mb-I). Although we have recently observed compound I of the F43H/H64L Mb mutant, F43H and wild type Mb react with *m*CPBA to give Mb-II without any accumulation of Mb-I. The results unambiguously indicate that His-64 plays a key role in destabilizing wild type Mb-I. Furthermore, Mb-I is found to be capable of performing two-electron oxidation of styrene, thioanisole and H_2O_2.

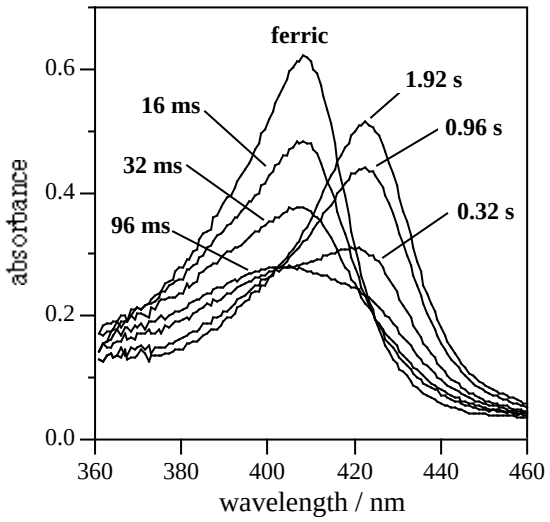

Figure 1. Time dependent spectral changes in the reaction of H64A Mb with *m*CPBA at 5.0°C in 50 mM sodium phosphate buffer, pH 7.0.

V-A-2 Effects of the Location of Distal Histidine in the Reaction of Myoglobin with Hydrogen Peroxide

Toshitaka MATSUI, Shin-ichi OZAKI and Yoshihito WATANABE

[*J. Biol. Chem.* in press]

In order to clarify how the location of distal histidine affects on the activation process of H_2O_2 by heme proteins, we have characterized reactions with H_2O_2 for L29H/H64L and F43H/H64L mutants of sperm whale myoglobin (Mb) designed to locate the histidine farther from the heme iron. While the L29H/H64L double substitution retards the reaction with H_2O_2, an 11-fold rate increase *versus* wild type Mb is observed for the F43H/H64L mutant. The Vmax values for one-electron oxidations by the Mbs are well correlated to the varied reactivities with H_2O_2. The functions of the distal histidine as a general acid-base catalyst are examined based on the reactions with cumene hydroperoxide and cyanide, and only the histidine in F43H/H64L Mb is suggested to facilitate the heterolysis of peroxide bond. The X-ray crystal structures of the mutants confirm that the distal histidines in F43H/H64L Mb and peroxidase are similar in distance from the heme iron while the distal histidine in L29H/H64L Mb is located too far to enhance the heterolysis (Figure 1). Our results indicate that the proper positioning of the distal histidine is essential for the activation of H_2O_2 by heme enzymes.

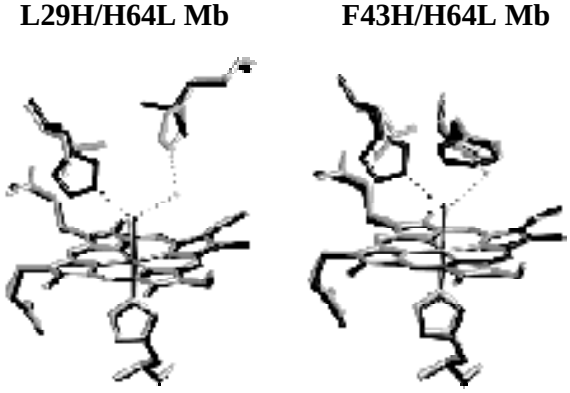

Figure 1. Crystal structures of L29H/H64L (left, gray) and F43H/H64L (right, gray) Mb mutants superimposed by wild type Mb (black).

V-A-3 Mechanistic Studies of Suicidal meso-Oxidation of Novel Iron Porphyrin Complexes as Models for the Formation of α-*Meso*-Hydroxyheme by Heme Oxygenase

Tatsuya MURAKAMI *(Kyoto Univ.)*, **Yoshihito WATANABE and Isao MORISHIMA** *(Kyoto Univ.)*

For the mechanistic studies on the formation of α-*meso*-hydroxyheme catalyzed by Heme Oxygenase (HO), we have prepared a novel iron porphyrin complex, in which less hindered *p*-chlorophenyl groups are introduced to the 5- and 15-*meso*-positions and the other two meso-positions are protected by mesityl groups; Fe^{III}BMB*p*CPP (**1a**) [BMB*p*CPP: 5,15-bis(mesityl)-10,20-bis(*p*-chlorophenyl)porphyrin]. The reaction of **1a**-trifluoroacetate (Tfa) and a small excess of *p*-nitroperbenzoic acid (*p*NPBA) has been carried out in dichloromethane containing 4 equiv of trifluoroacetic acid at -70°C. The oxidation product (2a) shows two intense absorption bands in a near-IR region and g values (6.18, 5.68, and 1.98) typical of iron(III) rhombic high spin complexes. In NMR measurements, four-splitting resonances assignable to β-pyrrole H of **2a** suggest the ring structure of C_s symmetry. These spectroscopic features readily lead us to identify **2a** as a ferric isoporphyrin complex. Further, IR and electrospray ionization (ESI) mass spectral measurements indicate **2a** bearing a *p*-nitrobenzoyloxy group at a *meso*-position. On the basis of the kinetic profile of the reaction between **1a**-Tfa and *p*NPBA, the reaction has been concluded to proceed via the formation of a *p*-nitroperbenzoate-iron(III) complex followed by an O-O bond cleavage, and more importantly, an intermediate (**3a**) prior to **2a** formation has been observed. Substituent effect of perbenzoic acid on the rate of the O-O bond cleavage shows that electron-withdrawing substituents accelerate the reaction, indicative of heterolysis of the O-O bond. When the reaction of **1a** and ^{18}O labeled *m*CPBA (Ar-C(=^{16}O)-$^{18}O_2H$) is carried out, *m*-chlorobenzoate is attached to a *meso*-position as Ar-C(=^{16}O)^{18}O-. These results demonstrate that the iron(III) isoporphyrin complex (**2a**) is formed via a *p*NPBA-iron(III) porphyrin complex and the following intermediate (**3a**) by the heterolytic O-O bond cleavage coupled with a intramolecular migration of *p*-nitrobenzoyloxy group to the *meso*-position.

V-A-4 Characterization of Polyethylene Glycolated Horseradish Peroxidase in Organic Solvents: Generation and Stabilization of Transient Catalytic Intermediates at Low Temperature

Shin-ichi OZAKI, Yuji INADA *(Toin Univ. Yokohama)* **and Yoshihito WATANABE**

[*J. Am. Chem. Soc.* **120**, 8020 (1998)]

Polyethylene glycolated horseradish peroxidase (PEG-HRP) can catalyze one- and two-electron oxidation reactions in organic solvents as well as in aqueous buffer. Even though the oxidation of guaiacol in benzene and chlorobenzene is five order of magnitude slower than in phosphate buffer, compound I and II are also involved in the catalytic cycle in organic media. Factor analysis and global fittings of rapid scan data set reveal that the formation of compound I of PEG-HRP in organic media consists of two steps: the first fast and the second slow process, and suggest the involvement of a H_2O_2-HRP complex in the catalytic cycle. The labile precursor of compound I is stabilized when PEG-HRP reacts with hydrogen peroxide in chlorobenzene at -20°C. The absorption spectrum of the precursor does not exhibit the features of hyperporphyrin spectrum but has a normal Soret as previously observed in R38L HRP. More importantly, compound I of PEG-HRP can be maintained for more than an hour at -20°C in chlorobenzene.

V-B Molecular Mechanisms of Substrate Metabolism by Heme Enzymes

Heme enzymes oxidize a variety of substrates, however, the detailed molecular mechanisms for many types of reactions including *N*-demethylation of amines, heme oxygenation, etc, are still obscure. Our efforts have been concentrated on the elucidation of the *N*-demethylation and heme oxygenation.

V-B-1 The Mechanisms of *N*-Demethylation Catalyzed by Heme Enzymes: Direct Observation of *N*-Demethylation by Compound I of Horseradish Peroxidase and Its Model Complex

Yoshio GOTO, Yoshihito WATANABE, Shunichi FUKUZUMI *(Osaka Univ)*, **Jeffry P. JONES** *(Univ. Rochester)* **and Joseph P. DINNOCENZO** *(Univ. Rochester)*

[*J. Am. Chem. Soc.* in press]

To elucidate the mechanisms of *N*-demethylation catalyzed by heme enzymes, we have employed two direct observation systems i.e., the *N*-demethylation of *p*-substituted *N*,*N*-dimethylaniline (DMA) both by horseradish peroxidase (HRP) compound I and by TMPFe(IV)=O cation radical, and evaluated the kinetic profiles. In HRP system, stepwise reduction of compound I to ferric state via compound II was observed. Linear correlation of the rate constants of each step with the oxidation potential of DMAs and no observation of kinetic isotope effect are consistent with the sequential one electron oxidation mechanism of the enzyme. On the other hand, O=$Fe^{IV}TMP^{+\bullet}$ showed isosbestic UV- spectral change to Fe^{III}TMP for the reaction with DMAs at 223K and rate constants are

linearly dependent on the oxidation potential of DMAs. Thus the demethylation by $O=Fe^{IV}TMP^{\bullet+}$ also proceeds via electron transfer. **The observed *kinetic* and *product* deuterium isotope effect profiles indicate that the electron transfer is followed by hydrogen atom transfer from $DMAs^{\bullet+}$ to $O=Fe^{IV}TMP$ in competition with the back electron transfer** (Scheme 1)**.**

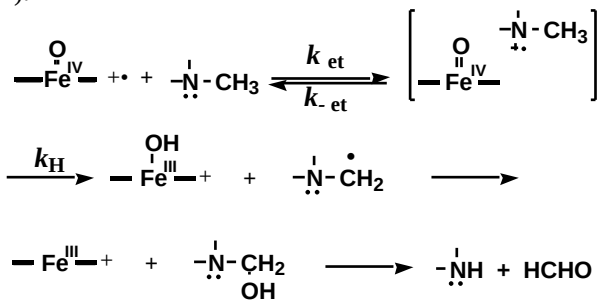

Scheme 1. *N*-Demethylation of amines by O=Fe(IV) porphyrin π-cation radical.

V-B-2 Effects of the Arrangement of a Distal Catalytic Residue on Regioselectivity and Reactivity in the Coupled Oxidation of Sperm Whale Myoglobin Mutants

Tatsuya MURAKAMI *(Kyoto Univ.)*, **Isao MORISHIMA** *(Kyoto Univ.)*, **Toshitaka MATSUI, Shin-ichi OZAKI, Isao HARA, Hui-Jun YANG and Yoshihito WATANABE**

The coupled oxidations of sperm whale myoglobin (Mb) mutants (Figure 1) are performed to examine active site residues controlling the regiospecific heme degradation. HPLC analysis of biliverdin isomers shows that L29H/H64L Mb almost exclusively gives biliverdin IXγ although H64L and wild type Mb mainly affords the α-isomer. Relocation of the distal histidine at the 43, and 107 position increases the amount of γ-isomer to 44 and 22%, respectively. Interestingly, the increase in the ratio of γ-isomer is also observed by a single replacement of either His-64 with Asp or Phe-43 with Trp. It appears that the polarity of the active site as well as hydrogen bonding between oxygen molecule bound to the heme iron and His or Trp is important in controlling the regioselectivity. The results of coupled oxidation kinetics, autooxidation kinetics, and redox potential of Fe^{3+}/Fe^{2+} couple are discussed with regards to their implications for the active site and mechanism of heme oxygenase.

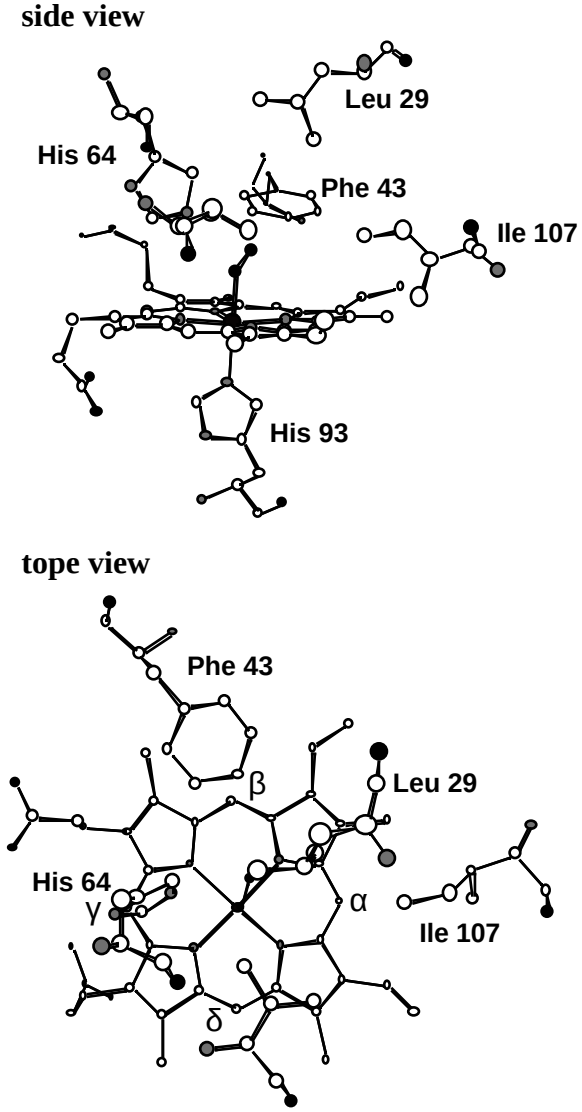

Figure 1. Top and side views of an oxy-form of the myoglobin active site.

V-C Model Studies of Non-heme Proteins

Non-heme proteins play important roles in biological redox processes. Many reactions catalyzed by the non-heme enzymes are quite similar to those by hemoproteins. We are interested in the active intermediates responsible for oxidation and oxygenation by non-heme enzyme, especially the similarity and differences.

V-C-1 A Model Complex for an Active Form of Soybean Lipoxygenase-1

Seiji OGO, Senji WADA, Masakazu IWASE *(Nagoya Inst. Tech.)*, **Akira WADA** *(Nagoya Inst. Tech.)*, **Manabu HARATA** *(Nagoya Inst. Tech.)*, **Koichiro JITSUKAWA** *(Nagoya Inst. Tech.)*, **Hideki MASUDA** *(Nagoya Inst. Tech.)*, **Hisahiko EINAGA** *(Nagoya Inst. Tech.)* **and Yoshihito WATANABE**

[*Angew. Chem. Int. Ed. Engl.* **37**, 2102 (1998)]

Lipoxygenases (LOs) are mononuclear non-heme iron enzymes which catalyze the peroxidation of polyunsaturated fatty acids and fatty acid esters containing the *cis,cis*-1,4-diene moiety to the corresponding 1-hydroperoxy-*trans,cis*-2,4-diene. We have studied synthesis, structure, and spectroscopic properties of a 6-coordinate (hydroxo)iron(III) complex

[Fe(TNPA)(OH)(PhCOO)]ClO_4 (**1**, TNPA = tris-(6-neopentylamino-2-pyridylmethyl)amine) which is the first structural model for the active center of ferric SLO-1 with a hydroxo ligand. Complex **1** has been characterized by X-ray structure analysis (Figure 1), UV/Vis, IR, EPR, and electrospray ionization mass spectrometry (ESI-MS). Complex **1** has cis-configuration between the OH^- ligand and the PhCOO- or three NH ligands of TNPA. The proposed core structure of ferric SLO-1 also has *cis*-configuration between the hydroxo ligand and the carboxylato ligand of C-terminal isoleucine or carboxamidato ligand of asparagine. The *cis*-configurations appear to be important for the formation of intramolecular hydrogen bonds which stabilize the (hydroxo)iron core structure of ferric SLO-1.

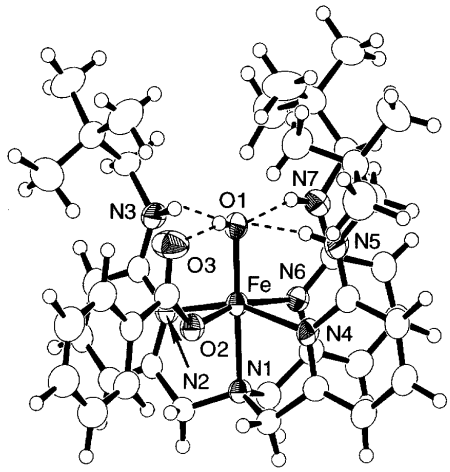

Figure 1. ORTEP drawing of [Fe(TNPA)(OH)(PhCOO)]-ClO_4 (**1**).

V-C-2 Functional Model Chemistry for Manganese(II)-Dependent Catechol Dioxygenases

Takuzo FUNABIKI *(Kyoto Univ.)*, **Tomoyuki ITO** *(Kyoto Univ.)*, **Hajime MATSUI** *(Kyoto Univ.)*, **Atsushi FUKUI** *(Kyoto Univ.)*, **Satohiro YOSHIDA** *(Kyoto Univ.)*, **Seiji OGO and Yoshihito WATANABE**

Catechol dioxygenases play key roles in the metabolism of various aromatic compounds, converting aromatics to aliphatics with insertion of molecular oxygen between a C-C bond of a benzene ring. It is well known that this reaction is catalyzed by nonheme iron oxygenases: Fe^{3+} enzymes catalyze mainly the intradiol oxygenation by a C1-C2 bond fission, and Fe^{2+} enzymes catalyze the extradiol oxygenation by a C2-C3 or C1-C6 bond fission. Besides the iron enzymes a manganese-dependent catechol dioxygenase is known to catalyze the extradiol cleavage. The similarity of the coordination environment to the iron(II) enzymes has been suggested, but little has been studied about its reactivity from both sides of enzymatic and model studies. An example reported is the oxygenation by a penicillamine-manganese complex(II), but no product analysis has been performed to confirm the extradiol oxygenation. As the first step for the functional model study for manganese-dependent catechol dioxygenases, we here first report the intradiol cleavage by a nonheme manganese complex via a semiquinonatomanganese(II) species. The present results give the support for the radical intermediate species in the oxygenation of catechols proposed for iron enzymes. In the iron system, the semiquinonate radical character caused by an electron transfer from the ligand to iron(III) has been suggested by the NMR and UV/VS spectroscopic data, but the radical species has not been detected. We here report EPR and UV/VS evidences for that species which reacts with oxygen.

V-D Transition Metal Oxide Clusters

Organometallic oxide clusters with cubic and incomplete cubic frameworks have useful applications as homogeneous and heterogeneous catalysts for reactions such as the oxidation and metathesis of propene. Understanding of the formation mechanisms of such oxide clusters may lead to the further development of synthetic methodologies for the construction of desired clusters having efficient catalytic ability for hydrocarbon transformations.

V-D-1 Direct Observation by Electrospray Ionization Mass Spectrometry of a Key Transient Intermediate in the Formation of a Double Bookshelf-Type Oxide Cluster

Satoshi TAKARA *(Osaka City Univ.)*, **Seiji OGO, Takanori NISHIOKA** *(Osaka City Univ.)*, **Isamu KINOSHITA** *(Osaka City Univ.)*, **Kiyoshi ISOBE** *(Osaka City Univ.)* **and Yoshihito WATANABE**

An organometallic oxide cluster $[(n\text{Bu})_4\text{N}]_2[(\text{Cp*-Rh}^{\text{III}})_2\text{Mo}^{\text{VI}}_6\text{O}_{20}(\text{OMe})_2]$ (**1**) with a multi-incomplete cubic framework was obtained from the reaction of $[\{\text{Cp*Rh}(\mu\text{-Cl})\text{Cl}\}_2]$ and $[(n\text{Bu})_4\text{N}]_2[\text{Mo}_2\text{O}_7]$ in MeOH. We have investigated the formation mechanism of **1**, by electrospray ionization mass spectrometry (ESI-MS) which is a powerful tool used in identification and characterization of unstable intermediates generated in solution. A transient intermediate, $[\text{Cp*RhMo}_3\text{O}_8\text{-(OMe)}_5]^-$ (**P_{im}**) in the formation of cluster **1** in MeOH at -78˚C was observed by ESI-MS. In order to gain further insight into the mechanism of the formation of **P_{im}**, time-dependent and deuterium-labeling experiments using $[(\text{Cp*-d6})\text{RhCl}_2]_2$ and CD_3OD have also been carried out. ESI-MS results established that the labeled Cp*-d6 and methoxo (OCD_3) ligands are incorporated into **P_{im}**.

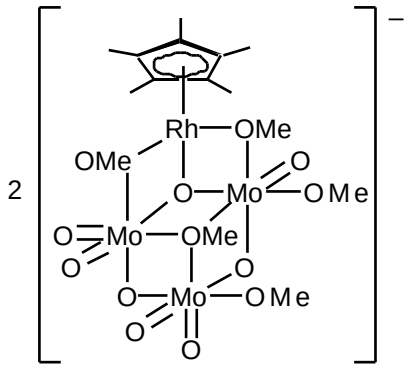

(**P$_{im}$**)

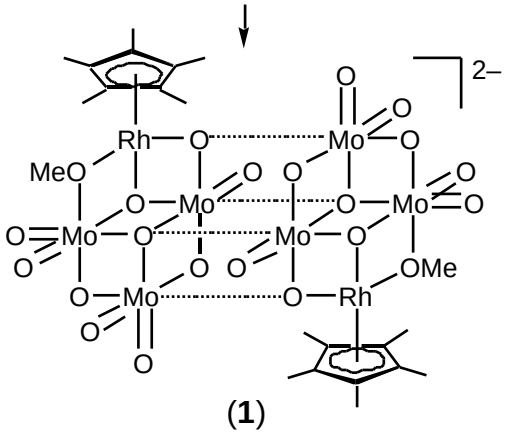

(**1**)

V-E Aqueous Organometallic Chemistry

Aqueous organometallic chemistry is a relatively new and exciting area that has primarily focused on the reactions of organometallic compounds with water soluble substrates in aqueous solution. We have studied chemo- and diastereoselective reactions of organometallic complexes as catalyst precursors in aqueous solution.

V-E-1 Synthesis and Structure of a New Water Soluble Rhodium(III) Complex

Nobuyuki MAKIHARA, Seiji OGO and Yoshihito WATANABE

Refluxing $RhCl_3 \cdot {}_3(H_2O)$ with 2-(tetramethylcyclopentadienyl)-4-methylphenol (Cp^t–H_2)[1)] in methanol generates the organometallic complex $[(Cp^t–H)Rh^{III}Cl_2]_2$ (**1**); the crystal structure of **1** was determined by X-ray analysis. Complex **1** reacts with $AgBF_4$ in water at ambient temperature to form the water soluble organometallic complex $[(Cp^t)Rh^{III}(OH_2)_2]\cdot(BF_4)$ (**2**). ^{1}H-NMR and electrospray ionization mass spectrometry (ESI-MS) have shown that complex **2** has two perpendicular (Cp^t and 4-methylphenolato) planes as the result of the formation of Rh–O(4-methylphenolato) bond. Applications of complex **2** as a catalyst precursor for selective oxidations and reductions of water soluble substrates in aqueous solution are currently under investigation.

Reference

1)Y. Chen, P. Fu, C. L. Stern and T. J. Marks, *Organometallics* **16**, 5958 (1997).

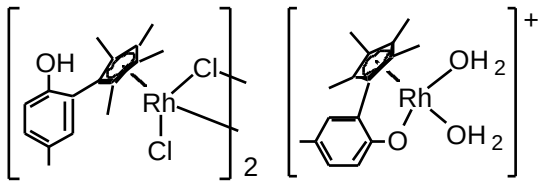

(**1**) (**2**)

V-F Construction of New Molecule-Based Magnets

Construction of molecular based magnetic materials which have well-defined one- or two-dimensional magnetic structure is a scientific subject of increasing interest. Heterospin systems consisting of paramagnetic transition metal

ions and organic free radicals as ligands constitute one of the mainstreams of such studies. Several of these materials have been established to have finite critical temperature of a ferro- or ferrimagnetic transition.

We have introduced a new strategy of employing π-conjugated polyaminoxyls as ligands in which the 2*p*-spins of the NO groups interact ferromagnetically ($J_1 > 0$). The dimensionality of the complex and the sign and magnitude of the exchange coupling between the neighboring spins may be readily tuned by this strategy. Depending on the nature of the additional interchain or interlayer interaction, the polymers are expected to become an antiferromagnet or ferri/ferromagnet. By modifying and extending this design strategy to bis- and tris(aminoxyl) radicals having triplet and quartet ground states, respectively, we have been able to construct with the aid of magnetic metal ions one-dimensional (1D) chain, two-dimensional (2D) network and three-dimensional (3D) parallel-crosses structures in which both the organic 2p and metallic 3d spins have been ordered in macroscopic scales. Since such a rational approach by self-assembly to the tailored extended systems having relevant physical properties is of great importance in materials synthesis.

V-F-1 Tacticity vs. Dimension of the Extended Structures in the Crystals of Heterospin Magnets Made of Transition Metal Complexes with Poly(aminoxyl) Radical

Hiizu IWAMURA *(Kyushu Univ.)*, **Katsuya INOUE and Noboru KOGA** *(Kyushu Univ.)*

[*New J. Chem.* **22**, 201 (1998)]

Bis- and tris(aminoxyl) radicals form with $M(hfac)_2$ {M = Mn(II) or Cu(II), and hfac = hexafluoroacetyl-acetonate} crystalline complexes having extended structures. Organic 2p and metal 3d spins in the complexes order at 3.4-46 K depending on the dimensions of the extended structures and the magnitude of exchange coupling between the adjacent spins. We have studied the crystal structures more carefully in a systematic manner to find that dimensionality of the crystal structures in these heterospin magnets is closely related to tacticity of the polymeric structures. The results obtained hereby will be of use in establishing a design strategy for tailored 3-D magnetic structures with high transition temperature on the basis of magnetic metal ions and high-spin organic polyradicals. In the crystals of one-dimensional systems, the polymeric chains are isotactic in that free radical have the same sign of chirality along any given chain (Figure 1). The polymeric chains are syndiotactic and crosslink to form two-dimensional honeycomb (Figure 2) or three-dimensional parallel-crosses networks (Figure 3).

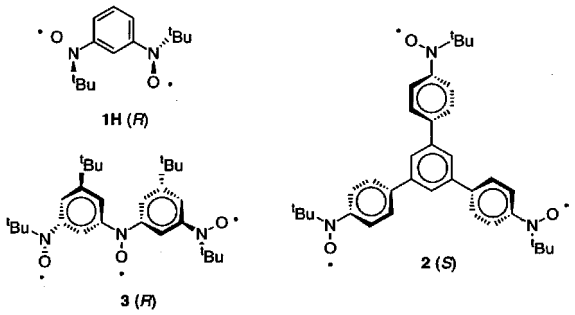

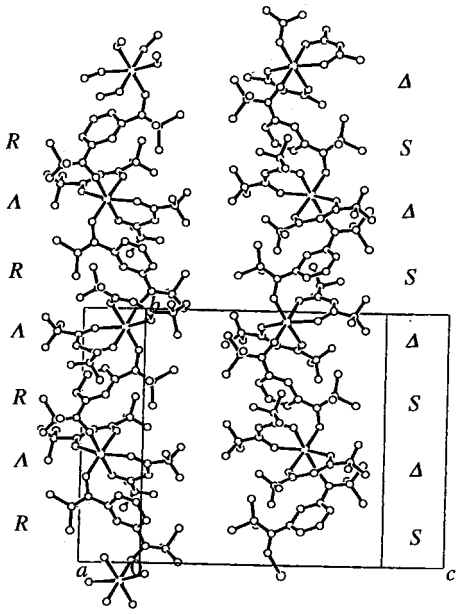

Figure 1. The one dimensional chains of $[Mn^{II}(hfac)_2 \cdot \mathbf{1H}]$ extending along the b axis.

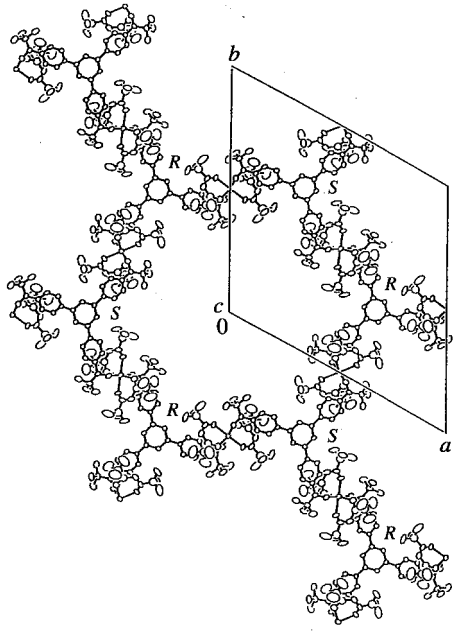

Figure 2. The complex $[\{Mn^{II}(hfac)_2\}_3 \cdot \mathbf{2}_2 \cdot n\text{-}C_7H_{16}]$ viewed down the c axis, showing the formation of two dimensional hexagonal nets. The n-C_7H_{16} molecules are disordered and not shown.

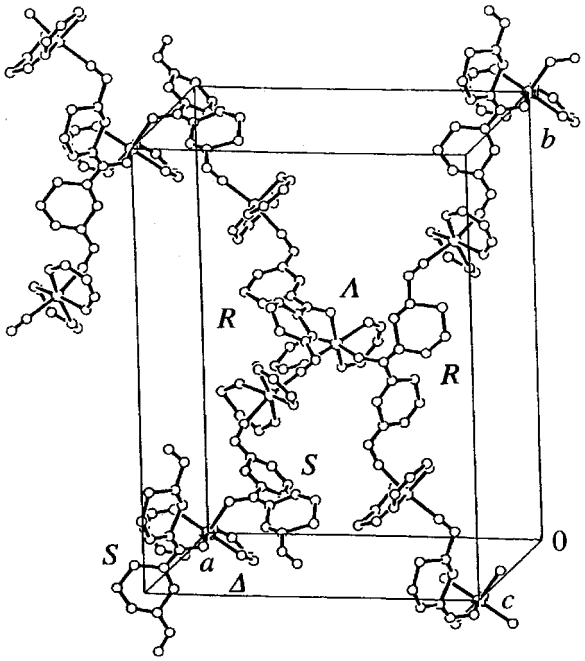

Figure 3. Three dimensonal crossed parallel structure of $[\{Mn^{II}(hfac)_2\}_3 \cdot \mathbf{3}_2]$. The CF_3 and $(CH_3)_3C$ groups are not shown for clarity.

V-F-2 Study of Magnetization and Magnetic Anisotropy of the Organometallic Complex between the Trinitroxide Radical and Bis(Hexafluoroacetylacetonato)Manganese(II)

Ashot S. MARKOSYAN, Takashi HAYAMIZU *(Kyushu Univ.)*, **Hiizu IWAMURA** *(Kyushu Univ.)* **and Katsuya INOUE**

[*J. Phys., Condens. Matter* **10**, 2323 (1998)]

A single crystal of the metal-radical complex $\{Mn(hfac)_2\}_3(\mathbf{3})_2$, where (**3**) is a trisaminoxyl radical (See previous part) with a quartet ground state, was grown. The magnetization was measured along the principal crystallographic axes in the range 1.8-300K. The compound was found to order ferrimagnetically at T_C = 45 ± 1K with collinear antiparallel alignment of the Mn- and (**3**)-magnetic spins along the c-direction. The paramagnetic susceptibility was treated in the quantum-classical approximation by taking into account the weak positive exchange interaction between the Mn(2) ions and one-dimensional ferrimagnetic ···-Mn(*1*)-(3)-Mn(*1*)-··· chains, in which trimer molecules composed of one Mn(*1*) and two 1/2 spins of different triradicals can be isolated (Figure 1). The anisotropy constants were evaluated and the anisotropy energy was estimated. Anisotropy of the paramagnetic susceptibility, which can be detected up to 55 K, was observed (Figure 2). The anisotropic effects are attributed both to the single-ion splitting of the Mn energy levels and the dipole-dipole interaction between the magnetic spins.

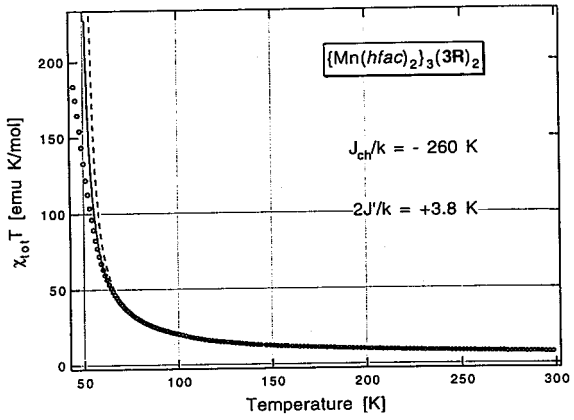

Figure 1. The temperature dependence of the product χ T of the $\{Mn(hfac)_2\}_3(\mathbf{3})_2$ complex in the paramagnetic temperature range. Open circles show the experimental data; the solid and dashed lines were calculated for the fixed trimer spin $S = 2/3$ in the quantum-classical and classical-classical approximations, respectively.

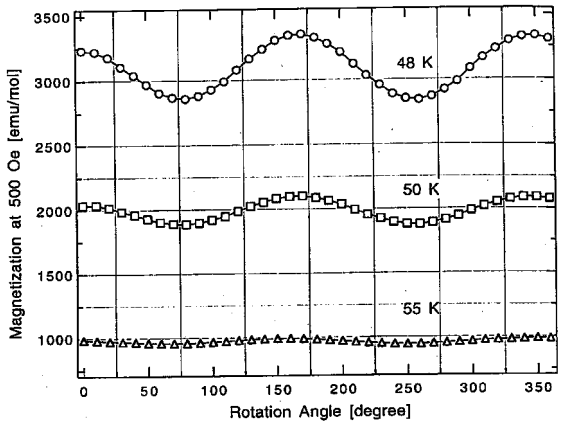

Figure 2. The angilar dependence of the low-field magnetization of the complex at different temperatures in the paramagnetic region measured in the (*ac*) crystallographic plane.

V-F-3 Magnetic Properties of Polymeric Chain Complex Made by 5-Bromo-1,3-Bis(*N-tert*-butyl-*N*-oxy-amino)benzene and Cu(II)(hfac)$_2$

Katsuya INOUE, Fumiyasu IWAHORI and Hiizu IWAMURA *(Kyushu Univ.)*

Bis(hexafluoroacetylacetonato)copper(II), $Cu(hfac)_2$, reacts with the triplet bisaminoxyl radical 5-bromo-1,3-bis(*N-tert*-butylaminoxyl) benzene **1**, to yield a distorted square-pyramidal adduct of formula $\mathbf{1}_2 \cdot [Cu(hfac)_2]_3$. The X-ray crystal structure shows that it crystallizes in the space group *P*1, with a = 12.469(2) Å, b = 15.278(2) Å, c = 11.602(2) Å, a = 104.59(1)°, b = 111.86(1)°, g = 88.32(1)°, and Z = 1. The complex makes 1-dimensional polymeric (···M-**1**-M-M-**1**-M-**1**-M-M-**1**···, M = Cu $(hfac)_2$) chain. (Scheme I) The magnetic data shows that a structural transition at ca. 48K. The structural transition shows temperature hystereisis (Figure 1). From the structural and magnetic analysis, the 1-D chain consisting of three different interaction ferro- (J_1, $J_2 > 0$) and antiferromagnetic ($J_3 \ll 0$) couplings has been realized. The exchange interaction value of 30.3 K ($2J/k_B$ value) between Cu_A

and NO group was estimated by linear three spin analysis. A structural transition occurred at ca. 48 K, the transition was assumed that the one of ferromagnetic interactions between three linear spins (NO—Cu_A—NO) changes to antiferomagnetic. (Scheme Ib)

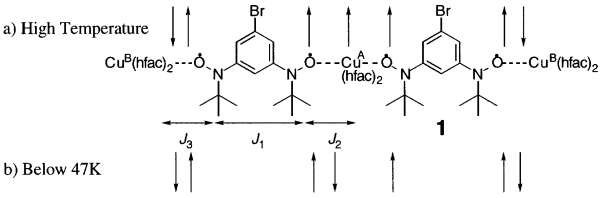

Scheme 1.

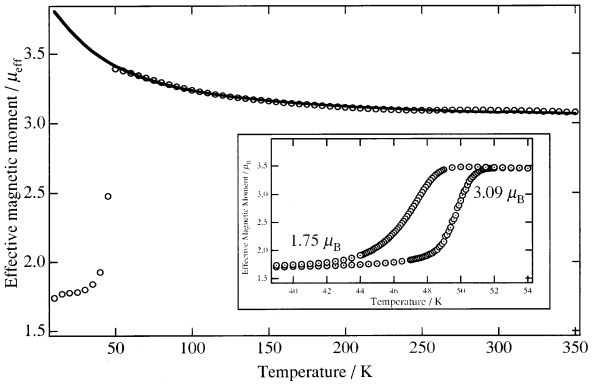

Figure 1. Observed magnetic moment versus *T* plots for the complex $\mathbf{1}_2 \cdot [Cu(hfac)_2]_3$ measured at a magnetic field of 50000 Oe. The inset shows the m_{eff} versus *T* plots of 40-55 K region. Solid lines are calculated with the linear trimer model (50-300 K).

V-G Synthesis of Chiral Molecule-Based Magnets

There is a phenomenological resemblance between natural and magnetic optical activity. The former is due to the handedness of molecular structure, whereas the latter is due to the magnetic field-induced circular dichroism. In 1984 Barron and Vrbancich call "magneto-chiral dichroism" (MChD) for a link between two phenomena. In 1997, Rikken and Raupach observed the MChD effect of tris(3-trifluoroacetyl-±-camphorato)europium (III) in the paramagnetic state. However, the MChD effect in the paramagnetic state is small. It's important to make the fully chiral molecule-based magnets, which expected to be strong MChD effect. There are still no examples of molecule-based chiral magnet. Novel properties are expected for such compounds.

The design of molecular materials with interesting electrical and/or magnetic properties is one of the major challenges of science in the last few years. It's possible to modify the molecular structure in the molecule-based magnetic materials. Recently, we introduced a strategy of using π-conjugated polyaminoxyl radicals with high-spin ground states as bridging ligands for magnetic metal ions in order to assemble and align the electron spins on a macroscopic scale. The crystal structures of these complexes are known, and some cases, the magnetic structures are analyzed. The dimensionality of the complex and the sign and magnitude of the exchange coupling between the neighboring spins may be readily tuned by this strategy. When we use a bidendate bisaminoxyl radicals as ligand and manganese(II) hexafluoroacetylacetonate, $Mn(II)(hfac)_2$, we can make one-dimensional complexes. If we use chiral triplet bisaminoxyl radicals for the construction of one-dimensional magnet, we can expect to make chiral molecule-based magnets.

V-G-1 Synthesis and Magnetic Properties of Chiral Organic Triplet Bisaminoxyl Radical

Hitoshi KUMAGAI and Katsuya INOUE

It is important to synthesize chiral magnetic compounds having ligating sites for construct chiral magnets. Nevertheless, only one example of pure organic chiral radical was reported. Novel properties are expected for such compounds. 1,3-substituted bisaminoxyl benzene biradical has been established to have a triplet ground state with a large intramolecular ferromagnetic interaction (J_1/k_B > 300 K) and has ligating capabilities. Here we report for the synthesis and characterization of a triplet organic diradical having not only a chiral carbon center but also ligating sites. A chiral triplet organic diradical 1,3-bis(*N-tert*-butyl-amino-*N*-oxyl)-5-{1-methyl-1-((*S*)-2-methylbutoxy)-ethyl}benzene (1) was synthesized and characterized. The temperature dependence of magnetic susceptibility was analyzed by a Bleany-Bowers type singlet-triplet model. (Figure 1) This result indicates that the two aminoxyl radical centers which are coupled ferro-magnetically within the organic radical molecule ($-2J/k_B$ = 461.8 K).

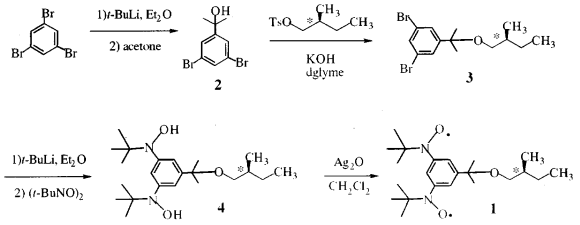

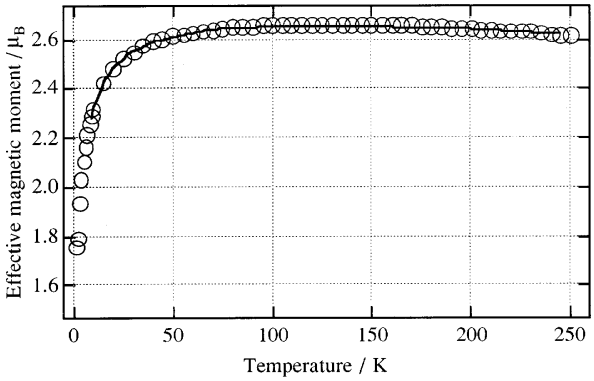

Figure 1. Observed effective magnetic moment vs. T plot for the diradical **1** measured in a magnetic field of 5000 Oe. Solid line is calculated by a Bleany-Bowers type model for the diradical **1**.

V-G-2 A Chiral Molecule-Based Metamagnet Made by Chiral Triplet Organic Radical and Manganese Ion

Hitoshi KUMAGAI and Katsuya INOUE

When we use a chiral bisaminoxyl radical for the ligand, a chiral one-dimensional structure was expected. Brown crystals of $\{\mathbf{1}\cdot Mn(II)(hfac)_2\}_n$ were obtained by mixing the 1,3-Bis (*N-oxy-tert*-butylamino)-5-{(S)-2'-methylbutyloxy}-*iso*-propylbenzene (**1**) and bis(hexafluoroacetylacetonato)manganese(II) $\{Mn(II)\cdot(hfac)_2\}$ in diethyl ether/*n*-heptane. A single crystal is triclinic, space group *P*1 (No. 1), with a = 11.0001 Å, b = 11.8204 Å, c = 17.7155 Å, α = 81.6093°, β = 84.8131°, γ = 63.5208°, V = 2038.9523 Å^3, and D_X = 1.380 g/cm^3 for Z = 1. An X-ray crystal structure analysis revealed the formation of a DNA strand type (*R*)-helical one-dimensional polymeric structure. It not only contains a (*S*) chiral carbon center but also (*R*) *C2* chiral skeleton of the organic ligand (Figure1). Each of the two aminoxyl radical centers which are mutually coupled ferromagnetically within the organic radical molecule is coupled antiferromagnetically to the d^5 manganese(II) ions. The temperature dependence of the magnetization revealed that the heterospin system behaves as a metamagnet below 5.4 K (Figure 2).

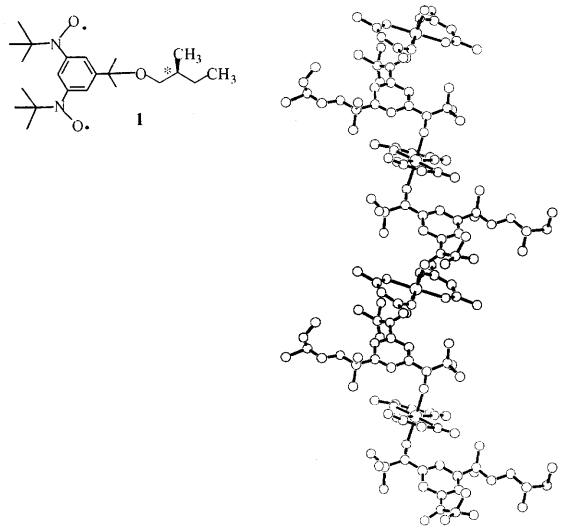

Figure 1. The X-ray crystal structure of the complex of $[\mathbf{1}\cdot Mn(II)(hfac)_2]_n$. Hydogen atoms are omitted for clarity. View along the *b* axis.

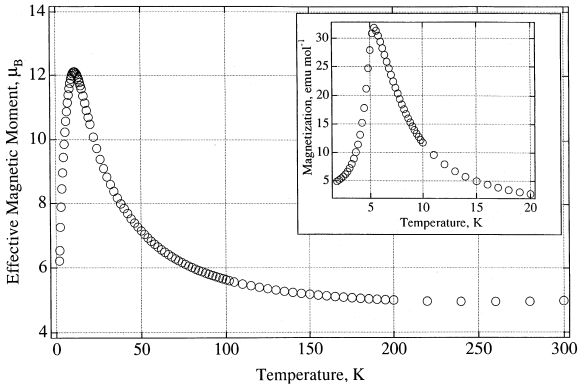

Figure 2. Temperature dependence of magnetic moment in a field of 5000 Oe of a polycrystalline sample of $[\mathbf{1}\cdot Mn(II)(hfac)_2]_n$. Inset shows the temperature dependence of magnetization at a field of 5 Oe of a polycrystalline sample.

V-H Synthesis and Characterization of Light Induced Spin-Crossover Complexes

The first transition metal compounds with d^4, d^5, d^6 and d^7 electron configuration are usually classified into two categories, i.e. high-spin and low-spin compounds depending on the strength of ligand field. However, there are compounds of which the ligand field strength is comparable to a spin-pairing energy, these complexes exhibit a temperature dependent spin-transition and this phenomenon is called spin-crossover. Spin-crossover complexes exhibit a temperature or pressure dependent spin transition. The spin-atate transition takes place through the thermal population of the high-spin and low-spin levels. A quantitative light-induced $^1A_1$(low-spin) $\rightarrow$ $^5T_2$(high-spin) transformation has been achieved in a number of iron(II) spin-crossover complexes in solid state, at a temperature much lower than that of the thermal transition (« 40 K), by irradiation the sample into the spin-allowed d-d or MLCT absorption bands of the stable low-spin species. The metastable high-spin state which forms in these conditions can remain trapped, with a practically infinite lifetime. This phenomenon is explained on the basis of light-induced excited spin state trapping; LIESST. We report the spin-state transition of the iron(III) complexes occurs by a new strategy which consists in varying ligand field strength under photochemical cis-trans isomerization of ligands, of which phenommenon has been able to be observed by using azobis(4-pyridine) analogs at relatively high temperature.

V-H-1 Synthesis and Magnetic Properties of Binuclear Iron(III) Complex Containing Photoisomerization Ligand

Shinya HAYAMI, Katsuya INOUE and Yonezo MAEDA *(Kyushu Univ.)*

[*Chem. Lett.* in press]

Binuclear iron(III) spin-crossover complexes with salten and az ligands $[Fe_2(salten)_2(az)](BPh_4)_2$ (salten is 1:2 condensation products of dipropylenetriamine and salicylaldehyde, and az is azobis(4-pyridine) (Scheme 1) were synthesized. The crystal structure, Mössbauer spectra, magnetic susceptibilities, electronoc spectra of the complex were examined. The X-ray structure of the complex were determined (Figure 1). Crystal data for the complex: $Fe_2O_4N_{10}C_{98}B_2H_{94}$, space group $P2_1/c$, Z = 2, a = 16.422(7), b = 16.005(6), c = 16.565(8) Å, β = 108.47(3)°, V = 4129(2) Å^3, R = 0.075, R_w = 0.060, 8608 reflections. The complex exhibited spin-crossover behavior depending on temperature, interexchange the rates of which are rapid compared to the Mössbauer time scale (10^7/s). The electronic spectra of the complex with photoisomerization ligamd (az) shifted reversibly by light irradiation in solution and irreversibly in solid state on the LMCT bands (Figure 2).

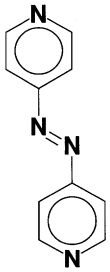

Scheme 1. Structure of az.

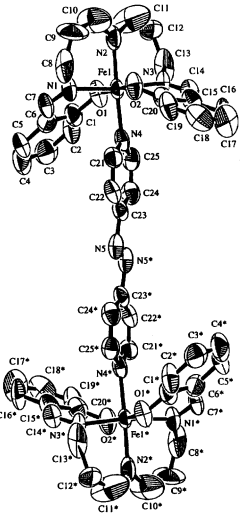

Figure 1. ORTEP view of the cation for $[Fe_2(salten)_2(az)](BPh_4)_2$. All hydrogen atoms are ommited for clarity.

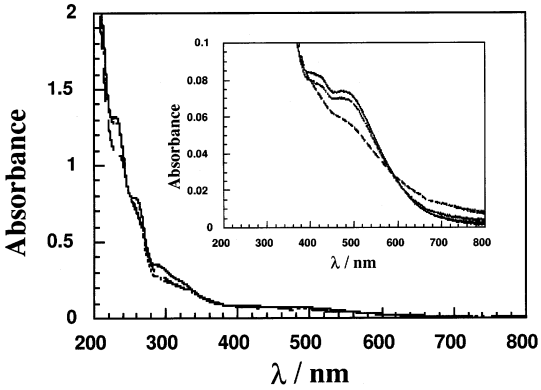

Figure 2. Absorption spectra at room temperature of $[Fe_2(salten)_2(az)](BPh_4)_2$ in acetonitrile solution before (——) and after (----) irradiation at lexc=300 nm, and 3 days after discontinuance of the irradiation (——). Insert: corresponding absorbance evolution in the LMCT band area.

V-I Synthesis and Characterization of Quantum-Spin Systems

Quantum spin systems have been much attracted for several decades. Quite different ground state is expected and the properties are open to research. In order to realize quantum spin systems, the spin-source should be isotropic. Organic radicals consisting only of light elements are regarded as ideal isotropic spin systems and are suitable for such studies. Focusing on this character, we are designing novel organic polyradicals to construct various lattice systems whose ground state is interested.

In 1983, Haldane conjectured the difference between a Heisenberg antiferromagnetic chain of integer-spin magnitude and that of half-integer-spin magnitude: Properties of integer-spin antiferromagnetic Heisenberg chain are characterized by the existence of a finite excitation gap above the unique ground state. Using organic biradicals, we can realize the intermediate spin state between spin-1/2 and spin-1. We have succeeded in tuning the intramolecular exchange couplings in organic biradicals by chemical modifications and arranging the biradicals to form low-dimensional antiferromagnetic lattices. The ground state properties are also studied in detail.

V-I-1 Ground State Properties of One- and Two-Dimensional Antiferromagnetic Heisenberg Spin Systems Made of Stable Organic Biradicals

Yuko HOSOKOSHI, Hiroki NAKANO *(ISSP Univ. Tokyo)***, Kohichi TAKIZAWA** *(ISSP Univ. Tokyo)***, Tsuneaki GOTO** *(ISSP Univ. Tokyo)***, Minoru TAKAHASHI** *(ISSP Univ. Tokyo)* **and Katsuya INOUE**

The ground state properties of antiferromagnetic

lattice systems of organic biradicals with $S = 1$ are examined. Among them, only F_2PNNNO exhibits an energy gap above the singlet ground state. The temperature dependence of the paramagnetic susceptibilities (χ_p's) of F_2PNNNO has a maximum at around 16 K and goes down to zero as temperature decreases. The magnetization isotherm of F_2PNNNO was measured at 0.5 K upto 40 T. The magnetization values below 8 T keep zero, take a constant value between 15-25 T at the half-value of the saturated magnetization and above 30 T, reach the saturated value corresponding to the parallel alignment of 2 mol of S = 1/2 species. (Figure 1). This behaviour is quite different from that of PNNNO, which shows monotonous increase of the magnetization. Both crystals of PNNNO and F_2PNNNO involve very similar chain structures, but interchain short contacts exist only in F_2PNNNO. We analyze the magnetic properties of PNNNO and F_2PNNNO based on the one-dimensional and two-dimensional model, respectively. The exchange parameter sets of $2J_F/k_B$ = 638 and $2J_{AF}/k_B$ = -14.5 K for PNNNO, and $2J_F/k_B$ = 407 and $2J_{AF}/k_B$ = -7.4, and $2J'_{AF}/k_B$ = -76 K for F_2PNNNO well reproduce the experimental results, where J_F, J_{AF}, and J'_{AF} represents the intramolecular ferromagnetic coupling, intrachain antiferromagnetic coupling, and interchain antiferromagnetic coupling, respectively. We must mention that F_2PNNNO is a quite rare example of two-dimensional system with an energy gap.

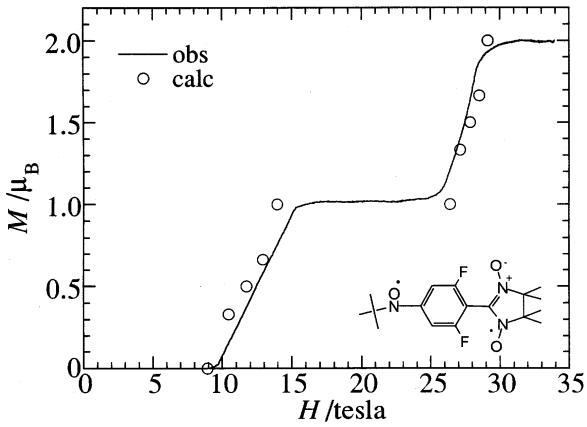

Figure 1. Magnetization process of F_2PNNNO at 0.5 K. Circles represent the calculation based on the two-dimensional model.

V-I-2 Construction of One-Dimensional Chain and Railroad-Trestle Using Organic Radicals

Yuko HOSOKOSHI, Keiichi KATOH *(Sci. Univ. Tokyo and IMS)***, Kenji MORI** *(Sci.Univ. Tokyo)* **and Katsuya INOUE**

We have synthesized organic monoradicals, F_2-PIMNH and Cl_2PIMNH to form chain structures using the hydrogen bonding between the NO and NH groups (-NO—HN-). In fact, both crystals involve such a hydrogen bonding, which yield small antiferromagnetic exchange coupling of *ca*. 3 K. Moreover, the crystals of F_2PIMNH has another hydrogen bonding as the second nearest contact to form a railroad trestle, whereas Cl_2-PIMNH form a simple uniform chain. The existence of an energy gap in F_2PIMNH is suggested from the temperature dependence of the static susceptibility measurements.

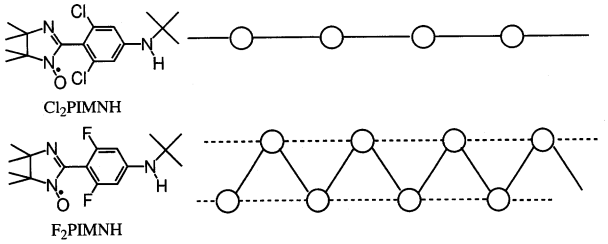

Figure 1. Schematic display of magnetic models with molecular structures.

V-J Pressure Effects on Molecular Magnetism

'Pressure' is a powerful tool to control the molecular packings and physical properties. The molecule-based materials with small densities are 'soft' and can be expected to exhibit large pressure effects. For the magnetic measurements with high-accuracy, we have developed a small high-pressure clamp cell made of Cu-Ti alloy which can be equipped to a Quantum Design SQUID magnetometer for the dc and ac magnetic measurements. The inner pressure of the clamp cell has been calibrated by the superconducting transition temperature of Pb. The maximum pressure maintained is ca. 7 kbar, the reproducibility is good, and the temperature variation of pressure in the cell is within ca 0.3 kbar.

We have already discovered that some kind of structural change can be suppressed by pressurization. We are now studying the pressure effects on the molecule-based magnetic materials in wider range. In molecular materials, the spin density are delocalized and distributed in a molecule and the spin-density-distribution plays an important role in the exchange interactions. It is attractive to control the sign of the exchange coupling by pressurization. The pressure effects on the related compounds with similar crystal structures are studied, and observed is the dimensional crossover and the change of the sign of magnetic interactions induced by pressure.

V-J-1 Pressure Effects on Organic Radicals with Ferromagnetic and Antiferromagnetic Interactions

Yuko HOSOKOSHI and Katsuya INOUE

Magnetic properties of stable organic biradicals under pressure are presented. The dimensional crossover from two-dimension to one-dimension induced by pressure is observed in F_2PNNNO, whereas the properties of the corresponding one-dimensional material, PNNNO is almost independent of the pressure. The energy gap in F_2PNNNO disappear under 3 kbar, reflecting the disappearance of the interchain interactions. (Figure 1). In the case of a quasi-one-dimensional antiferromagnet, PIMNO, the phase transition temperature become higher with applied pressure. The increase of the interchain interactions by pressurization has been observed, whereas the intrachain interactions are almost independent of the pressure.

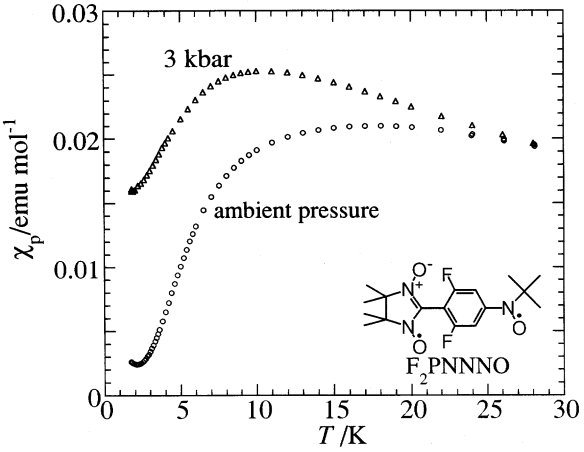

Figure 1. Temperature dependence of the paramagnetic susceptibilities of F_2PNNNO under 3 kbar compared with that at ambient pressure.

V-J-2 Pressure Effect on Mn Complexes of Bisaminoxyl Radicals

Yuko HOSOKOSHI, Kentaro SUZUKI *(Grad. Univ. Adv. Stud.)***, Katsuya INOUE and Hiizu IWAMURA** *(Kyushu Univ.)*

Organic biradical, 1,3-bis(*N*-tert-butylaminoxyl-benzene) (**1H**) makes a complex of [Mn(hfac)$_2$]·**1H** with one-dimensional chain and undergoes a metamagnetic phase transition at 5.4 K. The halogen derivatives of the biradical **1H**, replaced the hydrogen atom at 5 position by chlorine (**1Cl**) and bromine atoms (**1Br**), also form 1:1 complex with [Mn(hfac)$_2$] with one-dimensional chain and undergo ferrimagnetic phase transitions at 4.8 K and 5.3 K, respectively. The different ground states are attributed to the different sign of the interchain interactions. The slight change of the relative packing of the chain structure results in the different sign of the interchain interactions. Then, we apply pressure to these materials to change the magnitude and sign of the interchain exchange couplings.

The pressurization of the complex of [Mn(hfac)$_2$]·**1H** increases the magnitude of the antiferromagnetic interchain interactions. The transition temperature and the critical field of metamagnetic phase transition increases as increasing pressure. The critical field increases from *ca.* 200 Oe at ambient pressure to *ca.* 600 Oe under 7 kbar. The transition temperature under 7 kbar is 5.8 K.

On the other hand, the behaviour of the complex of chlorine derivative, [Mn(hfac)$_2$]·**1Cl**, under pressure is rather complicated. The temperature dependence of the ac susceptibilities under pressure shows a peak, whereas the one at ambient pressure diverges below *ca.* 4.8 K. The maximum temperature of the ac susceptibility under 4 and 7 kbar is 5.0 and 5.5 K, respectively. Moreover, the saturation rate of the magnetization at 1.8 K under pressure is slow, whereas the magnetization at 1.8 K at ambient pressure shows rapid saturation. Therefore, it is suspected that pressurization reduces the ferromagnetic distribution and induces the antiferromagnetic distribution in the interchain interactions.

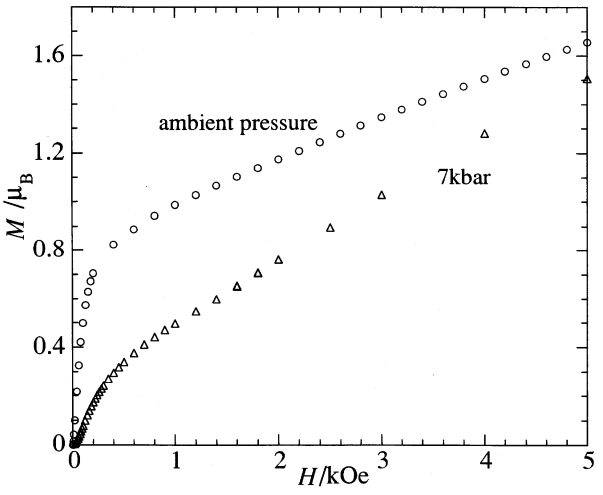

Figure 1. Magnetization isotherms at 1.8 K of [Mn(hfac)$_2$]·**1Cl**.

V-K New Charge-Transfer Complexes Exhibiting Novel Magnetic Properties

In 3d transition metals of iron, cobalt and nickel ferromagnetic state can be maintained at extremely high temperature. In contrast, a highest critical temperature (T_c) of ferromagnetic phase transition is 1.48 K in entirely s/p orbital-based organic ferromagnets, of which the first one has been discovered in a nitronylnitroxide radical crystal and successively about twenty ones have till now been prepared by using other organic radical crystals and charge-transfer (CT) complexes. In the present study we investigated the synthesis and magnetic properties of new

CT complexes with aim at achieving purely organic ferromagnets with high T_c.

V-K-1 1:2 Dimethyl-Substituted Tetracyanoquinodimethane/Its Radical Anion Mixed Salts: Ferromagnetic Behavior and High Electrical Conductivity at Room Temperature

Toyonari SUGIMOTO *(Osaka Pref. Univ. and IMS)*, **Kazumasa UEDA, Satoshi ENDO, Naoki TOYOTA, Toshiji TADA, Kei-ichiro NISHIMURA, Masakado KOHAMA, Kaoru SHIWAKU, Koji YAMAMOTO** *(Osaka Pref. Univ.)*, **Toshiyuki YAMAGUCHI, Yusaku SUENAGA and Megumu MUNAKATA** *(Kinki Univ.)*

[*Chem. Phys. Lett.* **288**, 767 (1998)]

So far, we prepared TCNQ/$TCNQ^{-\cdot}$ and $TCNQF_4$ /$TCNQF_4^{-\cdot}$ (1:2) mixed NMe_4^+ salts, which exhibited low electrical conductivities (< 10^{-2} S cm^{-1}) at room temperature. Nevertheless, for these mixed salts ferromagnetic behavior albeit in very small saturation magnetization was observed at room temperature. In order to confirm whether this anomalous magnetic behavior can also occur for the 1:2 mixed salts of the other substituted TCNQ derivatives, 1:2 mixed NMe_4^+ (**1**) and PMe_4^+ salts (**2**) of dimethyl-substituted TCNQ (DMTCNQ) with its radical anion ($DMTCNQ^{-\cdot}$) were prepared. The new 1:2 mixed salts exhibited both ferromagnetic behavior and high electrical conductivity at room temperature. The crystal structure of **2** (Figure 1) showed a composition of two different DMTCNQ /$DMTCNQ^{-\cdot}$ (1:1) and $DMTCNQ^{-\cdot}$ columns, which have significant contact with each other.

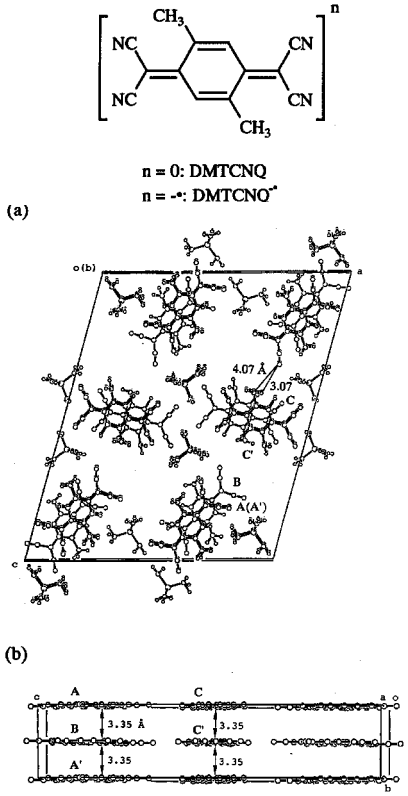

Figure 1. The crystal structure of **2**: the projections along the (a) *b* and (b) *a* axes.

V-K-2 Room-Temperature Ferromagnetic Behavior in 2,5-Diethyltetracyanoquinodimethanide Salts

Toyonari SUGIMOTO *(Osaka Pref. Univ. and IMS)*, **Kaoru SHIWAKU, Masakado KOHAMA, Kazumasa UEDA** *(Osaka Pref. Univ.)* **and Hideo FUJITA** *(Kyoto Univ.)*

Three years ago we found out room-temperature ferromagnetic behavior with small saturation magnetization for an 1:2 mixed NMe_4^+ salt of tetrafluoro-substituted TCNQ ($TCNQF_4$) with its radical anion. Subsequently, this phenomenon also was observed in 1:2 mixed Cs^+, NMe_4^+ and PMe_4^+ salts of TCNQ and dimethyl-substituted TCNQ (DMTCNQ) with their radical anions. In addition, the DMTCNQ salts exhibited high room-temperature electrical conductivities of 10-40 S cm^{-1}. Now, we investigated crystal structures, and electrical conducting and magnetic properties of NMe_4^+, PMe_4^+ and $AsMe_4^+$ salts of radical anion ($DETCNQ^{-\cdot}$) of diethyl-substituted TCNQ (DETCNQ). The crystal structure analyses showed that for the NMe_4^+ and PMe_4^+ salts one-dimensional column composed of dimerized $DETCNQ^{-\cdot}$ molecules is formed, while the two different $DETCNQ^{-\cdot}$ stacks are uniform for the $AsMe_4^+$ salt. These $DETCNQ^{-\cdot}$ salts also exhibited ferromagnetic behavior with very small saturation magnetization and coercive force, as was observed for the 1:2 mixed salts of TCNQ and DMTCNQ with their radical anions.

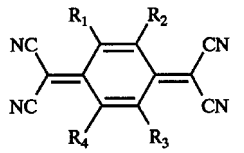

$TCNQF_4$: $R_1 = R_2 = R_3 = R_4 = F$
TCNQ: $R_1 = R_2 = R_3 = R_4 = H$
DMTCNQ: $R_1 = R_3 = Me$, $R_2 = R_4 = H$
DETCNQ: $R_1 = R_3 = Et$, $R_2 = R_4 = H$

V-K-3 Electrical Conducting and Magnetic Properties of Cesium Salts of Radical Anions of Dimethyl- and Diethyl-Substituted Tetracyanoquinodimethanes, and Tetracyanonaphthoquinodimethane

Toyonari SUGIMOTO *(Osaka Pref. Univ. and IMS)*, **Kaoru SHIWAKU, Masakado KOHAMA, Kazumasa UEDA, Satoshi ENDO, Naoki TOYOTA** *(Osaka Pref. Univ.)* **and Hideo FUJITA** *(Kyoto Univ.)*

A number of TCNQ radical anion ($TCNQ^{-\cdot}$) salts and 1:1 TCNQ/$TCNQ^{-\cdot}$ mixed salts have so far been prepared, but an 1:2 TCNQ/$TCNQ^{-\cdot}$ mixed salt is only known for the Cs^+ salt, which shows moderate room-temperature electrical conductivity on the single crystal. Furthermore, room-temperature ferromagnetic behavior with very small saturation magnetization was observed for the Cs^+ salt. The new Cs^+ salts of radical anions

(DMTCNQ$^{-\cdot}$, DETCNQ$^{-\cdot}$ and TNAP$^{-\cdot}$) of dimethyl- and diethyl-substituted TCNQ's (DMTCNQ and DETCNQ), and tetracyanonaphthoquinodimethane (TNAP) were prepared, which have molecular formulae of $Cs^+ \cdot DMTCNQ^{-\cdot}$, $\{Cs^+ \cdot DETCNQ^{-\cdot}/(Cs^+ \cdot DETCNQ^{-\cdot}) \cdot 1/2DETCNQ\}$ and $(Cs^+ \cdot TNAP^{-\cdot}) \cdot 1/2TNAP$, respectively. The $\{Cs^+ \cdot DETCNQ^{-\cdot}/(Cs^+ \cdot DETCNQ^{-\cdot}) \cdot 1/2DETCNQ\}$ and $(Cs^+ \cdot TNAP^{-\cdot}) \cdot 1/2TNAP$ salts exhibited considerably high room-temperature electrical conductivities of ca. 0.1 S cm^{-1} on the compressed pellets. The room-temperature ferromagnetic behavior was observed for the three Cs^+ salts, of which large saturation magnetization (7.3 emu mol^{-1}) was obtained for the $(Cs^+ \cdot TNAP^{-\cdot}) \cdot 1/2TNAP$ salt.

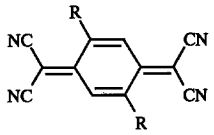

TCNQ: R = H
DMTCNQ: R = Me
DETCNQ: R = Et

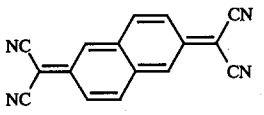

TNAP

V-K-4 Synthesis and Electrical Conducting Properties of Unsymmetrical Spiro Compounds Bearing a Tetrathiafulvalenyl Group

Masaki IWAMATSU, Kazumasa UEDA *(Osaka Pref. Univ.)*, **Toyonari SUGIMOTO** *(Osaka Pref. Univ. and IMS)* **and Hideo FUJITA** *(Kyoto Univ.)*

Single-component organic metals and furthermore superconductors are still not known, although their development is continuing to draw much attention. The first single-component organic conductor was realized in the TTF derivatives substituted with long-alkylthio or methyltelluro groups. The single-crystal electrical conducting property was semiconducting. We were rather interested in spiro compounds substituted with each of electron-donating and electron-accepting groups, which are arranged in a perpendicular manner and separated from each other, since a metallic state is expected to be increasingly stabilized by significant interaction between hole-carrying donor and electron-carrying acceptor stacks through a spiro conjugation, if the donating and accepting groups can be segregatedly stacked. As the first step, we prepared new spiro compounds (**1a** - **1d**) bearing each of dialkylthiotetrathiafulvalenyldithio and benzene- or toluene-dithio groups, and investigated their electrical conducting properties. One spiro compound, **1a** exhibited high room-temperature electrical conductivity (ca. 10^{-3} S cm^{-1}) on the compressed pellet.

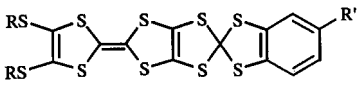

1a: R = CH_3, R' = H
1b: R = R' = CH_3
1c: R, R = -CH_2CH_2-, R' = H
1d: R, R = -CH_2CH_2, R' = CH_3

V-K-5 Synthesis, and Electrical Conducting and Magnetic Properties of Neutral Bis(tetrathiafulvalenyldithiolato) Cobalt Complexes

Kazumasa UEDA, Makoto GOTO, Yutaka KAMATA *(Osaka Pref. Univ.)*, **Toyonari SUGIMOTO** *(Osaka Pref. Univ. and IMS)*, **Satoshi ENDO, Naoki TOYOTA, Koji YAMAMOTO** *(Osaka Pref. Univ.)* **and Hideo FUJITA** *(Kyoto Univ.)*

Since the study on electrical conducting and magnetic properties of a prototype of π-d cooperative system, metallophthalocyanines, much effort has been paid for constructing various types of π-d cooperative systems and for elucidating their electrical conducting and magnetic properties. Our interest has been directed toward the synthesis of such a new type of organic complexes that an electron-donating organic ligand is bound to a magnetic metal ion through a covalent bond, and that two- or three-dimensional π conducting network is expected to be formed by π-d interaction in the crystal. Previously, we synthesized neutral bis(tetrathiafulvalenyldithiolato) copper complexes, which showed high room-temperature electrical conductivities (σ_{rt}'s) (10^{-4}-10^{0} S cm^{-1}) as result of preferential one-electron transfer from the Cu(II) atom to the TTF dithiolate radical cations. Now, the corresponding cobalt complexes (**1a-1c**) were synthesized, whose σ_{rt} values were 10^{-4}-10^{-10} S cm^{-1}. The SQUID measurement showed that the cobalt atom is in the Co(II) sate (S = 1/2). Addition of an equimolar amount of tetramethylthio-substituted TTF to **1a** brought about marked increase by ca. 10^7 in the σ_{rt} value.

V-L Desorption Induced by Electronic Transitions at the Surface of Van der Waals Condensates

The electronic excitation on the surface of a van der Waals condensate may lead the desorption of neutral and charged molecules, either in a ground state or in excited ones. The phenomena discussed here are neither thermal desorption nor direct mechanical sputtering but processes through a transformation of an electronic excitation energy into a kinetic energy of a desorbing particle. Close investigation of this DIET (Desorption Induced by Electronic Transitions) phenomena will reveal the dynamical aspect of the electronic excitation and its relaxation process at the surface. In this research project, we have revealed the desorption of the excimer, Ne_2*, and determined the absolute total desorption yield at the surface of solid Ne.

V-L-1 Exciton Induced Desorption at the Surface of Rare Gas Solids

Ichiro ARAKAWA *(Gakushuin Univ. and IMS)*

[*Mol. Cryst. Liq. Cryst.* **314**, 47 (1998)]

The nature of the exciton in rare gas solids have extensively been investigated by various experimental methods: photo-absorption, luminescence, electron energy loss spectroscopy, etc. The observation of the desorbed metastable is complementary one to the above approaches and is one of the most direct means to reveal the dynamic nature of the exciton, especially on a surface, because it detects the excited neutral species directly originated from the exciton. Many unclarified problems still remain in this field. As concerns the desorption from the S1 exciton, for example, the initial excitation and the deexcitation cascade leading to the desorption of the metastable have not been clarified yet. It is necessary to examine the fine structures in the relation between the exciton excitation and the desorption by using higher resolution spectroscopy. It has also been noticed that the phenomena are acutely sensitive to impurities adsorbed on a surface. As to some characteristic features observed in the present study, it should be clarified whether it is the nature intrinsic in a pure rare gas solid or is originated from impurities. Close investigation of the interaction with the impurities will provide a field of the study of the excitation transfer process between heteromolecules in a thick environment of condensate.

V-L-2 Desorption of Metastable Particles Induced by Electronic Excitation at the Surface of Rare Gas Solid with Hydrogen Physisorbed

Akira HAYAMA *(Gakushuin Univ.)*, **Takafumi KUNINOBU** *(Gakushuin Univ.)*, **Takato HIRAYAMA** *(Gakushuin Univ.)* **and Ichiro ARAKAWA** *(Gakushuin Univ. and IMS)*

[*J. Vac. Sci. Technol. A* **16**, 979 (1998)]

The effect of physisorption of hydrogen on the desorption of metastable particles induced by electronic excitation from the surface of rare-gas solids (Ar, Kr, and Xe) was investigated systematically. When the surface of rare-gas solid was exposed to a very small quantity of hydrogen at a temperature of about 30 K, in all cases, the desorption of hydrogen metastables was observed, and new desorption species of Kr* via cavity ejection process appeared in TOF spectra for Kr. For Ar, although no significant increase of desorption yield was found, the kinetic energy of Ar* desorbed through cavity ejection process was increased by hydrogen adsorption. These results will be discussed in terms of the change of electron affinity of the matrix and the interaction between hydrogen and rare gas molecules in excited states.

V-L-3 Desorption of an Excimer from the Surface of Solid Ne by Low Energy Electron and Photon Impact

Takato HIRAYAMA *(Gakushuin Univ.)*, **Akira HAYAMA** *(Gakushuin Univ.)*, **Takashi ADACHI** *(Gakushuin Univ.)* **and Ichiro ARAKAWA** *(Gakushuin Univ.and IMS)*

[submitted]

Desorption of an excited dimer from the surface of solid Ne initiated by a creation of an exciton was confirmed experimentally using a low energy electron and a monochromatic VUV light as excitation sources. The kinetic energy of desorbed excimer (Ne_2^* $^3\sum_u$) was found to be about (0.2±0.1) eV, which is consistent with a recent quantum mechanical calculation by Chen et al.[1] Desorption yield of the excimer in vibrationally excited states has been found to be about 10 times larger than that of vibrationally relaxed excimers. Desorption of excimers at the excitation of the first order surface exciton was found to be inefficient compared to that by the creation of bulk excitons opposed to the atomic desorption case.

Reference

1)L. F. Chen, G. Q. Huang and K. S. Song, *Nucl. Instrum. Meth. Phys. Res. B* **116**, 61 (1996).

V-M Synthesis and Physical Properties of Novel Molecular Metals

Development of organic materials which exhibit interesting electrical properties such as metallic conductivity and superconductivity has received considerable attention. A bis-fused TTF, 2,5-bis(1,3-dithiol-2-ylidene)-1,3,4,6-tetrathiapentalene (TTP) is a promising π-electron framework for preparation of stable metals down to low temperatures, because it has a ladder-like array of sulfur atoms indispensable for constructing two-dimensional network of the donors. In fact, we have found that the unsubstituted TTP has a strong tendency to afford highly conducting radical cation salts retaining metallic conductivity down to ≤ 1.2 K regardless of shape and size of counter anions. In the present study, we have developed several organic metals by means of comprehensive modification of TTP, namely i) introduction of substituents, ii) exchange of sulfur atoms in the TTP framework with selenium, iii) synthesis of TTP analogs possessing non-TTF donor unit.

V-M-1 Structural Feature of Radical Cation Salts Based on TTP and Its Selenium Analogs

Yohji MISAKI *(Kyoto Univ. and IMS)*, **Tatsuro KOCHI** *(Kyoto Univ.)*, **Masateru TANIGUCHI** *(Kyoto Univ.)*, **Tokio YAMABE** *(Kyoto Univ.)*,

Kazuyoshi TANAKA *(Kyoto Univ.)*, **Kazuo TAKIMIYA** *(Hiroshima Univ.)*, **Atsushi MORIKAMI** *(Hiroshima Univ.)*, **Tetsuo OTSUBO** *(Hiroshima Univ.)* **and Takehiko MORI** *(Tokyo Inst. Tech.)*

Two selenium analogs of TTP (2,5-bis(1,3-dithiol-2-ylidene)-1,3,4,6-tetrathiapentalene), ST-TTP and BDS-TTP have been prepared. Both donors afford many cation radical salts showing metallic conducting behavior down to liquid helium temperature. All the AsF_6 salts based on TTP, ST-TTP and BDS-TTP are isostructural to each other. The donors form conducting sheets along the *ac* plane, which are separated by insulating anion layers. The array of donors is classified as the so-called β-type (Figure 1), but the degree of dimerization in the stack is much smaller than that of β-$(BEDT\text{-}TTF)_2I_3$. It is noted that replacement of sulfur atoms with larger selenium atoms does not affect the donor array in the radical cation salts at all, whereas such a modification largely influences donor packing in the BEDT-TTF systems. For example, BETS affords κ- and λ-type salts with tetrahedral anions such as $GaCl_4^-$ and $FeCl_4^-$. In contrast, no such phase has been found in the BEDT-TTF salts with the similar anions. In a cationic state, the present TTP donors are completely planar and have a more rigid molecular skeleton compared to BEDT-TTF, which has flexible and non-planar ethylenedithio groups. Such a high planarity, as well as a long molecular skeleton (twice as large as TTF), is electronically and sterically favorable to form a β-type donor packing.

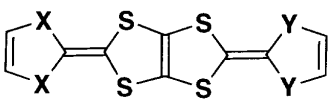

X = Y = S: TTP
X = S, Y = Se, ST-TTP
X = Y = Se, BDS-TTP

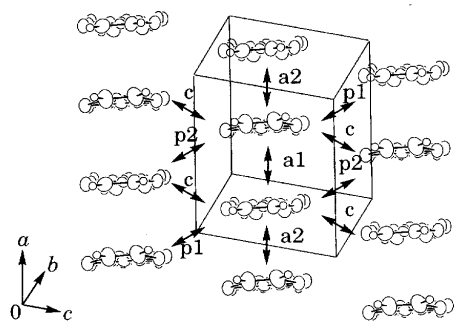

Figure 1. Donor sheet structure of $(BDS\text{-}TTP)_2AsF_6$.

V-M-2 Novel Oxygen Containing π-Electron Donors for Organic Metals: 2-(1,3-Dithiol-2-ylidene)-5-(pyran-4-ylidene)-1,3,4,6-tetrathiapentalenes

Yohji MISAKI *(Kyoto Univ. and IMS)*, **Hideki FUJIWARA** *(Kyoto Univ. and IMS)*, **Takashi MARUYAMA** *(Kyoto Univ.)*, **Masateru TANIGUCHI** *(Kyoto Univ.)*, **Tokio YAMABE** *(Kyoto Univ.)*, **Takehiko MORI** *(Tokyo Inst. Tech.)*, **Hatsumi MORI** *(ISTEC)* **and Shoji TANAKA** *(ISTEC)*

A bis-fused π-electron donor incorporating pyran-4-ylidene moiety, 2-(1,3-dithiol-2-ylidene)-5-(pyran-4-ylidene)-1,3,4,6-tetrathiapentalene (PDT-TTP), and its derivatives have been synthesized as donor components for organic conductors. The cyclic voltammograms of PDT-TTPs in benzonitrile are composed of two-pairs of single redox waves and one pair of two-electron one. The ethylendithio derivative ET-PDT have produced metallic salts with octahedral and liniear anions, which are stable down to 1.5-4.2 K. X-Ray structure analysis of the metallic PF_6^- salt of ET-PDT reveals that its composition is $(ET\text{-}PDT)_4PF_6(cn)$, where cn is 1-chloronaphthalene. The donors form conducting sheets, each of which is separated by the insulating layers composed of the anions and solvents. Two crystallographically independent ET-PDT molecules A and B form a face-to-face stack with four-folded period as A'ABB', in which the donors are stacked in a head-to-tail manner for molecules AA' and BB', and in a head-to-head manner for AB. The array of donors is close to that of an organic superconductor $\lambda\text{-}(BETS)_2GaCl_4$ (Figure 1). In the present salt, the head-to-tail overlap of the unsymmetrical π-electron framework of PDT-TTP prevents from an effective intrastack overlap. As a result, it has a strongly dimerized electronic structure along the stack direction in spite of its apparently uniform stack from the viewpoint of the interplanar distances. A tight-binding band calculations indicates it has an opened Fermi surfaces characteristic of quasi-one-dimensional metals.

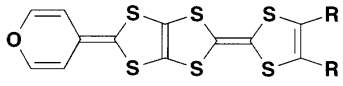

1a, R = H, PDT-TTP
1b, R = CO_2Me
1c, R = SMe
1d, 2R = $-S(CH_2)_2S-$, ET-PDT

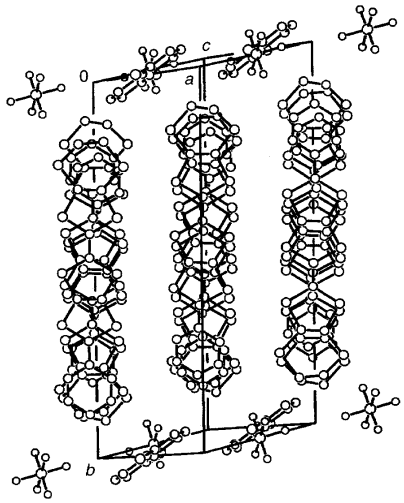

Figure 1. Crystal structure of $(ET\text{-}PDT)_4PF_6(cn)$.

V-M-3 Structures and Physical Properties of TMEO-ST-TTP Salts

Yohji MISAKI *(Kyoto Univ. and IMS)*, **Masateru TANIGUCHI** *(Kyoto Univ.)*, **Tadahiro KAIBUKI** *(Kyoto Univ.)*, **Koji TANAKA** *(Kyoto Univ.)*, **Tokio YAMABE** *(Kyoto Univ.)*, **Kazuyoshi TANAKA** *(Kyoto Univ.)*, **Kazuo TAKIMIYA** *(Hiroshima Univ.)*, **Atsushi MORIKAMI** *(Hiroshima Univ.)*, **Tetsuo OTSUBO** *(Hiroshima Univ.)* **and Takehiko MORI** *(Tokyo Inst. Tech.)*

A new donor TMEO-ST-TTP, where TMEO-ST-TTP is 2-[4,5-bis(methylthio)-1,3-diselenol-2-ylidene]-5-(4,5-ethylendioxy-1,3-dithiol-2-ylidene)-1,3,4,6-tetrathiapentalene, has been prepared. It affords highly conducting PF_6^- and AsF_6^- salts retaining metallic conductivity down to 4.2 K, while the TCNQ complex and ClO_4^- salt are low conductive semiconductors. X-Ray structure analysis of $(TMEO\text{-}ST\text{-}TTP)_2AsF_6$ reveals that this salt has the so-called β-type array of donors (Figure 1). A tight-binding band calculation suggests the present salt has a quasi one-dimensional Fermi surface opened along the stacking direction because the donors are dimerized in the stack.

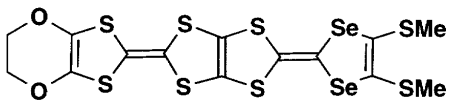

TMEO-ST-TTP

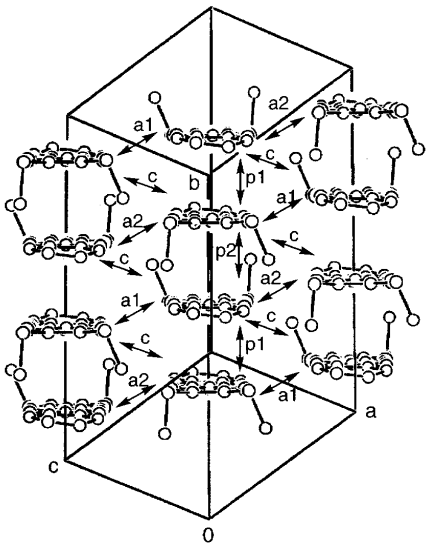

Figure 1. Donor sheet structure of $(TMEO\text{-}ST\text{-}TTP)_2AsF_6$.

V-M-4 Preparation and Properties of Gold Complexes with TTF-Dithiolato Ligands

Yohji MISAKI *(Kyoto Univ. and IMS)*, **Kazuyoshi TANAKA** *(Kyoto Univ.)* **and Klaus BECHGAAD** *(Risø National Lab.)*

A new family of metal complex with TTF-dithiolato ligands, $Au(dt)_2$ and $Au(tmdt)_2$, where dt and tmdt are 2-(1,3-dithiol-2-ylidene)- and 2-[4,5-bis(methylthio)-1,3-dithiol-2-ylidene]-1,3-dithiole-4,5-dithiolato, have been prepared. Cyclic voltammograms of tetrahexylammonium salts of $Au(dt)_2$ and $Au(tmdt)_2$ showed three and two pairs of irreversible waves, respectively. X-Ray structure analysis of $Bu_4N{\cdot}Au(dt)_2$ reveals that the $Au(dt)_2$ anion takes a slightly folded chair conformation with the dihedral angles of 8.6°. The neutral $Au(dt)_2$ and $Au(tmdt)_2$ exhibited high conductivity ($\sigma_{rt} = 10^0$ S cm^{-1}) on a compressed pellet, both of which showed semiconductive behavior with very low activation energies (E_a = 0.017-0.035 eV).

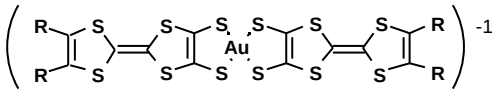

R'_4N^+

R = H, $(n\text{-}C_6H_{13})_4N{\cdot}Au(dt)_2$
R = SMe, $Bu_4N{\cdot}Au(tmdt)_2$

V-N Theoretical Study of the Electronic Structures of Weakly Bound Molecules

The electronic structures of weakly bound molecules such as van der Waals molecules are investigated by using sophisticated methods for electronic states, i.e., multi-reference single and double excitation configuration interaction (MRSDCI) and multi-reference coupled pair approximation (MRCPA) calculations.

V-N-1 Multi-Reference Coupled Pair Approximation (MRCPA) Calculations for the Ground State of the ArI_2 Complex

Eisaku MIYOSHI, Jun MAKI *(Hokkaido Univ.)*, **Takeshi NORO** *(Hokkaido Univ.)* **and Kiyoshi TANAKA** *(Hokkaido Univ.)*

[*J. Mol. Struct. Theochem* in press (1998)]

To investigate the relative stability of the T-shaped and linear isomers of the ArI_2 complex, multi-reference coupled pair approximation (MRCPA) and multi-reference single and double excitation configuration interaction (MRSDCI) calculations as well as single-reference CPA (SRCPA) and single-reference SDCI (SRSDCI) calculations were performed using relativistic model core potentials (MCPs) which included major relativistic effects. The localized natural orbitals (LNOs) set approach was used to calculate the correlation energy.

The T-shaped and linear isomers have almost the same binding energies. MRCPA calculations give a potential surface on which the T-shaped minimum is lower than the linear minimum by 9 cm^{-1}, which is in sharp contrast to those obtained by the SR approaches by Kunz *et al.*[1] who predicted that the linear isomer was more stable than the T-shaped isomer by 27, 18 and 13 cm^{-1} at the MP2, MP4 and CCSD(T) levels, respectively. Thus, the MR approach prefers the T-shaped isomer and is indispensable for investigating the relative stability of the linear and T-shaped isomers of halogen-rare gas van der Waals complexes.

Reference

1) C. F. Kunz, I. Burghardt and A. Hess, *J. Chem. Phys.* **109**, 359 (1998).

V-N-2 *Ab Initio* Study of the Ground and Excited States of ArHF

Tapas Kumar GHOSH, Eisaku MIYOSHI and Kiyoshi TANAKA *(Hokkaido Univ.)*

The class of van der Waals molecules involving the bonding between a rare gas atom and a hydrogen halide has gained intense impetus to both experimental and theoretical investigations because of its weakly intermolecular forces. In this study we have investigated the electronic structures of a van der Waals molecule, Ar-HF, to obtain the spectroscopic parameters and intermolecular potential energy surfaces for the ground $X\,^1\sum_g^+$ and excited $2\,^1\sum_g^+$ states. Calculations have been performed with a linear Ar-H-F structure. The dependence of both Ar-F and H-F distances have been studied. The excited $2\,^1\sum_g^+$ state is of ionic type (H^+F^-) and dissociates to a negative fluorine ion. This ,in turn, enlightens the photochemical reaction of the ionic excited HF with Ar correlating to the production of negative F ion:

$ArHF + h\nu \rightarrow Ar + (H^+F^-)^* \rightarrow (ArH^+)^* + F^-$.

V-N-3 *Ab Initio* Molecular Orbital Study of $Fe(CO)_n$ (n = 1, 2, and 3)

Hiroaki HONDA *(Hokkaido Univ.)*, **Takeshi NORO** *(Hokkaido Univ.)* **and Eisaku MIYOSHI**

Various unsaturated iron carbonyl complexes $Fe(CO)_n$ (n = 1 to 4) have been produced by the UV photolysis of iron pentacarbonyl $Fe(CO)_5$.[1] Among them the spectroscopic studies of the FeCO radical has been extensively performed from both experimental and theoretical points of view and there have been a few experimental spectroscopic constants of $Fe(CO)_2$ and $Fe(CO)_3$.

Although there have been published several theoretical studies for $Fe(CO)_2$ and $Fe(CO)_3$, there are few comprehensive studies for the change of bonding nature in the $Fe(CO)_n$ (n = 1 to 3) radicals. In this study we will investigate spectroscopic constants of the $Fe(CO)_n$ (n = 1 to 3) radicals by the use of *ab initio* calculations and discuss the change of the bonding nature through the donation and back-donation scheme in the radicals. Going from FeCO to $Fe(CO)_3$, the σ donation and π back-donation per CO decrease, which is consistent with the increase of vibrational frequencies of C-O stretch.

Reference

1) K. Tanaka, K. Sakaguchi and T. Tanaka, *J. Chem. Phys.* **106**, 2118 (1997).

V-O Molecular Dynamics Study Using Potentials by *Ab Initio* Molecular Orbital Calculations

Using potentials obtained by *ab initio* molecular orbital calculations, molecular dynamics calculations were performed to investigate physical properties of liquid mercury.

V-O-1 Molecular Dynamics Study of Liquid Mercury in the Density Region between Metal and Nonmetal

Tomonari SUMI *(Kyushu Univ.)*, **Eisaku MIYOSHI and Kiyoshi TANAKA** *(Hokkaido Univ.)*

We performed SDCI, SDCI(+Q), and CPA calculations for the ground $^1\sum_g^+$ state of Hg_2 incorporating the 5d and 6s electron correlations and major relativistic effects. The many-electron-excitation effect produces spectroscopic constants close to the experimental values. Although the metal-nonmetal (M-NM) transition can be explained as a simple band-crossing transition in one-electron theory, the many-electron-excitation effect is very important for describing the interaction between mercury atoms.

MD calculations for expanded liquid mercury were

performed using the potential energy curve of Hg_2, in the regions including the M-NM transition range. The volume (V) dependence of the thermal pressure coefficient, γ_v, and the internal pressure, P_0, estimated by the MD calculations agree well with experimental results. Thus, many-body interactions or the qualitative change in the form of interatomic interactions arising from density dependence are not necessarily essential to explain the behavior of the γ_v vs. V and the P_0 vs. V curves. The change of calculated pair distribution function between metallic and nonmetallic state qualitatively demonstrates the change of experimental ones. The temperature dependence of the isochoric electrical conductivity was estimated using interatomic distances obtained from the calculated pair distribution functions. It was shown that the increase of the isochoric electrical conductivity accompanying an increase in temperature can be realized through the increase of the density of states at the Fermi energy. In the preceding paper,[1] we reported that the MD calculations near the melting point using the potential curve of Hg_2 reproduce the cooperative motion corresponding to the collective short-wavelength excitations in the dynamic structure factor. These results suggest that pair-potential approximation using the potential curve of the dimeric molecule gives a good qualitative description of the metallic interatomic force for liquid mercury, and MD calculations using this approximation demonstrate the characteristic change of force fields between liquid metal and liquid semiconductor. However, the both γ_v vs. V and P_0 vs. V curves estimated by the MD calculations seem to deviate from the observed values slightly in the high-density metallic region. These differences between the observed and calculated values may be attributed to the lack of the many-body effects.

It has been pointed out[2] that the relative importance of three-body interactions compared with two-body interactions in the liquid-vapor critical range for mercury is larger than for other van der Waals molecules. The boiling point determined by the present MD calculations is much higher than the observed value. This higher temperature should be corrected by considering three-body effects, such as the Axilrod-Teller interaction, because the three-body dispersion forces are repulsive while the two-body dispersion force is a long-range attractive force. It is interesting to determine the liquid-vapor coexistence curve with pair-potential approximation using the potential energy curve of Hg_2 and to investigate the contribution of three-body effects to the liquid-vapor transition phenomena, especially in liquid-vapor critical range.

References

1) T. Sumi, E. Miyoshi, Y. Sakai and O. Matsuoka, *Phys. Rev. B* **57**, 914 (1998).
2) M. W. Pestak, R. E. Goldstein, M. W. Chan, J. R. de Bruyn, D. A. Balzarini and N.W. Ashcroft, *Phys. Rev. B* **36**, 599 (1987).

V-O-2 Molecular Dynamics Study for the Liquid-Vapor Coexistence Curve of Mercury

Tomonari SUMI *(Kyushu Univ.)* **and Eisaku MIYOSHI**

Critical behaviors in liquid-vapor coexistence curves of alkali metals such as Rb and Cs and of inert gases such as Ar and Xe and of mercury (Hg) have been shown to belong to different types of class.[1] The alkali metals and inert gases violate the particle-hole symmetry, which is valid for the universality class of three-dimensional Ising model, and the coexistence curves of alkali metals are extremely asymmetric.[1] It has been predicted that many-body interactions lead to the symmetry breaking in these fluids.[2] The coexistence curve of Hg is much more symmetric than that of the alkali metals and inert gases. We performed molecular dynamics (MD) calculations of fluid mercury using the potential energy curve of dimeric mercury obtained from ab initio molecular orbital calculations to determine the coexistence curve of mercury. Our MD calculations reproduced the symmetric coexistence curve of mercury.

References

1) F. Hensel, *J. Phys. C* **2**, SA33 (1990).
2) R.Goldstein and N.E. Aschcroft, *Phys. Rev. Lett.* **55**, 2164 (1985).

V-P Structures and Dynamics of Negatively-Charged Molecular Clusters

Negatively-charged molecular clusters continues to receive much attention as subjects for numerous theoretical and experimental investigations. The main interest has been focused on their fundamental properties concerning the electronic structures: i.e., how the aggregates of molecules bind an excess electron and how the electronic structures evolve with cluster size. Of particular interest are (1) the extent of charge localization/delocalization in the negatively-charged clusters, and (2) the existence of "electronic isomers" having different electronic structures. In our recent study, negative-ion photoelectron spectroscopy, in combination with *ab initio* calculations, have provided valuable information on the electronic properties of negatively-charged molecular clusters.

V-P-1 Formation of $N_3O_3^-$ anion in $(NO)_n^-$: Photoelectron Spectroscopy and *Ab Initio* Calculations

Tatsuya TSUKUDA *(Univ. Tokyo)***, Morihisa SAEKI, Lei ZHU and Takashi NAGATA**

[*Chem. Phys. Lett.* in press]

Anions of dimeric molecules often form tightly

bound species where the excess electron is delocalized to some extent over the dimer framework. For example, our recent photodetachment experiment has provided an evidence for a covalent $(CS_2)_2^-$ anion.[1)] In the present study, we have shown for the first time that anions of trimeric molecules can form covalent molecular anion. The photoelectron spectra of $(NO)_n^-$ ($1 \le n \le 7$) are recorded at a photon energy of 4.66 eV (Figure 1), and the vertical detachment energies (VDEs) are determined as a function of the cluster size. The VDE shows an abrupt increase from 2.93±0.05 eV at n = 2 to 3.70± 0.02 eV at n = 3. This large VDE shift is attributed to the formation of an $N_3O_3^-$ molecular anion, which acts as a core in the larger clusters; hence, the $(NO)_n^-$ clusters with $n \ge 3$ are well described as $N_3O_3^-\cdot(NO)_{n-3}$. *Ab initio* calculations are also performed at the MP2/6-31+G* level of theory. The calculations predict that the $N_3O_3^-$ anion has either normal or branched chain configuration shown in Figure 2.

Reference

1)T. Tsukuda, T. Hirose and T. Nagata, *Int. J. Mass Spectrum. & Ion Proc.* **171**, 273 (1997).

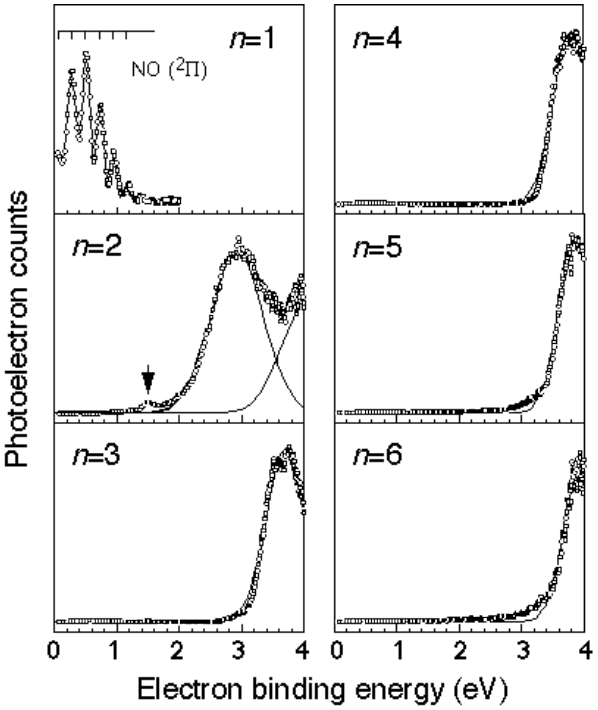

Figure 1. Photoelectron spectra of $(NO)_n^-$ with $1 \le n \le 6$. The open circles represent the experimental data. In the n = 1 spectrum the vibrational combs are shown for the ν_1 progression of NO. The best-fit Gaussian curves for $n \ge 3$ are shown by the solid lines.

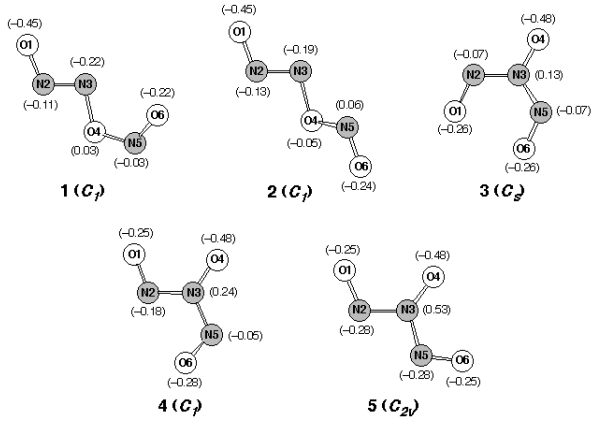

Figure 2. Optimized geometries of $N_3O_3^-$ obtained at the MP2/6-31+G* level. The shaded circles correspond to N atoms and open circles to O atoms. The numbers in parentheses indicate the net atomic charges.

V-P-2 Coexistence of Electronic Isomers in $[(CO_2)_nROH]^-$: Photoelectron Spectroscopy and *Ab Initio* Calculations

Tatsuya TSUKUDA *(Univ. Tokyo)*, **Morihisa SAEKI and Takashi NAGATA**

[*J. Chem. Phys.* submitted]

The electronic structures of $[(CO_2)_{n-1}ROH]^-$ (R = H, CH_3) have been investigated using negative-ion photoelectron spectroscopy. Analysis of the photoelectron band envelopes has revealed that spectra of $[(CO_2)_{n-1}H_2O]^-$ with size $3 \le n \le 5$ and $[(CO_2)_2CH_3OH]^-$ are characterized by two vertical detachment energies (VDE). In the photoelectron-depletion measurement,[1)] we have found that the low-VDE component of the $[(CO_2)_2ROH]^-$ photoelectron band can be selectively photodepleted, whereas the depletion is observed to be recovered to some extent in the case of $[(CO_2)_4H_2O]^-$. From these experimental findings, in conjunction with the theoretical results obtained in our MP2/6-31+G* calculations, we have drawn the following conclusions: (1) The electronic structures of $[(CO_2)_nROH]^-$ (R = H, CH_3) are categorized into two groups according to the extent of charge localization /delocalization: one formulated as $CO_2^-\cdot ROH(CO_2)_{n-2}$ and the other as $C_2O_4^-\cdot ROH(CO_2)_{n-3}$. These "electronic isomers" exhibit the VDE difference of ≈ 1 eV, which can be probed directly by negative-ion photoelectron spectroscopy; (2) The electronic isomers, $CO_2^-\cdot ROH(CO_2)_{n-2}$ and $C_2O_4^-\cdot ROH(CO_2)_{n-3}$, coexist in $[(CO_2)_{n-1}H_2O]^-$ with size $3 \le n \le 5$ and in $[(CO_2)_{n-1}CH_3OH]^-$. In the $[(CO_2)_2ROH]^-$ clusters the $CO_2^-\cdot ROH(CO_2) \leftrightarrow C_2O_4^-\cdot ROH$ interconversion is hindered by an insurmountable potential barrier along the isomerization pathway. Therefore, $CO_2^-\cdot ROH(CO_2)$ and $C_2O_4^-\cdot ROH$ coexist without interconversion (*static coexistence*). On the other hand, the $[(CO_2)_4H_2O]^-$ clusters occur with the $CO_2^-\cdot ROH(CO_2)_3 \leftrightarrow C_2O_4^-\cdot ROH(CO_2)_2$ interconversion (*dynamic coexistence*); (3) The occurrence of the dynamic coexistence implies that the $CO_2^-\cdot ROH(CO_2)_{n-2} \leftrightarrow C_2O_4^-\cdot ROH(CO_2)_{n-3}$ isomerization pathway, which is not opened in the smaller clusters,

becomes accessible in the larger analogues. A possible model for the isomerization is proposed, where the CO_2 neutrals surrounding the CO_2^-·ROH complex alternately take part in the formation of $C_2O_4^-$·ROH.

Reference

1)T. Tsukuda, M. A. Johnson and T. Nagata, *Chem. Phys. Lett.* **268**, 429 (1997).

V-P-3 Relaxation of Photoexcited $(C_6F_6)_n^-$ Using Time-Resolved Photoelectron Spectroscopy

Tatsuya TSUKUDA *(Univ. Tokyo)*, **Morihisa SAEKI and Takashi NAGATA**

Sub-ps time-resolved photoelectron spectroscopy was applied to probe the relaxation process of photo-excited $(C_6F_6)_n^-$ cluster anion. When $(C_6F_6)_n^-$ is photo-excited at ≈ 800 nm, photodissociation leading to the loss of one or two C_6F_6 molecules occurs competitively with the direct photodetachment. As the electronic excitation is possibly localized in the chromophore of $(C_6F_6)_n^-$, the conversion and dissipation of the electronic energy precede the evaporation of the C_6F_6 solvent:

$$\begin{array}{c}[C_6F_6^-(C_6F_6)_{n-1}] + h\nu \\ \downarrow \\ [C_6F_6^{-*}(C_6F_6)_{n-1}] \\ \downarrow \\ [C_6F_6^-(C_6F_6)_{n-1}]^{\dagger} \\ \downarrow \\ (C_6F_6)_m^- + (n\text{-}m)C_6F_6.\end{array}$$

In our experiment, the pump and probe pulses were generated by dividing the 790 nm output (390 fs) of a femtosecond laser system installed at the Laser Research Center for Molecular Science of IMS. The first pulse prepares the $(C_6F_6)_n^-$ in an electronically excited state, and the second pulse photodetaches the dissociating $(C_6F_6)_n^-$ clusters. While either pump or probe pulse itself detaches $(C_6F_6)_n^-$ to produce photoelectrons, additional photoelectron signals are observed when the pump and probe pulses are temporally overlapped. The signals appear around the kinetic energy of $2h\nu$ - VDE, where VDE represents the vertical detachment energy of the $(C_6F_6)_n^-$ clusters. The signal intensity decrease monotonically with the delay time Δt between the pump and probe laser pulses. The intensity vs Δt plots provide the characteristic decay time of ≈ 1.5 ps for the photoprepared electronic states of $(C_6F_6)_n^-$ with n = 3 and 4.

V-Q Millimeter-Wave Spectroscopy Combined with Pulsed-Jet Expansion Technique for the Detection of the Novel Unstable Species and the van der Waals Mode Transitions of Molecular Clusters

Molecular clusters have inherently low-frequency vibrations, so called van der Waals (vdW) vibrational modes, which are characteristic of the weakly bound complexes. The frequency of the vdW mode usually falls in the far-infrared region (30 - 300 cm^{-1}). However, if a cluster is extremely floppy, it sometimes falls in the submillimeter-wave (SMMW) region below 30 cm^{-1}.

The ArHCN cluster is a typical example which has extremely low-frequency vdW bending mode vibrations. Although the frequency of the vdW stretching is estimated to be 23.8 cm^{-1}, those for the bending vibrations are calculated to be as low as 4 - 7 cm^{-1}. Following the observation of the pure rotational spectra in the microwave region below 20 GHz, the vdW bending transitions of ArHCN have been measured in the millimeter-wave region near 180 GHz by molecular beam electric resonance optothermal spectroscopy (EROS).

In this project, a millimeter-wave absorption spectrometer combined with pulsed-jet expansion technique has been devised and applied to the direct observation of the rovibrational transitions of the vdW bending band of molecular clusters.

In the supersonic jet expansions short lived species can survive thanks to the collision-less environment and ultra low rotational as well as vibrational temperature. The millimeter-wave spectrometer combined with supersonic jet nozzle and glow discharge electrodes, as well as the UV excimer laser photolysis devices, also have been set up for the detection of novel unstable species, such as radicals, molecular ions, and ionic and radical clusters.

V-Q-1 Direct Absorption Observation of the van der Waals Bending Band of the ArDCN Cluster by Millimeter-Wave Spectroscopy Combined with Pulsed-Jet Expansion Technique

Stéphane BAILLEUX, Asao MIZOGUCHI, Kensuke HARADA, Tsuyoshi BABA *(Kyushu Univ.)*, **Mitsuaki SHIRASAKA** *(Kyushu Univ.)* **and Keiichi TANAKA** *(Kyushu Univ. and IMS)*

Millimeter-wave spectroscopy combined with a pulsed supersonic jet nozzle was applied to observe the absorption spectra of the van der Waals bending band of the ArDCN cluster in the frequency region 180 - 300 GHz. In total 53 rovibrational lines split into hyperfine structure due to nitrogen nucleus were observed and assigned to those for the $\sum_1$ - $\sum_0$ and $\prod_1$ - $\sum_0$ subbands of the j = 1 - 0 vdW fundamental bending band. The spectrum of the $Q(2)$ line of the $\prod_1$ - $\sum_0$ band observed at 196 GHz is shown in Figure 1.

The pure rotational spectrum in the ground $\sum_0$ state has been measured with the same spectrometer in the frequency region 40 - 71 GHz. The high-J transitions up

to J = 23 - 22 were observed and the molecular constants including the higher order centrifugal distortion constants in the ground state were derived.[1)]

The simultaneous analysis of the vdW bending mode transitions together with the pure rotational lines provided an accurate set of molecular constants, including the band origins, rotational constants, quadrupole coupling constants, and the Coriolis coupling constant between the $\sum_1$ and $\prod_1$ bending substates. Analysis of the hyperfine structure gives the *eqQ* values to be -3.1429, 0.8129, and 0.8022 MHz for the $\sum_0$, $\sum_1$, and $\prod_1$ states. The average angle $<\theta>$ between the principal axis of the cluster and the DCN part are derived to be 28, 62.5, and 62 degree, respectively. It means the average structure of the ArDCN cluster changes drastically by the excitation of the vdW bending mode from *linear* in the ground state to *T-shaped* in the first excited state. The band origins determined are unordinary higher, by 24.1 and 13.6 GHz, than those of the ArHCN species.[2)] Present molecular constants will be essential to improve the intermolecular potential surface between Ar and H(D)CN which is supposed to be double minimum corresponding to the linear and T-shape structures.[3)]

References

1)M. Shirasaka and K. Tanaka, *J. Mol. Spectrosc.* **185**, 189 (1997).
2)K. Uemura, A. Hara and K. Tanaka, *J. Chem. Phys.* **104**, 9747 (1996).
3)S. Drucker, A. L. Cooksy and W. Klemperer, *J. Chem. Phys.* **98**, 5158 (1993).

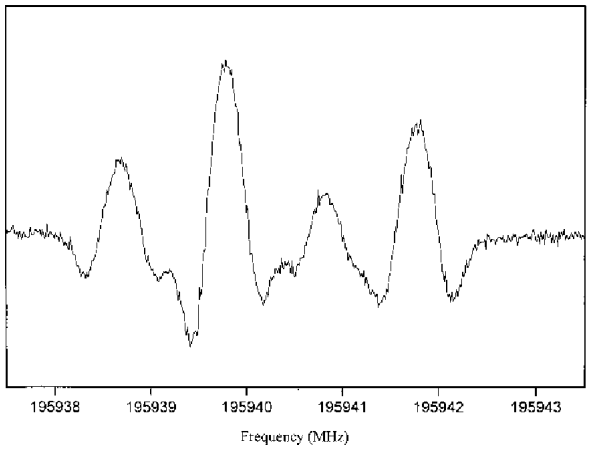

Figure 1. Hyperfine structure of the $Q(2)$ line of the $\prod_1 - \sum_0$ subband of the j = 1 - 0 vdW fundamental bending band of ArDCN.

V-Q-2 Millimeter-Wave Spectroscopy of the Iron Carbonyl Radical (FeCO) in the ν_2 State

Keiichi TANAKA *(Kyushu Univ. and IMS)*, **Mitsuhiro NAKAMURA** *(Kyushu Univ.)*, **Mitsuaki SHIRASAKA** *(Kyushu Univ.)* **and Takehiko TANAKA** *(Kyushu Univ.)*

The pure rotational spectrum of the iron carbonyl radical FeCO produced by a dc discharge of iron pentacarbonyl $Fe(CO)_5$ has been observed in the millimeter-wave (MMW) region. Seven rotational lines split into sextets, the electron spin components and Λ-type doubling components, were observed and assigned to those of the ν_2 bending vibrational state of FeCO. Although the symmetry of the ground electronic state is $^3\sum^-$, a large spin-orbit interaction constant A_{eff} = 14.0746 (57) GHz was obtained as well as the Λ-type doubling constants of o = -18.2899 (55) GHz, p = -355.36 (64) MHz and q = 9.5167 (69) MHz. The anomalously large fine structure splitting in the ν_2 state is explained by the vibronic interaction between the ν_2 bending vibrational state and the $^3\prod$ excited electronic state which is located very close (-6500 cm^{-1}) to the ground state.[1)]

The rotational and centrifugal distortion constants were determined to be B_0 = 4374.3908 (18) MHz and D_0 = 1.2497 (13) kHz. The spin-spin interaction constant and its higher order term are as large as λ_0 = 679.37 (29) GHz and λ_D = -454.8 (39) kHz, similar to those of the ground state. The spin-rotation interaction constant is γ_0 = -1180.0 (19) MHz, where the figures in parentheses are standard errors to be attached to the last digit.

Reference

1)K. Tanaka, M. Shirasaka and T. Tanaka, *J. Chem. Phys.* **106**, 6820 (1997)

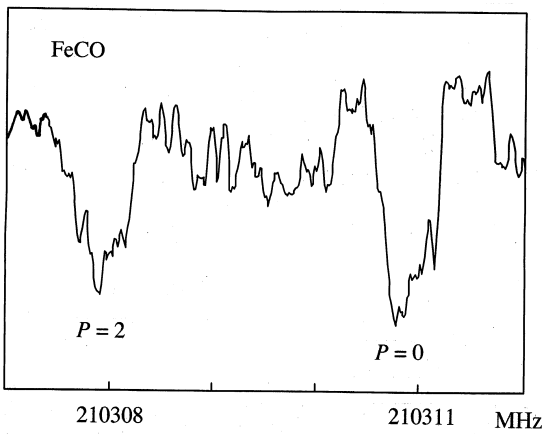

Figure 1. The Λ-type doubling component $P = 0^f$ and 2^f of the J = 24 ← 23 rotational transition of the FeCO radical in the ν_2 vibrational state.

V-R Ion-Molecule Reactions in the Troposphere

Ion chemistry in the troposphere is the most complicated among all level of earth's atmosphere because of the presence of a variety of trace compounds. We have been studying ion-molecule reactions in the troposphere by

investigating ion mobility distribution and its dependence on reaction time, pressure and temperature using an ion mobility spectrometer.[1,2] In order to confirm the ion-molecule reactions occurring in the troposphere, we designed high-resolution ion mobility/mass spectrometer which is capable of chemical identification of ion species forming ion peaks in mobility spectra. Using this spectrometer, we will investigate the ion processes in conditioned laboratory air as well as in natural air.

References

1)K. Nagato and T. Ogawa, *J. Geophys. Res.* **103**, 13917 (1998)
2)K. Nagato, D. J. Tanner, H. R. Friedli and F. L. Eisele, *J. Geophys. Res.* submitted.

V-R-1 Development of High-Resolution Ion Mobility/Mass Spectrometer for the Study of Ion-Molecule Reactions in the Troposphere

Kenkichi NAGATO

We have designed a high-resolution ion mobility/mass spectrometer which can make simultaneous measurements of mobility and mass spectra of cluster ions generated by ion-molecule reactions under atmospheric pressure. The spectrometer consists of a drift tube, a mass analyzer, and an interface chamber between the drift tube and the mass analyzer. Ions to be analyzed are generated by irradiation of sample air with an americium source and enter into the drift tube. In the drift tube, ions experience a chain of ion-molecule reactions with trace species in the sample air and are separated into different ion groups according to their mobility by an uniform electric field. The length of the drift tube can be varied up to about 40 cm, which allows measurements of ions aged for about 5 s. Ions are introduced through an aperture (100-200 μm) into the interface chamber which is differentially pumped by a rotary pump (800 l/min) and a turbo molecular pump (230 l/s). Ions are finally mass-analyzed by a quadrupole mass filter in a detection chamber which is pumped by a 10" diffusion pump. A preliminary experiment with this spectrometer is underway.

RESEARCH ACTIVITIES VI
Department of Vacuum UV Photoscience

VI-A Electronic Structure and Decay Mechanism of Inner-Shell Excited Molecules

This project is being carried out in collaboration with Photon Factory (KEK-PF). We are interested in ionic fragmentations and electron emission via inner-shell excitation of molecules and in their polarization dependence. We have investigated vibronic couplings in the inner-shell excited states of some polyatomic molecules. Recently we have developed a new and simple method, the measurement of kinetic energy dependence of angle-resolved ion yields, to extend our approaches to other molecules. This method can be an alternative in comparison with mass-resolved techniques.

VI-A-1 Antisymmetric Stretching Vibrations in the O1*s* $\rightarrow$ 3*p*π_u Rydberg Excited States of CO_2

Jun-ichi ADACHI, Nobuhiro KOSUGI, Eiji SHIGEMASA *(KEK-PF)* **and Akira YAGISHITA** *(KEK-PF)*

We have measured angle-resolved photoion-yield spectra (ARPIS) for the O1*s* excited states of CO_2 using linearly polarized synchrotron radiation. Vibrational structures with relatively large spacing (about 0.3 eV) are observed at about 538.4 eV in the I_{90} spectrum. These structures are assigned to the ν_3 = 0, 1, and 2 levels (antisymmetric stretching mode) in the O1*s* $\rightarrow$ 3*p*π_u Rydberg state. The dipole-allowed 1σ_g $\rightarrow$ 3*p*π_u Rydberg state ($^1\Pi_u$) is coupled with the forbidden 1σ_u $\rightarrow$ 3*p*π_u Rydberg state ($^1\Pi_g$) through the ν_3 (σ_u^+) mode excitation. On the other hand, the prominent O1*s* $\rightarrow$ 4*s*σ_g peak is observed in the I_0 spectrum. The enhancement of the 4*s*σ_g Rydberg state is attributed to the mixing with the O1*s* $\rightarrow$ 5σ_g* valence excited state.

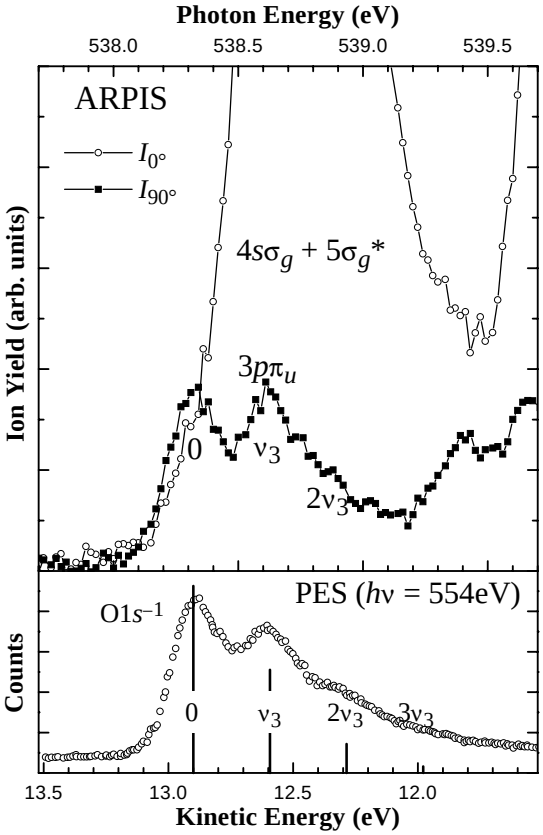

Figure 1. Angle-resolved ion-yield spectra for the O1*s* $\rightarrow$ 3*p*π_u and 4*s*σ_g Rydberg excited states of CO_2. The open circle (I_0) and square (I_{90}) show the ion yields in the 0° and 90° directions to the electric vector of the incident light, respectively. The O1*s* photoelectron spectrum of CO_2 obtained by Kivimäki *et al.*[1] is shown to compare with the present spectra.

References

1) A. Kivimäki, B. Kempgens, K. Maier, H. M. Köppe, M. N. Piancastelli, M Neeb, and A. M. Bradshaw, *Phys. Rev. Lett.* **79**, 998 (1997).

VI-A-2 Renner-Teller Splitting in the C1*s* $\rightarrow$ π* Excited States of CS_2, OCS, and CO_2

Jun-ichi ADACHI, Nobuhiro KOSUGI, Eiji SHIGEMASA *(KEK-PF)* **and Akira YAGISHITA** *(KEK-PF)*

[*J. Chem. Phys.* **107**, 4919 (1997)]

Fragment ions energetically emitted following the perpendicular ($\Delta\Lambda$ = +1) transitions of C1*s* $\rightarrow$ π* of

CS_2, OCS, and CO_2 are observed not only in the perpendicular (90°) direction but also in the parallel (0°) to the linear polarization; that is, ions have a momentum orthogonal to the linear molecule. This arises in the Renner-Teller (RT) vibronic coupling of bending vibrations in the C1*s* → in-plane π* excited state with a bent equilibrium geometry, though the RT splitting between C1*s* → out-of-plane π* excited state with a linear geometry and the C1*s* → in-plane π* state is not visible directly due to the lifetime broadening. The half-width at half-maximum on the lower energy side of the π* peak is sensitive to the RT splitting; 0.08, 0.11, and 0.29 eV for CS_2, OCS, and CO_2. The 0° ion yield is relatively small in CS_2 but is comparable to the 90° yield in CO_2; in the latter the peak maximum at 0° is 0.06 eV lower than at 90° and the anisotropy parameter β is heavily dependent on the photon energy. In CO_2 a great number of unresolved bending vibrations are coupled. In CS_2 the π* peak and β value are sharp and symmetric, indicating that the zero-point vibrational levels are only involved. In OCS three fine structures observed with separations of 0.21 eV are assigned to the ν_3 mode, which is comparable to the stretching mode in CO.

VI-A-3 Kinetic Energy Dependence of the Anisotropy Parameters for the Fragmentation of the C1*s* Excited States of C_2H_4

Jun-ichi ADACHI, Yasutaka TAKATA, Nobuhiro KOSUGI, Eiji SHIGEMASA *(KEK-PF)* **and Akira YAGISHITA** *(KEK-PF)*

We have measured angle-resolved ion-yield spectra for the C1*s* ($1a_g$ and $1b_{3u}$) excited states of C_2H_4 using linearly polarized synchrotron radiation. The anisotropy parameter for the fragment ions emitted following the C1*s* excitations of C_2H_4 is not directly related to the symmetry of the excited state because of some fragmentation patterns; the C-C bond and C-H bond breakings and other many-body fragmentations. However, it is found that the symmetries of valence and Rydberg states of C_2H_4 can be identified by measuring the kinetic energy dependence of the fragment ion yields. The relative H^+ yield to the other ion ones increases as the lower limit of the kinetic energy of the detected ions becomes higher. Then, the increasing, constant, and decreasing behaviors in the β_R value with increasing the lower limit of the kinetic energy (R) indicate that the transitions are due to the $1a_g \rightarrow b_{2u}/1b_{3u} \rightarrow b_{1g}$, $1a_g \rightarrow b_{1u}/1b_{3u} \rightarrow b_{2g}$, and $1a_g \rightarrow b_{3u}/1b_{3u} \rightarrow a_g$, respectively. The β_R values for the C1*s* → $2b_{2u}$* valence and $3pb_{1u}$ Rydberg transitions are almost constant within the bands. On the other hand, the β_R values for the $4a_g$* valence are changed just on the higher energy side. This result indicates that the peak at about 287.4 eV can be attributed to other electronic states or to vibronic states coupled in the bending or torsional mode.

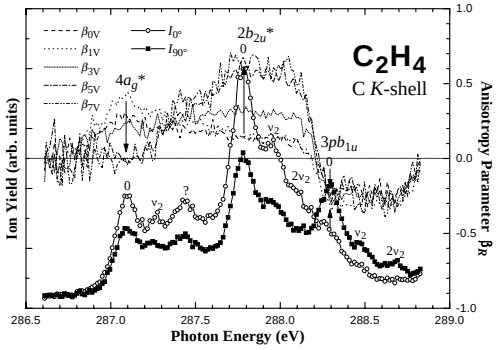

Figure 1. Angle-resolved ion-yield spectra with the larger kinetic energy than 3 eV for the C1*s* → Rydberg / σ* valence excited states of C_2H_4. The open circle (I_0) and square (I_{90}) show the ion yields in the 0° and 90° directions to the electric vector of the incident light, respectively. Various broken lines show the anisotropy parameter β_R with R = 0, +1, +3, +5, and +7 eV.

VI-A-4 Kinetic Energy Dependence of Anisotropic Yields of Ionic Fragmentations Following S 1*s* Excitations of SO_2

Jun-ichi ADACHI, Yasutaka TAKATA, Nobuhiro KOSUGI, Eiji SHIGEMASA *(KEK-PF)***, Akira YAGISHITA** *(KEK-PF)* **and Yoshinori KITAJIMA** *(KEK-PF)*

[*Chem. Phys. Lett.* in press (1998)]

Several S 1*s* excited states of SO_2 are investigated in high-resolution angle-resolved ion-yield spectra using linearly polarized synchrotron radiation. The anisotropy parameter for the triatomic molecule is not directly related to the symmetry of the excited state due to the three-body fragmentation. The present work shows that the symmetries of the lowest three valence states and some low-lying Rydberg states are clearly identified by measuring the kinetic energy dependence of the fragment ion yields at two angles, where the oxygen ion yields are increased and the sulfur ion yields are decreased for the higher kinetic energy.

VI-A-5 Direct Determination of Partial Waves Contributions in the σ* Shape Resonance in CO Molecules

Eiji SHIGEMASA *(KEK-PF)***, Jun-ichi ADACHI, Koichi SOEJIMA** *(Niigata Univ.)***, Naoki WATANABE** *(Hokkaido Univ.)***, Akira YAGISHITA** *(KEK-PF)* **and Nikolai A. CHEREPKOV** *(State Acad. Aerospace Instrum.)*

[*Phys. Rev. Lett.* **80**, 1622 (1998)]

The first complete experiment for the C *K*-shell of CO molecules in the region of the σ* shape resonance has been performed by detecting photoelectrons in coincidence with fragment ions. Four ratios of dipole matrix elements and four phase shift differences have been extracted from the experimental data. Their analyses show that, in the σ* shape resonance due to the

ℓ mixing, *d* and *f* partial waves give the main contribution to the cross section, and *f* and *g* waves give the main contribution to a rapid increase of phase shift by π.

VI-B Soft X-Ray Photoelectron-Photoabsorption Spectroscopy and Electronic Structure of Transition Metal Compounds

We have investigated electronic structures of molecular Ni complexes with planar structure by means of inner-shell photoabsorption and photoelectron spectra at the soft X-ray double crystal monochromator beamline BL1A of the UVSOR facility. Recently we have found that a one-electron picture is appropriate to interpret the Ni 2p photoabsorption and the resonant photoelectron spectra, and that the metal-to-ligand charge transfer (MLCT) is essential to describe the photoexcited states. This year we extended our study to Ni 1s and S 1s photoabsorption spectra, and also to other Ni compounds, to discuss intermolecular interaction and chemical bonds between metal and ligand.

VI-B-1 Metal-to-Ligand Charge Transfer Bands Observed in Polarized Ni 2*p* Photoabsorption Spectra of $[Ni(mnt)_2]^{2-}$

Takaki HATSUI *(Grad. Univ. Adv. Stud.)*, **Yasutaka TAKATA and Nobuhiro KOSUGI**

[*J. Electron Spectrosc. and Relat. Phenom.* submitted]

Linearly polarized Ni 2*p* photoabsorption spectra were measured for a planar Ni complex $[(n\text{-}C_4H_9)_4N]_2[Ni(mnt)_2]$ (mnt: 1,2-dicyanovinylene-1,2-dithiolato) as shown in Figure 1. The spectra show some characteristic bands above the strongest peak A. Because this complex has low-spin $3d^8$ configuration in the ground state, we expect intra-atomic transitions: strong one-electron transition to Ni $3d_{xy}$* and weak structure arising from intra-atomic correlation. Peak A is assigned to intra-atomic transition to Ni $3d_{xy}$*, which is confirmed by the observed polarization dependence of peak A. However, the polarization dependence shows that the characteristic bands B, C, and D can not be interepreted in terms of the correlation satellites. On the other hand, two mnt ligands produce two low-lying unoccupied orbitals L_{yz}* and $L_{x2\text{-}y2}$*, which may combine with Ni $3d_{yz}$ and Ni $3d_{x2\text{-}y2}$ orbitals, respectively. The polarization dependence shows that bands B and C are attributable to metal-to-ligand charge transfer (MLCT) transitions to L_{yz}* and $L_{x2\text{-}y2}$* in good agreement with ab initio molecular orbital predictions. Since stronger backbonding results in stronger MLCT bands, the in-plane backbonding ($3d_{x2\text{-}y2} \rightarrow L_{x2\text{-}y2}$*) is as important as the out-of-plane one ($3d_{yz} \rightarrow L_{yz}$*) in $[Ni(mnt)_2]^{2-}$ complex.

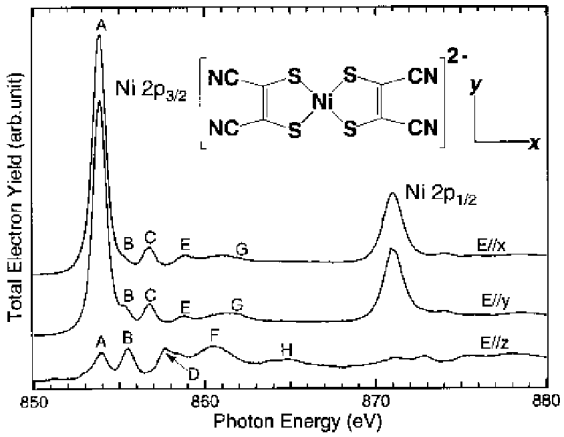

Figure 1. Polarized Ni 2*p* photoabsorption spectra of $[(n\text{-}C_4H_9)N]_2[Ni(mnt)_2]$.

VI-B-2 Polarized Ni 1*s* and 2*p*, and S 1*s* Photoabsorption Spectra of $[Ni(III)(mnt)_2]^{1-}$

Takaki HATSUI *(Grad. Univ. Adv. Stud.)*, **Yasutaka TAKATA and Nobuhiro KOSUGI**

[*J. Synchrotron Rad.* submitted]

In formally trivalent Ni compounds with 1,2-dithiolates, the ligands are partially oxidized and the Ni metals have oxidation numbers between 2 and 3. In a molecular orbital picture, such compounds have a singly occupied molecular orbital (SOMO) which is delocalized over Ni and ligand. In order to characterize SOMO, polarized Ni 1*s* and 2*p*, and S 1*s* photoabsorption spectra have been measured for a formally trivalent Ni planar complex with local D_{2h} symmetry, $[(C_2H_5)_4N][Ni(III)(mnt)_2]$ (mnt: dicyanovinylene-1,2-dithiolato). In the Ni 2*p* photoabsorption spectra (Figure 1), two strong peaks X and A are observed. The higher peak in energy is assigned to Ni $2p_{3/2} \rightarrow$ Ni $3d_{xy}$* and the lower one to a transition to SOMO (coordinates were chosen as Figure 1 of VI-B-1 section). The polarization dependence shows that SOMO has the b_{2g} (d_{yz}) symmetry (out-of-plane π*). Polarized S 1*s* photoabsorption spectra also show that the lowest transition (to SOMO) is of π* character. These results indicate strongly delocalized character of the SOMO in the

formally trivalent Ni complex $[Ni(mnt)_2]^{1-}$.

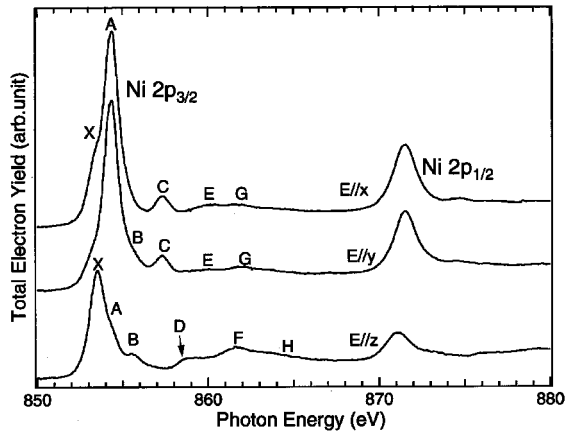

Figure 1. Polarized Ni 2*p* photoabsorption spectra of $[(C_2H_5)_4N][Ni(mnt)_2]$.

VI-B-3 Strong Pre-Edge Peaks Found in Ni 1*s* Photoabsorption Spectra of Ni Planar Complexes

Takaki HATSUI *(Grad. Univ. Adv. Stud.)*, **Yasutaka TAKATA and Nobuhiro KOSUGI**

In order to obtain information on the low-lying unoccupied orbitals with *p* symmetry, we have measured linearly polarized Ni 1*s* photoabsorption spectra of bis(dimethylglyoximato)nickel(II) [Ni-(Hdmg)$_2$] and $[(n\text{-}C_4H_9)_4N]_2[Ni(II)(mnt)_2]$ (mnt: 1,2-dicyanoethylene-1,2-dithiolato). These are planar complexes with D_{2h} symmetry and have low-spin $3d^8$ configuration. The molecular structures and coordinates are shown in Figure 1 and inset of Figure 1 in VI-B-1. The Ni(Hdmg)$_2$ molecules are perpendicular to *z* axis and are rotated 90° around *z* axis. Therefore, the E z spectrum corresponds to an average of the E//x and E//y spectra, where E is the electric vector of incident photon. For $[(n\text{-}C_4H_9)_4N]_2[Ni(II)(mnt)_2]$, all the $[Ni(II)(mnt)_2]^{2-}$ anions are parallel to one another. Figure 1 shows the polarized Ni 1*s* photoabsorption spectra. For Ni(Hdmg)$_2$, the lowest weak band A is assigned to a quadruple transition to Ni $3d_{xy}$*. Bands B and C are strong in E//z and are very weak in E z. $(Hdmg)_2^{2-}$ has some low-lying unoccupied orbitals. One of them has p_z symmetry, which split Ni $4p_z$* into two orbitals. Thus, bands B and C correspond to the transitions to unoccupied orbitals of metal $4p_z$* character with large mixing with ligand π* orbital. For $[(n\text{-}C_4H_9)_4N]_2[Ni(II)(mnt)_2]$ (Figure 1b), the lowest band A is unambiguously assigned to a quadruple transition to Ni $3d_{xy}$* based on the polarization dependence; band A is strong in the spectra for (E//x, k//y) and (E//y, k//x) and very weak in the spectrum for (E//y, k//z) (not shown here), where *k* is the wave vector of incident photon. Band B is allowed for (E//z, *k*//x), and is assigned to out-of plane Ni 1*s* → $4p_z$* transition. In contrast to Ni-(Hdmg)$_2$, no splitting of Ni 1*s* → $4p_z$* transition is observed. This is because $(mnt)_2^{4-}$ has no low-lying unoccupied ligand orbital with p_z symmetry.

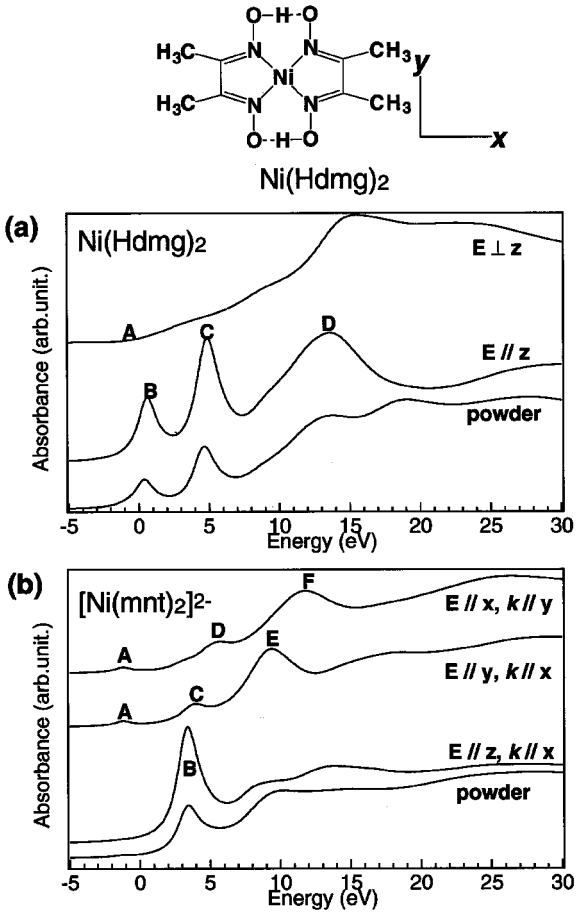

Figure 1. Polarized Ni 1*s* photoabsorption spectra of (a) Ni(Hdmg)$_2$ and (b) $[(n\text{-}C_4H_9)_4N]_2[Ni(mnt)_2]$.

VI-B-4 Effect of Intermolecular Interaction on Resonant Behavior of Satellite Photoelectrons in Ni Planar Complexes

Yasutaka TAKATA, Takaki HATSUI *(Grad. Univ. Adv. Stud.)* **and Nobuhiro KOSUGI**

We have measured resonant photoelectron spectra of Ni(Hdmg)$_2$ [bis(dimethylglyoximato)nickel(II)] and Ni-(Hgly)$_2$ [bis(glyoximato)nickel(II)] in order to investigate the effect of the intermolecular interaction on resonant behavior of satellite photoelectrons. Both the complexes have nearly the same local bonding character around a Ni atom, but their Ni-Ni distances, 3.25 Å for Ni(Hdmg)$_2$ and 4.20 Å for Ni(Hgly)$_2$, are rather different. As expected, their Ni 2p photo-absorption spectra are very similar. Figure 1 shows the off-resonant (0), on-resonant photoelectron spectra (1-9) in the Ni 3p and 3s region and the normal Auger spectrum of Ni(Hdmg)$_2$. The enhanced satellite band (a-e) lowers the kinetic energy for the higher resonance energy and is converging to the normal Auger final state. This behavior is characteristic of the molecular solid system as observed in $K_2Ni(CN)_4$. In Ni(Hgly)$_2$ (not shown here), the photon energy dependence of the kinetic energy shift (slope) is relatively large, -0.42± 0.05, as in $K_2Ni(CN)_4$ (slope = -055). However, the slope is very small, -0.09±0.05 in Ni(Hdmg)$_2$ with strong intermolecular interaction as shown in Figure 1.

These results indicate that the slope is dependent on the intermolecular interaction.

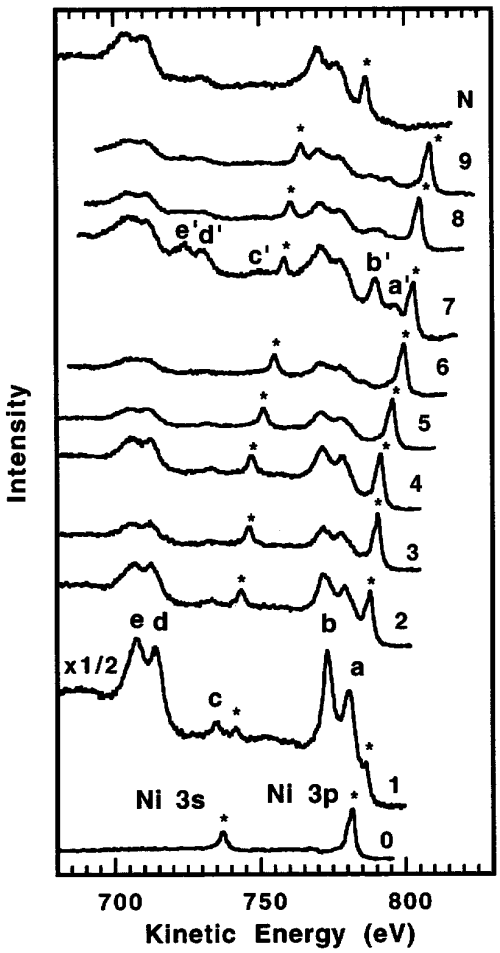

Figure 1. Off-resonant (0), on-resonant (1-9) photoelectron spectra in the Ni 3p and 3s region and the normal Auger spectra of $Ni(Hdmg)_2$.

VI-B-5 Resonant Photoelectron Spectra of Ni Metal Following the Ni 2p Excitation

Yasutaka TAKATA, Takaki HATSUI *(Grad. Univ. Adv. Stud.)* **and Nobuhiro KOSUGI**

We have measured resonant photoelectron spectra of Ni metal to get a unified interpretation of resonant behaviors of satellite photoelectrons at the Ni 2p edge. Figure 1 shows the off-resonant (0), on-resonant (1-6) photoelectron spectra in the Ni 3p and 3s region and the normal Auger spectrum. The kinetic energies of all the enhanced satellite bands (a-e) shows linear dispersion as a function of the excitation energy, namely, constant binding energies, below the Ni $2p_{3/2}$ resonance maximum (0) and show constant kinetic energies above the maximum with the same energies as the $3p^{-1}3d^8$ ($L_3M_{2,3}M_{4,5}$) Auger final states. This is reasonable considering that the localized states are embedded in the continuum band. The "$2p^{-1}3d^{10}$" photoexcited state is not strongly localized, and both the "$3p^{-1}3d^9$" singly ionized satellite state and "$3p^{-1}3d^8$" doubly ionized Auger final state are well screened by the conduction electron. These behaviors are quite different from those of a strongly correlated system, NiO, and a molecular system such as $K_2Ni(CN)_4$ and $Ni(Hdmg)_2$.

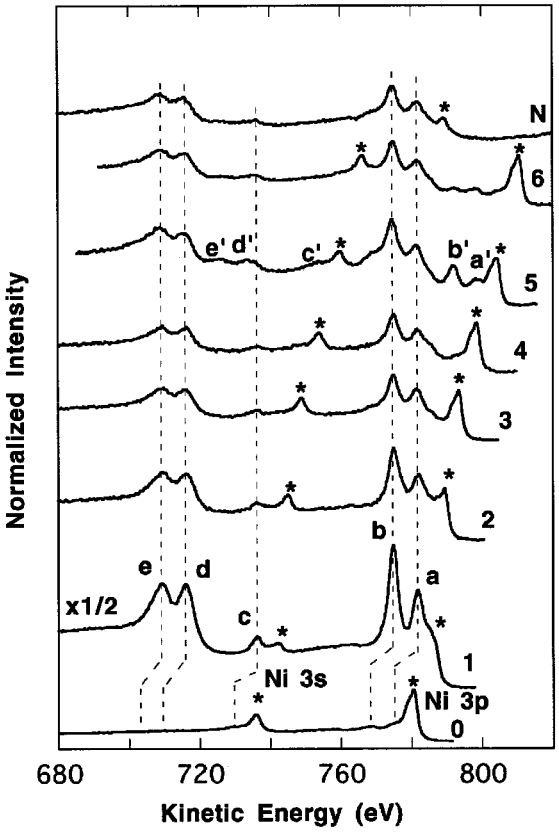

Figure 1. Off-resonant (0), on-resonant (1-6) photoelectron spectra in the Ni 3p and 3s region and the normal Auger spectra of Ni metal.

VI-C Studies on Primary Photochemical/physical Processes Using Femtosecond Time-Resolved Electronic Spectroscopy

Ultrafast spectroscopy is playing an essential role in the elucidation of photochemical reactions. Thanks to recent advances of the laser technology, we are now even able to observe wavepacket evolution in the course of chemical reactions with femtosecond time-resolution. In this project, we are studying primary photochemical /physical processes in the condensed phase using several types of femtosecond time-resolved spectroscopy. We already constructed three experimental setups so far; a femtosecond time-resolved fluorescence up-conversion spectrometer, a femtosecond optical heterodyne detected impulsive stimulated Raman scattering (OHD-ISRS) spectrometer and a femtosecond UV-VIS-NIR transient absorption spectrometer. In this year, while continuing research with these setups, we have also constructed a setup for generating femtosecond mid-infrared pulses down

to 10 μm.

VI-C-1 Generation of a Femtosecond Pulse in the Near- to Mid-Infrared Region

Satoshi TAKEUCHI and Tahei TAHARA

We have constructed an experimental setup to generate a femtosecond pulse in the near- to mid-infrared region which is applicable to a variety of ultrafast vibrational spectroscopies (Figure 1). This system is driven by regeneratively-amplified Ti:sapphire laser pulses (800 nm, 100 fs, 0.5 mJ), and is composed of two parts: (i) optical parametric amplifier (OPA) to generate a near-infrared pulse and (ii) difference-frequency mixer to generate a mid-infrared pulse. In the first part, a seed pulse is generated by self-phase modulation in a thin sapphire plate. A near-infrared portion of the seed pulse (850-1000 nm region) is amplified in a double-pass β-BaB_2O_4 OPA pumped by the second harmonic at 400 nm. The group-velocity mismatch between the interacting pulses is minimized by employing the noncollinear interaction scheme. The energy of the seed pulse amounts to several microjoules after amplification. In the second part, the amplified seed pulse is mixed with the fundamental pulse (800 nm) in a $AgGaS_2$ crystal (0.5 mm thickness) to generate the mid-infrared pulse in the 4-11 μm region (900-2500 cm^{-1}). The wavelength of the mid-infrared pulse can be changed by simultaneous angle-tuning of the two crystals. The output spectra were measured by using a monochromator and a HgCdTe detector, and are shown in Figure 2. The bandwidth is about 80 cm^{-1} independent of the center wavelength, and it is determined mainly by the phase-matching condition of the $AgGaS_2$ crystal.

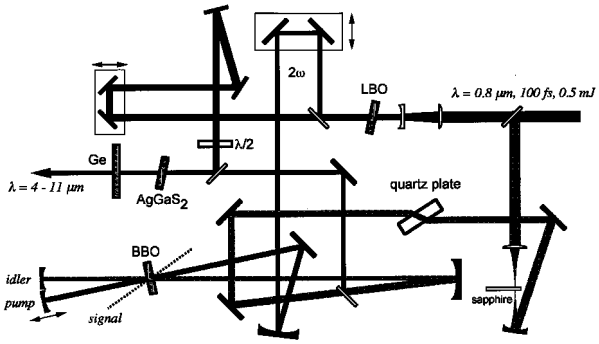

Figure 1. Apparatus for the femtosecond infrared pulse generation.

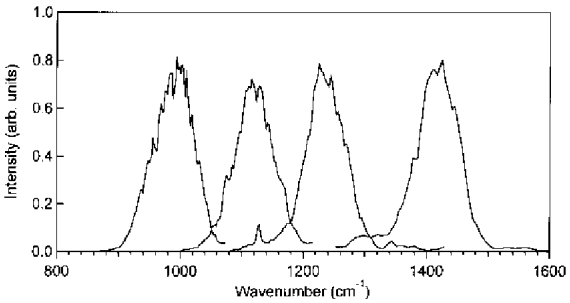

Figure 2. Spectra of the generated pulses in the mid infrared region.

VI-C-2 Femtosecond UV - VIS Fluorescence Study on the Excited-State Proton Transfer Reaction of 7-Azaindole Dimer

Satoshi TAKEUCHI and Tahei TAHARA

[*J. Phys. Chem.* in press]

The dynamics of the excited-state proton transfer reaction of 7-azaindole dimer has been investigated in hexane with use of the femtosecond fluorescence up-conversion method. Time-resolved measurements were performed in a wide fluorescence wavelength region from near ultraviolet to visible (320-620 nm) (Figure 1). Three fluorescence components due to the dimer were observed in addition to the fluorescence from coexisting monomer. We assigned the first (τ = 0.2 ps) and the second (τ = 1.1 ps) fluorescence components to two different dimeric excited states having different transition moment directions. The decay of the second component agrees with the rise of the third component which is attributable to the fluorescence from the tautomeric excited state (τ = 3.2 ns) formed by the proton transfer reaction. The fluorescence spectra of these three excited states were reconstructed from time-resolved fluorescence traces taken at 27 wavelengths, and they show intensity maxima around 330, 350, and 490 nm, respectively. This sequential red-shift reflects the cascaded population relaxation after the photo-excitation. Combining the spectral data with fluorescence quantum yield data, the oscillator strengths of the three excited states were evaluated as 0.13, 0.048 and 0.023. We assigned the higher- and the lower-energy dimeric excited states to the "^1L_b" and "^1L_a" states of the dimer on the basis of the obtained photochemical information. The deuterium substitution effects were also examined for two isotopic analogues. It was concluded that the proton transfer proceeds exclusively from the lowest "^1L_a" excited state with a time constant of 1.1 ps, after the electronic relaxation takes place from the initially-populated "^1L_b" state to the "^1L_a" state (Figure 2). The excited-state reaction pathway as well as quantitative characterization of each excited state is discussed.

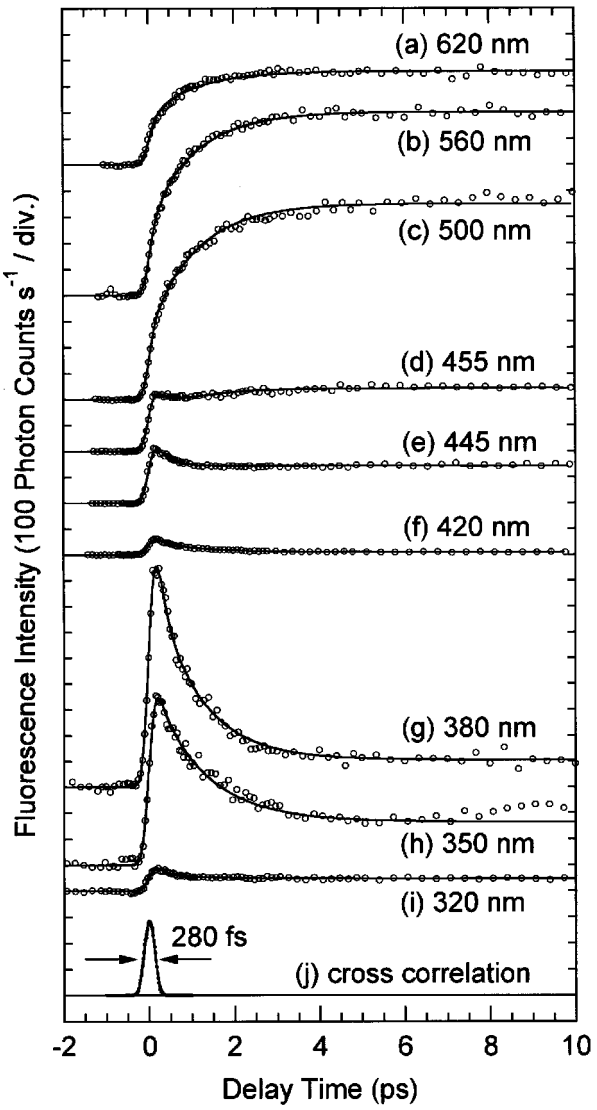

Figure 1. Femtosecond time-resolved fluorescence signals obtained from 7-azaindole in hexane (1×10^{-2} mol dm^{-3}, 270 nm excitation). Fluorescence signals at 620 nm (a), 560 nm (b), 500 nm (c), 455 nm (d), 445 nm (e), 420 nm (f), 380 nm (g), 350 nm (h), 320 nm (i), and a typical cross-correlation trace between the excitation and the gate pulses (j). The open circles are experimental data points, and the solid curves are results of the fitting analysis. The instrumental time resolution given by the fwhm of the cross-correlation trace is 280 fs.

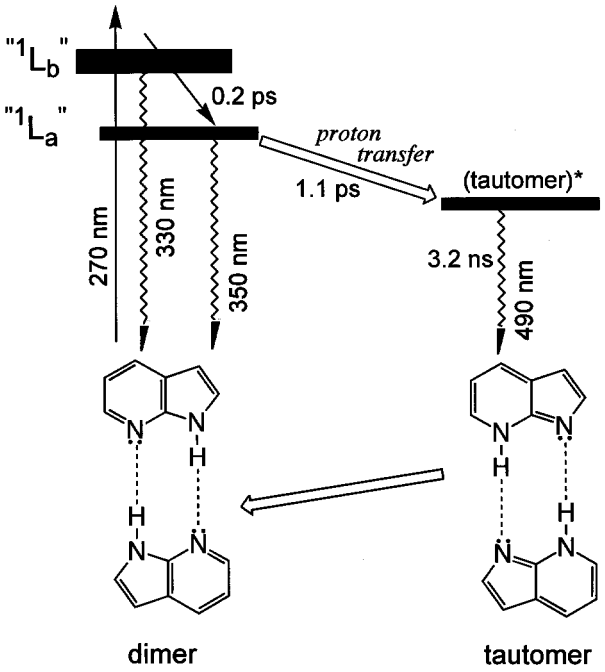

Figure 2. Schematic energy diagram illustrating the dynamics of the excited-state double proton transfer reaction of 7-azaindole dimer.

VI-C-3 Femtosecond Fluorescence Anisotropy Study of 7-Azaindole Dimer in Solution

Satoshi TAKEUCHI and Tahei TAHARA

Time-resolved anisotropy measurements have been widely utilized so far to investigate phenomena such as the orientational diffusion of molecules in solution and the migrational motion of excitations in solids. However, in the sub-picosecond time region, the orientational motion of molecules is negligible in solution. The anisotropy change observed in this short time region does not arise from the molucular motion but from the rotation of the excited-state transition moment direction itself, i.e., the change of the electronic excited state. Femtosecond time-resolved anisotropy measurements, therefore, can afford an unique experimental evidence which enables us to distinguish the internal conversion process from the dynamics within a single electronic excited state. In order to confirm the proton transfer reaction mechanism of 7-azaindole dimer which we propose, the fluorescence anisotropy of this molecule has been measured with a 280-fs time resolution (Figure 1). We observed a very rapid decrease of the anisotropy immediately after photoexcitation (0.2 ps), in addition to a slow component (12 ps) attributable to the orientational diffusion of the 7-azaindole dimer. Since the time constant of the rapid anisotropy change agrees with the observed lifetime of the "ultrafast" population decay component, we concluded that the internal conversion takes place from the initially-populated excited state to the lowest excited state having a different transition moment direction with a time constant of 0.2 ps. The quantitative analysis of the anisotropy data is now in progress to reveal relative directions of the two excited-state transition moments.

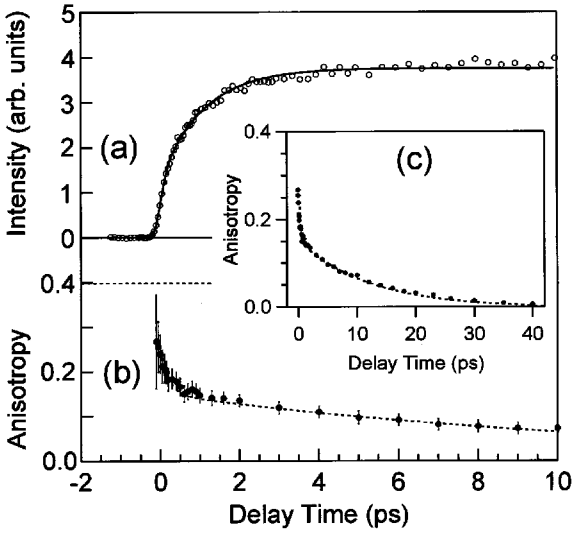

Figure 1. Time-resolved fluorescence signal (a) and fluorescence anisotropy (b) of 7-azaindole dimer in hexane at 500 nm. The longer-time behavior of the anisotropy is also shown in the inset (c). The dotted curve in the anisotropy data is the best-fitted biexponential function with decay time constants of 0.2 ps and 12 ps.

VI-C-4 Ultrafast Quenching of Biphenyl Fluorescence by Carbon Tetrachloride Observed with Time-Resolved Fluorescence Spectroscopy

Koichi IWATA *(Univ. Tokyo)*, **Satoshi TAKEUCHI and Tahei TAHARA**

Reaction kinetics of an ultrafast bimolecular reaction was successfully interpreted by the Smoluchowski model of diffusion-controlled reactions. When biphenyl is photoexcited to the first excited singlet (S_1) state in carbon tetrachloride solutions, it reacts with the solvent carbon tetrachloride. Because of this reaction, the fluorescence lifetime of biphenyl in carbon tetrachloride is anomalously shortened to a few picoseconds. We observed the kinetics of this ultrafast fluorescence quenching by using the fluorescence up-conversion method with the time resolution of 320 fs. Observed time dependence of the fluorescence signal from biphenyl in carbon tetrachloride is shown in the Figure 1 (dots). Although the observed decay curve was not fitted well with single exponential decay functions, it was well explained by a model function derived from the Smoluchowski model of diffusion-controlled reactions (solid curve). The fitting parameter for this analysis is distance *R* where the density of the reacting molecules becomes zero. The best fit was obtained when the distance *R* was 0.4 nm, which matched the actual size of the molecules well. The success of the Smoluchowski model suggests that the translational motion of biphenyl and carbon tetrachloride can be well described as a diffusion motion in a time scale of a few picoseconds.

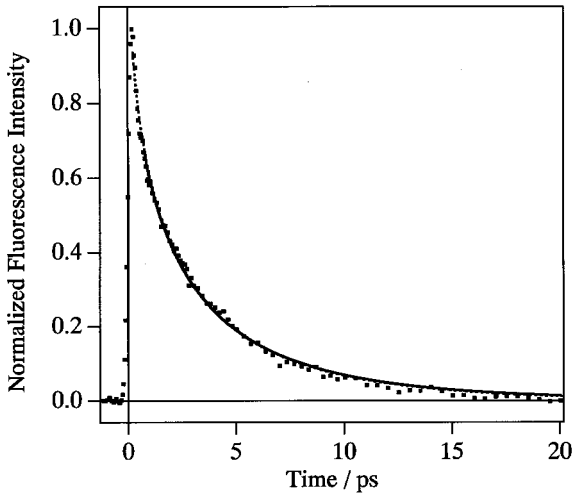

Figure 1. Observed fluorescence decay kinetics of biphenyl in carbon tetrachloride (dots). Decay kinetics simulated with the Simlukowski model of diffusion-controlled reaction is also shown (solid curve).

VI-C-5 Femtosecond Fluorescence from the Higher Excited State of Tetracene

Nilmoni SARKAR, Satoshi TAKEUCHI and Tahei TAHARA

In most of all cases, only fluorescence from the lowest excited singlet state is observed even if molecule is photoexcited initially to the higher excited singlet state. This rule, Kasha rule, was originally found for the steady-state fluorescence, but is also valid for time-resolved fluorescence up to picosecond time range. The implication of this rule is that the electronic relaxation from the higher excited state to the lowest one takes place much faster than fluorescence emission. However, if time-resolution of the measurement is high enough, it is expected that the fluorescence from the higher excited state is also observed before the electronic relaxation. With this idea, we studied fluorescence of tetracene with femtosecond time-resolution. Tetracene shows two prominent absorption bands in the ultraviolet-visible region. The absorption band in the ultraviolet is due to the ^1B_b-S_0 transition and the other in the visible is ascribed to the lowest ^1L_a-S_0 transition. We excited the molecule to the ^1B_b state with 270 nm excitation and found very short-lived fluorescence signal in the ultraviolet region where the intensity of steady-state fluorescence is negligible (Figure 1). The lifetime of this ultraviolet fluorescence was determined as 120 fs by fitting analysis which takes account of finite instrumental response. This lifetime agreed very well with rise of the ^1L_a (S_1) fluorescence observed in the visible region. We concluded that the fluorescence found in the ultraviolet is the fluorescence from the higher ^1B_b state and that the electronic relaxation from the ^1B_b state to ^1L_a state takes place with a time constant of 120 fs.

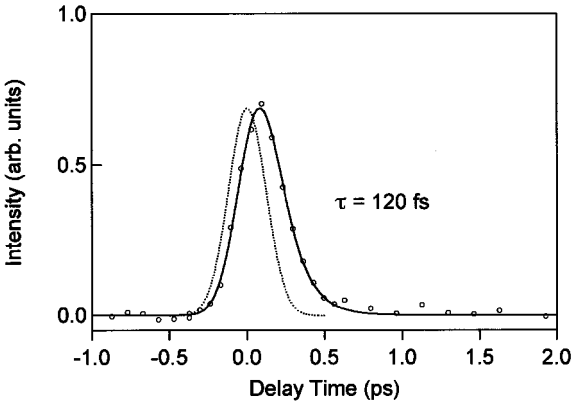

Figure 1. Femtosecond time-resolved fluorescence signal of tetracene at 340 nm (solid curve) and the instrumental response function (dotted curve).

VI-C-6 Ultrafast Relaxation Dynamics of Photo-excited Cu(II)(TMpy-P4) in Water

Sae Chae JEOUNG, Satoshi TAKEUCHI and Tahei TAHARA

We have conducted femtosecond pump-probe experiments to understand the relaxation process of a copper porphyrin, Cu(II)(TMpy-P4), in aqueous solution. It was found that both the spectral feature and the temporal behavior of the transient absorption strongly depend on the excitation density. From the comparison with a reference experiment for the solvent only, we concluded that the transient absorption signal obtained with the high excitation density arises not only from the excited-state dynamics of the porphyrin but also from solvated electrons generated from the water solvent. By carefully lowering the excitation density to remove the contribution from the solvated electrons, the transient absoption spectra purely due to Cu(II)(TMpy-P4) were obtained with photoexctation at the Soret band (Figure 1). We observed a broad transient absorption band from 450 nm to near infrared region. This band exhibits a spectral sharpening in early delay times, and then becomes broader again. On the basis of the analysis of the spectral changes, the excited-state dynamics of Cu(II)(TMpy-P4) and a possible involvement of a five-coordinated complex with a water molecule are discussed.

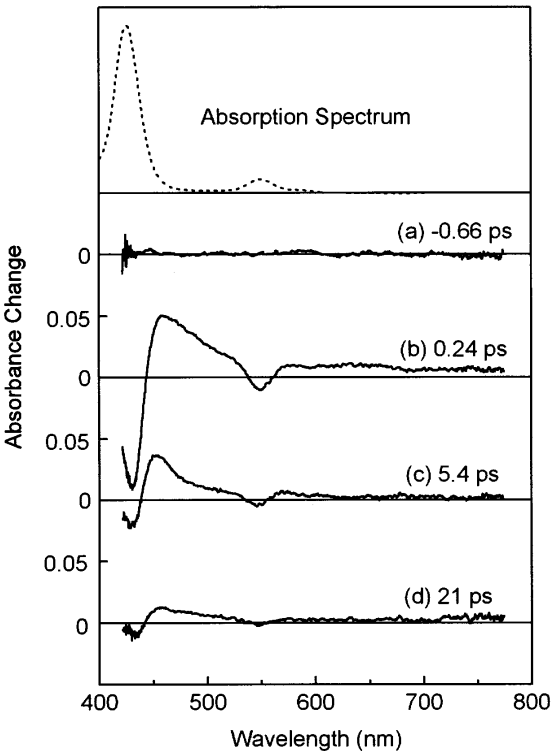

Figure 1. Transient absorption spectra of Cu(II)(TMpy-P4) in water measured at -0.66 (a), 0.24 (b), 5.4 (c), and 21 ps (d). Steady-state absorption spectrum of the porphyrin is also shown at the top.

VI-D Studies on Photochemical Reactions Using Picosecond Time-Resolved Vibrational Spectroscopy

Time-resolved vibrational spectroscopy is a very powerful tool for the study of chemical reactions. It often affords detailed information about the molecular structure of short-lived intermediates, which is not obtainable with time-resolved electronic spectroscopy. However, for molecules in the condensed phase, we need energy resolution as high as 10 cm^{-1} in order to obtain well-resolved vibrational spectra. This energy resolution is compatible only with time-resolution slower than picosecond because of the limitation of the uncertainty principle. In this sense, picosecond measurements are the best compromise between energy resolution and time resolution for time-resolved frequency-domain vibrational spectroscopy. In this project, we study photochemical processes and short-lived transient species by using picosecond time-resolved vibrational spectroscopy.

VI-D-1 Vibrational Dynamics in the Lowest Excited Triplet State Immediately after Intersystem Crossing

Atsuhiko SHIMOJIMA and Tahei TAHARA

Picosecond time-resolved spontaneous resonance Raman spectra of *all-trans* retinal were measured. Although it had been thought that the fluorescence background makes it difficult to obtain clear picosecond Raman signals from retinal, we succeeded in observing transient Raman bands due to the T_1 state by using the probe laser which is rigorously resonant with the T-T absorption. In order to reveal the initial photodynamics of the T_1 state, quantitative analysis was carried out for the 1553 cm^{-1} and 1183 cm^{-1} bands of the *all-trans* T_1 state. The intensities of these two Raman bands increase with a time constant of 25 ps which is in good agreement with the reported intersystem crossing time constant of *all-trans* retinal. In addition, it was found

that their peak position and band width change with time (Figure 1). They show frequency up-shift and band narrowing in the time range from 5 ps to 30 ps. The peak shifts were well fitted to single exponential functions with time constants of 14 ps (1553 cm^{-1}) and 18 ps (1183 cm^{-1}). These observations imply that the T_1 state generated by the intersystem crossing is initially vibrationally hot, and then the vibrational cooling takes place within a few tens of picosecond in the triplet manifold.

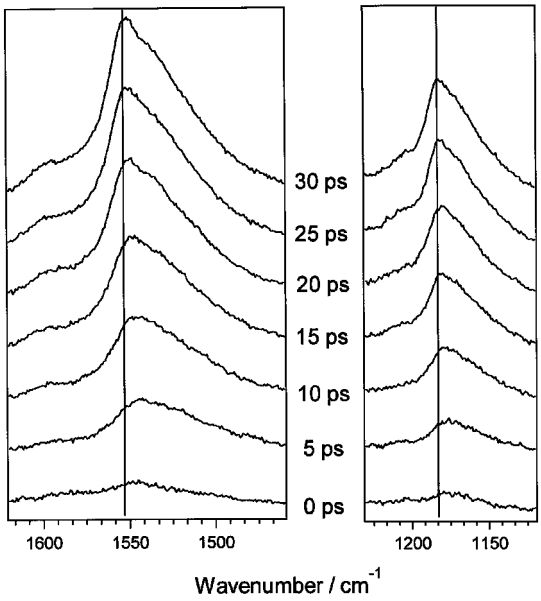

Figure 1. The initial photodynamics of the T_1 state of *all-trans* retinal observed in picosecond time-resolved Raman spectra (hexane solution, 10^{-3} mol dm^{-3}, pump 385 nm, probe 458 nm).

VI-D-2 Cis-Trans Photoisomerization Mechanism of Retinal Studied by Picosecond Time-Resolved Raman Spectroscopy

Atsuhiko SHIMOJIMA and Tahei TAHARA

Cis-trans photoisomerization of 9-cis and 13-cis retinal was studied by picosecond time-resolved resonance Raman spectroscopy. The time-resolved spectra were measured with the time and frequency resolution of 2 ps and 10 cm^{-1}, respectively, using an apparatus based on a picosecond mode-locked Ti: sapphire laser. The obtained spectra are shown in Figure 1. In the case of 9-cis retinal, the transient Raman bands assignable to the "all-trans" T_1 state slowly appear with a time constant of about 900 ps after photoexcitation, which indicates that cis-trans structural change takes place in the triplet manifold. On the other hand, with the photoexcitation of 13-cis retinal, the transient Raman signals attributable to the mixture of the "13-cis" and the "all-trans" T_1 states appear within several tens of picoseconds. In addition, the 1550 cm^{-1} band having contribution from both the "13-cis" and the "all-trans" T_1 states rises significantly faster than the 1182 cm^{-1} band which is solely due to the "all-trans" T_1 state. The time constant of rise of the 1182-cm^{-1} band agrees well with the intersystem crossing time of all-trans retinal. We concluded that the structural change from the 13-cis to the all-trans form takes place in the excited singlet state and that the "13-cis" and the "all-trans" T_1 states are separately generated from the S_1 state having each conformation. The cis-trans photoisomerization mechanism clarified in the present study is shown in Figure 2.

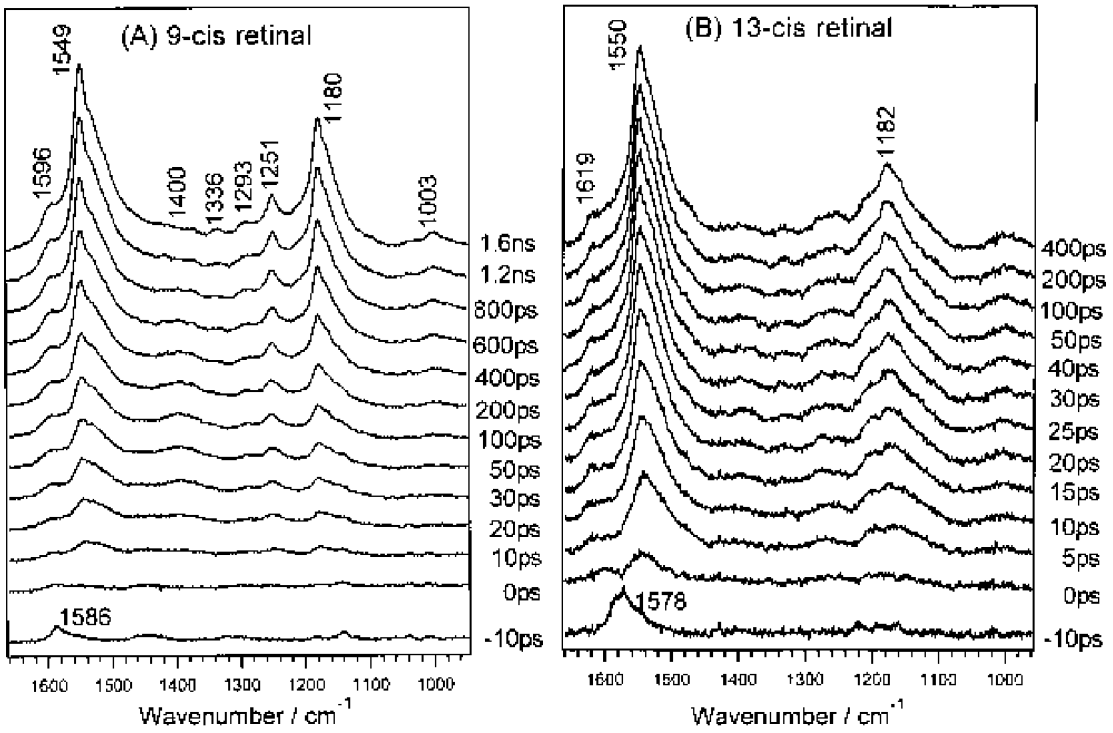

Figure 1. Time-resolved resonance Raman spectra of 9-cis (A) and 13-cis (B) retinal in hexane (10^{-3} mol dm^{-3}, pump 385 nm, probe 458 nm). Solvent Raman bands were subtracted from each spectrum.

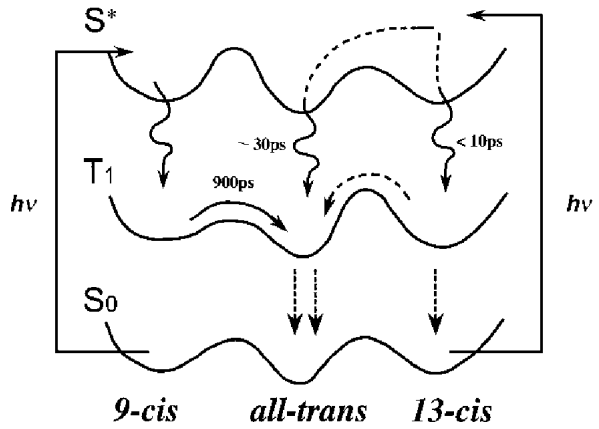

Figure 2. The cis-trans photoisomerization mechanism of retinal.

VI-D-3 Vibrational Cooling Dynamics of Solvated Structures of para-Nitroaniline in Acetonitrile

Kathaperumal MOHANALINGAM *(Waseda Univ.)*, **Hiro-o HAMAGUCHI** *(Univ. Tokyo)*, **Atsuhiko SHIMOJIMA and Tahei TAHARA**

Recently it has been shown that p-nitroaniline (pNA) in acetonitrile exists in two distinct solvated structures, the 1:1 form and 1:2 forms.[1)] In the 1:1 form, acetonitrile is associated with the amino group of pNA while it is associated with both the amino and nitro groups in the 1:2 form. These two structures exhibit different charge transfer characteristics which are manifested in the difference in their absorption spectra. We have measured picosecond time-resolved Raman spectra of pNA in acetonitrile by using the pump laser at 400 nm and the probe laser at 454 nm. Under this experimental condition, only the 1:2 form is selectively photoexcited. Immediately after photoexcitation, we observed bleach and the following very fast recovery for the intensity of the Raman band due to the symmetric stretch of the nitro group in the ground-state 1:2 form (1315 cm^{-1}). In addition, the bandwidth of this band changed with the time delay, reflecting vibrational cooling taking place in the solvent structure. These observations are consistent with the result of the earlier femtosecond time-resolved absorption studies which indicated that very fast dissociation and reassociation processes occurs with a time constant as fast as 0.7 ps after photoexcitation of the 1:2 form.

Reference

1)K. Mohanalingam and H. Hamaguchi, *Chem. Lett.* 157 (1977); K. Mohanalingham and H. Hamaguchi, *Chem. Lett.* 537 (1997).

VI-E Development of Time-Resolved Spectroscopy Using Synchrotron Radiation

Synchrotron radiation affords photons in a wide energy region from X-ray to far-infrared, and is intrinsically produced in the form of a picosecond pulse train. The unique characteristics of synchrotron radiation are very attractive for time-resolved spectroscopy. In this project, by utilizing the combination of laser and synchrotron radiation, we attempt time-resolved measurements in energy regions which are not accessible only with the existing lasers. We have constructed a setup for subnanosecond time-resolved far-infrared measurements at beamline BL6B in UVSOR. In this year, we made attempts to measure time-resolved spectra of several solid samples with use of this set-up.

VI-E-1 Trial to Measure Time-Resolved Far-Infrared Spectra of β'-(BEDT-TTF)$_2$ICl$_2$ Using Synchrotron Radiation

Tahei TAHARA and Akito UGAWA *(Univ. Florida, U.S.A.)*

Far-infrared spectra contain much information about low-frequency motion in the material including intermolecular vibrations in liquid and phonons in solid. It is highly desirable to develop time-resolved far-infrared spectroscopy, since it is expected to afford unique information on photo-induced processes in the material. In order to examine potentiality of synchrotron radiation for time-resolved far-infrared spectroscopy, we tried to measure time-resolved spectra of an organic semiconductor, β'-(BEDT-TTF)$_2$ICl$_2$, by using a setup at beamline BL6B in our synchrotron radiation facility (UVSOR). In this measurement, we used picosecond laser pulses for the excitation of the sample, and utilized far-infrared synchrotron radiation for probing. The picosecond laser pulse was the second harmonic of the output of a mode-locked Nd:YAG laser which was synchronized to the synchrotron radiation. Far-infrared/infrared synchrotron radiation was introduced to a Michelson-type Fourier Transform spectrometer through a Si or a KRS-5 optical window. The pumping laser pulse and the probing synchrotron radiation pulse were focused and overlapped on the sample, and the reflected synchrotron radiation beam was detected with a bolomer. Time-resolution of the measurements was predominantly determined by the duration of synchrotron radiation which is about 1 ns. Figure 1 shows time-resolved difference reflectance spectra obtained from β'-(BEDT-TTF)$_2$ICl$_2$ at 8K. With the irradiation of the laser pulse, the reflectance change was recognized for several phonon bands. The most prominent change was observed at the band around 230 cm^{-1}. This reflectance change, however, does not depend on the delay time, indicating that the relaxation time of the photo-induced change is much slower than the repetition rate of the photoexcitation (90 MHz). It is highly likely that the observed spectral change is due to the temperature change of the sample induced by the

laser irradiation.

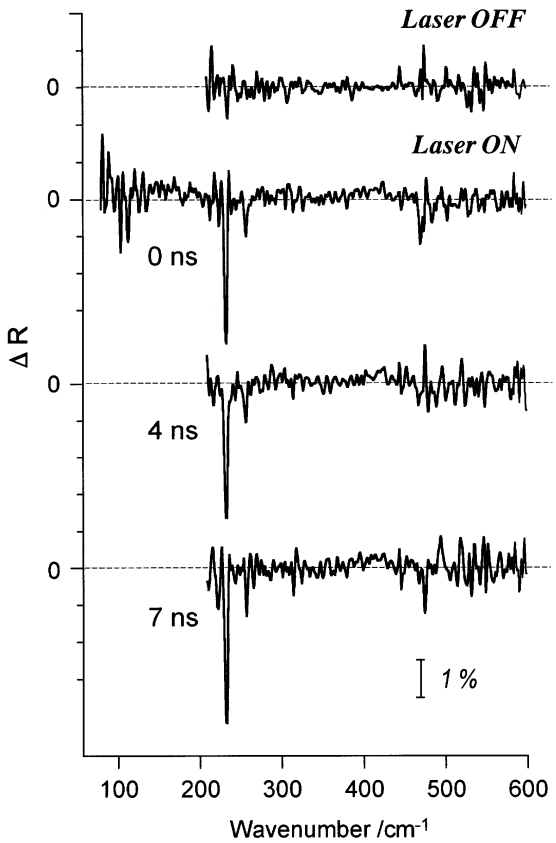

Figure 1. Time-resolved far-infrared spectra of β'-(BEDT-TTF)$_2$ICl$_2$ at 8 K.

VI-F Synchrotron Radiation Stimulated Surface Reactions

Study of synchrotron radiation (SR) stimulated surface reaction is a promising topic in fundamental science, because dynamical processes induced by the photostimulated core-electron excitations on surfaces are scarcely explored so far. This field is important also in applied science, since the fundamental study is expected to develop the new techniques for semiconductor processing such as SR stimulated etching and SR stimulated epitaxial growth.

VI-F-1 The Direct Observation of Synchrotron Radiation Stimulated Desorption of Thin SiO_2 Films on Si (111) by Scanning Tunneling Microscopy

Takayuki MIYAMAE, Hironaga UCHIDA *(Toyohashi Univ. Tech.)*, **Tsuneo URISU and Ian H. MUNRO** *(UMIST and IMS)*

This is the first report of the use of scanning tunneling microscopy (STM) to study changes in the surface morphology during synchrotron radiation (SR) stimulated desorption of SiO_2 films on Si(111). An atomically flat and clear surface was obtained after two hours SR irradiation at a surface temperature of 700 °C as shown in Figure 1. The STM topograph indicates that the SR desorption mechanism is quite different for the thermal desorption of SiO_2. The non-formation of voids indicates that the desorption of oxygen atoms and molecules by SR excitation leaving volatile SiO is an important mechanism.

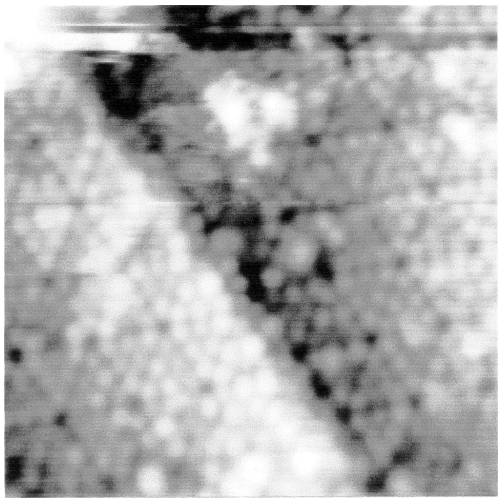

Figure 1. STM topograph of occupied states (sample vias = -2.1 V) of a Si (111) surface after 2 h SR-irradiation at 700 °C. Image size = 150 × 150 Å.

VI-F-2 Chemisorption of Deuterium on an Ultrathin Ge Film Deposited over Si(100)-2x1: Existence of a Dihydride Phase

Syed Irfan GHEYAS, Tsuneo URISU, Shinya HIRANO, Hidekazu WATANABE, Suehiro IWATA, Mutsumi AOYAGI, Mitsuhiro NISHIO *(Saga Univ.)* **and Hiroshi OGAWA** *(Saga Univ.)*

[*Phys. Rev. B* in press]

Adsorption of atomic deuterium on ultrathin Ge film deposited over Si(100) has been studied using Fourier transformed infrared reflection absorption spectroscopy and reflection high-energy electron diffraction (RHEED) measurements. Figure 1 shows the IR spectra of Ge/Si(100) as a function of deuterium exposure at 85 °C. At a low temperature of about 300 L, only one vibrational mode at about 1438 cm^{-1} can be observed clearly. This mode is assigned to GeD symmetric stretching. The RHEED pattern corresponding to an exposure of 320 L, which shows a strong 2 × 1 pattern, justifies this assignment. Notably, no Si-related peak was detected corresponding to this exposure. A deuterium exposure of 1200 L of higher, on the other hand, visibly weakens the GeD peak intensity. Interestingly, the IR spectra reveal a decrease in GeD intensity by about 40% but still no appearance of a Si-related peak as we proceed from Figures 1(a) to 1(c). We established that high atomic deuterium exposure on a Ge/Si(100) surface leads to a change in the RHEED pattern from 2 × 1 to 1 × 1. This change possibly is due to an overwhelming conversion on Ge monodeuterides to dideuteride. Etching of the Ge atoms has also clearly been observed.

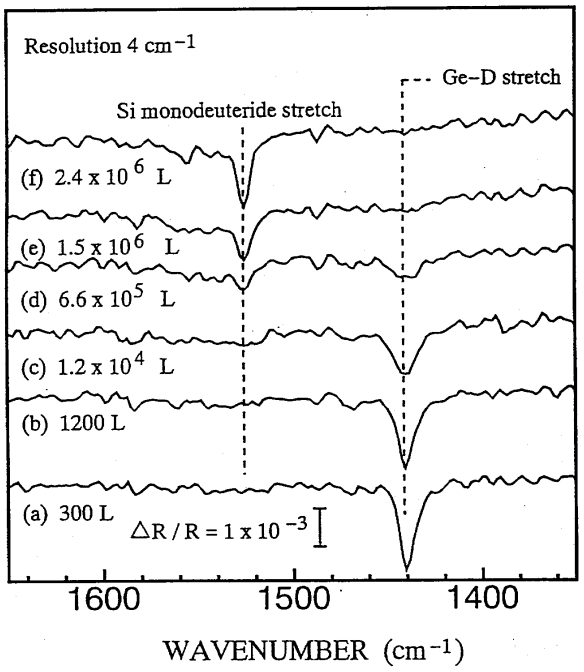

Figure 1. IR spectra taken after a series of deuterium exposures of Ge/Si(100) at 85 °C. All measurements were carried out at 85 °C.

VI-F-3 Structure of Hydrogen Terminated Si(100) Surfaces and Modification by Synchrotron Radiation Irradiation

Shinya HIRANO, Hideyuki NODA, Akitaka YOSHIGOE *(Japan Atomic Energy Research Institute)***, Syed Irfan GHEYAS** *(Emory Univ.)* **and Tsuneo URISU**

[*Jpn. J. Appl. Phys.* submitted]

The structure of the hydrogen (deuterium) saturation adsorbed Si(100)1×1 (H(D)-Si(100)1×1) surface generated at 400 K, and its change by annealing and synchrotron radiation (SR) irradiation were investigated by infrared reflection absorption spectroscopy (IRRAS) using $CoSi_2$ buried metal layer (BML) substrate and reflection high energy electron diffraction (RHEED) measurements. It was found that the structure of the H-Si(100)1×1 surface is disordered 3×1 consisting of coupled monohydride (H-Si-Si-H) + dihydride (H-Si-H) unit. By 650 K annealing, the D-Si(100)1×1 surface changes to 2×1 structure consisting of only D-Si-Si-D, which gives an SiD stretching vibration band with a sharp and symmetric shape peaked at around 1525 cm^{-1}. If the SR irradiation is added to the annealing of the D-Si(100)1×1 surface, the shape of the SiD stretching vibration band at 1525 cm^{-1} after 650 K annealing becomes broad and asymmetric. This is explained by that D-Si-D is etched (desorbed) by the SR irradiation.

VI-F-4 Design and Performance of a Multi-layered Mirror Monochromator in the Low Energy Region of Vacuum Ultra Violet

Harutaka MEKARU, Tsuneo URISU, Yoshiyuki TSUSAKA *(Himeji Inst. Tech.)***, Shin MASUI** *(Sumitomo Heavy Industries Ltd.)***, Eijiro TOYOTA** *(Sumitomo Heavy Industries Ltd.)* **and Hisataka TAKENAKA** *(NTT-AT)*

[*J. Synchrotron Rad.* **5**, 714 (1998)]

The vacuum ultra violet (VUV) photons in the SR can excite almost all the electronic states of molecules, so a large variety of chemical reaction channels different from that in the usual thermal-CVD are expected to be opened by the SR irradiation. In particular, core electrons, which cannot be excited using lasers are efficiently excited by the VUV photons in the SR. The excitation energy dependence of a photo-chemical reaction is important basic data. However it has not been sufficiently investigated in the VUV region, because of the difficulty of obtaining energy-tunable monochromatized light with sufficient photon flux in the VUV region.

In this work, a double-crystal-type MLM monochromator equipped with a C filter has been designed on the basis of trial fabrication of Mo/Si MLM and its performance has been evaluated by calculating what the basic characteristics such as output photon flux, resolution, monochromaticity and tuning range would be if the monochromator were set up as the part of the beamline (BL4A1) at the UVSOR. However,

considering a MLM monochromator to use in SR stimulated processes, it is known that extremely large total reflection components appear at less than 40 eV in the case of Mo/Si.

Therefore, a C thin-film filter was used to reduce drastically the low-energy background noise. The higher-order photons background noise is less than 4%. The calculated photon flux is $1 \sim 5 \times 10^{14}$ photons/s and the resolution is 5-9 eV. We conclude that the background noise due to the total reflection can be sufficiently reduced by using double MLM monochromator at low incident angles combined with the C thin-film filter.

VI-F-5 Construction of the Multilayered-Mirror Monochromator and the Beam Line for the Study of Synchrotron Radiation Stimulated Process

Harutaka MEKARU, Yoshiyuki TSUSAKA *(Himeji Inst. Tech.)*, **Takayuki MIYAMAE, Toyohiko KINOSHITA, Tsuneo URISU, Shin MASUI** *(Sumitomo Heavy Industries Ltd.)*, **Eijiro TOYOTA** *(Sumitomo Heavy Industries Ltd.)* **and Hisataka TAKENAKA** *(NTT-AT)*

[*Rev. Sci. Inst.* submitted]

The double crystal type multilayered-mirror (MLM) monochromator was developed and the beamline (BL4A1) using this monochromator was constructed at the UVSOR in the IMS. The low-energy background noise due to the total reflection component is reduced by using MLMs at low incident angles combined with a suitable thin-film filter. In the case of using Mo/Si MLMs and a C filter, the output beam photon flux, the monochromaticity, the low-energy background noise and the flux of the higher order photons were evaluated by measuring the transmission of the Al filter at around the Al $L_{2,3}$ absorption edge by a silicon photodiode and also by measuring the photo-emission spectra of Ta XPS spectra using the output beam as an excitation light source.

The transmission of the Al filter at around the Al $L_{2,3}$ absorption edge was measured by using the output beam of the monochromator as a function of the incident angle. The experimental results are compared with the calculation in Figure 1A. From the good agreement between the calculated and experimental results, it is concluded that the spectrum width should be almost equal to the calculated width (5 ~ 9 eV). The observed photo-emission spectra excited by output beam with the C filter at the incident angle of $\theta = 20°$ is shown in Figure 1B. The clear peak assigned to the Ta 5d state is observed indicating that the C filter reduces sufficiently the low-energy background.

It has been confirmed that the present MLM monochromator using Mo/Si MLM combined with C filter works well as predicted by the calculation. The output beam photon flux, the spectrum width, the low-energy background and the higher-order (second-order) photon background were evaluated to be 1.0×10^{12} (at 10 degree) ~ 1.5×10^{14} (at 55 degree) photons/s, 5 eV ~ 9 eV, less than 7.2% and less than 12%, respectively. We conclude that the MLM monochromator beamline BL4A1 constructed here have sufficient performance for the study of the excitation-energy dependence in the SR stimulated process.

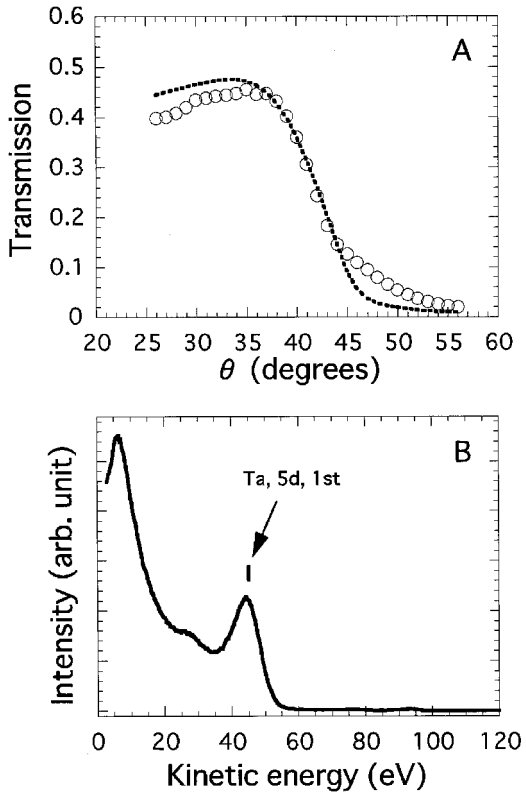

Figure 1. (A) The transmission of the Al filter in the vicinity of the Al $L_{2,3}$ absorption edge measured by using output beam of the monochromator for each mirror incident angle θ. ---: calculated value (the Al filter thickness of 180 nm and the transmission of the mesh holding the thin Al film of 74.8% are assumed) and ○: measured value, and (B) The photo-emission spectra of Ta measured by using the MLM monochromator output beam as the excitation light source. Mo/Si MLMs are used at θ = 20 degrees combined with the C filter (~120 nm thickness).

VI-F-6 Influence of Residual Fluorine Gases on the Adsorption of Atomic H on Si(100)-2×1 Surfaces

Hideyuki NODA, Shinya HIRANO, Youichi NONOGAKI, Mineo HIRAMATSU *(Meijo Univ.)* **and Tsuneo URISU**

We have investigated chemical reaction of atomic hydrogen (H) on Si(100)-2×1 surfaces and the effect of synchrotron radiation (SR) irradiation using buried metal layer - infrared reflection absorption spectroscopy (BML-IRRAS). In ultra high vacuum (UHV) chamber, we have found that a very small amount of residues influence Si clean surfaces. Figure 1 shows the intensity of each mass number measured by quadruple mass spectroscopy (QMS) in UHV chamber (2.0×10^{-10} Torr). The peak at the mass number of 19 for F component was observed, as shown in Figure 1. Figure 2 shows the IRRAS spectra of the time dependence after forming Si(100)-2×1 surface by gas source MBE

using disilane. As the time increased, the intensity of 820-1100 cm^{-1} peaks increased. These peaks are assinged to vibrations of Si-F (820 cm^{-1}), Si-F_2 and Si-F_3 (930 cm^{-1}), Si-F_4 (1010 cm^{-1}), respectively.[1)] It is considered that residual fluorine gases or hydrogen fluoride adsorbes on Si clean surfaces.

The influence of residual fluorine or fluoride gases on the adsorption of atomic H on Si(100)-2×1 surfaces is under investigations.

Reference

1)C. J. Fang et al., *Phys. Rev. B* **22**, 6140 (1980).

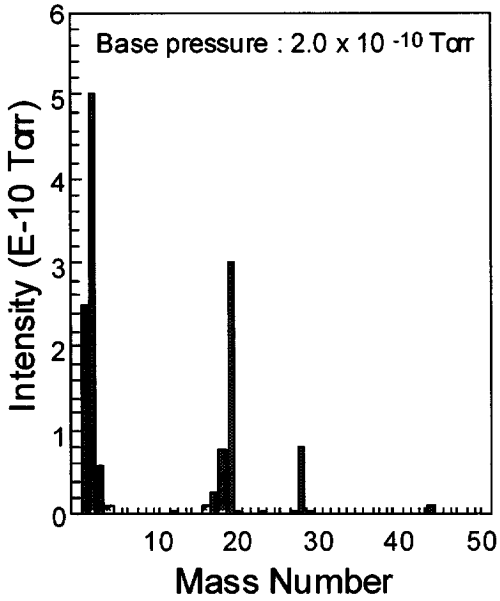

Figure 1. Intensities of each mass number measured by QMS.

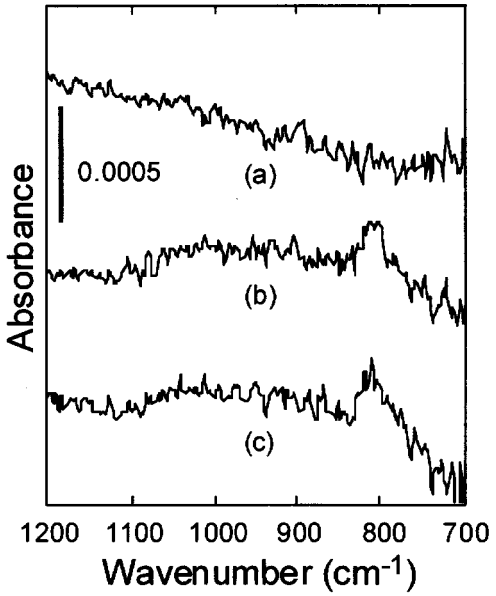

Figure 2. Change of the IRRAS spectra of the Si(100) surface under fluorine or fluoride residual gases (a : after epitaxial growth, b : (a) + 30 min, c : (a) + 50 min).

VI-G Ion Desorption Induced by Core-Electron Transitions Studied by Electron Ion Coincidence Spectroscopy Combined with Synchrotron Radiation

Ion desorption induced by core-electron transitions has been studied using energy-selected electron ion coincidence spectroscopy combined with synchrotron radiation. Auger electron photo-ion coincidence (AEPICO) and photoelectron photo-ion coincidence (PEPICO) spectroscopies proved to be an ideal tool for investigations of the ion desorption induced by core-level excitations. AEPICO results show that the character of the orbitals where holes are created, as well as the effective hole-hole Coulomb repulsion are important factors in the Auger-stimulated ion desorption from covalent molecules. The PEPICO spectroscopy, on the other hand, provided direct evidences of site-specific ion fragmentation induced by core-level excitations.

VI-G-1 Auger Electron Photoion Coincidence (AEPICO) Technique Combined with Synchrotron Radiation for the Study of Ion Desorption Mechanism in the Region of Resonant Transitions of Condensed H_2O

Kazuhiko MASE, Mitsuru NAGASONO, Shin-ichiro TANAKA, Tsuneo URISU, Eiji IKENAGA *(Hiroshima Univ.)*, **Tetsuji SEKITANI** *(Hiroshima Univ.)* **and Kenichiro TANAKA** *(Hiroshima Univ.)*

[*J. Chem. Phys.* **108**, 6550 (1998)]

Auger electron photoion coincidence (AEPICO) technique has been applied for the study of H^+ desorption induced by resonant excitations of O 1*s* of condensed H_2O. The peak positions of the AEPICO yield spectrum at the $4a_1 \leftarrow$ O 1*s* resonance ($h\nu$ = 533.4 eV) are found to correspond to spectator-Auger transitions leaving $(O\ 2s)^{-2}(4a_1)^1$, $(O\ 2s)^{-1}(O\ 2p)^{-1}(4a_1)^1$, and $(O\ 2p)^{-2}(4a_1)^1$ states. The H^+ AEPICO yield is greatly enhanced at $4a_1 \leftarrow$ O 1*s* while suppressed at $3p \leftarrow$ O 1*s* ($h\nu$ = 537 eV) as compared with that at the O 1*s* ionization ($h\nu$ = 560 eV). On the basis of these results, the ultrafast ion desorption mechanism is

suggested to be favorable for the H^+ desorption at $4a_1 \leftarrow$ O 1s, that is, the repulsive potential energy surface of the $(O\ 1s)^{-1}(4a_1)^1$ state is responsible for the H^+ desorption. For H^+ desorption at $3p \leftarrow$ O 1*s*, spectator-Auger stimulated ion desorption mechanism is concluded to be probable. The suppression of the H^+ AEPICO yield is ascribed to the reduction of the hole-hole repulsion due to the shield effect of the 3*p* electron. These results demonstrate the power of AEPICO technique to clarify the mechanism of ion desorption induced by core-electron excitations.

VI-G-2 Study of Ion Desorption Induced by Resonant Core-Electron Excitation of Isolated NH_3 Monolayer Adsorbed on a Xe Film Using Auger Electron Photoion Coincidence Spectroscopy

Mitsuru NAGASONO, Kazuhiko MASE, Shin-ichiro TANAKA and Tsuneo URISU

Mechanism of ion desorption induced by resonant core-electron excitation of isolated NH_3 monolayer adsorbed on a Xe film (NH_3/Xe) is studied using Auger electron photoion coincidence (AEPICO) spectroscopy. The total ion yield spectrum of NH_3/Xe exhibits a threshold peak at the resonant excitation from N 1*s* to the $4a_1$ N-H antibonding orbital. The Auger electron spectrum of NH_3 at the $4a_1 \leftarrow$ N 1*s* resonance is found to be mainly due to spectator Auger transitions. A series of AEPICO spectra at the $4a_1 \leftarrow$ N 1*s* resonance is measured for the electron kinetic energies corresponding to the spectator Auger transitions. The AEPICO spectra show that the H^+ is the only desorbed ion species. The electron kinetic energy dependence of the H^+ AEPICO yield displays a structure similar to that of the spectator Auger electron spectrum. This result indicates that the H^+ desorption probabilities are independent of the spectator Auger final states. We suggest that the repulsive potential surface of the $(N\ 1s)^{-1}(4a_1)^1$ state is responsible for the H^+ desorption, that is, ultrafast ion desorption mechanism is favorable in this system.

VI-H Photoionization Dynamics Studied by Electron Spectroscopy Combined with a Continuous Synchrotron Radiation Source

Molecular photoionization is a major phenomenon in vacuum UV excitation and provides a large amount of information on fundamental electron-core interactions in molecules. Especially, autoionizing and shape resonances become of main interest, since they often dominate photoabsorption cross sections and lead to various vibronic states which are inaccessible in direct ionization. In order to elucidate dynamical aspects of photoionization, we have developed a versatile machine for photoelectron spectroscopy. Introduction of a new methodology, two-dimensional photoelectron spectroscopy, allows us to investigate autoionization and predissociation of superexcited states of acetylene, nitric oxide, carbonyl sulfide, sulfur dioxide and so on. In this method, the photoelectron yield is measured as a function of both photon energy and electron kinetic energy (binding energy). The spectrum, usually represented as a contour plot, contains rich information on photoionization dynamics.

VI-H-1 Spectator- and Participant-Like Behavior of a Rydberg Electron on Predissociation of Superexcited States of OCS

Yasumasa HIKOSAKA, Hideo HATTORI and Koichiro MITSUKE

[*J. Chem. Phys.* submitted]

Predissociation of superexcited states of OCS is studied by two-dimensional photoelectron spectroscopy using synchrotron radiation in the photon energy range of 15-16.5 eV. A two-dimensional photoelectron spectrum exhibits two kinds of characteristic patterns both of which are ascribed to autoionization of sulfur atoms. To clarify the point, we show a photoelectron spectrum of Figure 1 which is obtained as a cut through the two-dimensional spectrum along the electron kinetic energy axis at the phootn energy of 15.95 eV. The superexcited atom S* is produced by predissociation of a Rydberg state OCS*(R_B) converging to $OCS^+(\tilde{B}^2\Sigma^+)$. The pattern of the first kind results from predissociation processes in which the effective principal quantum number *n* of the Rydberg electron is almost conserved. This suggests that the Rydberg electron behaves as a spectator because of its negligibly weak interaction with the ion core (spectator predissociation). On the contrary, *n* of S* does not accord with that of OCS*(R_B) in the pattern of the second kind, indicating that the Rydberg electron participates directly into the electron exchange mechanism controlling conversion from OCS*(R_B) to a predissociating state (participant predissociation). With increasing *n*, OCS*(R_B) decays more preferentially by the spectator than by the participant predissociation. The spectator predissociation of OCS*(R_B) proceeds through a two-step conversion which involves Rydberg states converging to $OCS^+(\tilde{A}^2\prod$ and $\tilde{X}^2\prod)$ and a dissociative multiple-electron-excited state OCS*(*SAT*) asymptotically correlating with S* + $CO(\tilde{X}^1\Sigma^+)$. In contrast, the participant predissociation may be accounted for by a direct conversion from OCS*(R_B) to OCS*(*SAT*). The quantum yields are estimated from Figure 1 to be 0.07 and 0.02 for the participant and spectator predissociation, respectively, at the incident photon energy of 15.95 eV where OCS*(R_B) states with $n \sim 12$ lie. A simulation is performed to reproduce the partial cross section curve for the spectator predissociation by using a model in which the decay

rates for the participant and spectator predissociation are assumed to be proportional to n^{-3} and n^0, respectively. The simulated and experimental cross section curves are in good agreement with each other at the photon energy higher than 15.8 eV.

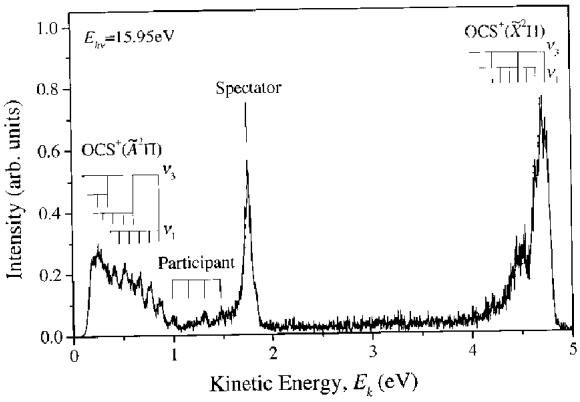

Figure 1. Photoelectron spectrum of OCS at the photon energy of 15.95 eV where OCS*(R_B) states with $n \sim 12$ are located.

VI-I Laser Photionization of Polarized Atoms Produced by Excitation with Synchrotron Radiation

In conventional photoionization experiments, the most standard method has generally been taken to be measurement of energy and angular distributions of photoelectrons from randomly oriented (unpolarized) atoms or molecules. However, information obtained from these experiments is insufficient, since the initial state constituted of atoms and photons is not selected and the internal properties of final photoions and electrons are not analyzed. In this project, we have performed photoelectron spectroscopy of polarized atoms using linearly-polarized laser light, aiming at complete quantum-mechanical photoionization experiments. Initial excitation with a linearly polarized synchrotron radiation permits ensemble of atoms to be aligned along the electric vector of the light. From an angular distribution of photoelectrons from polarized atoms, we are able to gain insight into the magnitude and phase shift difference of dipole transition moments of all final channels which are allowed by selection rules.

VI-I-1 Laser Photoionization of Polarized Ar Atoms Produced by Excitation with Synchrotron Radiation

Koichiro MITSUKE, Yasumasa HIKOSAKA *(Inst. for Mater. Struct. Sci.)* **and Kota IWASAKI**

Photoionization dynamics of poalrized Ar atom has been studied by photoelectron spectroscopy. Linearly polarized synchrotron radiation is used to pump a ground state atom to Rydberg states lying below the first ionization potential of Ar (15.759 eV). The polarized Ar atom is then ionized by absorbing a single photon of a Nd:YAG laser (λ = 532 nm) which is also linearly polarized. This photoionization process can be expressed by

$$Ar \xrightarrow{\text{Synchrotron}} Ar^*(\xi_0, J_0 = 1) \xrightarrow{h\nu} Ar^+(\xi_f, J_f = \tfrac{1}{2} \text{or} \tfrac{3}{2}) + e^-(\ell, j) \qquad (1)$$

where J_0 and J_f are the total angular momentum quantum numbers of Ar* and Ar^+, respectively, ξ_0 and ξ_f are the sets of quantum numbers other than J_0 and J_f, respectively, is the orbital angular momentum quantum number of the photoelectron e^-, and j is the total angular momentum quantum number of e^-. The total angular momentum quantum number J of the final state, which is given by a relation of $\vec{J} = \vec{J}_f + \vec{j}$, is restricted to 0, 1, and 2 from selection rules of the electric dipole transition. We have measured a two-dimensional spectrum as shown in Figure 1. Major spots are found to form two straight lines with a slope of unity which are attirbuted to two final ionic states of Ar^+ ($^2P_{1/2}$, $^2P_{3/2}$). Rotating the direction of the electric vector of the laser allows us to measure the angular distribution of energy-analyzed photoelectrons from a particular Ar* state. It is possible in some cases that we can estimate the dipole transition moments involving partial waves of photoelectrons designated by a combination of three angular momenta , j and J.

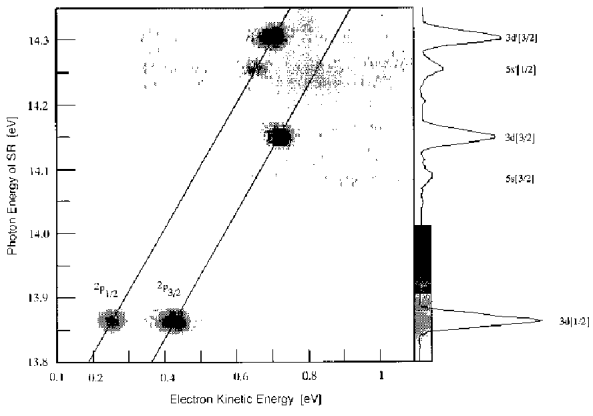

Figure 1. Laser-ionization two-dimensional photoelectron spectrum of polarized Ar atoms prepared by excitation with synchrotron radiation.

VI-I-2 Laser Photoionization Electron Spectroscopy of Polarized Kr Atoms Excited with Synchrotron Radiation

Kota IWASAKI, Yasumasa HIKOSAKA *(Inst. Mater. Struct. Sci.)* **and Koichiro MITSUKE**

Laser photoionization spectroscopy of polarized Kr atoms have been carried out to study spin-orbit interactions of a many-electron system. Krypton atoms are excited to Rydberg states with synchrotron radiation (λ = 900-950 nm) and aligned along the electric vector of the light. The beam of a Nd:YAG laser (λ = 532 nm) intersects the synchrotron radiation beam at 90° in a gas cell and ionizes the polarized Kr atoms. Photoelectrons emitted in the perpendicular direction to both the synchrotron radiation and laser beams are detected by using 160° spherical electrostatic energy analyzer.

We have measured a two-dimensional spectrum as shown in Figure 1. Major spots are found to form two straight lines with a slope of unity which are attirbuted to two final ionic states of $Kr^+(^2P_{1/2}, ^2P_{3/2})$. Since every Rydberg state is properly described by a J_c- coupling scheme, its ion core is assumed to release an excited electron without changing J_c on laser ionization. Here, the total angular momentum quantum number J_c of the ion core takes a value of either 1/2 or 3/2. We can therefore expect the conservation of the total angular momentum between J_f of the final Kr^+ state and J_c of the Rydberg state. However, several spectral features in Figure 1 appear to show a reverse trend. For example, the intensity of $Kr^+(^2P_{1/2})$ from the 5*d*[1/2] Rydberg state is higher than that of $Kr^+(^2P_{3/2})$, though Jc of this Rydberg state is 3/2. There are two possible interpretations for this observation: mixing of J_c = 1/2 and 3/2 components in the initial Rydberg state, or angular momentum exchange between the ejected electron and the ion core during photoionization.

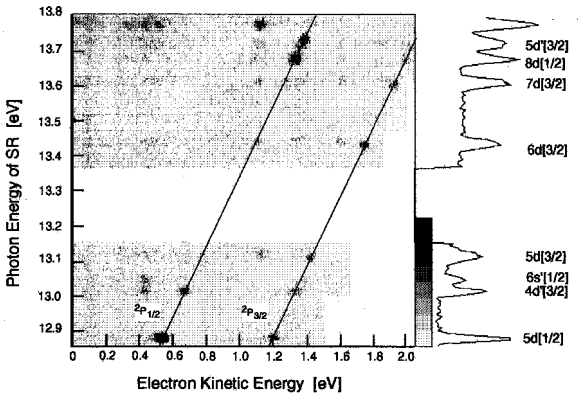

Figure 1. Laser-ionization two-dimensional photoelectron spectrum of polarized Kr atoms prepared by excitation with synchrotron radiation.

VI-J Vacuum UV Spectroscopy Making Use of a Combination of Synchrotron Radiation and a Mode-Locked or Pulsed UV Laser

An ultraviolet laser system has been developed which synchronizes precisely with the undulator radiation from the storage ring of the UVSOR facility. A mode-locked Ti:sapphire laser is made to oscillate at the frequency of the ring in a multibunch operation mode. The delay timing between undulator and laser pulses can be changed from 0 to 11 ns. The following two synchrotron radiation-laser combination studies have been performed. (1) Two-photon ionization of helium atoms studied as the prototype of the time-resolved experiment, and (2) fluorescence excitation spectroscopy of $N_2^+(X\ ^2\Sigma_g^+)$ ions produced by synchrotron radiation photoionization of N_2 or N_2O. On the other hand, we have developed another system, a pulsed dye laser pumped by an excimer laser, for synchrotron radiation-laser combination experiments. The second harmonic of the dye laser is tunable at 265-280 nm with a pulse energy of ca. 2 mJ pulse^{-1} at a repetition rate of 10-100 Hz. This laser system is mainly devoted to observing neutral species produced by neutral or ionic photofragmentation induced by synchrotron radiation excitation of molecules. This year, $S(3s^23p^4\ ^3P_{J''}, J'' = 0, 2)$ from Rydberg states of OCS is detected by resonance enhanced multiphoton ionization (REMPI) spectroscopy.

VI-J-1 Pump-Probe Spectroscopy of N_2 and N_2O by Using a Laser-Synchrotron Radiation Combination Technique

Koichiro MITSUKE, Masakazu MIZUTANI, Hiromichi NIIKURA *(Grad. Univ. Adv. Stud.)* **and Kota IWASAKI**

[*Rev. Laser Engin.* **26**, 458 (1998)]

Gas-phase N_2 or N_2O is photoionized with the fundamental light of an undulator radiation into $N_2^+(X\ ^2\Sigma_g^+, v'' = 0)$ which is then probed by laser induced fluorescence excitation spectroscopy in the laser wavelength region of the $(B\ ^2\Sigma_u^+, v' = 0) \leftarrow (X\ ^2\Sigma_g^+, v'' = 0)$ transition at 389-392 nm. The fluorescence excitation spectra of N_2^+ exhibit two maxima due to the *P* and *R* branches in which rotational lines are heavily overlapped. By fixing the laser wavelength at the maximum position of the *P* branch, partial cross sections for production of $N_2^+(X\ ^2\Sigma_g^+, v'' = 0)$ are measured as a function of the undulator photon energy. The cross section curve for N_2^+ from N_2 shows peaks originating from transitions to autoionizing Rydberg states converging to $N_2^+(A\ ^2\Pi_u, v = 0 \text{ or } 1)$. In the case of N_2O, several Rydberg states converging to $N_2O^+(C\ ^2\Sigma^+, v_1 = v_2 = v_3 = 0)$ are discernible in the cross section curve for N_2^+, as shown in Figure 1. It is likely that these Rydberg states autoionize into $N_2O^+(B\ ^2\Pi)$ which is subsequently predissociated by a repulsive

state correlating with $N_2^+(X\ ^2\sum g^+, v'' = 0) + O$.

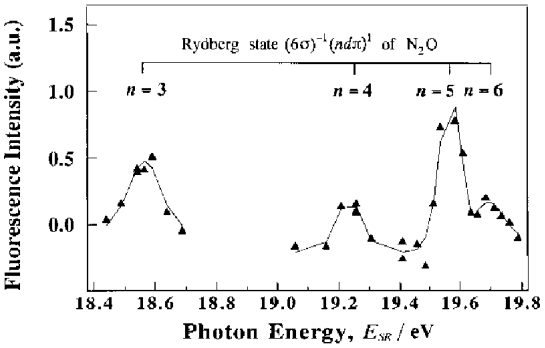

Figure 1. Photodissociation cross section curve of $N_2^+(X\ ^2\sum g^+, v'' = 0)$ obtained by plotting the laser induced fluorescence count rate of N_2^+ produced from N_2O as a function of the undulator photon energy.

VI-J-2 Apparatus for Resonance Enhanced Multiphoton Ionization Spectroscopy of Neutral Fragments Produced by VUV Photoexcitation

Masakazu MIZUTANI, Hiromichi NIIKURA *(Grad. Univ. Adv. Stud.)***, Kota IWASAKI and Koichiro MITSUKE**

We have developed pump-probe spectroscopy making use of the combination of UV laser and synchrotron radiation to investigate neutral dissociation of molecular superexcited states. Superexcited molecules are produced by excitation with monochromatized synchrotron radiation and neutral fragments resulting from predissociation are observed by means of (2+1)-resonance enhanced multiphoton ionization (REMPI) spectroscopy.

Undulator radiation emitted from beamline BL3A2 of UVSOR is crossed perpendicularly with a molecular beam discharged from a pulsed nozzle. Produced ions are extracted toward electrode 1 by a retarding field between electrodes 1 and 2. A part of neutral fragments produced by VUV excitation are sampled through an aperture of electrode 2 and ionized by a frequency-doubled dye laser (1-2 mJ pulse^{-1}) focused with an f = 500 mm lens on the space between electrodes 2 and 3. Ions produced by (2+1)-REMPI of the neutral fragments are detected with a quadrupole mass filter equipped with a channeltron electron multiplier.

The most serious problem in this REMPI experiment is that the real signal is smeared out by the background ion counts which originate from undulator radiation alone. In the case of detection of $S(3s^23p^4\ ^3P_2)$ from superexcited OCS molecules, the background count rate of S^+ is not less than 0.07 cps. These ions may be produced by electron impact ionization of residual gas of OCS near the aperture of electrode 2, since a number of electrons produced by VUV photoionization are accelerated to electrode 2. In order to suppress the background, we are planning to replace the ion lens system.

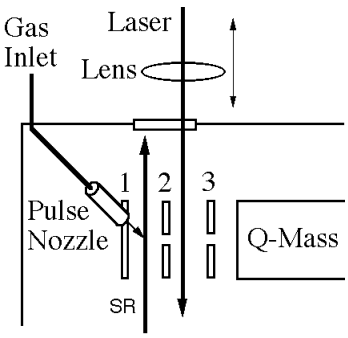

Figure 1. Schematic experimental setup for REMPI spectroscopy of neutral fragments produced by synchrotron radiation excitation.

VI-J-3 Laser Spectroscopy of Neutral Fragments from Superexcited States Prepared by Synchrotron-Radiation Photoexcitation

Hiromichi NIIKURA *(Grad. Univ. Adv. Stud.)***, Masakazu MIZUTANI, Kota IWASAKI and Koichiro MITSUKE**

We have measured a REMPI spectrum of $S(3s^23p^4\ ^3P_{J''}, J'' = 0, 2)$ dissociated from superexcited states of OCS prepared by photoexcitation with undulator radiation (BL3A2, UVSOR) in the range of 13-17 eV. The spectral resolution of the second harmonic of a probe laser was 0.015 nm. Figure 1 shows a REMPI spectrum of $S(3s^23p^4\ ^3P_2)$ as a function of the probe laser wavelength in the region involving the two-photon transitions, $S(3s^23p^35p\ ^3P_{J'}) \leftarrow S(3s^23p^4\ ^3P_2)$. The undulator photon energy was fixed at 16.5 eV. The maximum at 269.290 nm is considered to comprise two peaks resulting from transitions from $S(3s^23p^4\ ^3P_2)$ to $S(3s^23p^35p\ ^3P_1)$ and to $S(3s^23p^35p\ ^3P_2)$, though they are not separated because of a low signal-to-background ratio. As well as $S(3s^23p^4\ ^3P_2)$, we have been able to detect the REMPI signal of $S(3s^23p^4\ ^3P_0)$ at 271.375 nm where the two-photon transition from $S(3s^23p^4\ ^3P_0)$ to $S(3s^23p^35p\ ^3P_0)$ is allowed. Next, we fixed the laser wavelength at the maximum of Figure 1, *i.e.*, 269.290 nm, and measured the REMPI signal intensity as a function of the energy of the undulator radiation in the range of 13-17 eV. The resultant spectrum is considered to represent a relative photodissociation cross section curve for the formation of $S(3s^23p^4\ ^3P_2)$ from OCS. Band features existing at 13-16 and 16-17eV are ascribed to the Rydberg series converging to the $B\ ^2\sum^+$ and $C\ ^2\sum^+$ states, respectively, of OCS^+. In summary, we can obtain direct evidence for the first time for the formation of nonfluorescing and non-autoionizing neutral species dissociated from molecular superexcited states, by means of pump-probe spectroscopy combining synchrotron radiation and laser.

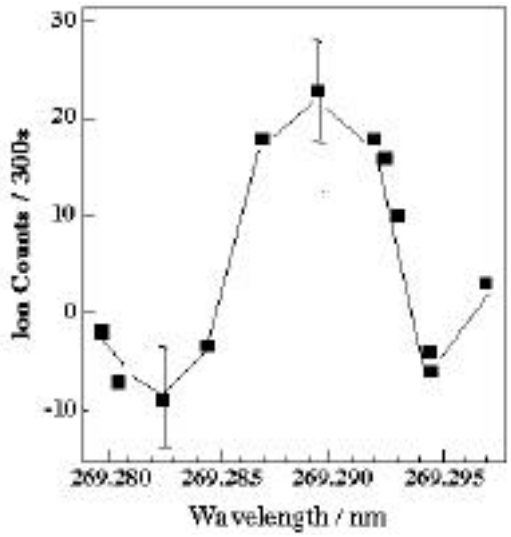

Figure 1. Laser REMPI spectrum of S($3s^2 3p^4\ ^3P_2$) produced by photoexcitation at the undulator photon energy of 16.5 eV.

VI-K Monochromator Newly Developed on Beamline BL2B2 in UVSOR

A grazing incidence monochromator has been constructed which supplies photons in the energy region from 20 to 200eV. This monochromator will bridge the energy gap between beamlines BL3A2 and BL8B1, thus providing for an accelerating demand for the high-resolution and high-flux photon beam from the research field of photoexcitation of inner-valence electrons or *L*-shell electrons in the third-row atom. A resolving power ($E/\Delta E$) of 5000 and photon flux of more than 10^{10} photons s^{-1} are expected at a 100 mA ring current.

VI-K-1 Design of an 18 m Spherical Grating Monochromator at UVSOR

Hideo HATTORI, Hiroaki YOSHIDA *(Hiroshima Univ.)* **and Koichiro MITSUKE**

An 18m spherical grating monochromator (SGM) has been constructed on the bending-magnet beamline BL2B2 of the UVSOR facility. Figure 1 shows the outline of the monochromator which consists of chambers for a prefocusing mirror (M1), an entrance slit (S1), gratings, an exit slit (S2), and a refocusing mirror (M4). Three gratings (G1-G3) and two mirrors (M2, M3) are accommodated in the grating chamber. The energy range of 20 - 200 eV is covered by exchanging G1-G3. When G3 is chosen, M2 and M3 are made to act as optical filters to reduce the second and higher-order lights. A computer controls mechanical motion for the wavelength scanning, *i.e.* rotation of the gratings and translation of the exit slit. From a preliminary optical adjustment, the zero-order light is found to be focused into a 1 × 1 mm^2 square spot at the focusing point. We are planning to connect a differential pump (XIA, DP-03.1) with the refocusing mirror chamber. In spite of a relatively short pump length we may attain a pressure difference of six orders of magnitude between this chamber and an experimental station, since this pump has the line of sight passing through the active pumping region of a Penning style ion pump.

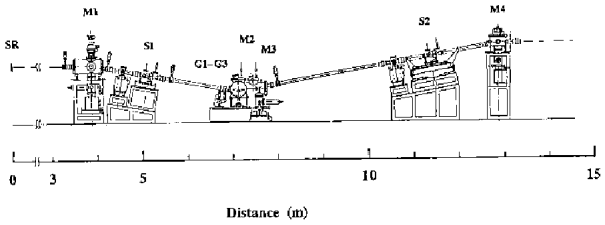

Figure 1. Schematic side view of the 18 m spherical grating monochromator at beamline BL2B2. SR, synchrotron radiation source; M_1, spherical mirror; S1, entrance slit; G1-G3, spherical gratings; M2 and M3, plane mirrors; S2, exit slit; M4, toroidal mirror.

VI-L Ultraviolet Photoelectron Spectroscopy on Organic Thin Films Using Synchrotron Radiation

The electronic structure and molecular orientation of organic thin films were investigated by angle-resolved UPS with synchrotron radiation. Furthermore corresponding spectroscopies, such as low-energy electron transmission, electron energy loss spectroscopy and Penning ionization electronspectroscopy, were used in investigating the electronic states of the thin films. The radiation inducedreaction at the surface of organic films were also studied by UPS and ion time-of-flight spectroscopy.

VI-L-1 Angle-Resolved UV Photoelectron Spectra (UPS) of Thin Films of Perylene-3,4,9, 10-Tetracarboxylic Dianhydride on MoS_2

Yasushi AZUMA *(Chiba Univ.)*, **Takehiko HASEBE** *(Chiba Univ.)*, **Takayuki MIYAMAE, Koji K. OKUDAIRA** *(Chiba Univ.)*, **Yoshiya HARADA** *(Chiba Univ.)*, **Kazuhiko SEKI** *(Nagoya Univ.)*, **Eizi MORIKAWA** *(Louisiana State Univ.)*, **Volker SAILE** *(Louisiana State Univ.)* **and Nobuo UENO**

[*J. Synchrotron Rad.* **5**, 1044 (l998)]

Angle resolved UV photoelectron spectra (ARUPS) were measured for thin films of perylene-3,4,9,10-tetracarboxylic dianhydride (PTCDA) deposited on cleaved MoS_2 Surfaces. The take-off angle (θ) dependence of the photoelectron intensity of the highest π band showed a sharp maximum at θ = 32-34°. A spectral feature of the binding energy at ~ 8.9 eV, which is believed to originate from a π State, showed a remarkably different dependence from that of the π band. A quantitative analysis of the observed θ dependencies clearly indicates that (a) the feature at ~ 8.9 eV originates from the oxygen 2p nonbondipg states and (b) the molecules lie flat on the substrate surface.

VI-L-2 Temperature Dependence of Photo-electron Angular Distribution from Thin Films of Chloroaluminum Phthalocyanine on MoS_2

Yasushi AZUMA *(Chiba Univ.)*, **Masahiko TSUTSUI** *(Chiba Univ.)*, **Satoshi KERA** *(Chiba Univ.)*, **Masaru AOKI** *(Univ. Tokyo)*, **Takayuki MIYAMAE, Koji K. OKUDAIRA** *(Chiba Univ.)*, **Yoshiya HARADA** *(Chiba Univ.)* **and Nobuo UENO**

[*J. Synchrotron Rad.* **5**, 1047 (1998)]

Angle-resolved UV photoelectron spectra were measured for thin films of chloroaluminum phthalocyanine deposited on cleaved MoS_2 Surfaces. The take-off angle (θ) dependence of the photoelectron intensity of the highest π band showed a remarkable sharpening upon cooling the film, indicating that thermal excitation of molecular vibrations gives a considerable broadening of the photoelectron angular distribution. The π dependence observed at ~ 120 K agrees well with that calculated.

VI-L-3 Photoemission Study of Pristine and Photodegraded Poly(Methyl Methacrylate)

Koji K. OKUDAIRA *(Chiba Univ.)*, **Shinji HASEGAWA, Phillip T. SPRUNGER** *(Louisiana State Univ.)*, **Eizi MORIKAWA** *(Louisiana State Univ.)*, **and Volker SAILE** *(Louisiana State Univ.)*

[*J. Appl. Phys.* **83**, 4292 (1998)]

Degradation of poly(methyl methacrylate) (PMMA) thin films by vacuum ultraviolet (VUV) monochromatic synchrotron radiation was investigated by ultraviolet photoelectron spectroscopy. The photodegradation reaction was analyzed, for the first time, by different spectrometry techniques and ab initio molecular orbital calculations. It is concluded that the main degradation mechanism in PMMA by VUV photons is ascribed to the disappearance of ester groups and formation of double bonds in the polymer chain. The hal product of the degradation seems to possess a relatively dch conjugation of unsaturated bonds. The rate constant of the degradation by VUV photons is evaluated to be 2.4×10^{-17} photons^{-1} cm^2.

VI-L-4 Site-Specific Chemical-Bond Scission in Poly(Methyl Methacrylate) by Inner Shell Excitation

Nobuo UENO and Kenichiro TANAKA *(Hiroshima Univ.)*

[*Jpn. J. App1. Phys.* **36**, 7605 (1997)]

The results of photon-stimulated ion desorption (PSID) from thin solid films of poly(methyl methacrylate) (PMMA) and corresponding polymers, poly(methyl acrylate) (PMA) and poly(methacrylic acid) (PMAA), owing to inner-shell excitation, are briefly reviewed. The results show that an enhancement of PSID takes place effectively upon electron excitation to a particular antibonding molecular orbital, indicating that the excitation to the antibonding state plays a major role in PSID enhancement. As a typical example, CH_3^+ desorption via oxygen 1s electron excitation was shown as a function of photon energy. By comparison of the photon energy dependences of PSID yields of CH_3^+ from the three polymers, it was found that the excitation of oxygen ls electron at OCH_3 to the cr* state localized at $COCH_3$ in PMMA results in the enhanced emission of CH_3^+ by bond scission at the side chain (0-CH_3), not at the main chain. The results indicate that there is a strong correlation between the sites of excitation and the following chemical-bond rupture. It is pointed out that monochromatic synchrotron radiation can be used as a "scalpel" to cut a chemical bond selectively in a molecular solid.

VI-L-5 Study of Solid Surfaces by Metastable Electron Emission Microscopy: Energy-Filtered Images and Local Electron Spectra at the Outermost Surface Layer of Silicon Oxide on Si(100)

Susumu YAMAMOTO *(Univ. Tokyo)*, **Shigeru MASUDA** *(Univ. Tokyo)*, **Hideyuki YASUFUKU** *(Chiba Univ.)*, **Nobuo UENO, Yoshiya HARADA** *(Chiba Univ.)*, **Takeo ICHINOKAWA** *(Waseda Univ.)*, **Makoto KATO** *(JEOL)* **and Yuji SAKAI** *(JEOL)*

We have observed images and local electron spectra of an oxide pattern on Si(100) using metastable electron emission microscopy (MEEM) recently developed at our laboratory. Low-energy electron microscopy (LEEM) was also used. For both MEEM and LEEM, the energy-filtered images were obtained for the first time. It was shown that MEEM gives the

information on the outermost surface layer selectively, while LEEM provides averaged information on several surface layers. The intensity of the band in the local electron spectrum of MEEM can be related to the distribution of the relevant orbitals exposed outside the surface, with which metastable atoms interact effectively. Thus, using energy-filtered MEEM, we can observe the map reflecting the distribution of individual orbltals at the outermost surface layer.

VI-L-6 Low-Energy Electron Transmission Spectroscopy of Thin Films of Chloroaluminum Phthalocyanine on MoS_2

Nobuo UENO, Yasushi AZUMA *(Chiba Univ.)*, **Takayuki YOKOTA** *(Chiba Univ.)*, **Masaru AOKI** *(Univ. Tokyo)*, **Koji K. OKUDAIRA** *(Chiba Univ.)* **and Yoshiya HARADA** *(Chiba Univ.)*

[*Jpn. J. Appl. Phys.* **36**, 5731 (1997)]

The growth of chloroaluminum phthalocyanine (CIAIPc) thin films on MoS_2 Surfaces was studied by low-energy electron transmission (LEET) spectroscopy. We observed that the as-grown monolayer, prepared by vacuum deposition, consists of islands of CIAIPc multilayers and the molecules spread over the substrate surface to form a uniform monolayer by heat treatment. Furthermore, we found that for heat-treated films the vacuum level of the sample system oscillates with increasing the film thickness from 0 to 2 monolayers. For the monolayer, the change of the vacuum level with respect to the substrate $\Delta\varphi$ ($= \varphi_{film} - \varphi_{substrate}$) was positive, while for the doublelayer it was negative. These results indicate that in the monolayer the molecules lie flat with the Cl atoms protruding outside the film to form an electric dipole layer directing to the substrate and in the doublelayer the molecules in the outer layer are turned over with the Cl atoms protruding inside the film to compensate the dipole originating from the first monolayer. Furthermore the thickness independent characteristics of LEET spectra above the doublelayer suggest that thicker films consist of a stack of a double layer-like structures.

VI-L-7 Photon Stimulated Ion Desorption of Deuterated Polystyrene Thin Films Induced by Core Excitation

Kentaro FUJII *(Hiroshima Univ.)*, **Tetsuji SEKITANI** *(Hiroshima Univ.)*, **Kenichiro TANAKA** *(Hiroshima Univ.)*, **Shuuhei YAMAMOTO** *(Chiba Univ.)*, **Koji K. OKUDAIRA** *(Chiba Univ.)*, **Yoshiya HARADA** *(Chiba Univ.)* **and Nobuo UENO**

[*J. Electron Spectr. & Related Phenom.* **88-91**, 837 (1998)]

Photon stimulated ion desorption (PSID) of thin films of selectively deuterated polystyrene ($[\text{-}CD_2\text{-}CD(C_6H_5)\text{-}]_n$, $[\text{-}CH_2\text{-}CH(C_6D_5)\text{-}]_n$ and $[\text{-}CD_2\text{-}CD(C_6D_5)\text{-}]_n$) have been investigated to reveal the mechanism of surface photochemical reactions following core excitation. Desorbing ions were measured using the time-of-flight mass spectrometer (TOF-MS) combined with a pulsed synchrotron radiation. From the total electron yield spectrum and partial ion yield spectrum of each sample, it is concluded that D^+ ions are mainly desorbed from the phenyl group and the yield of D^+ is enhanced at the C-D* resonance. From the ion kinetic energy distribution obtained from analysis of the TOF spectrum, the ions desorbed from the phenyl group have different kinetic energy distribution. The results are discussed in connection with the mechanism of PSID.

VI-L-8 Characterization of Self-Assembled Monolayer of Thiophenol on Gold by Penning Ionization Electron Spectroscopy

Abuduaini ABDUREYIM *(Chiba Univ.)*, **Satoshi KERA** *(Chiba Univ.)*, **Masaru AOKI** *(Univ. Tokyo.)*, **Koji K. OKUDAIRA** *(Chiba Univ.)*, **Nobuo UENO and Yoshiya HARADA** *(Chiba Univ.)*

[*J. Electron Spectr. & Related Phenom.* **88-91**, 849 (1998)]

The molecular orientation in self-assembled monolayers (SAMs) of thiophenol chemisorbed on polycrystalline gold from aqueous solutions has been investigated by Penning ionization electron spectroscopy (PIES) and ultraviolet photoelectron spectroscopy (UPS). The analysis of the relative band intensity of the Penning spectrum indicates that the phenyl ring in phenyl thiolate stands perpendicular to the substrate plane at room temperature. Upon heating the phenyl ring becomes tilted in the layer.

VI-L-9 High-Resolution Electron Energy Loss Spectroscopy of Chloroalminum Phthalo-cyanine Ultrathin Films

Yasushi AZUMA *(Chiba Univ.)*, **Takayuki YOKOTA** *(Chiba Univ.)*, **Satoshi KERA** *(Chiba Univ.)*, **Masaru AOKI** *(Univ. Tokyo)*, **Koji K. OKUDAIRA** *(Chiba Univ.)*, **Yoshiya HARADA** *(Chiba Univ.)* **and Nobuo UENO**

[*J. Electron Spectr. & Related Phenom.* **88-91**, 881 (1998)]

High-resolution electron energy loss spectra (HREELS) were measured for ultrathin films of chloroaluminum phthalo-cyanine (CIAIPc) deposited on a cleaved HOPG surface in order to investigate the molecular orientation and its thickness dependence. It was found that for the monolayer film CIAIPc molecules lie flat on the HOPG surface without heat treatment. With increase in the film thickness, the molecules become oriented at a tilt. The result show a marked difference from the orientation of CIAIPc molecules on MoS_2, where the molecules lie tilt on MoS_2 in the as-grown monolayer.

VI-L-10 Angle-Resolved UPS Study and Simulation with IAC Approximation for Oriented Monolayer of Tetratetracontane (*n*-$C_{44}H_{90}$) on Cu (100)

Daisuke YOSHIMURA *(Nagoya Univ.)*, **Hisao ISHII** *(Nagoya Univ.)*, **Yuhiko OUCHI (Nagoya Univ.), Eisuke ITO** *(Nagoya Univ.)*, **Takayuki MIYAMAE Shinji HASEGAWA, Nobuo UENO and Kazuhiko SEKI** *(Nagoya Univ.)*

[*J. Electron Spectr. & Related Phenom.* **88-91**, 875 (1998)]

The electronic structure and orientation of tetratetracontane (n-$C_{44}H_{90}$, TTC) monolayer film on Cu(100) were studied by angle-resolved UPS (ARUPS). We observed a 2×1 LEED pattern at room temperature. This indicates that the TTC molecule lies on the Cu(100) surface with its chain axis parallel to the Cu(110) direction. The application of the dipole selection rules to normal emission spectrum revealed that the C-C-C plane of TTC is parallel to the surface (flat-on orientation). We also examined the dependence of the photoemission spectra on the take off angle. The simulated spectra for flat-on orientation based on independent atomic center (IAC) approximation combined with *ab initio* MO calculations are in good agreement with the observed spectra. These results verify the deduced molecular orientation and demonstrate the reliability of theoretical simulation with IAC approximation.

VI-M Formation of Nanometer-Scale InAs Island on GaP (001) Substrate

For three-dimensional confinement of electrons and holes, new physical phenomena and improvement of optoelectronic devices, such as extremely sharp emission line, phonon relaxation bottleneck, and temperature independent threshold current density for lazing, have been predicted. InAs quantum dots on GaP are very attractive since the band-offset in the conduction band is expected to be as large as 1 eV. Furthermore, there is a large mismatch of 11% in lattice constants between InAs and GaP, which modifies their energy band structures.

VI-M-1 Nanometer-Scale InAs Islands Grown on GaP (001) by Organometallic Vapor Phase Epitaxy

Youichi NONOGAKI, Tadashi IGUCHI *(Nagoya Univ.)*, **Shingo FUCHI** *(Nagoya Univ.)*, **Yasufumi FUJIWARA** *(Nagoya Univ.)*, **Yoshikazu TAKEDA** *(Nagoya Univ.)*

[*Appl. Surf. Sci.* **130-132**, 724 (1998)]

We have successfully grown nanometer-scale InAs islands on GaP (001) by low-pressure organometallic vapor phase epitaxy (LP-OMVPE). Effects of substrate temperature and InAs deposition rate on the shape, size and areal density of InAs islands were investigated by *ex-situ* atomic force microscope (AFM) and high-energy electron diffraction (HEED). The AFM observations showed that the island size decreased with the substrate temperature while the areal density increased, indicating that migration play a role on island formation. The HEED patterns provided significant result that the island grown at high temperature (650°C) consisted of a few grains, while the island grown at low temperatures (550 and 500°C) was single crystalline.

VI-M-2 Effects of Post Annealing on Self-organized InAs Islands Grown on (001) GaP by Organometallic Vapor Phase Epitaxy

Shingo FUCHI *(Nagoya Univ.)*, **Youichi NONOGAKI, Tadashi IGUCHI** *(Nagoya Univ.)*, **Hiromitsu MORIYA** *(Nagoya Univ.)*, **Yasufumi FUJIWARA** *(Nagoya Univ.)*, **Yoshikazu TAKEDA** *(Nagoya Univ.)*

[*J. Surf. Analysis* **4**, 259 (1998)]

Using atomic force microscopy (AFM) and transmission electron microscopy (TEM), we have investigated effects of post annealing on self-organized InAs islands grown on (001) GaP by low-pressure organometallic vapor phase epitaxy (LP-OMVPE). The morphology of InAs islands without the cap layer depended strongly on the growth temperature, which was related to migration of InAs adsorbed on GaP. Subjected to the annealing at temperatures higher than the growth temperature, the small islands coalesced each other to form larger islands. The resultant morphology was quite similar to that of the samples grown at the annealing temperature. Cross-sectional TEM observation was carried out on the buried InAs islands. Almost relaxed InAs islands buried by the GaP cap layer with stacking faults were clearly observed. The size and density of the buried InAs islands were similar to those in the samples post-annealed at the growth temperature of the GaP cap layer, suggesting that the change on the InAs islands was induced during the increase in the substrate temperature for the GaP cap-layer growth. These results indicated that the growth temperature for the GaP cap layer played an important role in fabricating the sandwich structures with frozen small InAs islands.

VI-N Desorption Induced by Electronic Transitions (DIET) from Cryogenic Surfaces

Desorption processes of particles from cryogenic surfaces are studied using synchrotron radiation in soft X-ray and vacuum ultraviolet region. As a result of decay processes after an electronic excitation of surface layers by synchrotron radiation, various kinds of particles are released from the surface. For example, solid rare gases have particular excitation channels for the desorption of electronically excited neutral particles that are pronounced at the creation energy region of exciton. Experiments are performed at BL2B1 and BL5B of UVSOR. At BL5B the energy range is mainly on valence exciton region, and excited neutral particles and photons emitted during the desorption process are measured. On the other hand, SR in core excitation region is used at BL2B1, and desorbed ions are measured in a coincidence with Auger electron from molecules which produce fragment ions.

VI-N-1 Absolute Desorption Yield of Metastable Atoms from the Surface of Solid Rare Gases Induced by Exiton Creation

Takato HIRAYAMA *(Gakushuin Univ.)*, **Akira HAYAMA** *(Gakushuin Univ.)*, **Toshihiro KOIKE** *(Gakushuin Univ.)*, **Takafumi KUNINOBU** *(Gakushuin Univ.)*, **Ichiro ARAKAWA** *(Gakushuin Univ.)*, **Koichiro MITSUKE, Makoto SAKURAI and E. V. SAVCHENKO** *(B. Verkin Inst. for Low Temp. Phys. and Eng.)*

[*Surface Sci.* **390**, 266 (1997)]

Absolute yields of the metastable excited atoms desorbed from the surfaces of solid Ne and Ar by the creation of surface and bulk excitons have been measured using monochromatized synchrotron radiation as a selective excitation source. We have obtained the absolute yields of $(2.3\pm0.7) \times 10^{-3}$, $(1.4\pm0.4) \times 10^{-3}$, and $(7.8\pm2.3) \times 10^{-4}$ (atoms/photon) at the excitation of S1, B1 and S' exciton for Ne, respectively, and 1×10^{-5} (atoms/photon) at S1 excitation for Ar. The probability for metastable atom desorption is found to be about 2 to 10% at the excitation of S1 exciton on the surface of solid Ne.

VI-N-2 Long Lifetime Emission of the Excited Species Ejected from the Surface of Solid Ne

E. V. SAVCHENKO *(B. Verkin Inst. for Low Temp. Phys.)*, **Takato HIRAYAMA** *(Gakushuin Univ.)*, **Akira HAYAMA** *(Gakushuin Univ.)*, **Toshihiro KOIKE** *(Gakushuin Univ.)*, **Takafumi KUNINOBU** *(Gakushuin Univ.)*, **Ichiro ARAKAWA** *(Gakushuin Univ.)*, **Koichiro MITSUKE and Makoto SAKURAI**

[*Surface Sci.* **390**, 261 (1997)]

Desorption of long-lived neutral particles from solid Ne is studied using selective photoexcitation and time of flight (TOF) technique. The luminescence due to direct light from the sample surface is blocked by rotating the sample. Two new prominent features are revealed in the TOF spectra measured at a special geometry: a prominent long tail and a maximum at the delay time of ~ 0.5 ms. From the analysis of the excitation spectra recorded by the time window technique and the TOF spectra at selective excitation it is assumed that the new features are closely related to Ne_2* excimer desorption. Analysis of probable mechanisms of the long lifetime emission is presented.

VI-O Structure and Vibrational Spectra of Molecules Physisorbed on Metal Surfaces

Molecular layers physisorbed on metal surfaces at low temperature show specific structures which depend on the interaction between molecules and substrate, and vibrational spectra for physisorbed molecules reveal the details of the interaction. We use dynamical analysis of low-energy electron diffraction (LEED) to investigate the structure of adsorbed layers, and high-resolution electron energy loss spectroscopy has been utilized for vibrational spectroscopy for adsorbed molecules. As a complemental method for vibrational spectroscopy of surfaces, infrared reflection absorption spectroscopy will be combined with our experimental system. A new cryogenic sample holder for surface vibrational spectroscopy is also under development in order to provide a substrate at less than 4.2K.

VI-O-1 Upgraded Infrared Beamline BL6A1 at UVSOR

Makoto SAKURAI, Hidekazu OKAMURA *(Kobe Univ.)*, **Katsumi WATANABE** *(Kobe Univ.)*, **Takao NANBA** *(Kobe Univ.)*, **Shin-ichi KIMURA and Masao KAMADA**

[*J. Synchrotron Rad.* **5**, 578 (1998)]

BL6A1, a far-infrared (FIR) beamline at UVSOR originally built in 1986, has been upgraded recently. The upgrade included the introduction of a second FT-IR spectrometer, and now it is possible to cover the entire FIR-IR range (3 cm^{-1} to 10000 cm^{-1}) in one sequence of measurements, without having to open the sample chamber; the beamline has become a more convenient and powerful experimental station than before. The upgrade is also expected to enable such experiments as IR studies of molecules adsorbed on the solid surfaces, and time-resolved IR spectroscopies.

VI-O-2 Development of High Sensitivity EELS

Makoto SAKURAI

Electron energy loss spectroscopy (EELS) is a powerful tool for the structural analysis of molecules adsorbed on a solid surface. However, since ordinary EELS system uses a single channel electron analyzer, the measurement time for one spectrum usually amount to several minutes. This has been a disadvantage of EELS for real time analysis of surface reaction. We develop a new electron analyzer for EELS. The analyzer is a simulated hemispherical analyzer with a position sensitive detector. The components are made of aluminum (YH75), and mean radius of the deflector is 104 mm. The detector has CR chain type anode, and the signal is stored to a histogramming memory via posision analyzer. The spectrum can be measured as frequent as every 100 μs. This feature make it possible to perform a time resolved measurement of repetitive reaction processes.

VI-O-3 Electronic Structure of a Pt(111)-Ge Surface Alloy and Adsorbed CO

Katsuyuki FUKUTANI *(IIS Univ. Tokyo)*, **Tamerlan MAGKOEV** *(IIS Univ. Tokyo)*, **Yoshimasa MURATA** *(Univ. Electro-Communications)*, **Masuaki MATSUMOTO, Taizou KAWAUCHI** *(IIS Univ. Tokyo)*, **Tamotsu MAGOME** *(IIS Univ. Tokyo)*, **Yasuhisa TEZUKA** *(ISSP Univ. Tokyo)*, **Shik SHIN** *(ISSP Univ. Tokyo)*

[*J. Electron Spectrosc. Relat. Phenom.* **88-91**, 597 (1998)]

Angle-integrated photoemission spectra are observed for Pt(111) and a Pt(111)-Ge surface alloy. The spectra for Pt(111)-Ge show d-band filling compared with those for Pt(111). Although the chemisorption energy of CO is noticeably reduced by alloy formation, the binding energies of the occupied levels for adsorbed CO are almost the same as those on pure Pt(111). The results are discussed by the d band filling due to s-d hybridization of Ge s electrons and the Pt d band and by two-level hybridization of the 5 σ and 2 π states with the modified d band.

VI-O-4 LEED and STM Measurement of NO /Pt(111) at Low Temperature

Masuaki MATSUMOTO, Toshiyuki YAMADA *(Tsukuba Univ., CREST)*, **Natsuo TATSUMI** *(IIS Univ. Tokyo)*, **Tadashi ITOYAMA** *(IIS Univ. Tokyo)*, **Kouji MIYAKE** *(Tsukuba Univ., CREST)*, **Kenji HATA** *(Tsukuba Univ., CREST)*, **Hidemi SHIGEKAWA** *(Tsukuba Univ., CREST)*, **Katsuyuki FUKUTANI** *(IIS Univ. Tokyo)* **and Tatsuo OKANO** *(IIS Univ. Tokyo)*

The chemisorption of nitric oxide on Pt(111) at low temperature has been studied by electron energy loss spectroscopy (EELS), infrared absorption spectroscopy (IRAS) and low energy electron diffraction (LEED). The vibrational spectroscopy showed that N-O stretching frequency is 1490 cm^{-1} at low coverage (< 0.5 L) and 1710 cm^{-1} at high coverage (> 0.5 L). At high coverage, 2×2 LEED pattern was observed and its structure was attributed to the fcc hollow site by LEED dynamic theory. But there is no reasonable account for the difference of the N-O stretching frequency between low and high coverage regions and the structure is controversial yet. We measured the LEED I-V curves and STM images of NO/Pt(111) surface at several temperature and coverage conditions. At 175K, diffuse 2×2 LEED pattern could be seen even at low dosage (0.05L) and the I-V curve was the same as that at high dosage (1L). This indicates that (2×2)-NO islands grow with coverage increase but the local structure does not change at this temperature region.

RESEARCH ACTIVITIES VII
Coordination Chemistry Laboratories

Prof. Masa-aki Haga, Prof. Takeshi Sakurai, Dr. Hideaki Monjushiro and Dr. Hidemi Nagao finished their term in March 1998 in the laboratory of Synthetic Coordination Chemistry. Prof. Haga moved to Chuou Univ. Prof. Sakurai, Dr Monjushiro and Dr. Nagao returned to Kanazawa Univ. and Osaka Univ. Their contribution to the coordination Chemistry Laboratory (CCL) during their term is highly acknowledged. Prof. Yuzou Nishida, Prof. Yasushi Tsuji, Dr. Tomohiro Ozawa and Dr. Hiroyuki Kawaguchi took the position of Synthetic Coordination Chemistry from April 1998. Prof. Yuzou Yoshikawa (Okayama Univ.) and Assoc. Prof. Hiroshi Nakazawa (Hiroshima Univ.) finished their term as Adjunct Prof. in March 1998 in the Laboratory of Coordination Bond. Their effort during their term is gratefully appreciated. Prof. Ginya Adachi (Osaka Univ.) and Assoc. Prof. Hiromi Tobita (Tohoku Univ.) continued their position as Adjunct Prof. of Laboratory of Coordination Bond. Prof. Hiromu Sakurai (Kyoto Pharmacy Univ.) and Assoc. Prof. Yuji Mizobe (Univ. Tokyo) took the position of the laboratory of Complex Catalysis.

VII-A Surface Coordination Chemistry towards Molecular Protonic Devices

The design and fabrication of molecular arrays or layers at the surface is one of the important and attractive area in the future material science. In order to control the molecular arrays in two dimensions, the incorporation with coordination bond has advantage compared to the other molecular interactions such as hydrogen bonding and electrostatic interaction from the viewpoint of strength of interaction and molecular geometry around metal ion. However, the incorporation with coordination bond at the interface has not extensively studied so far. Our aim is to construct a supramolecular assembly in the controlled manner through the coordination bond at the surface, and to search an electrochemical and photochemical function towards the molecular electronic devices. We have developed the chemical principle underlying the proton-induced switching in 2-(2-pyridyl)benzimidazole Ru complexes. In order to achieve the proton-induced switching systems, the interlocking between the potential change by protonation/deprotonation and the pKa change by Ru(II) to Ru(III) oxidation is responsible. The judicious molecular design of the Ru complexes containing benzimidazole ligands allows us to synthesize the novel supramolecular metal complexes with bistable property not only in solution but also at the surface. Our synthetic strategy is the following: (1) The intrinsic properties of molecular inorganic complex are thoroughly examined from the viewpoint of photoactive, electroactive, or proton-responsive building blocks for molecular devices. (2) The molecular inorganic complex modules are organized or integrated for building up the molecular assemblies. Particularly, "complexes-as-ligands" method is useful to synthesize the supramolecular systems.

VII-A-1 Proton-Coupled Electron Transfer Reaction of Self-Assembled Monolayer of Ruthenium(II) Complex Containing Tridentate 2,6-Bis(benzimidazol-2-yl)pyridine

Masa-aki HAGA, Hun-Gi HONG, Hideaki MONJUSHIRO, Yasushi KAWATA and Ryuichi ARAKAWA

[*Langmuir* submitted]

The self assembled monolayer(SAM) of novel bis-[Ru(bzimpyH_2)(bzimpy)]-substituted octyl disulfide(**1**) and mixed monolayers with octanethiol on a polycrystalline gold electrode were characterized by means of MALDI-TOF mass spectrometry, XPS, and cyclic voltammetry. The shape of cyclic voltammograms for Ru(II/III) couple is strongly dependent on the surface coverage, and is close to the ideal voltammogram for the monolayer species. The oxidation potential of the Ru monolayer shows a linear dependence on solution pH, which indicates that the proton-coupled oxidative reactions occurred on the gold surface. The pKa values of Ru(bzimpyH_2) group on the gold surface were determined from the analysis for the plot of the oxidation potential vs pH. The pKa values of SAM depend on the amounts of surface covarage because of the change of localized pH.

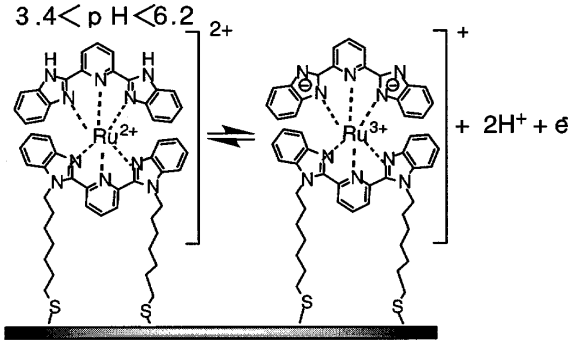

Scheme 1. Proton-coupled Redox Reaction of Ru Complex (**1**).

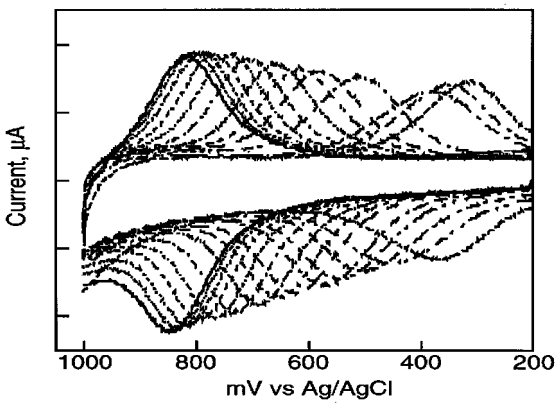

Figure 1. pH Dependence of cyclic voltammograms of the Ru complex modified on Au (From right to left, pH 1.33, 1.83, 2.21, 2.59, 3.10, 3.58, 4.09, 4.52, 4.86, 5.36, 5.83, 6.35, 6.88, and 7.35 respectively)

VII-A-2 Proton-Coupled Electron Transfer Reaction of Langmuir-Blodgett Monolayer of Ruthenium(II) Complex Containing Tridentate 2,6-Bis(benzimidazol-2-yl)pyridine

Masa-aki HAGA, Hun-Gi HONG, Hideaki MONJUSHIRO and Kezhi WANG

Proton translocation coupled to redox reaction is often seen in a biological membrane, and plays an important role for the energy transduction. In the present paper, we report the electrochemical pH response of Ru(II) complex Langmuir-Blodgett films on an indium-tin oxide(ITO) glass in order to simulate such a direction-controlled proton translocation. A novel amphiphilc Ru complex containing 2,6-bis(benzimidazolyl)pyridiene group in Scheme 1, [Ru(L18)(bimpyH_2)]$^{2+}$(**1**) (L18 = 2,6-bis(2'-(1'-octadecylbenzimidazolyl))pyridine; bimpyH_2 = 2,6-bis(2'-benzimidazolyl)pyridine), was synthesized. This Ru complex **1** acts as a diprotic acid (pK_{a1} ~ 5.35 and pK_{a2} ~ 6.94 in Triton micelle condition). Surface pressure-area (π-A) isotherms of this complex **1** are strongly dependent on the subphase pH (Figure 1). At the subphase pH = 2.89, a phase transition was observed at surface pressure at 20 mNm^{-1}. The molecular area obtained from the second condensed solid state is 1.3 nm^2 molecules^{-1}, which is almost coincided with that obtained at the subphase pH = 9.21. Proton equilibria at the air-water interface were also observed by *in situ* UV spectra. The vertical molecular orientation at the air-water interface was also proved from *in situ* UV spectra by the selection rule of metal-to-ligand charge transfer (MLCT) band around 500 nm. The Ru complex **1** was successfully transferred from the subphase onto the ITO glass with the transfer ratio of nearly 1 both at pH 2.89 and 9.21. The absorption maxima of MLCT band around 500 nm in the transferred LB films is shifted to a longer wavelength, accompanied by changing the subphase pH from 2.89 to 9.21. This trend is exactly consistent with the solution chemistry. The plot of absorbance vs the number of layers gave a linear line, which indicates a good measure of multilayer formation.

Cyclic voltammograms of Ru complex monolayer on an ITO electrode at different pH are shown in Figure 2. At pH 1.7, the peak-to-peak separation for the film transferred at 25 mNm^{-1} was 42 mV and the peak width at half-height was 140 mV. The transferred surface pressure affects the peak width at half-height: *i.e.*, lower pressure gave smaller peak width. Among the pH region of 1 < pH < 8, the oxidation potential is linearly shifted to a negative direction when the solution pH is increased. This indicates proton-coupled redox reaction occurred.

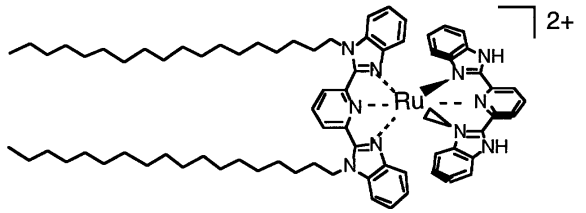

Scheme 1. Structure of [Ru(L18)(bimpyH_2)]$^{2+}$ (**1**)

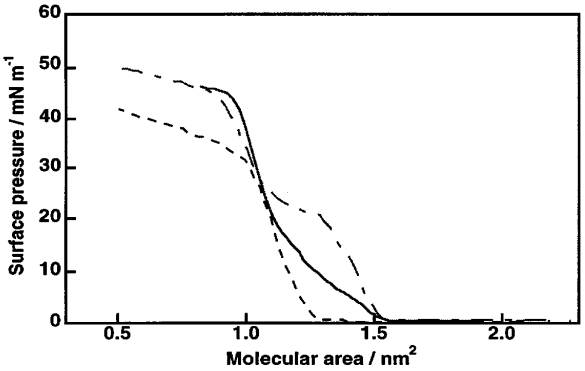

Figure 1. π-A isotherm of Ru complex **1** at different pH subphases at 20°C. (pH 2.89 (–·–·–), 5.40 (——) and 9.21 (– – –))

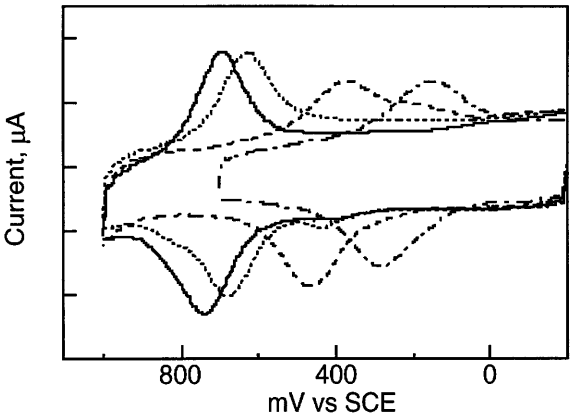

Figure 2. Cyclic voltammograms of Ru complex LB monolayer films on ITO in different pH: pH = 1.59, 2.66, 5.55 and 9.61 from left to right.

VII-A-3 Metal Coordination to Amphiphilic Ru Complexes at the Air-Water Interface

Masa-aki HAGA, Noriaki KATO, Hideaki MONJUSHIRO and Kezhi WANG

[*J. Supramol. Sci.* in press]

We have examined the applicability of "metal

complex as a ligand" strategy at the interface by using the Ru complexes acting as a ligand. New amphiphilic ruthenium complexes containing 2,6-bis(N-octadecylbenzimidazolyl)-pyridine (L18), $[Ru(L18)(X)]^{2+}$, were synthesized, where X = 2,3,5,6-tetrakis(2'-pyridyl)-pyrazine (tppz) and 1,4-bis(2,2':6', 2''-terpyridine-4'-yl)-benzene (bteb), in which the bis-tridentate ligand (tppz or bteb) of $[Ru(L18)(X)]^{2+}$ can act not only as a hydrophilic head group but also as a coordination site to a metal ion from the subphase at the air-water interface. These amphiphilic Ru complexes lead to a stable Langmuir-Blodgett (LB) film formation. The incorporation of metal ion from subphase at the air-water interface was proved by the measurements of π-A isotherms, UV spectra, angular dependent XPS spectra. The AFM images showed the formation of a circular domain structure at low surface pressures. The domains gathered with progessive compression. The weak intermolecular interaction between the Ru complexes is responsible for the domain formation at the air-water interface.

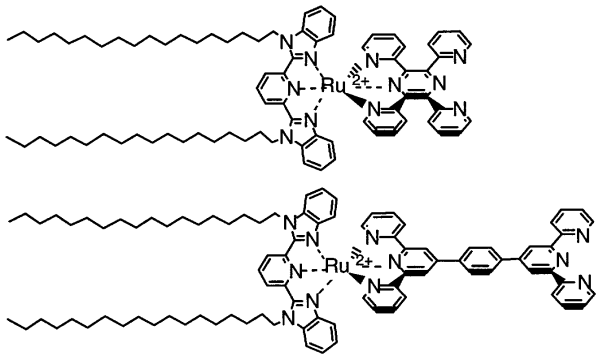

Scheme 1. Structure of amphiphilic Ru complex

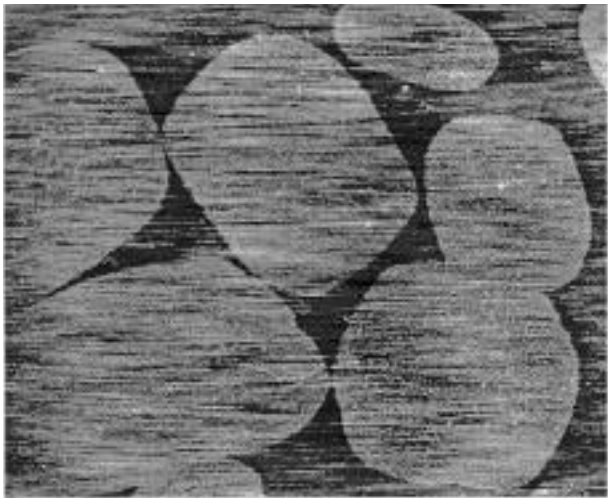

Figure 1. AFM image (5 μm × 5 μm) of the LB monolayer film of $[Ru(L18)(tppz)](PF_6)_2$ transferred onto mica at a surface pressure of 10 mNm^{-1}.

VII-A-4 Synthesis and Characterization of Amphiphilic Ru Complex with 2,2':6',2"-Terpyridine-4'-phosphonic Acid at the Air-Water Interface

Kezhi WANG, Md. Delower HOSSAIN, and Hideaki MONJUSHIRO and Masa-aki HAGA

[*Langmuir* submitted]

A novel amphiphilic Ru(II) complex with its molecular structure shown below, $Ru(L18)(tpy\text{-}PO_3H)\text{-}PF_6$ (L18 = 2,6-bis(N-octadecylbenzimidazolyl)pyridine and $tpy\text{-}PO_3H$ = monoprotonated-2,2':6",2'-terpyridine-4-phosphonate), was designed and synthesized for this purpose.

Surface pressure-area (π-A) isotherms were measured in detail by changing a subphase condition such as pH or metal ion (Zn^{2+},Cd^{2+} and Mn^{2+}). A freshly prepared dichloroethane solution of the complex (1.8-2.5 mg/5ml) was spread on the various subphases. The complex had a stable Langmuir-film forming property with a limiting molecular area of 1.4 $nm^2 \cdot molecule^{-1}$, which is consistent with that observed previously for $[Ru(L18)(tppz)]^{2+}$ (tppz = 2,3,5,6-tertakis(2'-pyridyl)pyrazine). The π-A isotherms are strongly dependent on the subphase pH. An expansion of the limiting molecular area was observed with increasing the subphase pH. In *in-situ* uv-vis spectra, we found that the Ru-to-ligand charge transfer (MLCT) band at the air-water interface is very sensitive to the subphase conditions, which is relevant to the molecular orientation of Ru complex. The intensity of MLCT band at the air-water interface was suppressed at pH 2.8 compared to that for the solution spectra, but at pH 9.4 the normal MLCT intensity was obtained. Thus, the molecular orientation of Ru complex can be controlled by the solution pH. Transferred LB films on hydrophilic and hydrophobic glass substrates have been studied by uv-vis, angle-resolved X-ray photoelectron spectroscopy (XPS), low angle x-ray diffraction (XRD), cyclic voltammetry and atomic force microscopy. A plot of absorbance at λ = 340 nm of LB films prepared at various experimental conditions used, as a function of number of LB layers is a straight line, indicative of a reproducible film transfer. Further, the transfer ratio onto an ITO substrate falls within 0.9 ~ 1.

When the metal ion contained subphase was used, the monolayer became stabilized as expected. Molar ratios of the Ru complex to the metal ions (Zn^{2+},Cd^{2+} and Mn^{2+}) in the transferred LB films from the corresponding metal ion-containing subphases, were found to be approximately 1:1, consistent with known layered solid of divalent metal organophosphonates, $M(O_3PR)H_2O$ (M = Mg, Mn, Zn, Cd; R = n-alkyl, aryl groups). A similar structure could thus be inferred for our case. Furthermore, an angle-resolved XPS of transferred LB films from metal ion contained subphase revealed that the relative intensity ratio of Ru $3d_{5/2}$ to metal ion peak reveals the angular dependence due to ordered layered structure of the LB films. Cyclic voltammetry of the monolayer film on ITO working electrode in 0.1 M $HClO_4$ as supporting electrolyte showed a reversible oxidation wave at +1.02 V vs SCE which is independent of pH. Furtheremore, $[Ru(L18)(tpy\text{-}PO_3H)]\text{-}TiO_2$ composite was successfully transferred onto an ITO electrode when the exfoliated TiO_2 suspension was used as a subphase, which shows a photoelectrochemical response.

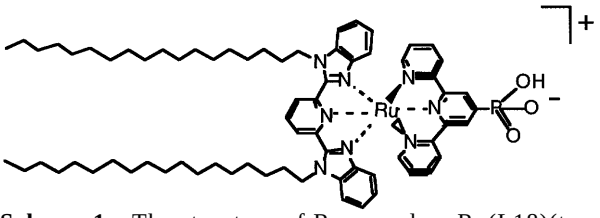

Scheme 1. The structure of Ru complex, Ru(L18)(tpy-PO_3H)PF_6

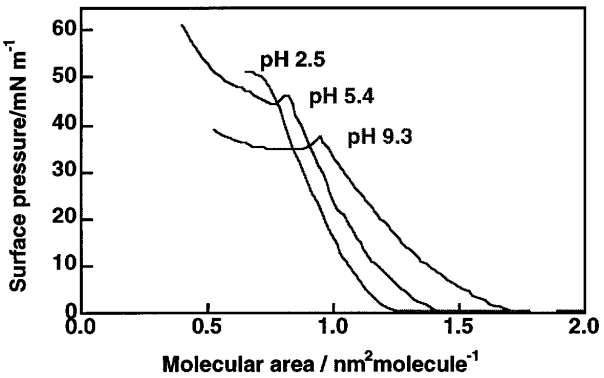

Figure 1. pH Dependence of subphase on π-A isotherms for Ru(L18)(tpy-PO_3H)PF_6 at 20°C.

VII-A-5 Metal-to-Ligand Charge Transfer (MLCT) Band of [Ru(L18)(tridentate ligand)]$^{2+}$ as a Molecular Orientation Probe at the Air-water Interface

Masa-aki HAGA, Kezhi WANG, Yuzo NISHIDA and Hideaki MONJUSHIRO *(Osaka Univ.)*

[submitted]

Metal-to-ligand charge transfer(MLCT) band of Ru(II) complexes has been investigated in detail for the last few decades. The present Ru(II) complexes, [Ru(L18)(tridentate ligand)]$^{2+}$, where L18 = 2,6-bis(N-octadecylbenzimidazolyl)pyridine and tridentate ligand = 2,3,5,6-tertakis(2'-pyridyl)pyrazine etc, which has a C_2 symmetry, show a characteristic MLCT band around 500 nm. Considering the molecular symmetry of these Ru complexes, the MLCT transition is polarized to z axis. Therefore, the drastic change of absorption intensity on MLCT band is expected when all the molecules of Ru complex is oriented to the z-axis direction. The *in-situ* UV spectra of [Ru(L18)(tppz)]$^{2+}$ shows a drastic decrease of MLCT band around 500 nm, which indicates the vertical orientation of molecules with respect to the air-water interface. On the other hand, a clear MLCT band of [Ru(L18)(betb)]$^{2+}$ (bteb = 1,4-bis(2,2':6',2''-terpyridine-4'-yl)benzene) was observed around 500 nm at the air-water interface. When the addition of Cu^{2+} ion into the subphase for [Ru(L18)(betb)]$^{2+}$, the MLCT band was disappeared but the π-π* bands are still observed.(Figure 1) This spectral change was rationalized by the change of molecular orientation from tilted form to vertical one by the Cu^{2+} ion coordination from the subphase. This interpretation was further supported by the surface pressure-area isotherm measurement. Therefore, the MLCT band of [Ru(L18)(tridentate ligand)]$^{2+}$ acts as a molecular orientation probe at the air-water interface.

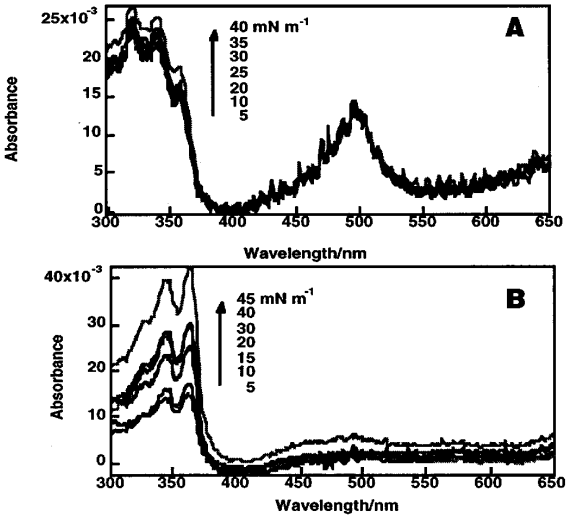

Figure 1. *in-situ* UV spectra of [Ru(L18)(bteb)]$^{2+}$ by Cu^{2+} coordination: (A) On a pure water subphase (B) on a Cu^{2+} (1 mM) containing subphase.

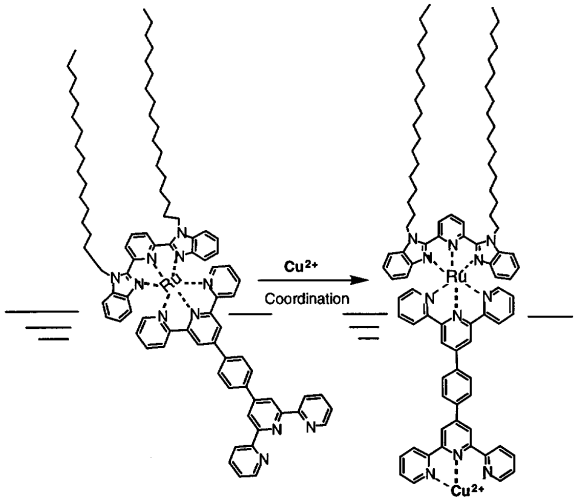

Scheme 1. The change of molecular orientation from tilted form to vertical one by the Cu^{2+} ion coordination from the subphase

VII-B Redox Chemistry of Inorganic Metal Complexes

The fundamental understanding and deeper knowledge of the redox processes in inorganic metal complexes are needed in order to build in the supramolecular inorganic complexes as components of molecular based devices. Molecular electrochemistry of inorganic and organometallic metal complexes in solution has been investigated in order to elucidate the redox chemistry of metal complexes and get relationships between structure and electrochemical behavior.

VII-B-1 1,8-Diphenyl-octa-1,3,5,7-tetraene Complexes of Ruthenium(II): Crystal Structures of [μ-(s-*cis*-1,2,3,4-η:s-*cis*-5,6,7,8-η-PhCH=CHCH=CHCH=CHCH=CHPh)(RuClCp*)$_2$] and [μ-(s-*trans*-1,2,3,4-η:s-*trans*-5,6,7,8-η-PhCH=CHCH=CHCH=CHCH=CHPh)-{Ru(acac)$_2$}$_2$]

Kazushi MASHIMA *(Osaka Univ)*, **Hiroki FUKUMOTO** *(Osaka Univ)*, **Kazuhide TANI** *(Osaka Univ)*, **Masa-aki HAGA and Akira NAKAMURA** *(Osaka Univ)*

[*Organometallics* **17**, 410 (1998)]

Reaction of 1,8-diphenyl-1,3,5,7-octatetraene with [Ru(μ-Cl)Cp*]$_4$ (**1**) (Cp* = η^5-pentamethylcyclopentadienyl) gave [μ-(s-*cis*-1,2,3,4-η:s-*cis*-5,6,7,8-η-PhCH=CHCH=CHCH=CHCH=CHPh)(RuClCp*)$_2$] (**2**), whose crystal structure revealed that **2** has a planar tetraene backbone coordinated by two Cp*RuCl moieties in s-*cis*-η^4-fashion; while the reaction with Ru(acac)$_3$/Zn system resulted in the formation of [μ-(s-*trans*-1,2,3,4-η:s-*trans*-5,6,7,8-η-PhCH=CHCH=CHCH=CHCH=CHPh){Ru(acac)$_2$}$_2$] (**3**), where both of the two Ru(acac)$_2$ moieties prefer s-trans coordination and thus the plane of the octatetraene backbone of **3** is deformed into an S-shape. Electrochemical studies for complexes **2** and **3** revealed that complex **3** has a strong coupling between the two ruthenium centers and is a conjugatively interacted dπ-pπ organometallic system, whereas complex **2** has a longer π-conjugation of the tetraene backbone without electronic communication between the two RuClCp* moieties

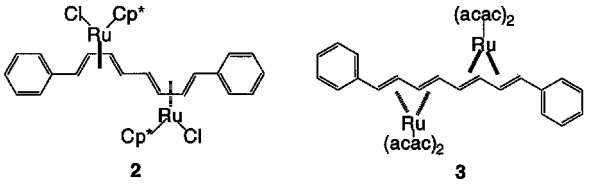

2 **3**

VII-B-2 Spectroelectrochemical Analysis of Intervalence Band in Mixed-Valence Di- and Tetranuclear Ru Complexes by Flow-Through Method

Masa-aki HAGA, Md. Meser ALI *(Mie Univ)*, **Hiroyasu SATO** *(Mie Univ)*, **Hideaki MONJUSHIRO, Koichi NOZAKI** *(Osaka Univ)* **and Kenji KANO** *(Kyoto Univ)*

[*Inorg. Chem.* **37**, 2320 (1998)]

Novel dendritic tetranuclear Ru and Os-2,2'-bipyridine complexes bridged by 2,2'-bis(1-methylbenzimidazo-2-yl)-4,4'-bipyridine (Scheme 1) showed four closely spaced one-electron oxidation processes; i.e., the central one-electron oxidation occurs first, followed by three peripheral metal oxidations at almost same potentials. During the progress of electrochemical oxidation, a characteristic near-infrared(NIR) band was observed, which can be assigned to intervalence charge transfer (IT) transition within the mixed-valence state. Since the potential separations among these three processes are generally small, the selective oxidation could not be achieved and even the one-electron oxidized species might be easily disproportionated into the original and two electron oxidized species. Therefore, the accurate determination of the absorption spectra for the mixed valence complexes should be determined by considering the comproportionation equilibria. In order to reconstruct the corrected absorption spectra of each mixed-valence complex, we have developed a new spectral analysis method based on the combination of digital simulation analysis of the reversible CV curves and the electrochemical titration by flow-through cell (Figure 2), which gives the complete spectra of IT band for the partially oxidized species in the dendritic tetranuclear complexes. This method can be applicable not only for the dendritic Ru tetranuclear complexes but also dinuclear Ru complexes.

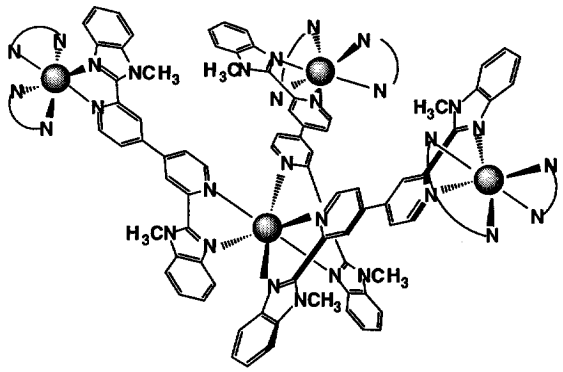

Scheme 1. Structure of dendritic tetranuclear Ru/Os-2,2'-bipyridine complexes

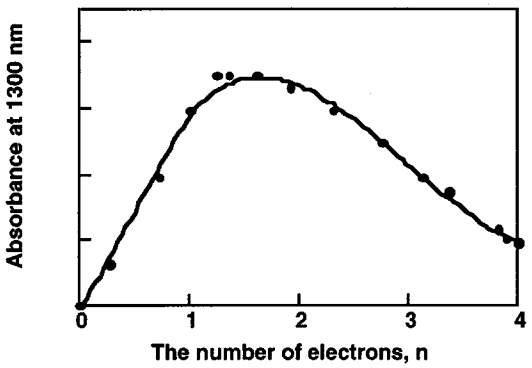

Figure 1. A plot of absorbance at 1300 nm vs the number of electrons, n,obtained from tthe current ratio for the complex, [{(bpy)$_2$Ru(dmbbbpy)}$_3$Ru]$^{8+}$ (2.3 × 10^{-4} M)

VII-C New Insight into Mechanism of Biological Oxygenation Reactions

One of the remaining frontiers in organic chemistry is the direct functionalization of saturated hydrocarbons. The catalytic cycle that oxidizes a hydrocarbon RH to an alcohol R-OH employing cytochrome P-450 and methane monooxygenase is a well-establised reaction, however, no reasonable mechanism for activation of dioxygen and for formation of a R-OH is available at present. Recently the present author has proposed a new idea that elucidates many biological oxygenation reactions comprehensively. In this consideration, the importance of electrophilic nature of a metal-peroxide adduct and role of the substrate as an electron donor were emphasized. This idea suggests that formation of a high-valent iron-oxo species occurs most likely when the metal-peroxide intermediate is activated through electronic interaction with both the peripheral organic group and substrate; the latter two act as a elelctron donor to the peroxide adduct. We are now continuing the study on the reactivity of the metal-peroxide adduct in order to ascertain that my idea is applicable to other reactions, such as degradation of DNA and proteins, etc.

VII-C-1 Mechanism of Double-Strand DNA Cleavage Effected by Iron-Bleomycin

Teruyuki KOBAYASHI, Li Li GUO and Yuzo NISHIDA

[*Z. Naturforsch.* **53C** (1998) in press]

We have observed that in the absence of hydrogen peroxide the Fe(III)-bleomycin (BLM) complex exhibits high DNA cleavage efficiency converting supercoiled Form I DNA (pBR322 or φx174) to Form II (nicked, relaxed circular); the present study may give an important clue to elucidate the fact that iron-bleomycin mediated double-strand DNA cleavage requires at least one molecule of oxygen(O_2) over the amount required to form "activated bleomycin."

VII-C-2 Contribution of a Peroxide Adduct of Copper(II)-Peptide Complex to Modify the Secondary Structure of Albumin

Yoshihiro ISHIKAWA, Sayo ITO, Satoshi NISHINO, Shigeru OHBA and Yuzo NISHIDA

[*Z. Naturforsch.* **53C**, 378 (1998)]

We have found that copper(II) compounds containing a peptide group in the chelate exhibit high activity for modification or degradation of albumin in the presence of hydrogen peroxide, whereas no activity was detected for the copper(II) complexes without an amide-group. It is suggested that presence of amide group in the ligand may play an important role in the formation of the peroxide adduct and in activation of the peroxide ion, leading to cleavage of peptide bond of a neighboring protein. It is implied that conversion of normal cellular prion protein PrP^{C} into a disease-causing isoform, PrP^{Sc} is attributed to the activated peroxide ion coordinated to a copper(II) ion captured in the NH_2-terminal domain of PrP^{C}.

VII-D Metal Ions in Biological Systems

In order to reveal the biological roles of transition metal ions, structures and reactions of metalloproteins and metalloenzymes such as NO reductase, laccase, ascorbate oxidase, and several blue copper proteins have been studied by absorption, CD, MCD, and EPR spectroscopies and by magnetic susceptibility measurements. V-haloperoxidase has also been isolated and characterized.

VII-D-1 Isolation and Characterization of Nitric Oxide Reductase from *Paracoccus halodenitrificans*

Nobuhiko SAKURAI and Takeshi SAKURAI

[*Biochemistry* **36**, 13809 (1997)]

Nitric oxide reductase was isolated from the membrane fraction of a denitrifying bacterium, *Paracoccus halodenitrificans*, in the presence of n-dodecyl-β-D-maltoside. A relatively simple and effective procedure to purify NO reductase using DEAE-Toyopearl and hydroxyapatite (ceramic) chromatographies has been developed. The enzyme consisted of two subunits with molecular masses of 20 and 42 kDa associated with the *c* type heme and two *b* type hemes, respectively. The optical and MCD spectra of the oxidized (as isolated) and reduced enzymes indicated that the heme *c* is in the low spin state and the hemes *b* are in the high and low spin states. The EPR spectrum also showed the presence of the split high spin component (g = 6.6, 6.0) and two low spin components ($g_{z,\,y,\,x}$ = 2.96, 2.26, 1.46, g_z = 3.59). Although the presence of an extra iron was suggested from atomic absorption spectroscopy, a non-heme iron could not be detected by colorimetric titrations using ferene and nitro-PAPS. One of extra signals at g = 4.3 and 2.00 might come from a non-heme iron, while they may originate from an adventitious iron and a certain non-metallic radical, respectively. When CO acted on the reduced enzyme, both of the low spin hemes were not affected, and when NO acted on the reduced enzyme, the optical and MCD spectra were of a mixture of the

oxidized and reduced enzymes. Consequently, the reduction of NO was supposed to take place at the high spin heme *b*. The heme c and the low spin heme *b* centers were considered to function as electron mediators during the intermolecular and intramolecular processes.

VII-D-2 Spectral Properties of Cytochrome c_{553} and a Membrane-Bound Cytochrome *b* from *Alcaligenes xylosoxidans* GIFU 1051

Nobuhiko SAKURAI, Hideyuki KUMITA *(Nagoya Inst. Tech.)*, **Takeshi SAKURAI and Hideki MASUDA** *(Nagoya Inst. Tech.)*

[*Bull. Chem. Soc. Jpn.* **70**, 135 (1998)]

Cytochrome c_{553} and cytochrome *b* were isolated from soluble and membrane fractions of *Alcaligenes xylosoxidans* GIFU 1051, respectively, and their spectroscopic characterization has been performed. Cytochrome c_{553} has been shown to be in the low spin state both in the oxidized and reduced forms at room temperature by the absorption and magnetic circular dichroism (MCD) spectra, while the high spin heme has been also observed in the cryogenic electron paramagnetic resonance (EPR) spectra. Exogenous small ligands such as NO and CO bind to cytochrome c_{553} by expelling the axial His ligand. The membrane-bound cytochrome *b* has two heme *b* centers in a protein molecule which are the active centers of NO reductase, the cytochrome *bc* complex, although the enzyme activity was considerably low. The absorption, MCD, and EPR spectra of the membrane-bound cytochrome *b* showed that two heme b centers are in the different electronic states, the high and low spin states. Cytochrome c_{553} is the natural electron donor to the membrane-bound NO reductase, although the interprotein electron-transfer could not been studied because of the low enzyme activity of the cytochrome *b* subunit

VII-D-3 Observation of Cu-N_3^- Stretching and N_3^- Asymmetric Stretching Bands for Mono-Azide Adduct of *Rhus vernicifera* Laccase

Shun HIROTA *(Nagoya Univ.)*, **Hiroki MATSUMOTO** *(Nagoya Univ.)*, **Hong-wei HUANG, Takeshi SAKURAI, Teizo KITAGAWA and Osamu YAMAUCHI** *(Nagoya Univ.)*

[*Biochem. Biophys. Res. Commun.* **243**, 435 (1998)]

Mono-azide adduct of *Rhus vernicifera* laccase was investigated with resonance Raman and FT-IR spectroscopies as a step forward elucidation of the structure and function of the trinuclear center. The Cu-N_3^- stretching RR band was observed for azide-bound multicopper oxidases for the first time. The Cu-N_3^- band was located at 400 cm^{-1} for mono-$^{14}N_3^-$ laccase, which shifted to 396 cm^{-1} with the $^{15}N^{14}N^{14}N^-$ analog. The Cu-N_3^- asymmetric stretching band was observed by FT-IR spectroscopy at 2035 cm^{-1} for $^{14}N_3^-$ laccase and at 2025 cm^{-1} with the $^{15}N^{14}N^{14}N^-$ analog. These spectra were comparable with those for hemocyanin with a stronger π bank donation from the copper to the bound N_3^- molecule.

VII-D-4 Genomic Cloning of the Region Encoding Nitric Oxide Reductase in *Paracoccus halodenitrificans* and a Structure Model Relevant to Cytochrome Oxidase

Nobuhiko SAKURAI and Takeshi SAKURAI

[*Biochem. Biophys. Res. Commun.* **243**, 400 (1998)]

The structural genes for the NO reductase in *Paracoccus halodenitrificans*, *norC*, *norB*, and *norQ* were sequenced. The *norC* and *norB* encode the cytochrome *c* (NorC) and cytochrome *b* (NorB) subunits, respectively. The matured NorC (17258 Da, 148 residues) has a binding motif (CXYCH) for heme c, which is axially coordinated by His65 and Met115. NorB (52337 Da, 451 residues) has twelve putative transmembrane helices and the 19% sequence homology with the subunit I of cytochrome oxidase from *Paracoccus denitrificans*. Several histidine and glutamate residues were identified as the ligands for two hemes *b* and *a* non-heme iron in comparison with the sequence of cytochrome oxidase. The higher-order model structures constructed from the amino acid sequences of NorC and NorB showed the topology of the helical segments and the locations of the metal centers.

VII-D-5 Magnetic Studies of the Trinuclear Center in Laccase and Ascorbate Oxidase Approached by EPR Spectroscopy and Magnetic Susceptibility Measurements

Hong-wei HUANG, Takeshi SAKURAI, Hideaki MONJUSHIRO and Sadamu TAKEDA

[*Biochim. Biophys. Acta* **160**, 1384 (1998)]

The trinuclear centers in laccase and ascorbate oxidase have been studied by EPR spectroscopy and magnetic susceptibility measurements over the wide range of temperature, 5 K to 300 K. The EPR spectra showed that type 2 Cu receives increasing tetrahedral distortion with raising temperature. Magnetic susceptibilities of laccase showed that both of type 1 and type 2 Cu's are almost fully paramagnetic since the antiferromagnetic interaction between type 3 Cu's is extremely strong from 5 K to 300 K. On the other hand, the effective magnetic moment of ascorbate oxidase is contributed by ca. 1.7 Cu^{2+} even below ca. 100 K, since type 2 Cu is partly in the reduced form. The effective magnetic moment continuously increased with raising temperature because the antiferromagnetic interaction between type 3 Cu's is not as strong as in the case of laccase. The type 2 Cu EPR signals in laccase and ascorbate oxidase were conspicuously broadened with raising temperature because of the increasing contribution of the triplet state by type 3 Cu's and/or of the rapid relaxation which finally led to only ca. 30 % detection of the type 2 Cu signal at room temperature.

The stepwise binding of azide to one of type 3 Cu's made the type 3 Cu to be EPR detectable. According to the SQUID measurements type 2 Cu and one of type 3 Cu's antiferromagnetically coupled through a bridging group, possibly not an azide ion but a hydroxide ion. All these findings indicate that the steric structure and magnetic property of the trinucelar center change depending on temperature and the magnetic data at room temperature reflect the inherent property of the trinuclear center composed of type 2 and type 3 Cu's in multicopper oxidases.

VII-D-6 Isolation and Characterization of Vanadium Bromoperoxidase from a Marine Macroalga, *Ecklonia stolonifera*

Isao HARA and Takeshi SAKURAI

[*J. Inorg. Biochem.* in press]

The bromperoxidase has been isolated from the brown seaweed *Ecklonia stolonifera* (83 kDa) and has been characterized. Bromoperoxidase requires vanadium for enzyme activity as has been evidenced by EPR spectroscopy. On addition of V^{5+} to the isolated enzyme, the enzyme activity was increased ca. 250%, indicating that more than 2/3 of the protein molecules were in the apo form. The increases in the enzyme activity was specific to V^{5+}, while Fe^{2+}, Fe^{3+}, and Cu^{2+} inhibited the enzyme activity. This V^{5+} addition effect was inhibited in the phosphate buffer, probably because phosphate and vanadate compete for the active site. The present bromoperoxidase exhibited a high thermo-stability (T_m = 68°C) and a high stability in organic solvents (completely intact even in the presence of 50 % of methanol, ethanol and 1-propanol).

VII-D-7 EPR and Magnetic Susceptibility Studies of the Trinuclear Copper Center in Native and Azide-Reacted Zucchini Ascorbate Oxidase

Hong-wei HUANG, Takeshi SAKURAI, Silvana MARITANO *(Osaka Univ.)*, **Augusto MARCHESINI** *(Ist. Sper. per la Nut. delle Piante)* **and Shinnichiro SUZUKI** *(Osaka Univ.)*

[*J. Inorg. Biol. Chem.* submitted]

The magnetic properties of the trinuclear center composed of type 2 Cu and a pair of type 3 Cu's in zucchini ascorbate oxidase have been studied by EPR spectroscopy and magnetic susceptibility measurements from cryogenic temperature to room temperature. The temperature-dependent EPR spectra showed that the Az value of the type 2 Cu signal decreases with increasing temperature. Concomitantly, the type 2 Cu signal was appreciably broadened at > 150 K differing from the type 1 Cu signal. While the EPR spectrum can be simulated for the 1 : 0.3-0.4 ratio of type 1 Cu and type 2 Cu per protein molecule, the total amount of the EPR detectable Cu^{2+} was not 1.3-1.4 but was 1.7-1.8 at < 150K and 1.3-1.4 at room temperature (Ascorbate oxidase is homodimer in which each subunit contains 1 type 1 Cu, 1 type 2 Cu and a pair of type 3 Cu's). The effective magnetic moment determined by SQUID measurements was 2.4 B. M. at < 200K, the value for 1.7 free spins per protein molecule. However, the magnetic moment increased at > 200 K, reaching 3.2 B. M. at room temperature, the value for 2.3 free spins. This decrease in the EPR detectable amount of Cu^{2+} and the increase in magnetic moment with increasing temperature are due to the contribution of the triplet state by the antiferromagnetcially coupled type 3 Cu's. The two-step binding of azide to the trinuclear center perturbs magnetic properties of the trinuclear center. Although no bridging group exists in the trinuclear center of the azide-ascorbate oxidase according to the X-ray crystal structure (Messerschmidt et al., *J. Mol. Biol.* **230**, 997-1014 (1993)), the magnetic susceptibility data indicated that two coppers in the trinuclear center are antiferromagnetically coupled. The binding modes for the one- and two-azide bound forms were discussed based on the temperature-dependent EPR and magnetic susceptibility data.

VII-D-8 The Putative Proton-Transfer Pathway in Membrane-Bound Nitric Oxide Reductase in Connection with Proton Transfers in Heme-Cu Terminal Oxidases

Takeshi SAKURAI and Nobuhiko SAKURAI

[*FEBS Lett.* submitted]

The amino acid sequence of the membrane-bound nitric oxide reductase from *Paracoccus halodenitrificans* was compared with that of cytochrome oxidase. There were strong similarities between NO reductase and cytochrome oxidase for the presence and topology of the twelve-transmembrane segments and the ligand groups for metal centers. In addition, it was also found that the acidic amino acids to assist the transfer of the vectorial proton from cytoplasm to the Heme a_3-CuB center in cytochrome oxidase are also present in the cytochrome *b* subunit of NO reductase, although the amino acids to transfer the vectorial proton from Heme a_3-CuB to periplasm and those to transfer the scalar proton are absent in NO reductase. This suggests the possibility of the presence of a specific pathway to transport protons utilized to transform 2NO to N_2O and H_2O at the binuclear center composed of the high spin heme *b* and the non-heme iron. This pathway to transport protons to be reacted might have evolved into the vectorial proton transfer pathway in cytochrome oxidase.

VII-D-9 Roles of Four Iron Centers in *Paracoccus halodenitrificans* Nitric Oxide Reductase

Takeshi SAKURAI, Nobuhiko SAKURAI, Hiroki MATSUMOTO *(Nagoya Univ.)* **Shun HIROTA** *(Nagoya Univ.)* **and Osamu YAMAUCHI** *(Nagoya Univ.)*

[*Biochem. Biophys. Res. Commun.* in press]

Reactions of *Paracoccus halodentrificans* nitric oxide reductase (NOR) containing four iron centers, a low spin heme *c*, a low spin heme *b*, a high spin heme *b* and a non-heme iron, have been studied to show the roles of each iron center. Soon after reacting the resting (oxidized) NOR with L-ascorbate the low spin heme *c* and low spin heme *b* were reduced to a considerable extent but the high spin heme *b* was still in the oxidized form and was reduced slowly. When CO was acted on the reduced NOR, the high spin heme *b* center changed to be a low spin state. On the other hand, when NO was acted on the resting NOR, no apparent spectral change was observed. However, when NO was acted on the reduced NOR (a steady state condition excess dithionite is present), both of the low spin centers changed to be partly in the oxidized form. A small but clear new EPR signal with g = 4.1 appeared together with some new signals at the g = 2 region soon after the action of NO on the reduced NOR. During incubation at room temperature the nitrosyl-heme signal typical of the 5-coordination developed. These results suggested that both of the high spin-heme *b* center and the non-heme iron are the reaction centers and their reductions are indispensable for the enzyme process in contrast to the reaction mechanism proposed for the P-450 type NOR (P-450nor).

VII-D-10 *Myrothecium verrucari* MT-1 Bilirubin Oxidase and Its Mutants for Potential Copper-Ligands

Atsushi SHIMIZU *(Aoyamagakuin Univ.)*, **Jung Hee KWON** *(Aoyamagakuin Univ.)*, **Takashi SASAKI** *(Aoyamagakuin Univ.)*, **Takanori SATOH** *(Aoyama - gakuin Univ.)*, **Nobuhiko SAKURAI, Takeshi SAKURAI, Shotaro YAMAGUCHI** *(Amano Pharm. Co.)* **and Tatsuya SAMEJIMA** *(Aoyamagkauin Univ.)*

[*Biochemistry* submitted]

Bilirubin oxidase [EC 1.3.3.5] which catalyzes the oxidation of bilirubin to biliverdin *in vitro* was purified from the culture medium of *Myrothecium verrucaria* MT-1 (authentic enzyme). The overexpression system of bilirubin oxidase gene was already established by using *Aspergillus oryzae* harboring an expression vector, thereby we obtained recombinant enzyme (wild type). The absorption and ESR spectra showed that the both bilirubin oxidases are a multicopper oxidase containing type 1, type 2, and type 3 coppers as similar with laccase, ascorbate oxidase, and ceruloplasmin. The cassette mutagenesis has been performed for the possible ligands of each type of coppers. In the mutants, Cys457 → Val, Ala, His94 → Val, and His134.136 → Val, the type 1 and type 2 copper centers were perturbed completely and the enzyme activity was completely lost. And these mutants showed the ESR spectra differing from the holoenzyme, showing the type 3 copper signal. However, the optical and magnetic property characteristic for the type 1 copper was retained even by mutating one of the type 1 copper ligand, *i.e.*, the mutant, Met467 → Gly, whose enzyme activity was also retained slightly. Futhermore, the mutant His456.458 → Val completely lost the enzyme activity and characteristics for type 2 and type3 coppers but still retained the type 1 copper. These results support that these above amino acids as the copper ligands and the peculiar sequence in the multicopper oxidases, His-Cys-His, also appeared in bilirubin oxidase to form the intramolecular electron transfer pathway between the type 1 copper site and the trinuclear center composed of the type 2 and type 3 copper sites.

VII-E Homogeneous Catalysis with Novel Reactivity

Highly active and selective homogeneous catalytic systems are developed. Mechanistic studies are carried out with isolated active catalyst species and related model complexes.

VII-E-1 Palladium Complex Catalyzed Cyanation of Allylic Carbonates and Acetates Using Trimethylsilyl Cyanide

Yasushi TSUJI, Tomohito KUSUI *(Gifu Univ.)*, **Takaharu KOJIMA** *(Gifu Univ.)*, **Yoshihiko SUGIURA** *(Gifu Univ.)*, **Naoaki YAMADA** *(Gifu Univ.)*, **Shinsuke TANAKA** *(Gifu Univ.)*, **Masahiro EBIHARA** *(Gifu Univ.)* **and Takashi KAWAMURA** *(Gifu Univ.)*

[*Organometallics* in press]

Allylic carbonates are cyanated in high yields to β,γ-unsaturated carbonitriles using trimethylsilyl cyanide in the presence of catalytic amount (5 mol%) of $Pd(PPh_3)_4$ in THF under reflux. In the reaction, cinnnamyl methyl carbonate affords cinnamyl cyanide in 98% yield. Allylic acetates also provide the corresponding carbonitriles, but often in lower yields. The cyanations of several *cis*- and *trans*-alicyclic substrates proceed cleanly (stereoselectivity > 99%) with overall retention. Characterization and reaction of palladium complexes relevant to the present catalysis indicate that transmetallation of η^3-allyl palladium complex with trimethylsilyl cyanide is facile, while the resulting cyano(η^3-allyl)palladium complexes afford the corresponding allylic cyanides only when excess trimethylsilyl cyanide is present. Stereochemistry of the product indicates that the CN attacks the η^3-allyl moieties from the palladium side.

VII-F Bio-Inspired Molecular Architecture

Nature has produced a limited number of molecular modules such as nucleosides and nucleotides, amino acids, and lipids. However, the chemical diversity of these biomolecules and the different ways they can be polymerized or assembled into precisely-defined three-dimensional shapes provide a wide range of possible structures and functions. Furthermore, owing to advances in chemical synthesis and biotechnology we can combine or chemically modify these molecular building blocks, almost at will, to produce new functional molecules that have not yet been made in Nature. Based on these concepts, we have been working on the following research projects. Our research programs also consciously focus on structures and functions that have been unknown in living, biological systems.

VII-F-1 Double-Strands Formation of Artificial DNAs Induced by Metal Complexation

Kentaro TANAKA, Honghua CAO *(Grad. Univ. Adv. Stud.)*, **Motoyuki TASAKA** *(Grad. Univ. Adv. Stud.)* **and Mitsuhiko SHIONOYA**

[*Nucleic Acids Res., Symp. Ser.* **39**, 171 (1998)]

An artificial DNA was synthesized, to which nonnatural bases were introduced as metal coordination sites, for the purpose of controlling higher-order structures of DNAs and for utilizing DNA as functionalized materials. The artificial DNA forms double stranded structure by metal complexation instead of hydrogen bonding in natural DNA. An artificial β-C-nucleoside **1** (Figure 1a) which has a phenylenediamine base as the metal coordination site was prepared by coupling reaction of lithiated *o*-phenylenediamine derivative and *O*-protected 1,4-ribonolactone followed by several steps to remove 2'-hydroxyl group. Figure 1b shows ^{1}H-NMR spectra of metal complex formation between C-nucleoside **1** and Pd^{2+}. The chemical shifts of the aromatic moiety shifted to lower field almost linearly with increasing concentration of Pd^{2+} until the concentration reached at a half of that for **1**. This result shows that **1** and Pd^{2+} form a stable 2:1 complex with a high binding constant. To control the number of charges of the metal complex moiety, the synthesis of new nucleobases bearing a catechol or an aminophenol as the nucleobase is now underway.

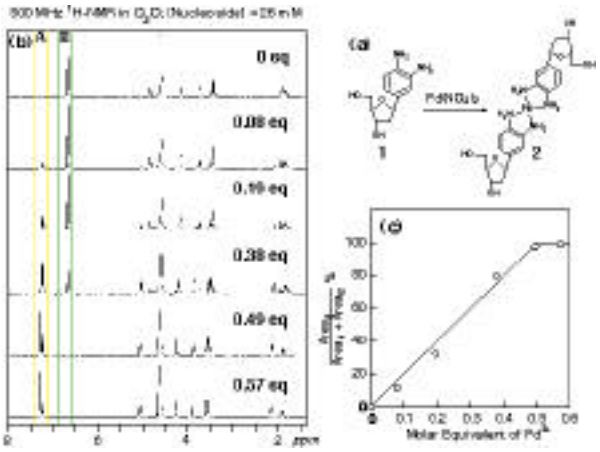

Figure 1. Complex formation of phenylenediamine-nucleoside with Pd^{2+}: (a) reaction scheme, (b) ^{1}H-NMR spectra of **1** with various concentrations of Pd^{2+}, (c) proportion of metal complex against molar equivalent of Pd^{2+} added.

VII-F-2 Metal-Assisted Formation of Artificial Nucleic Acids

Akihiko HATANO *(Grad. Univ. Adv. Stud.)*, **Hiromasa MORISHITA** *(Grad. Univ. Adv. Stud.)*, **Kentaro TANAKA and Mitsuhiko SHIONOYA**

[*Nucleic Acids Res., Symp. Ser.* **39**, 93 (1998)]

Self-assembly processes are used to create complex functional biological structures of nano scale dimensions with precision, and are now recognized as efficient tools in the construction of new systems with tailored functions. DNA, which is a genetic bio-molecule, forms a double helical structure with two complementary single strands through hydrogen bonding, and stores genetic information. In this work, we have designed a self-assembling nucleic acid which could be built up by molecular subunits with the cooperative participation of metal coordination, hydrogen bonding, and hydrophobic interaction etc. The compound **1** we first prepared in this work has a thymine base moiety and two amino carboxylic acid subunits. This chelating compound **1** was expected to be aligned on an adenine-rich single stranded DNA (or RNA) through hydrogen bonding and metal coordination. The interactions between poly dA, the compound **1**, and metal ions (Mg^{2+}, Zn^{2+}, Mn^{2+}, Ni^{2+}) were examined by UV absorption changes around 260 nm. Effective interactions between these three components would result in a decrease in the absorption compared with the total absorption of each component. However, there was only a little absorption change in the presence of the above ions. The synthesis of **2**, in which the metal coordination sites of **1** are replaced by ethylene diamine subunits, is now in progress.

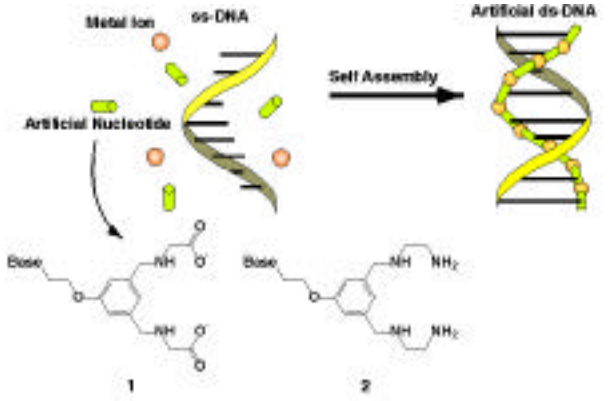

VII-F-3 An Efficient Strategy for the Liquid-Phase Synthesis of Cyclic Metallopeptides

Kazuki SHIGEMORI *(Grad. Univ. Adv. Stud.)*, **Kentaro TANAKA and Mitsuhiko SHIONOYA**

Synthetic cyclopeptides are interesting target molecules owing to their biological activity, their model character for enzymes or biomembranes, and their great potential as drugs and functional molecules such as nanotubes. New efficient synthetic methodology has been developed that can be utilized for the iterative construction of new families of cyclic metallopeptide oligomers of the general formula, cyclo[Gly-Cys-(terpyPt^{II})]$_3Cl_3$, **1**, and cyclo[Gly-Cys(terpyPt^{II})]$_4Cl_4$, **2**. The linear peptides (Gly-L-Cys)$_n$ trifluoroacetate salts (n = 3, 4) were synthesized on commercially available H-Cys(Trt)-2-ClTrt resin using standard Fmoc chemistry, cleaved from the solid support using trifluoroacetic acid in the presence of 1,2-ethanedithiol for the removal of triphenylmethyl groups from cystein residues, purified by RP-HPLC. [Gly-Cys(terpyPt^{II})]$_n$-Cl_n (n = 3, 4) were prepared from the above linear peptides and n eq [(terpy Pt^{II})Cl]Cl in H_2O at room temperature. The obtained linear metallopeptides were cyclized at 25°C in the presence of HOBt (10 mM) and EDC (100 mM) in H_2O-CH_3CN in high yields. A full analysis of these compounds by a variety of techniques, including UV-vis, ^{1}H NMR spectroscopies, electron spray mass, HPLC and capillary electrophoresis, has been performed. These cyclic metallopeptides proved to interact with DNA and cationic ions such as Mg^{2+}, Ca^{2+}, Gd^{3+}, Tb^{3+}, Eu^{3+} ions by circular dichroism spectroscopy.

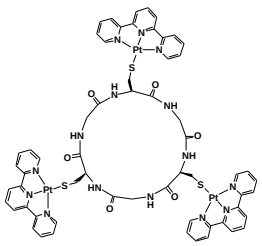

1

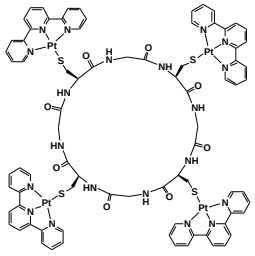

2

VII-F-4 Highly Controlled and Hierarchical Assembly of Metal Complexes

Hiromasa MORISHITA *(Grad. Univ. Adv. Stud.)*, **Xian-He BU** *(Nankai Univ., China and IMS)*, **Kentaro TANAKA and Mitsuhiko SHIONOYA**

Biological materials assembly on a very broad range of organizational length scales, and in both hierarchical and nested manners. The concept of a hierarchy of structures of increasing size was referred to repeatedly, and comparisons were inevitably made with the organization of living manner. Self-assembly features the cooperative participation of non-covalent interactions to construct thermodynamically minimized structures. The main purpose of this research is to arrange functional molecular subunits on DNA by non-covalent interactions, or to array designed molecules in a hierarchical manner assisted by metal ions. We have synthesized new families of tetradentate ligands which can be linked to other two subunits through metal coordination.

VII-F-5 Macrocyclic Metal Complexes for Selective Recognition of Nucleic Acid Bases and Manipulation of Gene Expression

Eiichi KIMURA *(Hiroshima Univ.)*, **Takuya IKEDA** *(Hiroshima Univ.)* **and Mitsuhiko SHIONOYA**

[*Pure & Appl. Chem.* **69**, 2187 (1997)]

Interaction of Zn-cyclen complexes **1**-**4** with uracil and thymine bases in double-stranded poly(A)-poly(U) and poly(dA)-poly(dT) has been investigated. These zinc(II) complexes lowered the melting temperatures (T_m) of poly(A)-poly(U) and poly(dA)-poly(dT) in 5 mM Tris-HCl buffer (pH 7.6) containing 10 mM NaCl as their concentrations increased, indicating that they destabilized the duplex structure of polynucleotides. The comparison of CD spectra of poly(A)-poly(U), poly(A), and poly(U) in the presence of zinc(II) complex **2** led us to conclude that the spectral changes of poly(A)-poly(U) were due to a structural change from double to single-strand, caused by zinc(II) complex **2** binding exclusively to uracils in poly(U). The destabilization effect of the zinc(II) complexes was not observed on poly(dG)-poly(dC) in the thermal denaturation experiments in 50 % formamide aqueous solution containing 2.5 mM Tris-HCl buffer (pH 7.6) and 5 mM NaCl. However, the acridine-pendant cyclen complex **2**, which associates with guanine at N7 and O6, and through π-π stacking, interacted with poly(dG) in the double helix to greatly stabilized the poly(dG)-poly(dC) double-strand, as was indicated by the higher T_m than those with reference intercalating agents. Poly(A)-poly(U) double-strand was most effectively broken with a bis(Zn-cyclen) bridged by para-xylyl group **3** that was designed as a host molecule to bind to two succeeding uracils in a 1:2 complex. Zn-cyclen complexes thus may become a prototype of small molecules that can affect the biological properties of nucleic acids at the molecular level.

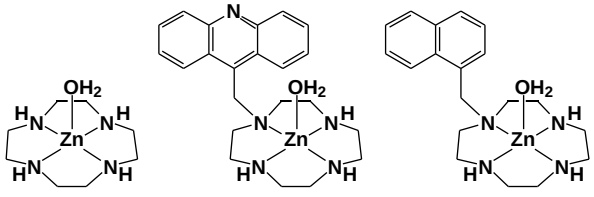

1 **2** **4**

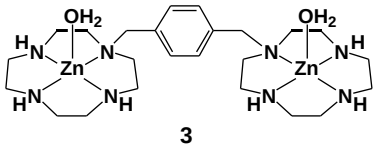

3

VII-F-6 Macrocyclic Zinc(II) Complexes for Selective Recognition of Nucleobases in Single- and Double-Stranded Polynucleotides

Eiichi KIMURA *(Hiroshima Univ.)*, **Takuya IKEDA** *(Hiroshima Univ.)*, **Mariko MURATA** *(Hiroshima Univ.)* **and Mitsuhiko SHIONOYA**

[*J. Bioinorg. Chem.* **3**, 259 (1998)]

Interaction of a series of Zn-cyclen complexes, which selectively bind to thymine and uracil nucleosides in aqueous solution at physiological pH, with polynucleotides has been examined. These complexes disrupt the A-U (or T) H-bonding to unzip the duplex of poly(A)-poly(U), as demonstrated by lowering melting temperatures of poly(A)-poly(U) and poly(dA)-poly(dT) with an increase in their concentrations. The order of the denaturing efficiency is well correlated with the order of the 1:1 affinity constants for each complex. The comparison of CD spectra of poly(A)-poly(U), poly(A), and poly(U) in the presence of the Zn-complex of acridine-pendant-cyclen revealed a structural change from poly(A)-poly(U) to single-stranded poly(A) and poly(U). This can be explained by the exclusive binding of this complex to uracils in poly(U). These Zn complexes, on the other hand, stabilized poly(dG)-poly(dC).

VII-G Stereochemistry of Coordination Compounds and Adsorption Phenomena of Various Gases on Inorganic Solids

Several coordination compounds including higher (than four)-coordinate silicon(IV) complexes are going to be synthesized and studied stereochemically and kinetically.

Dielectric properties of inorganic solids adsorbed water molecules, on which the two-dimensional condensation of water molecules occurs, were investigated as a function of surface coverage. Adsorption properties of dinitrogen (N_2) on copper-ion-exchanged mordenites were also investigated.

VII-G-1 Analysis of Active Sites on Copper Ion-Exchanged ZSM-5 for CO Adsorption through IR and Adsorption-Heat Measurements

Yasushige KURODA *(Okayama Univ.)*, **Yuzo YOSHIKAWA, Ryotaro KUMASHIRO** *(Okayama Univ.)* **and Mahiko NAGAO** *(Okayama Univ.)*

[*J. Phys.Chem. B* **101**, 6497 (1997)]

The state of copper ion exchanged in ZSM-5-type zeolite has been investigated through the IR and adsorption-heat measurements at 301 K by using CO as a probe molecule. As a result, it was proved that there are at least three kinds of adsorption sites for a CO molecule on the copper ion-exchanged ZSM-5, which are responsible for the IR bands at 2159, 2149, and 2136 cm^{-1}, as well as the differential adsorption-heats of 91, 82, and ~ 70 kJ mol^{-1}. Corresponding to these data, TPD also gives three desorption peaks at 363, 442, and 542 K. An excellent linear relationship has been established between the stretching vibrational frequencies due to the adsorbed CO species and the differential adsorption-heat values. When a CO gas is introduced to the 723 K-treated sodium ion-exchanged ZSM-5, this sample provides the adsorption-heat of about 35 kJ mol^{-1} in the whole adsorption region studied and the weak IR bands at 2175 and 2112 cm^{-1}. For the sodium ion-exchanged ZSM-5 and CO system, the above correlation does not hold in the same plot containing Cu-CO species. This fact is interpreted in terms of the difference in the nature of bonding between the electrostatic force for the sodium ion-exchanged ZSM-5 and CO system and the covalent nature for the copper ion-exchanged ZSM-5 and CO system. More detailed discussions are also made on the nature of Cu-CO bond.

VII-G-2 Preparative Study and Characterization of the *Cis*-Diamminetetranitro-Cobaltate(III) Ion — A Missing Link in the Ammine-Nitro Cobalt(III) Series

Miho FUJITA *(Nagoya City Univ.)*, **Takashi FUJIHARA** *(Saitama Univ.)*, **Masaaki KOJIMA** *(Okayama Univ.)*, **Yuzo YOSHIKAWA and Kazuo YAMASAKI, M.J.A.** *(Nagoya Univ.)*

[*Proc. Jpn. Acad.* **73B**, 161 (1997)]

The preparative conditions and stability of *cis*-$[Co(NO_2)_4(NH_3)_2]^-$, which had been a missing link in the nitro-ammine cobalt(III) series until recently, was studied using cobalt-59 NMR spectroscopy. The reaction of $Na_3[Co(NO_2)_6]$ with liquid ammonia mainly gave *cis*-$[Co(NO_2)_4(NH_3)_2]^-$ together with *mer*- and *fac*-$[Co(NO_2)_3(NH_3)_3]$ and *cis*-$[Co(NO_2)_2(NH_3)_4]^+$; the formation of *trans*-$[Co(NO_2)_4(NH_3)_2]^-$ was not observed. The reaction of aqueous $[Co(NO_2)_6]^{3-}$ with aqueous ammonia also gave the *cis*-isomer as a major product. On the contrary, the *cis*-isomer did not form during the conventional preparation from $CoCl_2$ in an aqueous solution. The *cis*-isomer was very stable in the solid state, but the isomer slowly isomerized in water ($t_{1/2}$ > 5 days at room temperature, *ca.* 0.1 mol/dm^3) to the *trans*-isomer. The reaction was accompanied by the formation of *fac*-$[Co(NO_2)_3(NH_3)_3]$ which then isomerized to the *mer*-isomer, and by the formation of several unknown species.

VII-G-3 Chromatographic Separation and Characterization of the Photoproduct of Tris(L-

cysteinesulfinato-*N,S*)cobaltate(III)

Masaaki KOJIMA *(Okayama Univ.)* **and Yuzo YOSHIKAWA**

[*J. Chromatogr. A* **789**, 273 (1997)]

The product of photolysis of K_3 (+)-[Co(L-cysi-*N,S*)$_3$] (**1**, L-cysi = L-cysteinesulfinate(2-) ion, cysi = $NH_2CH(COO^-)CH_2SO_2^-$) was separated by column chromatography on DEAE-Sephadex A-25. The main band contained [Co(L-cysi-*N,S*)$_2$(L-cysi-*N,O*)]$^{3-}$ (**2**); linkage isomerization from sulfinato-*S* to sulfinato-*O* took place. This complex (**2**) is thermally unstable and reverts to the starting complex (**1**). An anion-exchange high-performance liquid chromatographic (HPLC) method was successfully applied to the kinetic study of this linkage isomerization reaction from **2** to **1**.

VII-G-4 Stereochemistry of (*R*)-2 Methyl Aziridine Complex of Cobalt(III) and Dimerization of the Ligand

Masaaki KOJIMA *(Okayama Univ.)*, **Akiko SAKURAI** *(Okayama Univ.)*, **Mayumi MURATA** *(Okayama Univ.)*, **Kiyohiko NAKAJIMA** *(Aichi Univ. Educ.)*, **Setsuo KASHINO** *(Okayama Univ.)* **and Yuzo YOSHIKAWA**

[*J. Coord. Chem.* **42**, 95 (1997)]

A cobalt(III) complex containing (*R*)-2-methylaziridine (*R*-meaz), [Co(*R*-meaz)$(NH_3)_5]^{3+}$, was prepared and the two diastereomers arising from the presence of the chiral nitrogen atom (N(*R*) and N(*S*)) were separated by the column chromatographic method. Molecular mechanics calculations estimated the N(*R*)-isomer to be more stable. This result was supported by the X-ray structure determination of the more abundant (*ca.* 94%) isomer, N(*R*)-[Co(*R*-meaz)$(NH_3)_5]Br_3\cdot H_2O$. Crystal data: monoclinic, $P2_1$, a = 7.357(1), b = 9.780(1), c = 10.426(1) Å, β = 93.58(1)°, V = 748.7(3) Å^3, Z = 2. Kinetic studies of isomerization (epimerization) between the two isomers revealed that the inversion at the nitrogen center was very slow (5×10^{-2} M^{-1} s^{-1} at 25 °C). The small rate constant seems to be related to the strained three-membered structure of the meaz ligand. The reaction of $Na_3[Co(NO_2)_6]$ and *R*-meaz yielded a complex containing two dimerized *R*-meaz chelates, *trans*-[Co$(NO_2)_2$(di-*R*-meaz)$_2]^+$ (di-*R*-meaz = (*RR*)-α,2-dimethyl-1-aziridineethanamine). The crystal structure of *trans*-[Co$(NO_2)_2$(di-R-meaz)$_2$]-$ClO_4\cdot H_2O$ was established by the X-ray method. Crystal data: orthorhombic, $P2_12_12_1$, a = 11.784(6), b = 21.023(9), c = 8.608(7) Å, V = 2133(2) Å^3, Z = 4.

VII-G-5 Development of Site-Selective Copper-Ion-Exchanging Method of HZSM-5 by the Vapourization of Hexafluoroacetylacetonato-Copper Complex

Yasushige KURODA *(Okayama Univ.)*, **Kazunori YAGI** *(Okayama Univ.)*, **Yuzo YOSHIKAWA**, **Ryotaro KUMASHIRO** *(Okayama Univ.)* **and Mahiko NAGAO** *(Okayama Univ.)*

[*Chem.Comm.* 2241 (1997)]

The deposition of copper ion into one single ion-exchange site in HZSM-5-type zeolite was successful by using bis(1,1,1,5,5,5-hexafluoroacetylacetonato)-copper(II) as a volatile complex, and differing from the sample prepared by ion-exchanging operation, which gives a couple of bands at 2158 and 2151 cm^{-1}.

VII-G-6 A Stable Sulfonato-Cobalt(III) Complex: Δ-[Co{$OS(O)_2CH_2CH_2NH_2$-*N,O*}$(en)_2$]$(ClO_4)_2$

Mayumi MURATA *(Okayama Univ.)*, **Masaaki KOJIMA** *(Okayama Univ.)*, **Masakazu KITA** *(Naruto Univ.)*, **Setsuo KASHINO** *(Okayama Univ.)* **and Yuzo YOSHIKAWA**

[*Acta Cryst.* **C53**, 1761 (1997)]

A stable sulfonato complex, (2-aminoethanesulfonato-*N,O*)bis(ethylenediamine-*N,N'*)cobalt(III) perchlorate, [Co$(C_2H_6NO_3S)(C_2H_8N_2)_2](ClO_4)_2$, was prepared by oxidation of [Co{$OS(O)CH_2CH_2NH_2$-*N,O*}$(en)_2]^{2+}$ (en=$NH_2CH_2CH_2NH_2$) in acid media. This sulfonato complex was resolved by SP-Sephadex column chromatography and the absolute configuration of the slower eluted $(-)_{589}$-isomer was determined by X-ray analysis to be Δ.

VII-G-7 Complete Chromatographic Resolution of Axially Chiral β-Diketonate Complexes on Cellulofine C-200

Yoshiharu NAKANO *(Ibaraki Univ.)*, **Takeshi KAWAGUCHI** *(Ibaraki Univ.)* **and Yuzo YOSHIKAWA**

[*J. Coord. Chem.* **43**, 219 (1998)]

New chromatography on Cellulofine C-200 (modified polysaccharide ion exchanger) completely resolved the atropisomers reported previously [2]. The present technique needs no optically active eluting agents, differing from conventional chromatography on SP-Sephadex. The chromatographed atropisomers, axially chiral β-diketonate cobalt(III)-tren complexes, are listed in the table in the text.

VII-H Syntheses of Transition Metal-Sulfur Clusters and Development of Their Catalysis

This project focuses on the development of the new, reliable synthetic pathways affording the transition metal-

sulfur clusters with the tailored core structures in high yield, and also on the determination of the detailed structures of the novel clusters prepared in this study by the X-ray crystallography. Activation of the small molecules will be attempted by the use of polynuclear homo- or heterometallic site in these clusters to exploit the new catalytic reactions that are inaccessible by the mononuclear complex catalyst.

VII-H-1 Structures and Reactivities of Diruthenium Dithiolene Complexes and Triruthenium Sulfido Clusters Derived from a Hydrosulfido-Bridged Diruthenium Complex

Shigeki KUWATA *(Univ. Tokyo)*, **Masahiro ANDOU** *(Univ. Tokyo)*, **Kohjiro HASHIZUME** *(Univ. Tokyo)*, **Yasushi MIZOBE** *(Univ. Tokyo and IMS)* **and Masanobu HIDAI** *(Univ. Tokyo)*

[*Organometallics* **17**, 3429 (1998)]

The hydrosulfido-bridged diruthenium complex $[Cp^*RuCl(\mu_2\text{-}SH)_2RuClCp^*]$ (**1**; $Cp^* = \eta^5\text{-}C_5Me_5$) reacted with an excess of triethylamine to give the cubane-type tetraruthenium sulfido cluster $[(Cp^*Ru)_4(\mu_3\text{-}S)_4]$ through dimerization of the coordinatively unsaturated species $[Cp^*Ru(\mu_2\text{-}S)_2RuCp^*]$ (**2**) generated in situ. When the reaction was carried out in the presence of alkynes, **2** was trapped by the alkyne and the dithiolene-bridged diruthenium complexes $[(Cp^*Ru)_2(\mu_2\text{-}\eta^2\text{:}\eta^4\text{-}S_2C_2RR')]$ (**3**) were obtained. Treatment of **3** with CO afforded the carbonyl complexes $[(Cp^*Ru)(CO)(\mu_2\text{-}\eta^2\text{:}\eta^4\text{-}S_2C_2RR')RuCp^*]$ (**4**) containing a bent dithiolene ring. On the other hand, the reaction of **1** with an equimolar amount of $[RuH_2(PPh_3)_4]$ resulted in the formation of the triruthenium sulfido cluster $[(Cp^*Ru)_2(\mu_3\text{-}S)_2(\mu_2\text{-}H)RuCl(PPh_3)_2]$ (**5**). Cluster **5** reacted with an excess of $NaBH_4$ in ethanol to give the dihydrido cluster $[(Cp^*Ru)_2(\mu_3\text{-}S)_2(\mu_2\text{-}H)RuH(PPh_3)_2]$ (**6**), which was further converted to the dicarbonyl cluster $[(Cp^*Ru)_2(\mu_3\text{-}S)_2Ru(CO)_2(PPh_3)]$ (**7**) under CO. The structures have been determined in detail by the X-ray analyses for the new compounds, **3a** (R = H, R' = Bu^t), **4a** (R = H, R' = Bu^t), **5**, **6**, and **7**.

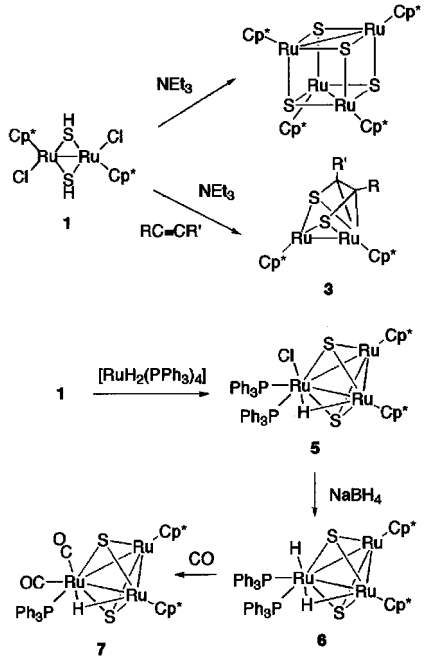

VII-H-2 Syntheses of Ruthenium Hydridotris(1-pyrazolyl)borate Complexes Having Sulfur-Donor Coligands

Yasushi MIZOBE *(Univ. Tokyo and IMS)*, **Masayuki HOSOMIZU** *(Univ. Tokyo)* **and Masanobu HIDAI** *(Univ. Tokyo)*

[*Inorg. Chim. Acta* **273**, 238 (1998)]

Treatment of $[TpRuCl(PPh_3)_2]$ (**1**; Tp = hydridotris(1-pyrazolyl)borate) with NaS_2CNMe_2 afforded the dithiocarbamate complex $[TpRu(\eta^2\text{-}S_2CNMe_2)(PPh_3)]$ in high yield, whose structure has been determined by the X-ray diffraction study. Complex **1** also reacted with a mixture of excess TolSSTol (Tol = *p*-MeC_6H_4) and Zn powder to give a novel trinuclear complex with bridging thiolate ligands $[\{TpRu(PPh_3)(\mu\text{-}STol)_2\}_2Zn]$ (**2**) in moderate yield, which has been characterized spectroscopically and by elemental analysis. Initial treatment of **1** with an equimolar amount of $AgBF_4$ followed by the reaction with a mixture of TolSSTol and Zn also resulted in the formation of **2** as the major product. However, from this reaction mixture, a dinuclear complex closely related to **2**, $[TpRu(PPh_3)(\mu\text{-}STol)_2Zn(STol)(MeOH)]$, was able to be isolated in quite a low yield, which has been fully characterized by the X-ray analysis.

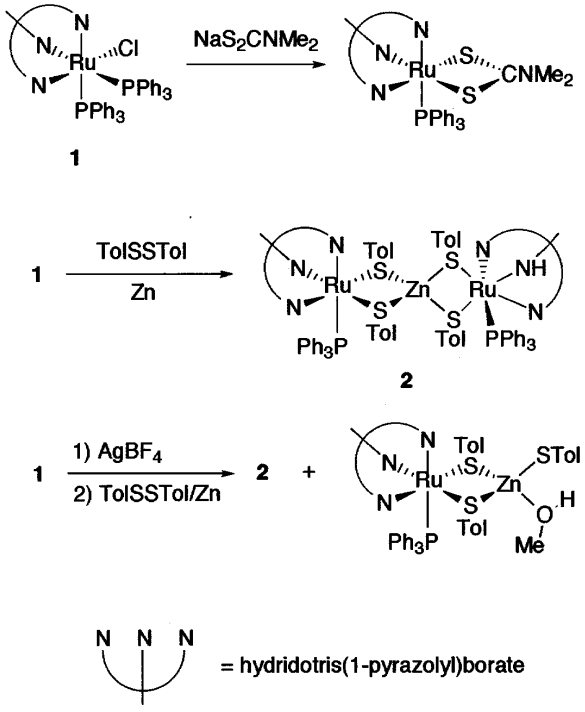

VII-H-3 Unprecedented Conversion of Benzylideneanilines into Aryl Isocyanides Promoted by a Low-Valent Molybdenum Complex. X-Ray Structure of *trans*-[Mo(CNPh)-

$(N_2)(Ph_2PCH_2CH_2PPh_2)_2$]

Goh NAKAMURA *(Univ. Tokyo)*, **Yuji HARADA** *(Univ. Tokyo)*, **Chirima ARITA** *(Univ. Tokyo)*, **Hidetake SEINO** *(Univ. Tokyo)*, **Yasushi MIZOBE** *(Univ. Tokyo and IMS)* **and Masanobu HIDAI** *(Univ. Tokyo)*

[*Organometallics* **17**, 1010 (1998)]

The molybdenum dinitrogen complex *trans*-[Mo-$(N_2)_2(dppe)_2$] (**1**; dppe = $Ph_2PCH_2CH_2PPh_2$) reacts with an excess of PhCH=NAr (Ar = Ph, *p*-MeC_6H_4, *p*-$MeOC_6H_4$) in benzene at reflux under N_2 to give novel isocyanide-dinitrogen complexes *trans*-[Mo(CNAr)-$(N_2)(dppe)_2$] (**2**) in moderate yield. The concurrent formation of benzene by the cleavage of the benzylidene C—Ph and C—H bonds have been confirmed by the GLC analysis of the reaction mixtures of **1** with PhCH=NAr (Ar = Ph, C_6H_4Me-*p*) in toluene or xylene. An X-ray diffraction study of **2** (Ar = Ph) has unambiguously disclosed the essentially linear Mo—C—N and C—N—C linkages in the PhNC ligand, which is trans to the N_2 ligand bound to the Mo atom in an end-on fashion. The reaction presumably proceeds via the iminoacyl species **3** as the key intermediate, which is formed by the oxidative addition of the benzylidene C—H bond to the coordinatively unsaturated, low-valent Mo center generated in situ from **1** upon thermolysis, although isolation or detection of **3** is still unsuccessful.

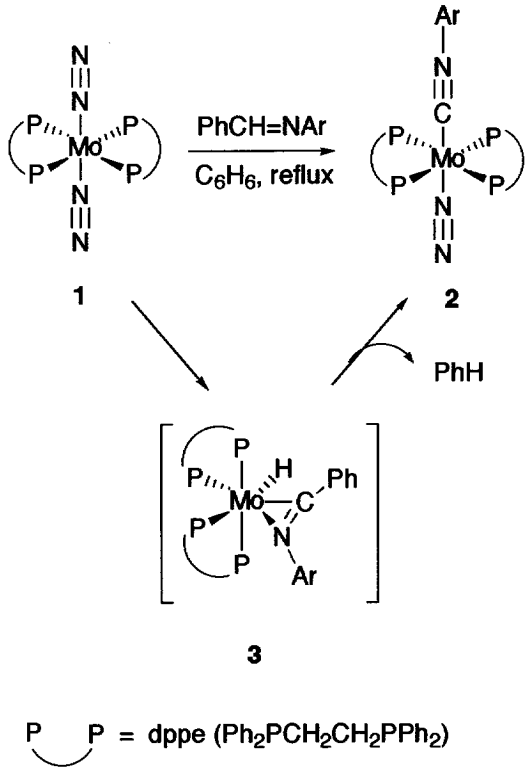

VII-I Activation of Carbon Dioxide and Energy Conversion from Proton Gradients to Electricity Mediated by Metal Complexes

An electrophilic attack of CO_2 to coordinatively unsaturated metal complexes produces M-η^1-CO_2 complexes, which can be converted to M-CO complexes as precursors to CO evolution. Metal complexes with a chelate ring that has an ability of ring-opening and -closing in a catalytic cycle of reduction of CO_2 would largely contributes the increment of thermal stability of low-valent coordinatively unsaturated metal complexes. Metal complexes used as homogeneous catalysts in the reduction of CO_2 have been desired to have a function of smooth CO evolution under mild conditions. On the other hand, reduction of M-CO bonds with depression of CO evolution in the reduction of CO_2 is expected to enable multi-electron reduction of CO_2 catalyzed by metal complexes. Thus, designing of molecular catalysts which have an ability of smooth conversion from CO_2 to CO without reductive cleavage metal-CO bonds would lead to new methodology for multi-electron reduction of CO_2 with carbon-carbon bond formation.

Biological system utilizes proton gradient for synthesis of ATP. The proton gradient (Δp) between inside and outside of a cell is depicted as the sum of electric activity ($\Delta\psi$) and chemical activity (ΔpH) components. $\Delta p = \Delta\psi - Z\Delta p$H ($Z = 2.303RT/F$). When we are concerned about chemical activity part, proton gradient is equivalent to the neutralization energy because the neutralization reaction takes place if the separating membrane is removed. Biological system creates various valuable energies from the neutralization, which, however, is just emitted as thermal energy on the disposition of waste acids or bases in industrial process. Basically, neutralization energy is originated from the binding energy of acid and base, namely is one of the chemical energies, which are able to be converted directly to valuable chemical, electric or mechanical energy in 100% efficiency in principal. Along this line, we tried to convert the neutral energy to electronic energy by using ruthenium-aqua complexes.

VII-I-1 Catalytic Generation of Oxalate through Activation of Two CO_2 Molecules on [$(IrC_p^*)_2$(Ir-η^4-$C_p^*CH_2CN$)(μ_3-S)$_2$]

Koji TANAKA, Yoshinori KUSHI, Kiyoshi TSUGE, Kiyotsuna TOYOHARA, Takanori NISHIOKA and Kiyoshi ISOBE

[*Inorg. Chem.* **37**, 120 (1998)]

Electrochemical reduction of CO_2 in the presence of $[(IrC_p^*)_3(\mu_3\text{-}S)_2](BPh_4)_2$ ($[Ir_3S_2](BPh_4)_2$) in CH_3CN at -1.30 V (*vs.* Ag/AgCl) produced $C_2O_4^{2-}$ with a current efficiency of 60%, and $[(IrCp^*)_2(Ir\text{-}\eta^4\text{-}C_p^*CH_2CN)(\mu_3\text{-}S)_2]^+$ ($[Ir_3S_2CH_2CN]^+$) was isolated from the electrolyte

solution. Crystal structure of $[Ir_3S_2CH_2CN](BPh_4)$ by X-ray analysis revealed that a linear CH_2CN group is linked at the exo-position of a C_p* ligand, and the C_p*CH_2CN group coordinates to an Ir atom with an η^4-mode. The cyclic voltammogram of $[Ir_3S_2CH_2CN]^+$ in CH_3CN under CO_2 exhibited a strong catalytic current due to the reduction of CO_2, while that of $[Ir_3S_2]^{2+}$ did not show an interaction with CO_2 in the same solvent. Thus, the reduced form of $[Ir_3S_2CH_2CN]^+$ works as the active species in the reduction of CO_2. The IR spectra of $[Ir_3S_2CH_2CN]^+$ in CD_3CN showed a reversible adduct formation with CO_2. The controlled potential electrolysis of $[Ir_3S_2CH_2CN]^+$ at -1.50 V under CO_2 evidenced the generation of $C_2O_4^{2-}$ through a 1:2 adduct between $[Ir_3S_2CH_2CN]^0$ and CO_2. A coupling reaction of two CO_2 molecules activated on adjacent μ_3-S and Ir in $[Ir_3S_2CH_2CN]^0$ is proposed for the first selective generation of $C_2O_4^{2-}$.

VII-I-2 Selective formation of $HCOO^-$ and $C_2O_4^{2-}$ in Electrochemical Reduction of CO_2 Catalyzed by Mono- and Dinuclear Ruthenium Complexes

Md. Meser ALI *(Mie Univ.)*, **Hiroyasu SATO** *(Mie Univ.)*, **Tetsunori MIZUKAWA, Kiyoshi TSUGE, Masa-aki HAGA and Koji TANAKA**

[*J. Chem. Soc., Chem. Commun.* 249 (1998)]

A key process for the activation of CO_2 on metals is how to create coordinatively unsaturated low valent metal centers under mild conditions. The first catalytic oxalate formation in the reduction of CO_2 catalyzed by $[(CpM)_3(\mu_3\text{-}S)_2]^{2+}$ (M = Co, Rh, Ir) is ascribed to creation of the reaction sites by an M-M bond cleavage upon the two electron reduction of these M_3S_2 clusters. Metal complexes with unsymmetrical chelating rings may also provide sites for activation of CO_2 by dechelation in the electrochemical reduction of CO_2. We introduced 2,2'-bis(1-methylbenzimidazo-2-yl)-4,4'-bipyridine (dmbbbpy) as an unsymmetrical chelating ligand into a $Ru(bpy)_2$ moiety to aim not only creation of reaction sites by opening of the chelate ring but also accumulation of electrons into the ligand required in the reduction of CO_2. Indeed, electrochemical reduction of carbon dioxide catalyzed by mono- and dinuclear ruthenium complexes produced HCOOH with a trace amount of CO and $C_2O_4^{2-}$ in the presence and absence of H_2O, respectively, in CH_3CN.

$[Ru(bpy)_2(dmbbbpy)](PF_6)_2$ (**1**) and dinuclear $[(bpy)_2Ru(dmbbbpy)Ru(bpy)_2](PF_6)_4$ (**2**) were synthesized by the reaction of $Ru(bpy)_2Cl_2$ with dmbbbpy with mole ratios of 1:1 and 2:1 respectively in ethyleneglycol. The controlled potential electrolysis of **1** and **2** (0.2-0.3 mmol/dm^{-3}) at -1.65 and -1.55 V (vs Ag/AgCl) was conducted in CO_2 saturated CH_3CN (20 ml) in the presence of H_2O (0.5 ml). After 80 C was passed in the electrolysis of **1**, $HCOO^-$ was produced with a current efficiencies (η) of 90% together with a trace amount of CO (η = 2~3%). On the other hand, the similar electrochemical reduction of CO_2 in dry CH_3CN selectively produced oxalate with an η of 60% without forming $HCOO^-$ and CO after 90 C was passed in the electrolysis. The electrochemical reduction of CO_2 catalyzed by **2** also generated almost selectively $HCOO^-$ (η = 90%) and $C_2O_4^{2-}$ (η = 70%) in the presence and the absence of H_2O, respectively, under the similar conditions.

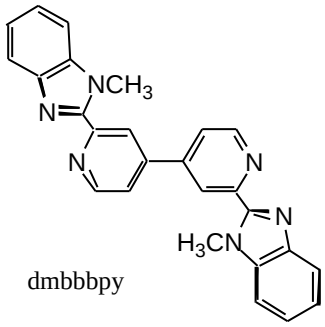

dmbbbpy

VII-I-3 Stabilization of $[Ru(bpy)_2(CO)(\eta^1\text{-}CO_2)]$ and Unprecedented Reversible Oxide Transfer Reactions from CO_3^{2-} to $[Ru(bpy)_2(CO)_2]^{2+}$ and from $[Ru(bpy)_2(CO)(\eta^1\text{-}CO_2)]$ to CO_2

Hiroshi NAKAJIMA, Kiyoshi TSUGE, Kiyotsuna TOYOHARA and Koji TANAKA

[*J. Organometallic Chem.* **569**, 61 (1998)]

Metal complexes with an η^1-CO_2 group are generally considered to be extremely labile to air, moisture and temeperature. Thermal stability of metal-η^1-CO_2 bonds will be improved by an increase of an electron donor ability of central metals, since a metal-η^1-CO_2 bond is formed by overlap of the filled dz^2 orbital of d^8 metals and the empty CO_2 π* orbital. Unusual thermal stability of $[Ru(bpy)_2(CO)(\eta^1\text{-}CO_2)]$ (**1**) as a metal-η^1-CO_2 complex was examined both in the solid state and in solutions. **1** dissolves in CH_3CN containing $LiCF_3SO_3$. Interaction between Li^+ and the η^1-CO_2 group enhances an electron flow from Ru to the CO_2 ligand and greatly contributes to the stabilization of the Ru-η^1-CO_2 bond. The reaction of $[Ru(bpy)_2(CO)_2](PF_6)_2$ with $[Crown{\cdot}K]_2CO_3$ in dry CH_3CN selectively produced **1** through the 1 : 1 adduct with the RuC(O)-OCO_2 moiety. Stoichimetric formation of **1** from the 1 : 1 adduct is also assisted by $[Crown.K]^+$ as a Lewis acid. Similarly, the reaction of $[Ru(bpy)_2(CO)_2](PF_6)_2$ with $(Me_4N)_2CO_3$ in DMSO gave the 1:1 adduct in the initial stage, which gradually changed to a metalloanhydride complex, $[Ru(bpy)_2(CO)((CO)_2O)]$ due to the absence of Lewis acids to stabilize **1**, since an addition of $LiCF_3SO_3$ to the solution gave $[Ru(bpy)_2(CO)(\eta^1\text{-}CO_2)]$ quantitatively.

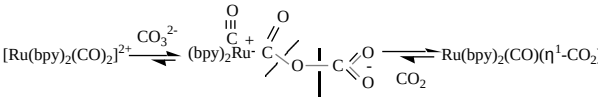

VII-I-4 Synthesis and Characterization of Ruthenium Terpyridine Dioxolene Complexes: Resonance Equilibrium between Ru^{III}-Catechol and Ru^{II}-Semiquinone Forms

Masato KURIHARA, Stephane DANIELE, Kiyoshi

TSUGE, Hideki SUGIMOTO and Koji TANAKA

[*Bull. Chem. Soc. Jap.* **71**, 867 (1998)]

A series of [RuX(dioxolene)(terpy)] (terpy = terpyridine; X = Cl, OAc) and one-electron oxidized complexes were prepared. The molecular structures of [RuCl($O_2C_6H_2$-3,5-Bu_2)(terpy)] (**1**) and [Ru(OAc)-($O_2C_6H_4$)(terpy)] (**3**) were determined by X-ray crystallography. Crystal data for **1**: monoclinic, space group $P2_1/c$, Z = 8, a = 11.548(1) Å, b = 18.224(5) Å, c = 30.002(8) Å, β = 96.51(2)°, and R = 0.077 (Rw = 0.068). Crystal data for **3**: monoclinic, space group C_2/c, Z = 8, a = 13.355(5) Å, b = 12.131(4) Å, c = 26.645(4) Å, β = 92.46(2)°, and R = 0.041 (Rw = 0.041). Although the binding mode of $O_2C_6H_2$-3,5-Bu_2 to Ru was not determined by the molecular structure of **1**, the carbon-oxygen and carbon-carbon bond lengths of $O_2C_6H_4$ in **3** were consistent with those of catecholato ligands. Electronic absorption spectra of [RuX(dioxolene)-(terpy)] were explained by the electronic structure of [Ru^{II}X(semiquinone)(terpy)] rather than [Ru^{III}X-(catecholato)(terpy)], while the reverse assignment was deduced from the IR spectra. Moreover, ESR spectra showed hyper-fine structures due to contribution of semiquinone superimposed on an axial pattern of the Ru(III) center indicating a resonance equilibrium between [Ru^{II}X(semiquinone)(terpy)] and [RuX-(dioxolene)(terpy)].

VII-I-5 Novel Intramolecular Rearrangement of Hepta-Coordinate Rhenium(V) Complex with Catecholato and Terpyridine Ligands

Hideki SUGIMOTO, Kiyoshi TSUGE and Koji TANAKA

[*Chem. Lett.* 719 (1998)]

An addition of $ReCl_3$(tpy) to a methanol solution containing 3,6-di-tert-butyl-catechol and triethylamine gave a clear blue-black solution. After exposure of the solution to air at room temperature and then the addition of NH_4PF_6 to the solution resulted in precipitation of [Re(tpy)(diBucat)$_2$]PF_6·CH_3CN ([**1**]PF_6·CH_3CN).

The ^{1}H NMR spectra of [**1**]$^+$ in CD_2Cl_2 reveal fluctuation of the catecholate ligands. Aromatic protons of two diBucat ligands emerge as two sharp singlet signals (δ = 6.98 and 6.67 ppm) at -20 °C. Despite the non-equivalence of 4,5-protons of diBucat containing O(1) and O(2), the appearance of the singlet signal is probably caused by an incidental agreement of the chemical shifts of the two protons. The two singlets broaden with increasing temperatures, and coalesced to one broad signals at 50 °C. On the other hand, no fluctuation was observed in the proton signals of tpy in the temperature range. Such chracteristic behavior of the proton signals of the diBucat and tpy ligands of [**1**]$^+$ is explained by the exchange of O(3) and O(1) in the equatorial position between two diBucat ligands. This is the first example of dynamic behavior between two mono-capped trigonal prism structures of hepta-coordinate metal complexes. Detailed thermodynamic behavior and parameters will be discussed in elsewhere.

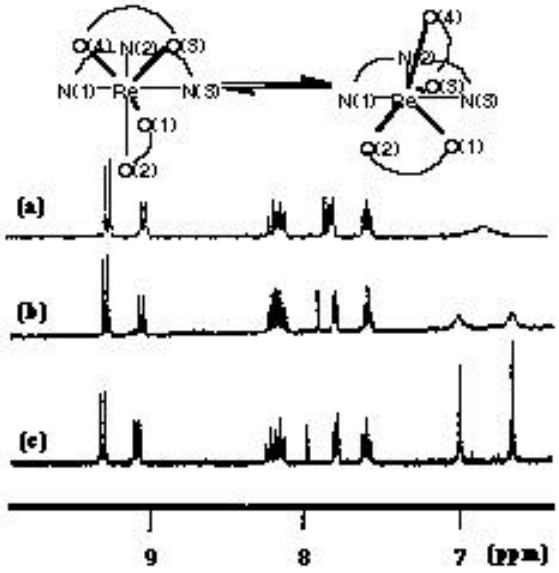

Figure 1. Temperature Dependent ^{1}H NMR spevtra of the complex [**1**]$^+$ in CD_2Cl_2; (a) 50°C, (b) 30°C, (c) -20°C.

VII-I-6 First Artificial Energy Conversion from Proton Gradient to Electricity

Kiyoshi TSUGE and Koji TANAKA

[*Chem. Lett.* 1069 (1998)]

Metal-aqua complexes are representative candidates for accumulation of proton gradient energy because they are expected to be converted to the corresponding hydroxy- and oxo-complexes by acid-base equilibria (eq 1), and the redox potentials of complexes change as

$$[M(H_2O)] \rightleftharpoons [M(OH)]^- \rightleftharpoons [M(O)]^{2-} \quad (1)$$

release of protons. We prepared the ruthenium-aqua complex having a redox active quinone ligand, [Ru-(trpy)(3,5-di-tert-butylquinone)$(H_2O)]^{2+}$ ([Ru-$H_2O]^{2+}$) to avoid dimerization and polymerization of hydroxy- and oxo complexes. The cyclic voltammogram (CV) of [Ru-$H_2O]^{2+}$ in acetone. [Ru-$H_2O]^{2+}$ undergoes two reversible redox couples at $E_{1/2}$ = -0.47 V and $E_{1/2}$ = 0.38V ($E_{1/2}$ = (E_{pc} + E_{pa})/2), which are assigned to the [Ru-$H_2O]^{0/+}$ and [Ru-$H_2O]^{+/2+}$ couples, respectively. When 0.7 equivalent of OH^- was added to the solution, the rest potential of the solution (Vrest) shifted from 0.60 V to 0.30 V across the $E_{1/2}$ of the [Ru-$H_2O]^{+/2+}$ couple (Figure 1b). At the same time, new redox couples appeared at $E_{1/2}$ = -0.80V and 0.00V assignable to the [Ru-$OH]^{0/+}$ and [Ru-$OH]^{+/2+}$ couples.

$$[Ru\text{-}H_2O]^{2+} + OH^- \rightarrow [Ru\text{-}OH]^+ + H_2O \quad (2)$$

$$[Ru\text{-}H_2O]^{2+} + [Ru\text{-}OH]^+ \rightarrow [Ru\text{-}H_2O]^+ + [Ru\text{-}OH]^+ \quad (3)$$

Further addition of OH^- caused deprotonation of [Ru-$OH]^{2+}$ to produce [Ru-O] (eq 4), which equilibrates with the reactant (eq 5).

$$[Ru\text{-}OH]^{2+} + OH^- \rightarrow [Ru\text{-}O]^+ + H_2O \quad (4)$$

$$[Ru\text{-}OH]^{2+} + [Ru\text{-}O]^+ \rightarrow [Ru\text{-}OH]^+ + [Ru\text{-}O]^+ \quad (5)$$

These redox reactions of this ruthenium aqua complex coupled with acid-base reactions enable the energy conversion from proton gradient to electricity. The energy conversion was conducted with two compartment cells (I and II) separated by an anion exchange membrane filled with an acetone solution of

$[Ru\text{-}H_2O]^{2+}$ (7.0 mmol/15 ml in each cell). Upon an addition of 1.6 equivalent of OH^- to cell(I), $[Ru\text{-}H_2O]^+$ and $[Ru\text{-}OH]^+$ formed and Vrest shifted from 0.60V to -0.13 V (eqs 2-5). The connection of two cells induced current flow from the cell(II) to cell(I). At the end of the discharge (12 hr later), Vrest of two cells were 0.33 ± 0.02 V, and 0.50 C of electricity was obtained. Because the only difference between two cells is the amount of OH^-, pH gradient produces electric energy with this complex. Thus the proton gradient is catalytically converted to electricity by ruthenium aqua complex $[Ru(trpy)(3,5\text{-di-tert-butylquinone})(H_2O)]^{2+}$. The first successful energy conversion from proton gradient to electricity is based on the redox reactions of this ruthenium complex coupled with acid-base reaction.

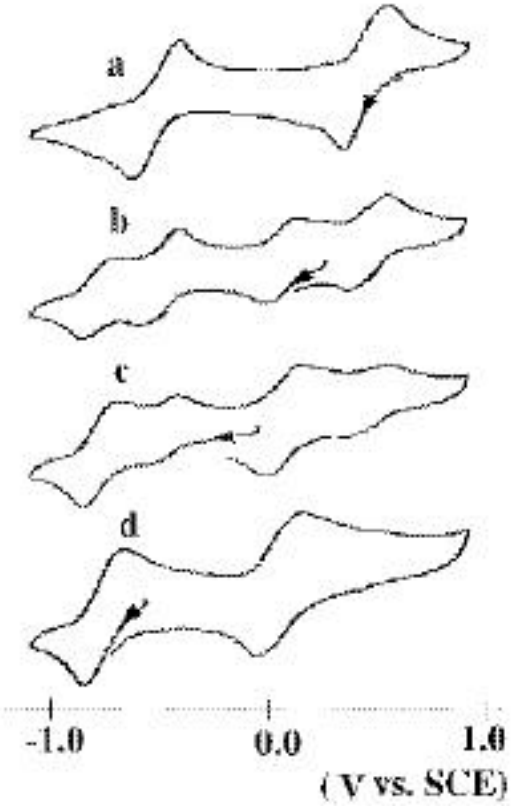

Figure 1. CV of $[Ru(H_2O)]^{2+}$ (a) in the presence of 0 (a), 0.7 (b), 1.3 (c) and 2.0 (d) equiv of OH^- in acetone.

VII-I-7 Two-Electron Reduction of $[\{(bpy)_2Ru(dmbbbpy)\}_3Ru]^{8+}$ from $(BNA)_2$ via Photoinduced Electron Transfer [dmbbbpy = 2,2'-Bis-(N-methylbenzimidazole-2-yl)-4,4'-bipyridine]

Md. Meser ALI *(Mie Univ.)*, **Hiroyasu SATO** *(Mie Univ.)*, **Koji TANAKA, Masa-aki HAGA, Akio YOSHIMURA** *(Osaka Univ.)* **and Takeshi OHNO** *(Osaka Univ.)*

[*Inorg. Chem.* in press]

Photoirradiation ($\lambda > 500$ nm) of $[\{(bpy)_2Ru(dmbbbpy)\}_3Ru]^{8+}$ ($\mathbf{1}^{8+}$) (dmbbbpy = 2,2'-Bis(N-methylbenzimidazole-2-yl)-4,4'-bipyridine and bpy = 2,2'-bipyridine) in the presence of dimeric N-benzyldihydronicotinamide, $(BNA)_2$ produced stable two-electron reduced species ($\mathbf{1}^{6+}$). Laser flash photolysis and emission spectroscopy were used to understand the reductive reaction pathways. The emission quenching k_q value (4.1×10^9 $M^{-1}s^{-1}$) obtained from Stern-Volmer plot is in excellent agreement with the electron transfer rate constant, k_{et} (4.7×10^9 $M^{-1}s^{-1}$) determined from the decay kinetics of transient $^3\mathbf{1}^{8+}$ triplet-triplet absorption at 650 nm indicating that photoreduction of $\mathbf{1}^{8+}$ proceeds via photoinduced electron transfer from $(BNA)_2$ to $^3\mathbf{1}^{8+}$*. After bimolecular electron transfer process, $\mathbf{1}^{8+}$ was reduced to $\mathbf{1}^{7+}$ and electron donor $(BNA)_2$ was oxidized. Oxidation of $(BNA)_2$ leads to the formation of highly reactive species, $BNA^{\cdot}$ which then reduces $\mathbf{1}^{7+}$ to $\mathbf{1}^{6+}$. The quantum yield for the formation of the photoreduction product was 0.026.

VII-I-8 Selective Production of Acetone in Electrochemical Reduction of CO_2 Catalyzed by Ru-Naphthyridine Complex

Tetsunori MIZUKAWA, Kiyoshi TSUGE, Hiroshi NAKAJIMA and Koji TANAKA

[*Angew. Chem.* in press]

Metal catalyzed reductive disproportionation of CO_2 proceeds through oxide transfer from metal-CO_2 to CO_2 followed by reductive cleavage of the resultant metal-CO bond. Acylation of the metal-CO bond derived from metal-CO_2 prior to CO evolution (eq 1),

$$[M\text{-}CO_2]^{n+} + CO_2 \rightarrow [M\text{-}CO]^{(n+2)+} + CO_3^{2-} \quad (1)$$

therefore, leads to new methodology for carbon-carbon bond formation in the reduction of CO_2. Polypyridyl ruthenium carbonyl complexes such as $[Ru(bpy)_2(quinoline)(CO)]^{2+}$ and $[Ru(bpy)(terpyridine)(CO)]^{2+}$ work as catalysts for the reduction of CO_2 of eq 1, and one electron reduction of these complexes causes bathochromic shift of their ν(CO) bands about by 30 - 40 cm^{-1}. The mono naphthyridine complex, $[Ru(bpy)_2(napy)(CO)](PF_6)_2$ (**1**) (napy = 1,8-naphthyridine-κN), undergoes pronounced bathochromic shift of the n(CO) band (Δ = 418 cm^{-1}) upon one-electron reduction due to a nucleophilic attack of the non-bonded nitrogen of monodentate napy to the carbonyl carbon (eq2).

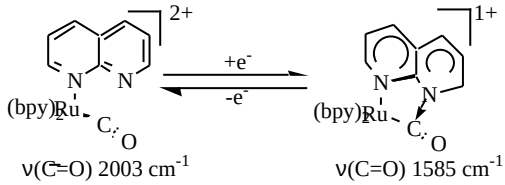

(2)

Such metallacyclization would suppress the reductive cleavage of the Ru-CO bond (CO evolution), and enable reduction of the CO group derived from CO_2.

Only CO and Li_2CO_3 were produced in the controlled potential electrolysis of **2** (0.6 mmol dm^{-3}) at -1.65 V (vs. Ag/Ag^+) with a glassy carbon (GC) electrode (4 cm^2) in CO_2-saturated DMSO (30 cm^3) containing $LiBF_4$ (0.1 mol dm^{-3}) as an electrolyte. On the other hand, when $(CH_3)_4NBF_4$ was used as an electrolyte under otherwise the same conditions, $CH_3C(O)CH_3$ was selectively generated with a trace amount

of CO. Besides these products, $(CH_3)_3N$ and $\{(CH_3)_4N\}_2CO_3$ were formed and no other product was detected in the solution. Thus, $(CH_3)_4N^+$ works as not only an electrolyte but also a methylation reagent for the catalytic generation of acetone in the electrochemical reduction of CO_2 catalyzed by **2** (eq 3). Based on the stoichiometry of eq 3, the curren

$$2CO_2 + 4e^- + 2(CH_3)_4N^+ \rightarrow CH_3C(O)CH_3 + CO_3^{2-} + 2(CH_3)_3N \quad (3)$$

efficiency of acetone was 70% at 100 C (turnover number 8.5) and that of CO was less than 1%.

VII-I-9 Basicity of μ_3-X and η^1-Y Ligands (X, Y = S, Se) of Reduced, Oxidized and Super-Oxidized Forms of $[Fe_4X_4(YAd)_4]^{2-}$ (Ad = 1-adamantane) in Aqueous Solutions

Masami NAKAMOTO, Kenji FUKAISHI, Tsuyoshi TAGATA, Hide KAMBAYASHI and Koji TANAKA

A series of $[Fe_4X_4(YAd)_4]^{2-}$ (X, Y= S, Se; Ad= 1-adamantane) were prepared as a model of high potential iron-sulfur proteins. Hydrolysis of those clusters were efficiently depressed in aqueous poly[2-dimethylamino-(hexanamide)] (PDAH) solutions due to the enbedding effect in hydrophobic environment and/or inhibition of dissociation of the terminal ligand into the aqueous media. Cyclic voltammetry of the clusters in aqueous PDAH solutions showed pH dependent redox potentials of not only $[Fe_4X_4]^{+/2+}$ but also $[Fe_4X_4]^{2+/3+}$ (X, Y = S and Se) couples, resulting from redox-linked protonation reactions of three oxidation states of $[Fe_4X_4(YAd)_4]^{n-}$ (n = 1- 3). pK Values of the reduced, oxidized, and super-oxidized forms of $[Fe_4X_4(YAd)_4]^{2-}$ were determined by computer simulation of the pH dependent redox potentials. The basicity of the μ_3-X cores (X= S and Se) of three oxidation states of $[Fe_4X_4(YAd)_4]^{n-}$ (n = 1, 2, 3) is stronger than the YAd (Y = S and Se) ligands: in the case of the mono-protonated $[Fe_4X_4(YAd)_4]^{3-}(H^+)$ and $[Fe_4X_4(YAd)_4]^{2-}(H^+)$, basicity of the η^1-Y ligand of $[Fe_4X_4(YAd)_4]^{2-}(H^+)$ becomes stronger than that of μ_3-X cores, although the μ_3-X cores of $[Fe_4X_4(YAd)_4]^{3-}(H^+)$ still show stronger basicity compared with those of η^1-Y ligands.

VII-J Supramolecular Self-Assembly through Coordination

Supramolecular self-assembly refers to the spontaneous generation of well-defined structures from component molecules under a well-defined set of conditions. Since 1990, we have been studying the self-assembly of finite and infinite structures based on coordination chemistry, where coordinate bonds induce the generation of defined structures. Our studies are focused on the self-assembly of such finite structures as macrocycles, catenanes (interlocked molecules), and cages, as well as infinite network structures. In the construction of the discrete structures, our strategy may be characterized by the use of palladium's 90 degree coordination angle because synthetic chemists have never employed this angle to constructed their target structures.

VII-J-1 Made-to-Order Assembling of [2]Catenanes from Palladium(II)-Linked Rectangular Molecular Boxes

Makoto FUJITA, Masaru AOYAGI *(Grad. Univ. Adv. Stud.)*, **Fumiaki IBUKURO** *(Grad. Univ. Adv. Stud.)*, **Katsuyuki OGURA** *(Chiba Univ.)* **and Kentaro YAMAGUCHI** *(Chiba Univ.)*

[*J. Am. Chem. Soc.* **120**, 611 (1998)]

Linked-ring molecules or catenanes have long intrigued chemists because mechanically connected structures are expected to show unique properties which chemically connected molecules have never possessed. An ideal methodology for catenane synthesis should allow chemists to design and prepare a variety of catenanes in quantitative yields without synthetic difficulties. Here we show such an ideal catenane synthesis can be provided by metal-mediated supramolecular self-assembly. That is, designed molecular boxes composed of transition metals and organic ligands are quantitatively catenated if the boxes involve parallelly arranged aromatic sides with the interplane separation of ca 3.5 Å. Thus eight building blocks — four metals and four ligands — are found to self-assemble into [2]catenanes **1** and **2** consisting of two rectangular molecular boxes.

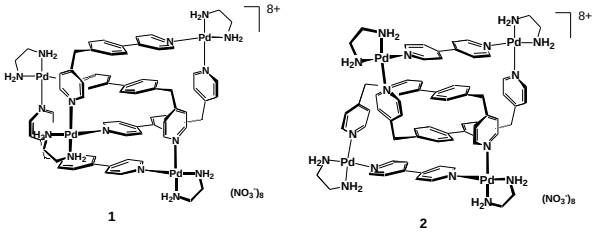

1 **2**

VII-J-2 Self-Assembled Molecular Ladders

Makoto FUJITA, Osamu SASAKI *(Chiba Univ.)*, **Kenya WATANABE** *(Chiba Univ.)*, **Katsuyuki OGURA** *(Chiba Univ.)* **and Kentaro YAMAGUCHI** *(Chiba Univ.)*

[*New. J. Chem.* 189 (1998)]

Coordination of a pyridine-based bridging ligand, 1,4-bis(4-pyridylmethyl)benzene, with cadmium nitrate afforded an infinite ladder complex, the unit structure of which involves a T-shaped assembly of three pyridine rings about a heptacoordinated Cd(II) atom. The ladder structure was found to expand its cavity volume by enclathrating *p*-dibromobenzene in the cavity. Nearly orthogonal interpenetration of infinite ladders was observed in the solid structure.

VII-J-3 Coordination Polymers Self-

Assembling from Cadmium(II) Ions and Flexible Pyridine-Based Bridging Ligands

Makoto FUJITA, Masaru AOYAGI *(Grad. Univ. Adv. Stud.)* **and Katsuyuki OGURA** *(Chiba Univ.)*

[*Bull. Chem. Soc. Jpn.* **71**, 1799 (1998)]

This paper describes coordination polymers assembling from cadmium nitrate and flexible bridging ligands, Py-X-Py (Py = 4-pyridyl, **1a**: X = CH_2, **1b**: X = $C(=CH_2)$, **1c**: X = CH_2CH_2). Single X-ray analysis of these complexes showed that their infinite topologies are quite different from each other despite the structural similarity of ligands **1a**-**1c**. Upon treatment with $Cd(NO_3)_2$, **1a** gave a sheet structure of an infinite two-dimensional network with a stoichiometry of ML_2 (M and L denote metal and ligand, respectively). Ligand **1b** also afforded an infinite polymer possessing the same ML_2 composition. However the polymer structure is characterized by a one-dimensionally bounded macrocyclic frameworks where adjacent Cd ions are linked by two ligand molecules. Interestingly, ligand **1c** gave an infinite polymer of $ML_{1.5}$ composition whose structure was shown to be a unique one-dimensional framework having macrocyclic frameworks (M_2L_2) linked by different L molecules.

VII-J-4 Nanometer-Sized Macrotricyclic Complexes Self-Assembled from Ten Small Component Molecules

Makoto FUJITA, Shu-Yan YU, Takahiro KUSUKAWA, Hidenori FUNAKI *(Chiba Univ.)*, **Katsuyuki OGURA** *(Chiba Univ.)* **and Kentaro YAMAGUCHI** *(Chiba Univ.)*

[*Angew. Chem. Int. Ed. Engl.* **37**, 2082 (1998)]

Self-assembly of nanoscale, highly positive charged macrotricycles **1** and **2** with a general formula of $[M_6L_4]^{12+}$ (where M = (en)Pd(II), L = tripyridyl ligands) is described. Both complexes have macrotricyclic structures with the dimension of *ca.* 3 nm × 2 nm × 2 nm which were unambiguously determined by X-ray crystallographic analysis. Having large hydrophobic cavities, they showed unique ability for molecular recognition of aromatic carboxylate ions. A proposed pathway leading to the $[M_6L_4]^{12+}$ macrotricycles involves an intermediate macrocycle $[M_2L_2]^{4+}$ which was isolated in a related system and structurally characterized by X-ray analysis.

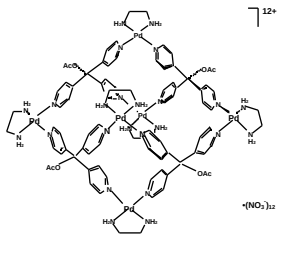

1

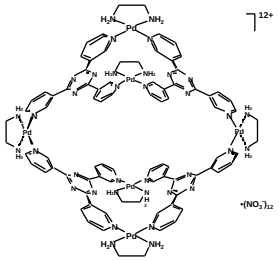

2

VII-J-5 Encapsulation of Large, Neutral Molecules in a Self-Assembled Nanocage Incorporating Six Palladium(II) Ions

Takahiro KUSUKAWA and Makoto FUJITA

[*Angew. Chem.* **110**, 2192 (1998)]

The synthesis of hollow, nanometer-scale molecular "container compounds" makes possible the creation of localized chemical micro-environments with properties different from those of the bulk phases. Recently, a hollow, roughly spherical nanocage framework (**1**, ca 2 nm in diameter) was constructed by self-assembly from ten species, four organic ligands held together by six metal ions.[1] Herein reported is binding property of nanocage 1 with large guest molecules. It is shown that self-assembled cage **1** can hold as many as four adamantane molecules inside its nanosized cavity. Thus efficient formation of $\mathbf{1}\cdot\mathbf{G}_4$ complex (**G** = adamantane) in a two-phase system was observed when D_2O solution of **1** was stirred with saturated hexane solution of adamantane at 60°C (Figure 1). Cage compound **1** also encapsulates as many as four molecules of o-carborane (8 Å in diameter). A large guest, 1,3,5-tri-tert-butylbenzene, once encapsulated through thermally-activated slippage, cannot escape from the cavity at room temperature since its dimension is slightly larger than that of the cavity entrance.

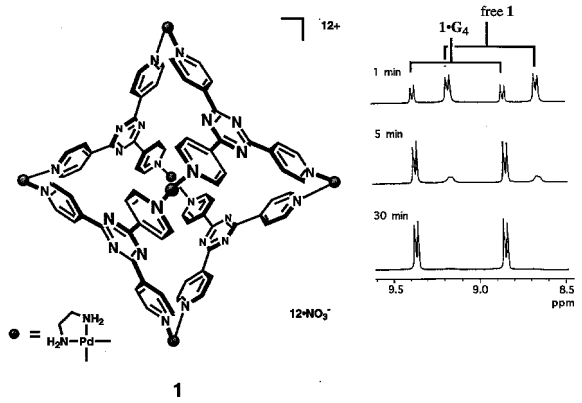

1

Figure 1. Time-dependent NMR observation of aq phase in the formation of $\mathbf{1}\cdot\mathbf{G}_4$ complex through liquid-liquid extraction (aq phase: D_2O solution of **1**; org phase: saturated hexane solution of **G**.)

VII-J-6 A Thermally Switchable Molecular Lock. The Guest-Templated Synthesis of a Kinetically Stable Nano-Sized Cage

Fumiaki IBUKURO *(Grad. Univ. Adv. Stud.)*, **Takahiro KUSUKAWA and Makoto FUJITA**

[*J. Am. Chem. Soc.* **120**, (1998)]

Metal-containing supramolecules are in general labile and not tolerant under acidic, basic, or nucleophilic conditions because they self-assemble as a result of thermodynamic equilibration. If the self-assembled structures can be converted to kinetically inert structures, then supramolecules in thermodynamic

equilibration can be trapped into kinetically stable forms. Such a conversion was achieved by exploiting the dual character of a Pt(II)-pyridine coordinate bond which is inert but temporally becomes labile by thermal stimuli. Thus, stable nano-sized cage complex **1** self-assembled under thermal stimuli and converted into an inert (stable) form by turning off the thermal stimuli. A large guest molecule showed remarkable template effect for the conversion. In addition, the complete switching of the binding property of cage **1** by pH control was achieved.

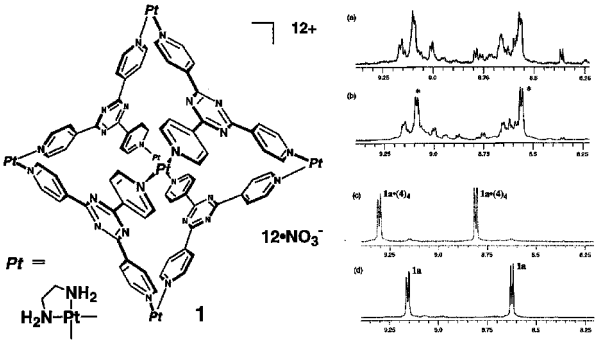

Figure 1. The ^{1}H NMR observation of the guest template synthesis of **1a** (500 MHz, D_2O, 25°C, TMS as an external standard). (a) A kinetically distributed oligomer mixture. (b) After 24 h at 100°C. Main peaks (*) assignable to 1a appear at δ 9.08 and 8.56, which are slightly upfield shifted (by ca 0.05 ppm) from those of empty **1a** presumably due to some interactions with other oligomer components. (c) After 24 h at 100°C in the presence of guest **4** (4 equiv). Signals appearing at δ = 9.31 and 8.81 are assigned to **1a**·(**4**)$_4$ and slightly downfield shifted from those of empty **1a**. (d) Empty cage **1a** obtained after the removal of guest **4** (acid form) by extraction with $CHCl_3$.

VII-J-7 Spontaneous Assembling of Ten Small Components into a Three-Dimensionally Interlocked Compound Consisting of the Same Two Cage Frameworks

Makoto FUJITA, Norifumi FUJITA *(Grad. Univ. Adv. Stud.)***, Katsuyuki OGURA** *(Chiba Univ.)* **and Kentaro YAMAGUCHI** *(Chiba Univ.)*

Recent developments in noncovalent syntheses are partly thanks to the achievement of the efficient syntheses of catenanes by metal-templating as well as by self-assembly. While a catenane framework stems form the topological isomerism of two rings, no example has been reported to date for an interlocked molecule arising from the isomerism of two cages. Here, we show that such a three-dimensionally interlocked compound consisting of two cages, as schematically shown in Figure 1a, is easily prepared by metal-mediated self-assembly. The framework of each cage is self-assembled from five components, two different exo-tridentate ligands held together with three metal ions. The cage framework possesses an interplanar separation with a distaince ideal to bind an aromatic ring. Thus, the two cage units efficiently bind each other through the formation of an efficient quadruple aromatic stack giving rise to a ten-component self-assembly into an unprecedented three-dimensionally interlocked molecule **1**.

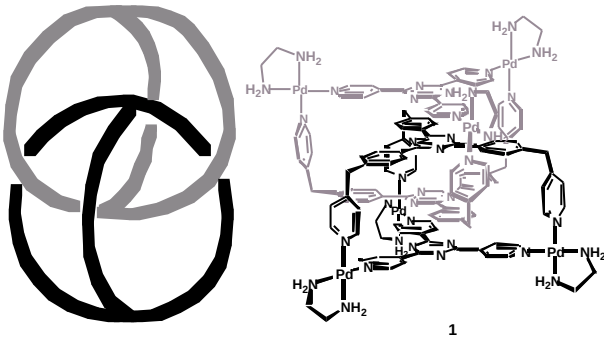

VII-J-8 A Nonometer-sized Hexahedral Coordination Capsule Assembled from Eighteen Metal Ions and Six Triangular Organic Ligands

Nobuhiro TAKEDA *(CREST, Science and Technology Corporation (JST) and IMS)***, Kentaro YAMAGUCHI** *(Chiba Univ.)* **and Makoto FUJITA**

Molecular cupsules create isolated microspace inside their frameworks where molecules, once encapsulated, cannot interact with any outside species. In such isolated space, the properties of molecules change and, for example, otherwise unstable molecules can be remarkably stabilized. Here we report the transition metal-induced assembly of a stable, nanometer sized coordination capsule **1** from twenty-four small components, eighteen metals and six triangular organic ligands. Cupsule **1** is roughly hexahedral and made up of six edge-sharing triangles with two metal ions at each side. The triangular unit is composed of four coplanar armatic rings. Thus, totally twenty-four aromatic rings surround the large cavity of capsule **1** making a closed shell structure with small pinhalls through which ordinary organic molecules can never come in nor escape.

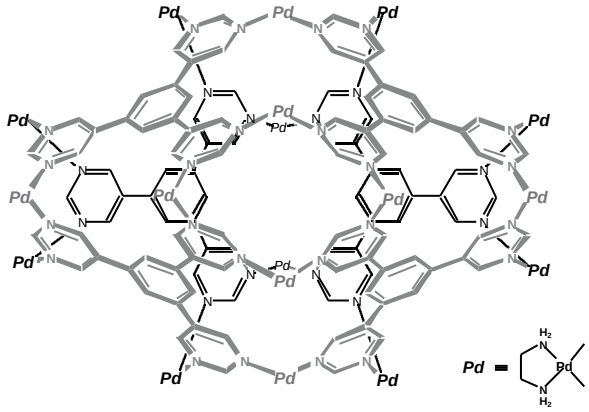

1

VII-J-9 "Ship-in-a-Bottle" Formation of Stable Hydrophobic Dimers of cis-Azobenzene and -Stilbene Derivatives in a Self-Assembled Coordination Nanocage

Takahiro KUSUKAWA and Makoto FUJITA

Stabilization and activation of molecules in the cavity of cage-like molecules have been receiving increasing attention. A recent rapid progress in this field is partly owing to the development of facile preparation of cage compounds by non-covalent synthesis exploiting hydrogen and coordination bonds. Nano-sized coordination cage **1**, recently constructed by transition metal-mediated self-assembly, has been shown to enclathrate large newtral guest molecules. Here we report the selective enclathration of "C-shaped" molecules such as cis-azobenzene and -stilbene derivatives by cage **1**. These guest molecules are enclathrated in the cavity through the "ship-in-a-bottle assembly" into a hydrophobically interacted dimer with a topology reminiscent of Rebek's hydrogen bonded "tennis ball" (eq 1). We also show that the hydrophobic dimers of azobenzene derivatives are considerably stabilized and do not undergo cis-trans isomerization.

VII-K Synthesis and Reactivity of Complexes Containing Peculiar Bonds between Transition Elements and Main Group Elements of Group 14

The bonds between transition elements and main group elements are attracting increasing attention in recent years. This is attributable not only to the great variety of the combination of elements but also to the peculiarity of their physical and chemical properties. We focused on transition metal complexes containing novel and peculiar bonds between transition elements and some main group elements of group 14, particularly multiple bonds to silicon and germanium. Some new silyl and silylene complexes and their germanium analogs were prepared and the reactivity of these complexes was examined to gain a better understanding on the unsaturated bond systems involving silicon and germanium atoms. In addition, the reactivity and properties of M-Si single bonds and the C-H bond activation by cationic metallocenes were investigated.

VII-K-1 Intramolecular Aromatic C-H Bond Activation by a Silylene Ligand in a Methoxy-Bridged Bis(silylene)-Ruthenium Complex

Hiroaki WADA *(Tohoku Univ.)*, **Hiromi TOBITA** *(Tohoku Univ. and IMS)* **and Hiroshi OGINO** *(Tohoku Univ.)*

[*Organometallics* **16**, 3870 (1997)]

When a solution of $Cp(Ph_3P)Ru\{SiMe_2\cdots O(Me)\cdots SiMe_2\}$ (**1**; Cp = η^5-C_5H_5) and a two-electron-donating ligand L was heated at 130°C, a C-H bond of a phenyl group was activated by the Ru=Si double bond, and the complexes $CpLRuSiMe_2(o\text{-}C_6H_4PPh_2)$ (**2a**, L = PPh_3; **2b**, L = PMe_3; **2c**, L = PEt_3; **2d**, L = $P(OMe)_3$; **2e**, L = ^{t}BuNC) were obtained. Heating **1** in the absence of a ligand at 130°C gave $CpLRuSiMe_2(o\text{-}C_6H_4PPh_2)$-(H)($SiMe_2OMe$) (**3**). A possible mechanism for formation of **2** involves the electrophilic attack of a silylene ligand to the ortho carbon of a phenyl group in the PPh_3 ligand to give **A**. Subsequent proton migration to the Ru center gives **3**, and when a two-electron donor L exists, reductive elimination of $HSiMe_2OMe$ and addition of L occur to afford **2**. This is the first example of C-H bond activation by a silylene complex.

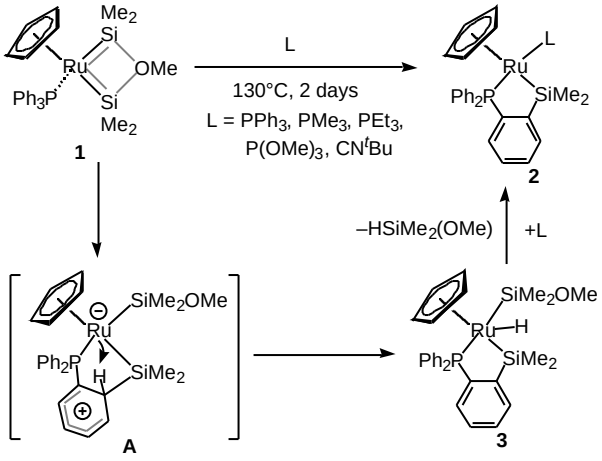

VII-K-2 Quantitative Transfer of a Methyl Group from a Methyl(hydrido)iridium Complex to $SiRH_3$ (R = *n*-butyl, pentyl or hexyl) to Give $SiR(Me)H_2$ and a Dihydridoiridium Complex

Masaaki OKAZAKI *(Tohoku Univ.)*, **Hiromi TOBITA** *(Tohoku Univ. and IMS)* **and Hiroshi OGINO** *(Tohoku Univ.)*

[*J. Chem. Soc., Dalton Trans.* 3531 (1997)]

Thermal reaction of $[Ir(Me)(H)\{\eta^2\text{-}Me_2Si(CH_2)_2\text{-}PPh_2\}(PMe_3)_2]$ with $SiRH_3$ (R = *n*-butyl, pentyl, or hexyl) resulted in silicon-carbon bond formation to give $SiR(Me)H_2$ and $[IrH_2\{\eta^2\text{-}Me_2Si(CH_2)_2PPh_2\}(PMe_3)_2]$. Isolation of $Si(n\text{-}C_6H_{13})MeH_2$ was achieved by preparative gas chromatography. A possible mechanism involving 1,2-methyl-shift in hydrido(methyl)(silylene) intermediate **A** was proposed.

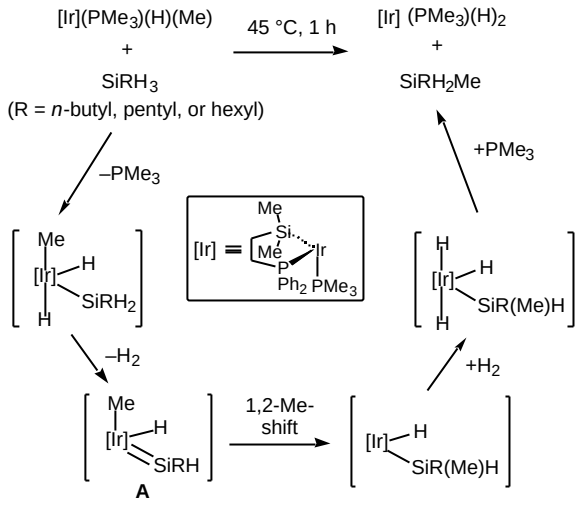

VII-K-3 Thermal Reaction of Ethyl(hydrido){(2-phosphinoethyl)silyl}iridium(III) Complex — Formation of a {(2-Phosphinoethyl)}(ethene)-iridium(I) Complex —

Masaaki OKAZAKI *(Tohoku Univ.)*, **Hiromi TOBITA** *(Tohoku Univ. and IMS)* **and Hiroshi OGINO** *(Tohoku Univ.)*

[*Chem. Lett.* 69 (1998)]

Thermolysis of $L_nIr(C_2H_5)(H)$ (**1**) [L_n = {η^2-$Me_2Si(CH_2)_2PPh_2$}$(PMe_3)_2$] led to the clean formation of a 1:1 mixture of ethene complex $L_nIr(C_2H_4)$ (**2**) and dihydrido complex $L_nIr(H)_2$ (**3**). The geometry of these products were unequivocally determined by NMR spectroscopy. A possible mechanism involves a parallel occurrence of two processes; (**A**) reversible β-elimination of ethene and (**B**) irreversible reductive elimination of ethane. The ethene generated in process **A** is effectively trapped by the coordinatively unsaturated species formed in process **B**. The ethene complex **2** is proved to be an efficient precursor of an unsaturated silyliridium(I) species through dissociation of ethene.

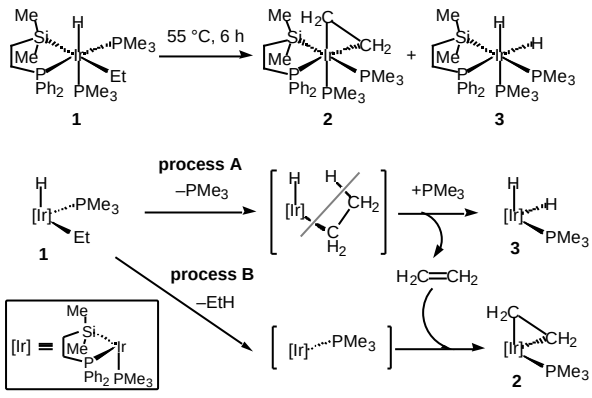

VII-K-4 Synthesis of Cationic Germyleneiron Complexes and X-Ray Structure of $[Cp^*(CO)_2Fe{=}GeMe_2{\cdot}DMAP]BPh_4{\cdot}CH_3CN$ ($Cp^* = C_5Me_5$, DMAP = 4-(Dimethylamino)pyridine)

Hiromi TOBITA *(Tohoku Univ. and IMS)*, **Kaoru ISHIYAMA** *(Tohoku Univ.)*, **Yasuro KAWANO** *(Tohoku Univ.)*, **Shinji INOMATA** *(Tohoku Univ.)* **and Hiroshi OGINO** *(Tohoku Univ.)*

[*Organometallics* **17**, 789 (1998)]

Chlorogermyl iron complexes $Cp^*(CO)_2FeGeMe_2Cl$ (**1**) and $Cp^*(CO)(PPh_3)FeGeMe_2Cl$ (**2**) undergo chloride abstraction by $AgBPh_4$ in the presence of 4-(dimethylamino)pyridine (DMAP) to afford cationic germylene complexes $[Cp^*(CO)_2Fe{=}GeMe_2{\cdot}DMAP]BPh_4$ (**3**) and $[Cp^*(CO)(PPh_3)Fe{=}GeMe_2{\cdot}DMAP]BPh_4$ (**4**), respectively. Structural determination by X-ray crystallography of **1** and **3·CH$_3$CN** revealed that both complexes have a gauche conformation with respect to the Fe-Ge bonds. The short Fe-Ge bond (2.329(3) Å) and very long Ge-N (DMAP) bond (1.989(8) Å) in **3·CH$_3$CN** demonstrate the unsaturated bond character of the former and the dative bond character of the latter. The complexes **3** and **4** in dichloromethane revert to the parent complexes **1** and **2**, respectively, via an electron transfer process from the counter anion, BPh_4^-, followed by chlorine abstraction from the solvent.

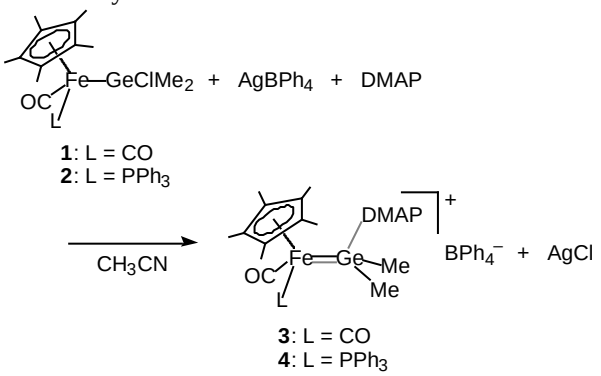

VII-K-5 Thermal Reactions of Alkyl(hydrido)-(hydrosilyl)iridium(III) Complexes: Generation of a Hydrido(silylene)iridium(I) Species via the Reductive Elimination of Alkane and 1,2-H-Shift from the Silicon Atom to the Ir(I) Metal Center

Masaaki OKAZAKI *(Tohoku Univ.)*, **Hiromi TOBITA** *(Tohoku Univ. and IMS)*, **Yasuro KAWANO** *(Tohoku Univ.)*, **Shinji INOMATA** *(Tohoku Univ.)* **and Hiroshi OGINO** *(Tohoku Univ.)*

[*J. Organomet. Chem.* **553**, 1 (1998)]

Heating of alkyl(hydrido)(hydrosilyl)iridium(III) complexes $L_nIr(R)(H)$ (**1**) [L_n = {η_2-$MesHSi(CH_2)_2PPh_2$}$(PMe_3)_2$, R = Me, Et] led to the reductive elimination of alkane. Subsequently, the resulting hydrosilyliridium(I) intermediate LnIr (A) activated the intramolecular carbon-hydrogen bond to give two geometrical isomers of $Ir(H)(\eta^3$-$CH_2C_6H_2(CH_3)_2SiH(CH_2)_2PPh_2\}(PMe_3)_2$ (**2** and **2'**). In the presence of MeOH, **A** was quickly trapped with MeOH to give a methoxysilyliridium(III) complex $Ir(H)_2\{\eta^2$-$Mes(MeO)Si(CH_2)_2PPh_2\}(PMe_3)_2$ (**3**). This reactivity of **A** with MeOH clearly supports the occurrence of a 1,2-H-shift from the silyl silicon atom to the iridium center to

generate a hydrido(silylene)iridium(I) species Ir(H)[η^2-{=SiMes$(CH_2)_2PPh_2$}]$(PMe_3)_2$ (**B**).

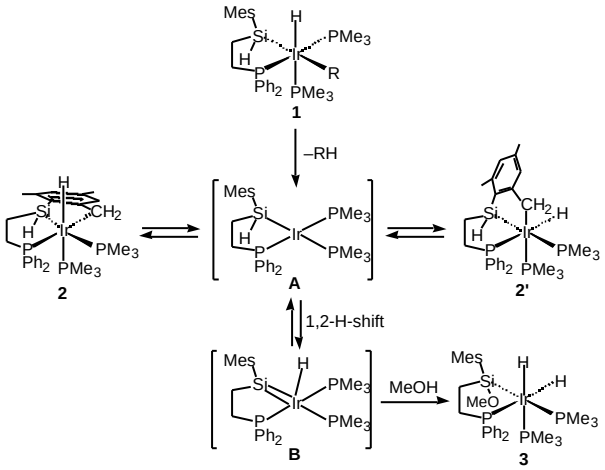

VII-K-6 Synthesis, Structure, and Reactivity of a Bis(silylene)(carbonyl)ruthenium Complex and a Novel Addition Reaction of Photochemically Generated Dimethylsilylene to Bis(silylene) Complexes Cp(OC)M{$SiMe_2$···O(Me)···SiMe$_2$} (M = Ru, Fe)

Hiromi TOBITA *(Tohoku Univ. and IMS)*, **Hitoe KURITA** *(Tohoku Univ.)* **and Hiroshi OGINO** *(Tohoku Univ.)*

[*Organometallics* **17**, 2844 (1998)]

Photolysis of $CpRu(CO)_2SiMe_2SiMe_3$ (**1a**) with a low or medium pressure Hg lamp for a long time caused the loss of a $SiMe_2$ moiety to give $CpRu(CO)_2SiMe_3$ (**2**) perhaps through the photochemical dissociation of a CO ligand. This mechanism was supported by the quantitative formation of bis(silylene)ruthenium complex Cp(OC)Ru{$SiMe_2$···O(Me)···SiMe$_2$} (**3a**) by photolysis of (methoxydisilanyl)ruthenium complex $CpRu(CO)_2SiMe_2SiMe_2OMe$ (**1b**). The X-ray crystal structure analysis of **3a** revealed that **3a** has an almost planar Ru-Si-O-Si four-membered chelate ring with short Ru-Si bonds (2.316(3) and 2.311(3) Å) and long Si···O bonds (1.801(7) and 1.793(7) Å).**3a** reacts with MeOH instantaneously to give Cp(OC)Ru(H)$(SiMe_2OMe)_2$ (**4**) quantitatively. Photolysis of $CpM(CO)_2SiMe_2SiMe_2OMe$ (**1b**: M = Ru, **1c**: M = Fe) or Cp(OC)M{$SiMe_2$···O(Me)···SiMe$_2$} (**3a**: M = Ru, **3b**: M = Fe) with a photochemical silylene precursor $(SiMe_2)_6$ by means of a low pressure Hg lamp afforded a mixture of **3a** or **3b**, disilanyl(silylene) complexes Cp(OC)M{=$SiMe_2$←O(Me)$SiMe_2SiMe_2$} (**5a**: M = Ru, **5b**: M = Fe), and $(SiMe_2)_5$. Two possible mechanisms for the addition of dimethylsilylene to **3** to give **5** were proposed.

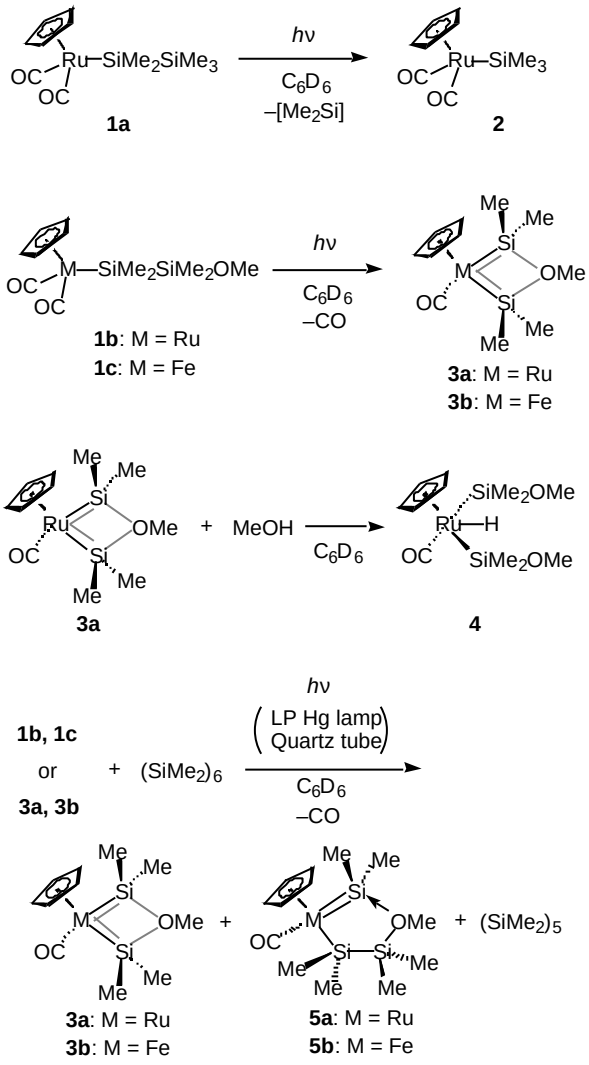

VII-K-7 Synthesis and Properties of Intramolecularly Base-Stabilized Disilanyl(silylene)ruthenium and -iron Complexes

Hiromi TOBITA *(Tohoku Univ. and IMS)*, **Hitoe KURITA** *(Tohoku Univ.)* **and Hiroshi OGINO** *(Tohoku Univ.)*

[*Organometallics* **17**, 2850 (1998)]

Photolysis of 3-methoxytrisilanyl complex $CpM(CO)_2SiMe_2SiMe_2SiMe_2OMe$ (**1a**: M = Ru, **1b**: M = Fe) afforded intramolecularly methoxy-stabilized disilanyl(silylene) complex Cp(OC)M{=$SiMe_2$←O(Me)$SiMe_2SiMe_2$} (**2a**: M = Ru, **2b**: M = Fe) as a primary product. Prolonged irradiation of the solution resulted in the decay of **2a**,**b** with release of a dimethylsilylene moiety to give methoxy-bridged bis(silylene) complex Cp(OC)M{$SiMe_2$···O(Me)···SiMe$_2$} (**3a**: M = Ru, **3b**: M = Fe). The X-ray crystal structure analysis of **2a** revealed that **2a** has a 5-membered chelate ring and the Ru-Si(silylene) bond (2.291(2) Å) is much shorter than the other Ru-Si bond (2.350(1) Å). It can be concluded from the bond lengths that the former possesses a partial double bond character while the latter is a normal Ru-Si single bond.

Photolysis of diisopropyl derivatives $CpM(CO)_2SiMe_2$-$Si^iPr_2SiMe_2OMe$ (**4a**: M = Ru, **4b**: M = Fe) gave Cp-(OC)M{=$SiMe_2 \leftarrow O(Me)SiMe_2Si^iPr_2$} (**5a**: M = Ru, **5b**: M = Fe) exclusively, in which the positions of substituents on silicon atoms in **5a** and **5b** were determined by ^{29}Si-^1H COLOC and NOESY NMR spectra. Mechanism involving 1,2-migration of the methoxydisilanyl group to the metal center was suggested.

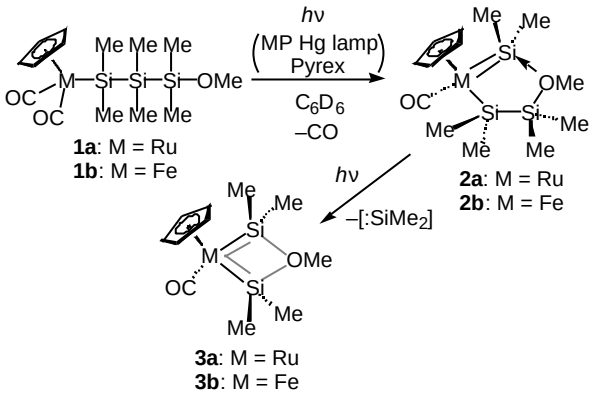

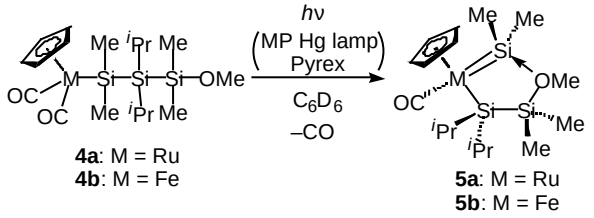

VII-K-8 Thermal and Photochemical Reactions of a Cationic Rhenocene-Acetonitrile Adduct: The First C-H Bond Activation by Rhenocene Cation

Hiromi TOBITA *(Tohoku Univ. and IMS)***, Kiyonari HASHIDZUME** *(Tohoku Univ.)***, Kouji ENDO** *(Tohoku Univ.)* **and Hiroshi OGINO** *(Tohoku Univ.)*

[*Organometallics* **17**, 3405 (1998)]

Photolysis of $[Cp_2Re(H)_2](BF_4)$ (**1**) in MeCN afforded $[Cp_2Re(NCMe)](BF_4)$ (**2**) as moderately air and moisture stable red crystals in 93% isolated yield. Complex **2** did not react with benzene or thiophene thermally at room temperature, but under UV irradiation **2** reacted with an excess of benzene and thiophene to give the C-H bond activation products $[Cp_2Re(H)Ph](BF_4)$ (**3**) and $[Cp_2Re(H)(2\text{-}C_4H_3S)](BF_4)$ (**4**) in 88% and 80% yields, respectively. Small kinetic isotope effect (k_H/k_D = 1.09) was measured for the formation reaction of **3**. The cationic complex **3** was readily deprotonated by DBU to give phenylrhenocene Cp_2RePh (**5**) in 70% yield. This reaction is reversible and the protonation of **5** with HBF_4 regenerated **3** in 85% yield.

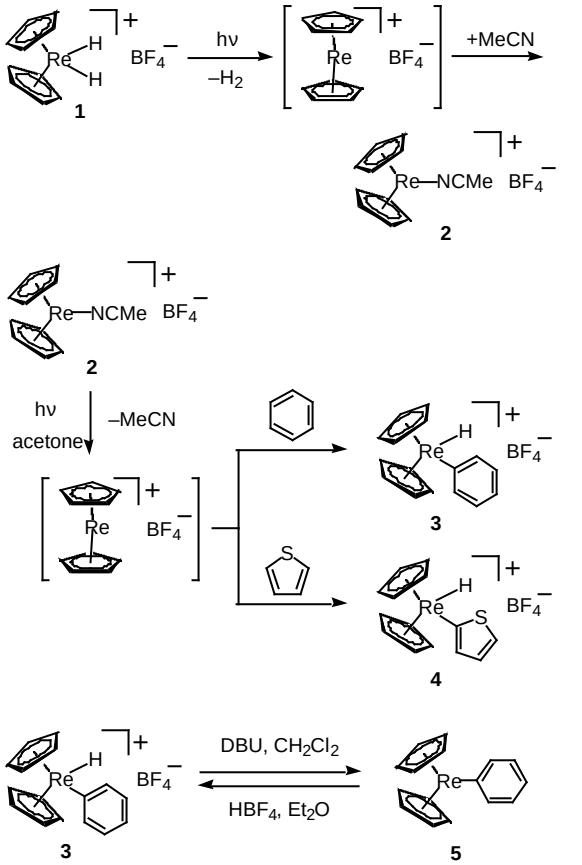

VII-K-9 Novel Reaction of Silyl Carbonyl Complexes with Hydride-Transfer Reagents: Reduction of a Carbonyl Ligand and Coupling with a Silyl Group

Rie SHIOZAWA *(Tohoku Univ.)***, Hiromi TOBITA** *(Tohoku Univ. and IMS)* **and Hiroshi OGINO** *(Tohoku Univ.)*

[*Organometallics* **17**, 3497 (1998)]

Treatment of $(\eta^5\text{-}C_5R'_5)Fe(CO)_2SiR_3$ (R' = H, CH_3; R = H, alkyl, aryl) with $LiAlH_4$ in ether or THF gave CH_3SiR_3 as a major product in moderate to high yield together with $HSiR_3$. Labeling experiments using $LiAlD_4$ and ^{13}C proved that the carbonyl ligand was reduced with $LiAlH_4$ and coupled with the silyl group to give the methylsilane.

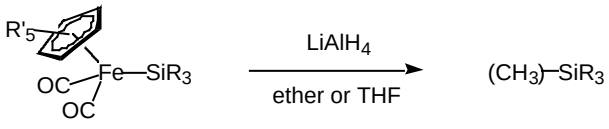

RESEARCH ACTIVITIES VIII
Computer Center

VIII-A Theoretical Studies on Electronic Structure and Dynamics of Electronically Excited States in Polyatomic Molecules

VIII-A-1 Wavepacket Study on the Photodissociation Dynamics of OCS

Toshinori SUZUKI, Hideki KATAYANAGI, Shinkoh NANBU and Mutsumi AOYAGI

[*J. Chem. Phys.* **109**, 6838(1998)]

Prof. Suzuki's experimental group has measured the speed, angular and alignment distributions of $S(^1D_2)$ atoms from the ultraviolet photodissociation of OCS by a photofragment imaging technique. It was found that the dissociation from A' state gives rise to high- and low-speed fragments, while the A" state only provides the high-speed fragment. In order to elucidate the dissociation dynamics, in particular the bimodal speed distribution of S atoms, two-dimensional potential surfaces of OCS were calculated for the C-S stretch and bending coordinates by ab initio State-Averaged CASSCF/MRSDCI method. Conical intersections of $^1\Delta$ and $^1\sum^-$ with $^1\prod$ were found as adiabatic dissociation pathways. Wave packet calculations on these adiabatic surfaces, however, did not reproduce the low-speed component of the $S(^1D_2)$ fragments. The discrepancy regarding the slow S atoms was attributed to the dissociation induced by non-adiabatic transition from $2A'(^1\Delta)$ to $1A'(^1\sum^-)$ in the bending coordinate. This was confirmed by wave packet calculations including non-adiabatic transitions. The slow recoil speed of S atom in the non-adiabatic dissociation channel is due to more efficient conversion of bending energy into CO rotation than the adiabatic dissociation on the upper surface.

VIII-A-2 Theoretical Study on the Predissociation Dynamics of Electronically Excited $^1\Delta$ state of HCP Molecule

Shinkoh NANBU, Tomoko KINOSHITA and Mutsumi AOYAGI

The potential energy surfaces and transition dipole moment surfaces of the low-lying electronically excited states of HCP molecule are calculated using the ab initio state averaged CASSCF and multi reference configuration interaction (CI) method. The photodissociation dynamics for $HCP(1^1\sum^+) + h\nu \rightarrow H(^2S) + CP(X)$; where $X = 1^2\sum^+$ and $2^2\prod$, are investigated by performing wave packet calculations on ab initio surfaces. The photoabsorption cross section of HCP $(1^1\sum^+) + h\nu$ (299-237nm) and the rovibrational state distribution of the CP product were evaluated. We found that the non-adiabatic transition between $1^1A'$ and $2^1A'$ states in the bent conformations plays an important role in the predissociation process.

VIII-A-3 Theoretical Study on the Unimolecular Reaction Dynamics of Acetyl Radical $CH_3CO \rightarrow CH_3 + CO$

Masakatsu ITO, Shinkoh NANBU and Mutsumi AOYAGI

Prof. Suzuki's group at IMS has shown that the RRKM unimolecular dissociation rate constant k(E) of internally excited acetyl radical did not reproduce the experimental values. We investigate the dissociation dynamics of acetyl radical with the classical trajectory method using the electronic model hamiltonian based on our ab initio calculations. At each time step in our classical trajectory calculations, the electronic hamiltonian is diagonalized to obtain the instantaneous adiabatic states and then the Hellmann-Feynmann forces are evaluated to drive the nuclear coordinates. Our hamitonian is based on the valence bond (VB) description of the electronic wavefunctions. Since acetyl radical and its dissociative products have completely different bonding characters, the wavefunctions along the dissociation process are approximately expanded by two correponding VB bases states.

UHF/MP2/6-311G** calculations at various nuclear conformations are carried out to fit the potential parameters in the model hamiltonian. The maximum deviation of the model potential energies from the ab-initio ones is 0.0038 hartree, which is about one-tenth of the barrier height. Although this level of calculation is accurate enough to describe the qualitative characters in dissociation processes of acetyl radical, the resulting barrier height is still 4 kcal/mol heigher than the experimentally proposed value. Hence we modified two parameters from the PUHF/MP4/6-311G** calculations, where barrier height is as accurate as the experimental value(15 kcal/mol).

The initial preparations of the trajectories are employed with a Monte Carlo "random walk" in conformational space for microcanonical sampling. We found that the energy of the CCO bending excitation does not efficiently transfer into the dissociation coordinate(C-C) over the time period of 30 ps. We suggested that this slow transfer or redistribution of internal energy could be one of the important sources for the discrepancy between the RRKM rate constants and the experimental values. We continue to analyze the detailed IVR processes of internally excited acetyl radical to clarify the reason for experimentally observed non-RRKM behavior.

VIII-A-4 Ab Initio Molecular Orbital Studies of Isomerization Reaction from c-$OSiH_2O$ to t-

OSiHOH

Shigeo KONDO *(Nat. Inst. of Material and Chemical Research)*, **Kazuaki TOKUHASHI** *(Nat. Inst. of Material and Chemical Research)*, **Hidekazu NAGAI** *(Nat. Inst. of Material and Chemical Research)*, **Akifumi TAKAHASHI** *(Nat. Inst. of Material and Chemical Research)* **and Mutsumi AOYAGI**

[*J. Mol. Struct. (THEOCHEM)* in press]

We have suggested in a previous study that the reaction route from $SiH_3 + O_2$ to OSiOH + 2H is a key to understand the spontaneous ignition at room temperature. The whole route of this reaction was found as follows;

$SiH_3 + O_2 \rightarrow$ SiH3OO*
$\rightarrow$ c-$OSiH_2O$ + H
$\rightarrow$ OSiHOH + H
$\rightarrow$ OSiOH + 2H

In this study, we investigated the detailed isomerization mechanism from c-$OSiH_2O$ to t-OSiHOH with *ab initio* Gaussian-2 theory and CASSCF(6,6) method. It was found that the reaction proceeds through two consecutive steps; i.e., c-$OSiH_2O$ undergoes isomerization to yield w-$OSiH_2O$, and then the latter is converted to t-OSiHOH. The G-2 energy of the transition state of the latter process is 4.3 kcal/mol higher than that of the former. However, the G-2 energy of this higher transition state plus H atom is still 4.8 kcal/mol lower than that of the original reactants of $SiH_3 + O_2$.

VIII-A-5 Ab Initio Study of $PH_2 + O_2$ Reaction Relevant to the PH_3 Combustion

Shigeo KONDO *(Nat. Inst. of Material and Chemical Research)*, **Kazuaki TOKUHASHI** *(Nat. Inst. of Material and Chemical Research)*, **Akifumi TAKAHASHI** *(Nat. Inst. of Material and Chemical Research)*, **Masaaki SUGIE** *(Nat. Inst. of Material and Chemical Research)* **and Mutsumi AOYAGI**

[*J. Phys. Chem.* submitted]

Ab initio calculations have been carried out for the $PH_2 + O_2$ reaction by using Gaussian-2 theory, which is considered as a key reaction to understand low temperature phosphine combustion. This reaction consists of two main branching routes at low temperatures. One is the reaction to yield OH radicals, and the other to yield hydrogen atoms, Of the two reactions, we found that a long reaction pathway;

$PH_2 + O_2 \rightarrow PH_2OO$
$\rightarrow$ c-OPH_2O
$\rightarrow$ w-OPH_2O
$\rightarrow$ OPHO + H
$\rightarrow$ OPO + 2H

has been concluded to be the chain branching process, which enables the spontaneous ignition of phosphine at room temperature.

VIII-A-6 Semiclassical Study of Nonintegrable Systems

Toshiya TAKAMI

We study nonadiabatic process in classically nonintegrable systems such as 2D billiards and kicked rotators to reveal essence of the dynamical characters in the highly excited states of molecules. Nonadiabatic transition between adjacent levels through an avoided crossing was studied first in pioneering works by Landau, Zener, etc. In the nonintegrable systems, however, Landau-Zener formula cannot be applied because the system contains essentially many levels and nonadiabatic couplings between adiabatic states are not vanish everywhere.

On the numerical experiments of nonintegrable systems, we found non-Landau-Zener behavior in the nonadiabatic process, and we pointed that this phenomenon arises from a boundary term which is missed in Landau-Zener formula. Applying this extra term, we construct new basis functions which can describe nonadiabatic transition locally even in many level systems. We use semiclassical methods to obtain the new basis and to study physical properties of them.

VIII-A-7 A Theoretical Study on Structures and Vibrational Spectra of C_{84} Fullerene Isomers

Takeshi NISHIKAWA, Tomoko KINOSHITA, Shinkoh NANBU and Mutsumi AOYAGI

[*J. Mol. Struct. (THEOCHEM)* in press]

The C_2, D_2, and D_{2d} isomers of C_{84} fullerene were investigated by ab initio molecular orbital calculations. Optimized geometries, relative stabilities, and vibrational spectra of eleven isomers are determined by restricted Hartree-Fock (RHF) calculations with STO-3G, 3-21G, and D95V basis sets. For the purpose of an assignment on the C_{84} structures, we discussed a way to distinguish a specific isomer by comparing the calculated vibrational spectra.

We found that the peaks located at higher than 1300 cm^{-1} are all belonging to the on-surface mode where each carbon atom moves on the surface of C_{84} skeleton. On the other hand, the peaks below 1000 cm^{-1} correspond to the breathing mode, in which atoms are moving perpendicularly to the surface. There exists a window region(around 1000-1300 cm^{-1}) in all calculated spectra, which split a character of normal mode vibrations. In D_2 symmetry, the vibrational spectra of isomer No. 1 has a noticeable difference in the locations of three main peaks. The isomer No. 2 with C_2 symmetry also has characteristic vibrational structure, where numbering scheme introduced by Fowler et. al. is used. For the rest of other isomers examined, it was hard to clearly predict the structure solely with calculated vibrational spectra. We suggested that the difference in the bands around 650 cm^{-1} and 1670 cm^{-1} can be used as a finger print of D_2

isomers, and that the vibrational bands below 900 cm^{-1} and peak around 1880 cm^{-1} can be used to distinguish C_2 species.

Laser Research Center for Molecular Science

VIII-B Zero Kinetic Energy Pulsed Field Ionization Spectroscopy of Very Highly Excited Rydberg States and van der Waals Complexes

Zero kinetic energy pulsed field ionization (ZEKE-PFI) spectroscopy is a very high resolution (~0.1 meV) photoelectron spectroscopic technique based on PFI of very highly excited Rydberg states. The very highly excited (n > 100) Rydberg states, which have unexpectedly long lifetimes, are investigated with a newly developed two-pulsed field ionization technique. The van der Waals complexes of aromatic compounds with rare gas atoms are also studied to clarify inter-molecular forces of cationic vdW complexes.

VIII-B-1 Energy Exchange between Electron and Ion Core in Very High-Lying Rydberg States of Poliatomic Molecules Evidenced by Sweep-Off-Probe Pulsed-Electric-Field Ionization

Shin-ichiro SATO, Yoshitaka NOZAKI *(Sigma Kouki Co.)* **and Katsumi KIMURA**

We have newly developed the Sweep-off-Probe Pulsed-Field Ionization (SOP-PFI) technique for detecting only the higher Rydberg states supplied from the lower Rydberg states due to the energy exchange. In this technique, the first pulsed electric field (F_1) discriminates free kinetic electrons and very high-lying Rydberg electrons just below the ionization threshold generated by the optically pumping. Some time after (typically ~ 1 μs), the second pulsed electric field (F_2) ionizes high-lying Rydberg states and these electrons are detected as ZEKE-PFI signal. The ZEKE-PFI signal consists of only the Rydberg electrons in the detection window determined by the strength of F_2. Both the Rydberg molecules initially populated by the optically pumping and supplied by the energy exchange may be observed under the condition $F_1 < F_2$. However, only the Rydberg molecules supplied by the energy exchange should be observed under the condition $F_1 > F_2$, since any initially populated Rydberg molecules are swept out by the stronger F_1. ZEKE-PFI signals were observed even under the condition $F_1 > F_2$ for poliatomic molecules like benzene and its derivatives, while not for the NO molecule. This fact strongly suggests that the internal energies of an ionic core excite Rydberg states to the higher excited Rydberg states.

VIII-B-2 Cation Vibrational Spectra of Pyrimidine and Its van der Waals Complexes with Ar and N_2 by ZEKE Photoelectron Spectroscopy

Shin-ichiro SATO, Kenji OMIYA *(Cyuubu Medical Co.)* **and Katsumi KIMURA**

[*J. Electron Spectrosc.* submitted]

Cation vibrational spectra of pyrimidine as well as the pyrimidine-Ar, -Ar_2 and -N_2 van der Waals (vdW) complexes have been obtained by means of ZEKE (zero kinetic energy) photoelectron spectroscopy for the first time. Four totally symmetric fundamental vibrations (ν_1, ν_{6a}, ν_{9a}, ν_{12}) and one non-totally symmetric vibration (ν_{6b}) of the pyrimidine cation have been assigned by using the respective five S1 vibrational levels as intermediate resonant states. *Ab initio* calculations (UHF/6-31G*, MP2/6-31G*, CASSCF/6-31G* and B3LYP/6-31G*) were also carried out for the vibrational frequencies of the pyrimidine cation to compare with the experimental values. The calculated frequencies of the 16*b* and 6*b* modes obtained from the UHF and CASSCF calculations are deviated from the experimental ones, but in good agreement with the experimental values in the B3LYP calculations under C_{2v} symmetry. Four additional vibrational levels (ν_{8a}, ν_{16a}, ν_{16b}, ν_{19a}) found from the ZEKE spectra have been assigned on the basis of the calculated frequencies. The I_a values of the complexes were found to be lowered from the I_a value of bare pyrimidine (I_a = 75 261 ± 6 cm^{-1}) by 261 cm^{-1} for the Ar complex, by 516 cm^{-1} for the Ar_2 complex, and by 95 cm^{-1} for the N_2 complex. In the ZEKE spectrum of pyrimidine-Ar, three low-frequency vibrational modes (b_x, b_y, s_z) were also observed at 36, 40, and 50 cm^{-1}, respectively. The change in structure along with the $D_0 \rightarrow S_1$ transitions was estimated from the Franck-Condon analysis of the relative band intensities for the pyrimidine-Ar complex. Some results obtained from the MP2/3-21+G** ab initio calculations were also presented for the pyrimidine-Ar complex.

VIII-C Developments and Researches of New Laser Materials

Although development of lasers is remarkable, there are no lasers which lase in ultraviolet and far infrared regions. However, it is expected that these kinds of lasers break out a great revolution in not only the molecular science but also in the industrial world.

In this project we research characters of new materials for ultraviolet and far infrared lasers, and develop new lasers by using these laser materials.

VIII-C-1 Spectrum Control of Intense THz-Radiation from InAs under Magnetic Field Irradiated with Stretched Femtosecond Laser Pulses

Shinji IZUMIDA, Shingo ONO, Hideyuki OHTAKE, Zhenlin LIU and Nobuhiko SARUKURA

We have reported the significant enhancement of THz-radiation power from InAs under magnetic field irradiated with femtosecond optical pulses. The THz-radiation power exhibits almost quadratic dependence on the excitation power and higher magnetic field. Furthermore, the radiation spectrum is found to be controlled by the excitation pulsewidth. For the control of the spectrum of this intense THz radiation, we introduced a high dispersion prism pair to stretch the pulse duration. The pulse duration was changed from 260 to 1100 fsec (FWHM) in auto correlation. With this stretched pulse for the excitation, we can control center frequency of THz radiation as shown in Figure 1. The longer excitation pulse width resulted in lower center frequency.

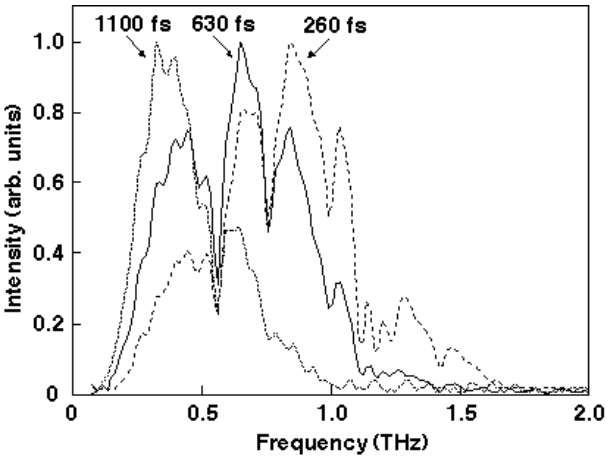

Figure 1. Spectrum of THz radiation excited with different pulse duration.

VIII-C-2 Estimation the Focusability of the THz Radiation

Shingo ONO, Shinji IZUMIDA, Zhenlin LIU, Takayuki YANO, Hideyuki OHTAKE, and Nobuhiko SARUKURA

We estimated the focusability of the THz radiation by measuring the intensity distribution of THz radiation. We can visualize the beam profile of THz-radiation propagation by using knife edge method as shown in Figure 1. THz radiation from the light source is collimated, focused, collimated, and focused onto a bolometer by four 10-cm off-axis parabolic mirrors. We measured in vertical and horizontal direction around the first focusing point using knife edge on the automatic translation stages. Figure 1 shows horizontal intensity distribution around the beam waist. The spot size at the beam waist reached about 1.5 mm. From this measurement, we propose that this spot size is good enough to perform pump and probe experiment in far infrared region.

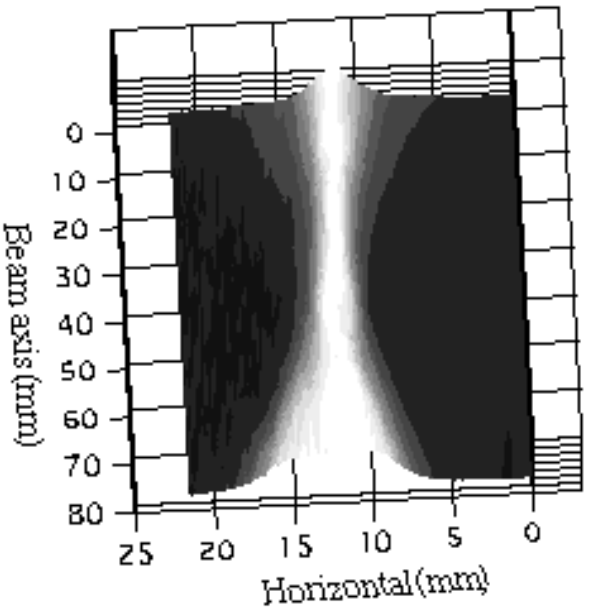

Figure 1. Horizontal intensity distribution of THz-radiation power around the beam waist.

VIII-C-3 Efficient, High Output Energy, Ultraviolet Ce:LiCAF Laser

Zhenlin LIU, Hideyuki OHTAKE, Nobuhiko SARUKURA, Kiyoshi SHIMAMURA *(Inst. Materials Research Tohoku Univ.)***, Na MUJILATU** *(Inst. Materials Research Tohoku Univ.)* **and Tsuguo FUKUDA** *(Inst. Materials Research Tohoku Univ.)*

The Ce^{3+}:$LiCaAlF_6$ (Ce:LiCAF) lasers have emerged as convenient, compact sources of tunable ultraviolet (UV) radiation in the spectral region from 281 to 315 nm. A UV solid-state Ce:LiCAF laser laser resonator is established by a flat high reflector and a flat output coupler with 30% reflection separated by 4 cm. The large Ce:LiCAF crystal (aperture 10 mm → 10 mm) which is doped with 1.2 mol% Ce^{3+} ions is located midway between the two cavity end mirrors. The fourth harmonic of a Q-switched Nd:YAG laser is used as the pumping source. The pump beam is focused with a 40-cm focal length lens to produce a spot size of φ4 mm at the surface of the Ce:LiCAF crystal. More than 85% of the incident pump energy was absorbed by the crystal. Figure 1 presents the obtained output energies at 290 nm as a function of the absorbed 266 nm pump energy. The laser oscillation threshold is 12 mJ, corresponds to a threshold fluence of approximately 100 mJ/cm^2. The measured output energy remained linear with pump fluence with an extremely good slope efficiency of 39%. The pulse energy as high as 21 mJ at 10 Hz at 290 nm, is the highest output energy reported from a Ce:LiCAF oscillator until now, to our knowledge.

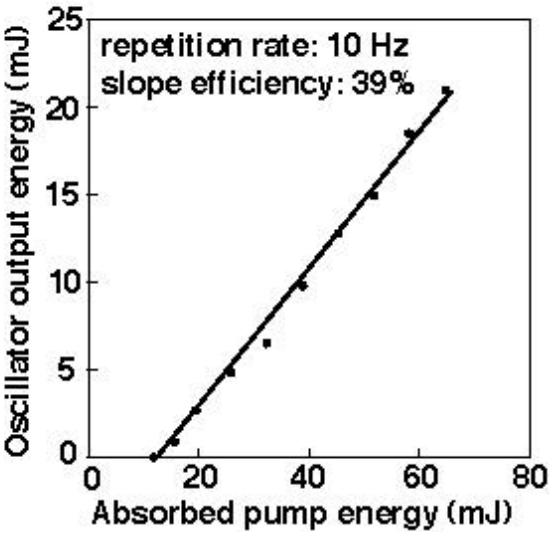

Figure 1. Laser output energy as a function of absorbed pump energy

VIII-C-4 All-Solid-State Tunable Ultraviolet Picosecond Ce^{3+}:$LuLiF_4$ Laser Pumped by the Fifth Harmonic of an Nd:YAG Laser

Zhenlin LIU, Hideyuki OHTAKE, Nobuhiko SARUKURA, Mark A. DUBINSKII *(Science & Engineering Services, Inc, USA)***, Ravil Yu. ABDULSABIROV** *(Kazan State Univ., Russia)* **and Stella L. KORABLEVA** *(Kazan State Univ., Russia)*

Due to the recent development of the fifth harmonic generation of Nd:YAG lasers, it becomes practical for the recently developed tunable solid-state UV laser material Ce^{3+}:$LiLuF_4$ (Ce:LLF) with tunability of about 305-340 nm to be directly pumped by the fifth harmonic of Nd:YAG lasers. Our optical layout for the short-cavity Ce:LLF laser is shown schematically in Figure 1. The Ce:LLF crystal with 0.2 at.% doping level was cut to form a cylinder ($\varphi 5 \rightarrow 25$ mm) with a flat polished window on the side. To geometrically reduce effective pumping penetration depth, the tilted-incidence-angle transverse pumping was used. To test the Ce:LLF laser tunability, a high-Q cavity was employed. The laser consisted of a dispersive Littrow-mounted 30°-prism with high reflection coated cathetus face and a low transmission flat output coupler (T = 20%). The 213-nm, 25-mJ, 5-nsec, horizontally polarized pulses (for σ-pumping) were stably obtained using the $(\omega + 4\omega)$ sum frequency generation process in $Li_2B_4O_7$ crystal. The Ce:LLF laser tunability obtained at the pumping energy of 22 mJ is from 309.5 nm to 312.3 nm and from 324.5 nm to 327.7 nm. For obtaining short pulses, a low-Q, short-cavity (6 cm) Ce:LLF laser was realized by replacing the above output coupler for an 80% transmission flat mirror. Using 16-mJ pumping pulses at 10-Hz repetition rate, we obtained 880-psec, 77-μJ, σ-polarized, and satellite-free pulses at 309-nm.

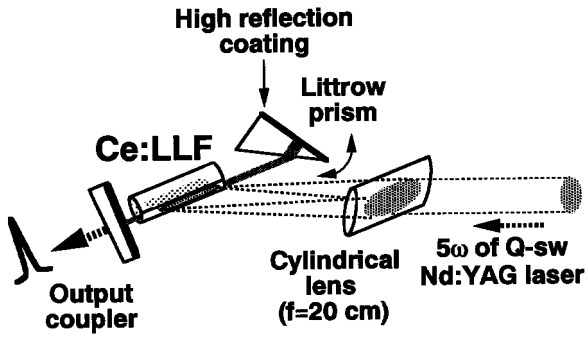

Figure 1. Short-cavity, tilted-incidence-angle ($\theta = 70°$) transverse pumping tunable Ce:LLF laser.

VIII-C-5 Broad-Band Gain Demonstration of New Yb:Glass

Zhenlin LIU, Hideyuki OHTAKE, Nobuhiko SARUKURA, Akihiko NISHIMURA *(Japan Atomic Energy Research Institute—Kansai Research Establishment)* **and Hiroshi TAKUMA** *(Japan Atomic Energy Research Institute—Kansai Research Establishment)*

Ytterbium:glass materials are interesting because they have long fluorescence lifetime, high saturation fluence and broad fluorescence band width. These characteristics make them particularly attractive for the generation of high peak power ultrashort pulses. A high power Yb:glass regenerative amplification has been demonstrated with the Chirped Pulse Amplification technique. The absorption and emission spectra of Yb:glass are much smoother than those of Yb:YAG. The broad gain of the Yb:glass was demonstrated through a pump-probe experiment. The pumping source was a dye (LDS925) laser pumped by the second harmonic of Q-SW Nd:YAG laser. It gave the pulse energy of 22 mJ at the wavelength of 930 nm. The probe beam came from a mode-locking Ti:sapphire laser (Tsunami, Spectra-Physics) pumped by an all solid-state green laser (Millennia X, Spectra-Physics). The 10 ps probe pulses are tunable ranging from 980 nm to 1065 nm. The pump and probe beams were overlapped colinearly through a dichroic mirror and then focused on to the Yb:glass (beam sizes: probe less than 300 μm/dia.; pump ~ 1 mm/dia.). The gain spectrum of the Yb:glass is shown in Figure 1. The gain spectrum of a Yb:YAG crystal is also shown in Figure 1 for comparison. The broad gain width of the Yb:glass has been confirmed with sufficient gain factors.

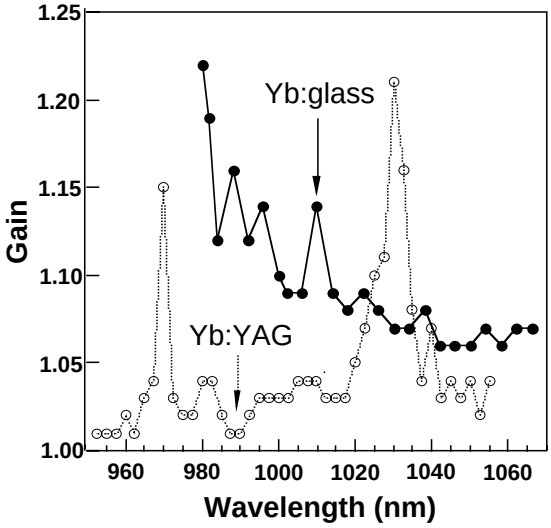

Figure 1. Gain spectrum of Yb:glass

VIII-C-6 Strong Enhancement of THz-Radiation Power from Femtosecond-Laser Irradiated InAs Clean Surface and Its Temperature Dependence

Hideyuki OHTAKE, Shingo ONO *(Science Univ. of Tokyo)***, Shinji IZUMIDA, Zhenlin LIU, and Nobuhiko SARUKURA, Kazuya WATANABE and Yoshiyasu MATSUMOTO**

We found strong enhancement of THz-radiation power from InAs (100) clean surface irradiated with femtosecond optical pulses. The clean surface was produced by Ar ion spattering method and we obtained clear LEED pattern after cleaning and 30 minutes annealing. The THz-radiation power became about three times larger than before cleaning. We have also found that THz-radiation power has strong temperature dependence. As shown in Figure 1, the power of THz-radiation at 50 K reaches about one order of magnitude higher than that at 450 K. Since we did not observe any changes of THz-radiation spectral shape, the origin of this radiation is the same at any temperature. This strong temperature dependence of THz-radiation power might be due to temperature dependence of carrier density.

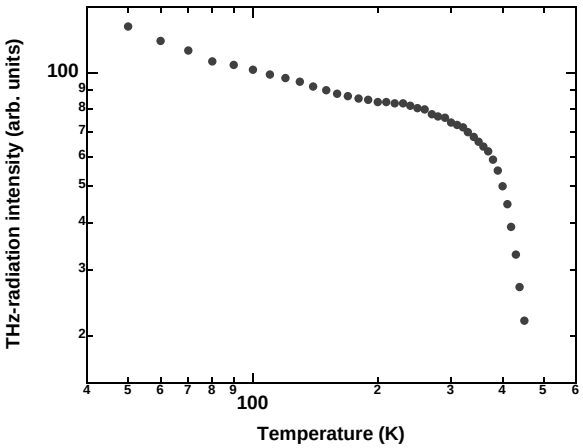

Figure 1. Temperature dependence of THz-radiation power. THz radiation from InAs (100) increases dramatically as temperature decreases.

VIII-D Development and Research of Advanced Tunable Solid State Laser Sources

The use of diode lasers to pump solid-state lasers leads to favorable performance characteristics. Diode-pumped solid-state lasers are compact, long-lived, and efficient sources of coherent radiation. They can provide excellent spatial mode quality and narrow linewidths. Because of the improved beam quality of diode-pumped solid-state lasers, nonlinear frequency conversion can readily be applied. Moreover, the availability of new and improved nonlinear optical crystals makes these techniques more practical. These kind advanced tunable solid-state light sources will assist the research of molecular science.

In this projects we research new Diode-Pumped Solid-State Lasers and new frequency conversion devices.

VIII-D-1 Intracavity Frequency Doubled Yb:YAG Miniature Laser

Takunori TAIRA, Jiro SAIKAWA, Eiji YAMAGUCHI *(Fukui Univ.)***, Takao KOBAYASHI** *(Fukui Univ.)* **and Robert. L. BYER** *(Stanford Univ.)*

Compact and efficient visible source of stable, single-frequency radiation are of potential interest for many applications such as display, interferometer and holographic systems. However, current argon-ion lasers suffer from low efficiency, short lifetimes and low coherency. Alternatively, as green lasers such as frequency doubled Nd-doped lasers are poor tunability and far from 515 nm.

In other hand, diode-pumped Yb:YAG laser which is promising material as a high power and high efficiency laser also have a potential for a wide tunable and high power mode lock lasers.[1-3] We also have reported a cw single-frequency and wide tunable Yb:YAG miniature laser.[4] Subsequently, frequency doubled Yb:YAG laser is one alternative technique to obtain single-frequency tunable light source around 515 nm region. We report our recent results for tunable single axial-mode oscillation of intracavity frequency doubled Yb:YAG miniature lasers.

The experimental configuration of the laser is shown in Figure 1. A maximum output power in single axial mode of 150 mW cw was achieved at 516nm with stability of ±1.7% during 15 minute. For frequency tuning, an intracavity birefringent filter was used. We obtained 10.9 nm(12.4THz) tunability around 516 nm by using 2-mm KTP crystal.

References
1)H. W. Bruesselbach, *et al*., *IEEE JSTQE.* **3**, 105 (1997).
2)A. Giesen, *et al.*, *OSA TOPS on Advanced Solid-State Lasers.* **10**, 280 (1997).
3)C. Honninger, *et al.*, *Opt. Lett.* **20**, 2402 (1995).
4)T. Taira, *et al*., *IEEE JSTQE.* **3**, 100 (1997).

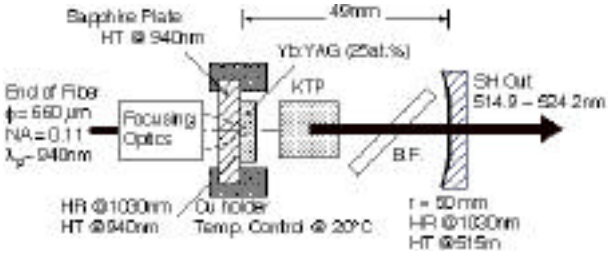

Figure 1. Schematic of the Intracavity frequency doubled Yb:YAG laser.

VIII-D-2 Design of Longitudinally Solid-State Lasers by Using M^2 Pump-Beam Factor

Takunori TAIRA, Nicolaie PAVEL *(Inst. Atm. Phy., ROMANIA)***, Mitsuyoshi FURUHATA** *(Fukui Univ.)***, Masato OHTAKA** *(Fukui Univ.)***, Takao KOBAYASHI** *(Fukui Univ.)* **and Hiromasa ITO** *(Tohoku Univ.)*

A model for optimization of longitudinally pumped solid-state lasers, in which the pump-beam was described by its M^2 factor, is proposed. Using the mode-overlap integrals, numerical investigations were carried out to obtain the optimum focusing position and pump beam waist, that ensure a minimum threshold pump power and maximum overlap efficiency, at a defined laser beam spot-size. The numerical data were fitted with analytical functions of pump beam M^2 factor, active medium absorption coefficient at the pump wavelength and laser beam volume. The experiments were performed with a Nd:YAG laser, longitudinally pumped with a maximum 10W fiber-coupled diode laser system and a Nd:YVO_4 miniature laser, pumped by a max. 1W array diode laser. Figure 1 shows Output power as a function of pump power for the Nd:YVO_4 laser. A fairly good agreement with theory was obtained.

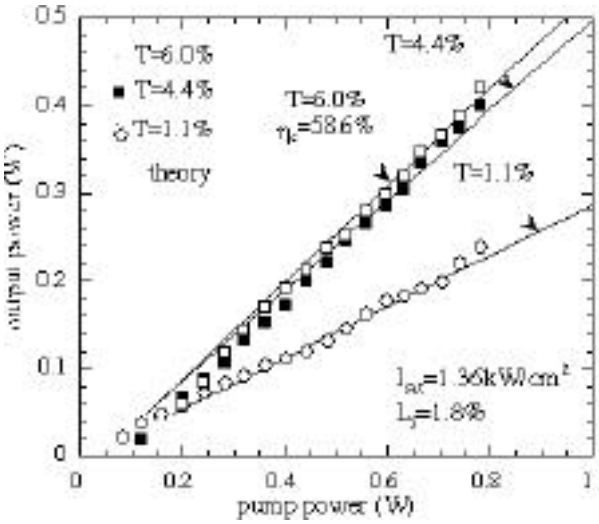

Figure 1. Output power as a function of pump power for the miniature Nd:YVO_4 system.

VIII-D-3 Diode-Pumped Nd:YAG Ceramics Lasers

Takunori TAIRA, Akio IKESUE *(Kurosaki Corp.)* **and Kunio YOSHIDA** *(Osaka Inst. Tech.)*

With the development of diode-pumped solid-state lasers during last decade, numerous laser materials have been developed and improved to achieve high efficiency and high power output. Nd:YVO_4 is in used as high efficiency miniature lasers because of its high absorption and emission cross-sections compare with Nd:YAG single crystal. However, its poor thermo-mechanical problems prevent high power operation. Much effort has gone into laser material research to find a high absorption coefficient laser medium with high thermal shock parameters.

Recently, we have developed a Nd:YAG ceramics with high optical quality.[1)] The YAG ceramics allows high neodymium-ion doping to overcome low absorption cross-section. Figure 1 shows the thermal conductivity of ceramics as a function of Nd concentration at 20°C. The YAG ceramic allows high neodymium-ion doping equal to high absorption and has high thermal conductivity compare with YAG single crystal and YVO_4. Therefore, Nd:YAG ceramics is promising new laser material for high efficiency and high power lasers.

We demonstrated, for the first time, a single-longitudinal-mode oscillation with ~ 213 mW output power, 17.6% slope efficiency using a Nd:YAG ceramics chip (4.8 at%). The threshold pump power was ~ 355 mW. For a 9.1 at% doped sample an effective absorption coefficien of 32.6 cm^{-1} was measured.

Reference
1) A. Ikesue, *et al.*, *J. Am. Ceram. Soc.* 78. 1033. (1995)

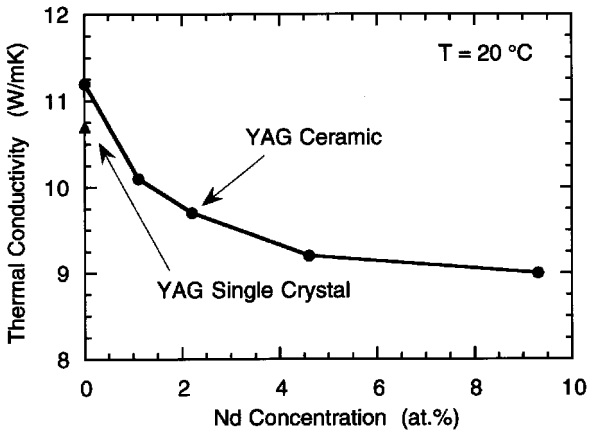

Figure 1. Thermal conductivity of the YAG ceramics as a function of Nd concentration.

Research Center for Molecular Materials

VIII-E Development of Novel Heterocyclic Compounds for Advanced Materials

Heterocycles containing chalcogen atoms are useful as components of organic conductors since heteroatoms in their rings are helpful to stabilize ions or ion-radical species, and extended π-conjugation decreases Coulombic repulsion. In addition intermolecular interactions caused by heteroatom contacts can be expected to form unique molecular assemblies. In this project novel electron acceptors, donors, and donor-acceptor compounds based on heterocycles such as 1,2,5-thiadiazole and 1,3-dithiole were synthesized and their properties including those of the charge-transfer complexes or ion-radical salts were investigated. Thiophene oligomers with rigid structures were also synthesized for molecular wires.

VIII-E-1 Synthesis and Characterization of New Electron Donors Containing 1,2,5-Thiadiazole and 1,1'-Dihydro-4,4'-bi(pyridylidene) Units

Yoshiro YAMASHITA, Katsuhiko ONO, Masaaki TOMURA and Kenichi IMAEDA

[*Chem. Commun.* 1851 (1997)]

Viologens **1** are widely used as electron-transfer reagents. However, their cation radical and neutral states are unstable toward oxygen due to their very low oxidation potentials. We have now introduced 1,2,5-thiadiazole rings to the dihydrobipyridine skeleton to give **2** in order to enhance the stability of the neutral state of viologens. The viologen derivatives **2** were prepared by reductive coupling of pyridinium compounds **3** which were obtained from 7-chloro-1,2,5-thiadiazolo[3,4-b]pyridine via several steps. The compounds **2a**,**b** are stable in air, in contrast to the unstable neutral viologens. They have absorption maxima in the long wavelength region [**2a**: 623, **2b**: 627 nm in CH_2Cl_2]. The oxidation potentials are lower than those of TTF, indicating that they are stronger electron donors than TTF. The donor **2a** gave PF_6 and AsF_6 salts of the cation radical upon electrochemical oxidation. They are 1:1 salts and show semiconducting behaviour. X-ray structure analysis of the PF_6 salt revealed that the planar donor molecules are stacked in an interesting mode where one donor molecule bridges two other molecules. Another interesting feature is that a tape-like network of the donor molecules is formed by short S···N contacts (3.05 Å).

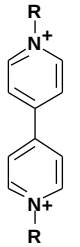

1

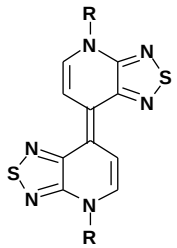

2a R = Me
2b R = Et

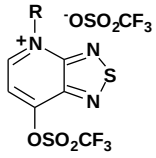

3

VIII-E-2 Synthesis and Properties of Bis(1,3-dithiol-2-ylidene) Compounds Containing a 2,2'-Bithienyl Unit

Akira OHTA and Yoshiro YAMASHITA

In order to develop new redox systems which undergo a reversible structural change by electron transfer, bis(1,3-dithiol-2-ylidene) compounds **1** containing a 2,2-bithienyl unit have been prepared by a Wittig-Horner reaction from the corresponding ketone. The cyclic voltammogram of **1a** shows an irreversible peak (E_{pa} = 0.82 V, E_{pc} = 0.28 V vs. SCE in PhCN). This result can be explained by considering that it undergoes an intramolecular oxidative cyclization and the resulting dication **2** reverts to **1** by reduction. In fact, chemical oxidation of **1a** with nitrosyl tetrafluoroborate afforded the corresponding cyclization products **2a** as a dication salt in 96% yield. The starting compound **1a** was reproduced by reduction of the dication salt with zinc dust in acetonitrile.

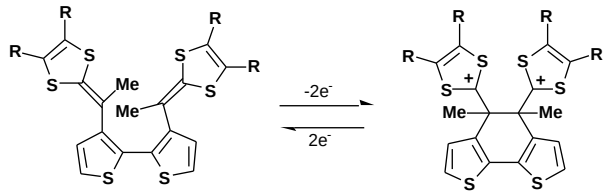

1 **a**: R, R = benzo **b**: R = SMe **2**

VIII-E-3 Synthesis and Properties of Novel Tetrathiafulvalene Vinylogues

Yoshiro YAMASHITA, Masaaki TOMURA, M. Badruz ZAMAN and Kenichi IMAEDA

[*Chem. Commun.* in press]

TTF vinylogues **1** bearing substituents at the vinyl positions have been considered to be non-planar due to the steric interactions between the substituents and the 1,3-dithiole parts. However, the TTF vinylogue skeletons can be planar when the aryl substituents are twisted from the π-conjugated framework. These compounds are expected to afford conductors with unusual structures since the bulky substituents disturb usual molecular overlapping. We have now synthesized

various derivatives **1** using an oxidative dimerization reaction of 1,4-dithiafulvene derivatives **2** with tris(4-bromophenyl)aminium hexachloroantimonate. The methyl, phenyl, and *p*- or *m*-substituted phenyl derivatives show reversible one-stage two-electron redox waves in their cyclic voltammograms, indicating that they are non-planar molecules and their cation radicals are unstable. In contrast, the derivatives with *o*-substituted phenyl groups show stepwise reversible oxidation potentials. This result suggests that the aryl part is twisted and the TTF vinylogue skeleton is planar in the cation radical states of the *o*-substituted phenyl derivatives. Actually, some compounds afforded the cation radical salts as single crystals upon electrochemical oxidation.

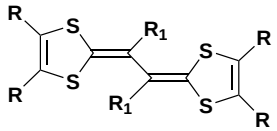

1

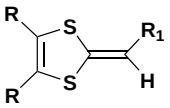

2

R, R = benzo, SCH_2CH_2S

VIII-E-4 Molecular and Crystal Structure of Novel Tetrathiafulvalene Vinylogues and Their Cation Radical Salts

Masaaki TOMURA and Yoshiro YAMASHITA

Molecular and crystal structures of novel tetrathiafulvalene (TTF) vinylogues and their cation radical salts with extended π-conjugated system and various functional groups in their vinyl part have been investigated by X-ray crystallographic analysis. In the compound **1a**, two 1,3-dithiole parts were twisted remarkably (dihedral angle: 61.1°). In contrast with the neutral state, the TTF vinylogue framework in the cation radical salt **1a**-PF_6 obtained by electrochemical oxidation was planar. Such a molecular structure causes an interesting two-dimensional stacking mode where one donor molecule bridges two molecules in the crystal of **1a**-PF_6, as shown in Figure 1. On the other hand, unique mixed stack was observed in the crystal of **1b**-$Au(CN)_2$ salt.

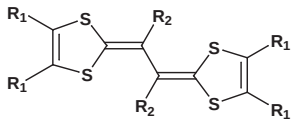

1

a: R_1,R_1 = benzo, R_2 = 2,6-$F_2C_6H_3$
b: R_1,R_1 = SCH_2CH_2S, R_2 = *o*-ClC_6H_4

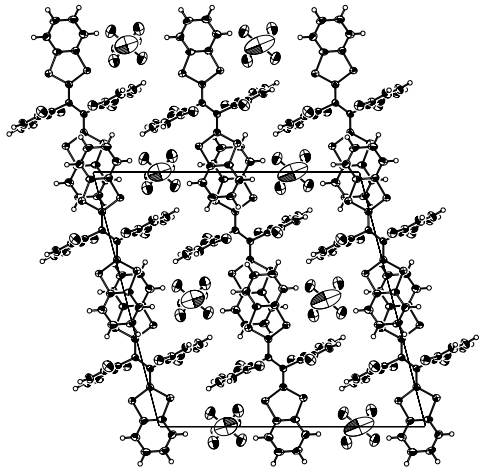

Figure 1. Crystal structure of **1a**-PF_6 salt viewed along b axis.

VIII-E-5 New Electron Acceptors Containing Thieno[3,4-b]pyrazine Units

Kazuharu SUZUKI, Masaaki TOMURA and Yoshiro YAMASHITA

[*J. Mater. Chem.* **8**, 1117 (1998)]

Sulfur containing TCNQ analogues are highly polarized and are expected to have strong intermolecular interactions by heteroatom contacts. Benzothiophene-TCNQ **1** is a weak electron acceptor due to the fused benzene ring. We have now replaced the benzene ring by electron-withdrawing pyrazine rings to give new acceptors **2**. We have also obtained π-extended acceptors **3** here. The acceptors **2** and **3** were prepared from 5,7-dibromothieno[3,4-b]pyrazines **4**. Thus, reaction of **4** with tetracyanoethylene oxide (TCNEO) in refluxing 1,2-dibromoethane afforded **2** and **3**. The cyclic voltammograms of **2** and **3** show reversible two-step one-electron redox waves. The reduction potentials are lower than those of TCNQ. The differences between the first and second reduction potentials are much lower in **3** than in **2** due to reduced on-site Coulomb repulsion. The single crystals of **2a** were obtained as two crystal forms, i.e. orthorhombic and monoclinic forms. In the orthorhombic crystal no short interheteroatom contact was observed. On the other hand, in the monoclinic crystal three kinds of short S···N contacts were observed, which result in an interesting helical structure. The acceptor **2a** gave two kinds of CT complexes with TTF (1:2 and 3:2 complexes) which have unique three-dimensional structures involving short S···N contacts.

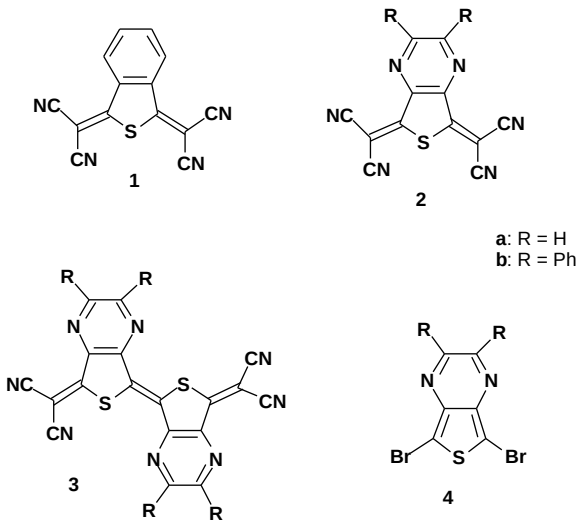

VIII-E-6 Design of Novel 4-Terminal Molecular Switching Unit Based on Multi-Stage Redox System

Shoji TANAKA and Yoshiro YAMASHITA

There has been a great deal of interest in utilizing π-conjugated organic molecules for nano-scale electronic devices. The main issue of molecular design in this area is to realize steady-state single-molecule conduction and quick switching of the conductivity (switching frequency > 1 T Hz). For this purpose, intensive efforts are now in place to synthesize transistor-like conjugated molecules with three or more distinct terminals, which would lead to dynamic control of information carries. As a novel building unit for this class of functional molecules, we have designed a "4-terminal" conjugated heterocyclic compound **2**. This molecule contains a pyrazine-dihydropyrazine multi-stage redox center **1** and the electronic structure can be switchable between low and high energy-gap states by chemical or electrochemical methods.

Compound **2red** was synthesized from 3',4'-diamino-2,2':5',2''-terthiophene. The reaction of **2red** with nickel peroxide gave the oxidized form **2ox**. AM1 calculations indicate that the unsubstituted redox center **1** has a much lower HOMO-LUMO gap in the oxidized form compared with that in the reduced form. Further, conformational analyses predict that the oxidized form **2ox** has a fully-conjugated π-system with all *s-trans* coplanar conformation, while the reduced form **2red** has a non-planar geometry. These theoretical predictions are consistent with the spectral data; the longest λ_{max} of **2ox** (1062 nm) appears at a much longer wavelength than that of **2red** (360 nm). We are trying to develop synthetic approaches for selective introduction of various types of molecular wires to each terminal (unsubstituted α or β-positions of the thiophene rings) of **2** to construct a molecular-scale transistor.

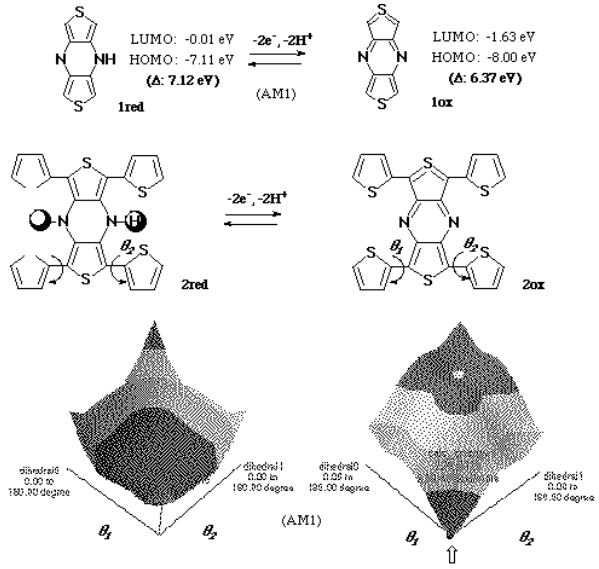

Figure 1. FMO levels of **1** and torsional potentials of **2** as a function of dihedral angles θ_1 and θ_2.

VIII-F Elecrtonic Structures and Rectivities of Active Sites of Metalloproteins

Metalloproteins are a class of biologically important macromolecules which have various functions such as oxygen transport, electron transfer, oxidation, and oxygenation. These diverse functions of metalloproteins have been thought to depend on the ligands from amino acid, coordination structures, and protein structures in immediate vicinity of metal ions. In this project, we are studying the relationship between the structures of the metal active sites and functions of metalloproteins.

VIII-F-1 Imidazole and *p*-Nitrophenolate Complexes of Oxo Iron(IV) Porphyrin π-Cation Radicals as Models for Compounds I of Peroxidase and Catalase

Hiroshi FUJII, Tetsuhiko YOSHIMURA *(Inst. for Life. Supp. Tech.)* **and Hitoshi KAMADA** *(Inst. for Life. Supp. Tech.)*

[*Inorg. Chem.* **36**, 6142 (1997)]

Oxo iron(IV) porphyrin π-cation radical species (compound I) have been identified or proposed as functional intermediates in the catalytic cycles of peroxidase, catalase, and cytochrome P-450. Since these enzymes have different axial ligands: peroxidase (imidazole), catalase (phenolate), and cytochrome P-450 (thiolate), the axial ligands are generally thought to control the reactivity of compounds I. To investigate the functional role of the axial ligand in compound I, we prepared and characterized imidazole, $(P^{\cdot})Fe^{IV}O(Im)$, and phenolate, $(P^{\cdot})Fe^{IV}O(OAr)$, complexes of oxo

iron(IV) 2,7,12,17-tetramethyl-3,8,13,18-tetramesityl porphyrin. $(P^{\cdot})Fe^{IV}O(Im)$ was prepared by titration of perchlorate oxo iron(IV) porphyrin π-cation complex, $(P^{\cdot})Fe^{IV}O(ClO_4)$, with one equivalent of imidazole. $(P^{\cdot})Fe^{IV}O(Im)$ was also formed when a mono imidazole complex of iron(III) porphyrin was oxidized by ozone in dichloromethane at -80°C. The successful formation of $(P^{\cdot})Fe^{IV}O(Im)$ can be attributed to the weak ligand character of the perchlorate anion which is easily displaced by imidazole and/or the use of ozone which does not form a coordinative ligand during the oxidation. The absorption spectrum of $(P^{\cdot})Fe^{IV}O(Im)$ closely resembled that of compound I in peroxidase. The paramagnetic ^{1}H-NMR of $(P^{\cdot})Fe^{IV}O(Im)$ indicates an a_{1u} radical state as well as imidazole coordination without reduction of the porphyrin π-radical. Similarly, a p-nitrophenolate complex of oxo iron(IV) porphyrin, $(P^{\cdot})Fe^{IV}O(OAr)$, was prepared by ozone oxidation of a mono *p*-nitrophenolate complex of iron(III) porphyrin in dichloromethane at -95°C. The absorption spectrum of $(P^{\cdot})Fe^{IV}O(OAr)$ closely resembled that of compound I of catalase. The results in this study indicate that the position of the absorption peak in compound I species correlates with the basicity of the axial ligand, but not the a_{1u}/a_{2u} porphyrin radical state.

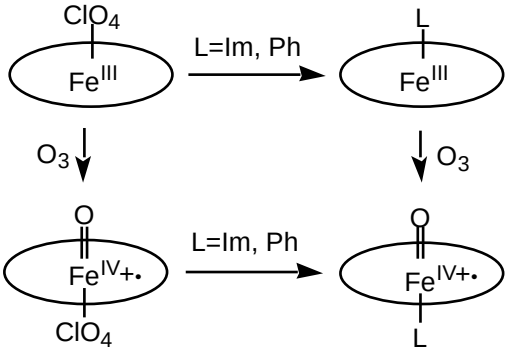

Figure 1. Synthesis of imidazole and *p*-nitrophenolate complexes of oxo iron(IV) porphyrin π-cation radicals.

VIII-F-2 Electron Configuration and Spin Distribution in Low-Spin (meso-Tetraalkylporphyrinato)iron(III) Complexes Carrying One or Two Orientationally Fixed Imidazole Ligands

Mikio NAKAMURA *(Toho Univ.)*, **Takahisa IKEUE** *(Toho Univ.)*, **Hiroshi FUJII, Tetsuhiko YOSHIMURA** *(Life for Supp. Tech.)* **and Kunihiko TAJIMA** *(Kyoto Inst. Tech.)*

[*Inorg. Chem.* **37**, 2405 (1998)]

To understand the orientation effect of coordinated imidazole ligands, a series of low-spin (tetraalkylporphyrinato)iron(III) complexes, $[Fe(TRP)(L)_2]^+$ and [Fe(TRP)(L)(CN)], carrying at least one orientationally fixed imidazole (L) have been prepared. The ^{1}H NMR pyrrole signals of a series of $[Fe(TRP)(2\text{-}MeIm)_2]^+$ have shown considerable downfield shifts as the meso substituent becomes bulkier, from -30.4 (R = H) to +5.6 ppm (R = iPr) at -71°C. The spread of the pyrrole signals decreases from 9.4 (Me) to 8.2 (Et) and then to 5.7 (iPr) ppm. The downfield pyrrole signals together with the small spread in $[Fe(TiPrP)(2\text{-}MeIm)_2]^+$ are in sharp contrast to the other low-spin complexes with orientationally fixed imidazole ligands; the chemical shifts and spreads of the pyrrole signals in [tetrakis-(2,4,6-trialkylphenyl)porphyrinato]iron(III) complexes $[Fe(R\text{-}TPP)(2\text{-}MeIm)_2]^+$ (R = Me, Et, iPr) are ca. -20 and ca. 9 ppm, respectively, at -71°C. The EPR spectra of a series of $[Fe(TRP)(2\text{-}MeIm)_2]^+$ were then taken at 4.2 K. While the R = H, Me, and Et complexes have shown so-called "large gmax type" spectra as in the case of $[Fe(R\text{-}TPP)(2\text{-}MeIm)_2]^+$, the iPr complex has exhibited an "axial type" spectrum. The result indicates that the electron configuration of the ferric ion of $[Fe(TiPrP)(2\text{-}MeIm)_2]^+$ is presented by the unusual $(dxz, dyz)^4(dxy)^1$ in contrast to the other low-spin complexes where ferric ions have the $(dxy)^2(dxz, dyz)^3$ configuration. When one of the 2-MeIm ligands in $[Fe(TRP)(2\text{-}MeIm)_2]^+$ is replaced by CN^-, not only the iPr but also the Me and Et complexes have shown the $(dxz, dyz)^4(dxy)^1$ configuration as revealed from the EPR spectra. The pyrrole signals of the iPr complex [Fe(TiPrP)(2-MeIm)(CN)] have been observed at 12.2, 14.1, 14.8, and 16.2 ppm at -71°C. Thus, the spread is only 4.0 ppm. The value is quite different from that of the corresponding [Fe(Me-TPP)(2-iPrIm)(CN)] where the spread reaches as much as 11.4 ppm. On the basis of these results, it is concluded that the spin distribution on the pyrrole -carbons in the complexes with $(dxz, dyz)^4(dxy)^1$ is rather homogeneous even if the coordinated imidazole is orientationally fixed. On the contrary, the fixation induces a larger asymmetric spin distribution on these carbons in the complexes with $(dxy)^2(dxz, dyz)^3$ configuration.

VIII-F-3 Raman Signature of the Fe_2O_2 "Diamond" Core

Elizabeth C. WILKINSON *(Univ. Minnesota)*, **Yanhong DONG** *(Univ. Minnesota)*, **Yan ZANG** *(Univ. Minnesota)*, **Hiroshi FUJII, Robert FRACZKIEWICZ** *(Univ. Houston)*, **Grazyna FRACZKIEWICZ** *(Univ. Houston)*, **Roman S. CZERNUSZEWICZ** *(Univ. Houston)* **and Lawrence QUE, JR.** *(Univ. Minnesota)*

[*J. Am. Chem. Soc.* **120**, 955, (1998)]

We report the resonance Raman (RR) spectra of iron complexes containing the $Fe_2(\text{-}O)_2$ core. Frozen CH_3CN solutions of the FeIIIFeIV intermediate $[Fe_2(\text{-}O)_2L_2](ClO_4)_3$ (where L = TPA, 5-Me_3-TPA, 5-Me_2-TPA, 5-MeTPA, 5-Et_3-TPA, or 3-Me_3-TPA) show numerous resonance-enhanced vibrations, and among these, an oxygen-isotope-sensitive vibration around 667 cm^{-1} that shifts ca. 30 cm^{-1} when the samples are allowed to exchange with $^{18}OH_2$, and whose Raman shift does not vary with methyl substitution of the TPA ligand. Spectra of iron-isotope-substituted samples of $[Fe_2(\text{-}O)_2(L)_2](ClO_4)_3$ (^{54}Fe and ^{57}Fe for L = TPA, and ^{54}Fe and ^{58}Fe for L = 5-Me_3-TPA) show that this vibration is also iron-isotope-sensitive. These isotopic data taken together strongly suggest that this vibration involves motion of the $Fe_2(\text{-}O)_2$ core that is isolated from motions of the ligand. A frozen CH_3CN solution of the

diiron(III) complex $[Fe_2(-O)_2(6\text{-}Me_3\text{-}TPA)_2](ClO_4)_2$ shows one intense resonance-enhanced vibration at 692 cm^{-1} that shifts -30 cm^{-1} with ^{18}O labeling. Normal coordinate analysis of the $Fe_2(-O)_2$ core in $[Fe_2(-O)_2(5\text{-}Me_3\text{-}TPA)_2](ClO_4)_3$ supports the assignment of the Fermi doublet centered around 666.2 cm^{-1} as an A_1 vibration of this core. Furthermore, we propose that this unique feature found in the region between 650 and 700 cm^{-1} is indicative of a diamond core structure and is the Raman signature of an iron cluster containing this core.

VIII-F-4 ^{63}Cu-NMR Study of Copper(I) Carbonyl Complexes with Various Hydrotris(pyrazolyl)-borates: Correlation between ^{63}Cu Chemical Shifts and CO Stretching Vibrations

Sadako IMAI *(Tokyo Inst. Tech.)*, **Kiyoshi FUJISAWA** *(Tokyo Inst. Tech.)*, **Takako KOBAYASHI** *(Tokyo Inst. Tech.)*, **Nobuhiko SHIRASAWA** *(Tokyo Inst. Tech.)*, **Hiroshi FUJII, Tetsuhiko YOSHIMURA** *(Inst for Life Supp. Tech.)*, **Nobumasa KITAJIMA** *(Tokyo Inst. Tech.)* **and Yoshihiko MORO-OKA** *(Tokyo Inst. Tech.)*

[*Inorg. Chem.* **37**, 3066 (1998)]

Copper(I) carbonyl complexes with a series of hindered LR_1,R_2 ligands (L: hydrotris(pyrazolyl)borate, R_1 and R_2 are substituents at the 3- and 5-positions of the pyrazole ring, respectively), LR_1,R_2CuCO [R_1, R_2 = Me, Me (1), i-Pr, i-Pr (2), t-Bu, Me (3), t-Bu, i-Pr (4), Ph, i-Pr (5), Ph, Ph (6)] have been synthesized and characterized by ^{1}H NMR and IR spectroscopy and elemental analysis. The molecular structures of 3 and 6 have been determined by X-ray crystallography. The electronic structures of copper(I) sites are characterized by means of ^{63}Cu NMR spectroscopy and by the CO stretching vibration. The sharp ^{63}Cu NMR signals are observed for LR_1,R_2CuCO complexes in toluene at room temperature. The ^{63}Cu NMR signals of copper(I) complexes with alkyl-substituted ligands (1-4) are observed in lower field than those of the phenyl derivatives (5, 6) correlating with the electron-density at the copper center. This argument is supported by the good correlation between the (^{63}Cu) value and CO stretching vibration which is a sensitive indicator of the extent of back-donation of the Cu d electrons to the antibonding CO orbitals.

VIII-G Molecular Mechanism of Heme Degradation and Oxygen Activation by Heme Oxygenase

Heme oxygenase (HO), an amphipathic microsomal proteins, catalyzes the regiospecific oxidative degradation of iron protoporphyrin IX (heme) to biliverdinIXα, carbon monoxide, and iron in the presence of NADPH-cytochrome P-450 reductase, which functions as an electron donor. Heme oxygenase reaction is the biosynthesis processes of bile pigments and CO which is a possible physiological messenger. Recent development in the bacterial expression of a soluble form of heme oxygenase has made it possible to prepare in the large quantities for structural studies. In this project, we are studying the molecular mechanism of heme degradation and oxygen activation by heme oxygenase using various spectroscopic methods.

VIII-G-1 Cobalt Porphyrin Heme Oxygenase Complex. EPR Evidences for the Distal Heme Pocket Hydrogen Bonding

Hiroshi FUJII, Yi DOU *(Case Western Reserve Univ.)*, **Hong ZHOU** *(Yamagata Univ.)*, **Tadashi YOSHIDA** *(Yamagata Univ.)* **and Masao IKEDA-SAITO** *(Case Western Reserve Univ.)*

[*J. Am. Chem. Soc.* **120**, 8251 (1998)]

Heme oxygenase (HO) is a microsomal enzyme which catalyzes the degradation of iron protoporphyrin IX (heme) to biliverdinIXα through the two heme derivatives, α-meso-hydroxyheme and verdohemeIXα. The key intermediate in the first step of the heme oxygenase reaction is the metastable ferrous O_2-bound form of the heme-HO complex. While our resonance Raman studies of the oxy-form indicated a highly bent structure of bound dioxygen, the electronic structure and the activation mechanism, including the proton relay system using hydrogen bond interaction with bound dioxygen, need to be elucidated. To this end, we have prepared the cobalt(II) porphyrin HO complex. The EPR spectrum of deoxy-form of the cobalt(II) porphyrin HO complex is similar to that of cobalt-myoglobin (Mb), indicating the similarity of the binding property of proximal histidine between them. In contrast, the EPR spectrum of the oxy-from of cobalt porphyrin HO complex is more anisotropic than that of cobalt-Mb. This reflects the difference in the structure of bound dioxygen between them. The EPR parameters seem to be consistent with the highly bent Co-dioxygen binding. When the measurement is carried out in a deuterated buffer system, the hyperfine structure of the EPR spectrum of the oxy form of the cobalt-HO complex is sharpened. This shows the formation of a hydrogen bond interaction between the bound dioxygen and the amino acid residue in the distal pocket of the enzyme. The finding of the hydrogen bond interaction could explain the high oxygen affinity of the heme-HO complex and the meso hydroxylation mechanism using proton relay system proposed for cytochrome P-450.

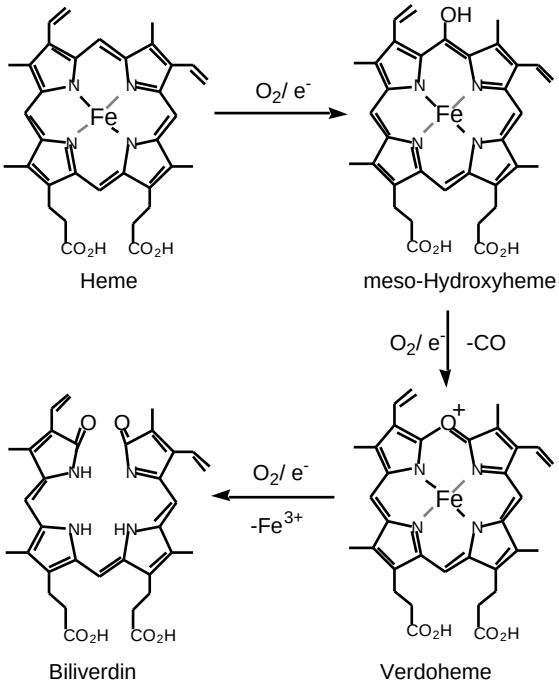

Figure 1. Reaction intermediates in the heme oxygenase-catalyzed oxidation of heme to biliverdinIXα.

VIII-G-2 The Oxygen and Carbon Monoxide Reactions of Heme Oxygenase

Catharina Taiko MIGITA *(Case Western Reserve Univ.)*, **Kathyln Mansfield MATERA** *(Case Western Reserve Univ.)*, **Masao IKEDA-SAITO** *(Case Western Reserve Univ.)*, **John S. OLSON** *(Rice Univ.)*, **Hiroshi FUJII, Hong ZHOU** *(Yamagata Univ.)* **and Tadashi YOSHIDA** *(Yamagata Univ.)*

[*J. Biol. Chem.* **273**, 945 (1998)]

Heme oxygenase is the central enzyme of heme degradation and associated carbon monoxide biosynthesis. We have prepared the heme, α-hydroxyheme, and verdoheme complexes of heme oxygenase, and their reactions with oxygen and carbon monoxide have been studied. The heme complexes of heme oxygenase isoforms-1 and -2 have similar oxygen and carbon monoxide binding properties. The oxygen affinities are very high, K_{O_2} = 30 - 80 μM^{-1}, which is 30 to 90-fold greater than those of mammalian myoglobins. The oxygen association rate constants are similar to those for myoglobins (k'_{O_2} = 7-20 $\mu M^{-1}s^{-1}$), whereas the oxygen dissociation rates are remarkably slow (k_{O_2} = 0.25 s^{-1}), implying the presence of very favorable electrostatic interactions between bound oxygen and protein residues in the heme pocket. The carbon monoxide association reactions with the heme-enzyme complexes are biphasic, while the CO dissociation reactions are monophasic. The carbon monoxide affinities estimated for both isoforms are only 1 to 6-fold higher than the corresponding oxygen affinities. Thus, both HO-1 and HO-2 discriminated much more strongly against CO binding than either myoglobin or hemoglobin. The carbon monoxide binding reactions with the ferrous a-hydroxyheme-HO complex are similar to those of the initial protoheme complex, and thus hydroxylation at the a-meso position does not appear to affect the reactivity of the iron atom. In contrast, the carbon monoxide affinities of the verdoheme-HO complexes are > 10,000 times weaker that those of the heme complexes due to a 100-fold slower association rate constant ($k'_{CO} \approx 0.004\ \mu M^{-1}$) and a 300-fold greater dissociation rate constant (kCO ≈ 3 s^{-1}) compared to the corresponding rate constants of the protoheme and a-OH heme complexes. The positive charge on the verdoporphyrin ring causes a large decrease in reactivity of the iron.

VIII-G-3 Identification that Histidine 45 is the Axial Heme Iron Ligand of Heme Oxygenase-2

Kazunobu ISHIKAWA *(Yamagata Univ.)*, **Kathyln Mansfield MATERA** *(Case Western Reserve Univ.)*, **Hong ZHOU** *(Yamagata Univ.)*, **Hiroshi FUJII, Michihiko SATO** *(Yamagata Univ.)*, **Tetsuhiko YOSHIMURA** *(Inst. for Life. Supp. Tech.)*, **Masao IKEDA-SAITO** *(Case Western Reserve Univ.)* **and Tadashi YOSHIDA** *(Yamagata Univ.)*

[*J. Biol. Chem.* **273**, 4317 (1998)]

A truncated, soluble, and enzymatically active form of human heme oxygenase-2(ΔHHO2) was expressed in *Escherchia coli*. To identify the axial heme ligand of HO-2, His-45 to Ala(ΔH45A) and His-152 to Ala (ΔH152A) mutants have been prepared using this expression system. ΔH45A could form a 1:1 complex with hemin but was completely devoid of the heme degradation acitivty. A 5-coordinate-type ferrous NO EPR spectrum was observed for the heme-ΔH45A complex. The ΔH152A mutant was expressed as an inclusion body and was recovered from the lysis pellet by dissolution in urea followed by dialysis. The solubilized fraction obtained, however, was composed of a mixture of a functional enzyme and an inactive fraction. The inactive fraction was removed by Sephadex G-75 column at the void volume. The gel filtration-purified ΔH152A exhibited spectroscopic and enzymatic properties identical to those of wild-type. We conclude, in contrast to the previous reports (McCoubrey and Mains, *Arch. Biochem. Biophys.* **302**, 402 (1993); McCoubrey, W. K., Jr., Huang, T. J. and Mains, M., *J. Biol. Chem.* **272**, 12568 (1997)), that His-45, but not H152, in heme oxygenase isoform-s is the proximal ligand of the heme and is essential for the heme degradation aciticty of the enzyme. His-152 appears to play a structural role in stabilization of the heme oxygenase protein.

VIII-H Designing Artificial Photosynthesis at Molecular Dimensions

Photosynthesis is one of the finest piece of molecular machinery that Nature has ever created. Its ultrafast electron transfer and following well-organized sequence of chemical transformation have been, and will continue to be, challenging goals for molecular scientists. We are trying to mimic the function of photosynthesis by assembling molecular units that perform individual physical/chemical action. The molecular units include porphyrins, redox active organic molecules, and transition metal complexes.

We have been so far focusing our efforts on manganese complexes (which are known to play a key role in oxygenic photosynthesis) and their interaction with porphyrins. Our ultimate goal is to design artificial molecular systems that effect multiple chemical reactions triggered by light, on the basis of molecular rationale.

VIII-H-1 Synthesis and Characterization of Manganese Complexes

Hitoshi IIKURA *(Kyoto Univ.)* **and Toshi NAGATA**

[*Inorg. Chem.* in press]

Four new manganese complexes of carboxylate-containing chelating ligands, L^1 and L^2 (L^1H = (bis(2-pyridylmethyl)amino)acetic acid, L^2H = 3-(bis(2-pyridylmethyl)amino)propionic acid), were synthesized and characterized by X-ray crystallography. In spite of the structural diversity in these complexes - two Mn^{II} dimers, one Mn^{II} chain complex, and one bis(μ-oxo) Mn^{IV} dimer - all of them were built up from a common structural motif, an "L^nMn" fragment, interconnected in various topology. These ligands L^1 and L^2 are potentially useful in controlling structures of manganese carboxylate complexes.

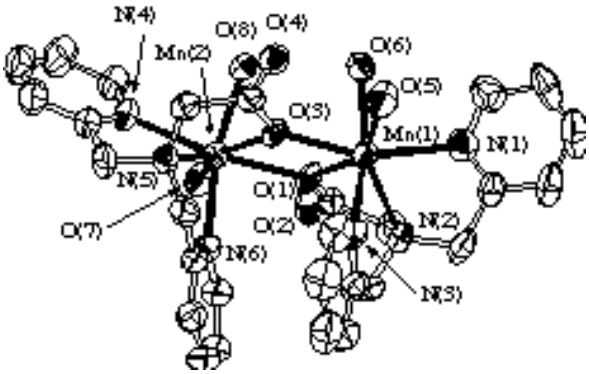

Figure 1. ORTEP view of the $[Mn_2L^1{}_2(H_2O)_4]^{2+}$ cation.

VIII-H-2 Synthesis and Photophysical Properties of Porphyrin-Dimanganese Composite Molecules

Katsuji AIKAWA *(Kyoto Univ.)***, Toshi NAGATA, Atsuhiro OSUKA** *(Kyoto Univ.)***, Yoshifumi KIMURA** *(Kyoto Univ.)***, Noboru HIROTA** *(Kyoto Univ.)***, Iwao YAMAZAKI** *(Hokkaido Univ.)* **and Yoshinobu NISHIMURA** *(Hokkaido Univ.)*

The first porphyrin-dimanganese composite molecules were synthesized. Fluorescence of the porphyrin moiety was effectively quenched by the dimanganese moiety (fluorescence lifetime decreased from 1.5 ns to 61 ps). Transient absorption spectoscopy revealed that intersystem crossing from S_1 of porphyrin to T_1 was enhanced by the presence of the manganese complex. Analogous compound with zinc in place of manganese did not show such enhancement, suggesting that the unpaired electrons on the manganese ions are involved in the process. Comparison of the electrochemical properties of the composite molecules with those of the component molecules (porphyrin and dimanganese complex), it was revealed that the oxidation potentials of dimanganese moieties showed about +0.1 V shift whereas the oxidation potentials of porphyrin showed no significant change.

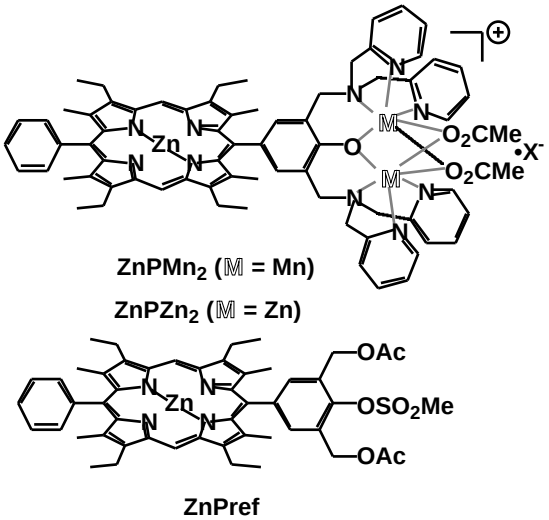

Figure 1. A porphyrin-dimanganese composite molecule and related compounds.

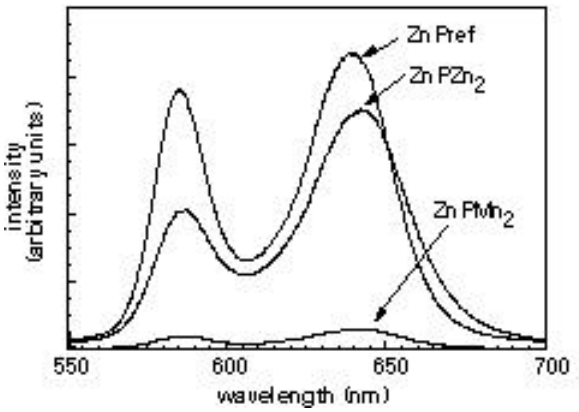

Figure 2. Steady-state fluorescence spectra (at room temperature, in CH_3CN).

VIII-I Organic Molecular Materials with Novel Electronic Properties

Some aromatic and heterocyclic compounds show intriguing physical properties, such as superconductivity, ferromagnetism, and electroluminescence, in the solid state. The aim of our research is to design and synthesize such molecules. We have been working on three research projects: synthesis of organic conductors, fullerene chemistry, and organic electroluminescent (EL) materials.

VIII-I-1 Functionalization of C_{60} by Acetylenes

Hiroshi YAMAGUCHI *(Nagoya Univ.)*, **Shizuaki MURATA** *(Nagoya Univ.)* **and Toshiyasu SUZUKI**

Unsaturated bonds in the organic groups on C_{60} are expected to interact with π orbitals of C_{60}, if the distance between these two π systems is close enough. Some of these examples are known to undergo unique intramolecular rearrangements. We are interested in constructing such C_{60} derivatives by using acetylenes.[1)] Thus, in the presence of Pd(0), two dimethyl acetylenedicarboxylate molecules react with C_{60} to give $(MeOCOC)_4C_{60}$. Under photochemical conditions, this derivative can be converted into the bis-methanofullerene isomer, which is easily oxidized to $(MeOCO)_4C_{60}O_2$ (Figure 1) with a large hole in the fullerene cage.

Reference

1)H. Yamaguchi, S. Murata, T. Akasaka and T. Suzuki, *Tetrahedron Lett.* **38**, 3529 (1997).

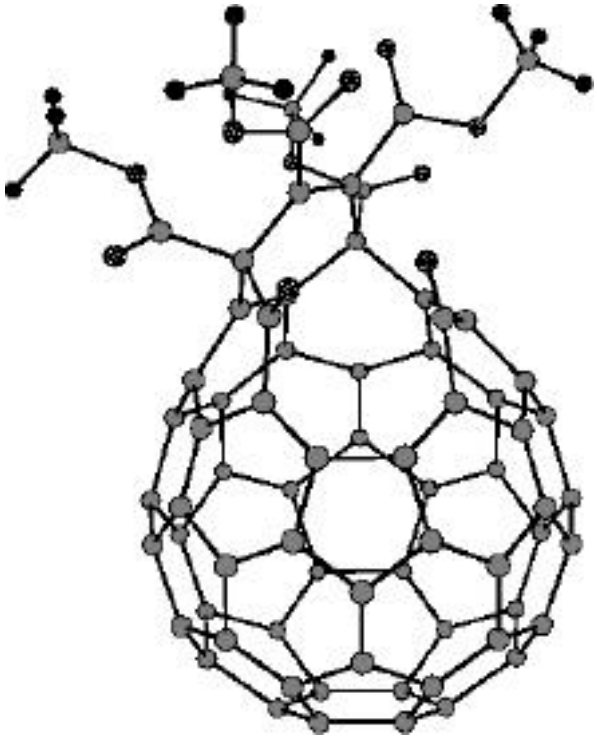

Figure 1. Molecular model of $(MeOCO)_4C_{60}O_2$.

VIII-I-2 New Electron-Transporting Materials for Organic EL Devices

Toshiyasu SUZUKI

Recently, organic EL devices have gained considerable attention because of their application to flat panel displays. These devices are composed of hole-transporting, emissive, and electron-transporting (ET) layers as well as two electrodes. Organic photoconductors (triaryl amine derivatives) and laser dyes can be adapted to hole-transporting and emissive materials, respectively. On the other hand, there have been few ET organic materials for practical use. We are trying to synthesize perfluorinated phenylene dendrimers which might form stable amorphous ET layers.

VIII-J Studies of Nanoscale Carbons

The sp^2 bonded nanometer scale carbons are studied in this project. Nanotubes and nano-graphite particles are the candidates of the materials. Electron microscopy, powder x-ray diffraction, Raman scattering, electron spin resonance and magnetic susceptibility measurements are all used to study the structural and solid state properties of nanoscale carbon materials.

VIII-J-1 Effect of Environment Temperature for Synthesizing the Single Wall Carbon Nanotubes by Arc Vaporization Method

Morio TAKIZAWA *(Japan Science & Technology Corporation)*, **Tatsuharu TORII and Shunji BANDOW** *(Japan Science & Technology Corporation)*

Single wall carbon nanotubes (SWNTs) can be synthesized either a pulsed laser vaporization at high temperature environment (~1200 °C) or an arc burning at room temperature of a carbon rod containing a few atomic % of bi-metallic catalysts such as Ni-Y, Ni-Co and Ni-Fe. The effect of the environment temperature for yielding SWNTs by the pulsed laser vaporization method has been reported previously.[1] Briefly, a synthesizing rate of SWNTs was accelerated at the temperature higher than 850 °C. In this study, we briefly report the effect of environment temperature to produce SWNTs via. the arc burning of a Ni-Y (0.6-0.6 atom %) catalyzed carbon rod. The arc burning of the carbon rod containing Ni-Y was carried out in a 50 mm diameter quartz tube under a 500 Torr of He gas. Environment temperature near the arcing was controlled by the electronic furnace surrounding the quartz tube. The number of SWNTs was estimated by measuring the diameter of tubule bundle D and by counting the number of bundles per unit area N. By using D^2N, we can estimate the number of individual tubules per unit area for each sample. Figure 1 shows the temperature effect for synthesizing the tubules. In Figure 1, we can find the SWNTs are well generated in the temperature range of 400 to 600 °C. According to the present study and to the laser vaporization study, it was found that the environment temperature is also important to synthesize SWNTs as well as to select the metal catalyst.

References

1) S. Bandow, S. Asaka, Y. Saito, A. M. Rao, L. Grigorian, E. Richter and P. C. Eklund, *Phys. Rev. Lett.* 80, 3779 (1998).

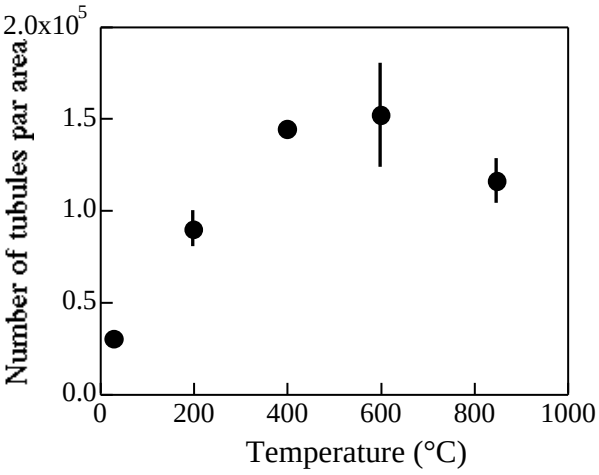

Figure 1. Environment temperature dependence on synthesizing the single wall carbon nanotubes via. arc burning of Ni-Y (0.6-0.6 atom %) composite carbon rod. The rod is 10 mm in diameter and is set at the end of the positive electrode. The arc current is 100 A under a 500 Torr of He gas with a flow rate of 100 sccm.

VIII-J-2 Radial Thermal Expansion of Purified Multiwall Carbon Nanotubes Measured by X-Ray Diffraction

Shunji BANDOW *(Japan Science & Technology Corporation)*

[*Jpn. J. Appl. Phys.* **36**, L1403 (1997)]

The thermal expansion in the radial direction (stacking axis of graphene sheets) of multiwall carbon nanotubes (MWNTs) is measured in the temperature range from 10 to 320 K. The sample includes in excess of 85 % by weight of MWNTs. The radial thermal expansion of MWNTs is found to be almost the same with the c-axis thermal expansion of graphite. This result strongly challenges the concentric structural model for MWNTs, suggesting the appropriateness of the scroll type model instead of the concentric one.

VIII-J-3 Effect of the Growth Temperature on the Diameter Distribution and Chirality of Single Wall Carbon Nanotubes

Shunji BANDOW *(Japan Science & Technology Corp.)*, **Shuji ASAKA, Yahachi SAITO** *(Mi'e Univ.)*, **Apparao M. RAO** *(Univ. Kentucky)*, **Leonid GRIGORIAN** *(Univ. Kentucky)*, **Ernest RICHTER** *(Univ. Kentucky)* **and Peter C. EKLUND** *(Univ. Kentucky)*

[*Phys. Rev. Lett.* **80**, 3779 (1998)]

Pulsed laser vaporization (PLV) of a heated, catalyzed carbon target in argon gas has been used to synthesize single-wall carbon nanotubes (SWNTs). Electron microscopy, x-ray diffraction and Raman spectroscopy were all used to study the effect of the catalyst on the tube yield, and the evolution of the tube diameter distribution with increasing growth environment temperature T. By controlling the temperature in the range $780 < T < 1050$ °C, we have been able to tune the diameter of the tubules from ~ 0.81 to ~ 1.51 nm. The threshold temperature for significant SWNT production was found to be ~ 850 °C.

VIII-J-4 Purification and Magnetic Properties of Carbon Nanotubes

Shunji BANDOW *(Japan Science & Technology Corp.)*, **Shuji ASAKA, X. ZHAO** *(Meijo Univ.)* **and Yoshinori ANDO** *(Meijo Univ.)*

[*Appl. Phys. A* **67**, 23 (1998)]

Purification procedures for both multi- (MWNTs) and single-wall carbon nanotubes (SWNTs) are introduced in this paper. Intermediate stages in the purification procedure are monitored by scanning electron microscopy, which clearly shows the increase of the nanotube content with increasing the purification. The magnetic properties are investigated by the electron spin resonance (ESR). Two kinds of samples are used in

the ESR measurements for MWNTs and for SWNTs. One is dispersed in hexane to make loosely contacting tubules, and the other is a dried-deposited tubules to realize a close contacting tubule state. By use of these samples, it is found that the ESR lineshape is closely related to the contact between nanotubes. The curved nature of the tube wall plays an important role to explain the ESR properties.

VIII-J-5 Raman Spectroscopy of Single Wall Carbon Nanotubes

Apparao M. RAO *(Univ. Kentucky)*, **Shunji BANDOW** *(Japan Science & Technology Corp.)*, **Ernest RICHTER** *(Univ. Kentucky)* **and Peter C. EKLUND** *(Univ. Kentucky)*

[*Thin Solid Films* in press]

Pulsed laser vaporization (PLV) of a heated, Fe/Ni or Co/Ni catalyzed carbon target in argon gas has been used to synthesize single-wall carbon nanotubes (SWNTs). The Raman spectrum of SWNTs is very different from that observed for graphite (the nanotube's flat parent) and these differences can be understood as a result of the cyclic boundary condition imposed on a graphene sheet rolled up to form a seamless nanotube. Optical resonances are observed which are associated with the one dimensional character of the electronic states of these novel quantum wires. The high frequency tangential mode frequency is significantly upshifted (downshifted) when the SWNT bundles are exposed to acceptor (donor) dopants.

VIII-J-6 The Structure and Electronic Properties of Graphite Nano-Particles

Odd E. ANDERSSON *(Tokyo Inst. Tech.)*, **B. L. V. PRASAD** *(Tokyo Inst. Tech.)*, **Hirohiko SATO** *(Tokyo Inst. Tech.)*, **Toshiaki ENOKI** *(Tokyo Inst. Tech.)*, **Yoshihiro HISHIYAMA** *(Musashi Inst. Tech.)*, **Yutaka KABURAGI** *(Musashi Inst. Tech.)*, **Masanori YOSHIKAWA** *(Tokyo Inst. Tech.)*, **Shunji BANDOW** *(Japan Science & Technology Corp.)*

[*Phys. Rev. B* submitted]

We have investigated the structure and electronic properties of graphite nano-particles prepared by heat-treating diamond nano-particles. The prepared nano-graphite forms a polyhedron with a hollow in its inside, whose faces comprise a stacking of 3-6 planar graphene sheets with the in-plane size of 7-8 nm and the inter-sheet distance of 0.353 nm. The large inter-sheet distance suggests a considerably large reduction in interlayer interaction compared to the case of bulk regular graphite. Electron spin resonance and magnetic susceptibility measurements show that there is a considerable enhancement in the density of states at the Fermi energy, indicating the presence of an additional band superimposed upon the bonding π and the antibonding π^* bands around the Fermi energy. Taking into consideration the discontinuous shape at an edge line formed by crossing adjacent graphene sheets, graphene sheets in a nano-graphite particle are considered to have open π-bond edges. On the basis of the theoretical suggestion that non-bonding π orbitals give edge-inherited surface states depending on the shape of the graphene edge, this is suggestive of the contribution of the novel edge states to the electronic structure of nano-sized graphene having open p-bond edges.

VIII-K The Measurement of Dipolar Interactions under Magic-Angle Sample Spinning

VIII-K-1 Dipolar Interactions between ^{13}C and ^{15}N

Daisuke KUWAHARA, Toshihito NAKAI *(Tsukuba Univ.)* **and Seiichi MIYAJIMA**

[*Chem. Phys. Lett.* **291**, 244 (1998)]

A novel and simple method for measuring heteronuclear dipolar spectra under magic-angle sample spinning is described; the present method utilizes a chemical-shift-anisotropy recovery technique exploited by Tycko, Dabbagh and Mirau in a two-dimensional NMR experimental scheme. ^{13}C-^{15}N dipolar powder spectrum was obtained to give a internuclear distance for a doubly labeled *L*-alanine. The present method will be extended to observe a heteronuclear dipolar interaction between ^{13}C and quadrupolar nuclei having integer spins such as ^{2}H or ^{14}N.

Equipment Development Center

VIII-L Development of "IMS Machines"

The technical staff of the Equipment Development Center is partly engaged in planning, researching, designing and constructing "IMS machines." This machine, crowned with the acronym of the Institute for Molecular Science, is a high-tech experimental instrument, with emphasis on new technical idea and co-operative work with members inside and outside the Institute including those in industries. We collect suggestions of new instruments once every year from all of the members of IMS.

In this fiscal year, 1997, three project themes (1 thorough 3) were adopted as IMS machines. IMS machine projects 3 and 4 (IMS machine 1996) below were completed.

1. **Surface Profiler of Mirrors for High-Resolution Monochromator**
   (proposed by Toyohiko KINOSHITA, developed with Hisashi YOSHIDA, Toshio HORIGOME, and Shuji ASAKA)
2. **Off-Axis Paraboloid Polarizing Mirror for Far-Infrared Light**
   (proposed and developed by Hideyuki OHTAKE and Takayuki YANO)
3. **Multi-Channel Detector for Mid-Infrared Light**
   (proposed by Takashi OGURA, developed with Hisashi YOSHIDA and Shuij ASAKA)
4. **Programmable Micro Current Source**
   (proposed and developed by Tomonori TOYODA)

Brief reports on the projects 3 and 4 are presented in the following.

VIII-L-1 Multi-Channel Detector for Mid-Infrared Light

Hisashi YOSHIDA, Shuji ASAKA and Takashi OGURA

We have developed a multi-channel detector for mid-infrared light by using a 256-channel MCT photoconductive array cell (HAMAMATSU, Figure 1). The block diagram of the present device is shown in Figure 2. The current signals from the MCT cells are amplified and integrated in respective 256 units of AC-coupled amplifier and gated integrators. The output from each integrator is fed to a computer channel by channel through a data multiplexer. There exists a difficulty in that the high gain amplifiers undergo large voltage drifts due to temperature change. We have overcome this point by adding a chopper in the incoming light source, gating the integrator to synchronize with the open and closed periods of the chopper, and finally taking the difference of the two integrated outputs. The subtraction is done in a software to reduce the loads to the hardware. Control and data processing are performed on a DOS machine, and this software was developed by use of VisualBasic. The appearance of the developed detector system is shown in Figure 3.

Figure 1. Outer view of 256-channel MCT photoconductive array cell.

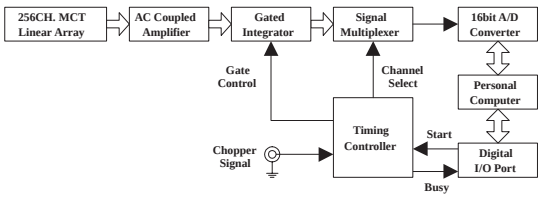

Figure 2. Block diagram of the multi-channel detector system.

Figure 3. Appearance of the multi-channel detector system.

VIII-L-2 Programmable Micro Current Source

Tomonori TOYODA

We have developed a programmable micro current source for growth of conductive organic crystals.

A group of organic crystals are grown by an electrolytic reaction under a constant micro current for a long period of time. The present current source, which can be digitally programmed and controlled, is suitable for such crystal grouth. The appearance of the device is shown in Figure 1. The source shown includes a single module which has eight output channels, and the number of output channels can be increased simply by adding the modules.

Furthermore, based on requests from chemical researchers, the device is equipped with a voltage monitor across both ends of the crystal. This voltage is one of the most important growth parameters since the electrolytic reaction varies according to the voltage. In other current sources, this voltage has not often been utilized to control the crystal growth. In the present device the output current can be controlled so that the voltage across both ends of the crystal under growth does not exceed a certain point. This feature may enable users to isolate crystals in a certain single oxidization (deoxidization) state out of many possible states. The device can also be used to find optimal growth conditions of the crystals by investigating the programmed current profiles.

Figure 1. Appearance of the programmable micro current source.

VIII-M Development of Experimental Devices

VIII-M-1 Prototype Apparatus for Synthesizing the Single Wall Carbon Nanotubes by Arc Discharge at High Temperature Environment

Tatsuharu TORII and Shunji BANDOW *(Japan Science & Technology Corporation)*

The single wall carbon nanotubes (SWNTs) can be synthesized by arc burning of the carbon rod containing bi-metallic catalysts such as Ni-Y, Co-Ni and Fe-Ni. Normally, the composite carbon rod is burnt by arcing at a room temperature environment. Recently, it was found that the synthesis rate of SWNTs was accelerated at high temperature environment (T < ~ 850 °C) by the laser evaporation method.[1)] Here we designed an apparatus for studying the temperature effect on yielding the SWNTs by the arc vaporization method.

Figure 1 is a schematic of the apparatus for arc vaporization of the composite carbon rod at high temperature. The composite carbon rod (10 mm in diameter) is set at the end of the positive electrode and the counter rod is pure carbon (number 3 in Fig. 1), both of which are set in the quartz tube(50 mm in diameter and 1000 mm in length, number 1 in Figure 1). The environment temperature around the arcing is controlled by a 300 mm electric tube furnace placed near the center of the quartz tube, whose furnace can elevate the temperature up to 1200 °C. The part number 2 in Figure 1 is a handle for feeding a composite carbon rod to adjust a spark gap. Most of the SWNTs prepared under high temperature environment are carried by the He flow (500 Torr,100 sccm) and gathered on the water cooled copper collector. The photographic picture of this apparatus is shown in Figure 2.

It is also planned for further study to construct an automatic spark gap adjusting system to realize a suitable sparking condition.

Reference

1) S. Bandow, et al., Phys. Rev. Lett. 80, 3779 (1998).

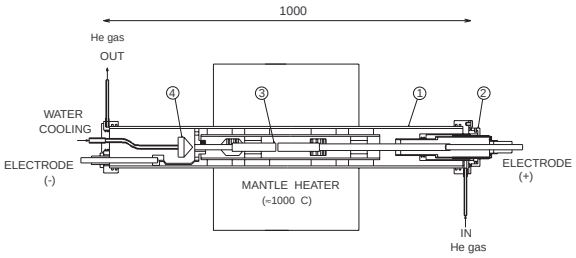

Figure 1. Schematic of the apparatus for arc vaporization of the composite carbon rod at high temperature.

Figure 2. Photographic picture of the apparatus.

VIII-N Development of Spectroscopic System with Combination of Synchrotron Radiation and Laser

VIII-N-1 Time-Gated Photon Counting Method for Two-Photon Spectroscopy Using Synchrotron Radiation and Laser

Shuji ASAKA, Shunsuke NAKANISHI *(Kagawa Univ.)*, **Hiroshi ITOH** *(Kagawa Univ.)*, **Masao KAMADA** *(UVSOR Facility)*, **Masayuki WATANABE** *(Kyoto Univ.)*, **Osamu ARIMOTO** *(Okayama Univ.)*, **Shigeki FUJIWARA** *(Okayama Univ.)*, **Toru TSUJIBAYASHI** *(Osaka Dental Univ.)* **and Minoru ITOH** *(Shinshu Univ.)*

[*Rev. Sci. Instrum.* **69**, 1931 (1998)]

A new measurement system has been developed for two-photon spectroscopy in solids with a combination of synchrotron radiation and laser. This system is based on a time-gated photon counting technique (Figure 1) to observe luminescence signals induced by two-photon excitation. It is demonstrated that this technique enables us to achieve a high sensitivity and a good signal-to-noise ratio because it is a kind of zero-method.

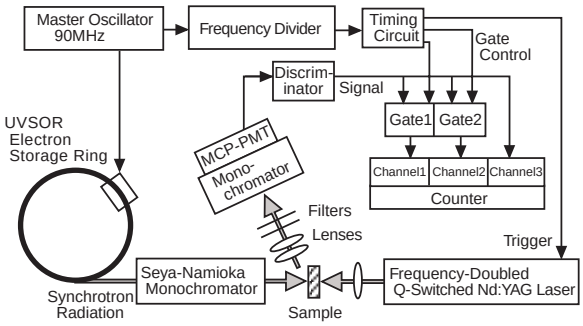

Figure 1. Block diagram of experimental setup for two-photon spectroscopy.

Ultraviolet Synchrotron Orbital Radiation Facility

VIII-O Development of the UVSOR Light Source

VIII-O-1 Non-linear Calibration of Beam Position Monitors

Masahito HOSAKA, Shiro TAKANO *(SPring-8)*, **Jun-ichiro YAMAZAKI, Toshio KINOSHITA, Hitoshi TANAKA** *(SPring-8)* **and Hiroyuki HAMA**

To deduce higher order terms of the dispersion function in the UVSOR storage ring by measuring slight changes of the beam equilibrium orbit, precise calibrations of the beam position monitors (BPMs) are crucial. A first order form of the solution of the Poisson equation for a vacuum chamber at the BPMs has been used so far. However there was a couple of difficulties and problems; (1) a very narrow region to be properly applied (< 3 mm) and (2) attenuation due to connectors and cables were not exactly known, so that experimental data derived from the BPMs has been less accuracy and reliability. To overcome these issues, a numerical evaluation for inductive electric fields in the chamber has been performed by using a boundary element method and a higher order expansion of the analytical solution of the Poisson equation up to 10-th order has been also evaluated. Both results are quite in good agreement in a very wide range (< 10 mm). Attenuation factors for all button monitors were obtained by using a least squares method to fit an identical position deduced from four different combinations of three button monitors in a BPM. Consequently the accuracies of the beam position of 5 μm and 10 μm for the horizontal and the vertical planes, respectively, were obtained.

VIII-P Researches by the USE of UVSOR

VIII-P-1 Time Response and Temperature Dependence of Photo-Stimulated Desorption of Sodium Atoms from Sodium Halides

Sayumi HIROSE *(Sumitomo Heavy Industries Ltd.)* **and Masao KAMADA**

[*J. Electron Spectroscopy and Related Phenomena* **92**, 109 (1998)]

Photo-stimulated desorption (PSD) of sodium atoms from sodium halide crystals has been investigated using intense synchrotron radiation from a planar-type undulator. The PSD intensities of ground-state and excited-state Na atoms showed different temperature dependence, indicating different desorption processes. The temperature dependence of the PSD intensities was also different from that of thermally-stimulated desorption. Moreover, time response of the excited-state Na desorption was found to consist of a nano-second component and a slower one. The temperature dependence of the nano-second component was also different from that of the slow PSD. These present results are consistent with the idea that the excited-state alkali desorption can be interpreted with two models, a fast desorption induced by electronic transition in the surface layer and a slow one due to thermal process of surface defects.

VIII-P-2 Laser-Induced Fluorescence Study of Fast Desorption of Ground-State K Atoms from Potassium Halides Excited by Synchrotron Radiation

Masao KAMADA and Sayumi HIROSE *(Sumitomo Heavy Industries Ltd.)*

[*Surface Science* **390**, 194 (1997)]

The nano-second desorption of ground-state K atoms from KCl was investigated for the first time by using a laser-induced fluorescence method with synchrotron radiation and laser pulses. It was found that the desorption consists of a nano-second component and a slow one more than 178 ns. The fast desorption is several orders of magnitude faster than the existing results of the time response of ground-state alkali desorption. Therefore, the fast desorption of ground-state alkali atoms can not be interpreted with the existing mechanisms and requires a new desorption model. We suggest that the lattice instability due to the electronic excitation in the surface layer may play an important role on the fast desorption of ground-state alkali atoms.

VIII-P-3 Circular Dichroism in the Angular Distribution of Core-Level Photoelectrons from GaAs (111)

Masao KAMADA, Yong Q. CAI *(Univ. Tokyo)*, **Naoshi TAKAHASHI** *(Heinrich-Heine-Univ. Duesseldorf)*, **Shin-ichiro TANAKA and D. A. WOOLF** *(Univ. Wales, UK)*

[*J. Electron Spectroscopy and Related Phenomena* **72**, 219 (1998)]

The circular dichroism of angle-resolved photoelectron spectra was investigated for core-levels from clean and hydrogen exposed GaAs (111) surfaces. It was found that the circular dichroism of Ga-3d and As-3d photoelectrons shows clear dependence on the emission angle of the photoelectrons and the sample surface. It is proposed that the experimental results may be interpreted primarily in terms of the interference of photoelectrons affected by the anisotropic field in the surface layer of GaAs (111).

VIII-P-4 Simultaneous Measurements of Photoelectron and Luminescence of Barium Halides

Masao KAMADA, Shigeki FUJIWARA *(Okayama Univ.)*, **Osamu ARIMOTO** *(Okayama Univ.)*, **Yasuo FUJII** *(Osaka City Univ.)* **and Shin-ichiro TANAKA**

[*J. Electron Spectroscopy and Related Phenomena* **88-91**, 297 (1998)]

Photoelectron and optical spectra are both important to know the electronic structures of solids, but they have been measured independently in insulating materials so far. In the present experiments, simultaneous measurements of photoelectron and luminescence spectra of BaF2 thin films were carried out. It was found that both photoemission and luminescence intensities decrease with increasing synchrotron-radiation doses, indicating the formation of radiation-induced defects. Also, the time-correlation between Ba-4d photoelectrons and Auger-free luminescence photons was observed for the first time, suggesting that these correlate with each other.

VIII-P-5 Temperature Dependence of Auger-Free Luminescence in Alkali and Alkaline-Earth Halides

Minoru ITOH *(Shinshu Univ.)*, **Masao KAMADA and Nobuhito OHNO** *(Osaka Electron-Communication Univ.)*

[*J. Phys. Soc. Jpn.* **66**, 2502 (1997)]

Auger-free luminescence (AFL) resulting from a radiative transition between the outermostcore bands and the valence in BaF2, RbF, CsF, CsCl and been studied in a wide range of temperatures from 10 to 300 K. The AFL spectra are separated from those originating from the valence-band excitation with use of time-resolved luminescence spectroscopy. It is found that the decay profile of AFL in each crystal is essentially the same throughout the spectrum. The remarkkable thermal broadening of the linewidth is verilied for all systems. This strongly suggests that the core hole generated on a positive ion induces considerable displacement of the surrounding ions within its lifetime. Based on the predent results, the spectral shape of AFL is discussed in terms of a cluster model and a two-band model, requiring further development of the investigations in theory and experiment.

VIII-P-6 Combinational Use of Synchrotron Radiation and Laser for Two-Photon Spectroscopy of BaF_2[1]

Osamu ARIMOTO *(Okayama Univ.)*, **Shigeki FUJIWARA, Toru TSUJIBAYASHI** *(Osaka Dental Univ.)*, **Masayuki WATANABE** *(Kyoto Univ.)*, **Minoru ITOH** *(Shinshu Univ.)*, **Shunsuke NAKANISHI** *(Kagawa Univ.)*, **Hiroshi ITOH** *(Kagawa Univ.)*, **Shuji ASAKA and Masao KAMADA**

[*J. Electron Spectroscopy and Related Phenomena* **88-91**, 219 (1998)]

We have carried out nonlinear spectroscopy by making use of tunable VUV ligt from synchrotron radiation (SR) together with intense lgt from a laser. The valence excitons of BaF2 with a large band gap of ~11 eV were chosen as our target. A single crystal of BaF2 was irradiated at 15 K by the two light pulses from the SR (6-9eV) and an Nd:YAG laser (2.33eV). Self-trapped exciton luminescence induced by two-photon excitation was detected with a time-gated photon-counting system developed for the present study. This zero-method technique is expected to be sensitive compared to early experiments by an Italian group monitoring transmittance changes. The energy of the 2P exciton is estimated to be 10.6 eV at 15 K.

VIII-P-7 Direct Excitation of Tl^+ Impurity Ions by Hot Photoelectrons in Wide-Gap Crystals

E. FELDBACH *(Inst. Physics)*, **Masao KAMADA, M. KIRM** *(Inst. Physics)*, **A. LUSHCHIK** *(Tartu Univ. and IMS)*, **Ch. LUSHCHIK** *(Inst. Physics)* **and I. MARTINSON** *(Lund Univ.)*

[*Phys. Rev. B* **56**, 13908 (1997)]

The reflection spectra of KCI and RbCl crystals and excitation spectra of *A* and *B* luminescence and recombination phosphorescence of Tl^+ centers for RbCl:Tl and KCl:Tl crystals have been measured in a spectral region from 5 to 30 eV. The energy distribution curvers of emitted electrons have been measured on the excitation of RbCl thin films by 13-30 eV photons. The comparative analysis of optical and photoelectric characteristics allowed us to reveal the effect of direct excitation of Tl^+ impurity ions up to *A* ($^3P_1$), *B* ($^3P_2$), and *C* ($^1P_1$) states by hot conduction electrons. The threshold photon energies of this effect are determined. The estimated energies of conduction electrons, formed by such photons, are close to the energies of direct optical transitions $^1S_0 \rightarrow {}^3P_1$ (5 eV) and $^1S_0 \rightarrow {}^3P_2$ (6eV) of Tl^+ centers in KCl:Tl and RbCl:Tl crystals. Similar to the case of ns^2 free atoms, the excitation functions for triplet states of Tl^+ centers have a sharp maximum at the energy just above the threshold in RbCl:Tl and KCl:Tl crystals. The peculiarities of electron impact spectroscopy of impurity ions in wide-gap crystals are discussed.

VIII-P-8 Study of Ion Desorption Induced by the Core-Level Excitation on the CaF_2(111) Surface

Shin-ichiro TANAKA, Kazuhiko MASE, Mitsuru NAGASONO and Masao KAMADA

[*J. Elec. Spec. and Rel. Phenom.* **92**, 119 (1998)]

Desorption of F^+ induced by core-level excitation with synchrotron radiation has been investigated on the

CaF_2 (111) film produced on Si(111). The ion yield is proportional to electron yield in the region of Ca-2p edge, while an enhancement of the ion yield is observed at the photon energy for the F-1s core-exciton. The peak corresponding to the F-1s excitation observed in the ion yield is shifted from that in the electron yield by about -1.2eV, which is predominantly ascribed to the change in the Madelung potential at the surface. The electron-ion coincidence study shows that the F^+ desorption is directly stimulated via a decay of the F-1s surface core-exciton, while secondary-electron stimulated desorption is the predominant process after the creation of Ca-2p hole.

VIII-P-9 Observation of the Surface States on CuCl(100)

Shin-ichiro TANAKA and Masao KAMADA

[*J. Elec. Spec. and Rel. Phenom.* **88-91**, 689 (1998)]

The surface electronic structure of the CuCl(100) film produced on the Si(100) surface was investigated by using the angle-resolved photoelectron spectroscopy with synchrotron radiation. Two surface states were observed, and assigned to Cl-3p and Cu-3d, respectively. The dispersions of them were measured (Figure 1). The photoelectron spectra of the CuCl(100) surface exposed to CO gas were also observed, and it was found that CO is adsorbed on CuCl(100) through a Cu atom.

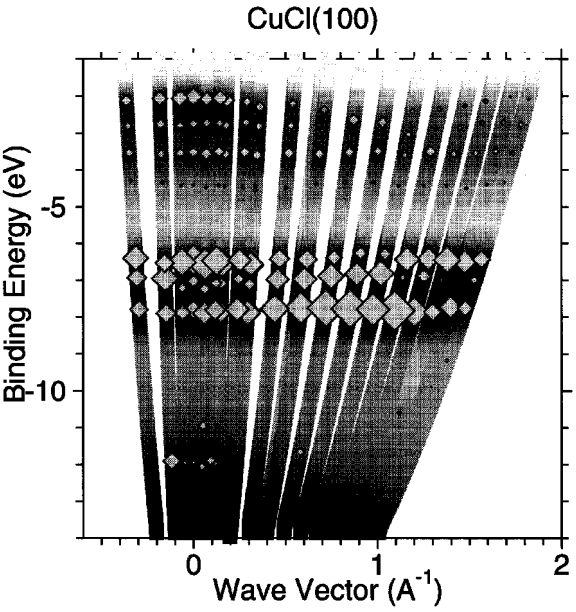

Figure 1. Band dispersions determined by angle resolved photoelectron spectroscopy. Grey tapes correspond to photoelectron spectra. Symbols correspond to the components of fitting calculations, and their size indicates the area intensity of components.

VIII-P-10 Electronic Structures of Organic Salts $(DI\text{-}DCNQI)_2M$ (M = Cu and Ag) Using Photo-electron Spectromicroscopy

Yuichi HARUYAMA, Shin-ichi KIMURA, Yüksel UFUKTEPE *(Univ. Cukurova-Turkey)***, Toyohiko KINOSHITA, Krishna Gopal NATH, Ko-ichi HIRAKI** *(Gakushuin Univ.)* **and Kazushi KANODA** *(Univ. Tokyo)*

The electronic structures of organic salts $(DI\text{-}DCNQI)_2M$ with M = Cu and Ag, where DI-DCNQI is 2,5-diiodo-N,N'-dicyanoquinonediimine, have been studied at various photon energies using the photo-electron spectromicroscopy. The experiments have been performed at the BL5B with VG ESCALAB 220i-XL system. From the photon energy dependence of the photoionization cross-section, the atomic orbital characters of the observed spectral features are determined. For both $(DI\text{-}DCNQI)_2Cu$ and $(DI\text{-}DCNQI)_2Ag$, the C and N 2*p* states originating in the cyano group and the quinone ring are located at ~ 4.0 eV and ~ 6.5 eV, respectively. The Cu 3*d* states for $(DI\text{-}DCNQI)_2Cu$ and the Ag 4*d* states for $(DI\text{-}DCNQI)_2Ag$ are located at ~ 3.5 eV and ~ 5.5 eV, respectively. This indicates that the $p\pi$-*d* hybridization at the Fermi level between the M ions and the N atoms of the DCNQI columns is larger for $(DI\text{-}DCNQI)_2Cu$ than for $(DI\text{-}DCNQI)_2Ag$. From the comparison between the observed photoemission spectra for $(DI\text{-}DCNQI)_2Cu$ and the previous ones for $(DMe\text{-}DCNQI)_2Cu$,[1] the energy shifts of the C and N 2*p* states originating in the quinone ring and the Cu 3*d* states are observed. These energy shifts probably reflect the difference in the chemical bond caused by the minor structural change.

Reference

1) A. Tanaka, A. Chainani, T. Miura, T. Takahashi, T. Miyazaki, S. Hasegawa and T. Mori, *Solid State Commun.* **93**, 1 (1995).

VIII-P-11 Resonant Photoemission Study of Temperature-Induced Valence Transition Material $EuNi_2(Si_{1-x}Ge_x)_2$

Heralu Pathirannehelage Nihal Jayalath GUNASEKARA *(Ceylon Inst. Sci. and Ind. Research, Sri Lanka)***, Yasutaka TAKATA, Shin-ichi KIMURA, Toyohiko KINOSHITA, Nobuhiro KOSUGI, Krishna Gopal NATH, Hirofumi WADA** *(Kyoto Univ.)***, Akihiro MITSUDA** *(Kyoto Univ.)***, Masayuki SHIGA** *(Kyoto Univ.)***, Haruhiko OGASAWARA** *(Univ. Tokyo)* **and Akio KOTANI** *(Univ. Tokyo)*

Among the intermediate valent systems of rare earth compounds, Eu compounds are known to exhibit strong temperature dependence of the mean valence. Very recently, it was found that the $EuNi_2(Si_{1-x}Ge_x)_2$ compounds with $0.70 \leq x \leq 0.82$ show a temperature induced valence transition below room temperature.[1] It has been known that the 3*d*-4*f* resonant photoemission of such kind of mixed valent 4*f* compounds is a rather useful technique to clarify the different 4*f* electronic states owing to different valence than the 4*d*-4*f* resonant photoemission. In this study, we have applied the 3*d*-4*f* resonant photoemission method to investigate the valence transition of the $EuNi_2(Si_{1-x}Ge_x)_2$ compound. The experiments were performed at BL1A with the SCIENTA SES-200 analyzer. Figures show the

resonant photoemission spectra along with the photoelectron total yield (TY) spectra around the Eu 3*d*-4*f* excitation region at about 300K and 80K. It is noticed that the peaks 2 and 3 for the TY spectrum are enhanced at the low temperature phase. This is due to the increase of the trivalent Eu ion component at low temperature. In the same manner, the trivalent components of Eu 4*f* photoemission states are enhanced at the excitation conditions of 2 and 3, whereas the divalent 4*f* states are dominant at 1, 4 and 5. From these results, the features around 0-4 eV binding energy are estimated to be mostly divalent 4*f* states and those around 6-12 eV are trivalent ones in these on-resonant spectra.The results were compared with the theoretical calculation based on an atomic model for divalent and trivalent Eu ions. The estimated values of the mean valence for both temperature were smaller than those reported before. This may be due to the effect of the oxidization of the samples in the previous experiments.[1)]

Reference

1) H. Wada, A. Nakamura, A. Mitsuda, M. Shiga, T. Tanaka, H. Mitamura and G. Goto, *J. Phys., Condens. Matter.* **9**, 7913 (1997).

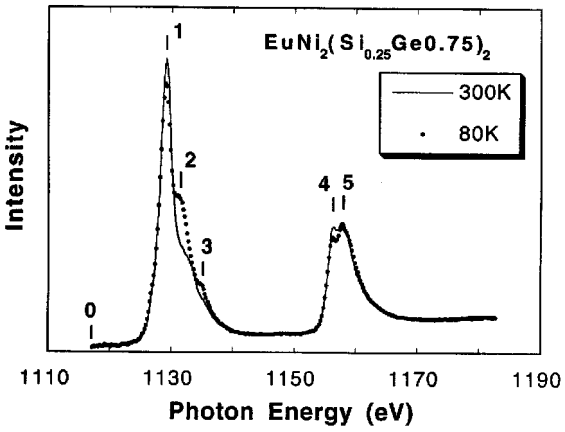

Figure 1. 3*d*-4*f* TY spectra for $EuNi_2(Si_{1-x}Ge_x)_2$ (x = 0.75) at 300K and 80K.

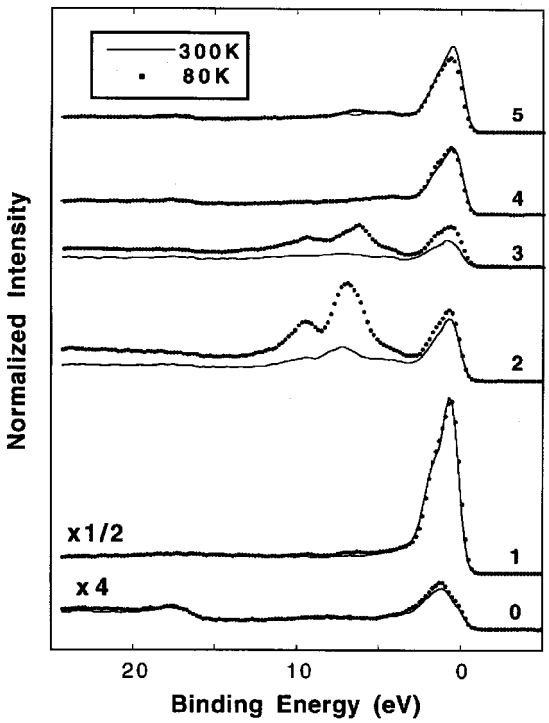

Figure 2. 3*d*-4*f* Resonant photoemission spectra for $EuNi_2(Si_{1-x}Ge_x)_2$ (x = 0.75).

VIII-P-12 Study of Magnetic Linear Dichroism (MLD) for Different Thickness of Ni-Thin Film Grown on Ferromagnetic Co (100) in Element Specific Photoemission

Krishna Gopal NATH, Yuichi HARUYAMA, Shinichi KIMURA, Yüksel UFUKTEPE *(Univ. Cukurova-Turkey)* **and Toyohiko KINOSHITA**

Study of the thin film magnetism is one of the expanding topics in the surface science. In order to investigate the magnetic behaviors of Ni/Co (100) and compare with those of Ni/Cu (100), we measured magnetic linear dichroism (MLD) for either the valence band or the core level (3*p*) photoelectrons of the different thickness of Ni-film grown on Co substrate. The VG ESCALAB 220i-XL system was connected to the beam line BL5B for the experiments. Thin film is magnetized along two orthogonal directions in the surface plane (in-plane magnetization) where one of these directions is along Cu [100] direction.

Figure 1 shows the MLD results for 3d bands of the Ni thin films on Co and Cu substrates, respectively, taken at the photon energy of 67.2eV, i.e. the Ni 3*p*-3*d* resonant condition. It is found in Figure 1(a) that both the main peak ($3d^9$) and the satellite peak ($3d^8$) show asymmetry but in opposite sign from each other for Ni/Co system. On the other hand, the Ni/Cu system does not show the MLD. This is an evidence that the Ni thin film around 10ML on Co shows in-plane magnetization at room temperature whereas the Ni/Cu does not show the in-plane magnetization. The MLD results in Figure 1(a) is similar to the previous MCDAD result but not similar to the MLDAD result reported by Ueda et al.[1)] The theoretical calculation is in progress, which will give us more clear understanding about resonant

effect on MLD for satellite region.

Reference

1) S. Ueda, S. Imada, Y. Saitoh, T. Mura, M. Kasashima, A. Kimura, A. Kakizaki and S. Suga, *J. Electron Spectrosc. Relat. Phenom.* **88-91**, 191 (1998).

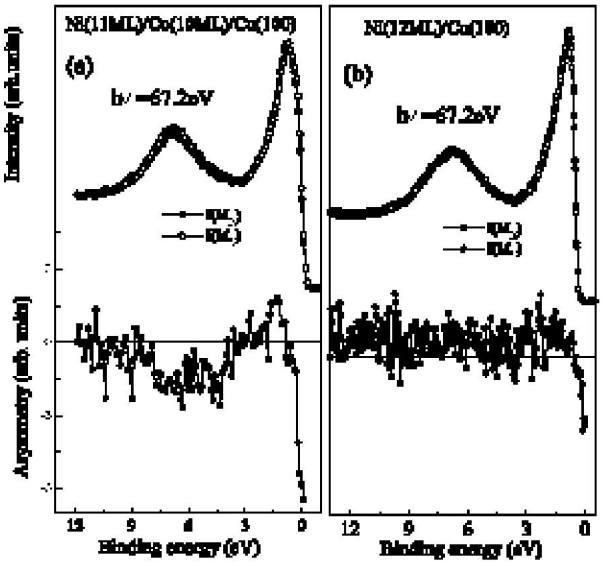

Figure 1. Ni 3*d* photoemission spectra for the two magnetized directions **M**//**E**(closed) and **M** **E**(open), where **M** is the vector of magnetization and **E** is of polarization of the light. The lower panel shows the MLD, i.e., asymmetry obtained from the two spectra. (a) is for Ni/Co system and (b) for Ni/Cu.

VIII-P-13 Tm5p Resonant Photoemission Study of TmX (X=S, Se and Te) around 4d-Excitation Region

Krishna Gopal NATH, Yüksel UFUKTEPE *(Univ. Cukurova-Turkey)***, Shin-ichi KIMURA, Toyohiko KINOSHITA, Takeshi MATSUMURA** *(Tohoku Univ.)***, Takashi SUZUKI** *(Tohoku Univ.)***, Haruhiko OGASAWARA** *(Univ. Tokyo)* **and Akio KOTANI** *(Univ. Tokyo)*

In the 4*d*-4*f* resonant process of rare earth compounds, study of resonant behavior of core levels (5*p* or 5*s*) is important to understand overall decay processes related to different electronic states. In fact, the core level photoemission spectra in rare earth systems show complex multiplet structures due to existence of unfilled and localized 4*f*-shell.[1)] Sometimes it is rather difficult to separate the spin-orbit peaks and the valence components if the system is mixed-valence. Followed by the recent resonant photoemission of 4*f*-states at the 4*d*-4*f* excitation condition of thulium compounds (TmS, TmSe, and TmTe) for divalent and trivalent Tm-ions,[2)] in this study, we present the Tm-5*p* photoemission results at the 4*d*-4*f* absorption edges (hν = 150-200 eV) of Tm-compounds. The experiments were performed at BL2B1.

Figure 1 shows the on- and off- resonant 5*p* resonant photoemission results of mostly divalent compounds TmTe. It is noticed that the resonance effect is larger for higher binding energy states, i.e. around 30 eV than lower ones around 24 eV. In Figure 2, the resonance behavior of trivalent Tm5*p* of TmSe, a typical mixed-valent compound, is shown. The photoemission spectra also show the both Tm^{3+} and Tm^{2+} components as seen in the comparison with the calculated curves for two valences. It is found that 4*d*5*p*4*f*-decay channel is also active but not so strong as 4*d*4*f*4*f* decay channel. The photoemission spectra for two Tm-valences are defined by complex multiplet structures, not only by single 5*p*3/2 or 5*p*1/2 peak.

References

1) A.Kotani, *Inner shell photoelectron process in solids* (Hand book on synchrotron Radiation), vol. 2, G. V. Marr, Ed., North-Holland Physics Publishing; Amsterdam (1987).
2) Y.Ufuktepe, S. Kimura, T. Kinoshita, K. G. Nath, H. Kumigashira, T. Takahashi, T. Matsumura, T. Suzuki, H. Ogasawara and A. Kotani, *J. Phys. Soc. Jpn.* **67**, 2018 (1998).

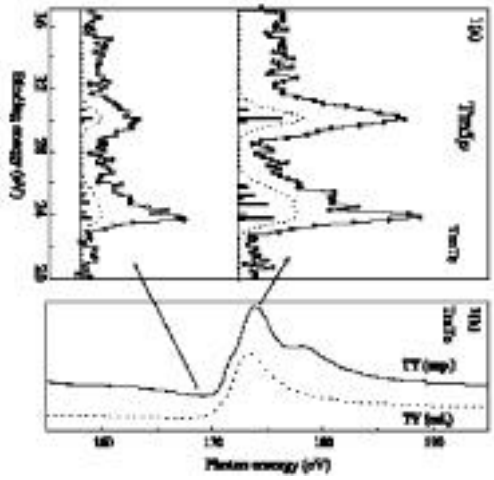

Figure 1. (a) On (upper)- and off (lower)-resonant photoemission spectra of Tm*5p* for TmTe, mostly divalent compounds. The calculated spectra for Tm divalent ion are shown for comparison.
(b) Photoelectron total yield spectrum of TmTe around the Tm*4d* edge. The calculated spectrum for Tm divalent ion is also shown.

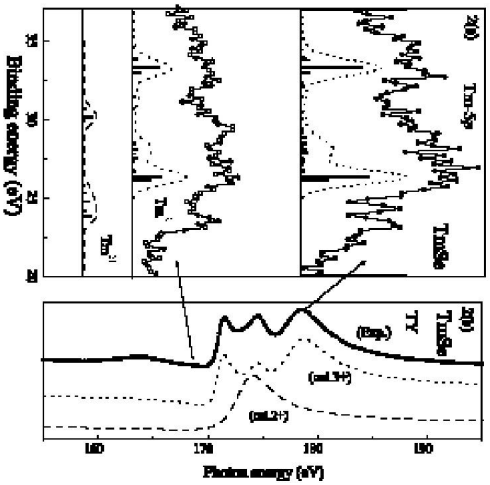

Figure 2. Same as in Figure 1, but for TmSe. Both the divalent and trivalent components are observed and calculated.

VIII-P-14 Photodissociation of Ozone in the K-Edge Region

Tatuso GEJO, Kazumasa OKADA *(Hiroshima Univ.)*, **Toshio IBUKI** *(Kyoto Univ. Education)*, **Norio SAITO** *(ETL)* **and Isao H. SUZUKI** *(ETL)*

Ozone is one of the most important molecules in chemistry since ozone in the stratosphere absorbs UV light emitted from the sun and prohibits humanity from the exposure by the UV light. We have investigated the photochemistry and photodissociation dynamics of Ozone in K-edge region with angle-resolved time-of-flight apparatus for the first time. TOF spectra were obtained at 0 and 90 degree relative to the axis of soft x-ray polarization. At π^* excitation from 1s level of terminal ones, O^+ and O_2^+ photofragments are observed to be emitted to the direction perpendicular to the polarization of light, which is consistent with our assignment.[1] TOF spectra at π^* excitation from that of center one, however, shows more isotropic ones. It suggests the overlap of several electronic states. This is consistent with our calculation which predict that π^* state ($2b_1$) are overlapped with σ^* ($5a_1$) state in this band. A π^* excitation from inner-1s of center oxygen atom generates preferably O^+, compared to that from inner-1s of terminal oxygen atoms.

Reference

1)T. Gejo, K. Okada and T. Ibuki, *Chem. Phys. Letters* **277** 497 (1997)